Characteristics of Environmental Data Layers for Use in Species Distribution Modelling in the Maritimes Region

L. Beazley, J. Guijarro, C. Lirette, Z. Wang, E. Kenchington

Ocean and Ecosystem Sciences Division
Maritimes Region
Fisheries and Oceans Canada

Bedford Institute of Oceanography
PO Box 1006
Dartmouth, Nova Scotia
Canada B2Y 4A2

2017

Canadian Technical Report of Fisheries and Aquatic Sciences 3212

Fisheries and Oceans Canada | Pêches et Océans Canada

Canada

Canadian Technical Report of Fisheries and Aquatic Sciences

Technical reports contain scientific and technical information that contributes to existing knowledge but which is not normally appropriate for primary literature. Technical reports are directed primarily toward a worldwide audience and have an international distribution. No restriction is placed on subject matter and the series reflects the broad interests and policies of Fisheries and Oceans Canada, namely, fisheries and aquatic sciences.

Technical reports may be cited as full publications. The correct citation appears above the abstract of each report. Each report is abstracted in the data base *Aquatic Sciences and Fisheries Abstracts*.

Technical reports are produced regionally but are numbered nationally. Requests for individual reports will be filled by the issuing establishment listed on the front cover and title page.

Numbers 1-456 in this series were issued as Technical Reports of the Fisheries Research Board of Canada. Numbers 457-714 were issued as Department of the Environment, Fisheries and Marine Service, Research and Development Directorate Technical Reports. Numbers 715-924 were issued as Department of Fisheries and Environment, Fisheries and Marine Service Technical Reports. The current series name was changed with report number 925.

Rapport technique canadien des sciences halieutiques et aquatiques

Les rapports techniques contiennent des renseignements scientifiques et techniques qui constituent une contribution aux connaissances actuelles, mais qui ne sont pas normalement appropriés pour la publication dans un journal scientifique. Les rapports techniques sont destinés essentiellement à un public international et ils sont distribués à cet échelon. II n'y a aucune restriction quant au sujet; de fait, la série reflète la vaste gamme des intérêts et des politiques de Pêches et Océans Canada, c'est-à-dire les sciences halieutiques et aquatiques.

Les rapports techniques peuvent être cités comme des publications à part entière. Le titre exact figure au-dessus du résumé de chaque rapport. Les rapports techniques sont résumés dans la base de données *Résumés des sciences aquatiques et halieutiques.*

Les rapports techniques sont produits à l'échelon régional, mais numérotés à l'échelon national. Les demandes de rapports seront satisfaites par l'établissement auteur dont le nom figure sur la couverture et la page du titre.

Les numéros 1 à 456 de cette série ont été publiés à titre de Rapports techniques de l'Office des recherches sur les pêcheries du Canada. Les numéros 457 à 714 sont parus à titre de Rapports techniques de la Direction générale de la recherche et du développement, Service des pêches et de la mer, ministère de l'Environnement. Les numéros 715 à 924 ont été publiés à titre de Rapports techniques du Service des pêches et de la mer, ministère des Pêches et de l'Environnement. Le nom actuel de la série a été établi lors de la parution du numéro 925.

Canadian Technical Report of
Fisheries and Aquatic Sciences 3212

2017

Characteristics of Environmental Data Layers for Use in Species Distribution Modelling in the Maritimes Region

by

L. Beazley, J. Guijarro, C. Lirette, Z. Wang, E. Kenchington

Ocean and Ecosystem Sciences Division
Maritimes Region
Fisheries and Oceans Canada
Bedford Institute of Oceanography
P.O. Box 1006
Dartmouth, N.S.
Canada B2Y 4A2

© Her Majesty the Queen in Right of Canada, 2017.
Cat. No. Fs97-6/3212 ISBN 978-0-660-08365-0 ISSN 1488-5379

Correct citation for this publication:

Beazley, L., Guijarro, J., Lirette, C., Wang, Z., and Kenchington, E. 2017. Characteristics of Environmental Data Layers for Use in Species Distribution Modelling in the Maritimes Region. Can. Tech. Rep. Fish. Aquat. Sci. 3212: vii + 327p.

TABLE OF CONTENTS

ABSTRACT vi
RÉSUMÉ vii
INTRODUCTION 1
MATERIALS AND METHODS 2
Study Area 2
Data Sources 3
Global Ocean Reanalyses and Simulations (GLORYS) 3
Sea Surface Chlorophyll *a* 4
Sea Surface Primary Production 5
World Ocean Database 2013 (WOD13) 7
Spatial Interpolation Methods 9
Data Exploration and Model Fitting (adapted from Beazley et al., 2016b) 9
Caveat for Spatial Interpolation Using Ordinary Kriging 10
Assessment of Model Performance (extracted from Beazley et al., 2016b) 11
RESULTS 13
Temperature 13
Bottom Temperature Mean 13
Bottom Temperature Minimum 16
Bottom Temperature Maximum 19
Bottom Temperature Range 22
Bottom Temperature Average Minimum 25
Bottom Temperature Average Maximum 28
Bottom Temperature Average Range 31
Surface Temperature Mean 34
Surface Temperature Minimum 37
Surface Temperature Maximum 40
Surface Temperature Range 43
Surface Temperature Average Minimum 46
Surface Temperature Average Maximum 49
Surface Temperature Average Range 52
Salinity 55
Bottom Salinity Mean 55
Bottom Salinity Minimum 58
Bottom Salinity Maximum 61
Bottom Salinity Range 64
Bottom Salinity Average Minimum 67
Bottom Salinity Average Maximum 70
Bottom Salinity Average Range 73
Surface Salinity Mean 76
Surface Salinity Minimum 79
Surface Salinity Maximum 82
Surface Salinity Range 85
Surface Salinity Average Minimum 88

Surface Salinity Average Maximum 91
Surface Salinity Average Range 94
Current Speed 97
Bottom Current Mean 97
Bottom Current Minimum 100
Bottom Current Maximum 103
Bottom Current Range 106
Bottom Current Average Minimum 109
Bottom Current Average Maximum 112
Bottom Current Average Range 115
Surface Current Mean 118
Surface Current Minimum 121
Surface Current Maximum 124
Surface Current Range 127
Surface Current Average Minimum 130
Surface Current Average Maximum 133
Surface Current Average Range 136
Maximum Seasonal Mixed Layer Depth 139
Maximum Spring Mixed Layer Depth 139
Maximum Summer Mixed Layer Depth 142
Maximum Fall Mixed Layer Depth 145
Maximum Winter Mixed Layer Depth 148
Maximum Average Spring Mixed Layer Depth 151
Maximum Average Summer Mixed Layer Depth 154
Maximum Average Fall Mixed Layer Depth 157
Maximum Average Winter Mixed Layer Depth 160
Bottom Shear 163
Bottom Shear Mean 163
Bottom Shear Minimum 166
Bottom Shear Maximum 169
Bottom Shear Range 172
Bottom Shear Average Minimum 175
Bottom Shear Average Maximum 178
Bottom Shear Average Range 181
Sea Surface Chlorophyll *a* 184
Spring Chlorophyll *a* Mean 184
Spring Chlorophyll *a* Minimum 187
Spring Chlorophyll *a* Maximum 190
Spring Chlorophyll *a* Range 193
Summer Chlorophyll *a* Mean 196
Summer Chlorophyll *a* Minimum 199
Summer Chlorophyll *a* Maximum 202
Summer Chlorophyll *a* Range 205
Fall Chlorophyll *a* Mean 208
Fall Chlorophyll *a* Minimum 211
Fall Chlorophyll *a* Maximum 214

Fall Chlorophyll *a* Range 217
Annual Chlorophyll *a* Mean 220
Annual Chlorophyll *a* Minimum 223
Annual Chlorophyll *a* Maximum 226
Annual Chlorophyll *a* Range 229
Primary Production 232
Spring Primary Production Mean 232
Spring Primary Production Minimum 235
Spring Primary Production Maximum 238
Spring Primary Production Range 241
Spring Primary Production Average Minimum 244
Spring Primary Production Average Maximum 247
Spring Primary Production Average Range 250
Summer Primary Production Mean 253
Summer Primary Production Minimum 256
Summer Primary Production Maximum 259
Summer Primary Production Range 262
Summer Primary Production Average Minimum 265
Summer Primary Production Average Maximum 268
Summer Primary Production Average Range 271
Fall Primary Production Mean 274
Fall Primary Production Minimum 277
Fall Primary Production Maximum 280
Fall Primary Production Range 283
Fall Primary Production Average Minimum 286
Fall Primary Production Average Maximum 289
Fall Primary Production Average Range 292
Annual Primary Production Mean 295
Annual Primary Production Minimum 298
Annual Primary Production Maximum 301
Annual Primary Production Range 304
Annual Primary Production Average Minimum 307
Annual Primary Production Average Maximum 310
Annual Primary Production Average Range 313
Dissolved Oxygen 316
Dissolved Oxygen 316
ACKNOWLEDGMENTS 319
REFERENCES 320
APPENDIX I - Summary of Variables with Negative Values in the Interpolated Prediction Surface Resulting from Ordinary Kriging 324
Bottom Temperature Range 325
Bottom Temperature Average Range 325
Bottom Salinity Range 326
Bottom Salinity Average Range 326
Spring Chlorophyll *a* Range 327
Annual Chlorophyll *a* Range 327

ABSTRACT

Beazley, L., Guijarro, J., Lirette, C., Wang, Z., and Kenchington, E. 2017. Characteristics of Environmental Data Layers for Use in Species Distribution Modelling in the Maritimes Region. Can. Tech. Rep. Fish. Aquat. Sci. 3212: vii + 327p.

Species distribution models (SDMs) are tools that combine species observations of occurrence, abundance, or biomass with environmental variables to predict the distribution of a species in unsampled locations. To produce accurate predictions of occurrence, abundance or biomass distribution, a wide range of physical and/or biological variables is desirable. Such data is often collected over limited or irregular spatial scales, and require the application of geospatial techniques to produce continuous environmental surfaces that can be used for modelling at all spatial scales. Here we provide a review of 102 environmental data layers that were compiled for the entire spatial extent of Fisheries and Oceans Canada's (DFO) Maritimes Region. Variables were obtained from a broad range of physical and biological data sources and spatially interpolated using geostatistical methods. For each variable we document the underlying data distribution, provide relevant diagnostics of the interpolation models and an assessment of model performance, and present the final standard error and interpolation surfaces. These layers have been archived in a common (raster) format at the Bedford Institute of Oceanography to facilitate future use. Based on the diagnostic summaries in this report, a subset of these variables has subsequently been used in species distribution models to predict the distribution of deep-water corals, sponges, and other significant benthic taxa in the Maritimes Region.

RÉSUMÉ

Beazley, L., Guijarro, J., Lirette, C., Wang, Z., et Kenchington, E. 2017. Characteristics of Environmental Data Layers for Use in Species Distribution Modelling in the Maritimes Region. Rapp. tech. can. sci. halieut. aquat. 3212 : vii + 327p.

Les modèles de répartition des espèces sont des outils qui rassemblent des observations d'espèces (occurrence, abondance ou biomasse) avec des variables environnementales pour prédire l'aire de répartition d'une espèce dans des emplacements non échantillonnés. Afin de produire des prévisions exactes de l'occurrence, de l'abondance ou de la répartition de la biomasse, il est souhaitable d'obtenir une vaste gamme de variables physiques ou biologiques (ou les deux). Ces données sont souvent recueillies sur des échelles spatiales limitées ou irrégulières et nécessitent l'application de techniques géospatiales pour produire des surfaces environnementales continues qui peuvent être utilisées pour la modélisation à toutes les échelles spatiales. Dans le présent document, nous offrons un examen de 102 couches de données environnementales qui ont été compilées pour l'ensemble de l'étendue spatiale de la région des Maritimes de Pêches et Océans Canada (MPO). Des variables ont été obtenues à partir d'une vaste gamme de sources de données physiques et biologiques interpolées sur le plan spatial à l'aide de méthodes géostatistiques. Pour chaque variable, nous documentons la répartition des données sous-jacentes, fournissons des analyses pertinentes des modèles de répartition et une évaluation du rendement des modèles. Nous présentons l'erreur type et les surfaces interpolées définitives. Ces couches de données ont été archivées dans un format commun (trame) à l'Institut océanographique de Bedford afin de simplifier leur utilisation future. En se fondant sur les résumés analytiques du présent rapport, un sous-ensemble de ces variables a par la suite été utilisé dans des modèles de répartition des espèces pour prévoir la répartition, en eau profonde, des coraux, des éponges et d'autres taxons benthiques importants dans la région des Maritimes.

INTRODUCTION

Species distribution modelling (SDM) is a tool that utilizes the relationship between a species and its environment in known (sampled) locations to predict the species' distribution in unsampled areas. SDM applications require continuous surfaces of each environmental predictor variable in order to predict across the spatial domain of the study extent to areas where environmental data do not exist. These variables are typically collected at different spatial and temporal resolutions, and are often spatially interpolated to provide continuous surfaces that can be used for predictive modelling at all spatial scales. Predictor variables may themselves be from direct measurements, modelled outputs, temporal averages, and derivations.

Continuous interpolated surfaces produced at high resolution often show very detailed spatial variation, implying that the surfaces are very precise. However, spatial interpolation methods are affected by sample size, sampling design and data quality properties, and variation within the data has very large impacts on the performance of the spatial interpolators (Li and Heap, 2008). There are over 60 methods to choose from, including geostatistical interpolators (e.g., kriging), non-geostatistical interpolators (e.g., inverse distance weighting, natural neighbours, nearest neighbours), and methods that combine both (Li and Heap, 2008).

The Scotian Shelf is a 700 km section of continental shelf off Nova Scotia that is bounded by the Laurentian Channel and Cabot Strait in the east and northeast, and the Gulf of Maine in the west. The shelf itself is broad, varying in width from 120 to 240 km, and is characterized by shallow offshore banks and deep basins, troughs, channels, and has a mean depth of ~116 m. Its steep slope is excised by a number of deep canyons and gullies. The oceanographic conditions on the Scotian Shelf and in Bay of Fundy are dynamic and vary seasonally and inter-annual, making broad characterization of this region difficult. Temperature and salinity conditions on the Scotian Shelf varies spatially due to its complex bottom topography, heat transfer between the ocean and atmosphere, inflow from the Gulf of St. Lawrence and Newfoundland Shelf, exchange with offshore slope waters, local mixing, freshwater runoff, direct precipitation, and melting of sea ice in the spring (Drinkwater et al., 2003; Hebert et al., 2013). The dynamicity of this region highlights the importance of including frequent and long-term time series data to describe mean oceanographic climate.

Here, we provide detailed information on 102 environmental data layers collected over different spatial and temporal resolutions and spatially interpolated using the ordinary kriging method to provide continuous surfaces across the entire domain of Fisheries and Oceans Canada's (DFO) Maritimes Region. For each variable, we show the distributional properties of the raw data prior to spatial interpolation, model performance indicators and assessment of model performance, and finally, maps of the prediction standard error and interpolation prediction surfaces. Our intention is that these variables are used in species distribution modelling or other ecosystem-based management applications. A subset of these variables have already been used in random forest and generalized additive models to predict the probability of occurrence and biomass distribution of deep-water corals, sponges, and other significant benthic taxa (see Beazley et al., 2016a; 2017), the results of which are currently being used to identify important areas in conservation planning applications.

MATERIALS AND METHODS

Study Area

Fisheries and Oceans Canada's (DFO) Maritimes Region, one of DFO's six administrative regions across Canada, was used as the spatial boundary for the construction of environmental variables in this report (Figure 1). This study area encompasses the Bay of Fundy, part of the Laurentian Channel and Cabot Strait, and the entire Scotian Shelf, Slope, Rise, and Abyssal Plain. The extent is delimited by the Canadian Maritime Boundary to the west in Gulf of Maine, the 200 nautical mile Exclusive Economic Zone (EEZ) in the south, the Placentia Bay-Grand Bank Large Ocean Management Area in the east, and the Gulf Region MPA Network Planning Boundary in the north. A 5 kilometre buffer was added around all land points.

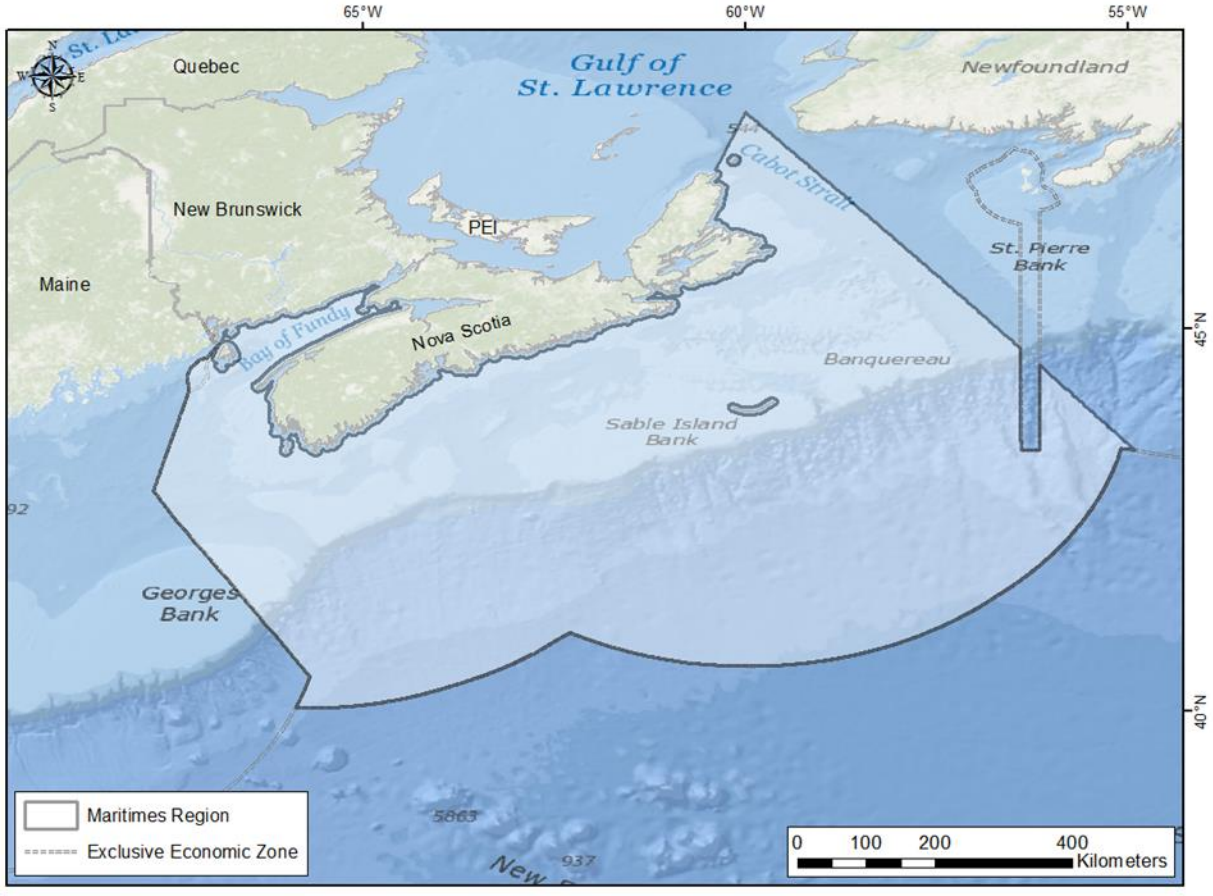

Fig. 1. Extent of the DFO Maritimes Region boundary used for creating interpolated surfaces of environmental variables.

Data Sources

Global Ocean Reanalyses and Simulations (GLORYS)

Data for surface and bottom temperature, salinity, current speed, bottom shear, and mixed layer depth were extracted from the Global Ocean Reanalyses and Simulations (GLORYS2V1). GLORYS2V1 is a numerical ocean general circulation model reanalysis product with ¼° horizontal resolution (approximately 20.4 km in the Maritimes Region; Fig. 2) that aims to provide the mean and time-varying state of the oceanic states with a focus on capturing variation of meso-scale eddies (http://www.mercator-ocean.fr/eng/science/GLORYS). Details on this model and its caveats can be found in Beazley et al. (2016b).

For each variable, two different sets of statistics were created from the GLORYS2V1 monthly data. First, the absolute minima, maxima, and range were calculated for each variable by taking the minimum and maximum values across all months and years at each location. Range was calculated as the difference between these values at each location. In this report these variables are denoted as Minimum/Maximum/Range. These 'absolute' variables are likely reflective of anomalous events over the time period. The second dataset was created by calculating the average minima, maximum and range by taking the minimum and maximum values at each location across all months within a year, and averaging across years. These variables are denoted as Average Minimum/Maximum/Range in this report, and are likely more representative of long-

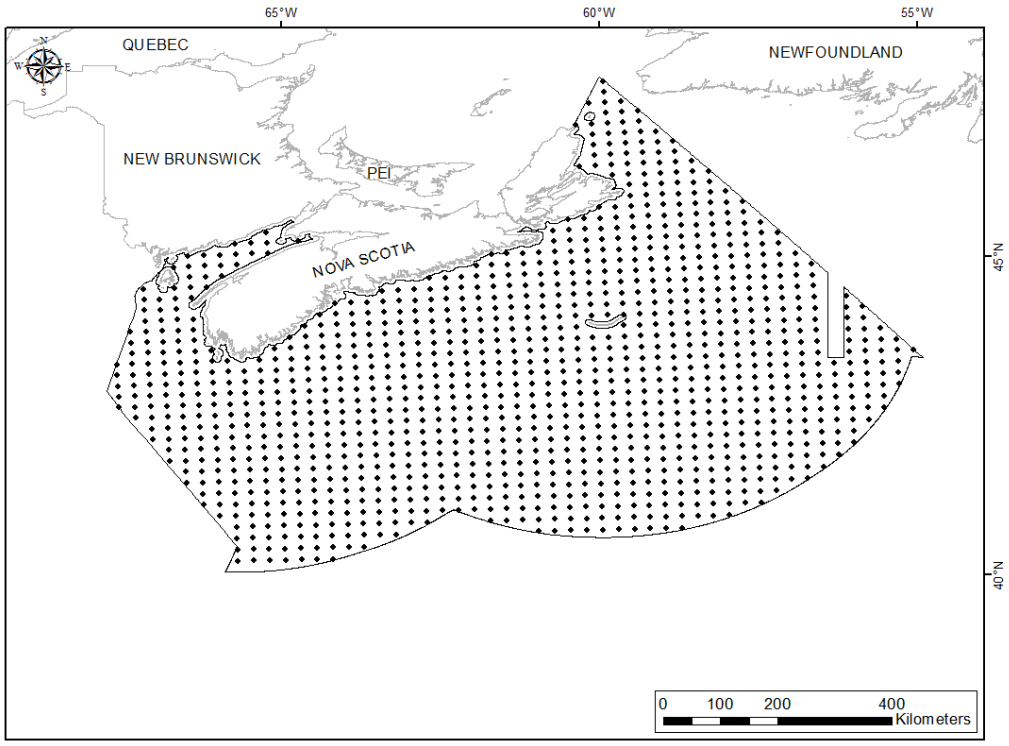

Fig. 2. Distribution of point data extracted from the GLORYS2V1 model from 1993 to 2011 for the Maritimes Region. Point data have a native resolution of ¼° (~20.4 km).

term oceanographic conditions in the region. Finally, the mean of each variable was calculated by averaging the values at each location across all months and years, and is denoted as the Mean in this report. For mixed layer depth, statistics were compiled quarterly to derive spring (April - June), summer (July - September), fall (October - December) and winter (January - March) variables. Zero values in the current and shear data, which were falsely generated from a model topography issue, were removed prior to calculating the statistics.

Sea Surface Chlorophyll *a*

Sea surface chlorophyll *a* data were derived from Aqua-MODIS (Moderate Resolution Imaging Spectroradiometer) Case I was processed by the Remote Sensing Unit at the Bedford Institute of Oceanography (RSU-BIO). In deep oceanic waters, optical properties are dominated by phytoplankton and the observed spectral features in the reflected light can be directly related to chlorophyll *a* concentration (Moses et al., 2009). These waters are referred to as Case I waters. In Case I waters, spectral algorithms that use reflectances in the blue green regions of the spectrum have shown to accurately estimate chl-*a* concentration. In contrast, most inland, estuarine, and coastal waters that are rich in suspended solids and dissolved organic matter are referred to as Case II waters. The optical properties of Case II waters are therefore not dominated by phytoplankton, and spectral algorithms based on reflectance in the red and near-infrared spectral regions are typically used to estimate chl-*a* concentration (Moses et al., 2009). Generally, Case I chlorophyll calculations should not be used for Case II waters. In the Maritimes Region, the Bay of Fundy is considered Case II waters due to its strong tidally-induced vertical mixing and resuspension of organic material (Harrison et al., 2007). A comparison of satellite-derived chlorophyll *a* to *in situ* measurements in Bay of Fundy revealed significant over-estimation of chlorophyll concentration by both MODIS Case I and MERIS Case II algorithms, although Case II was closer than Case I. Coastal waters less than 30 m deep are also considered Case II, however, these waters are generally excluded in our study due to the 5-km land buffer applied to land values. Given that the majority of the Maritimes Region is considered Case I, we therefore opted to include only MODIS Case I chlorophyll *a* data layers in this report but acknowledge that this algorithm does not adequately represent chlorophyll *a* concentration in Bay of Fundy.

Daily MODIS (Aqua Level-2) data from 2002 to 2012 were downloaded from NASA's OceanColor Web (http://oceandata.sci.gsfc.nasa.gov/]). Composite images were displayed in raster format with a resolution of 2 km. Data from 2003 to 2011 were used. Individual passes were filtered to eliminate extreme outliers using the median of a 3 x 3 pixel matrix (ENVI-IDL). The native resolution of the point data for MODIS Case I chlorophyll *a* data is shown in Fig. 3.

Annual and seasonal averages were computed for the MODIS Case I dataset. Seasons were delimited by the following 'day of year' ranges: days 91 – 181 (spring), 182 – 273 (summer), and 274 – 365 (fall). These seasonal delimitations capture the peak of the spring and fall phytoplankton blooms over most of the Scotian Shelf. Alternate seasonal ranges could be considered that would fully capture the spring phytoplankton bloom in all areas of the study extent. The minimum, maximum and range values for each season (except winter) and annually were derived from these using the 'Cell Statistics' tool in ArcMap's Spatial Analyst toolbox. Zero and N/A values in the chlorophyll data were removed prior to calculating the statistics.

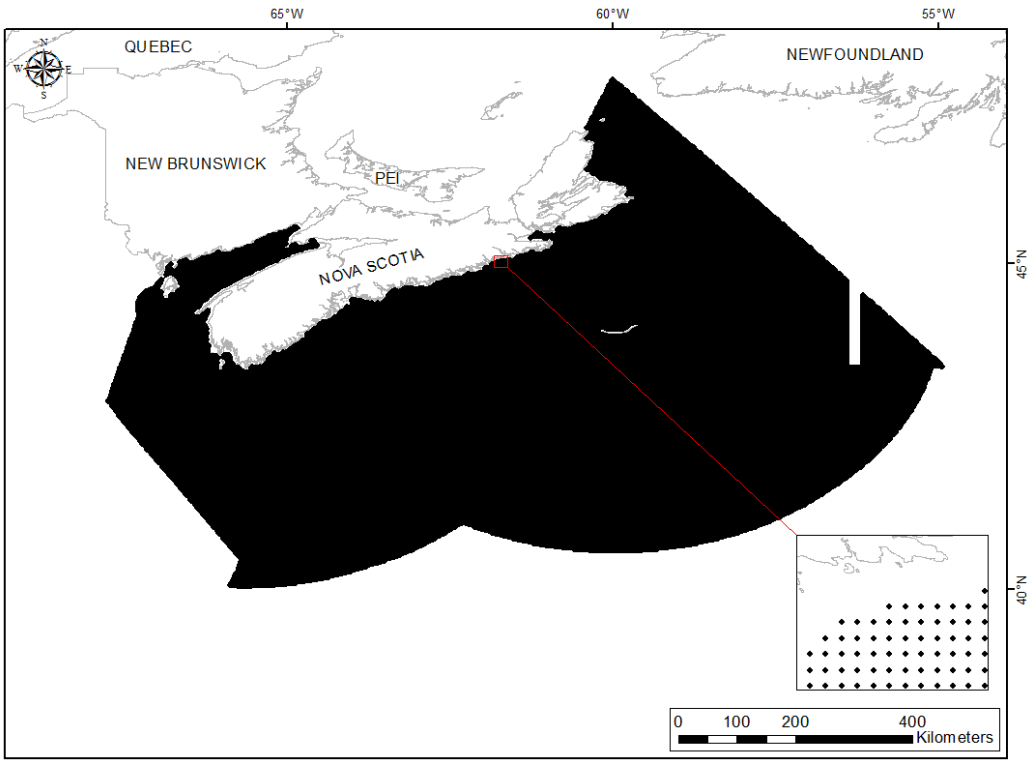

Fig. 3. Distribution of sea surface chlorophyll *a* (MODIS Case I) point data (spring, summer, fall and annual) for the Maritimes Region. Point data have a native resolution of 2 km.

Sea Surface Primary Production

Primary production was calculated following the method of Platt et al. (2008) using software developed by the RSU-BIO and the Department of Oceanography at Dalhousie University. The calculation of primary production requires input from multiple sources. Monthly mean surface chlorophyll *a* and photosynthetically active radiation (PAR) was obtained from NASA's Sea-viewing Field-of-view Sensor (SeaWiFS) Level 3, 9-km global coverage (reprocessing R2010.0; Feldman and McClain, 2012). Sea surface temperature (SST) was obtained from NOAA PathFinder version 5.2 data and was reprocessed from its native resolution of 4000 m^2 $pixel^{-1}$ to match the spatial and temporal resolution of chlorophyll data. Monthly images of total cloud fraction data used in the model were obtained in November 2014 from MYD08_M3, a monthly aggregation of MYD35, collection 51 (ftp://ladsweb.nascom.nasa.gov/allData/51/MYD08_M3/). The *in situ* parameters, such as photosynthetic performance, chlorophyll *a*, sea surface temperature, and water depth originate from ship-based observations made by DFO's Atlantic Zone Monitoring Program (AZMP; http://www.bio.gc.ca/science/monitoring-monitorage/azmp-pmza-en.php). Reliability of the resulting primary production data is therefore unknown for areas outside the AZMP region. The model described in Platt et al. (2008) results in pixel-by-pixel depth-integrated net primary production (mg C m^{-2} day^{-1}) calculated for the 15 day of each month from September 2006 to September 2010. Like the GLORYS2V1-derived variables, monthly values for primary production allowed for the calculation of both 'absolute' and 'average' minima, maxima, and range quantifications. However, for some months and years no

data was available (see Table 1), therefore only spring (April – June), summer (July – Sept.), fall (October to December) and annual layers were created. For the creation of these variables, we ensured that each point location across the study extent had at least two months of data in each of the five years contributing to the quantifications. Spring, summer and annual surfaces showed nearly full coverage across the Maritimes Region, whereas large areas off Cape Breton, southwest Nova Scotia and Bay of Fundy are not covered in the fall as these are locations with less than one month of data contributing across the 5-year data period.

Table 1. Contributing months to each of the 5 years of data for the primary production dataset. The √ indicates that data exists for this month. Note however that even though data exists for a particular month, each point location across the Maritimes Region study extent may not have observation data.

Season	Month	2006	2007	2008	2009	2010	Total number of years
	January	√	√		√	√	4
	February	√	√		√	√	4
	March	√	√		√	√	4
	April	√	√	√	√	√	5
Spring	**May**	√	√	√		√	4
	June	√	√	√	√	√	5
	July	√	√		√	√	4
Summer	**August**	√	√	√	√	√	5
	September	√	√	√		√	4
	October	√	√	√		√	4
Fall	**November**	√		√	√	√	4
	December			√	√	√	3

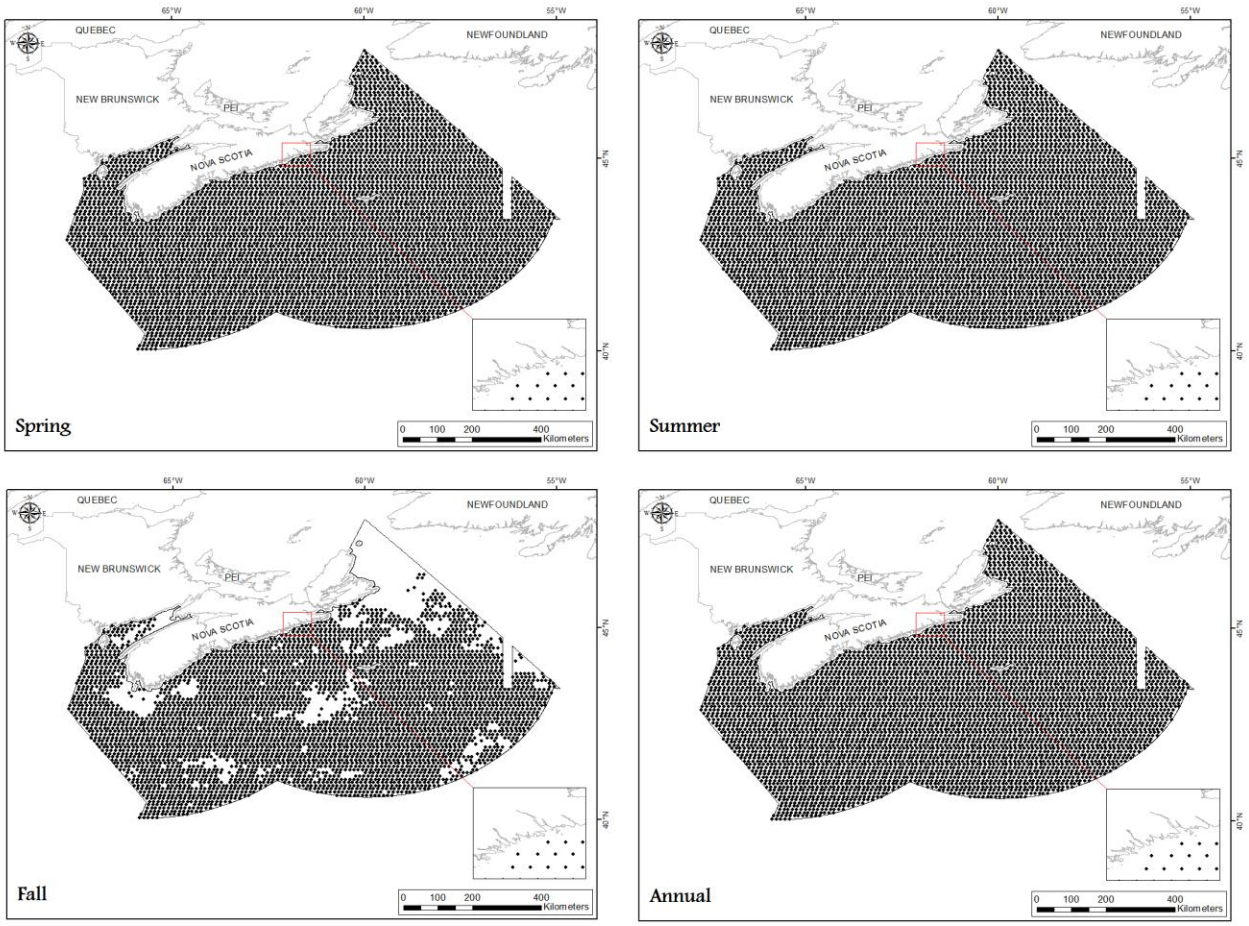

Fig. 4. Distribution of spring, summer, fall and annual primary production point data from 2006 to 2010 for the Maritimes Region. Point data have a native resolution of 9 km.

World Ocean Database 2013 (WOD13)

Dissolved oxygen and nutrients (nitrate, phosphate, and silicate) were extracted from the World Ocean Database 2013 (WOD13) (https://www.nodc.noaa.gov/OC5/WOD13/; Boyer et al., 2013) produced by the US National Oceanographic Data Center (NODC) Ocean Climate Laboratory (OCL). WOD13 houses ocean profile and plankton measurement data submitted by individual scientists and institutional, national, and regional data centres with the goal of providing a centralized source for large-scale oceanographic data and metadata that has been formatted in a similar way. Data in WOD13 are organized under four different operational definitions: profile, cast, station, and cruise. Each data value and profile in WOD13 are associated with their own quality control flag. Data collected in a similar manner are further grouped together into 11 different datasets.

The data were queried from the WODselect retrieval system (https://www.nodc.noaa.gov/OC5/SELECT/dbsearch/dbsearch.html) using user-specified search

criteria under the following four categories: geographic coordinates, observation dates, dataset, and measured variables. Nutrient data were queried from the Ocean Station Data (OSD) dataset from the period of 2006 to 2011, which corresponded to the start of when the highest quality control indicators accompanied the data, and end period of the GLORYS data layers. In the event where more than one value was measured at a single location, the data values were averaged. The OSD dataset groups together bottle (Nansen and Niskin) and bucket data, plankton data, and low resolution CTD and expendable CTD (XCTD) data, and is the only dataset in WOD13 that contains nutrient data. Only data collected within the top 10 metres of water and with the highest quality control flag ('Accepted') were used. Only dissolved oxygen showed good enough coverage over the Maritimes Region to spatially interpolate the data (see Fig. 5).

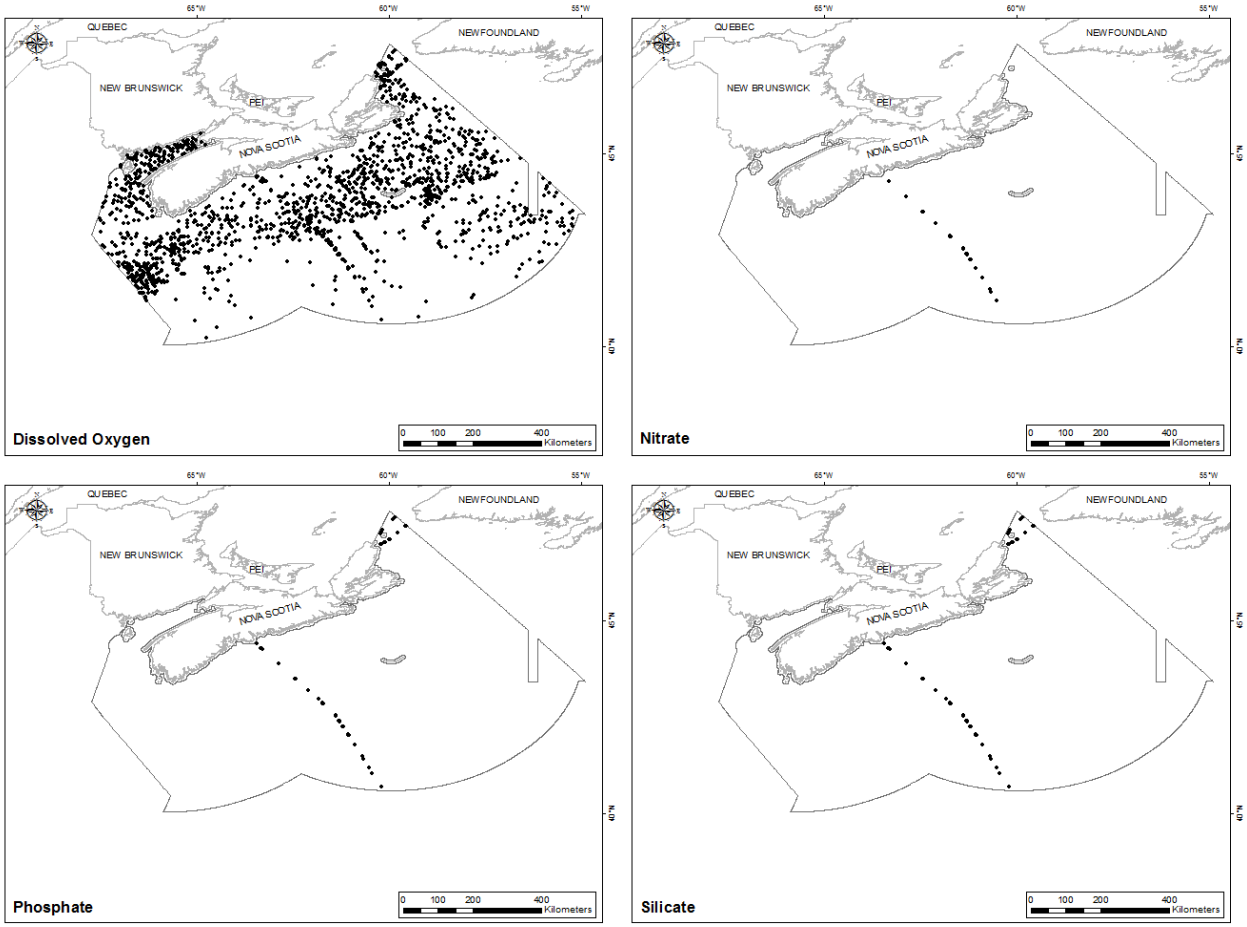

Fig. 5. Distribution of dissolved oxygen, nitrate, phosphate, and silicate point data from 2006 to 2011 extracted from WOD13 for the Maritimes Region. The spatial distribution of the data is not uniform across the study extent.

Spatial Interpolation Methods

Data Exploration and Model Fitting (adapted from Beazley et al., 2016b)

Kriging is a family of geostatistical estimators used to interpolate spatial data. It is a generalized least-square regression technique that allows for spatial prediction in unsampled locations by accounting for the spatial dependence between observed data (Goovaerts, 2000). Spatial dependence is captured by constructing an empirical semivariogram that shows the average semivariance between points by the distance between them. A semivariogram model is then fit to the points forming the empirical semivariogram, and predictions are generated for unmeasured locations based on a weighted average of neighbouring data and their spatial arrangement (Johnston et al., 2001).

Within the kriging family a number of different methods exist including but not limited to, ordinary kriging, universal kriging, and simple kriging. For this report, we chose ordinary kriging as the method of spatial interpolation as it assumes that the mean is unknown prior to modelling and approximately constant (stationary) only in the local neighbourhood of each estimation point and not over the entire data domain (Li and Heap, 2008; Krivoruchko, 2011). Thus ordinary kriging with a local search neighbourhood already accounts for trends in the data (Li and Heap, 2008). When compared against the Inverse Distance Weighting (IDW) interpolation method, ordinary kriging produced better overall mean prediction and root-mean-square errors and smoother prediction surfaces for the same variables interpolated in the Gulf Region (see Beazley et al., 2016b).

Ordinary kriging as a geostatistical interpolator does not require the data to follow a normal distribution (Krivoruchko, 2011). However, the generation of quantile and probability maps using ordinary kriging does require the data to meet this assumption (Krivoruchko, 2011). Transformation of highly skewed data prior to ordinary kriging may result in improved estimates and prediction errors, particularly if the dataset is small and contains outliers (Kravchenko and Bullock, 1999). If a variable shows positive skewness, the confidence limits on the variogram are wider than normal resulting in higher variance (Robinson and Metternicht, 2006; Yamamoto, 2007). Thus, data are often transformed prior to spatial interpolation in order to improve the calculation of statistics and weighted averages (Yamamoto, 2007). Transformation of the data results in estimates on a different scale than the original data, and so it is necessary to back-transform the kriging estimates to their original scale prior to creating the interpolation surface. However, for logarithmic transformation, back-transformation through exponentiation results in exaggerated interpolation-related errors, with extreme errors being the worst affected (Goovaerts, 1997; Robinson and Metternicht, 2006). In the Maritimes Region, variables that had been back-transformed within the Geostatistical Analyst package had poorer prediction errors when compared to variables that were log-transformed outside the ArcMap forum (and thus, were not back-transformed in ArcMap). Therefore, to avoid biased prediction errors, we chose not to transform our data prior to spatial interpolation.

Prior to interpolation we assessed the distributional properties of all variables by examining histograms and summary statistics generated in the ‘Explore Data’ option in ArcMap’s

Geostatistical Analyst package. These were reviewed to detect anomalous data points and to visually assess departures from a normal distribution (skewness, kurtosis) in advance of conducting geostatistics. Data distributions were described in terms of their skew (right, or positive, and left, or negative), and kurtosis. Kurtosis is a measure of the 'tailedness' of the distribution, where values equal to 3 are considered mesokurtic (zero tailedness), values < 3 platykurtic (thin-tailed), and values > 3 are leptokurtic (heavy-tailed) (DeCarlo, 1997). Normal Q-Q plots were then constructed to compare the distribution of the data against a standard normal (Gaussian) distribution. The data values are ordered and cumulative distribution values are calculated as $(i– 0.5)/n$ for the i^{th} ordered value out of n total values. If the data values are normally distributed they will form a perfect line at 45° to the origin. Data values that fell above and below the reference line were mapped to identify any spatial trend in the departure from normality.

Ordinary kriging models were created using all default settings in the Geostatistical Analyst wizard. Default settings are a stable semivariogram model type and a circular search neighbourhood with 4 sectors that capture a minimum of 2 and a maximum of 5 neighbours. The optimization function was set for each model, which determines the optimal partial sill, nugget, lag size, and number of lags based on the model range.

Caveat for Spatial Interpolation Using Ordinary Kriging

We noted that ordinary kriging of some GLORYS and chlorophyll *a* 'range' variables resulted in negative values in the prediction surfaces. This is in addition to some of the small negative values produced by the GLORYS model itself (see Beazley et al., 2016b for description). In the Maritimes Region this phenomenon occurred in the following variables:

1. Bottom Salinity Range
2. Bottom Salinity Average Range
3. Bottom Temperature Range
4. Bottom Temperature Average Range
5. Spring Chlorophyll *a* Range
6. Annual Chlorophyll *a* Range

This issue has been previously described by Deutsch (1996) and Ly et al. (2011), who found that negative weights were generated by ordinary kriging models when outlying data points occurred close to the location being estimated. Ly et al. (2011) suggested two methods for dealing with this issue: 1) apply an *a posteriori* correction as outlined in Deutsch (1996), or 2) to replace all negative interpolated values with zero. To determine the influence of these variables with negative values on a species distribution model, we ran several random forest models with these variables as-is (i.e. with the negative interpolated values), and models with the negative values changed to zero. We found very little difference in the resulting surfaces and accuracy measures between models run with the negative values and those negative values changed to zero (see Guijarro et al., 2016). We conclude that these negative values have a negligible impact on species distribution modelling applications. The location of negative values in the prediction surface of each variable are shown in Appendix I.

Assessment of Model Performance (extracted from Beazley et al., 2016b)

Model performance was examined by performing cross-validation, a process where each data point is removed in turn from the model and predicted by the remaining data points. Geostatistical Analyst provides several graphical summaries of the cross validation results, including a scatterplot of the measured versus predicted values (called the Prediction plot), a scatterplot of the residuals of the measured values versus the predicted values (Error plot), a standardized error plot, which shows measured values subtracted from the predicted values and divided by the estimated kriging standard errors, and finally a Q-Q plot, which shows the quantiles of the difference between the predicted and measured values and the corresponding quantiles from a standard normal distribution to assess the normality of the error distributions. Of these, we show only the Prediction plot in the report, although all plots were visually assessed. In the Prediction plot, a horizontal relationship indicates that the model has no information content. With autocorrelation and a good geostatistical model, the relationship between the measured and predicted values should be 1:1.

Also provided by cross validation are five prediction error statistics used for performance evaluation (see Table 2). The overall mean error represents the difference between the measured and predicted values, and should be near zero if the prediction errors are unbiased (i.e., centred on the measured values). However, this value depends on the scale and units of the data, therefore it is better to assess the standardized prediction errors, which are given as prediction errors divided by their prediction standard errors. The mean (Standardized Mean) of these should also be near zero. If the Average Standard Error is close to the Root-Mean-Square Prediction Error, variability in the predictions has been correctly assessed. The Standardized Root-Mean-Square error should be close to one. If the Average Standard Error is greater than the Root-Mean-Square Prediction Error, or if the Standardized Root-Mean-Square Prediction Error is less than one, then the variability of predictions has been overestimated. If the Average Standard Rrror is less than the Root-Mean-Square Prediction Error or if the Standardized Root-Mean-Square Prediction Error is greater than one, then the variability of predictions has been

Table 2. Prediction error statistics rules used to assess performance of ordinary kriging models.

Prediction error	**Rule**
Overall Mean Error	Close to 0
Root-Mean-Square Prediction Error	Close to 0 and approximately equal to the average standard error
Standardized Mean	Close to 0
Standardized Root-Mean-Square Prediction Error	Close to 1
Average Standard Error	Approximately equal to the root mean square prediction error

underestimated. In summary, a good geostatistical model has an Overall Mean Error and Standardized Mean near zero, a small Root-Mean-Square Prediction Error that is approximately equal to the Average Standard Error, an Average Standard Error approximately equal to the Root-Mean-Square Prediction Error, and a Standardized Root-Mean-Square Prediction Error close to one (Johnston et al., 2001). These five prediction error statistics are provided for each variable and are assessed against the rules in Table 2 to provide an overall assessment of model performance.

Finally, model performance was assessed through visual examination of a standard error map. A standard error map quantifies the uncertainty of the prediction and is calculated by taking the square root of the kriging variances. If the data comes from a normal distribution, the true value will be within ± 2 times the prediction standard errors about 95% of the time (Johnston et al. 2001). These maps were used to determine whether there was any spatial pattern in the error distribution.

During the assessment of model performance, we noted that data with a poor underlying distribution did not always result in poor cross validation statistics during the interpolation process. For instance, ordinary kriging on some variables displaying a bimodal distribution (e.g., Bottom Temperature Mean in Beazley et al. 2016b) produced a good fit between measured and predicted values and good to excellent cross validation statistics, suggesting the ordinary kriging is robust to non-normality. Similarly, a model displaying a good fit between measured and predicted values often showed poor cross validation statistics, particularly a higher-than-expected Standardized Root-Mean-Square Prediction Error, indicating that variability in the predictions has been underestimated.

RESULTS

Temperature

Both surface and bottom temperatures have biological relevance to benthic invertebrates. Temperature directly influences the rates of activities associated with feeding such as pumping, filtration and digestion, movement, and growth. Temperature can also influence larval duration and timing of metamorphosis (Vance, 1973). Surface water temperature can influence primary and secondary production and hence benthic food supply. Temperature, along with salinity, can be used to indicate water mass structure.

Bottom Temperature Mean

This variable displayed a slightly right-skewed, platykurtic distribution prior to interpolation (Table 3, Fig. 6). The data were greater than predicted by a normal distribution at the smallest values and upper mid-values and less than predicted at the highest and mid-values (Fig. 7). These areas of under- and over-prediction showed spatial pattern over the region (Fig. 7).

The semivariogram showed moderate autocorrelation present in the data (Fig. 8). The kriged model showed a good fit between measured and predicted value and good cross-validation statistics (Table 4), indicating it was good at prediction despite the distribution of the underlying data. The error map showed high error along the edges of the study extent (Fig. 9). The kriged surface is presented in Fig. 10.

Table 3. Distributional properties of Bottom Temperature Mean (°C).

Property	Value
Number of Observations	1160
Minimum	1.225
Maximum	11.179
Mean	3.958
Median	3.106
Standard Deviation	2.328
Skewness	0.984
Kurtosis	2.730

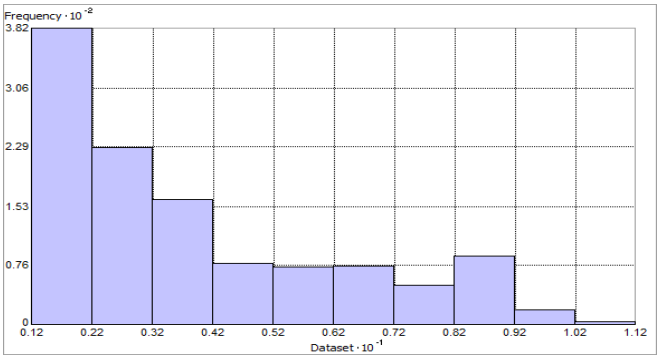

Fig. 6. Distribution of Bottom Temperature Mean (°C). Histogram was illustrated using 10 bins. X axis is shown at 10^{-1}; Y axis is shown at 10^{-2}.

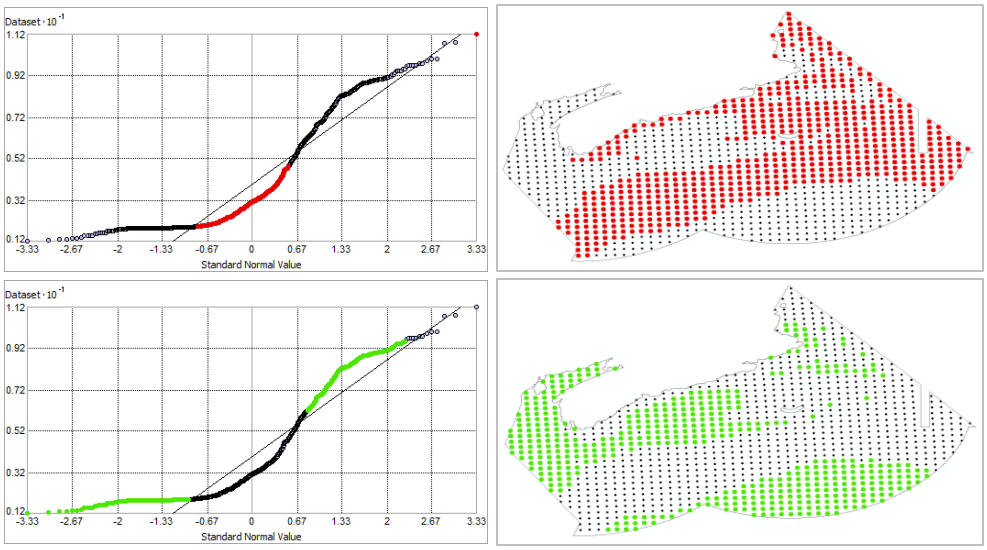

Fig. 7. Normal Q-Q plot for data values of Bottom Temperature Mean (°C). Points falling under (top right panel) and over (bottom right panel) the reference line are mapped.

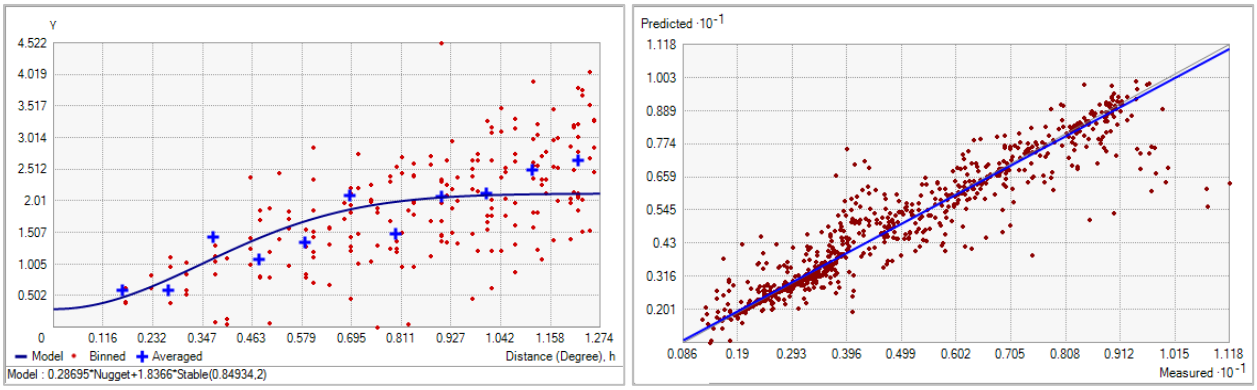

Fig. 8. Left panel: Semivariogram of Bottom Temperature Mean (°C). Binned values are shown as red dots; average points are shown as blue crosses; the model fit to the averaged values is shown as a blue line. Lag size: 0.106 degrees; number of lags: 12; Parameter: 2; Range: 0.849 degrees; Partial Sill: 1.837. Right panel: Scatterplot of predicted values versus observed values for the model of Bottom Temperature Mean (°C).

Table 4. Results of cross-validation of the kriged model for Bottom Temperature Mean (°C).

Prediction error	**Value**
Number of Observations	1160
Overall Mean Error	-1.100×10^{-3}
Root Mean Square Prediction Error	0.662
Standardized Mean	-1.821×10^{-3}
Standardized Root Mean Square Prediction Error	1.023
Average Standard Error	0.653

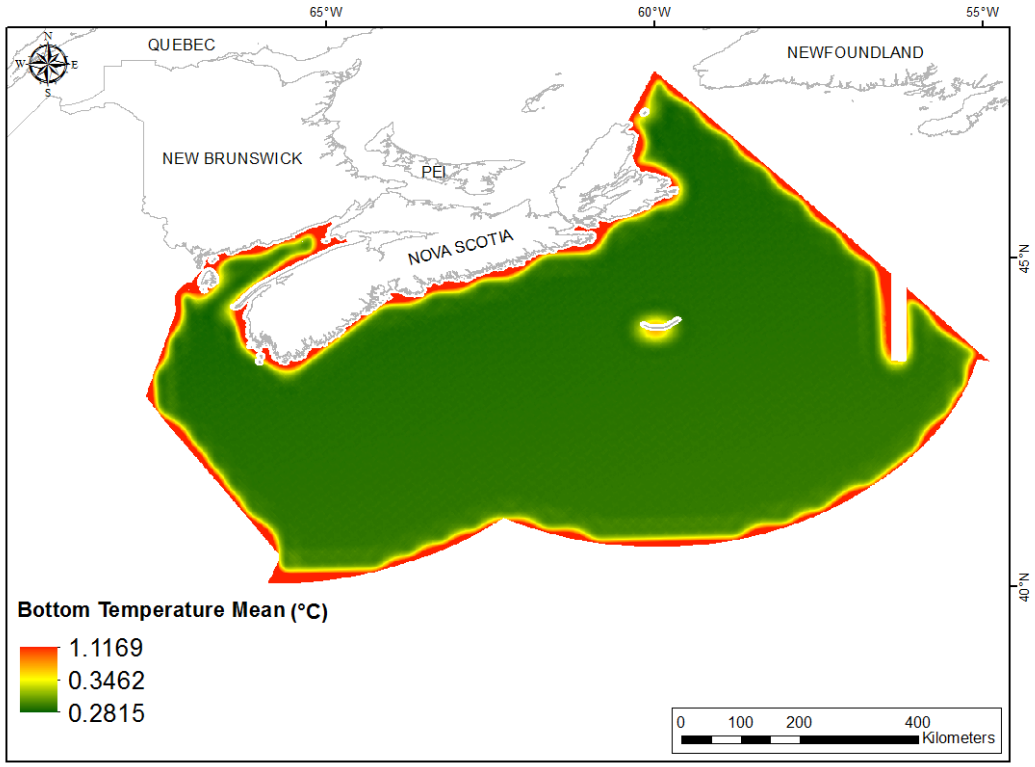

Fig. 9. Prediction standard error surface of Bottom Temperature Mean (˚C).

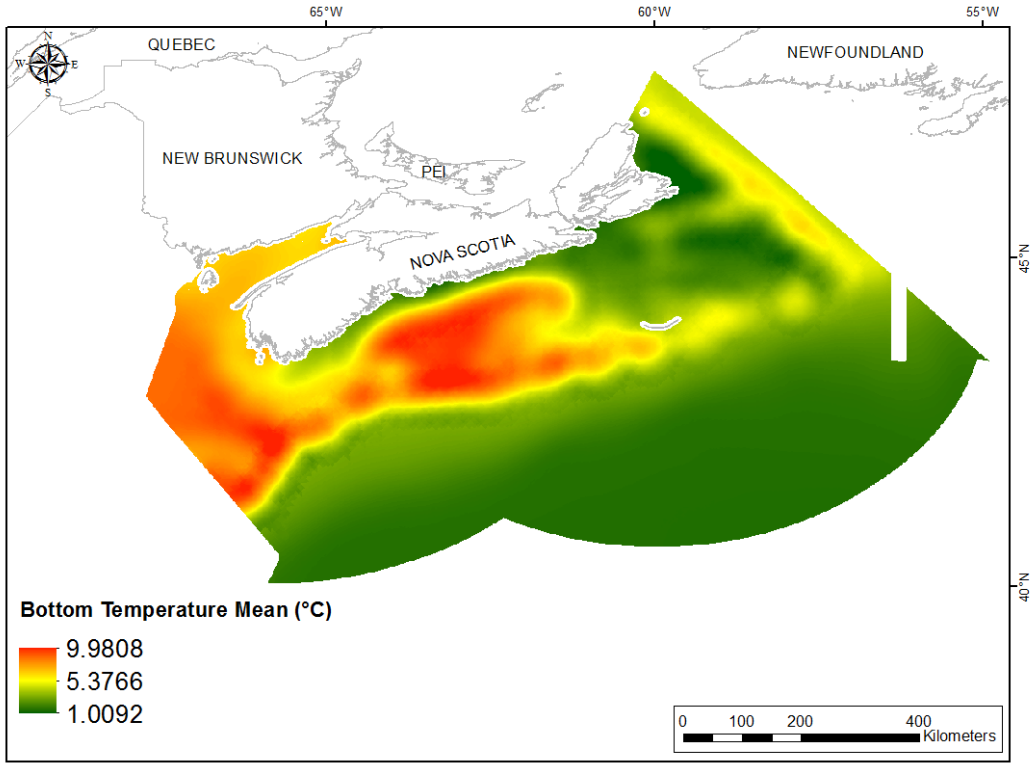

Fig. 10. Interpolated prediction surface of Bottom Temperature Mean (˚C).

Bottom Temperature Minimum

This variable displayed a right-skewed, leptokurtic distribution prior to interpolation (Table 5, Fig. 11). The data were greater than predicted by a normal distribution at the smallest and upper-mid-values and less than predicted at the highest and mid values (Fig. 12). These data points were somewhat spatially cohesive with specific areas of over- and under-prediction (Fig 12).

The semivariogram showed weak autocorrelation present in the data (Fig. 13). The kriged model showed a good fit between measured and predicted values (Fig. 13) and good cross-validation statistics (Table 6), indicating it was good at prediction. The error map showed high error along the edges of the study extent (Fig. 14). The kriged surface is presented in Fig. 15.

Table 5. Distributional properties of Bottom Temperature Minimum (°C).

Property	Value
Number of Observations	1160
Minimum	-2.167
Maximum	6.419
Mean	2.206
Median	1.862
Standard Deviation	1.546
Skewness	0.351
Kurtosis	3.750

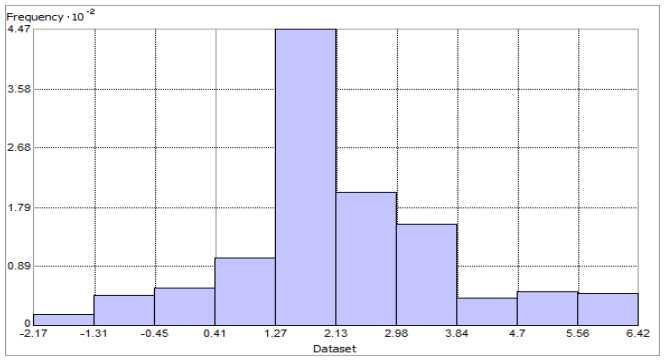

Fig. 11. Distribution of Bottom Temperature Minimum (°C). Histogram was illustrated using 10 bins. Y axis is shown at 10^{-2}.

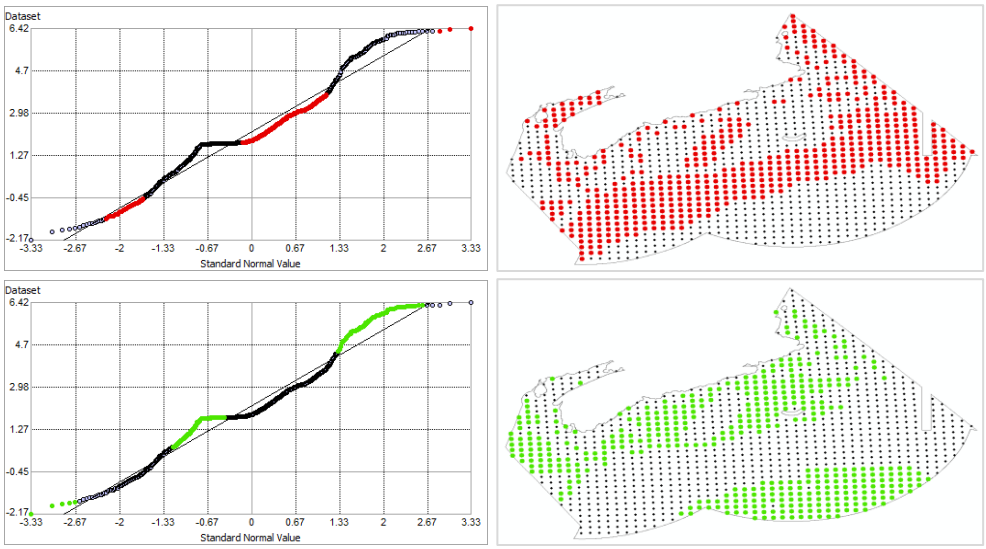

Fig. 12. Normal Q-Q plot for data values of Bottom Temperature Minimum (°C). Points falling under (upper panel) and over (bottom panel) the reference line are mapped.

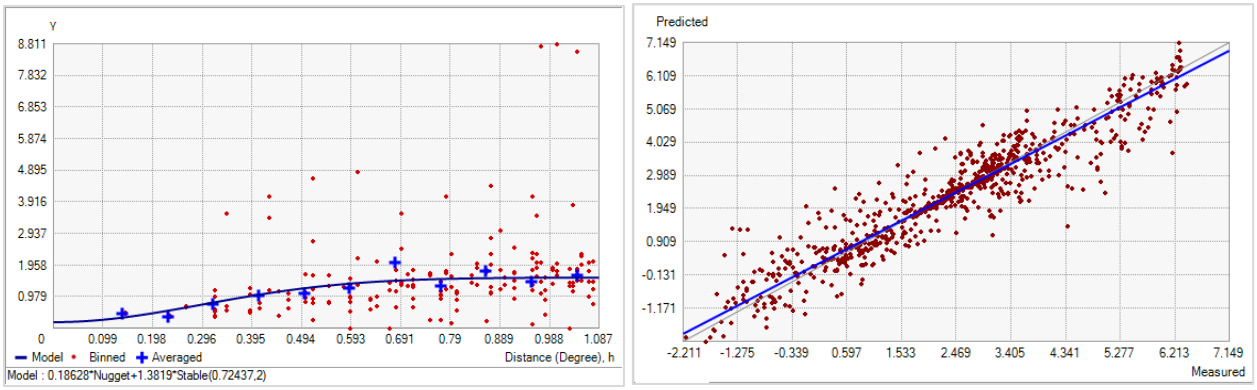

Fig. 13. Left panel: Semivariogram of Bottom Temperature Minimum (°C). Binned values are shown as red dots; average points are shown as blue crosses; the model fit to the averaged values is shown as a blue line. Lag size: 0.091 degrees; number of lags: 12; Parameter: 2; Range: 0.724 degrees; Partial Sill: 1.382. Right panel: Scatterplot of predicted values versus observed values for the model of Bottom Temperature Minimum (°C).

Table 6. Results of cross-validation of the kriged model for Bottom Temperature Minimum (°C).

Prediction error	**Value**
Number of Observations	1160
Overall Mean Error	5.544×10^{-3}
Root Mean Square Prediction Error	0.529
Standardized Mean	5.821×10^{-3}
Standardized Root Mean Square Prediction Error	0.949
Average Standard Error	0.566

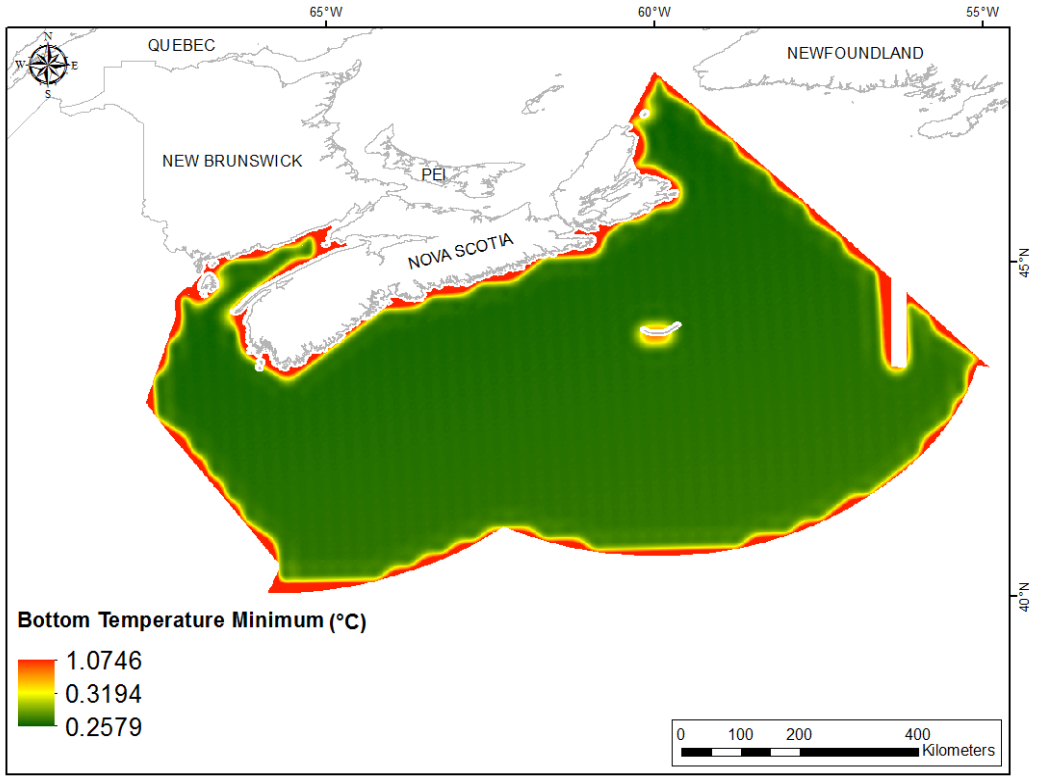

Fig. 14. Prediction standard error surface of Bottom Temperature Minimum (˚C).

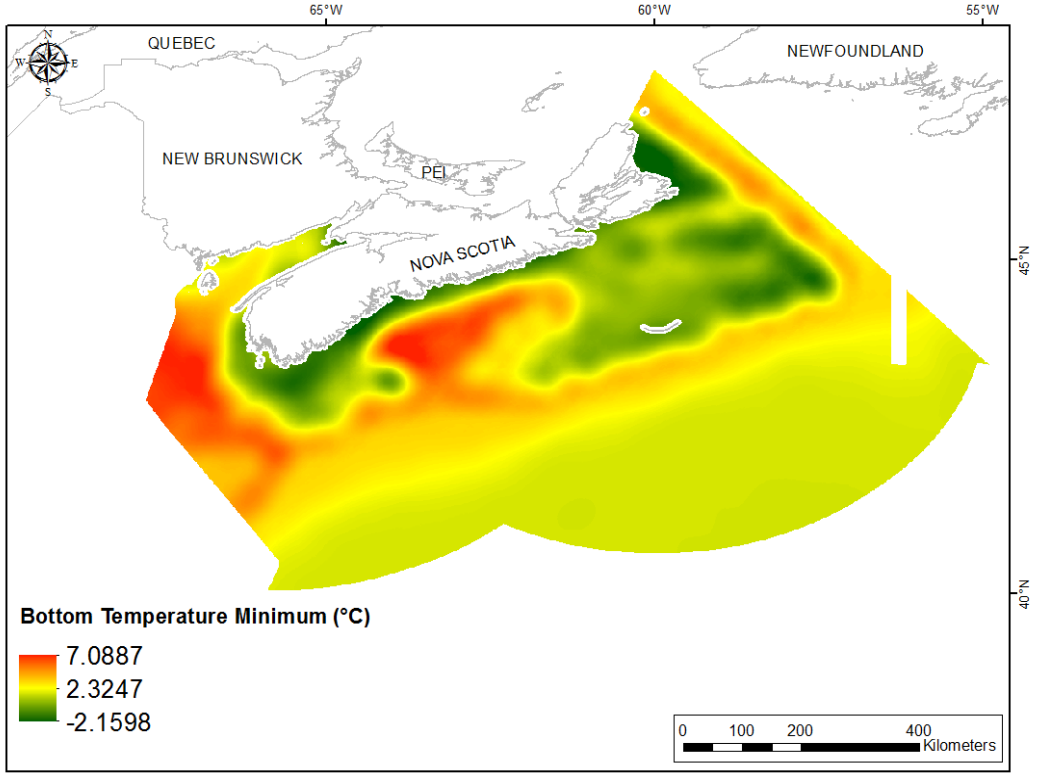

Fig. 15. Interpolated prediction surface of Bottom Temperature Minimum (˚C).

Bottom Temperature Maximum

This variable displayed a right-skewed, platykurtic and bimodal distribution prior to interpolation (Table 7, Fig. 16). The data were greater than predicted by a normal distribution at low and upper mid-values while the mid-range values of the data were under-predicted (Fig. 17). These data points were somewhat spatially cohesive with specific areas of over- and under-prediction (Fig. 17).

The semivariogram showed autocorrelation present in the data (Fig. 18). The model showed a good fit between measured and predicted values (Fig. 18). Good performance of the model was indicated by the cross-validation results (Table 8). The error map showed high error along the edges of the study extent (Fig. 19). The kriged surface is presented in Fig. 20.

Table 7. Distributional properties of Bottom Temperature Maximum (°C).

Property	Value
Number of Observations	1160
Minimum	1.909
Maximum	19.963
Mean	5.861
Median	4.022
Standard Deviation	4.022
Skewness	0.773
Kurtosis	2.316

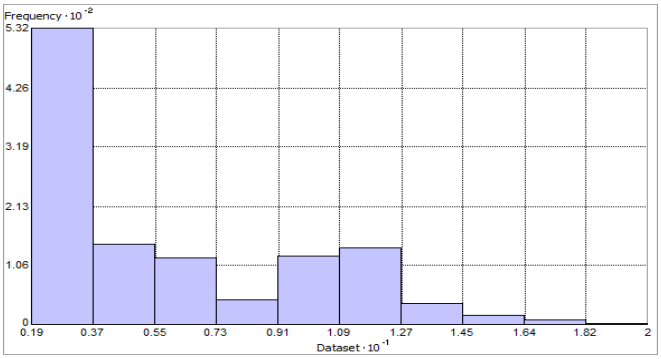

Fig. 16. Distribution of Bottom Temperature Maximum (°C). Histogram was illustrated using 10 bins. X axis shown at 10^{-1}; Y axis is shown at 10^{-2}.

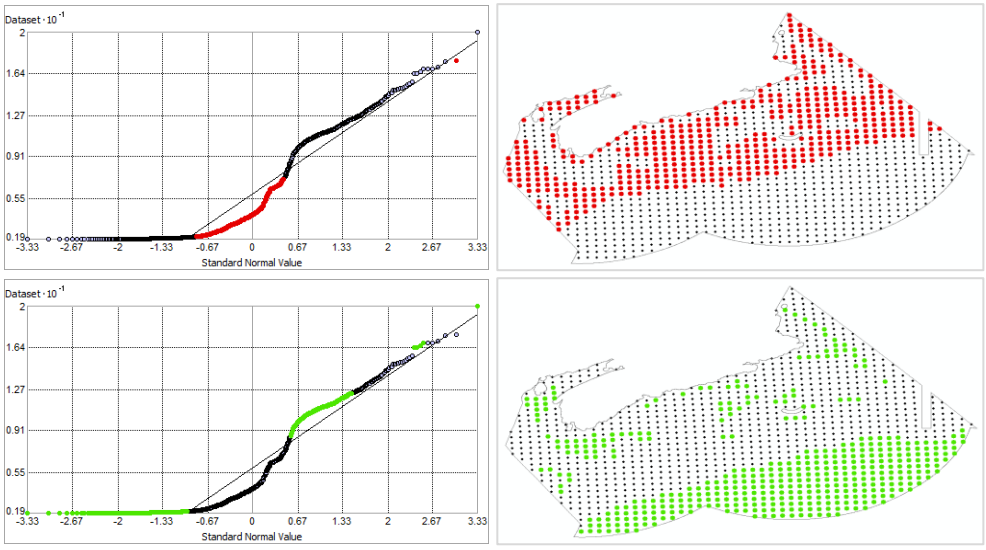

Fig. 17. Normal Q-Q plot for data values of Bottom Temperature Maximum (°C). Points falling under (upper panel) and over (bottom panel) the reference line are mapped.

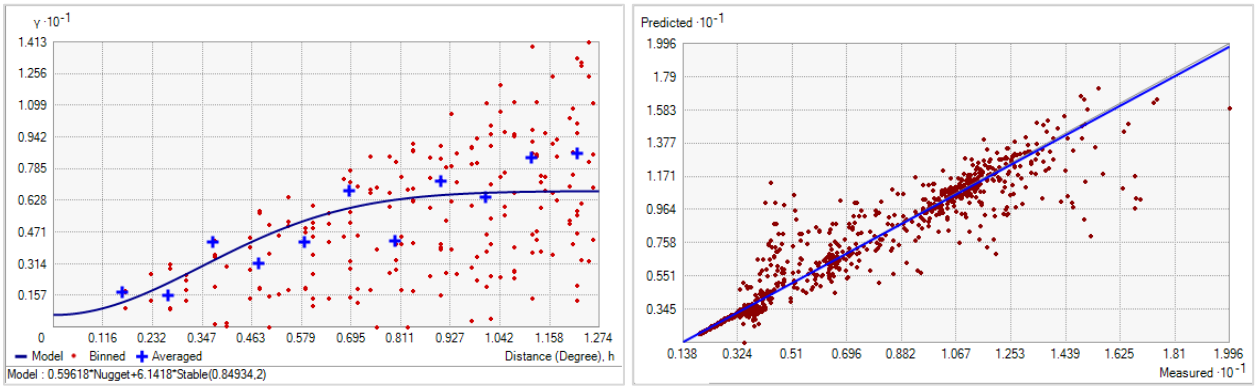

Fig. 18. Left panel: Semivariogram of Bottom Temperature Maximum (°C). Binned values are shown as red dots; average points are shown as blue crosses; the model fit to the averaged values is shown as a blue line. Lag size: 0.106 degrees; number of lags: 12; Parameter: 2; Range: 0.849 degrees; Partial Sill: 6.142. Right panel: Scatterplot of predicted values versus observed values for the model of Bottom Temperature Maximum (°C).

Table 8. Results of cross-validation of the kriged model for Bottom Temperature Maximum (°C).

Prediction error	**Value**
Number of Observations	1160
Overall Mean Error	-0.010
Root Mean Square Prediction Error	1.126
Standardized Mean	-4.913×10^{-3}
Standardized Root Mean Square Prediction Error	1.156
Average Standard Error	0.971

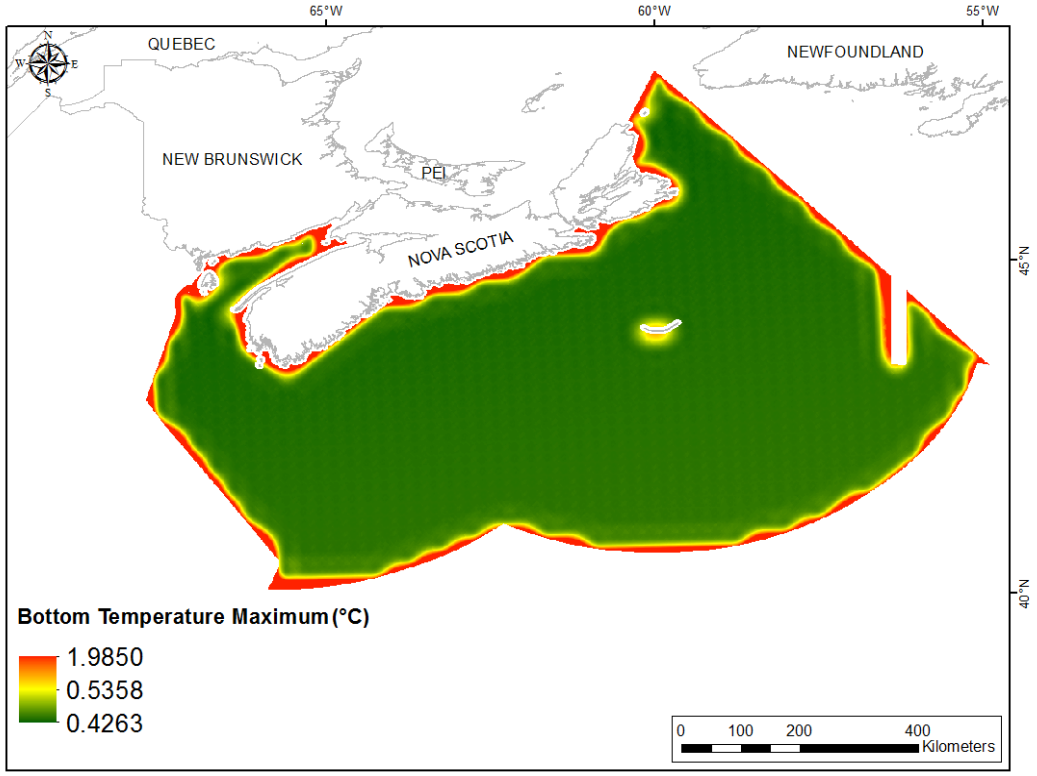

Fig. 19. Prediction standard error surface of Bottom Temperature Maximum (˚C).

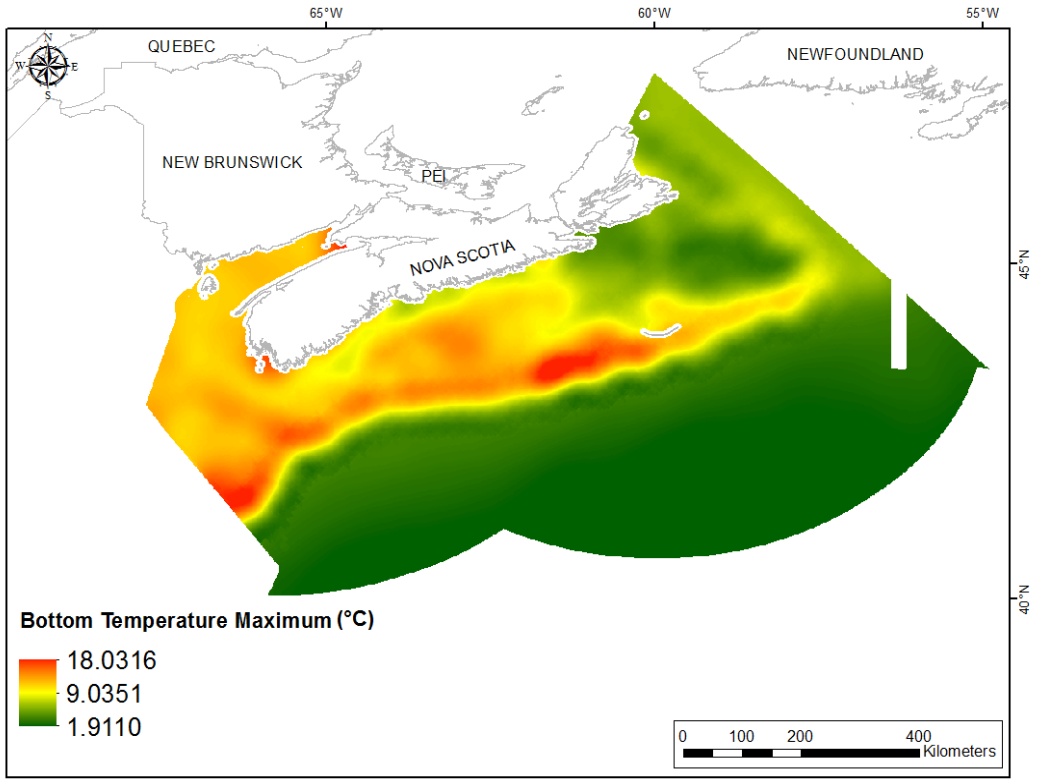

Fig. 20. Interpolated prediction surface of Bottom Temperature Maximum (˚C).

Bottom Temperature Range

This variable displayed a right-skewed distribution prior to interpolation (Table 9, Fig. 21). At both of the tails the actual data were greater than predicted by a normal distribution while there was an area of under-prediction at mid-range values (Fig. 22). These areas of under- and over-prediction showed spatial pattern over the region (Fig. 22).

The semivariogram showed moderate autocorrelation present in the data (Fig. 23). The kriged model showed a good fit between measured and predicted values (Fig. 23) and good cross-validation statistics (Table 10), indicating it was good at prediction. The error map showed high error along the edges of the study extent (Fig. 24). The kriged surface is presented in Fig. 25. Negative values resulted from the right-skewed nature of the raw data (Fig. 21). Of the 326,283 raster cells in the study extent, 1,970 contained negative values (see Table A1). These were located in a long band along the lower slope (Fig. A1).

Table 9. Distributional properties of Bottom Temperature Range (°C).

Property	Value
Number of Observations	1160
Minimum	0.182
Maximum	18.376
Mean	3.655
Median	1.002
Standard Deviation	3.930
Skewness	0.942
Kurtosis	2.846

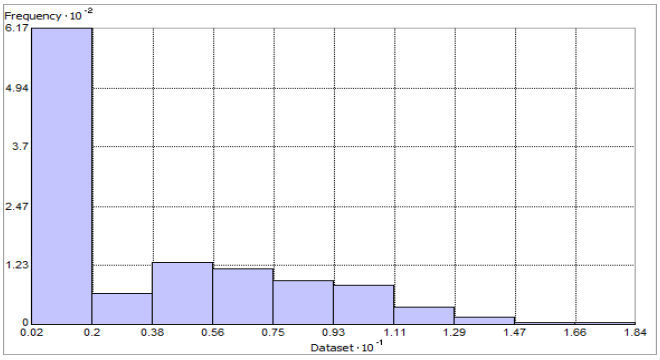

Fig. 21. Distribution of Bottom Temperature Range (°C). Histogram was illustrated using 10 bins. X axis shown at 10^{-1}; Y axis is shown at 10^{-2}.

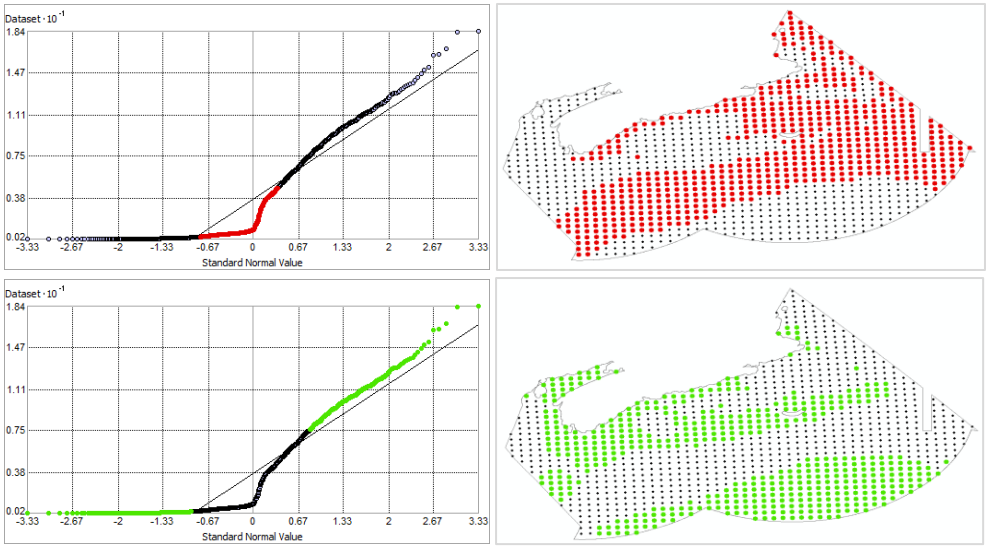

Fig. 22. Normal Q-Q plot for data values of Bottom Temperature Range (°C). Points falling under (upper panel) and over (bottom panel) the reference line are mapped.

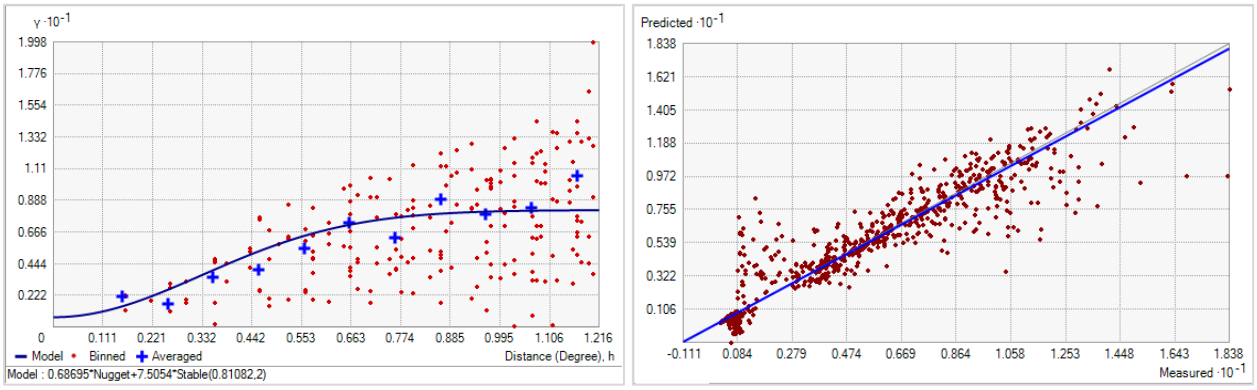

Fig. 23. Left panel: Semivariogram of Bottom Temperature Range (°C). Binned values are shown as red dots; average points are shown as blue crosses; the model fit to the averaged values is shown as a blue line. Lag size: 0.101 degrees; number of lags: 12; Parameter: 2; Range: 0.811 degrees; Partial Sill: 7.505. Right panel: Scatterplot of predicted values versus observed values for the model of Bottom Temperature Range (°C).

Table 10. Results of cross-validation of the kriged model for Bottom Temperature Range (°C).

Prediction error	**Value**
Number of Observations	1160
Overall Mean Error	-0.014
Root Mean Square Prediction Error	1.204
Standardized Mean	-5.932×10^{-3}
Standardized Root Mean Square Prediction Error	1.122
Average Standard Error	1.067

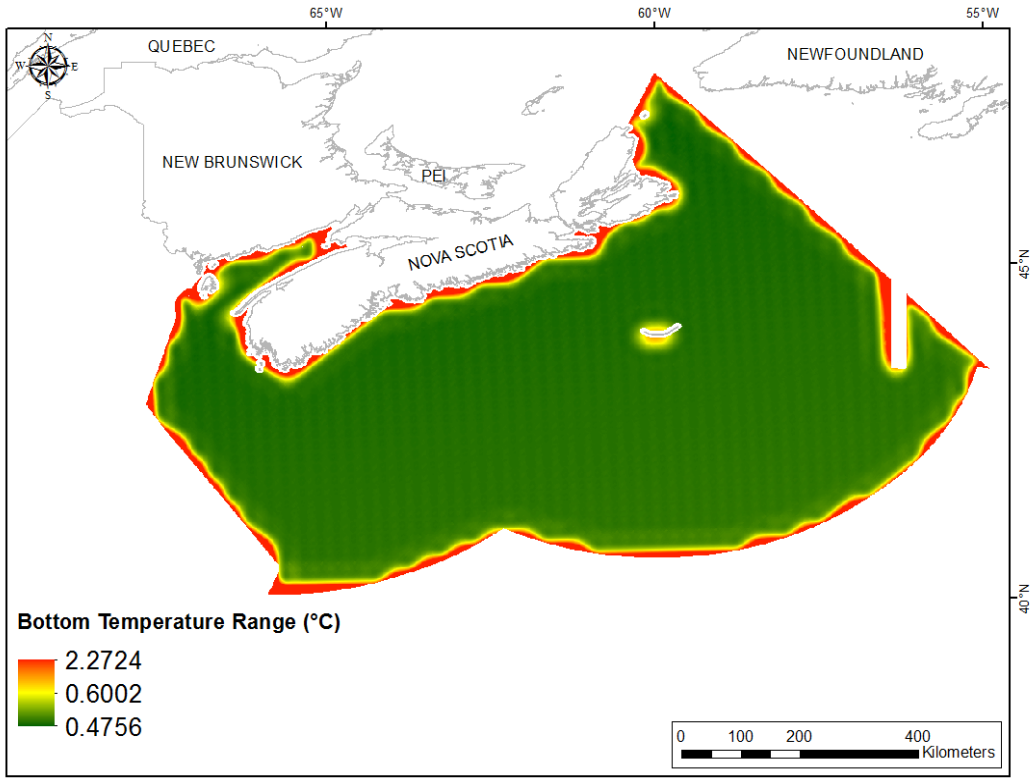

Fig. 24. Prediction standard error surface of Bottom Temperature Range (˚C).

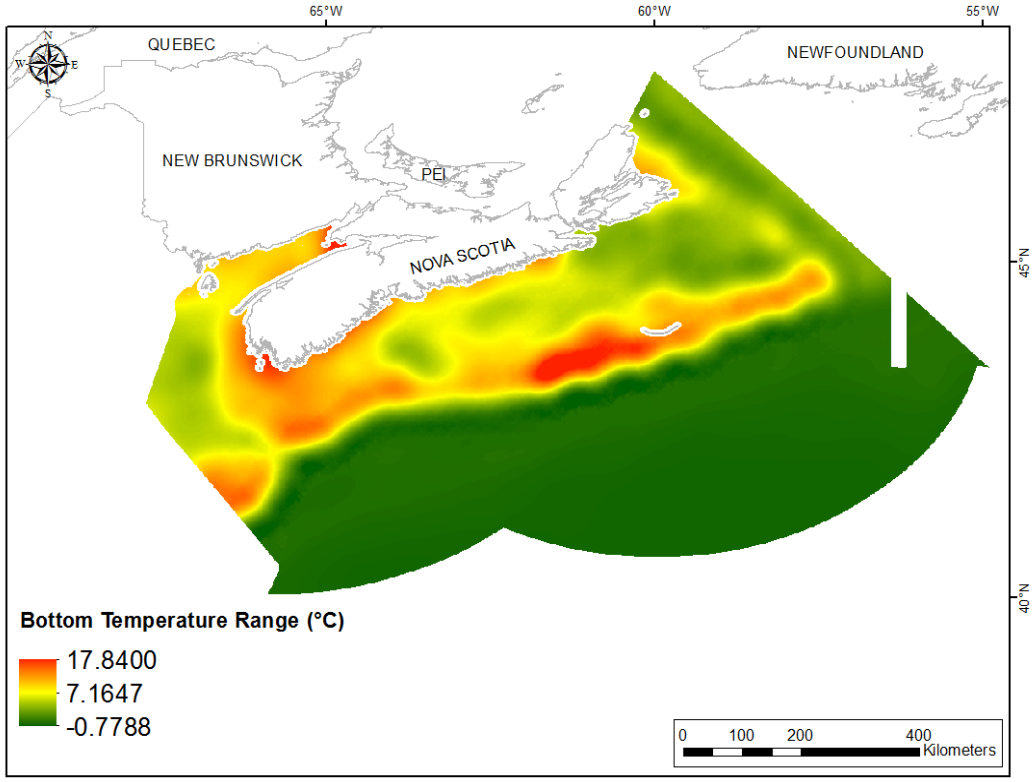

Fig. 25. Interpolated prediction surface of Bottom Temperature Range (˚C).

Bottom Temperature Average Minimum

This variable displayed a right-skewed, leptokurtic distribution prior to interpolation (Table 11, Fig. 26). The data were lower than predicted by a standard normal distribution in the highest and mid-range values and higher than predicted at low values and in the upper mid-data range (Fig. 27). These areas of under- and over-prediction showed some spatial pattern over the region (Fig. 27).

The semivariogram showed weak autocorrelation present in the data (Fig. 28). The model showed a good fit between measured and predicted values (Fig. 28). Good performance of the model was also indicated in the good cross-validation statistics (Table 12). The error map showed high error along the edges of the study extent (Fig. 29). The kriged surface is presented in Fig. 30.

Table 11. Distributional properties of Bottom Temperature Average Minimum (°C).

Property	Value
Number of Observations	1160
Minimum	-0.871
Maximum	8.756
Mean	3.158
Median	2.448
Standard Deviation	1.852
Skewness	1.143
Kurtosis	3.704

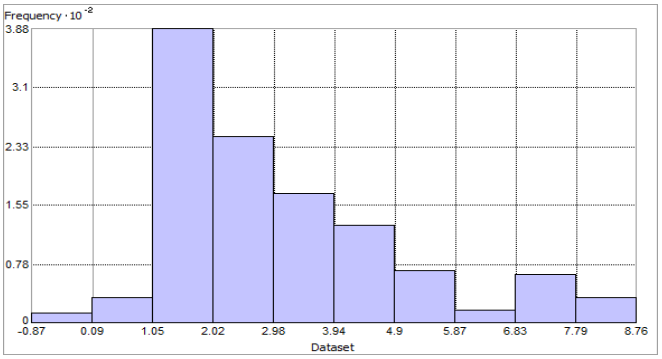

Fig. 26. Distribution of Bottom Temperature Average Minimum (°C). Histogram was illustrated using 10 bins. Y axis is shown at 10^{-2}.

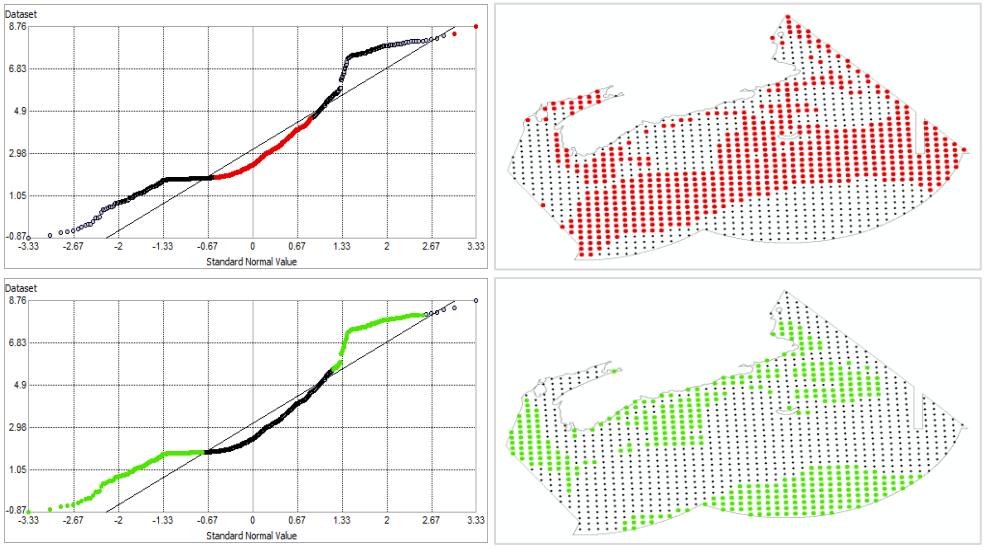

Fig. 27. Normal Q-Q plot for data values of Bottom Temperature Average Minimum (°C). Points falling under (top right panel) and over (bottom right panel) the reference line are mapped.

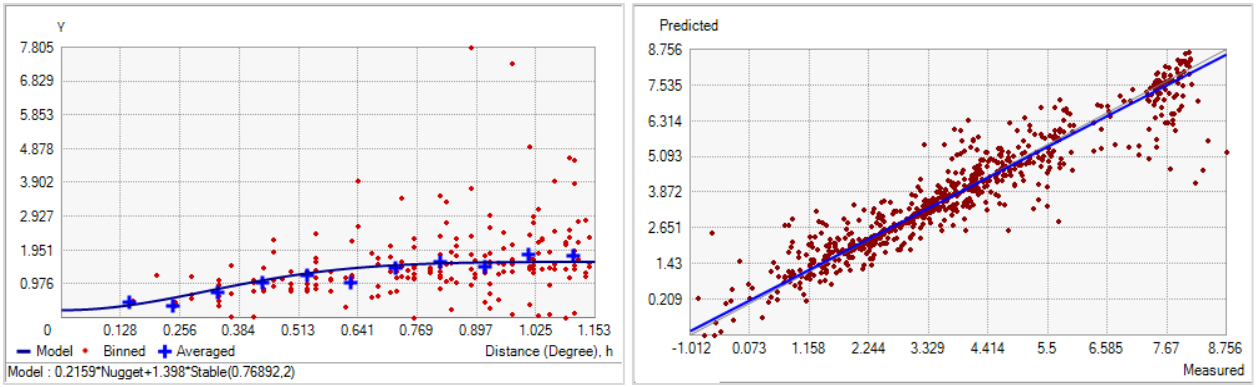

Fig. 28. Left panel: Semivariogram of Bottom Temperature Average Minimum (°C). Binned values are shown as red dots; average points are shown as blue crosses; the model fit to the averaged values is shown as a blue line. Lag size: 0.096 degrees; number of lags: 12; Parameter: 2; Range: 0.769 degrees; Partial Sill: 1.398. Right panel: Scatterplot of predicted values versus observed values for the model of Bottom Temperature Average Minimum (°C).

Table 12. Results of cross-validation of the kriged model for Bottom Temperature Average Minimum (°C).

Prediction error	**Value**
Number of Observations	1160
Overall Mean Error	6.758×10^{-3}
Root Mean Square Prediction Error	0.552
Standardized Mean	5.018×10^{-3}
Standardized Root Mean Square Prediction Error	0.943
Average Standard Error	0.587

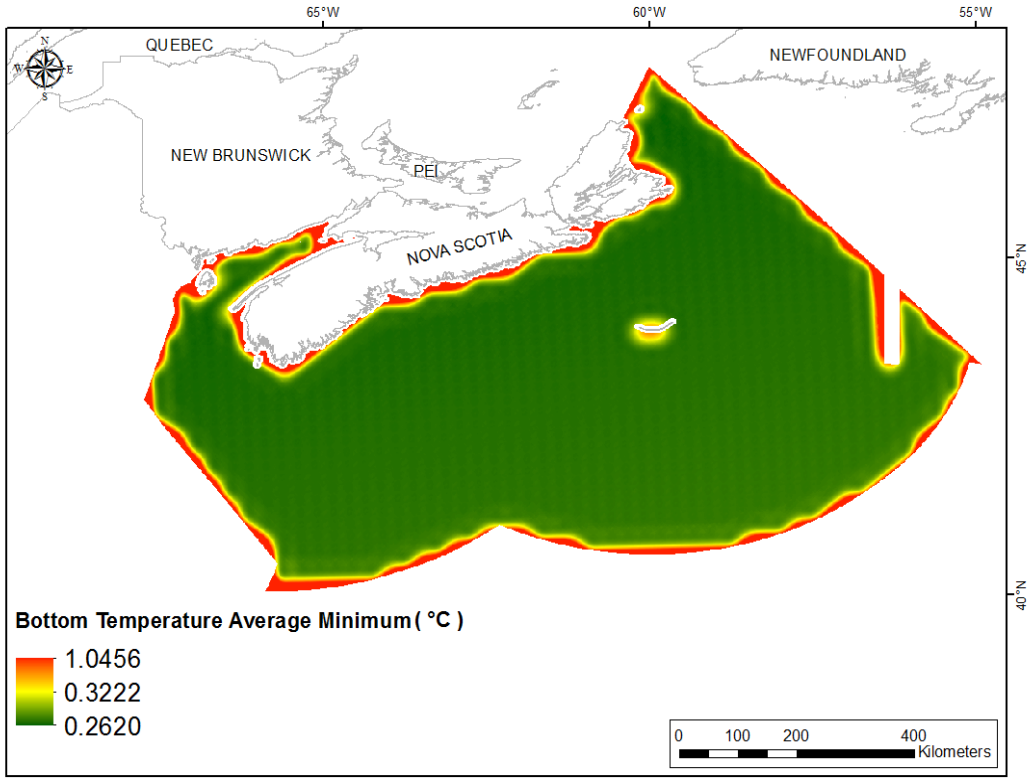

Fig. 29. Prediction standard error surface of Bottom Temperature Average Minimum (˚C).

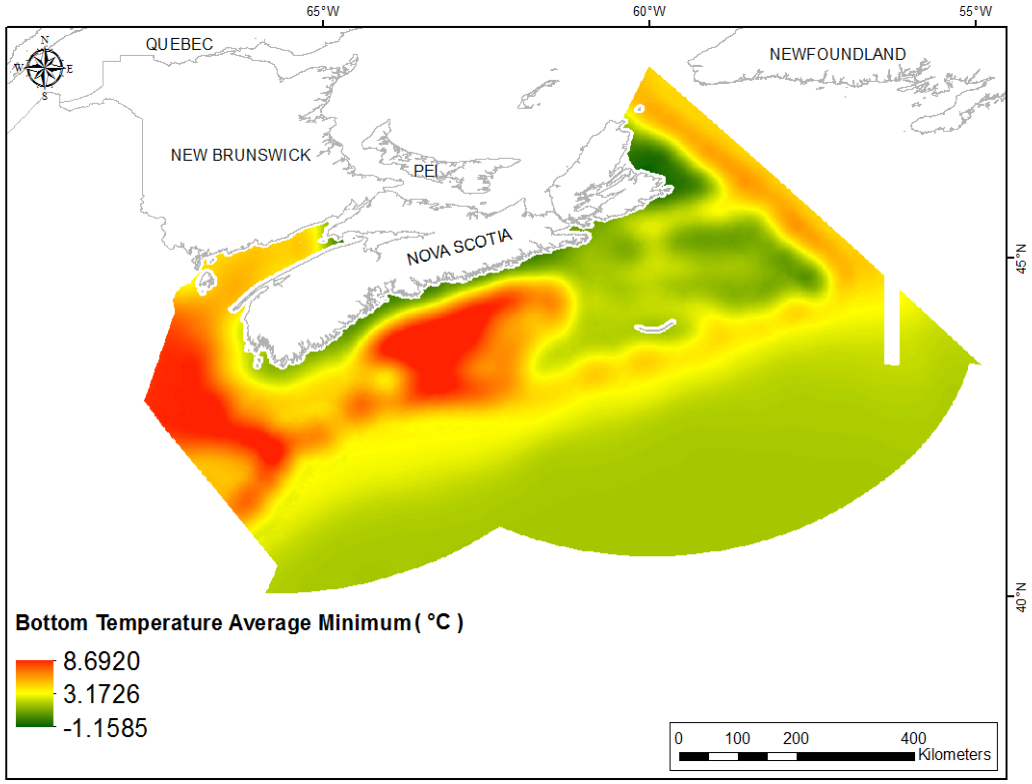

Fig. 30. Interpolated prediction surface of Bottom Temperature Average Minimum (˚C).

Bottom Temperature Average Maximum

This variable displayed a right-skewed, platykurtic distribution with outlying data in the upper range (Table 13, Fig. 31). The data were higher than predicted by a normal distribution at the tails of the distribution and under-predicted through the lower mid-range of the data (Fig. 32). These data points were somewhat spatially cohesive with specific areas of over- and under-prediction (Fig. 32).

The semivariogram showed moderate autocorrelation present in the data, and the model showed a good fit between measured and predicted values (Fig. 33). Good performance of the model was indicated by the good cross-validation statistics (Table 14). The error map showed high error along the edges of the study extent (Fig. 34). The kriged surface is presented in Fig. 35.

Table 13. Distributional properties of Bottom Temperature Average Maximum (°C).

Property	Value
Number of Observations	1160
Minimum	1.852
Maximum	18.566
Mean	4.846
Median	3.450
Standard Deviation	3.145
Skewness	0.923
Kurtosis	2.737

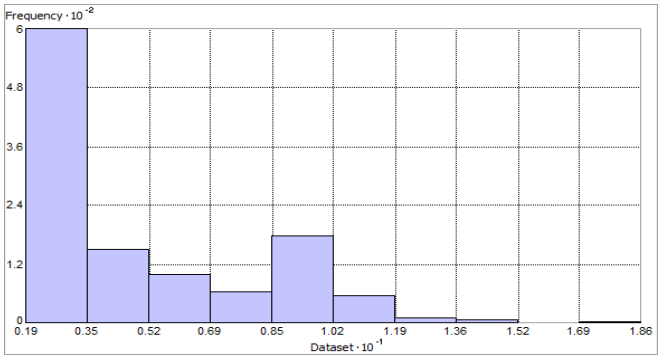

Fig. 31. Distribution of Bottom Temperature Average Maximum (°C). Histogram was illustrated using 10 bins. X axis is shown at 10^{-1}; Y axis is shown at 10^{-2}.

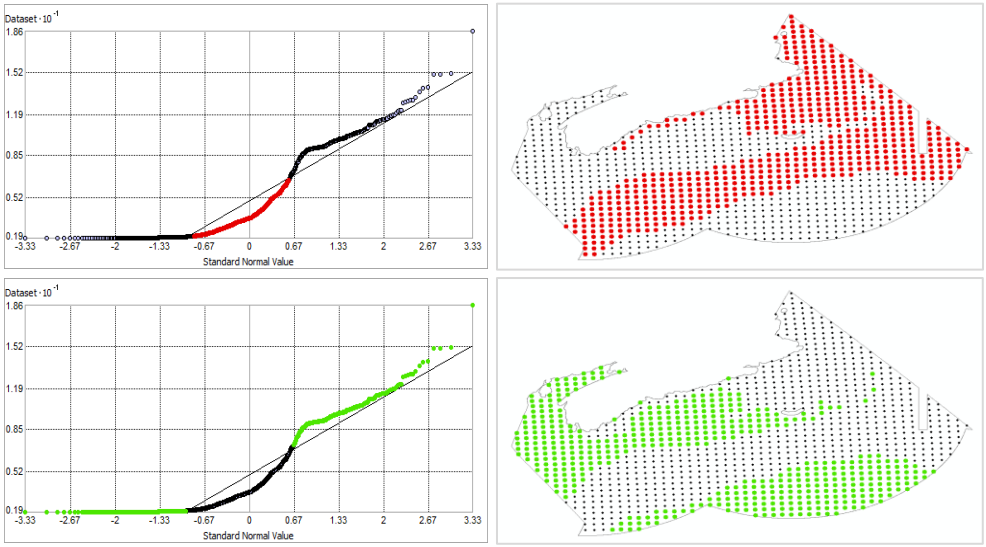

Fig. 32. Normal Q-Q plot for data values of Bottom Temperature Average Maximum (°C). Points falling under (upper panel) and over (bottom panel) the reference line are mapped.

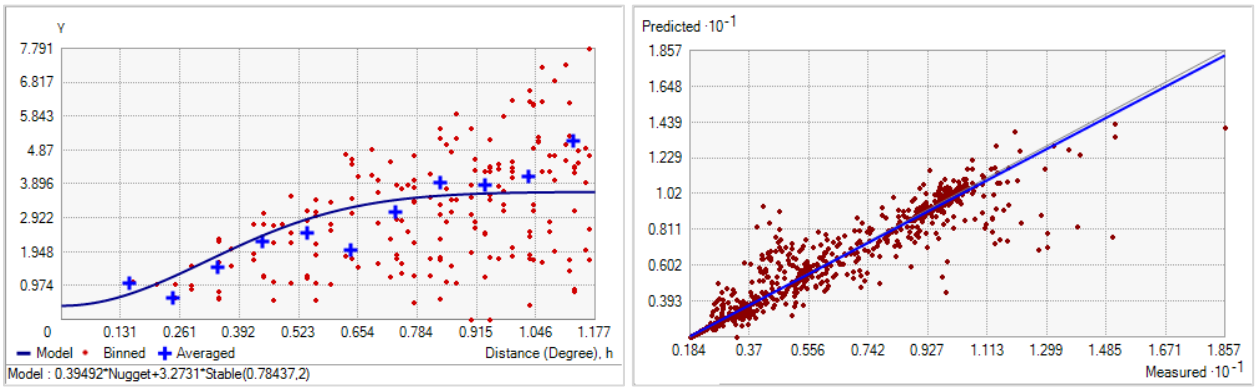

Fig. 33. Left panel: Semivariogram of Bottom Temperature Average Maximum (°C). Binned values are shown as red dots; average points are shown as blue crosses; the model fit to the averaged values is shown as a blue line. Lag size: 0.098 degrees; number of lags: 12; Parameter: 2; Range: 0.784 degrees; Partial Sill: 3.273. Right panel: Scatterplot of predicted values versus observed values for the model of Bottom Temperature Average Maximum (°C).

Table 14. Results of cross-validation of the kriged model for Bottom Temperature Average Maximum (°C).

Prediction error	**Value**
Number of Observations	1160
Overall Mean Error	-7.201×10^{-3}
Root Mean Square Prediction Error	0.909
Standardized Mean	-3.313×10^{-3}
Standardized Root Mean Square Prediction Error	1.113
Average Standard Error	0.803

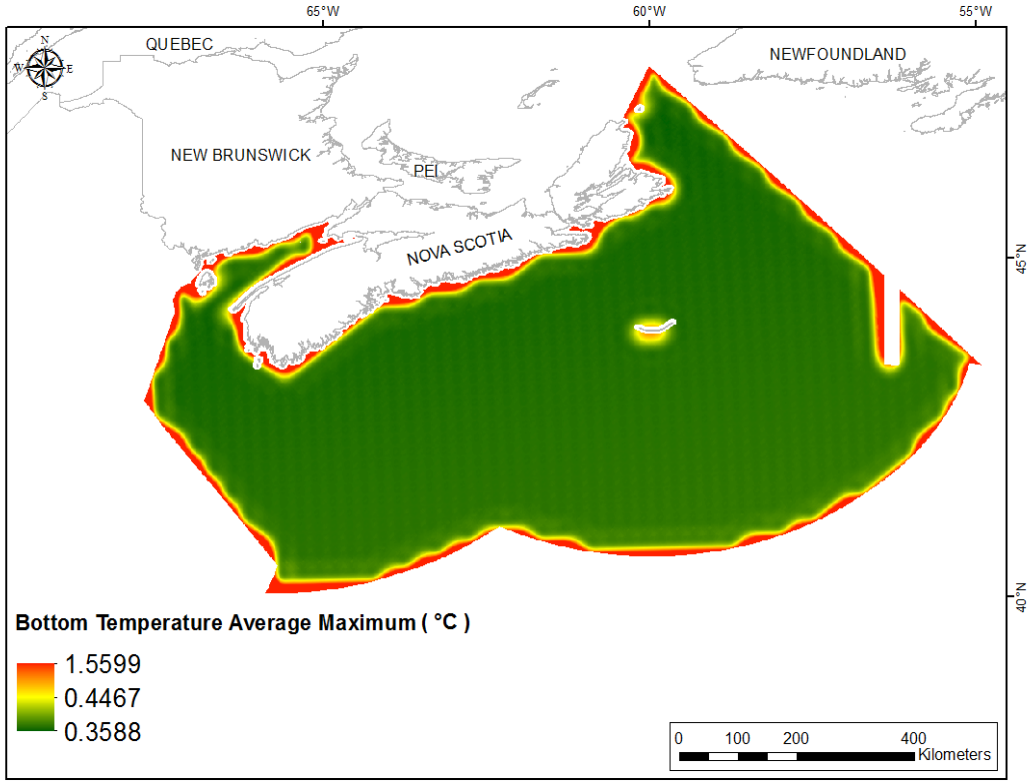

Fig. 34. Prediction standard error surface of Bottom Temperature Average Maximum (˚C).

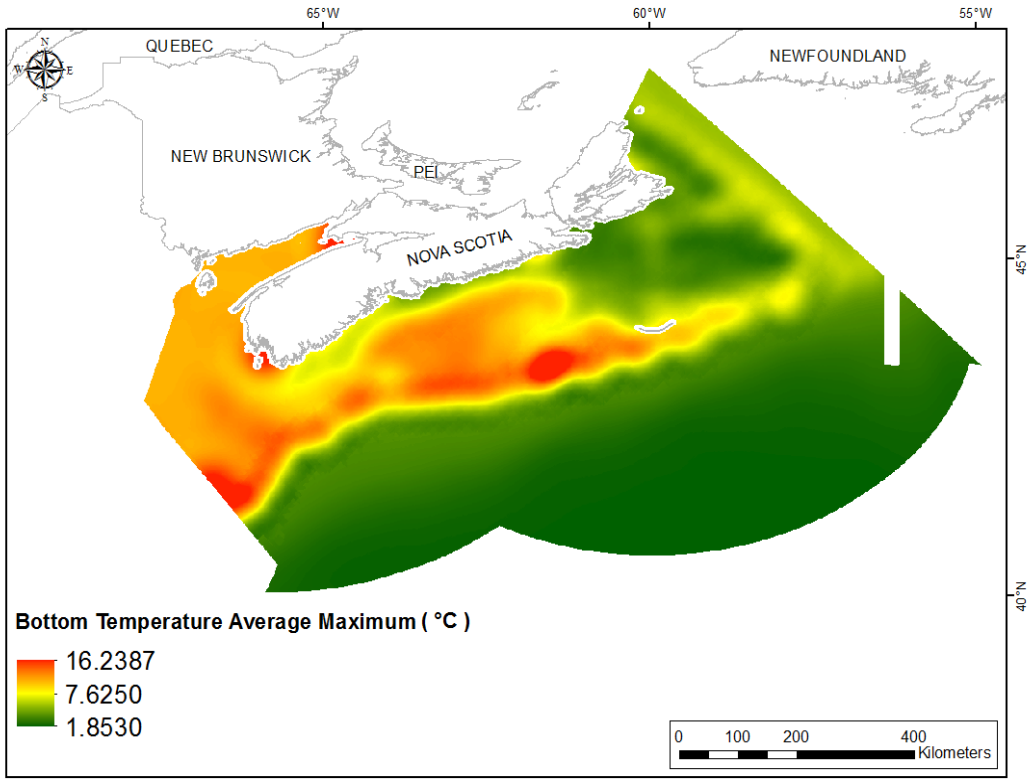

Fig. 35. Interpolated prediction surface of Bottom Temperature Average Maximum (˚C).

Bottom Temperature Average Range

This variable displayed a right-skewed, leptokurtic distribution with outlying data in the upper range (Table 15, Fig. 36). The data were higher than predicted by a normal distribution at the tails and lower than predicted through the mid-range of the data (Fig. 37). These areas of under- and over-prediction showed spatial pattern over the region (Fig. 37).

The semivariogram showed moderate autocorrelation present in the data, and the model showed a good fit between measured and predicted values (Fig. 38). Good performance of the model was indicated by the good cross-validation statistics (Table 16). The error map showed high error along the edges of the study extent (Fig. 39). The kriged surface is presented in Fig. 40. Negative values resulted from the right-skewed nature of the raw data (Fig. 36). Of the 326,283 raster cells in the study extent, 5,470 contained negative values (see Table A1). These were located in a long band along the lower slope (Fig. A2).

Table 15. Distributional properties of Bottom Temperature Average Range (°C).

Property	Value
Number of Observations	1160
Minimum	0.048
Maximum	15.879
Mean	1.677
Median	0.367
Standard Deviation	2.139
Skewness	1.796
Kurtosis	7.508

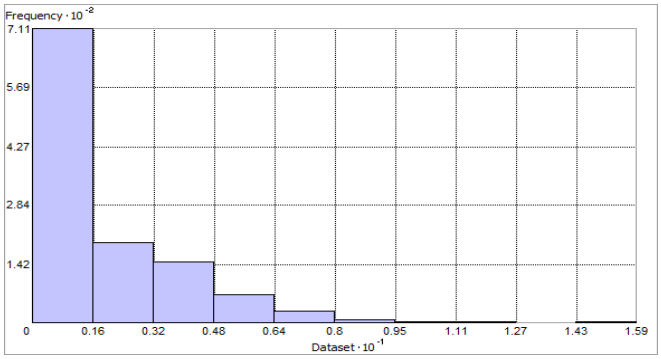

Fig. 36. Distribution of Bottom Temperature Average Maximum (°C). Histogram was illustrated using 10 bins. X axis is shown at 10^{-1}; Y axis is shown at 10^{-2}.

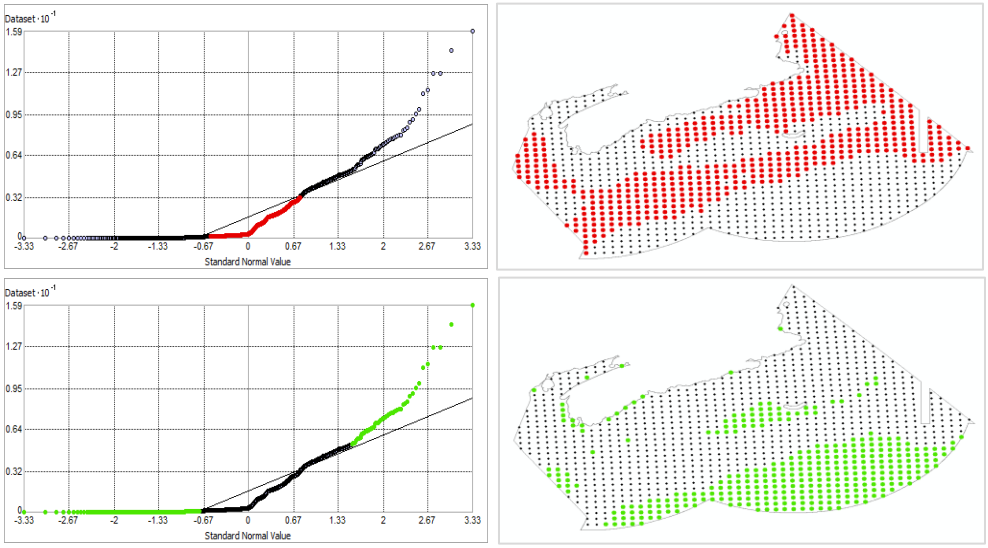

Fig. 37. Normal Q-Q plot for data values of Bottom Temperature Average Range (°C). Points falling under (upper panel) and over (bottom panel) the reference line are mapped.

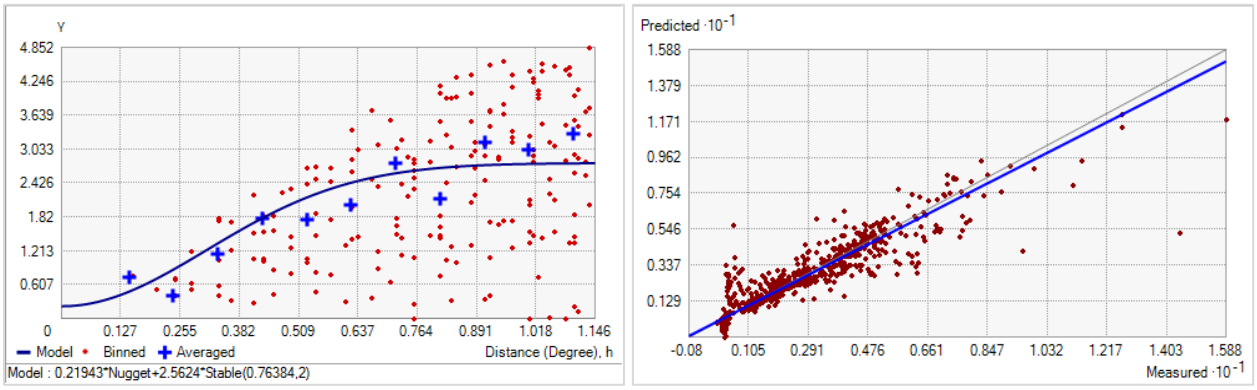

Fig. 38. Left panel: Semivariogram of Bottom Temperature Average Range (°C). Binned values are shown as red dots; average points are shown as blue crosses; the model fit to the averaged values is shown as a blue line. Lag size: 0.095 degrees; number of lags: 12; Parameter: 2; Range: 0.764 degrees; Partial Sill: 2.562. Right panel: Scatterplot of predicted values versus observed values for the model of Bottom Temperature Average Range (°C).

Table 16. Results of cross-validation of the kriged model for Bottom Temperature Average Range (°C).

Prediction error	**Value**
Number of Observations	1160
Overall Mean Error	-0.013
Root Mean Square Prediction Error	0.714
Standardized Mean	-8.354×10^{-3}
Standardized Root Mean Square Prediction Error	1.068
Average Standard Error	0.624

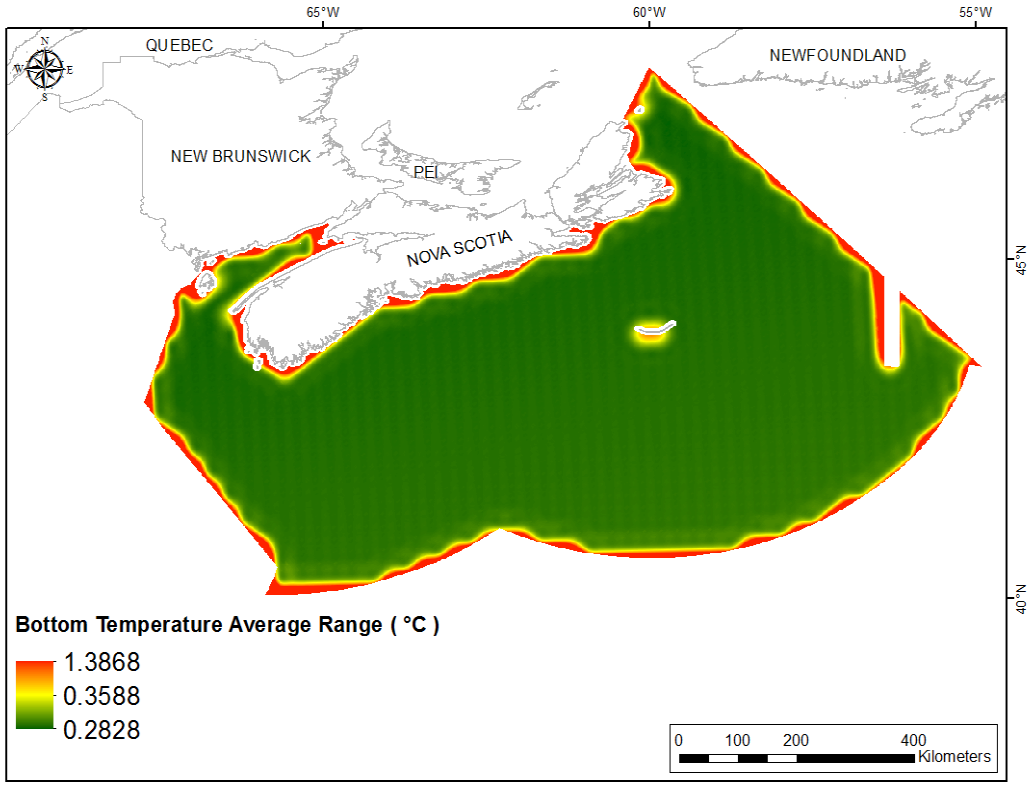

Fig. 39. Prediction standard error surface of Bottom Temperature Average Range (˚C).

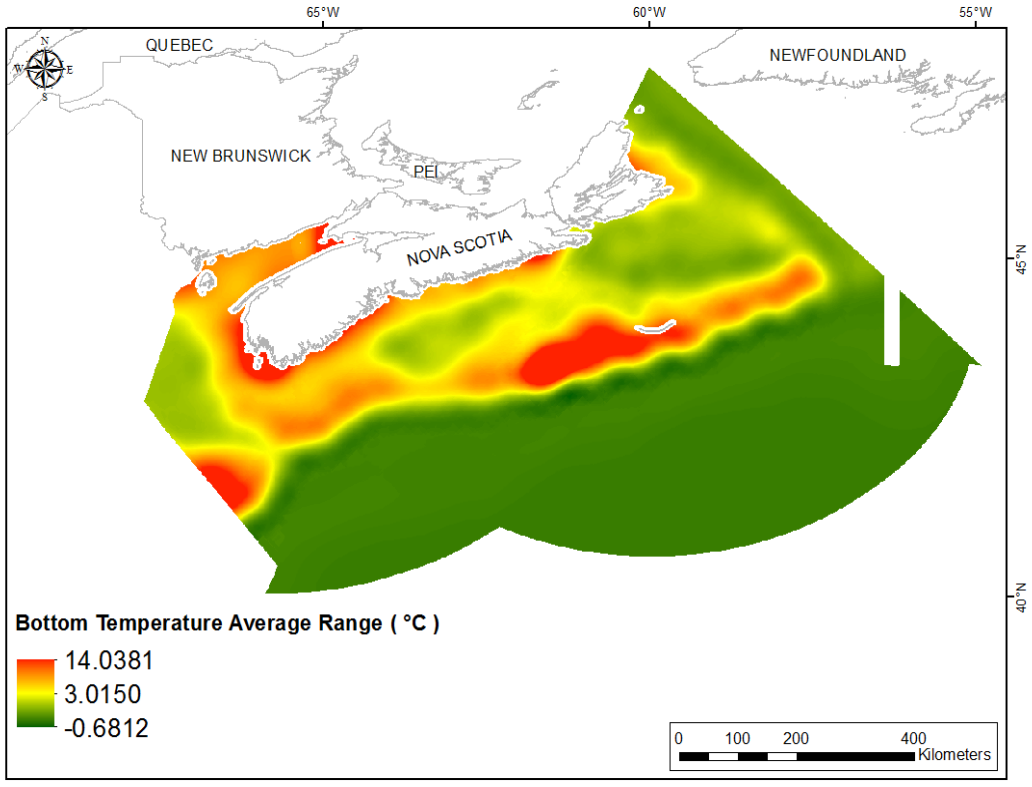

Fig. 40. Interpolated prediction surface of Bottom Temperature Average Range (˚C).

Surface Temperature Mean

This variable displayed a right-skewed, platykurtic distribution prior to interpolation (Table 17, Fig. 41). The data were higher than predicted by a standard normal distribution at low and upper mid-range values and lower than predicted at the highest and mid-values (Fig. 42). These areas of under- and over-prediction showed strong spatial pattern over the region (Fig. 42).

The semivariogram showed weak autocorrelation present in the data but an excellent fit between the predicted and measured values (Fig. 43). The kriged model showed poor cross-validation statistics (Table 18). The Standardized Root-Mean-Square Prediction Error was much lower than 1 indicating that variability in the predictions was overestimated. The error map showed a 'bullseye' pattern with error increasing with distance from data points (Fig. 44). The kriged surface is presented in Fig. 45.

Table 17. Distributional properties of Surface Temperature Mean (°C).

Property	Value
Number of Observations	1160
Minimum	6.234
Maximum	20.092
Mean	11.466
Median	10.104
Standard Deviation	3.819
Skewness	0.670
Kurtosis	2.178

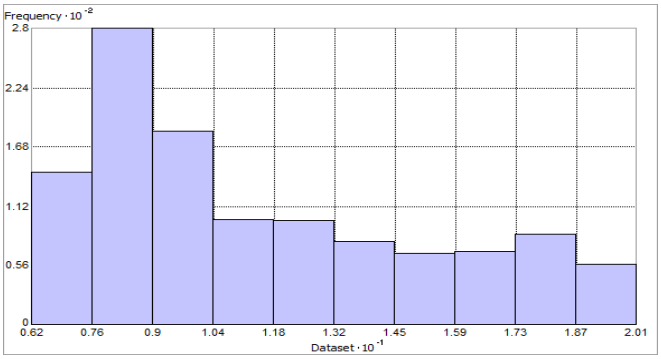

Fig. 41. Distribution of Surface Temperature Mean (°C). Histogram was illustrated using 10 bins. X axis is shown at 10^{-1}; Y axis is shown at 10^{-2}.

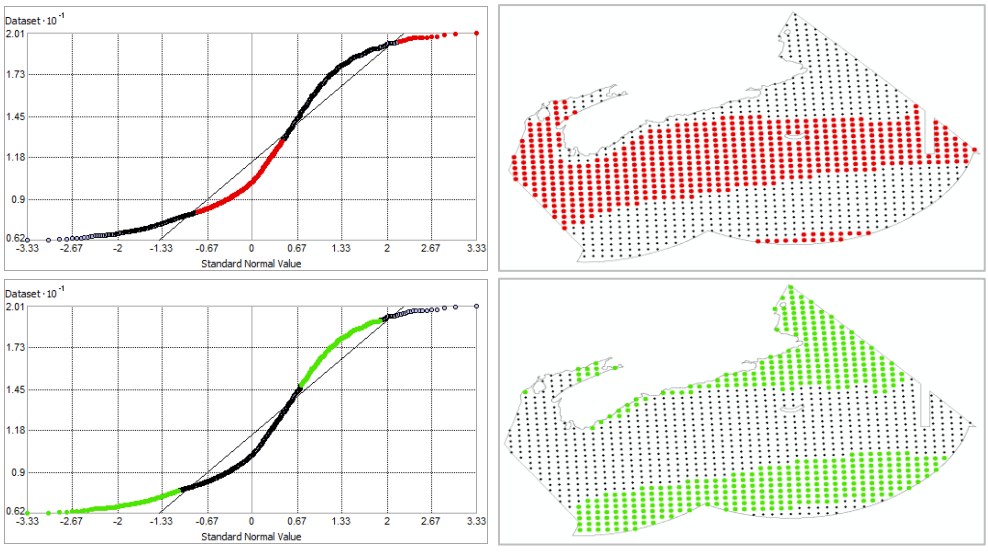

Fig. 42. Normal Q-Q plot for data values of Surface Temperature Mean (°C). Points falling under (upper panel) and over (bottom panel) the reference line are mapped.

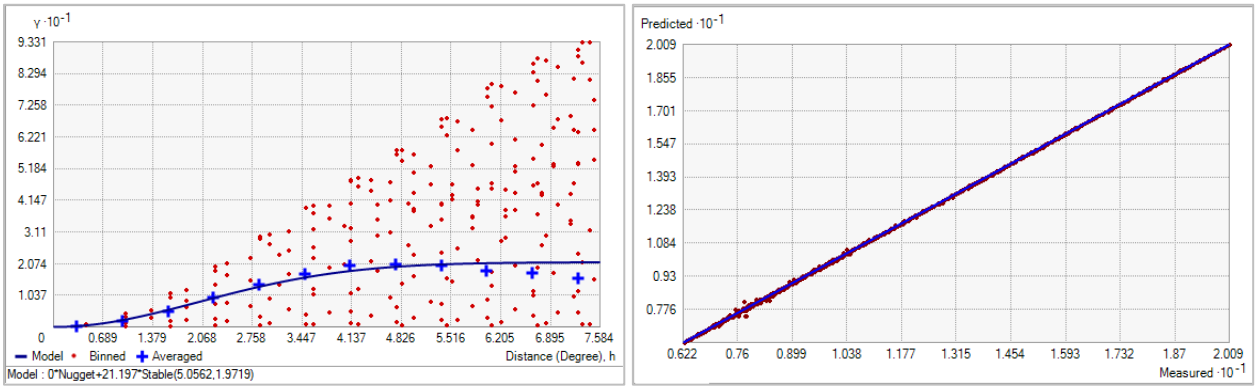

Fig. 43. Left panel: Semivariogram of Surface Temperature Mean (°C). Binned values are shown as red dots; average points are shown as blue crosses; the model fit to the averaged values is shown as a blue line. Lag size: 0.632 degrees; number of lags: 12; Parameter: 1.972; Range: 5.056 degrees; Partial Sill: 21.197. Right panel: Scatterplot of predicted values versus observed values for the model of Surface Temperature Mean (°C).

Table 18. Results of cross-validation of the kriged model for Surface Temperature Mean (°C).

Prediction error	**Value**
Number of Observations	1160
Overall Mean Error	-4.076×10^{-5}
Root Mean Square Prediction Error	0.034
Standardized Mean	6.080×10^{-5}
Standardized Root Mean Square Prediction Error	0.575
Average Standard Error	0.052

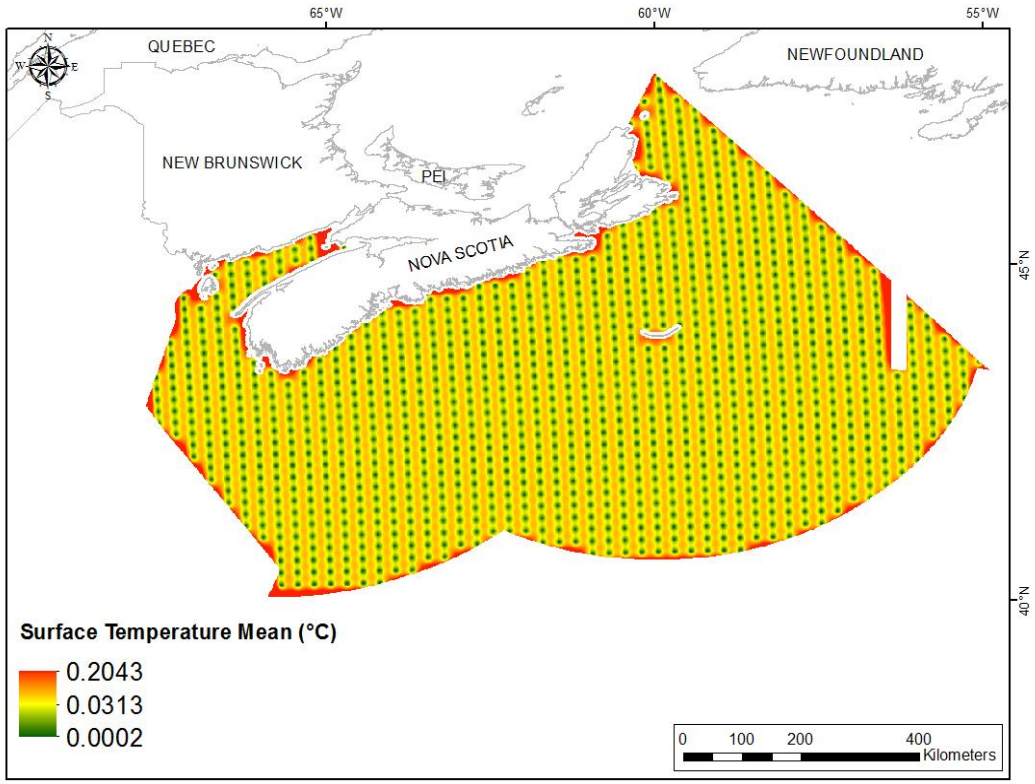

Fig. 44. Prediction standard error surface of Surface Temperature Mean (˚C).

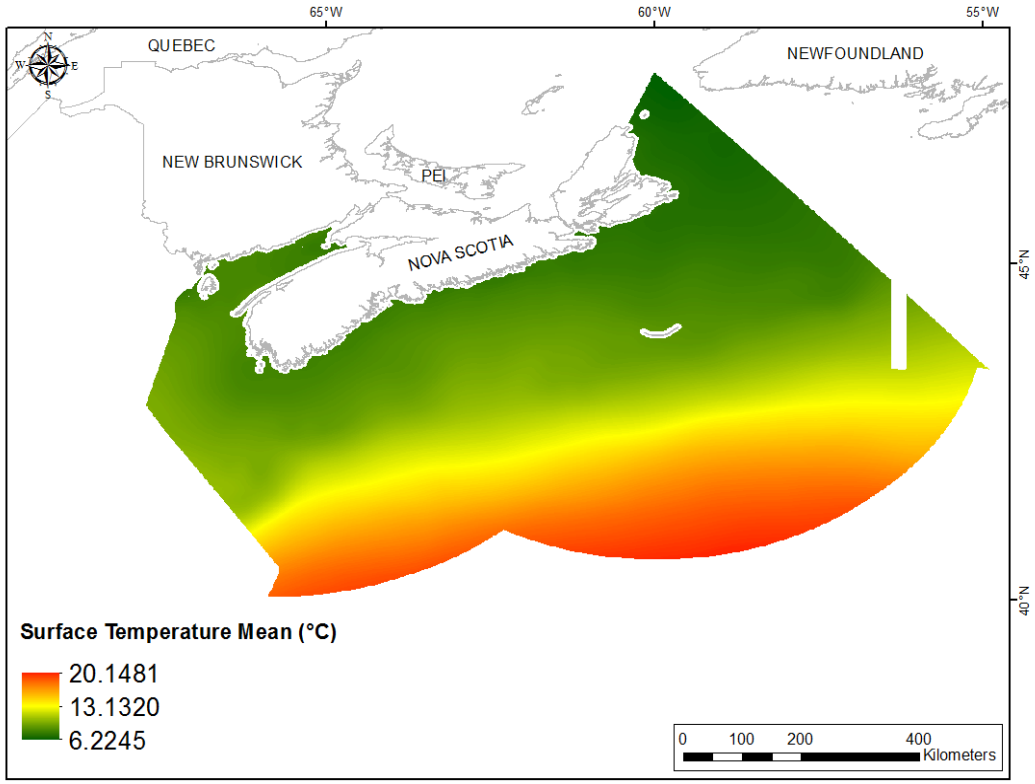

Fig. 45. Interpolated prediction surface of Surface Temperature Mean (˚C).

Surface Temperature Minimum

This variable displayed a right-skewed, leptokurtic distribution prior to interpolation (Table 19, Fig. 46). The data were higher than predicted by a standard normal distribution at the tails and were lower than predicted at mid-range values (Fig. 47). These data points were spatially cohesive with big areas of over- and under-prediction (Fig. 47), with the former being more prevalent.

The semivariogram showed weak autocorrelation present in the data but an excellent fit between the predicted and measured values (Fig. 48). The kriged model showed fair cross-validation statistics (Table 20). The error map showed a 'bullseye' pattern with error increasing with distance from data points (Fig. 49). The kriged surface is presented in Fig. 50.

Table 19. Distributional properties of Surface Temperature Minimum (°C).

Property	Value
Number of Observations	1160
Minimum	-1.606
Maximum	13.699
Mean	2.622
Median	1.660
Standard Deviation	3.732
Skewness	1.134
Kurtosis	3.491

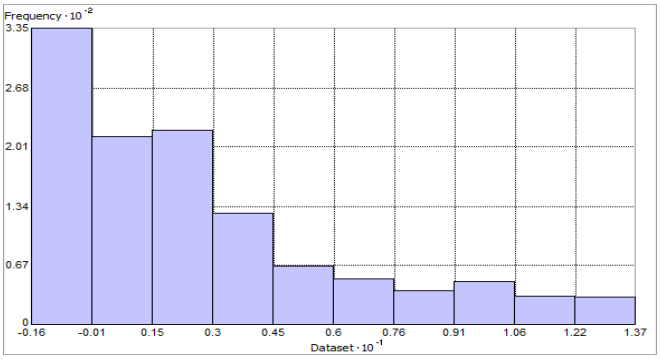

Fig. 46. Distribution of Surface Temperature Minimum (°C). Histogram was illustrated using 10 bins. X axis is shown at 10^{-1}; Y axis is shown at 10^{-2}.

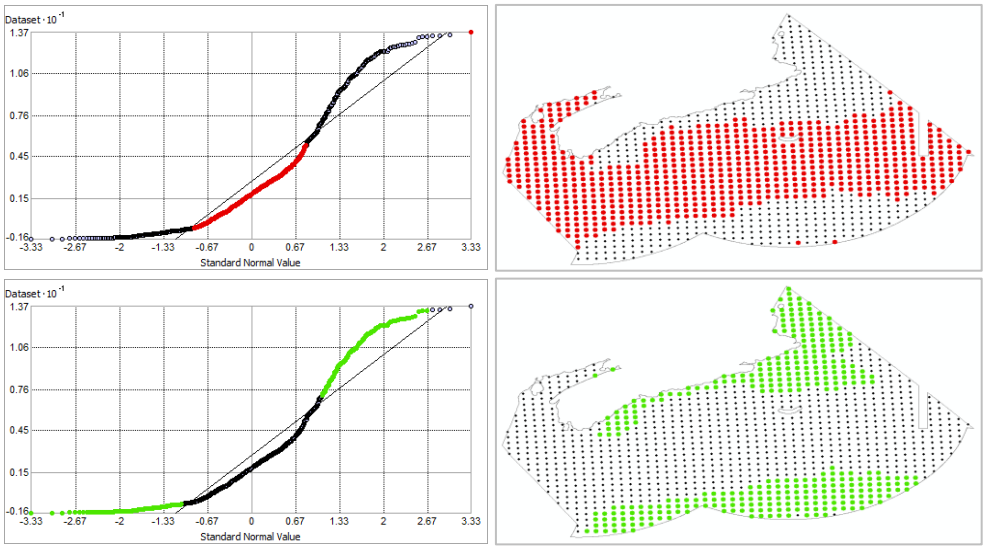

Fig. 47. Normal Q-Q plot for data values of Surface Temperature Minimum (°C). Points falling under (upper panel) and over (bottom panel) the reference line are mapped.

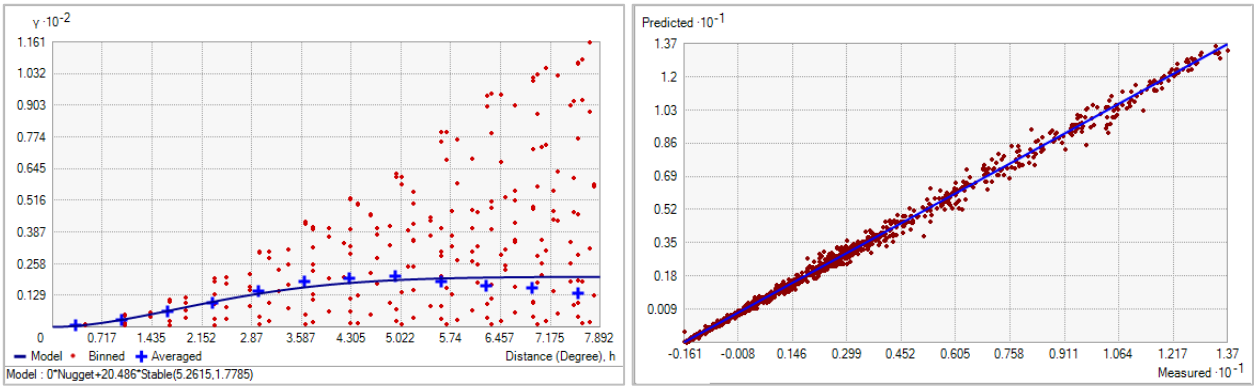

Fig. 48. Left panel: Semivariogram of Surface Temperature Minimum (°C). Binned values are shown as red dots; average points are shown as blue crosses; the model fit to the averaged values is shown as a blue line. Lag size: 0.658 degrees; number of lags: 12; Parameter: 1.779; Range: 5.261 degrees; Partial Sill: 20.486. Right panel: Scatterplot of predicted values versus observed values for the model of Surface Temperature Minimum (°C).

Table 20. Results of cross-validation of the kriged model for Surface Temperature Minimum (°C).

Prediction error	**Value**
Number of Observations	1160
Overall Mean Error	8.336×10^{-4}
Root Mean Square Prediction Error	0.229
Standardized Mean	1.175×10^{-3}
Standardized Root Mean Square Prediction Error	1.219
Average Standard Error	0.190

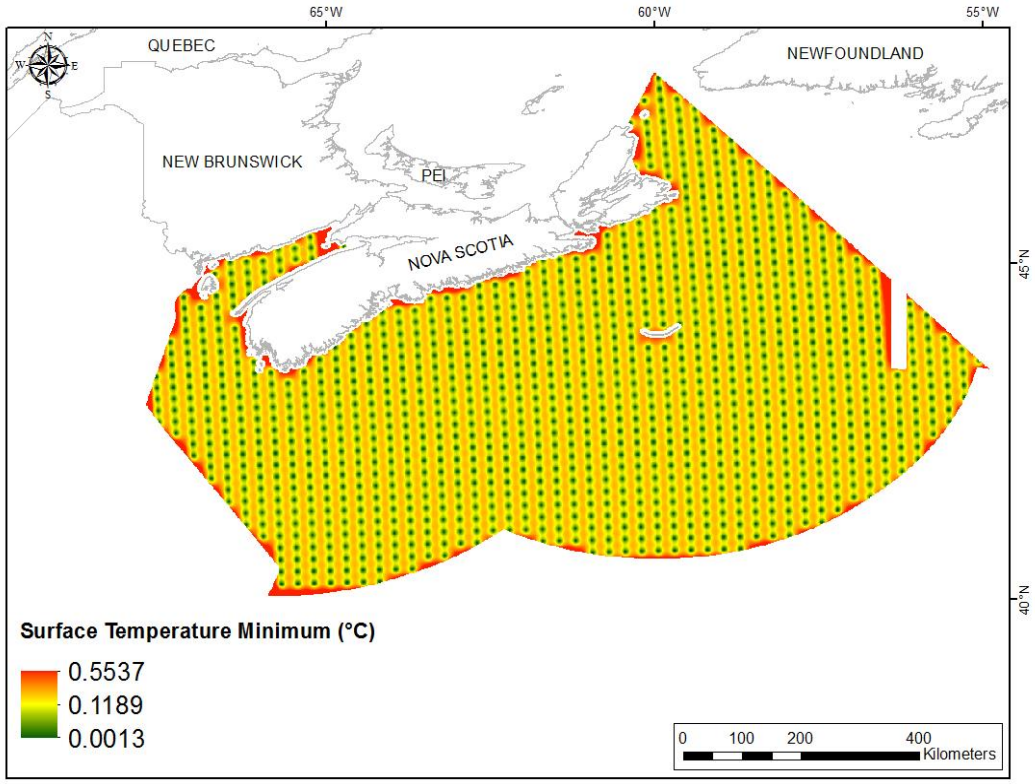

Fig. 49. Prediction standard error surface of Surface Temperature Minimum (˚C).

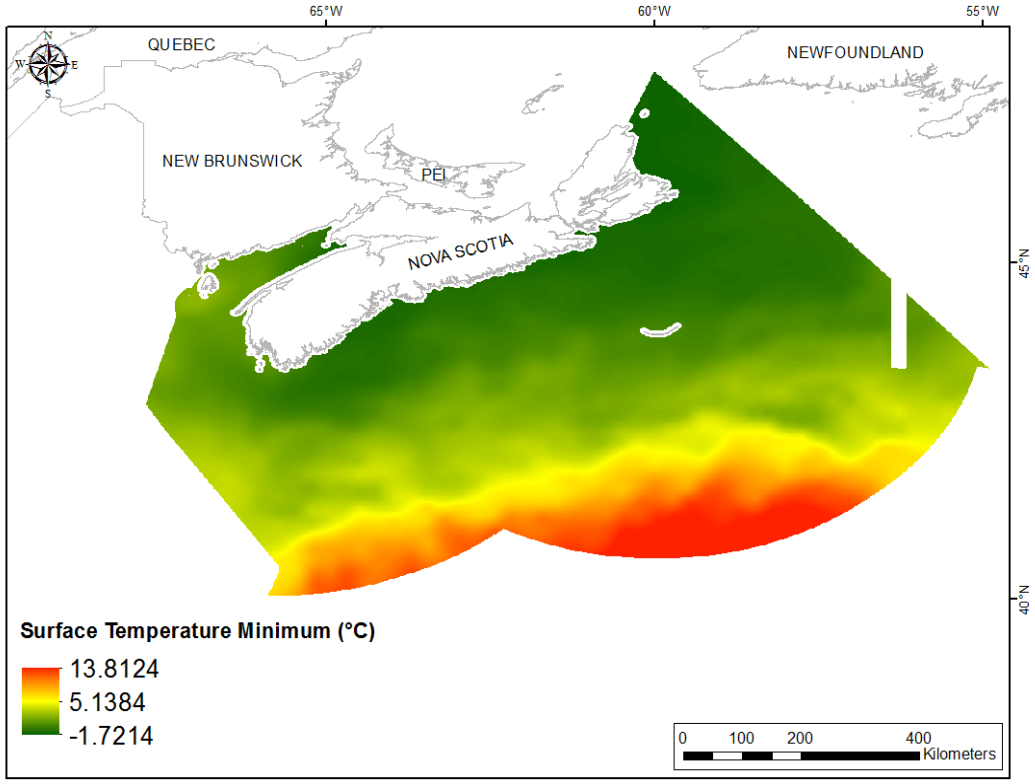

Fig. 50. Interpolated prediction surface of Surface Temperature Minimum (˚C).

Surface Temperature Maximum

This variable displayed a platykurtic, bimodal distribution prior the modeling (Table 21, Fig. 51). The data were higher than predicted by a standard normal distribution at low and upper mid-values and lower than predicted at high and mid-values (Fig. 52). These data points were spatially cohesive across the region (Fig. 52).

The semivariogram showed fair autocorrelation present in the data but an excellent fit between measured and predicted values (Fig. 53). The kriged model showed fair cross-validation statistics (Table 22). The Standardized Root-Mean-Square Prediction Error was higher than 1 indicating that variability in the predictions has been underestimated. The error map showed high error along the edges of the study extent (Fig. 54). The kriged surface is presented in Fig. 55.

Table 21. Distributional properties of Surface Temperature Maximum (°C).

Property	Value
Number of Observations	1160
Minimum	14.059
Maximum	27.009
Mean	21.512
Median	20.739
Standard Deviation	3.127
Skewness	0.092
Kurtosis	1.849

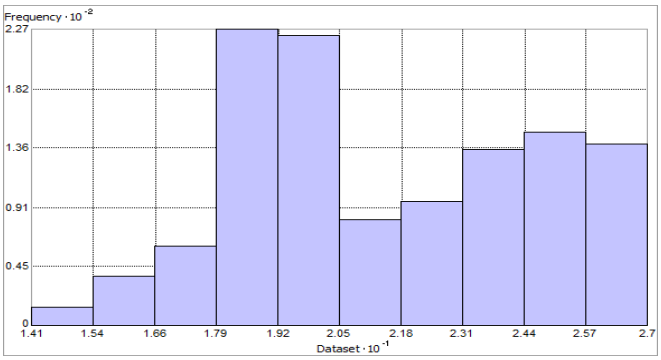

Fig. 51. Distribution of Surface Temperature Maximum (°C). Histogram was illustrated using 10 bins. X axis is shown at 10^{-1}; Y axis is shown at 10^{-2}.

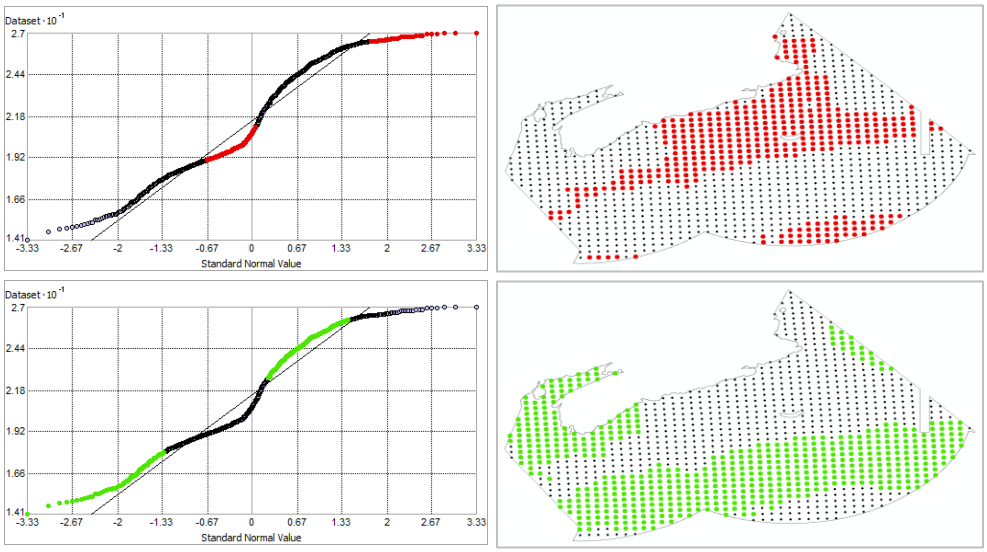

Fig. 52. Normal Q-Q plot for data values of Surface Temperature Maximum (°C). Points falling under (upper panel) and over (bottom panel) the reference line are mapped.

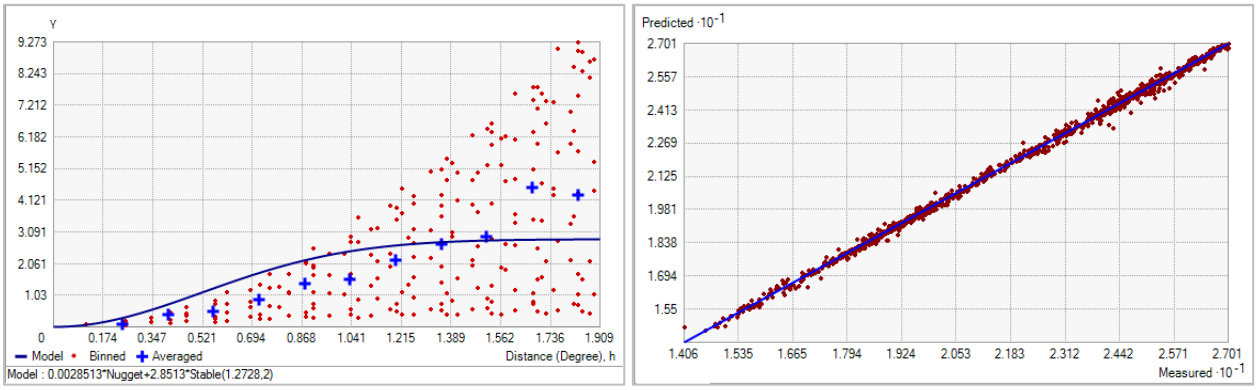

Fig. 53. Left panel: Semivariogram of Surface Temperature Maximum (°C). Binned values are shown as red dots; average points are shown as blue crosses; the model fit to the averaged values is shown as a blue line. Lag size: 0.159 degrees; number of lags: 12; Parameter: 2; Range: 1.273 degrees; Partial Sill: 2.851. Right panel: Scatterplot of predicted values versus observed values for the model of Surface Temperature Maximum (°C).

Table 22. Results of cross-validation of the kriged model for Surface Temperature Maximum (°C).

Prediction error	**Value**
Number of Observations	1160
Overall Mean Error	-9.786×10^{-4}
Root Mean Square Prediction Error	0.141
Standardized Mean	-9.983×10^{-3}
Standardized Root Mean Square Prediction Error	1.828
Average Standard Error	0.088

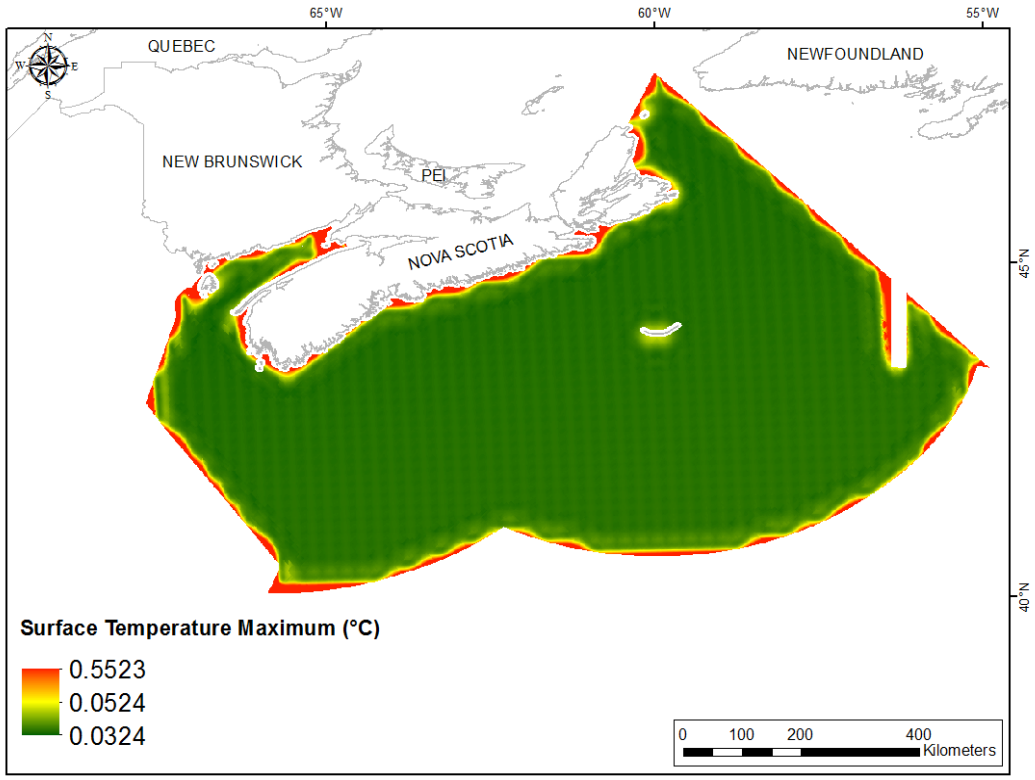

Fig. 54. Prediction standard error surface of Surface Temperature Maximum (˚C).

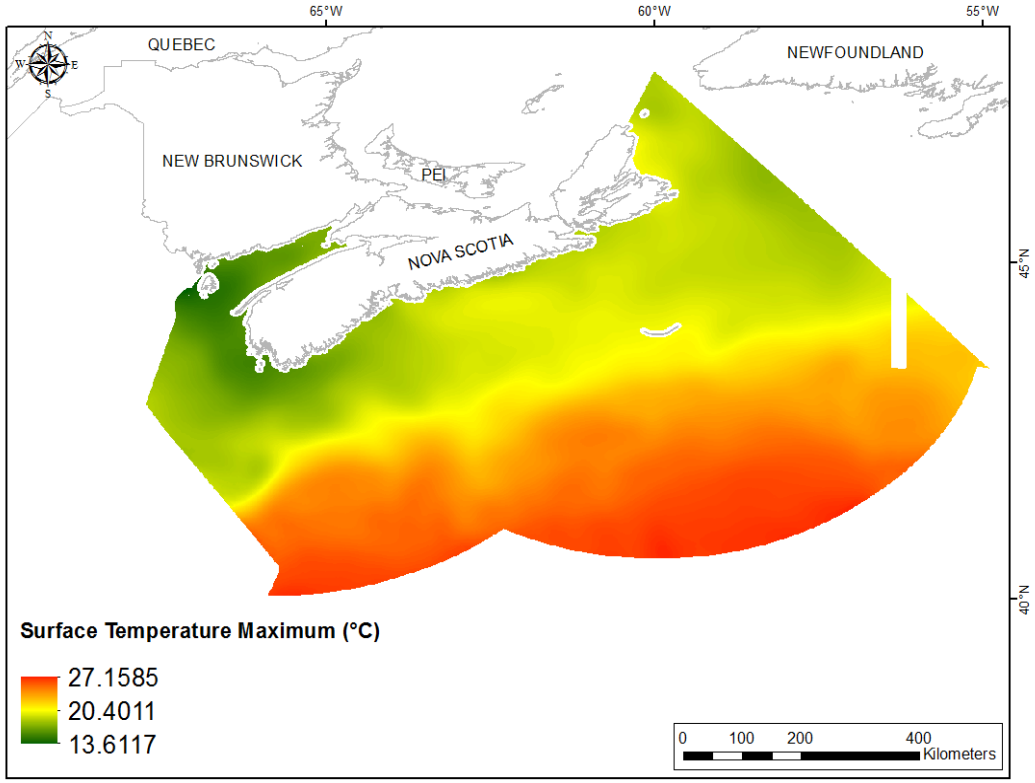

Fig. 55. Interpolated prediction surface of Surface Temperature Maximum (˚C).

Surface Temperature Range

This variable displayed a left-skewed, leptokurtic distribution prior to interpolation (Table 23, Fig. 56). The data were greater than predicted by a standard normal distribution at mid-values and lower than predicted at both tails (Fig. 57). These areas of under- and over-prediction showed no strong spatial pattern over the region (Fig. 57).

The semivariogram showed moderate autocorrelation present in the data and good predictive fit (Fig. 58). The kriged model showed good cross-validation statistics indicating that it was good at prediction (Table 24). The error map showed a 'bullseye' pattern with error increasing with distance from data points (Fig. 59). The kriged surface is presented in Fig. 60.

Table 23. Distributional properties of Surface Temperature Range (°C).

Property	Value
Number of Observations	1160
Minimum	12.013
Maximum	222.409
Mean	18.890
Median	19.492
Standard Deviation	1.992
Skewness	-1.041
Kurtosis	3.300

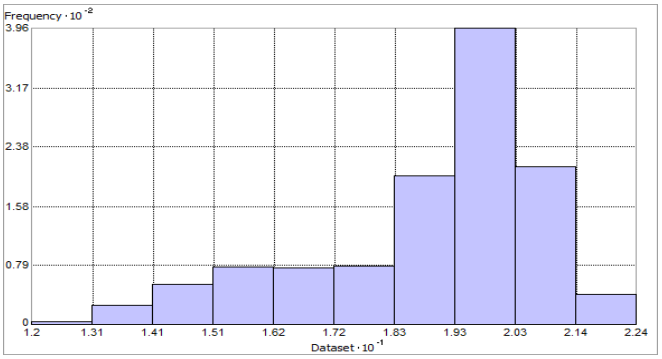

Fig. 56. Distribution of Surface Temperature Range (°C). Histogram was illustrated using 10 bins. X axis shown at 10^{-1}; Y axis is shown at 10^{-2}.

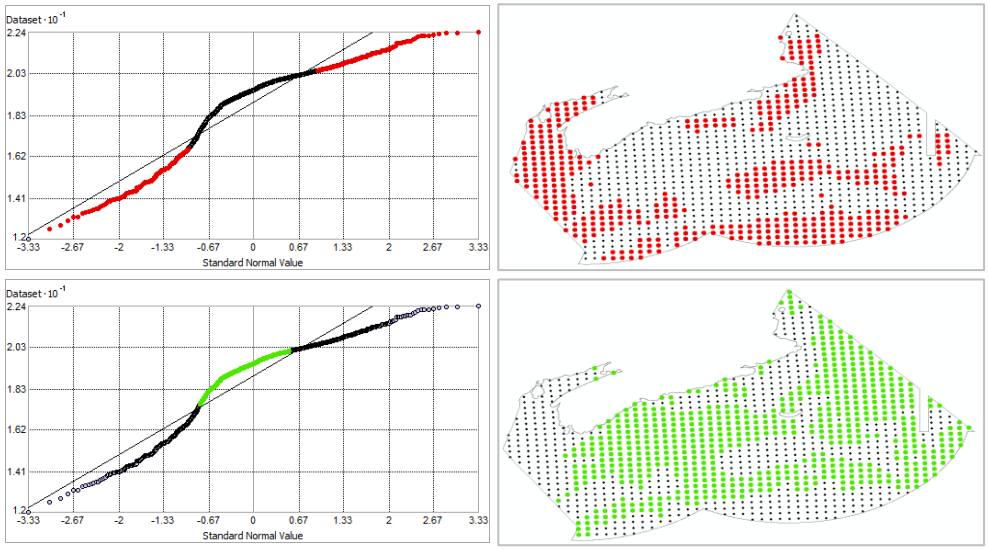

Fig. 57. Normal Q-Q plot for data values of Surface Temperature Range (°C). Points falling under (upper panel) and over (bottom panel) the reference line are mapped.

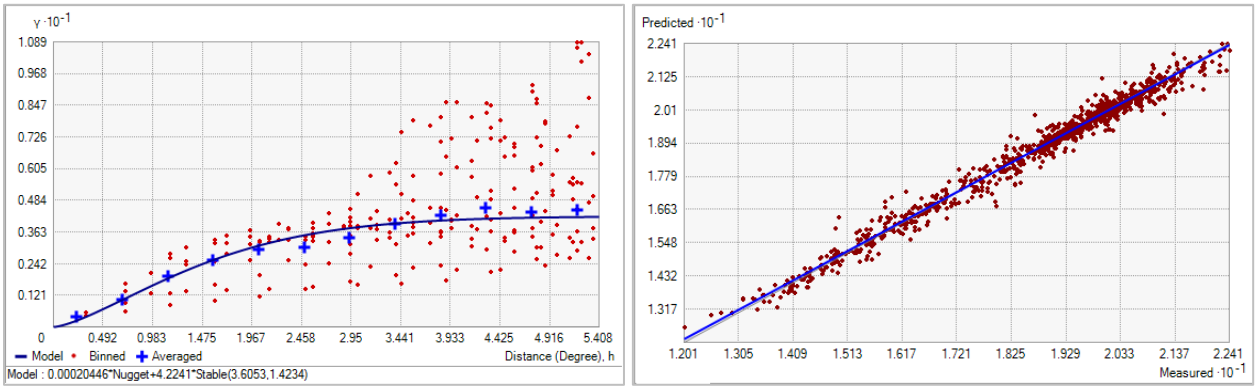

Fig. 58. Left panel: Semivariogram of Surface Temperature Range (°C). Binned values are shown as red dots; average points are shown as blue crosses; the model fit to the averaged values is shown as a blue line. Lag size: 0.451 degrees; number of lags: 12; Parameter: 1.423; Range: 3.605 degrees; Partial Sill: 4.224. Right panel: Scatterplot of predicted values versus observed values for the model of Surface Temperature Range (°C).

Table 24. Results of cross-validation of the kriged model for Surface Temperature Range (°C).

Prediction error	**Value**
Number of Observations	1160
Overall Mean Error	-1.376×10^{-3}
Root Mean Square Prediction Error	0.271
Standardized Mean	-1.967×10^{-3}
Standardized Root Mean Square Prediction Error	0.827
Average Standard Error	0.326

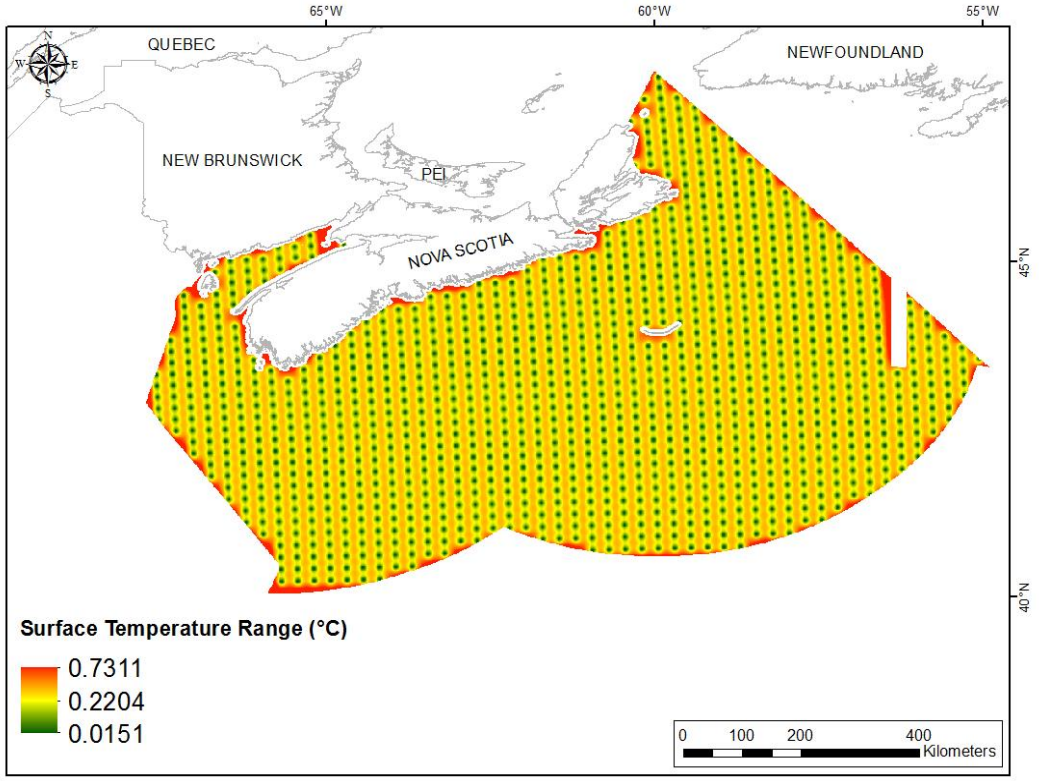

Fig. 59. Prediction standard error surface of Surface Temperature Range (˚C).

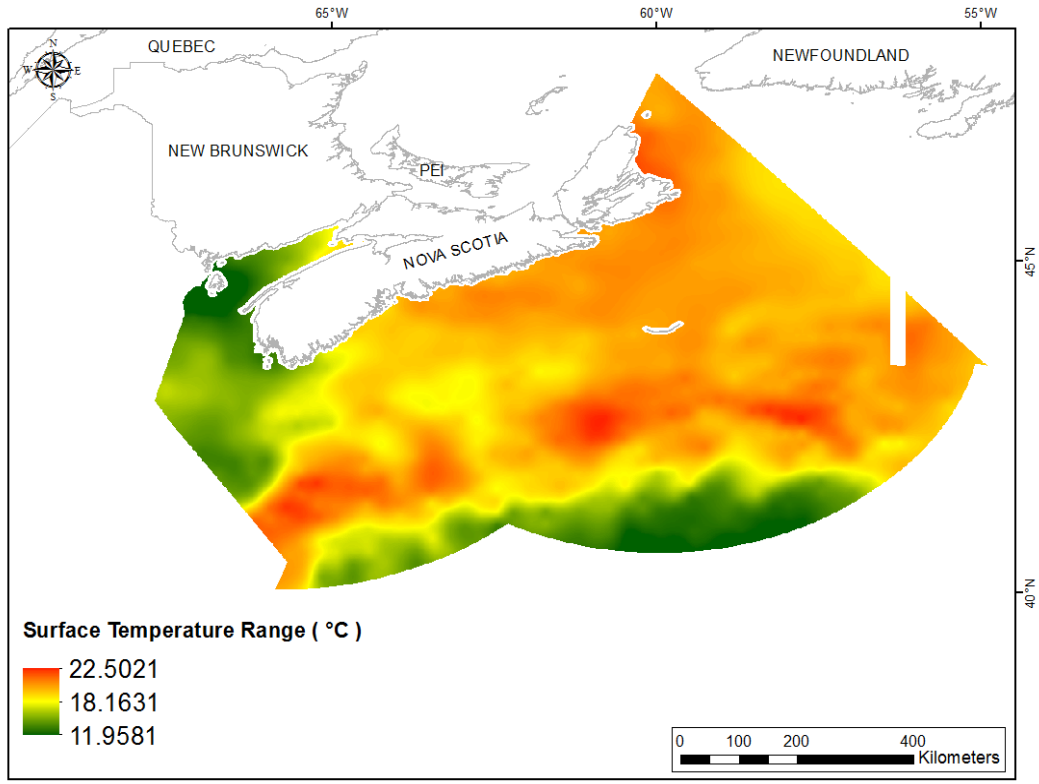

Fig. 60. Interpolated prediction surface of Surface Temperature Range (˚C).

Surface Temperature Average Minimum

This variable displayed a right-skewed, platykurtic distribution prior to interpolation (Table 25, Fig. 61). The data were greater than predicted by a standard normal distribution at upper mid-range and low values, and lower than predicted at lower mid-range and highest values (Fig. 62). These data points were spatially cohesive with specific areas of over- and under-prediction (Fig. 62).

The semivariogram showed weak autocorrelation present in the data but an excellent predictive fit (Fig. 63). However, the model showed poor cross-validation statistics (Table 26). The Standardized Root-Mean-Square Prediction Error was lower than 1 indicating that variability in the predictions has been overestimated. The error map showed a 'bullseye' pattern with error increasing with distance from data points (Fig. 64). The kriged surface is presented in Fig. 65.

Table 25. Distributional properties of Surface Temperature Average Minimum (°C).

Property	Value
Number of Observations	1160
Minimum	-1.277
Maximum	15.518
Mean	4.785
Median	3.477
Standard Deviation	4.333
Skewness	0.756
Kurtosis	2.512

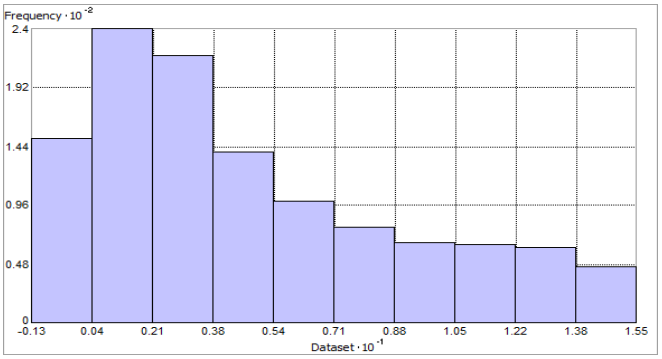

Fig. 61. Distribution of Surface Temperature Average Minimum (°C). Histogram was illustrated using 10 bins. X axis is shown at 10^{-1}; Y axis is shown at 10^{-2}.

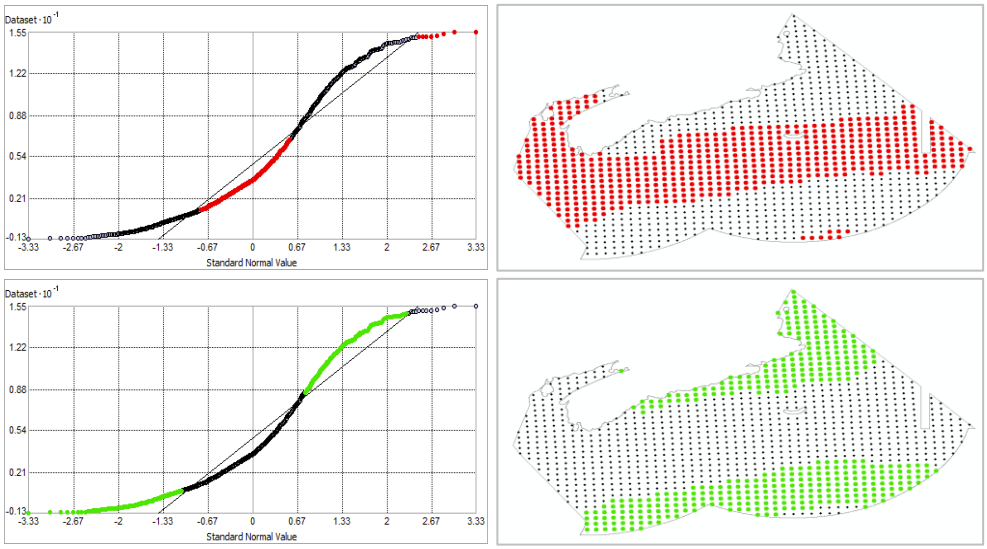

Fig. 62. Normal Q-Q plot for data values of Surface Temperature Average Minimum (°C). Points falling under (upper panel) and over (bottom panel) the reference line are mapped.

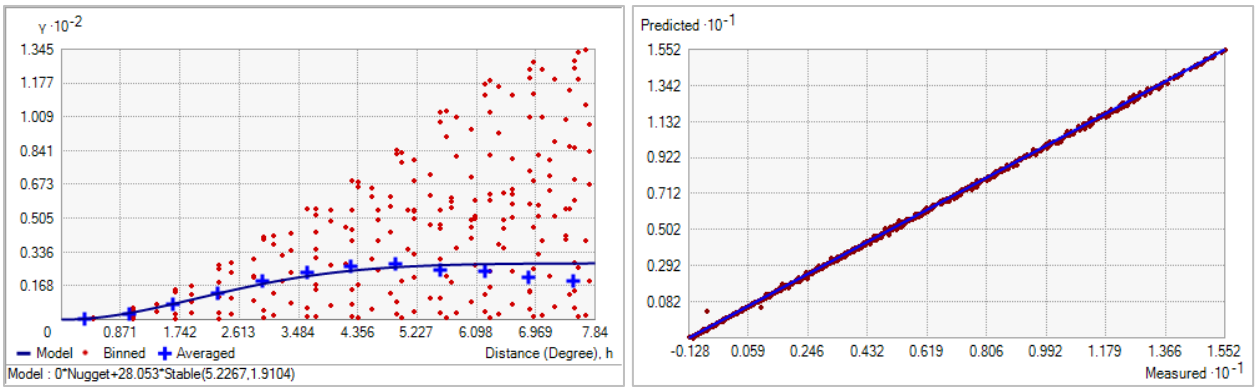

Fig. 63. Left panel: Semivariogram of Surface Temperature Average Minimum (°C). Binned values are shown as red dots; average points are shown as blue crosses; the model fit to the averaged values is shown as a blue line. Lag size: 0.653 degrees; number of lags: 12; Parameter: 1.910; Range: 5.227 degrees; Partial Sill: 28.053. Right panel: Scatterplot of predicted values versus observed values for the model of Surface Temperature Average Minimum (°C).

Table 26. Results of cross-validation of the kriged model for Surface Temperature Average Minimum (°C).

Prediction error	**Value**
Number of Observations	1160
Overall Mean Error	1.050×10^{-3}
Root Mean Square Prediction Error	0.067
Standardized Mean	1.623×10^{-3}
Standardized Root Mean Square Prediction Error	0.501
Average Standard Error	0.115

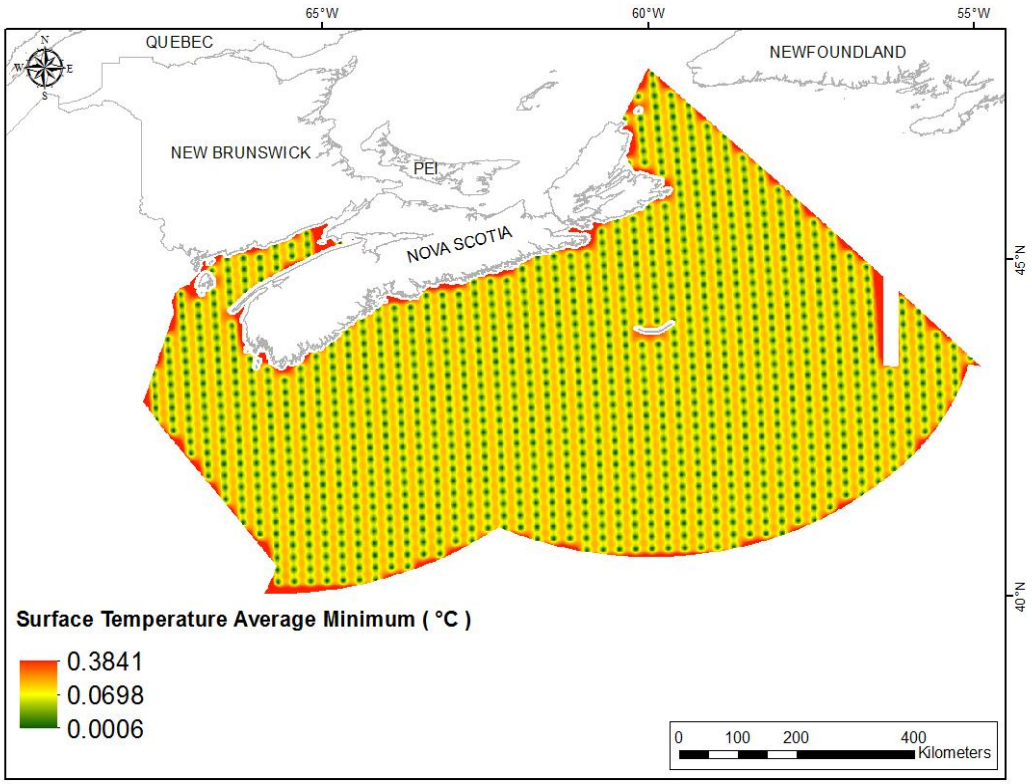

Fig. 64. Prediction standard error surface of Surface Temperature Average Minimum (˚C).

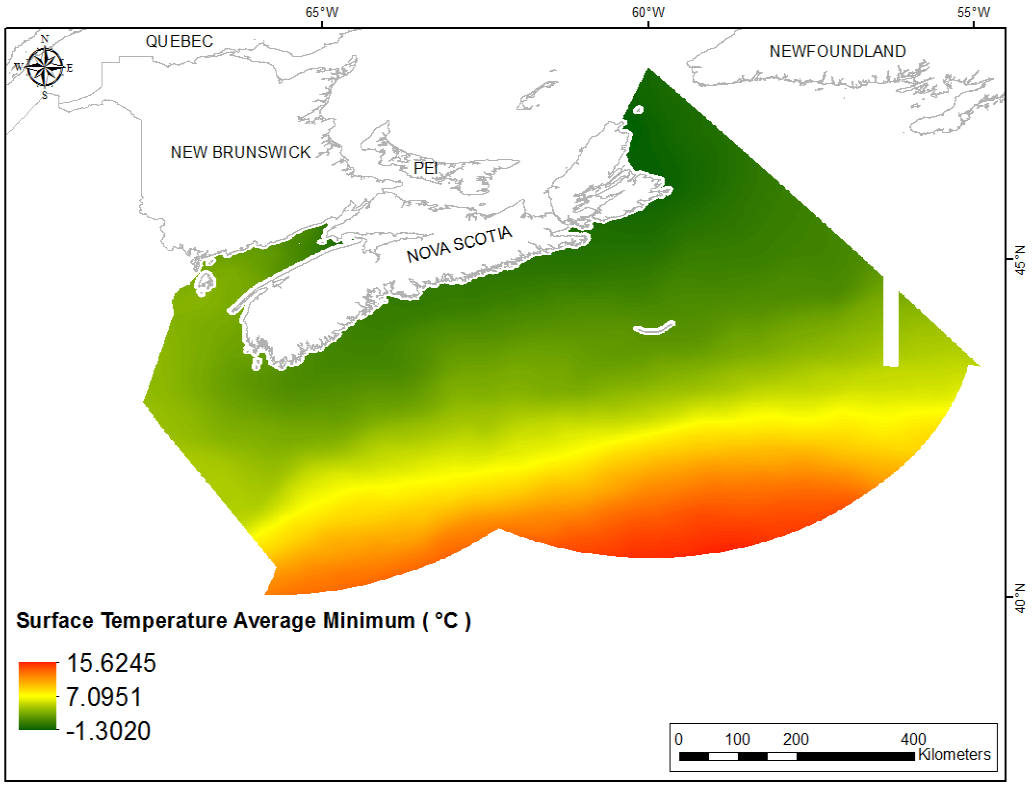

Fig. 65. Interpolated prediction surface of Surface Temperature Average Minimum (˚C).

Surface Temperature Average Maximum

This variable displayed a platykurtic, right-skewed distribution prior to interpolation (Table 27, Fig. 66). The data showed deviations from a standard normal distribution with the lower tail and the upper mid-range values being higher than predicted and the upper tail and mid-values being lower than predicted by a normal distribution (Fig. 67). These data points were spatially cohesive with specific areas of over-and under-prediction (Fig. 67).

The semivariogram showed weak autocorrelation present in the data but excellent predictive fit (Fig. 68). The model showed good cross-validation statistics (Table 28) indicating that it was good at prediction. The error map showed high error along the edges of the study extent (Fig. 69). The kriged surface is presented in Fig. 70.

Table 27. Distributional properties of Surface Temperature Average Maximum (°C).

Property	Value
Number of Observations	1160
Minimum	12.602
Maximum	25.660
Mean	19.678
Median	18.887
Standard Deviation	2.855
Skewness	0.312
Kurtosis	2.230

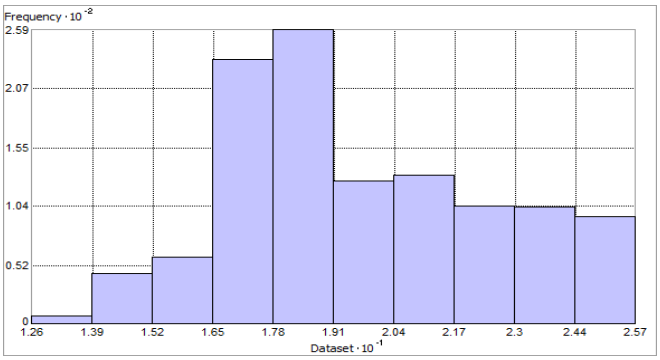

Fig. 66. Distribution of Surface Temperature Average Maximum (°C). Histogram was illustrated using 10 bins. X axis is shown at 10^{-1}; Y axis is shown at 10^{-2}.

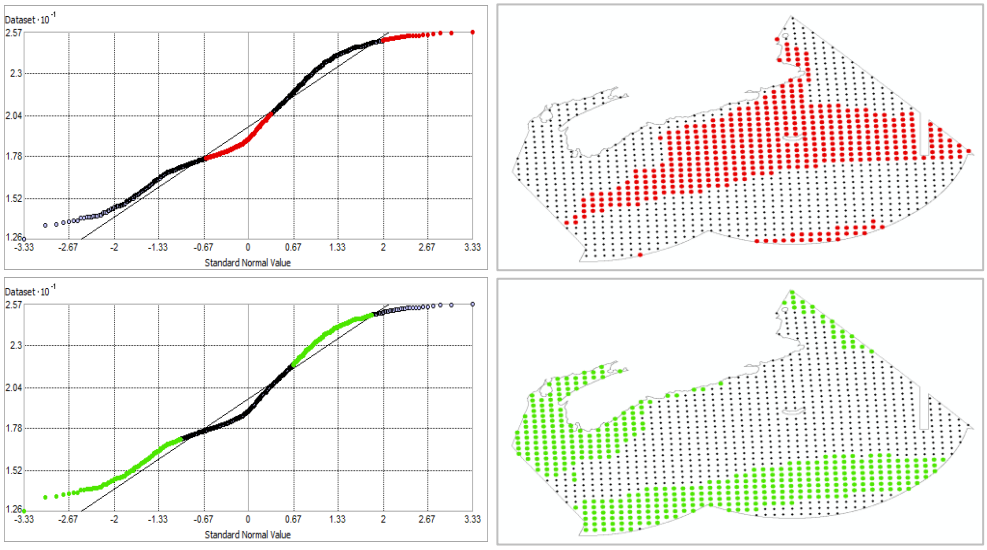

Fig 67. Normal Q-Q plot for data values of Surface Temperature Average Maximum (°C). Points falling under (upper panel) and over (bottom panel) the reference line are mapped.

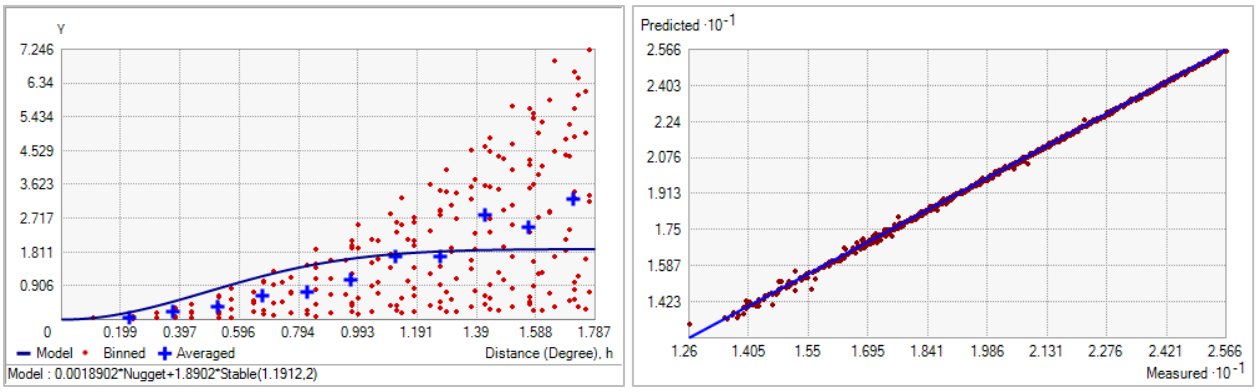

Fig. 68. Left panel: Semivariogram of Surface Temperature Average Maximum (°C). Binned values are shown as red dots; average points are shown as blue crosses; the model fit to the averaged values is shown as a blue line. Lag size: 0.149 degrees; number of lags: 12; Parameter: 2; Range: 1.191 degrees; Partial Sill: 1.890. Right panel: Scatterplot of predicted values versus observed values for the model of Surface Temperature Average Maximum (°C).

Table 28. Results of cross-validation of the kriged model for Surface Temperature Average Maximum (°C).

Prediction error	**Value**
Number of Observations	1160
Overall Mean Error	-8.547×10^{-4}
Root Mean Square Prediction Error	0.067
Standardized Mean	-6.215×10^{-3}
Standardized Root Mean Square Prediction Error	0.864
Average Standard Error	0.076

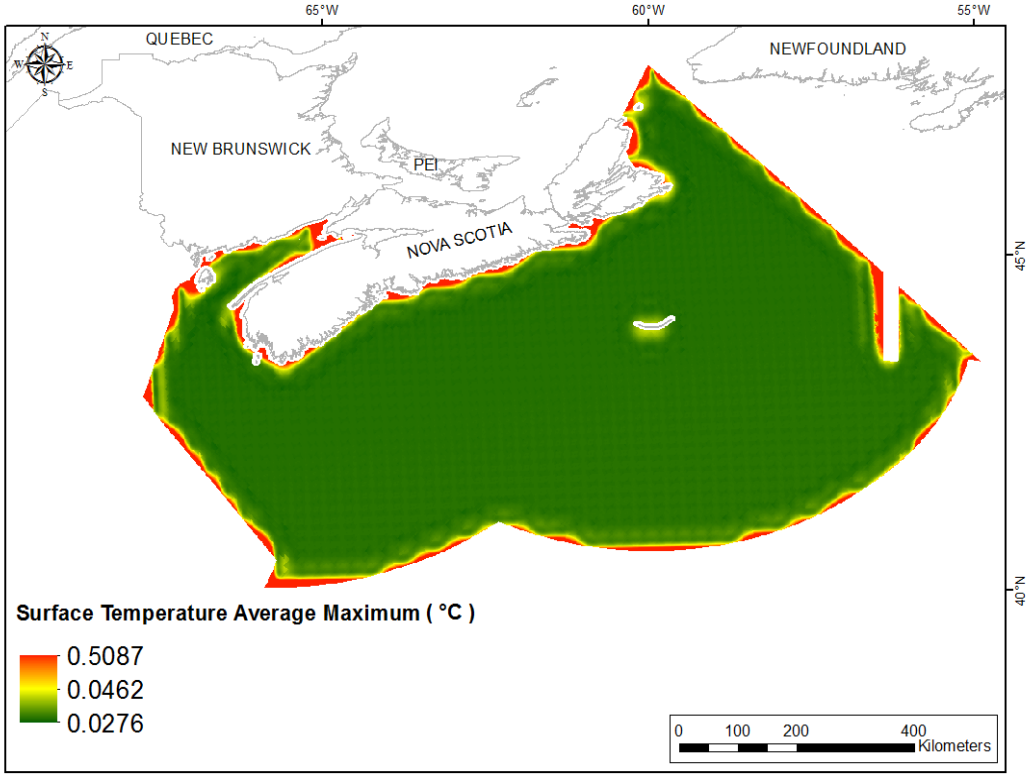

Fig. 69. Prediction standard error surface of Surface Temperature Average Maximum (˚C).

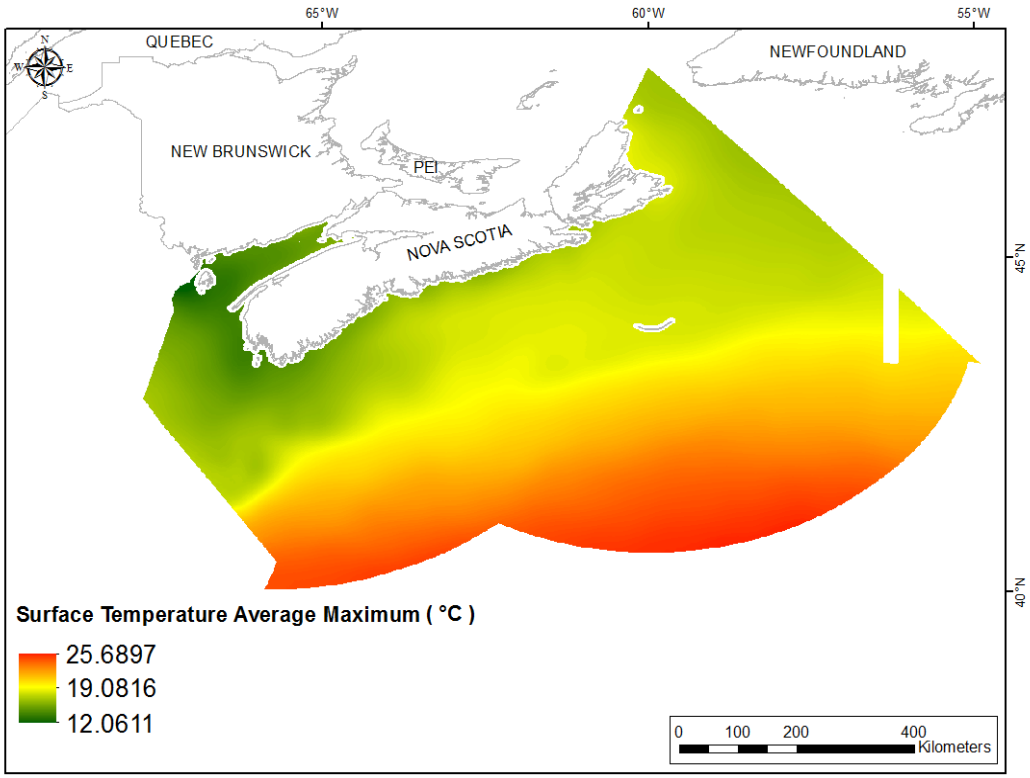

Fig. 70. Interpolated prediction surface of Surface Temperature Average Maximum (˚C).

Surface Temperature Average Range

This variable displayed platykurtic, left-skewed distribution prior to interpolation (Table 29, Fig. 71). The data were greater than predicted by a standard normal distribution at mid-range and lowest values, and lower than predicted at lower mid-range and the highest values (Fig. 72). These areas of under- and over-prediction showed little spatial pattern over the region (Fig. 72).

The semivariogram showed weak autocorrelation present in the data and a poor fit between measured and predicted values (Fig. 73). However, the model showed good cross-validation statistics (Table 30). The error map showed high error along the edges of the study extent (Fig. 74). The kriged surface is presented in Fig. 75.

Table 29. Distributional properties of Surface Temperature Average Range (°C).

Property	Value
Number of Observations	1160
Minimum	0.801
Maximum	23.915
Mean	14.790
Median	15.795
Standard Deviation	5.231
Skewness	-0.623
Kurtosis	2.697

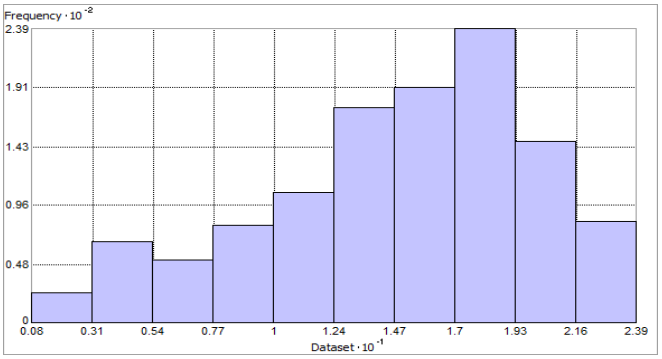

Fig. 71. Distribution of Surface Temperature Average Range (°C). Histogram was illustrated using 10 bins. X axis is shown at 10^{-1}; Y axis is shown at 10^{-2}.

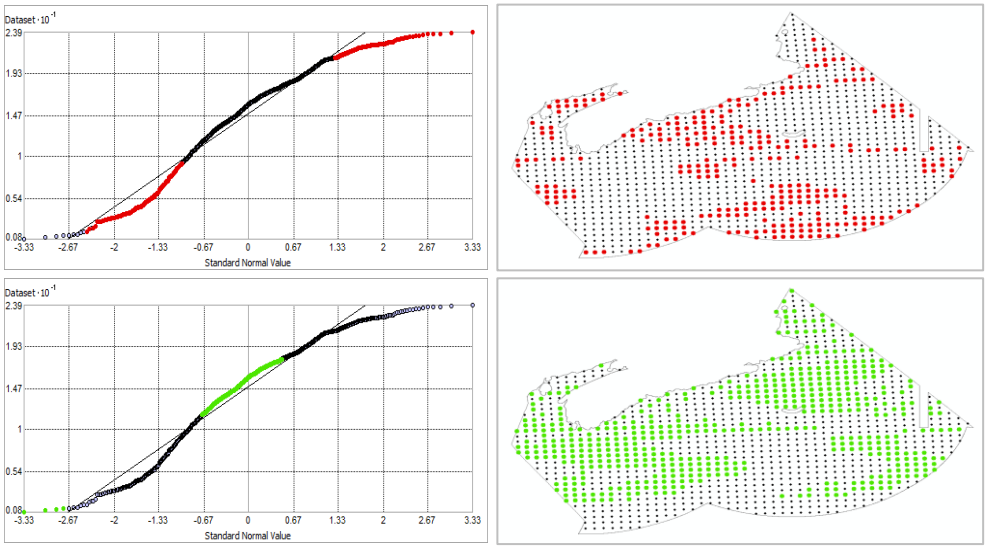

Fig. 72. Normal Q-Q plot for data values of Surface Temperature Average Range (°C). Points falling under (upper panel) and over (bottom panel) the reference line are mapped.

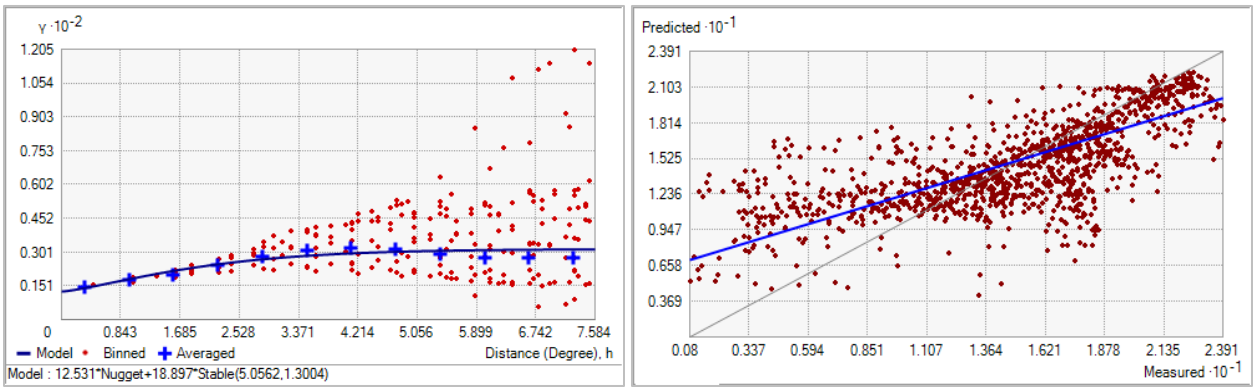

Fig. 73. Left panel: Semivariogram of Surface Temperature Average Range (°C). Binned values are shown as red dots; average points are shown as blue crosses; the model fit to the averaged values is shown as a blue line. Lag size: 0.632 degrees; number of lags: 12; Parameter: 1.300; Range: 5.056 degrees; Partial Sill: 18.897. Right panel: Scatterplot of predicted values versus observed values for the model of Surface Temperature Average Range (°C).

Table 30. Results of cross-validation of the kriged model for Surface Temperature Average Range (°C).

Prediction error	**Value**
Number of Observations	1160
Overall Mean Error	-2.792×10^{-3}
Root Mean Square Prediction Error	3.717
Standardized Mean	-3.349×10^{-4}
Standardized Root Mean Square Prediction Error	0.984
Average Standard Error	3.777

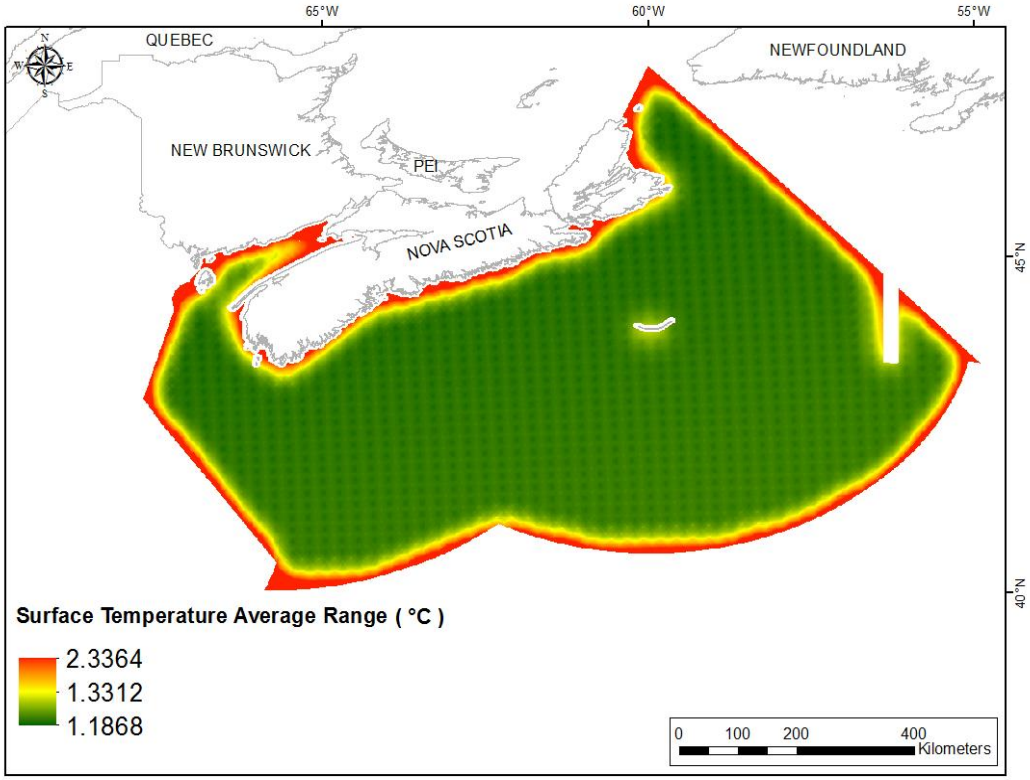

Fig. 74. Prediction standard error surface of Surface Temperature Average Range (˚C).

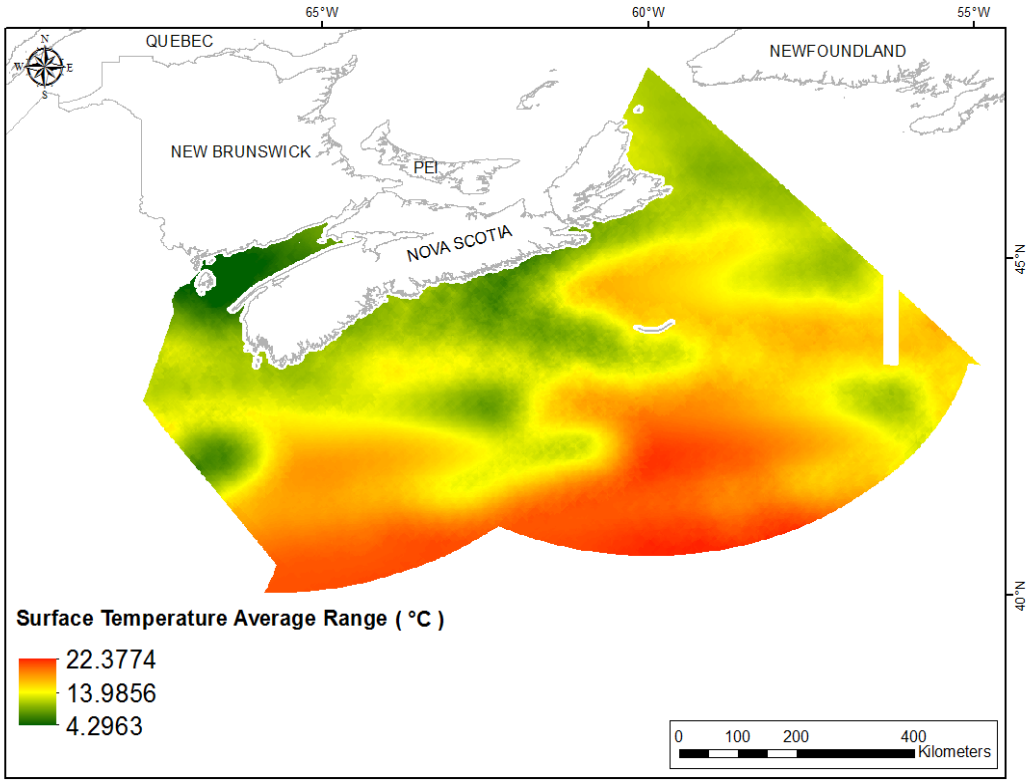

Fig. 75. Interpolated prediction surface of Surface Temperature Average Range (˚C).

Salinity

Salinity influences osmoregulation (control of osmosis and diffusion) and is a very important determinant of species distribution. Salinity also strongly influences the rate at which inorganic particles settle in response to changes in flocculation of the clay mineral kaolinite (Sutherland et. al., 2014). This is particularly important in estuaries and deltas where clay minerals mix with marine waters. Salinity and temperature together are diagnostics of water masses which maintain characteristic T/S signatures.

Bottom Salinity Mean

This variable displayed a left-skewed, leptokurtic distribution with outlying data in the lower range prior to interpolation (Table 31, Fig. 76). The data deviated from a standard normal distribution with lower and upper values falling under the reference line (Fig. 77), and mid-values falling over the reference line. These data points were spatially cohesive across the region (Fig. 77).

The semivariogram showed very weak autocorrelation present in the data. Aside from a few outliers there was a good fit between measured and predicted values (Fig. 78). The kriged model showed good cross-validation statistics (Table 32). The error map showed high error along the edges of the study extent (Fig. 79). The kriged surface is presented in Fig. 80.

Table 31. Distributional properties of Bottom Salinity Mean.

Property	Value
Number of Observations	1160
Minimum	27.415
Maximum	35.234
Mean	34.300
Median	34.892
Standard Deviation	0.941
Skewness	-1.524
Kurtosis	5.653

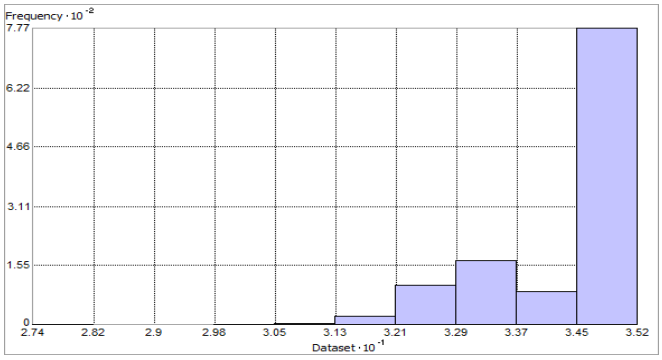

Fig. 76. Distribution of Bottom Salinity Mean. Histogram was illustrated using 10 bins. X axis shown at 10^{-1}; Y axis is shown at 10^{-2}.

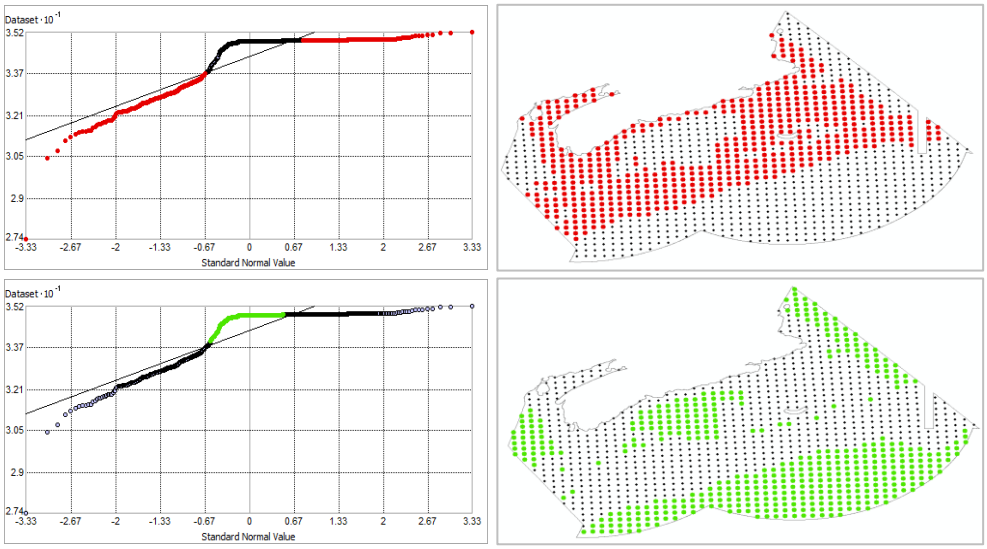

Fig. 77. Normal Q-Q plot for data values of Bottom Salinity Mean. Points falling under (upper panel) and over (bottom panel) the reference line are mapped.

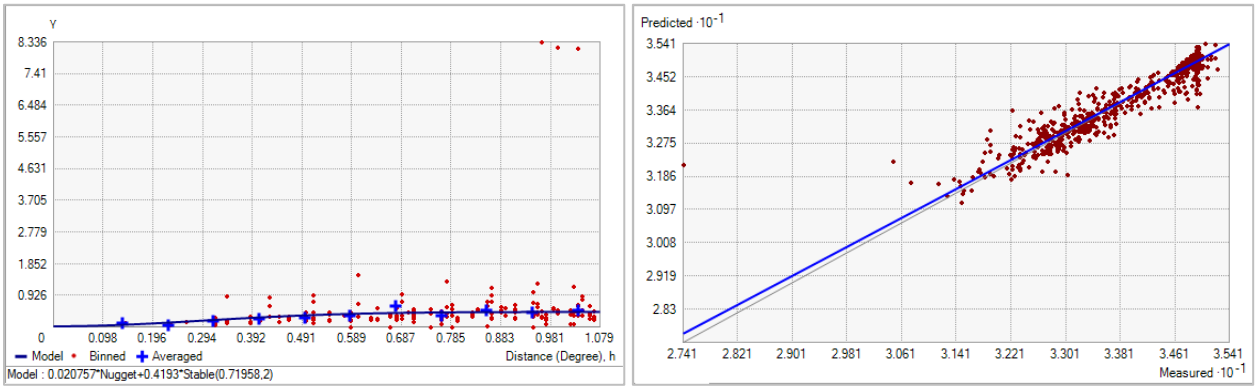

Fig. 78. Left panel: Semivariogram of Bottom Salinity Mean. Binned values are shown as red dots; average points are shown as blue crosses; the model fit to the averaged values is shown as a blue line. Lag size: 0.090 degrees; number of lags: 12; Parameter: 2; Range: 0.720 degrees; Partial Sill: 0.419. Right panel: Scatterplot of predicted values versus observed values for the model of Bottom Salinity Mean.

Table 32. Results of cross-validation of the kriged model for Bottom Salinity Mean.

Prediction error	**Value**
Number of Observations	1160
Overall Mean Error	9.528×10^{-3}
Root Mean Square Prediction Error	0.267
Standardized Mean	0.018
Standardized Root Mean Square Prediction Error	1.088
Average Standard Error	0.211

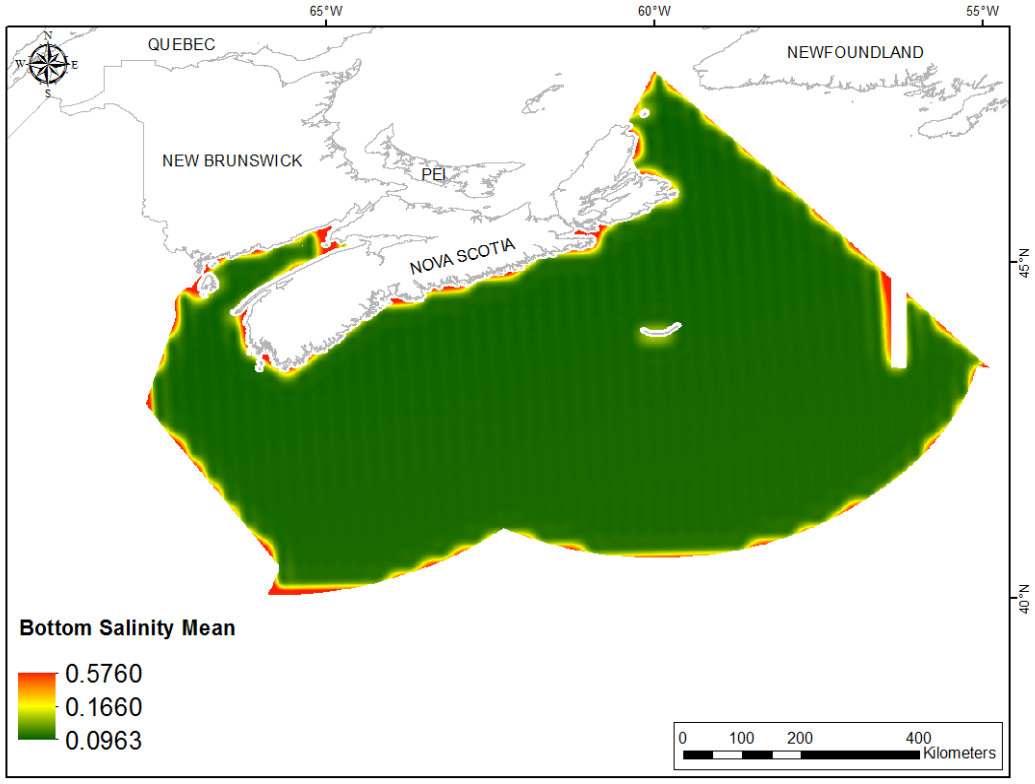

Fig. 79. Prediction standard error surface of Bottom Salinity Mean.

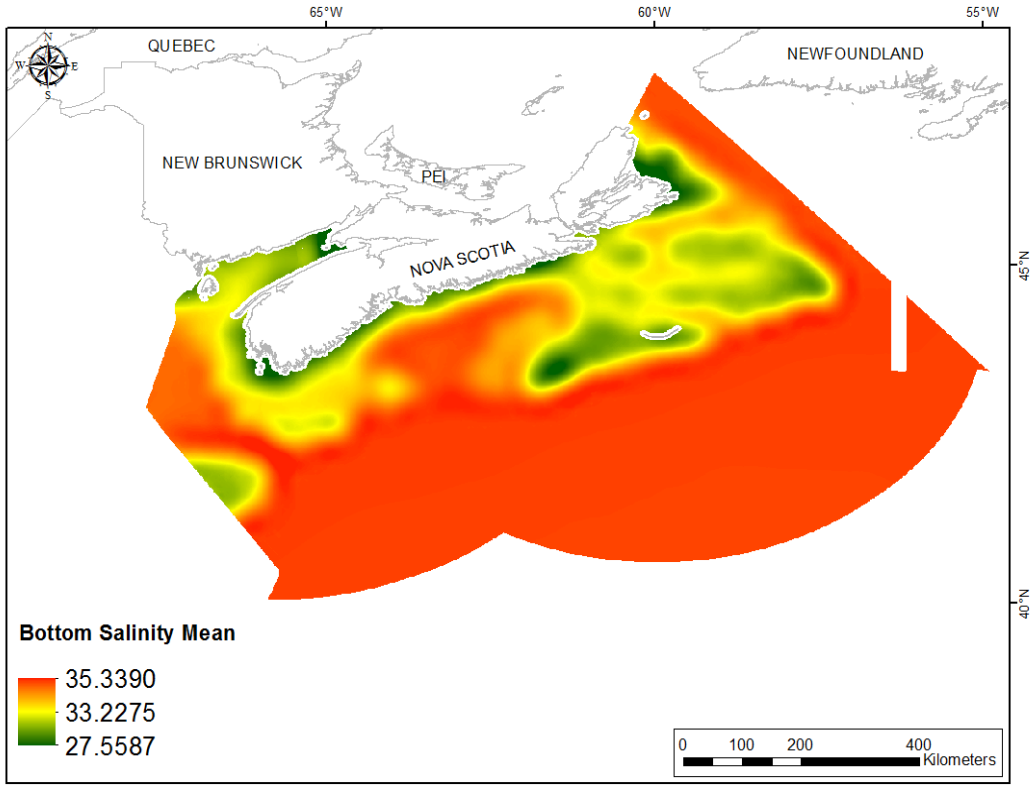

Fig. 80. Interpolated prediction surface of Bottom Salinity Mean.

Bottom Salinity Minimum

This variable displayed a left-skewed, leptokurtic distribution with outlying data in the lower range prior to interpolation (Table 33, Fig. 81). The data were lower than predicted by a normal distribution at low and high values (Fig. 82). Mid-range values were higher than the reference line. These data points showed some spatial cohesion across the region (Fig. 82).

The semivariogram showed very weak autocorrelation present in the data (Figure 83). Aside from a few outliers there was a good fit between measured and predicted values (Fig. 83). The kriged model showed good cross-validation statistics (Table 34). The error map showed high error along the edges of the study extent (Fig. 84). The kriged surface is presented in Fig. 85.

Table 33. Distributional properties of Bottom Salinity Minimum.

Property	Value
Number of Observations	1160
Minimum	24.897
Maximum	34.908
Mean	33.843
Median	34.836
Standard Deviation	1.398
Skewness	-1.270
Kurtosis	4.361

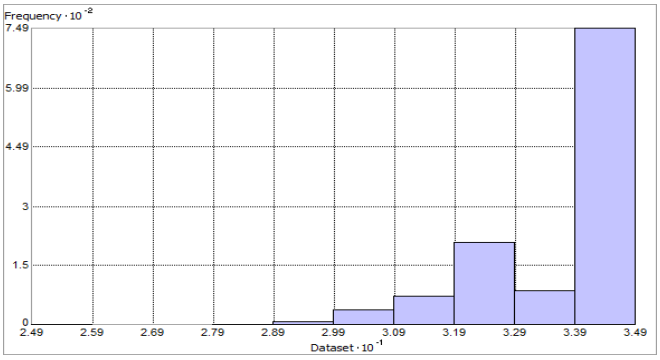

Fig. 81. Distribution of Bottom Salinity Minimum. Histogram was illustrated using 10 bins. X axis shown at 10^{-1}; Y axis is shown at 10^{-2}.

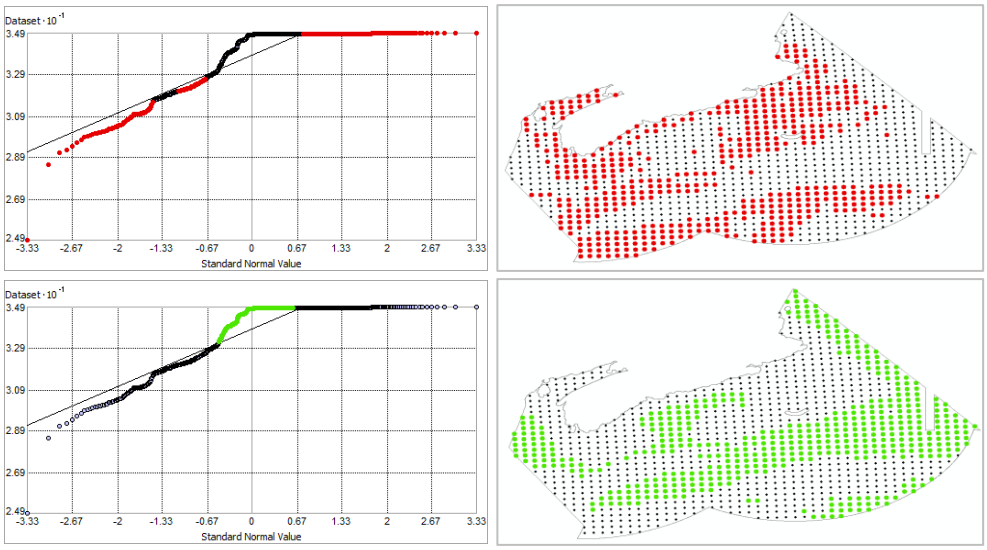

Fig. 82. Normal Q-Q plot for data values of Bottom Salinity Minimum. Points falling under (upper panel) and over (bottom panel) the reference line are mapped.

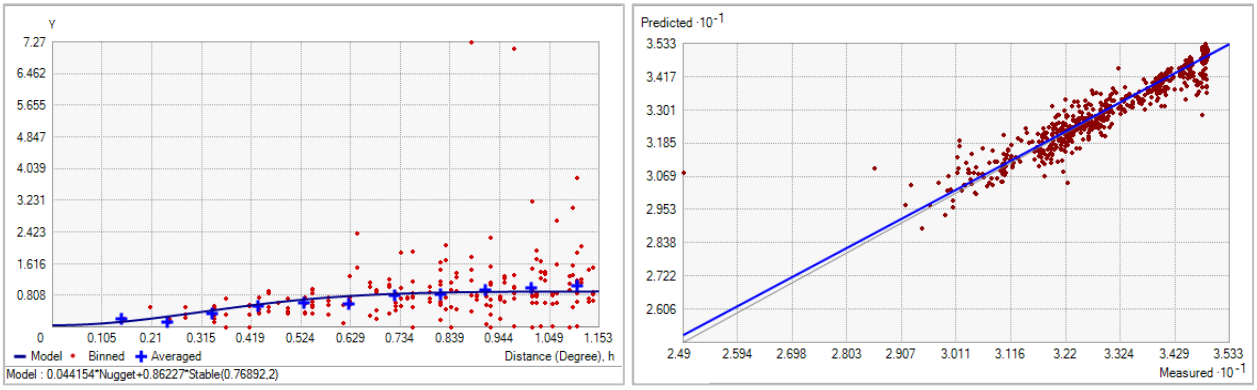

Fig. 83. Left panel: Semivariogram of Bottom Salinity Minimum. Binned values are shown as red dots; average points are shown as blue crosses; the model fit to the averaged values is shown as a blue line. Lag size: 0.096 degrees; number of lags: 12; Parameter: 2; Range: 0.769 degrees; Partial Sill: 0.862. Right panel: Scatterplot of predicted values versus observed values for the model of Bottom Salinity Minimum.

Table 34. Results of cross-validation of the kriged model for Bottom Salinity Minimum.

Prediction error	**Value**
Number of Observations	1160
Overall Mean Error	9.915×10^{-3}
Root Mean Square Prediction Error	0.359
Standardized Mean	0.013
Standardized Root Mean Square Prediction Error	1.079
Average Standard Error	0.294

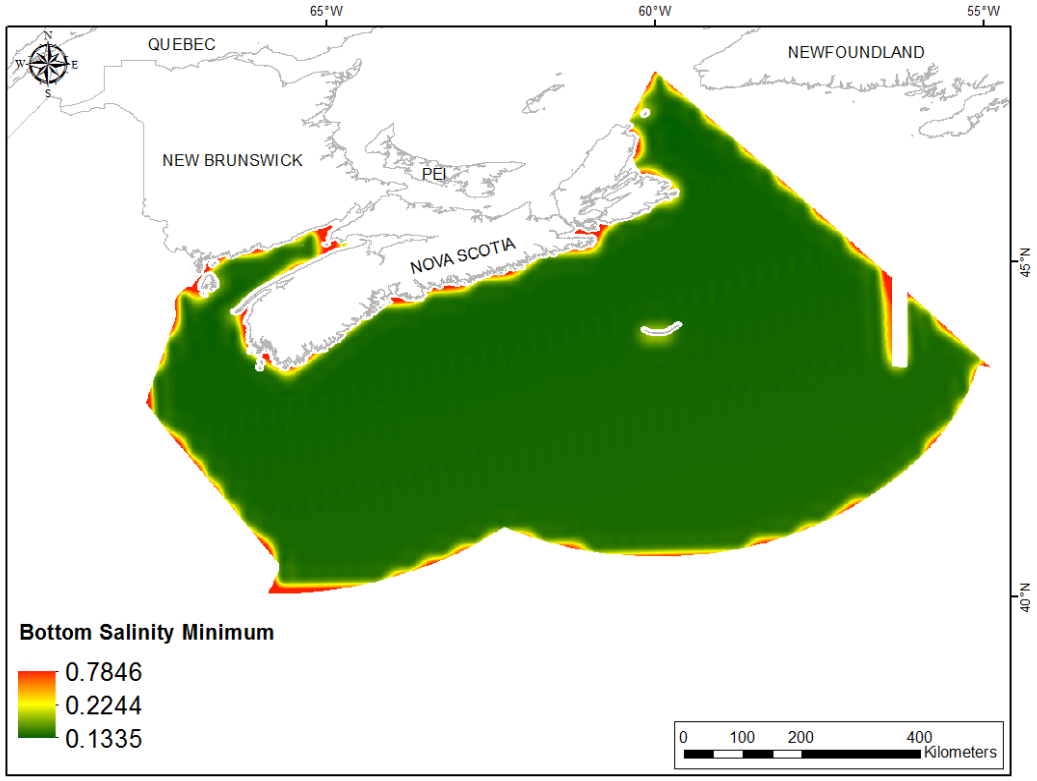

Fig. 84. Prediction standard error surface of Bottom Salinity Minimum.

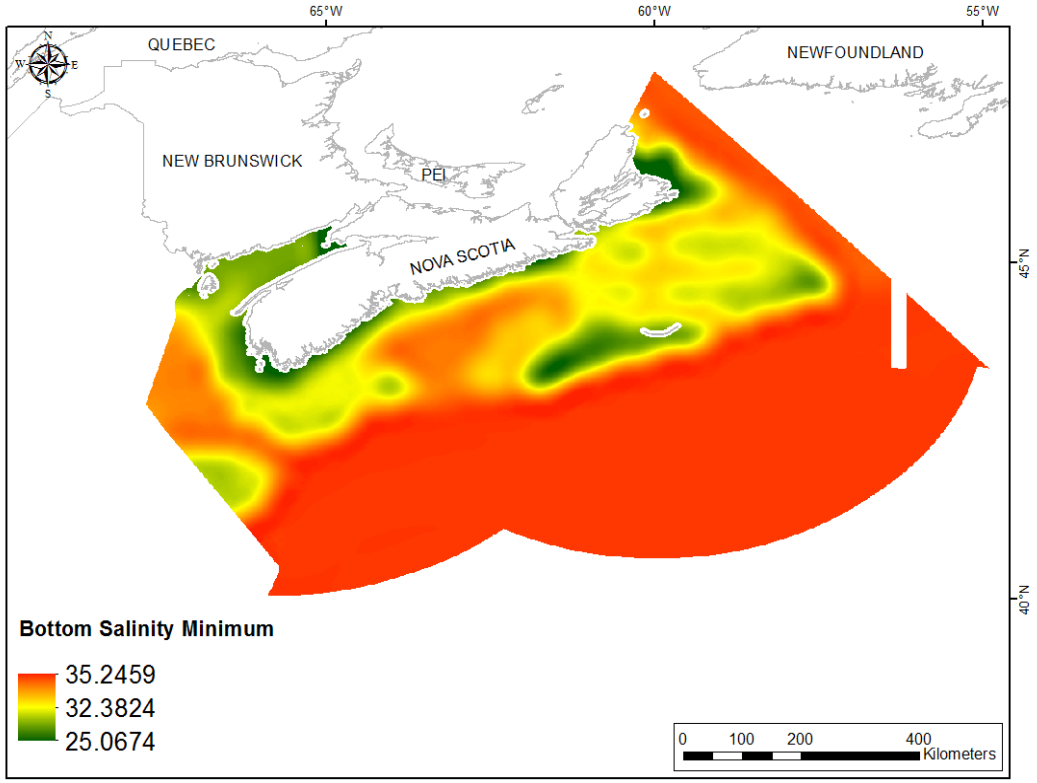

Fig. 85. Interpolated prediction surface of Bottom Salinity Minimum.

Bottom Salinity Maximum

This variable displayed a left-skewed, leptokurtic distribution with outlying data in the lower range prior to interpolation (Table 35, Fig. 86). The data were lower than predicted by a normal distribution at both tails (Fig. 87). Mid-range values were higher than the reference line. The areas of over- and under-prediction showed a spatial pattern through the study extent with points over the reference line located primarily in the deep water beyond the shelf (Fig. 87).

The semivariogram showed weak autocorrelation present in the data (Fig. 88). Aside from a single outlier there was a good fit between measured and predicted values (Fig. 88). The kriged model showed excellent cross-validation statistics (Table 36). The error map showed high error along the edges of the study extent (Fig. 89). The kriged surface is presented in Fig. 90.

Table 35. Distributional properties of Bottom Salinity Maximum.

Property	Value
Number of Observations	1160
Minimum	30.790
Maximum	36.305
Mean	34.750
Median	34.916
Standard Deviation	0.655
Skewness	-1.326
Kurtosis	5.410

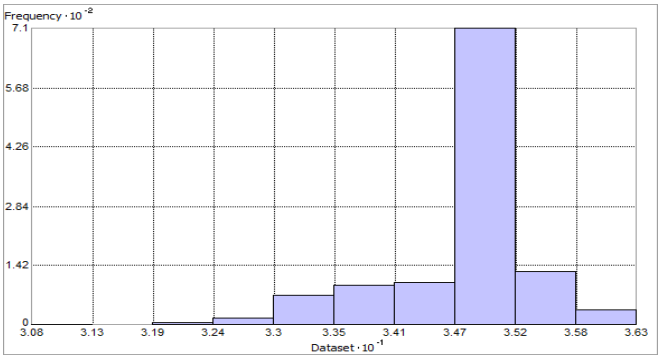

Fig. 86. Distribution of Bottom Salinity Maximum. Histogram was illustrated using 10 bins. X axis shown at 10^{-1}; Y axis is shown at 10^{-2}.

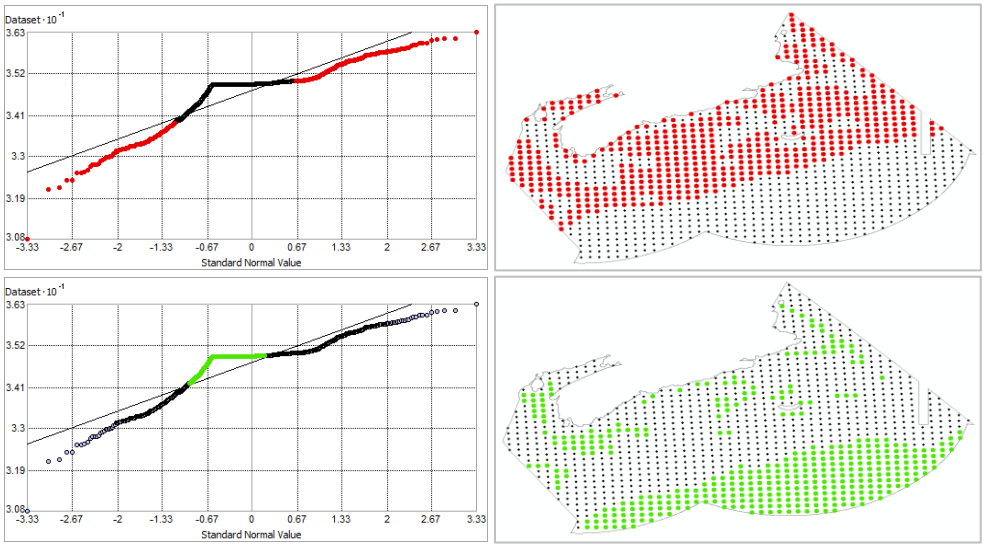

Fig. 87. Normal Q-Q plot for data values of Bottom Salinity Maximum. Points falling under (upper panel) and over (bottom panel) the reference line are mapped.

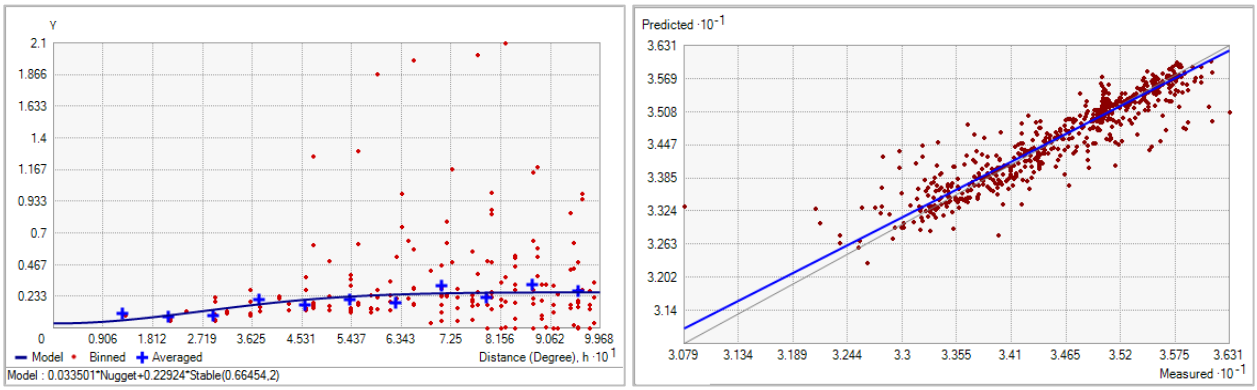

Fig. 88. Left panel: Semivariogram of Bottom Salinity Maximum. Binned values are shown as red dots; average points are shown as blue crosses; the model fit to the averaged values is shown as a blue line. Lag size: 0.083 degrees; number of lags: 12; Parameter: 2; Range: 0.665 degrees; Partial Sill: 0.229. Right panel: Scatterplot of predicted values versus observed values for the model of Bottom Salinity Maximum.

Table 36. Results of cross-validation of the kriged model for Bottom Salinity Maximum.

Prediction error	**Value**
Number of Observations	1160
Overall Mean Error	6.814×10^{-3}
Root Mean Square Prediction Error	0.254
Standardized Mean	0.013
Standardized Root Mean Square Prediction Error	0.980
Average Standard Error	0.248

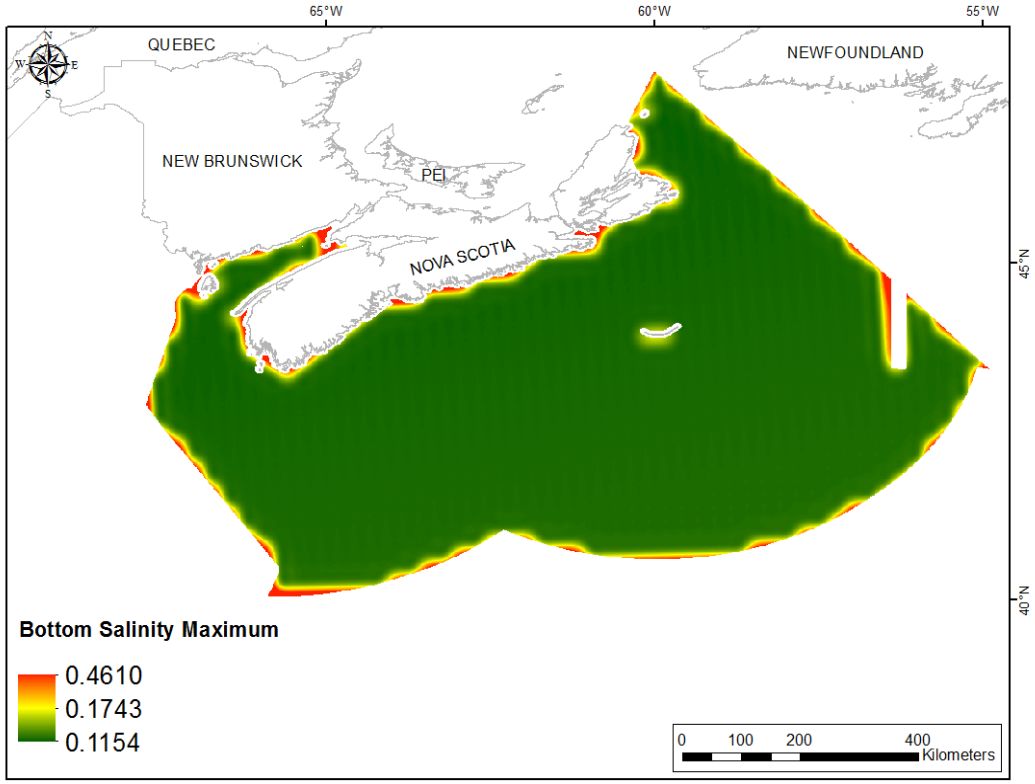

Fig. 89. Prediction standard error surface of Bottom Salinity Maximum.

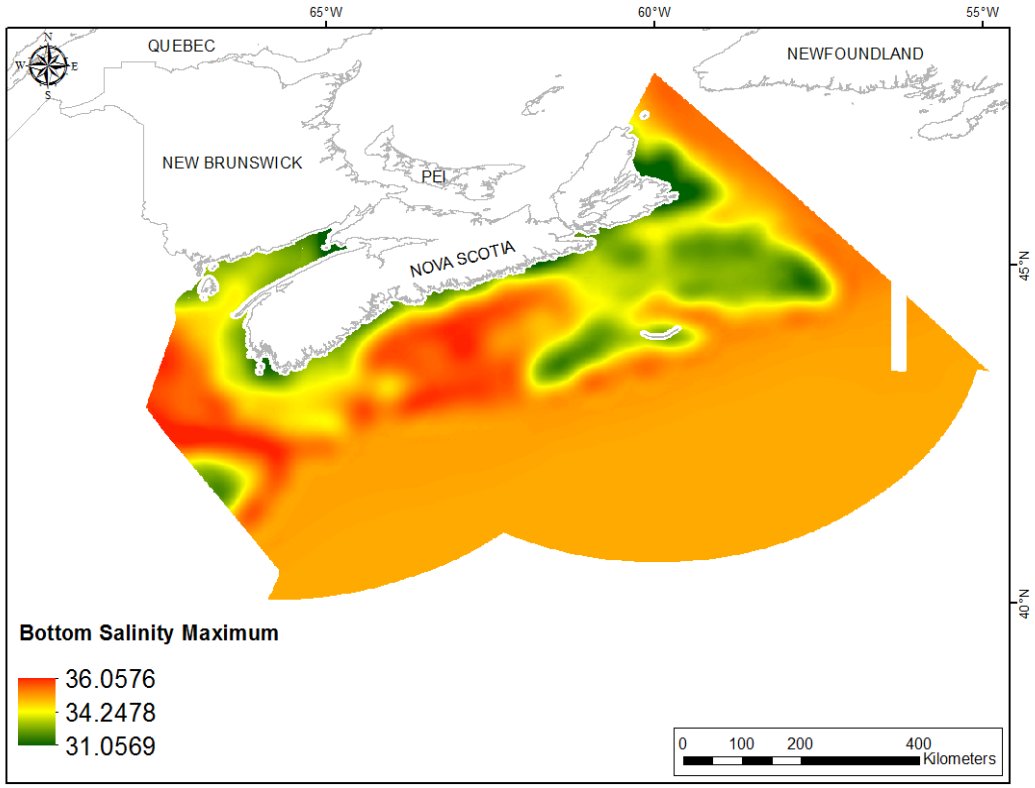

Fig. 90. Interpolated prediction surface of Bottom Salinity Maximum.

Bottom Salinity Range

This variable displayed a right-skewed, leptokurtic distribution with outlying data in the upper range (Table 37, Fig. 91). The data were higher than predicted by a normal distribution at low and upper mid-range values and lower than predicted at mid-range and high values (Fig. 92). Values under and over the reference line showed a spatial pattern in the region (Fig. 92).

The semivariogram showed moderate autocorrelation present in the data (Fig. 93). Aside from a single outlier there was a fair fit between measured and predicted values (Fig. 93). The kriged model showed good cross-validation statistics (Table 38). The error map showed high error along the edges of the study extent (Fig. 94). The kriged surface is presented in Fig. 95. Negative values resulted from the right-skewed nature of the raw data (Fig. 91). Of the 326,283 raster cells in the study extent, 4,032 contained negative values (see Table A1). These were located in a long band along the lower slope (Fig. A3).

Table 37. Distributional properties of Bottom Salinity Range.

Property	Value
Number of Observations	1160
Minimum	0.024
Maximum	5.893
Mean	0.907
Median	0.178
Standard Deviation	1.014
Skewness	0.802
Kurtosis	2.514

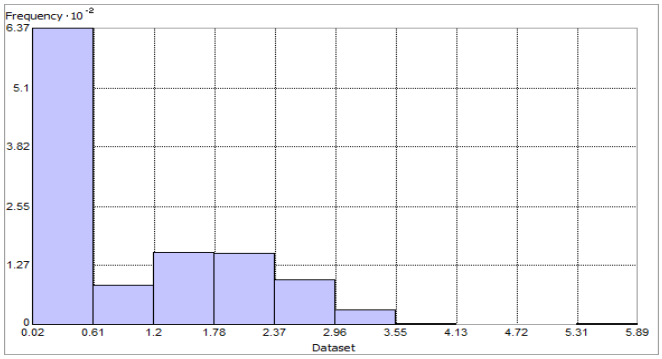

Fig. 91. Distribution of Bottom Salinity Range. Histogram was illustrated using 10 bins. Y axis is shown at 10^{-2}.

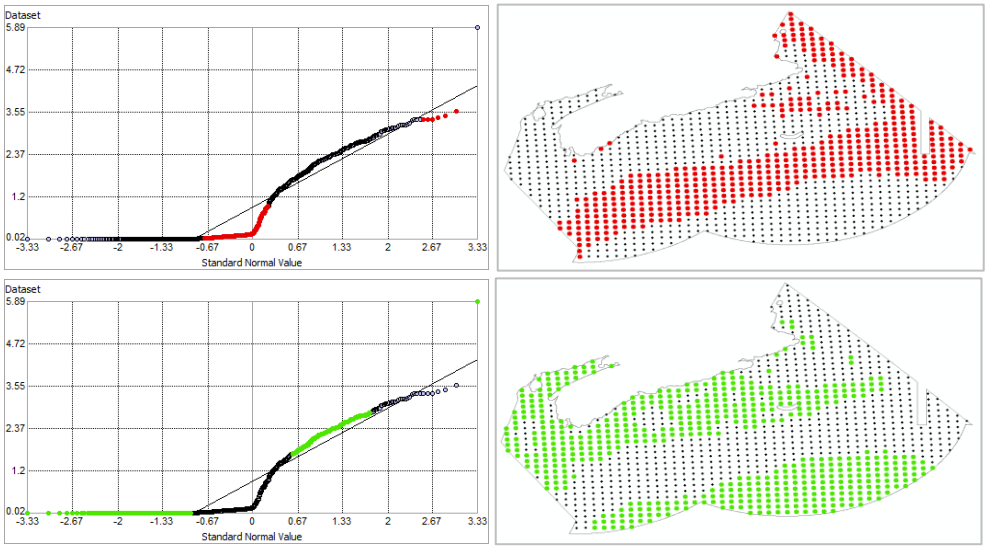

Fig. 92. Normal Q-Q plot for data values of Bottom Salinity Range. Points falling under (upper panel) and over (bottom panel) the reference line are mapped.

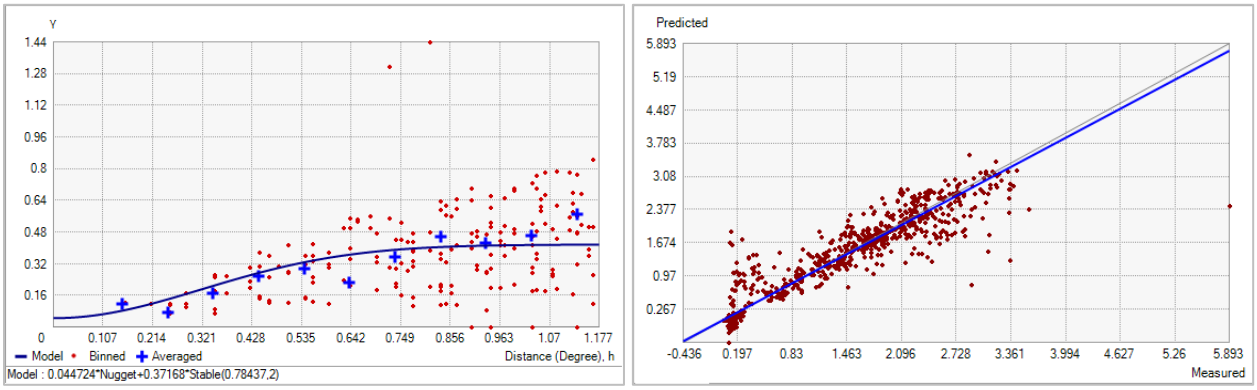

Fig. 93. Left panel: Semivariogram of Bottom Salinity Range. Binned values are shown as red dots; average points are shown as blue crosses; the model fit to the averaged values is shown as a blue line. Lag size: 0.098 degrees; number of lags: 12; Parameter: 2; Range: 0.784 degrees; Partial Sill: 0.372. Right panel: Scatterplot of predicted values versus observed values for the model of Bottom Salinity Range.

Table 38. Results of cross-validation of the kriged model for Bottom Salinity Range.

Prediction error	**Value**
Number of Observations	1160
Overall Mean Error	-3.224×10^{-3}
Root Mean Square Prediction Error	0.306
Standardized Mean	-4.835×10^{-3}
Standardized Root Mean Square Prediction Error	1.089
Average Standard Error	0.270

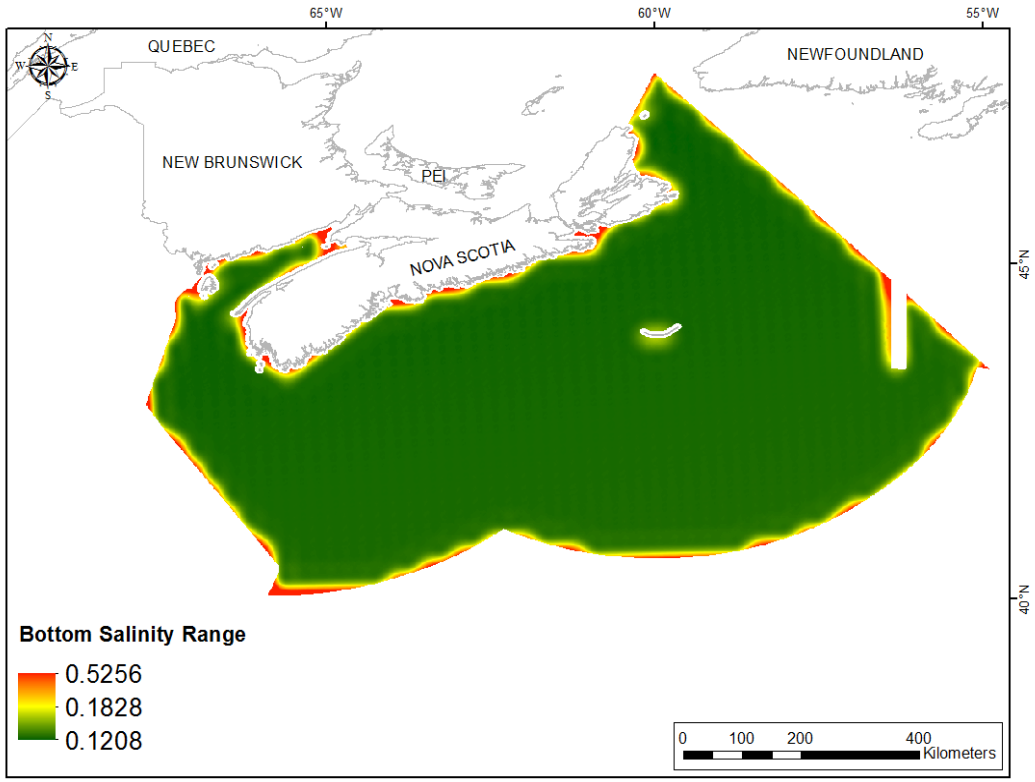

Fig. 94. Prediction standard error surface of Bottom Salinity Range.

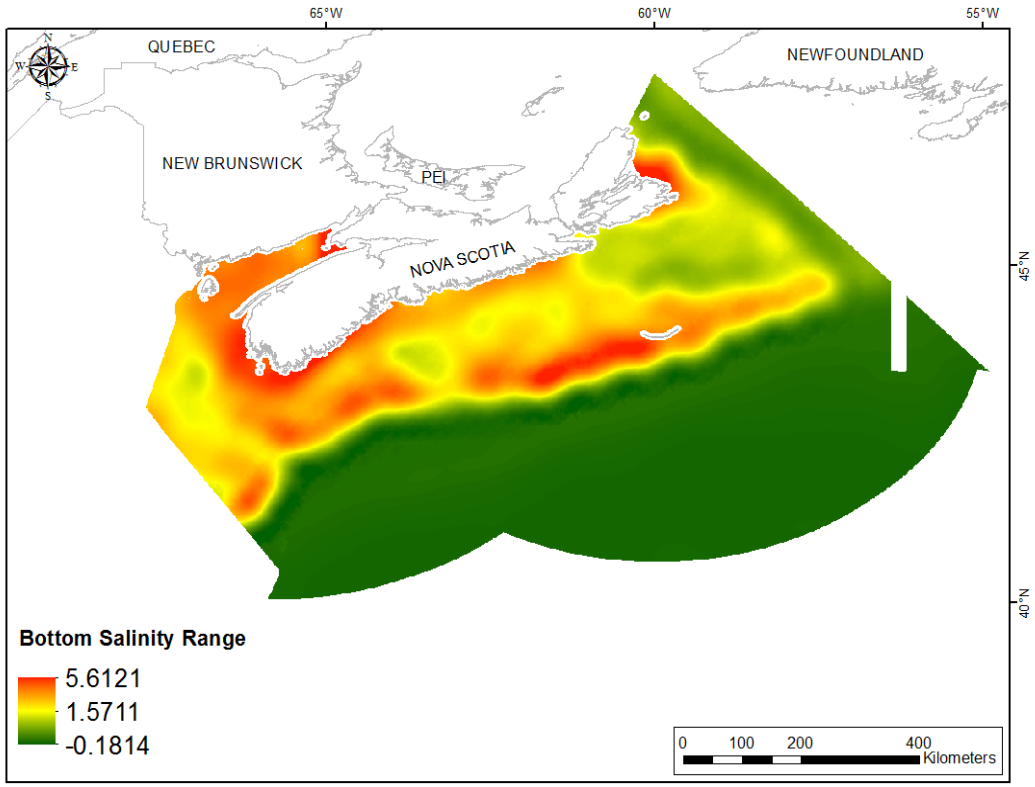

Fig. 95. Interpolated prediction surface of Bottom Salinity Range.

Bottom Salinity Average Minimum

This variable displayed a left-skewed, leptokurtic distribution with outlying data in the lower range prior to interpolation (Table 39, Fig. 96). The data were lower than predicted by a normal distribution at low and high values (Fig. 97). Mid-range values were higher than the reference line. The areas of over- and under-prediction a spatial pattern with over-predicted points located mainly in the deep waters beyond the shelf (Fig. 97).

The semivariogram showed very weak autocorrelation present in the data (Fig. 98). Aside from a single outlier there was a good fit between measured and predicted values (Fig. 98). The kriged model showed good cross-validation statistics (Table 40). The error map showed high error along the edges of the study extent (Fig. 99). The kriged surface is presented in Fig. 100.

Table 39. Distributional properties of Bottom Salinity Average Minimum.

Property	Value
Number of Observations	1160
Minimum	25.542
Maximum	34.946
Mean	34.101
Median	34.887
Standard Deviation	1.162
Skewness	-1.507
Kurtosis	5.867

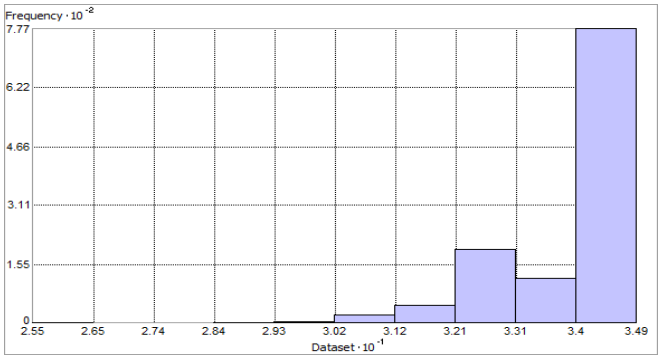

Fig. 96. Distribution of Bottom Salinity Average Minimum. Histogram was illustrated using 10 bins. X axis is shown at 10^{-1}; Y axis is shown at 10^{-2}.

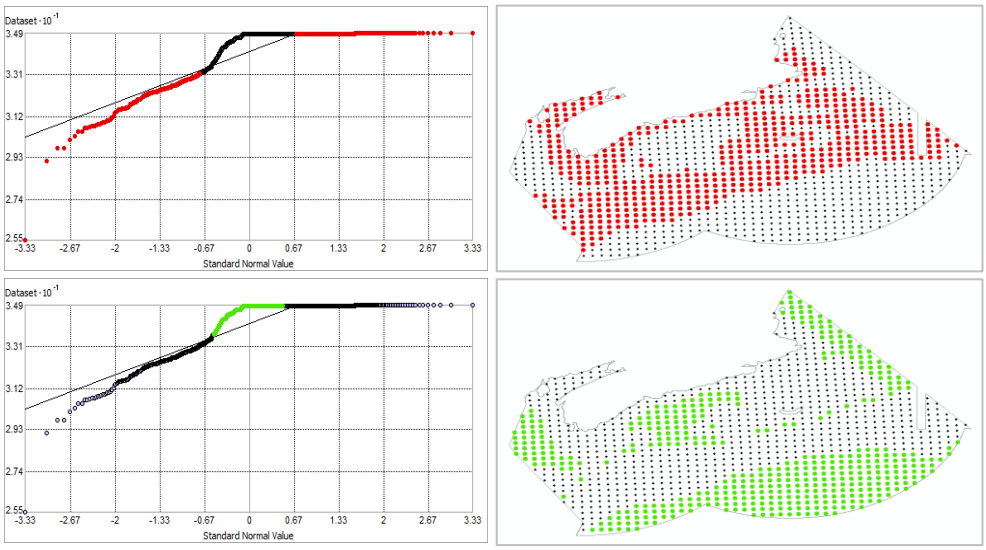

Fig. 97. Normal Q-Q plot for data values of Bottom Salinity Average Minimum (°C). Points falling under (upper panel) and over (bottom panel) the reference line are mapped.

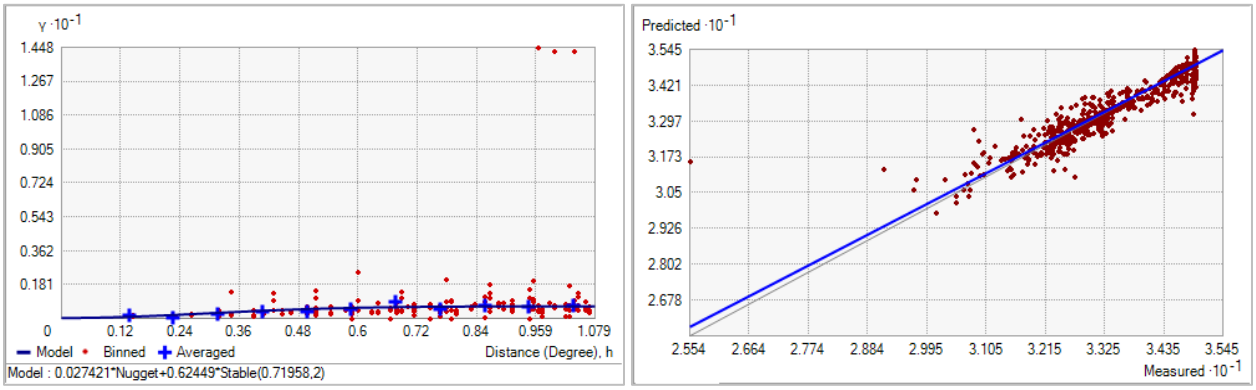

Fig. 98. Left panel: Semivariogram of Bottom Salinity Average Minimum. Binned values are shown as red dots; average points are shown as blue crosses; the model fit to the averaged values is shown as a blue line. Lag size: 0.090 degrees; number of lags: 12; Parameter: 2; Range: 0.720 degrees; Partial Sill: 0.624. Right panel: Scatterplot of predicted values versus observed values for the model of Bottom Salinity Average Minimum.

Table 40. Results of cross-validation of the kriged model for Bottom Salinity Average Minimum.

Prediction error	**Value**
Number of Observations	1160
Overall Mean Error	0.011
Root Mean Square Prediction Error	0.325
Standardized Mean	0.017
Standardized Root Mean Square Prediction Error	1.120
Average Standard Error	0.246

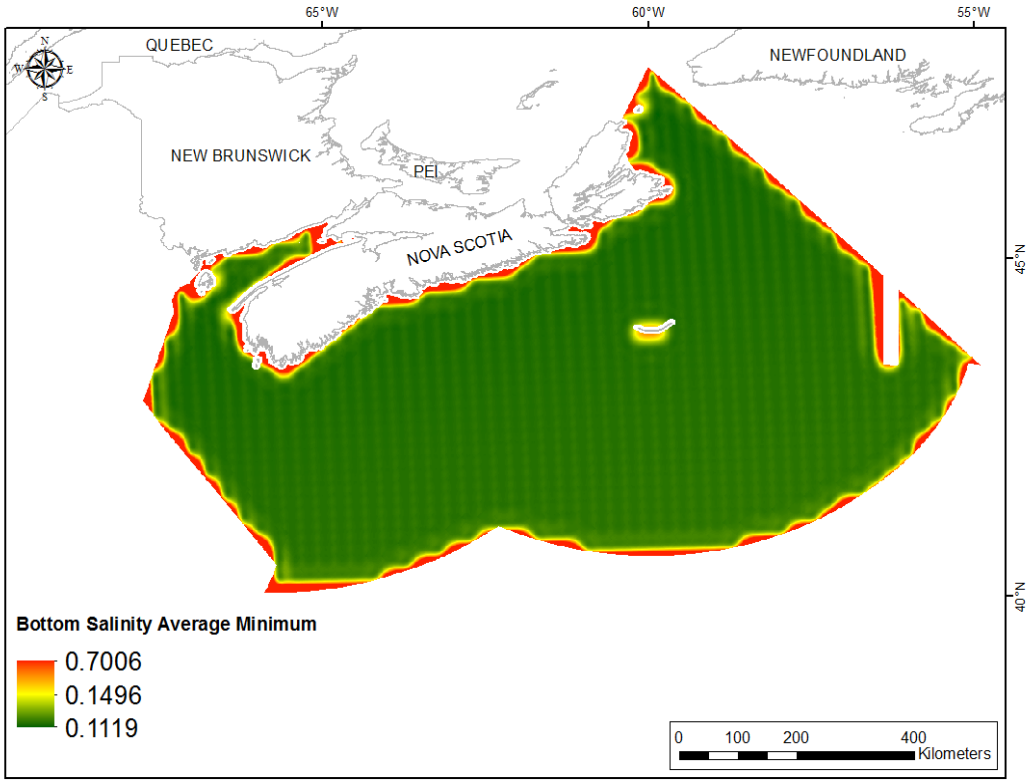

Fig. 99. Prediction standard error surface of Bottom Salinity Average Minimum.

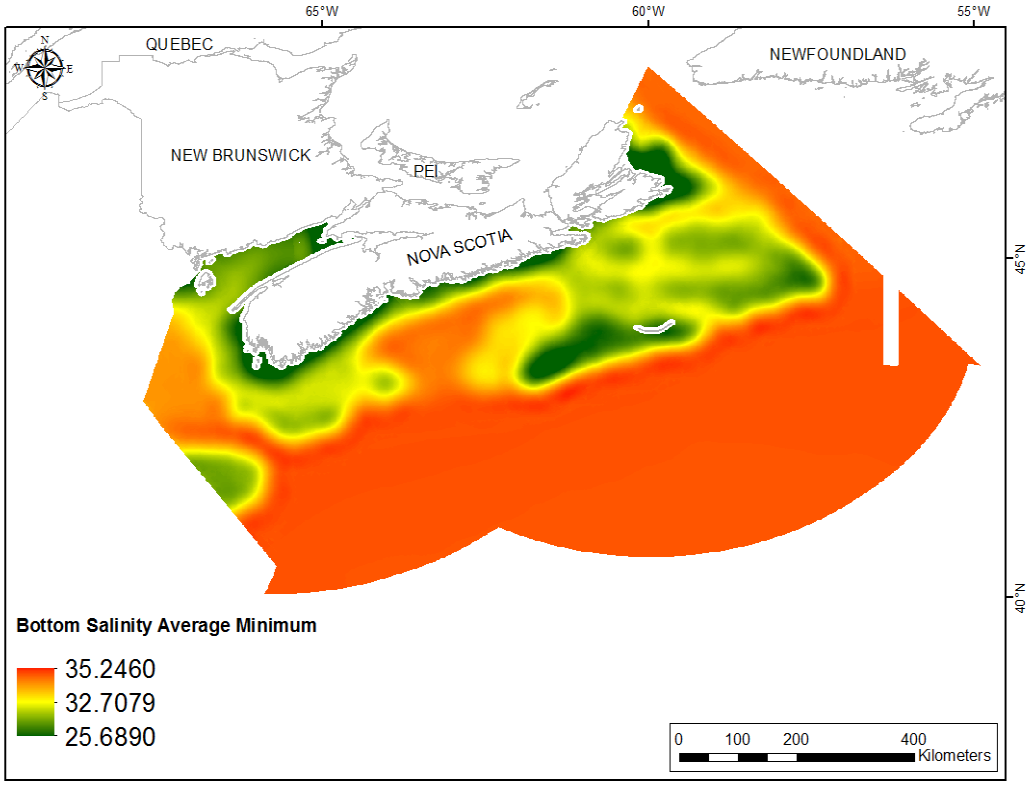

Fig. 100. Interpolated prediction surface of Bottom Salinity Average Minimum.

Bottom Salinity Average Maximum

This variable displayed a left-skewed, leptokurtic distribution with outlying data in the lower range prior to interpolation (Table 41, Fig. 101). The data were lower than predicted by a normal distribution at low and high values (Fig. 102). Mid-range values were higher than the reference line. The areas of over- and under-prediction a spatial pattern with over-predicted points located mainly in the deep waters beyond the shelf (Fig. 102).

The semivariogram showed weak autocorrelation present in the data (Fig. 103). Aside from a single outlier there was a good fit between measured and predicted values (Fig. 103). The kriged model showed good cross-validation statistics (Table 42). The error map showed high error along the edges of the study extent (Fig. 104). The kriged surface is presented in Fig. 105.

Table 41. Distributional properties of Bottom Salinity Average Maximum.

Property	Value
Number of Observations	1160
Minimum	29.382
Maximum	35.948
Mean	34.491
Median	34.899
Standard Deviation	0.762
Skewness	-1.559
Kurtosis	5.222

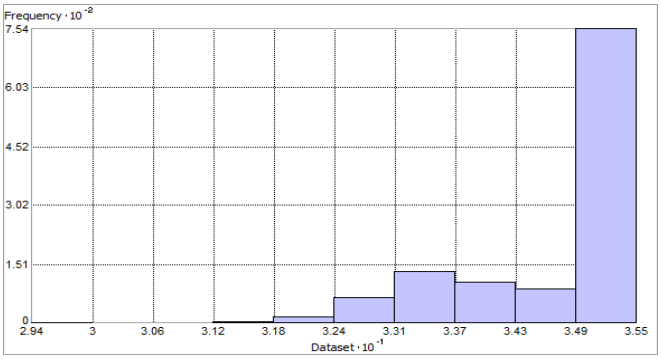

Fig. 101. Distribution of Bottom Salinity Average Maximum. Histogram was illustrated using 10 bins. X axis is shown at 10^{-1}; Y axis is shown at 10^{-2}.

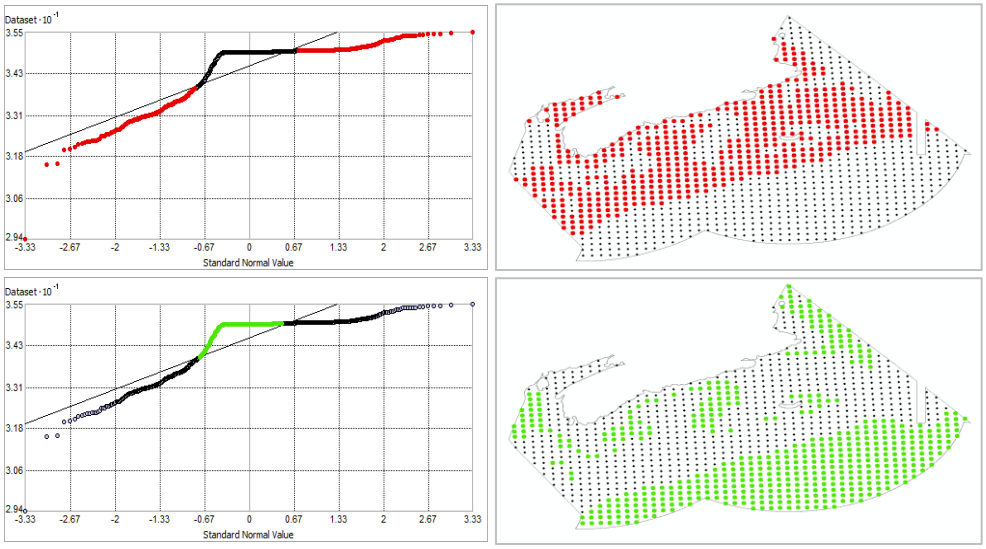

Fig. 102. Normal Q-Q plot for data values of Bottom Salinity Average Maximum. Points falling under (upper panel) and over (bottom panel) the reference line are mapped.

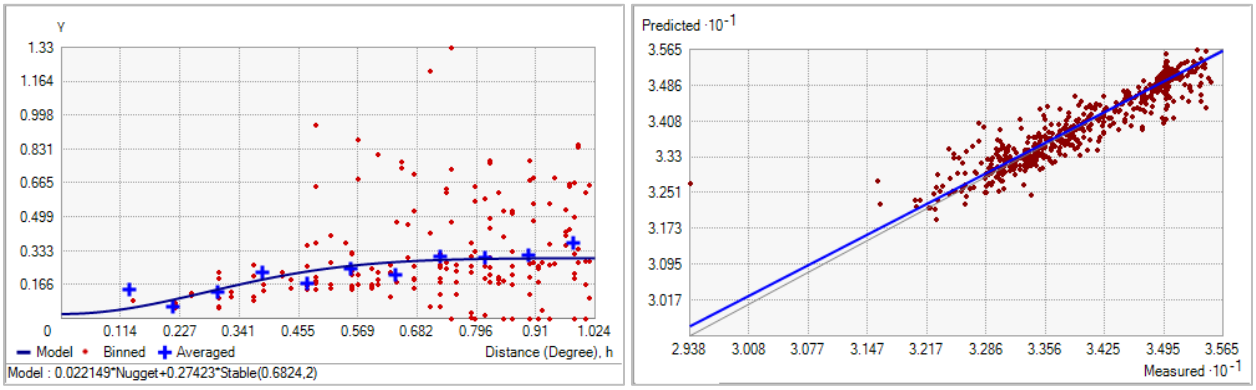

Fig. 103. Left panel: Semivariogram of Bottom Salinity Average Maximum. Binned values are shown as red dots; average points are shown as blue crosses; the model fit to the averaged values is shown as a blue line. Lag size: 0.085 degrees; number of lags: 12; Parameter: 2; Range: 0.682 degrees; Partial Sill: 0.274. Right panel: Scatterplot of predicted values versus observed values for the model of Bottom Salinity Average Maximum.

Table 42. Results of cross-validation of the kriged model for Bottom Salinity Average Maximum.

Prediction error	**Value**
Number of Observations	1160
Overall Mean Error	8.377×10^{-3}
Root Mean Square Prediction Error	0.235
Standardized Mean	0.018
Standardized Root Mean Square Prediction Error	1.012
Average Standard Error	0.213

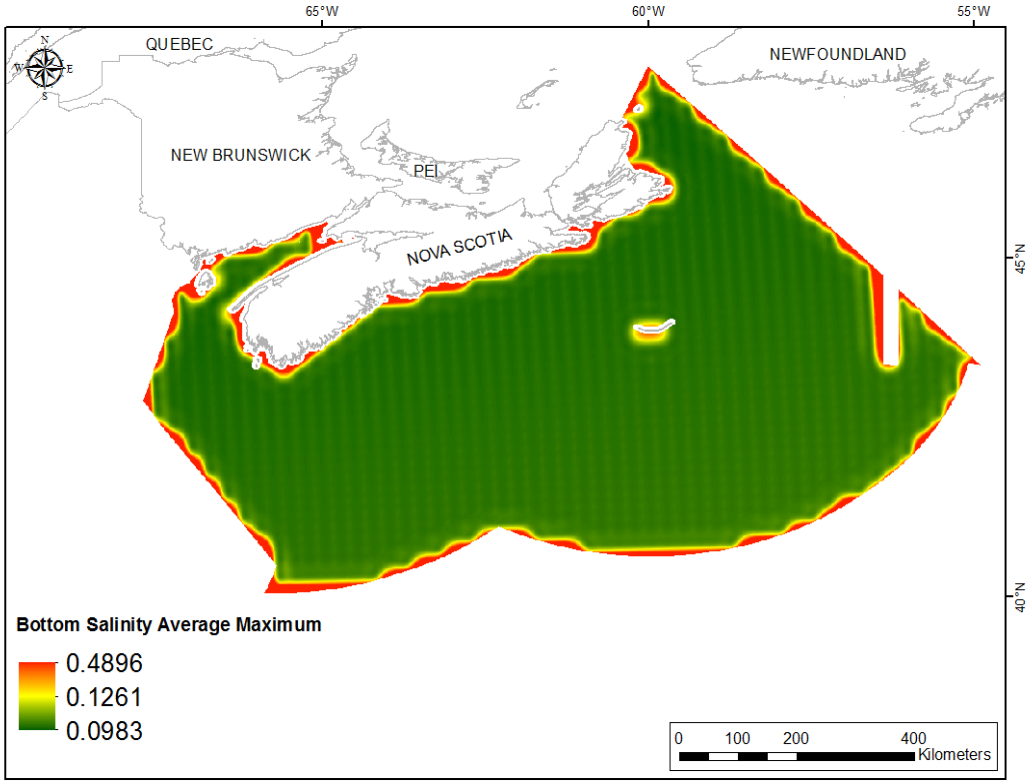

Fig. 104. Prediction standard error surface of Bottom Salinity Average Maximum.

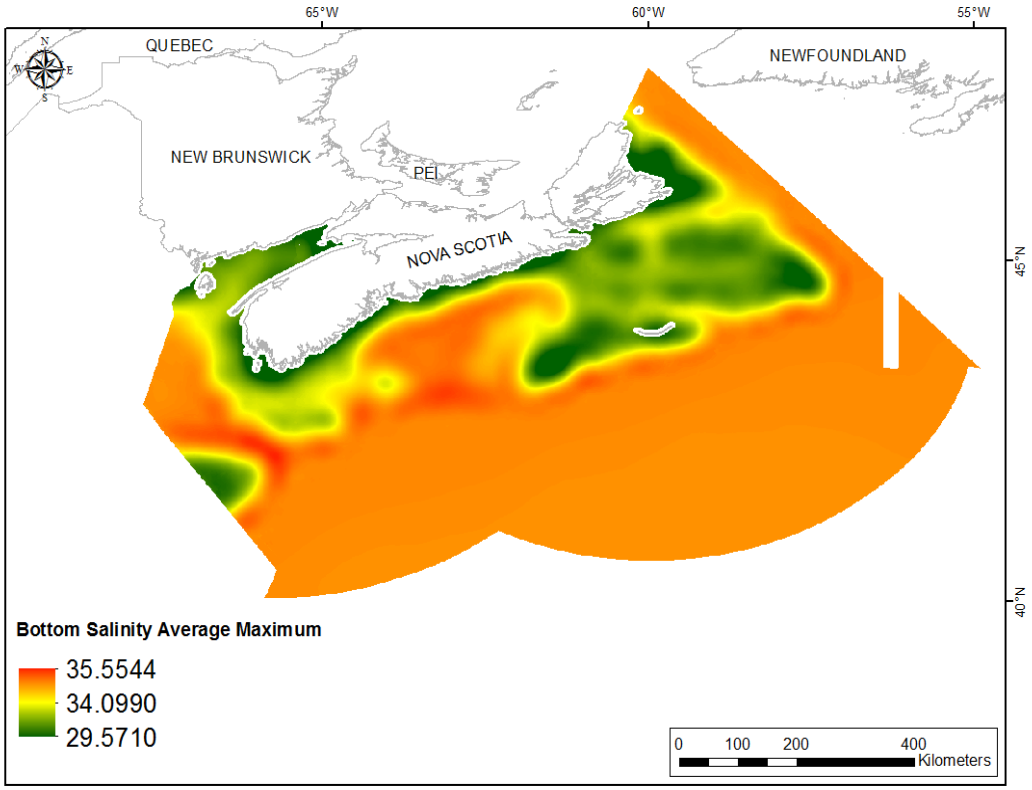

Fig. 105. Interpolated prediction surface of Bottom Salinity Average Maximum.

Bottom Salinity Average Range

This variable displayed a right-skewed, leptokurtic distribution with outlying data in the upper range prior to interpolation (Table 43, Fig. 106). The data were higher than predicted by a normal distribution at low and high values, and mid-range values were lower than the reference line (Fig. 107). There was a pattern to the under- and over-prediction (Fig. 107).

The semivariogram showed weak autocorrelation present in the data, however there was a good predictive fit (Fig. 108). The kriged model showed good cross-validation statistics (Table 44) indicating that it was good at prediction. The error map showed high error along the edges of the study extent (Fig. 109). The kriged surface is presented in Fig. 110. Negative values resulted from the right-skewed nature of the raw data (Fig. 106). Of the 326,283 raster cells in the study extent, 11,390 contained negative values (see Table A1). These were located in a long band along the lower slope (Fig. A4).

Table 43. Distributional properties of Bottom Salinity Average Range.

Property	Value
Number of Observations	1160
Minimum	0.005
Maximum	3.840
Mean	0.389
Median	0.049
Standard Deviation	0.489
Skewness	1.288
Kurtosis	5.106

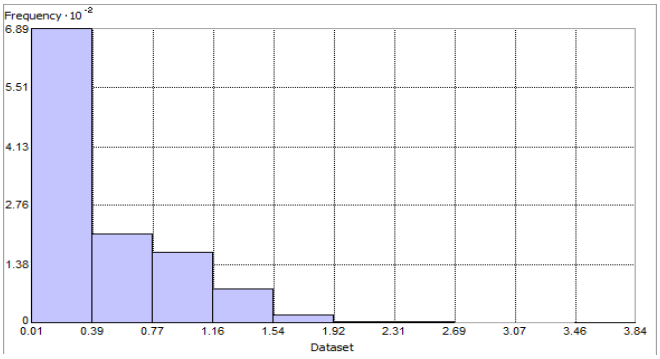

Fig. 106. Distribution of Bottom Salinity Average Range. Histogram was illustrated using 10 bins. Y axis is shown at 10^{-2}.

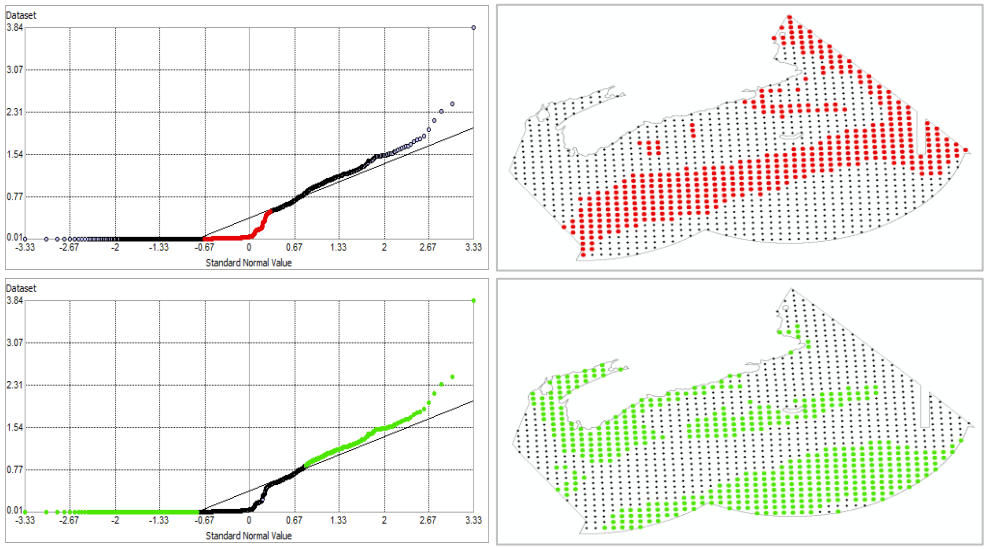

Fig. 107. Normal Q-Q plot for data values of Bottom Salinity Average Range. Points falling under (upper panel) and over (bottom panel) the reference line are mapped.

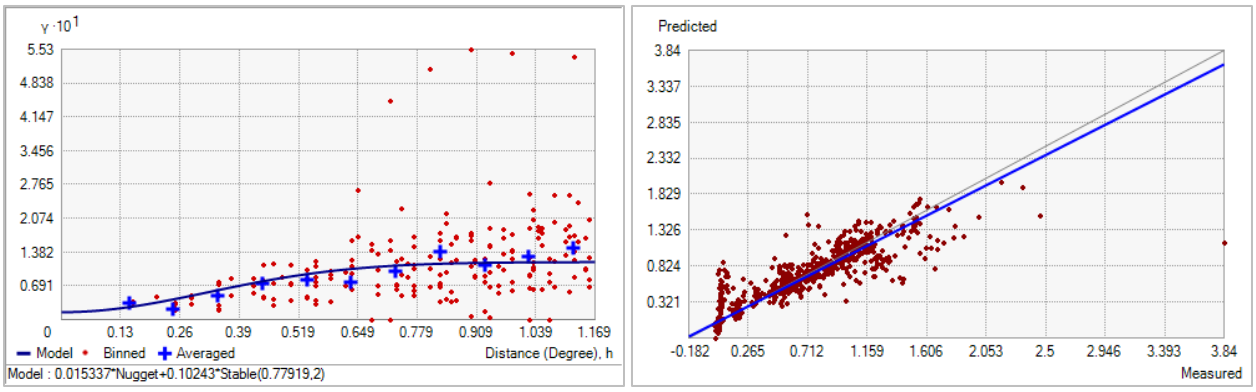

Fig. 108. Left panel: Semivariogram of Bottom Salinity Average Range. Binned values are shown as red dots; average points are shown as blue crosses; the model fit to the averaged values is shown as a blue line. Lag size: 0.097 degrees; number of lags: 12; Parameter: 2; Range: 0.779 degrees; Partial Sill: 0.102. Right panel: Scatterplot of predicted values versus observed values for the model of Bottom Salinity Average Range.

Table 44. Results of cross-validation of the kriged model for Bottom Salinity Average Range.

Prediction error	**Value**
Number of Observations	1160
Overall Mean Error	-2.485×10^{-3}
Root Mean Square Prediction Error	0.179
Standardized Mean	-5.670×10^{-3}
Standardized Root Mean Square Prediction Error	1.052
Average Standard Error	0.156

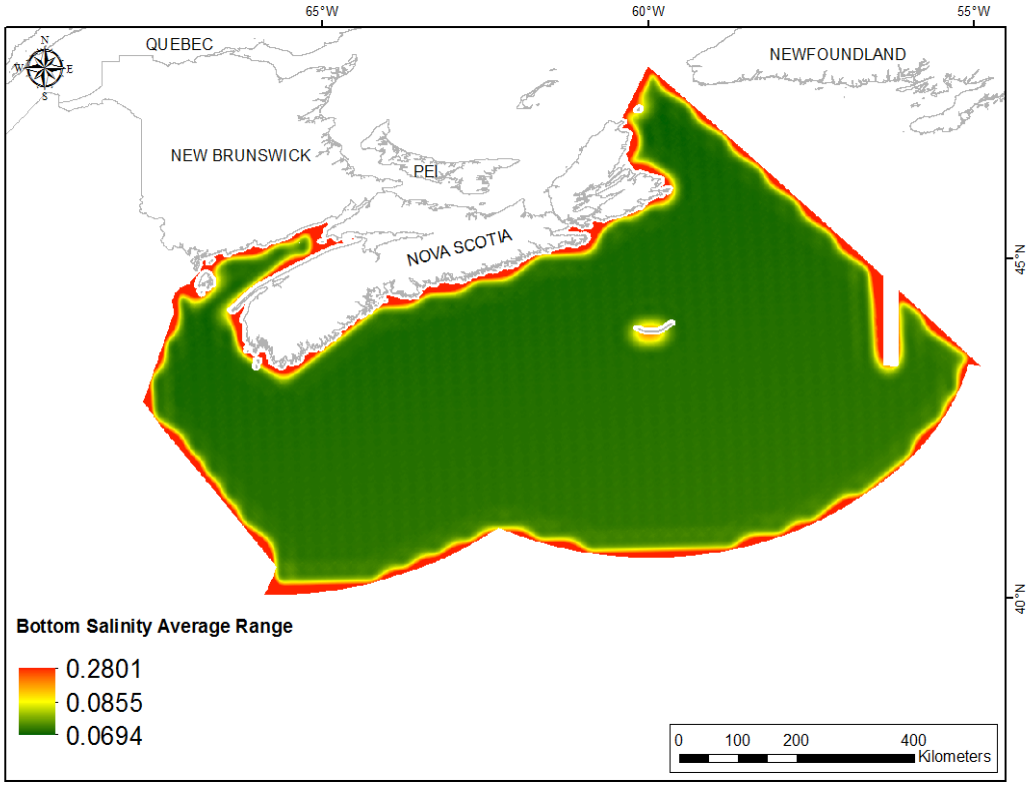

Fig. 109. Prediction standard error surface of Bottom Salinity Average Range.

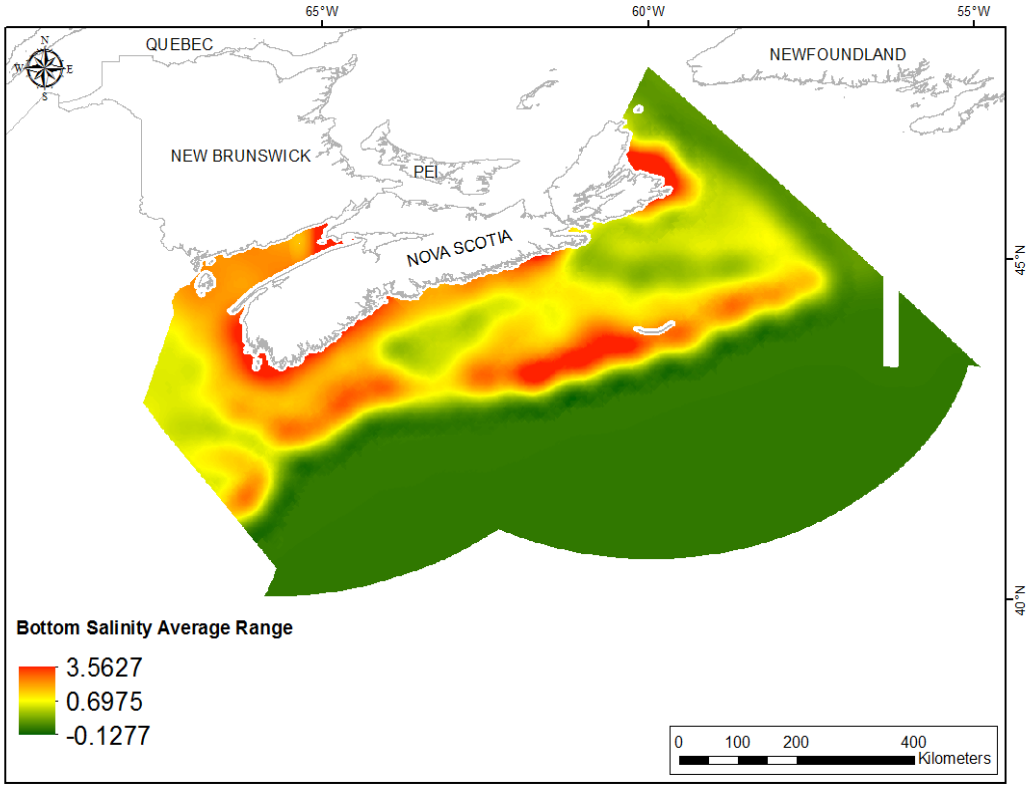

Fig. 110. Interpolated prediction surface of Bottom Salinity Average Range.

Surface Salinity Mean

This variable displayed a right-skewed, platykurtic distribution prior to interpolation (Table 45, Fig. 111). The data were lower than predicted by a normal distribution at mid-range and high values and higher than predicted at low and upper mid-range values (Fig. 112). There was a strong spatial pattern to the under- and over-predicted data points (Fig. 112).

The semivariogram showed moderate autocorrelation present in the data (Fig. 113). There was very good fit between the measured and predicted values (Fig. 113). However, the kriged model showed poor cross-validation statistics (Table 46). The Standardized Root-Mean-Square Prediction Error was less than 1 indicating that variability in the predictions has been overestimated. The error map showed high error along the edges of the study extent (Fig. 114). The kriged surface is presented in Fig. 115.

Table 45. Distributional properties of Surface Salinity Mean.

Property	Value
Number of Observations	1160
Minimum	26.805
Maximum	35.748
Mean	32.408
Median	32.098
Standard Deviation	1.705
Skewness	0.245
Kurtosis	2.209

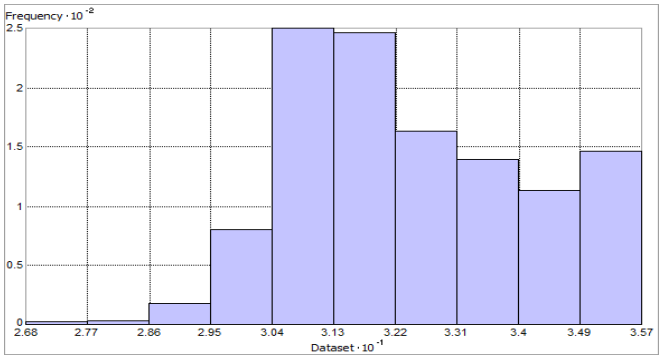

Fig. 111. Distribution of Surface Salinity Mean. Histogram was illustrated using 10 bins. X axis is shown at 10^{-1}; Y axis is shown at 10^{-2}.

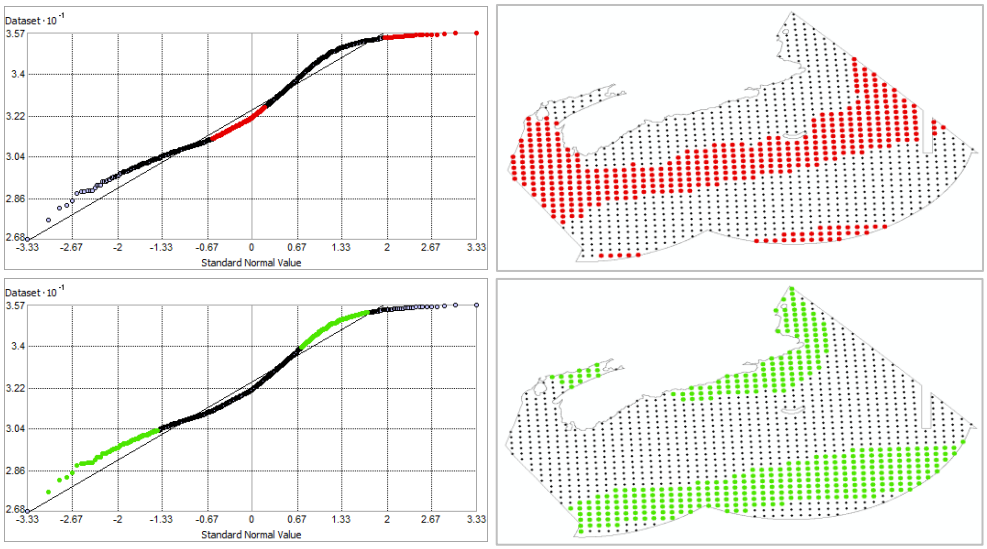

Fig. 112. Normal Q-Q plot for data values of Surface Salinity Mean. Points falling under (upper panel) and over (bottom panel) the reference line are mapped.

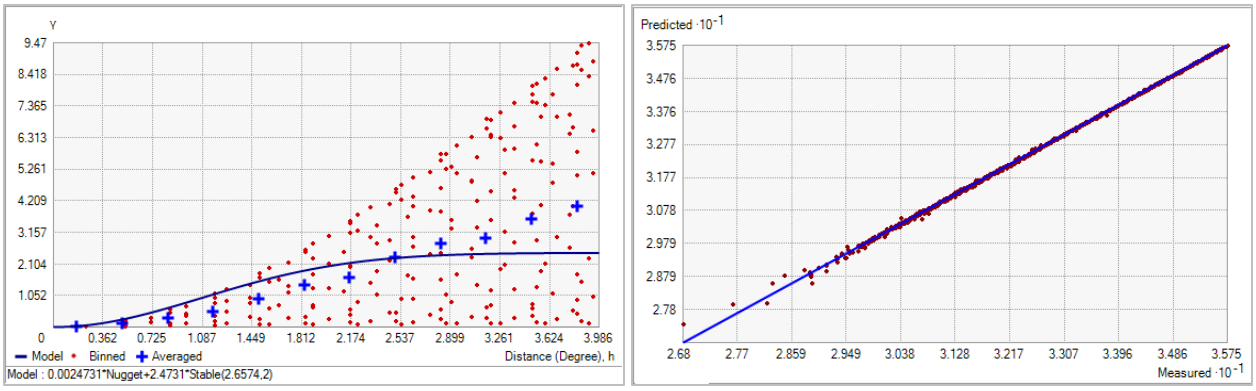

Fig. 113. Left panel: Semivariogram of Surface Salinity Mean. Binned values are shown as red dots; average points are shown as blue crosses; the model fit to the averaged values is shown as a blue line. Lag size: 0.332 degrees; number of lags: 12; Parameter: 2; Range: 2.657 degrees; Partial Sill: 2.473. Right panel: Scatterplot of predicted values versus observed values for the model of Surface Salinity Mean.

Table 46. Results of cross-validation of the kriged model for Surface Salinity Mean.

Prediction error	**Value**
Number of Observations	1160
Overall Mean Error	1.228×10^{-3}
Root Mean Square Prediction Error	0.037
Standardized Mean	9.698×10^{-3}
Standardized Root Mean Square Prediction Error	0.492
Average Standard Error	0.057

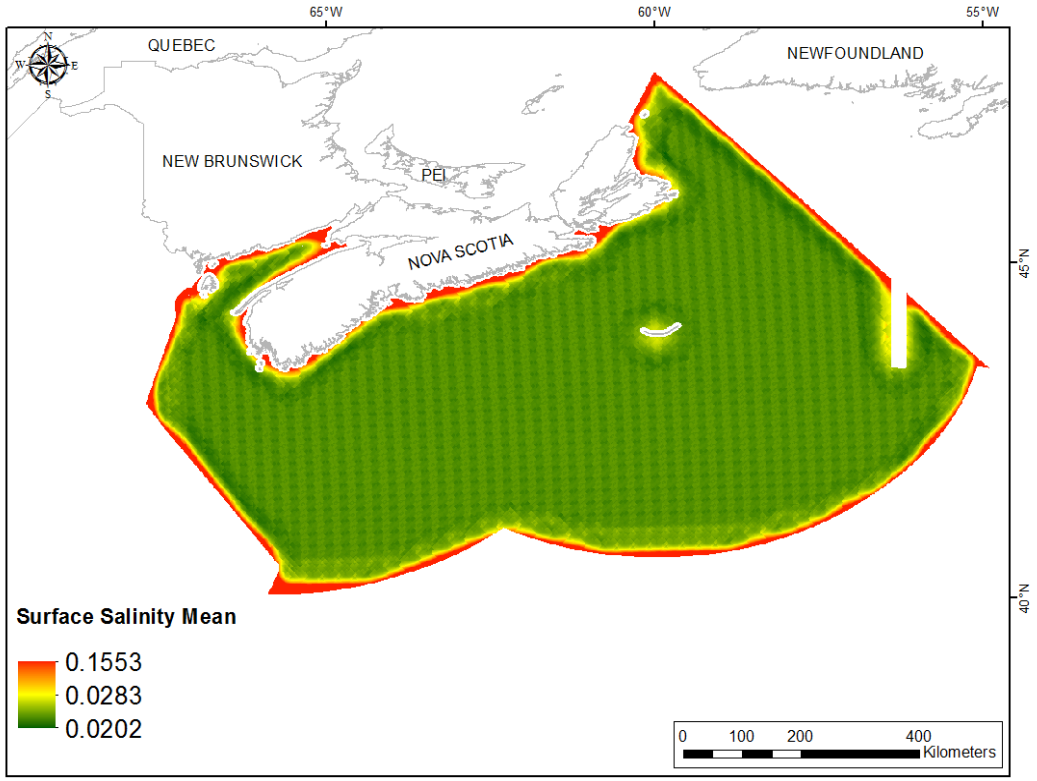

Fig. 114. Prediction standard error surface of Surface Salinity Mean.

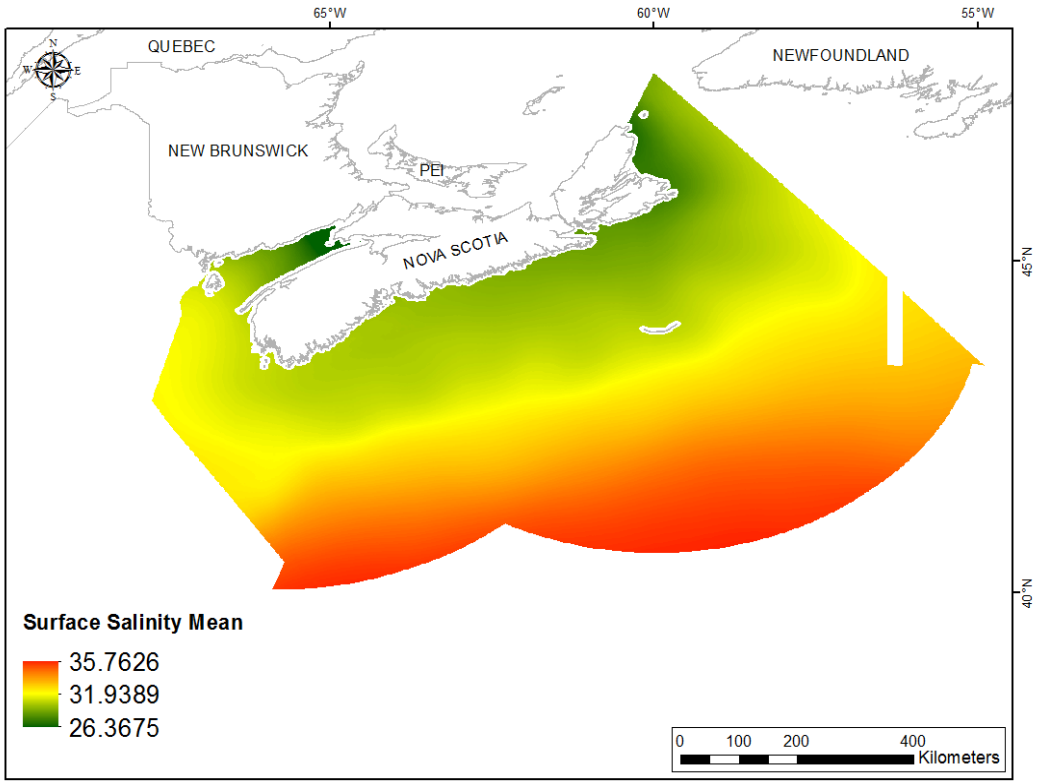

Fig. 115. Interpolated prediction surface of Surface Salinity Mean.

Surface Salinity Minimum

This variable displayed a left-skewed, leptokurtic distribution prior to interpolation (Table 47, Fig. 116). The data were lower than predicted by a normal distribution at both tails, while some mid-range values were above the reference line (Fig. 117). There was spatial pattern to the under- and over-prediction (Fig. 117).

The semivariogram showed weak autocorrelation present in the data (Fig. 118). The kriged model showed excellent fit between predicted and measured values (Fig. 118) but poor cross-validation statistics (Table 48). The Standardized Root-Mean-Square Prediction Error was greater than 1 indicating that variability in the predictions has been underestimated. The error map showed a 'bullseye' pattern with error increasing with distance from data points (Fig. 119). The kriged surface is presented in Fig. 120.

Table 47. Distributional properties of Surface Salinity Minimum.

Property	Value
Number of Observations	1160
Minimum	23.869
Maximum	34.245
Mean	30.538
Median	30.462
Standard Deviation	1.483
Skewness	-0.103
Kurtosis	3.413

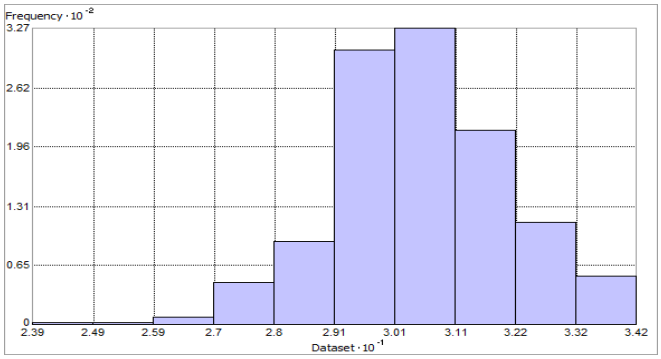

Fig. 116. Distribution of Surface Salinity Minimum. Histogram was illustrated using 10 bins. X axis is shown at 10^{-1}; Y axis is shown at 10^{-2}.

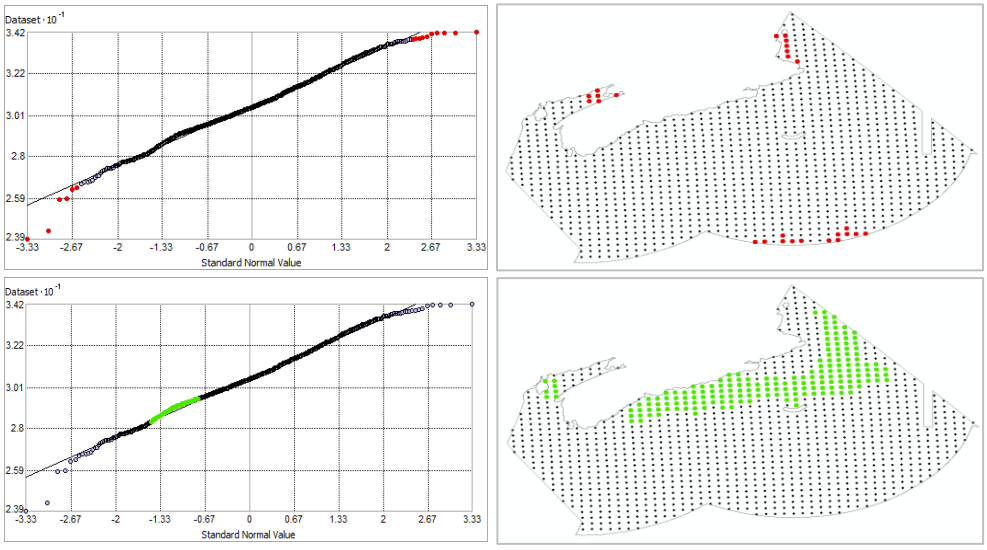

Fig. 117. Normal Q-Q plot for data values of Surface Salinity Minimum. Points falling under (upper panel) and over (bottom panel) the reference line are mapped.

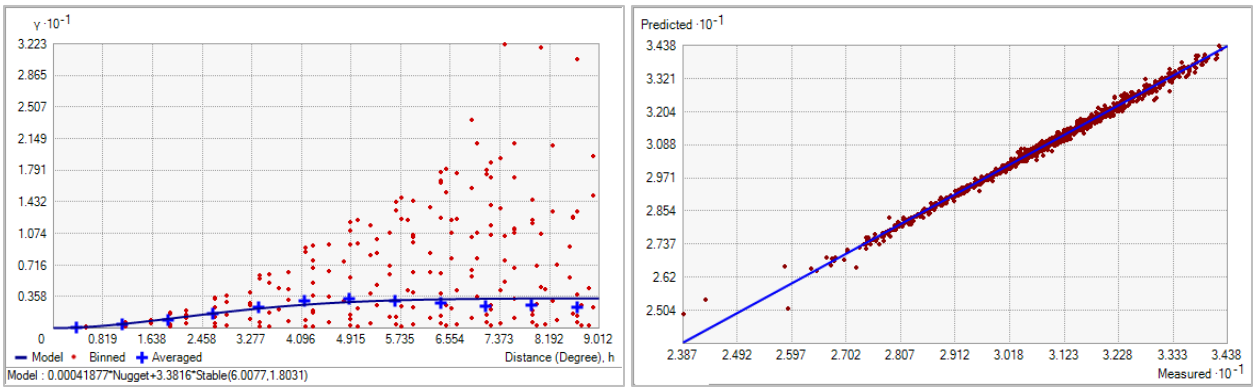

Fig. 118. Left panel: Semivariogram of Surface Salinity Minimum. Binned values are shown as red dots; average points are shown as blue crosses; the model fit to the averaged values is shown as a blue line. Lag size: 0.751 degrees; number of lags: 12; Parameter: 1.803; Range: 6.008 degrees; Partial Sill: 3.382. Right panel: Scatterplot of predicted values versus observed values for the model of Surface Salinity Minimum.

Table 48. Results of cross-validation of the kriged model for Surface Salinity Minimum.

Prediction error	**Value**
Number of Observations	1160
Overall Mean Error	1.895×10^{-3}
Root Mean Square Prediction Error	0.115
Standardized Mean	0.010
Standardized Root Mean Square Prediction Error	1.567
Average Standard Error	0.067

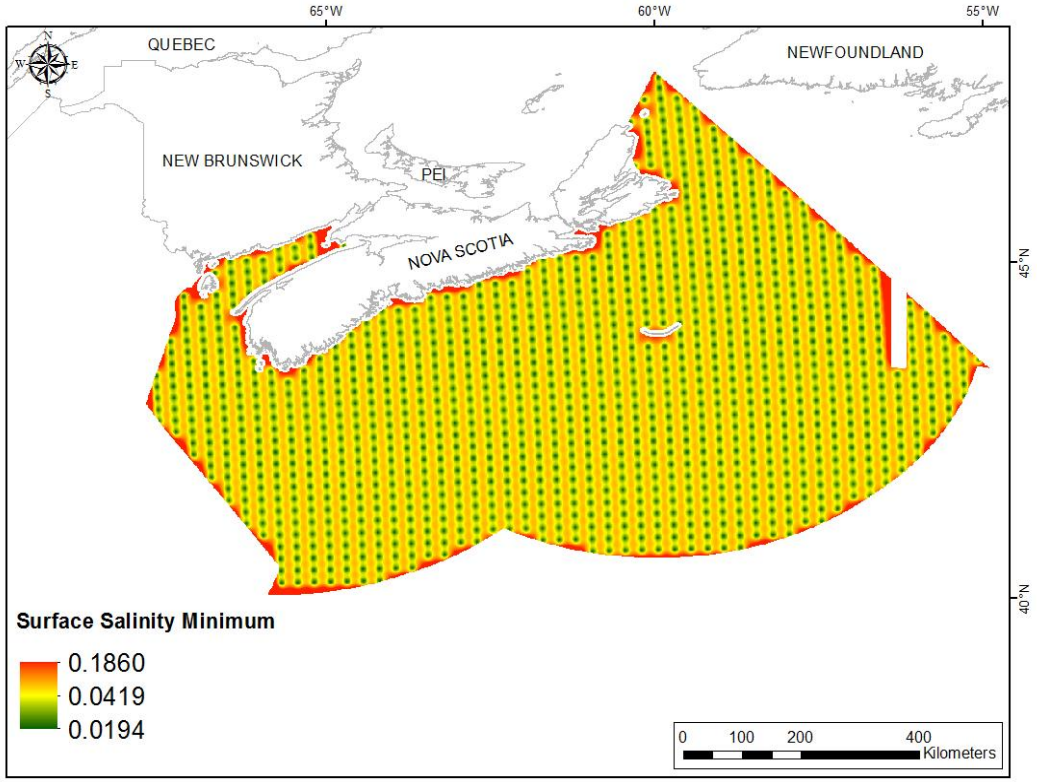

Fig. 119. Prediction standard error surface of Surface Salinity Minimum.

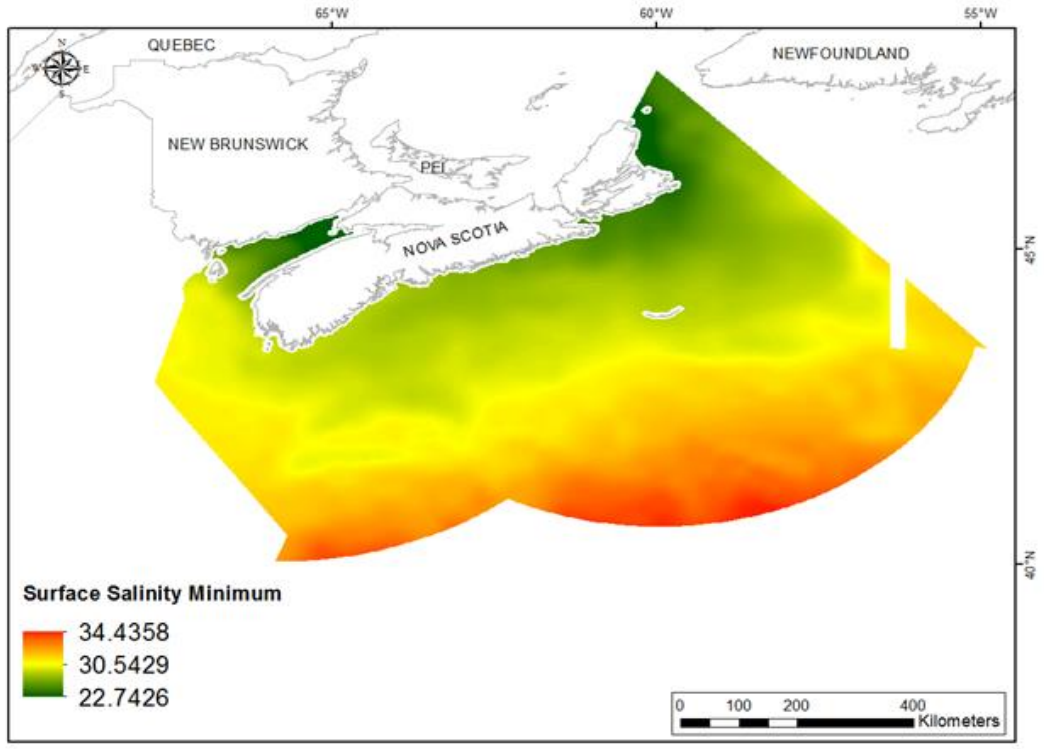

Fig. 120. Interpolated prediction surface of Surface Salinity Minimum.

Surface Salinity Maximum

This variable displayed a left-skewed, platykurtic and bimodal distribution prior to interpolation (Table 49, Fig. 121). The data were lower than predicted by a normal distribution at mid-range and high values (Fig. 122). Low-and upper mid-range values were higher than the reference line. There was spatial pattern to the under- and over-prediction (Fig. 122).

The semivariogram showed moderate autocorrelation present in the data and very good predictive fit (Fig. 123). The model showed fair cross-validation statistics (Table 50). The Standardized Root-Mean-Square Prediction Error was greater than 1 indicating that variability in the predictions has been underestimated. The error map showed a 'bullseye' pattern with error increasing with distance from data points (Fig. 124). The kriged surface is presented in Fig. 125.

Table 49. Distributional properties of Surface Salinity Maximum.

Property	Value
Number of Observations	1160
Minimum	30.416
Maximum	36.499
Mean	34.053
Median	33.787
Standard Deviation	1.730
Skewness	-0.013
Kurtosis	1.540

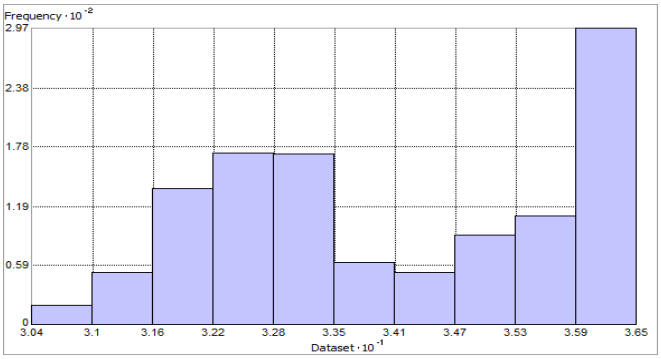

Fig. 121. Distribution of Surface Salinity Maximum. Histogram was illustrated using 10 bins. X axis is shown at 10^{-1}; Y axis is shown at 10^{-2}.

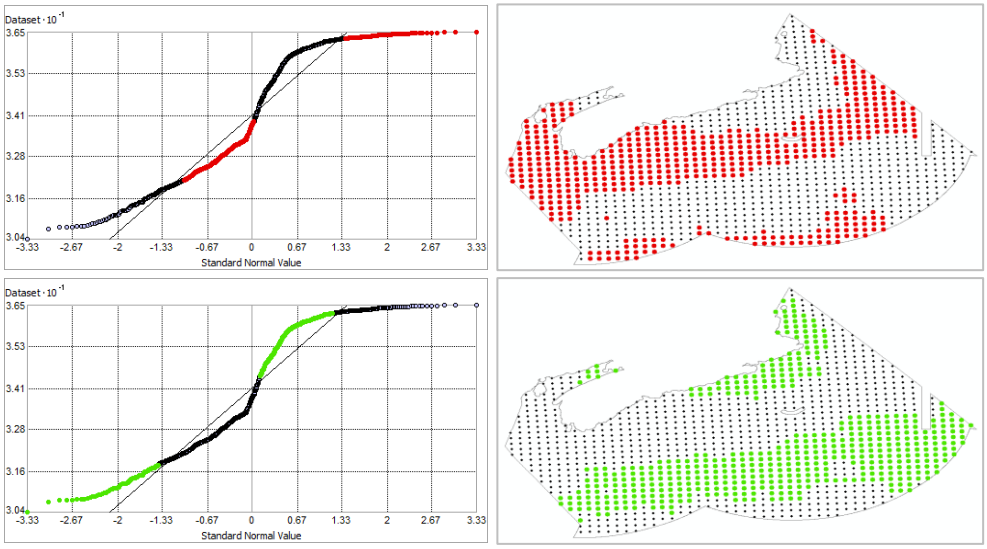

Fig. 122. Normal Q-Q plot for data values of Surface Salinity Maximum. Points falling under (upper panel) and over (bottom panel) the reference line are mapped.

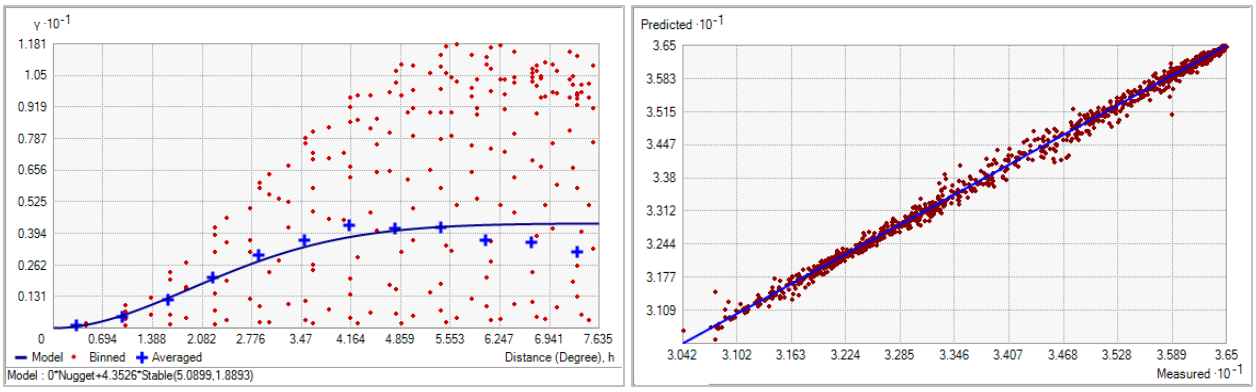

Fig. 123. Left panel: Semivariogram of Surface Salinity Maximum. Binned values are shown as red dots; average points are shown as blue crosses; the model fit to the averaged values is shown as a blue line. Lag size: 0.636 degrees; number of lags: 12; Parameter: 1.889; Range: 5.090 degrees; Partial Sill: 4.353. Right panel: Scatterplot of predicted values versus observed values for the model of Surface Salinity Maximum.

Table 50. Results of cross-validation of the kriged model for Surface Salinity Maximum.

Prediction error	**Value**
Number of Observations	1160
Overall Mean Error	8.534×10^{-4}
Root Mean Square Prediction Error	0.109
Standardized Mean	4.358×10^{-3}
Standardized Root Mean Square Prediction Error	2.104
Average Standard Error	0.053

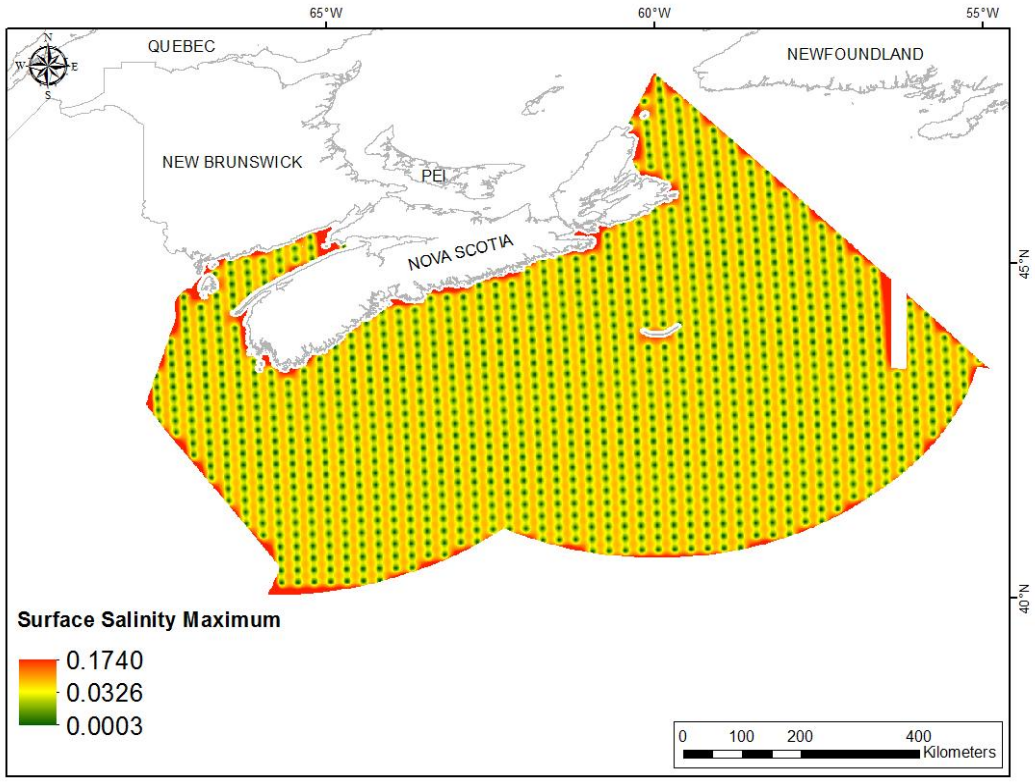

Fig. 124. Prediction standard error surface of Surface Salinity Maximum.

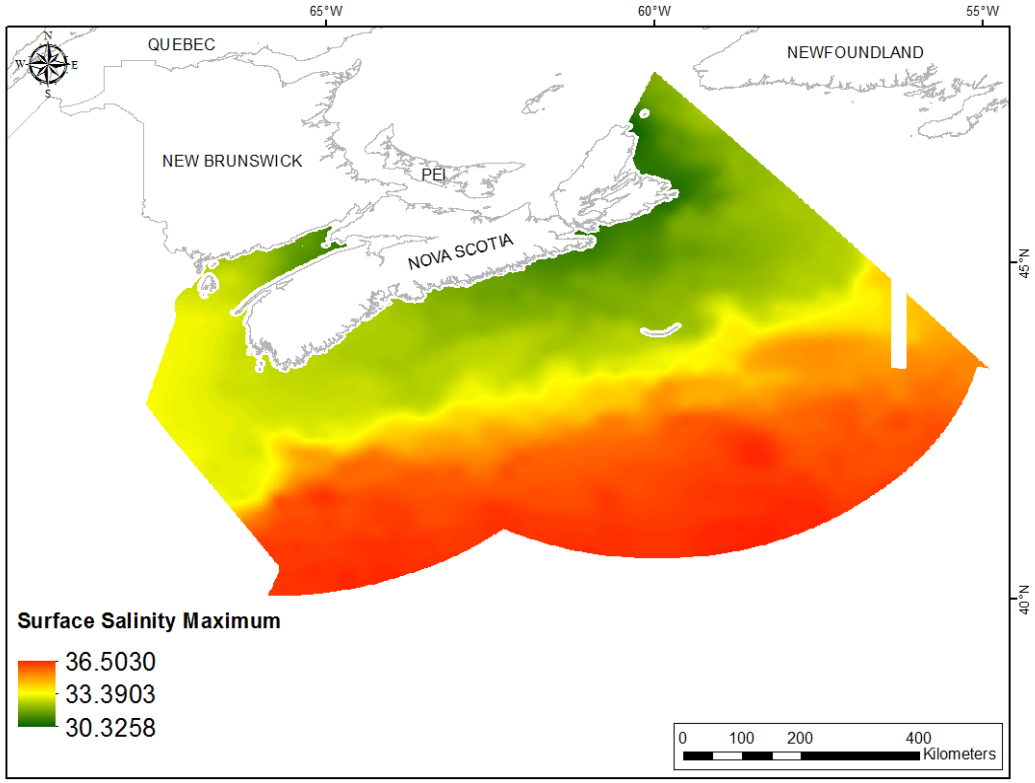

Fig. 125. Interpolated prediction surface of Surface Salinity Maximum.

Surface Salinity Range

This variable displayed a near-mesokurtic distribution with slight positive skew and outlying data in the upper range (Table 51, Fig. 126). The data were higher than predicted by a normal distribution at both tails, with mid-range values falling slightly below the reference line (Fig. 127). The areas of under- and over-prediction showed no strong spatial pattern over the study extent (Fig. 127).

The semivariogram showed autocorrelation present in the data (Fig. 128). The model showed a good fit between measured and predicted values (Fig. 128) and good cross-validation statistics indicating that it was good at prediction (Table 52). The error map showed a 'bullseye' pattern with error increasing with distance from data points (Fig. 129). The kriged surface is presented in Fig. 130.

Table 51. Distributional properties of Surface Salinity Range.

Property	Value
Number of Observations	1160
Minimum	2.173
Maximum	7.211
Mean	3.516
Median	3.368
Standard Deviation	0.740
Skewness	0.560
Kurtosis	3.056

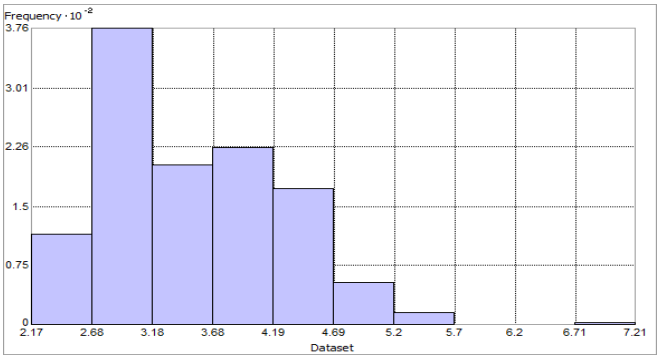

Fig. 126. Distribution of Surface Salinity Range. Histogram was illustrated using 10 bins. Y axis at 10^{-2}.

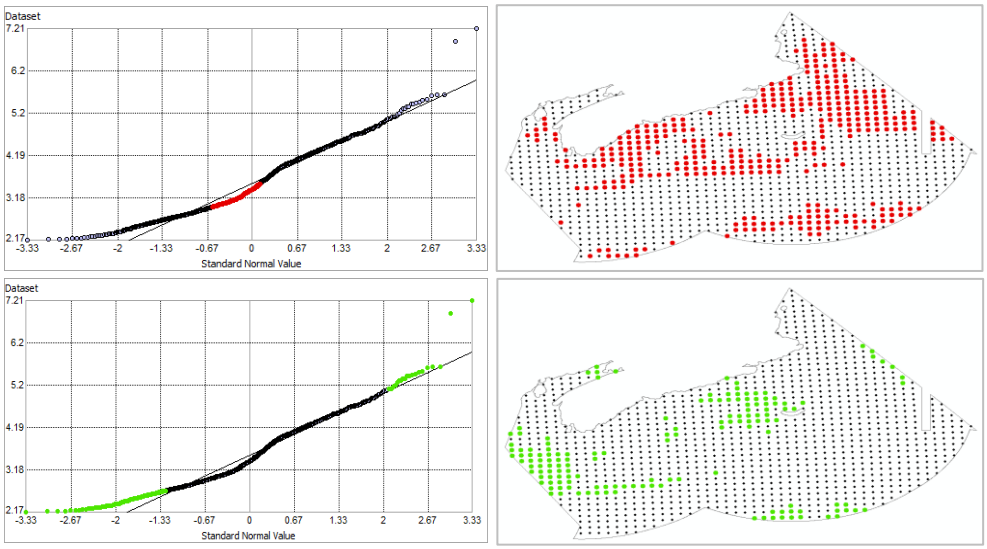

Fig. 127. Normal Q-Q plot for data values of Surface Salinity Range. Points falling under (upper panel) and over (bottom panel) the reference line are mapped.

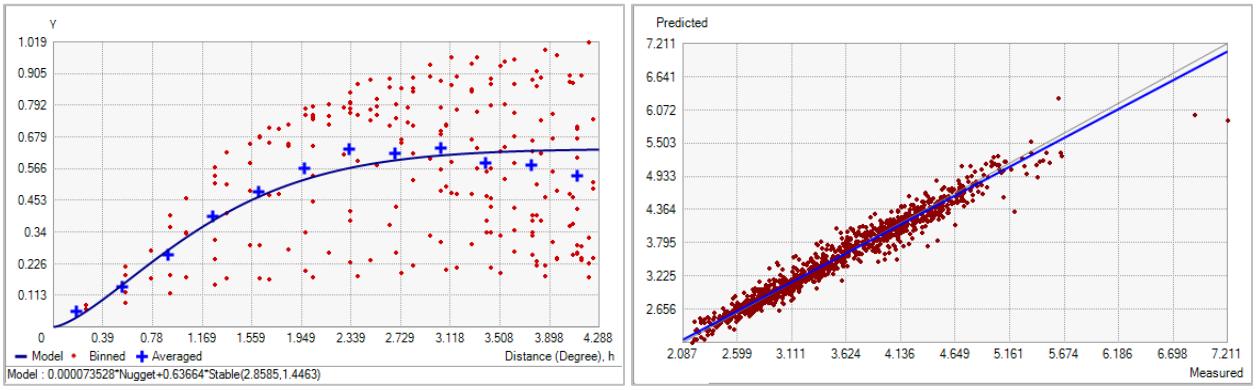

Fig. 128. Left panel: Semivariogram of Surface Salinity Range. Binned values are shown as red dots; average points are shown as blue crosses; the model fit to the averaged values is shown as a blue line. Lag size: 0.357 degrees; number of lags: 12; Parameter: 1.446; Range: 2.859 degrees; Partial Sill: 0.637. Right panel: Scatterplot of predicted values versus observed values for the model of Surface Salinity Range.

Table 52. Results of cross-validation of the kriged model for Surface Salinity Range.

Prediction error	**Value**
Number of Observations	1160
Overall Mean Error	-1.305×10^{-3}
Root Mean Square Prediction Error	0.154
Standardized Mean	-3.789×10^{-3}
Standardized Root Mean Square Prediction Error	1.057
Average Standard Error	0.143

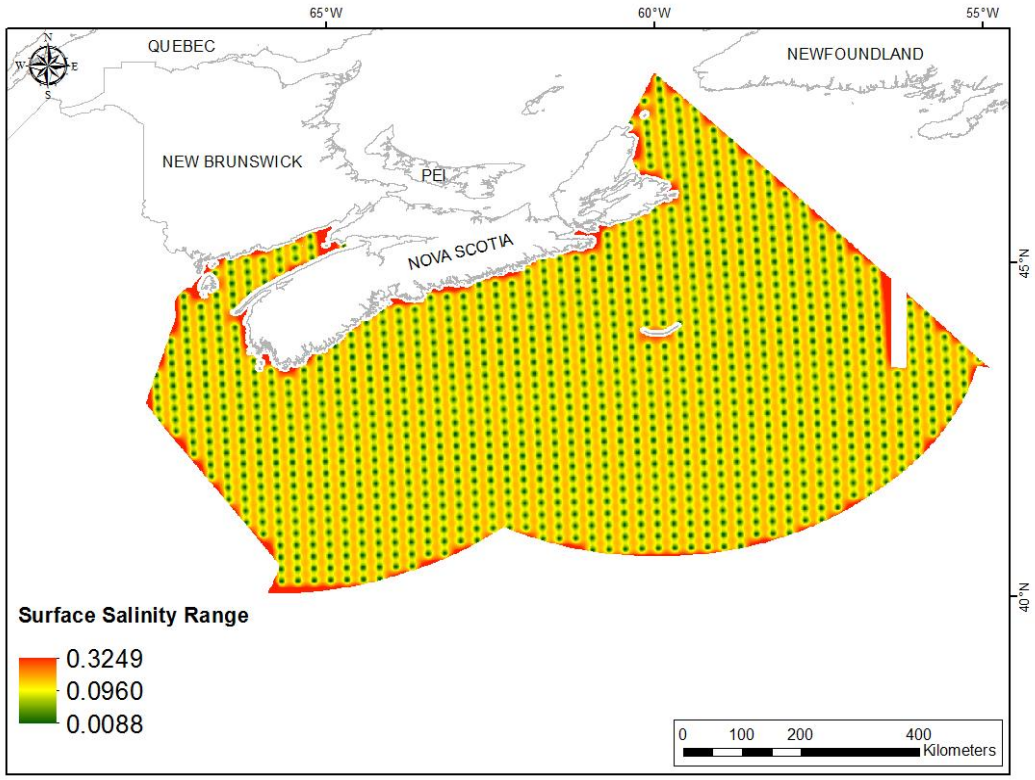

Fig. 129. Prediction standard error surface of Surface Salinity Range.

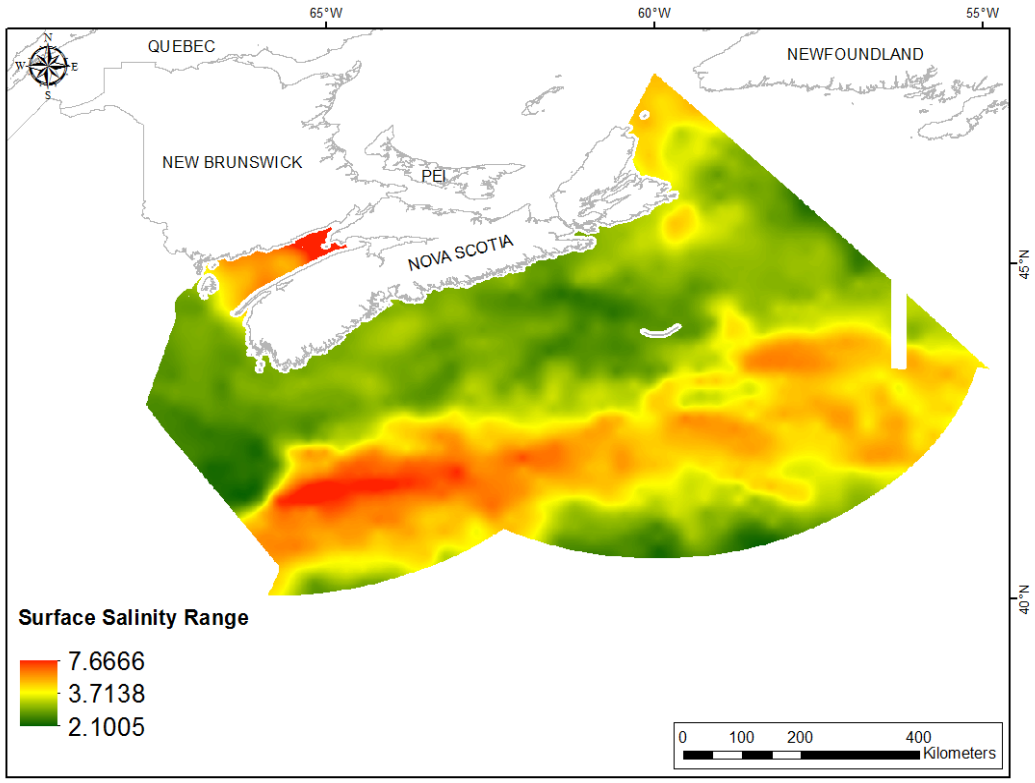

Fig. 130. Interpolated prediction surface of Surface Salinity Range.

Surface Salinity Average Minimum

This variable displayed a near-mesokurtic distribution with slight positive skew (Table 53, Fig. 131). The data were lower than predicted by a normal distribution at both tails with some mid-range values above the reference line (Fig. 132). There was a strong spatial pattern to the under- and over-prediction (Fig. 132).

The semivariogram showed weak autocorrelation present in the data (Fig. 133). There was an excellent fit between the measured and predicted values (Fig. 133), but the model showed poor cross-validation statistics (Table 54). The Standardized Root-Mean-Square Prediction Error was greater than 1 indicating that variability in the predictions has been underestimated. The error map showed a 'bullseye' pattern with error increasing with distance from data points (Fig. 134). The kriged surface is presented in Fig. 135.

Table 53. Distributional properties of Surface Salinity Average Minimum.

Property	Value
Number of Observations	1160
Minimum	24.653
Maximum	34.985
Mean	31.449
Median	31.310
Standard Deviation	1.590
Skewness	0.115
Kurtosis	2.972

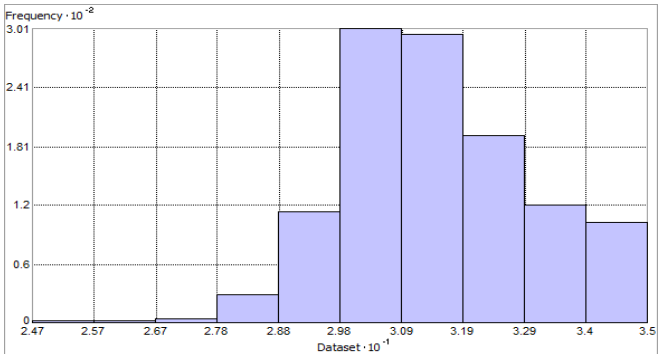

Fig. 131. Distribution of Surface Salinity Average Minimum. Histogram was illustrated using 10 bins. X axis is shown at 10^{-1}; Y axis is shown at 10^{-2}.

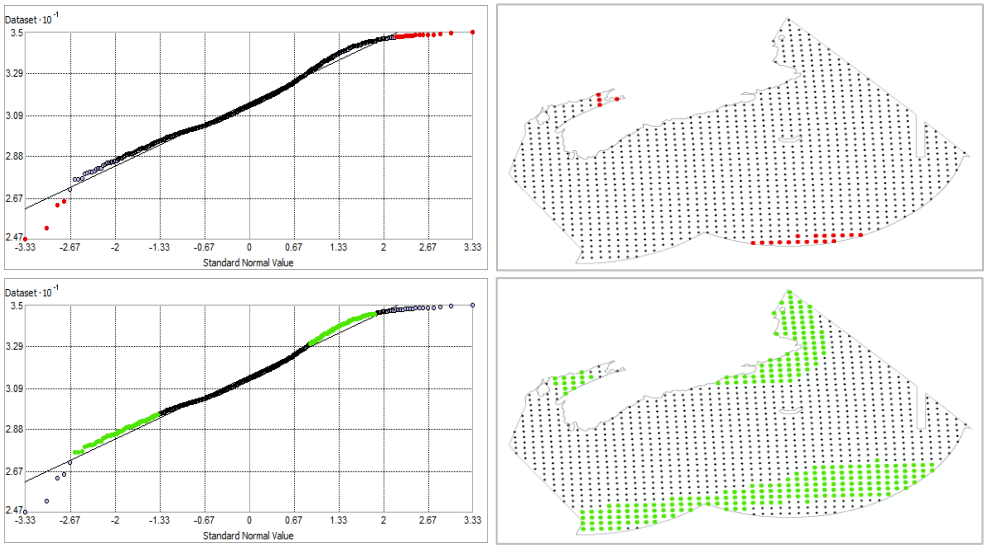

Fig. 132. Normal Q-Q plot for data values of Surface Salinity Average Minimum. Points falling under (upper panel) and over (bottom panel) the reference line are mapped.

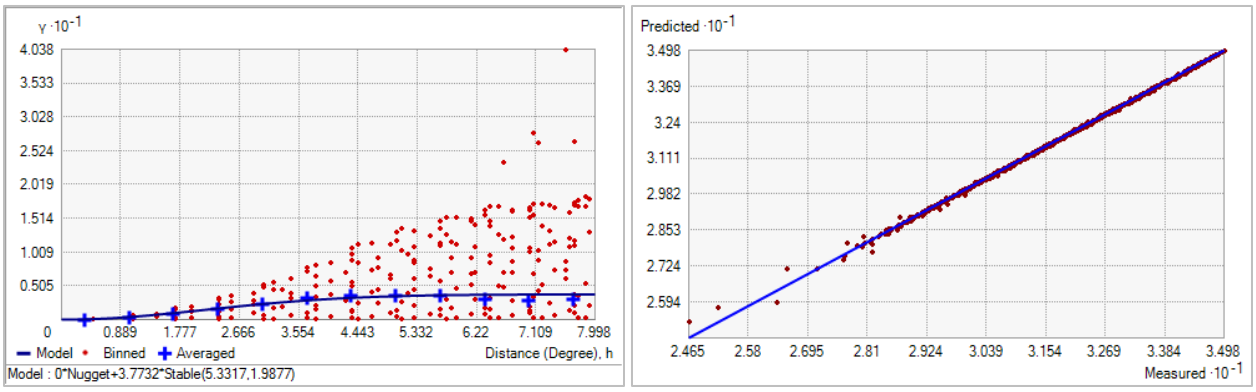

Fig. 133. Left panel: Semivariogram of Surface Salinity Average Minimum. Binned values are shown as red dots; average points are shown as blue crosses; the model fit to the averaged values is shown as a blue line. Lag size: 0.666 degrees; number of lags: 12; Parameter: 1.988; Range: 5.331 degrees; Partial Sill: 3.773. Right panel: Scatterplot of predicted values versus observed values for the model of Surface Salinity Average Minimum.

Table 54. Results of cross-validation of the kriged model for Surface Salinity Average Minimum.

Prediction error	**Value**
Number of Observations	1160
Overall Mean Error	1.193×10^{-3}
Root Mean Square Prediction Error	0.047
Standardized Mean	0.023
Standardized Root Mean Square Prediction Error	2.566
Average Standard Error	0.014

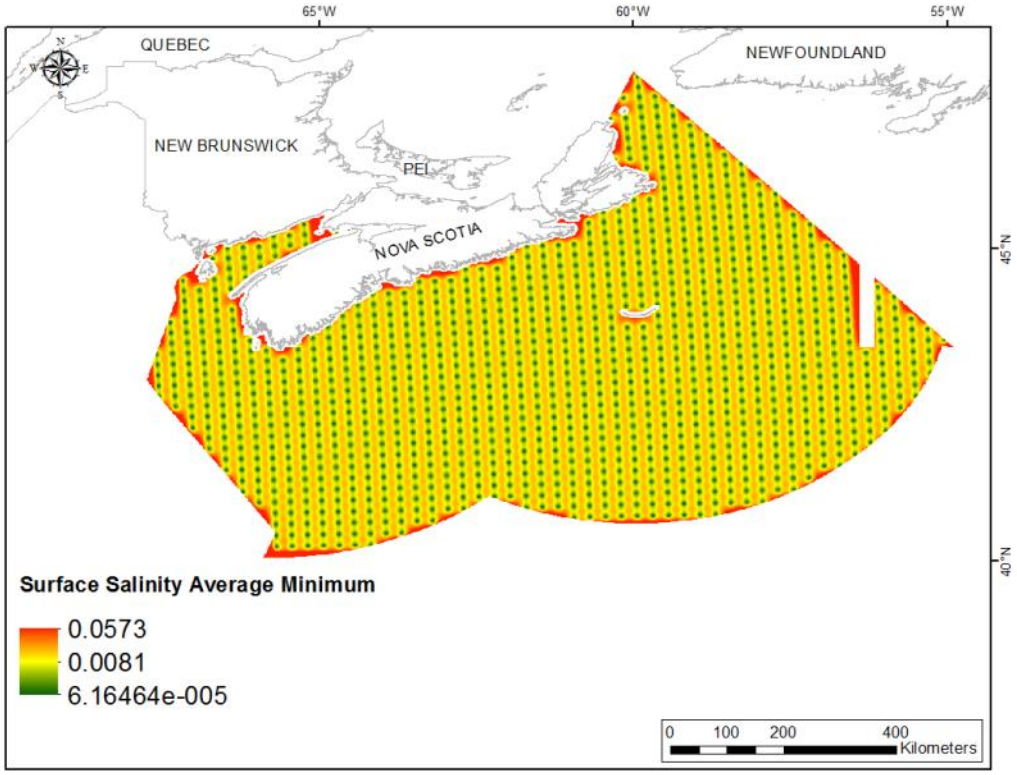

Fig. 134. Prediction standard error surface of Surface Salinity Average Minimum.

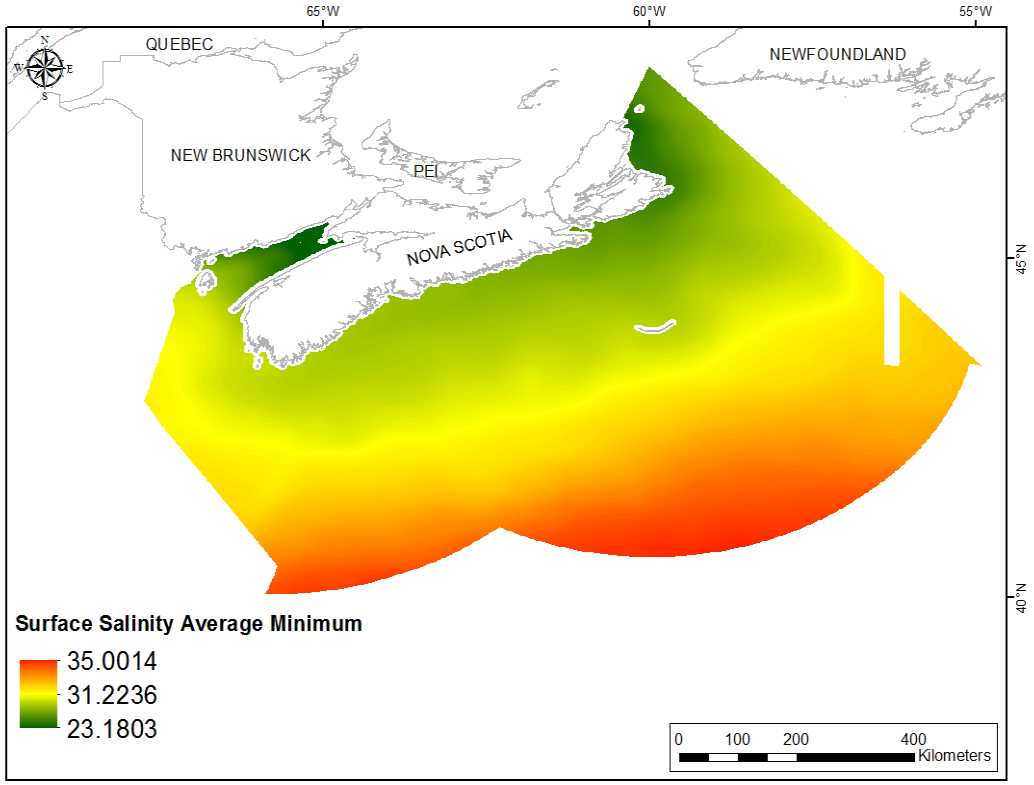

Fig. 135. Interpolated prediction surface of Surface Salinity Average Minimum.

Surface Salinity Average Maximum

This variable displayed a platykurtic, right-skewed distribution with bimodality prior to interpolation (Table 55, Fig. 136). The data were higher than predicted by a normal distribution at low and upper mid-range values and lower than predicted at mid-range and high values (Fig. 137). There was spatial pattern to the under- and over-prediction (Fig. 137).

The semivariogram showed weak to moderate autocorrelation present in the data (Fig. 138). There was an excellent fit between measured and predicted values (Fig. 138) and the model showed excellent cross-validation statistics (Table 56). The error map showed a 'bullseye' pattern with error increasing with distance from data points (Fig. 139). The kriged surface is presented in Fig. 140.

Table 55. Distributional properties of Surface Salinity Average Maximum.

Property	Value
Number of Observations	1160
Minimum	29.221
Maximum	36.226
Mean	33.320
Median	32.867
Standard Deviation	1.761
Skewness	0.183
Kurtosis	1.756

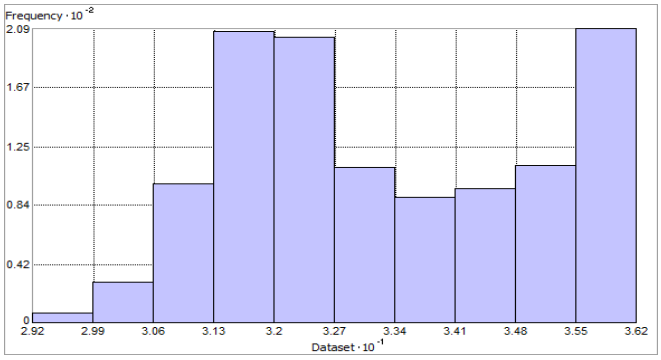

Fig. 136. Distribution of Surface Salinity Average Maximum. Histogram was illustrated using 10 bins. X axis is shown at 10^{-1}; Y axis is shown at 10^{-2}.

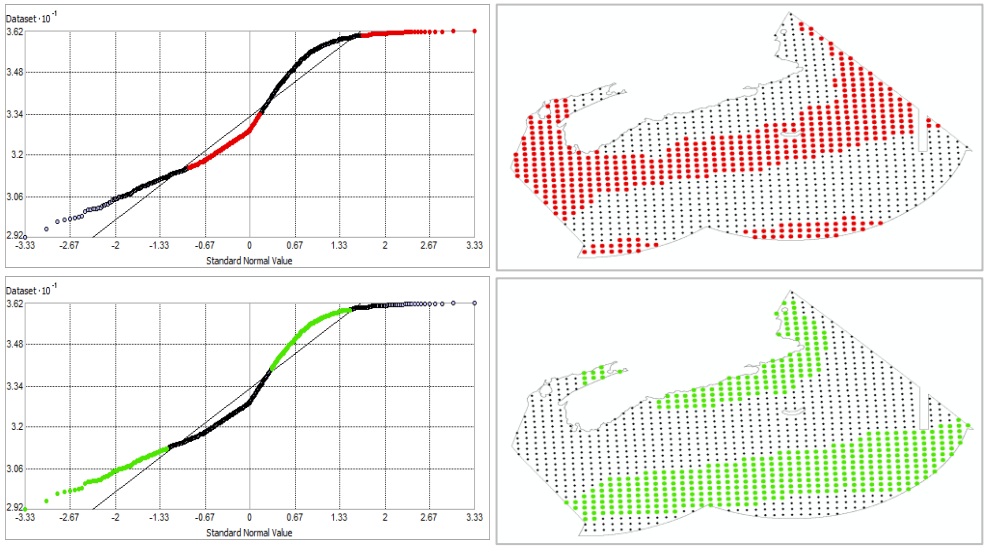

Fig. 137. Normal Q-Q plot for data values of Surface Salinity Average Maximum. Points falling under (upper panel) and over (bottom panel) the reference line are mapped.

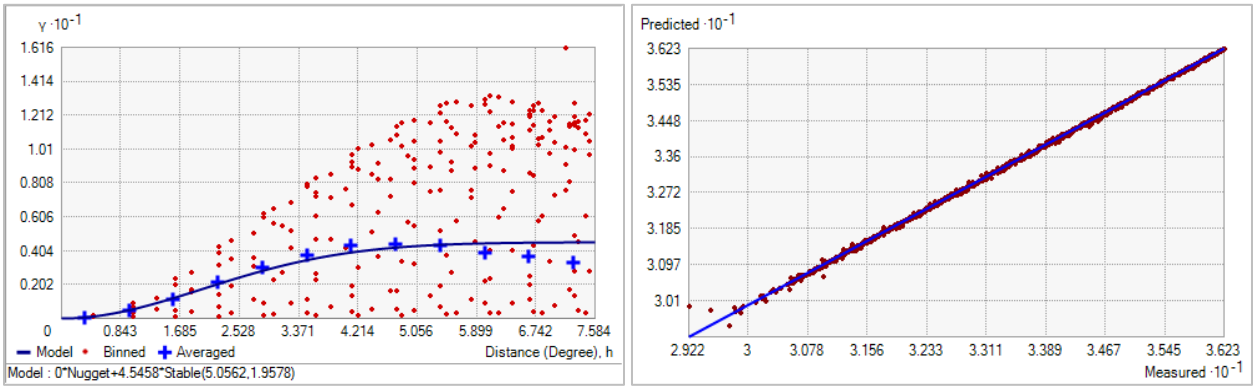

Fig. 138. Left panel: Semivariogram of Surface Salinity Average Maximum. Binned values are shown as red dots; average points are shown as blue crosses; the model fit to the averaged values is shown as a blue line. Lag size: 0.632 degrees; number of lags: 12; Parameter: 1.958; Range: 5.056 degrees; Partial Sill: 4.546. Right panel: Scatterplot of predicted values versus observed values for the model of Surface Salinity Average Maximum.

Table 56. Results of cross-validation of the kriged model for Surface Salinity Average Maximum.

Prediction error	**Value**
Number of Observations	1160
Overall Mean Error	6.543×10^{-4}
Root Mean Square Prediction Error	0.039
Standardized Mean	4.172×10^{-3}
Standardized Root Mean Square Prediction Error	0.981
Average Standard Error	0.030

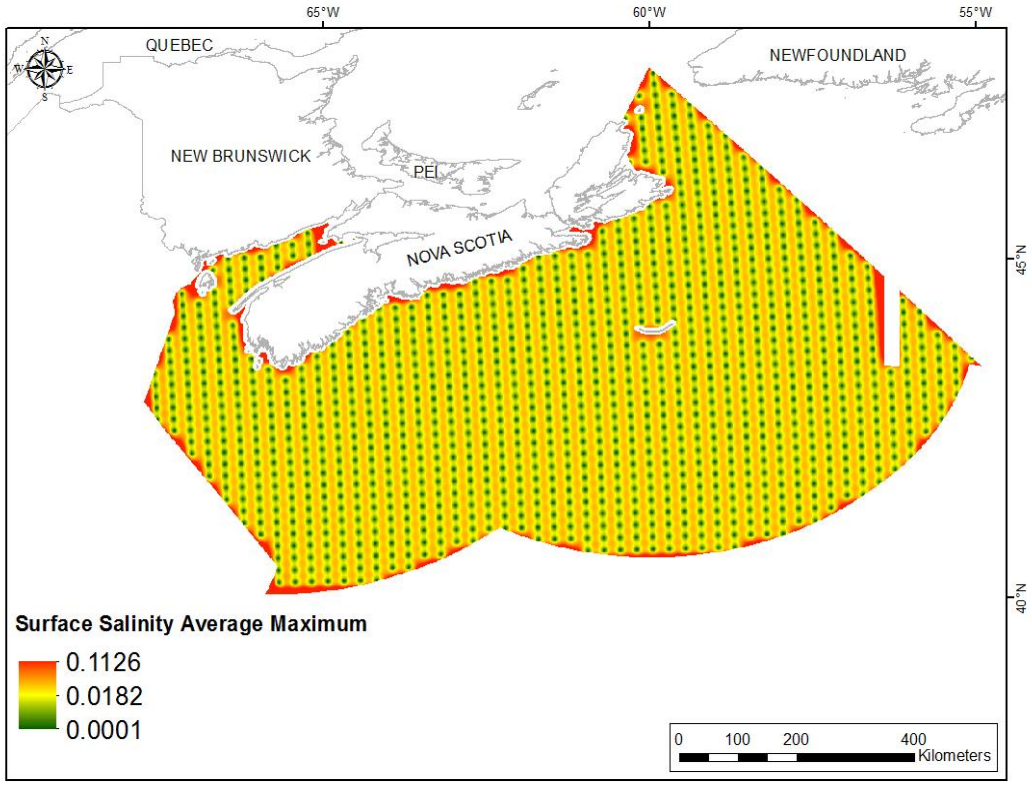

Fig. 139. Prediction standard error surface of Surface Salinity Average Maximum.

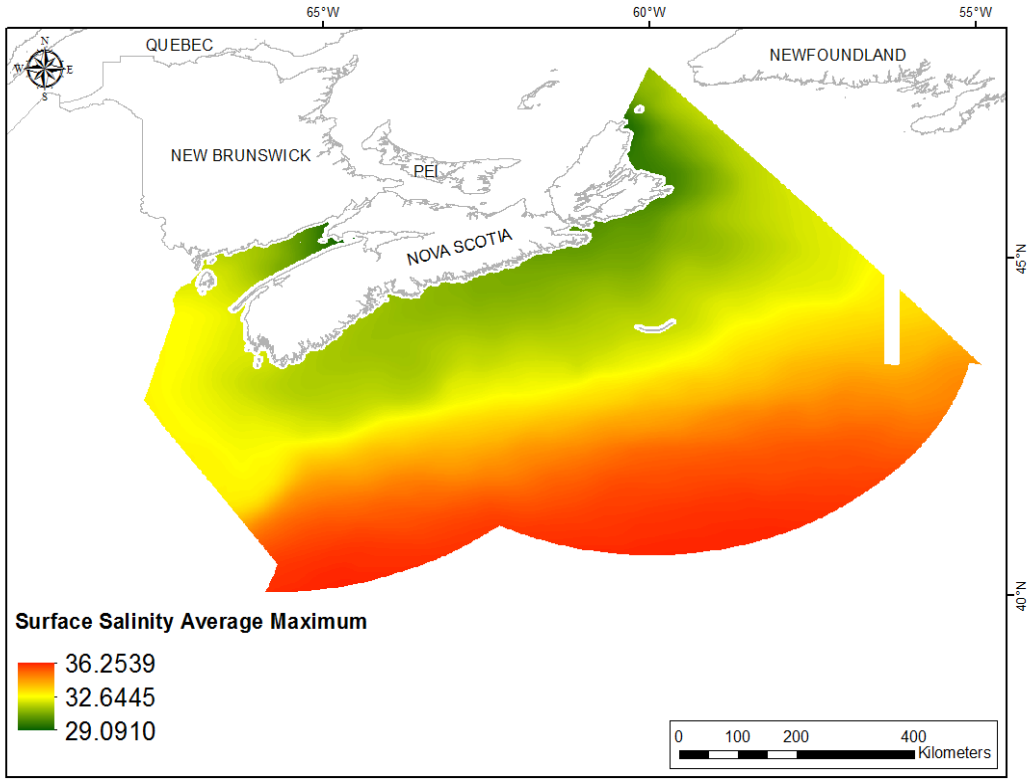

Fig. 140. Interpolated prediction surface of Surface Salinity Average Maximum.

Surface Salinity Average Range

This variable displayed a right-skewed, leptokurtic distribution prior to interpolation (Table 57, Fig. 141). The data were higher than predicted by a normal distribution at low and high values and slightly lower than predicted at mid-range values (Fig. 142). The areas of under- and over-prediction showed some spatial cohesion over the study extent (Fig. 142).

The semivariogram showed autocorrelation present in the data (Fig. 143). There was an excellent fit between measured and predicted values, particularly in the lower range (Fig. 143). However, the model showed poor cross-validation statistics (Table 58) with a standardized root mean square error greater than 1, indicating that variability in the predictions has been underestimated. The error map showed high error along the edges of the study extent (Fig. 144). The kriged surface is presented in Fig. 145.

Table 57. Distributional properties of Surface Salinity Average Range.

Property	Value
Number of Observations	1160
Minimum	1.031
Maximum	5.009
Mean	1.870
Median	1.730
Standard Deviation	0.484
Skewness	0.994
Kurtosis	4.776

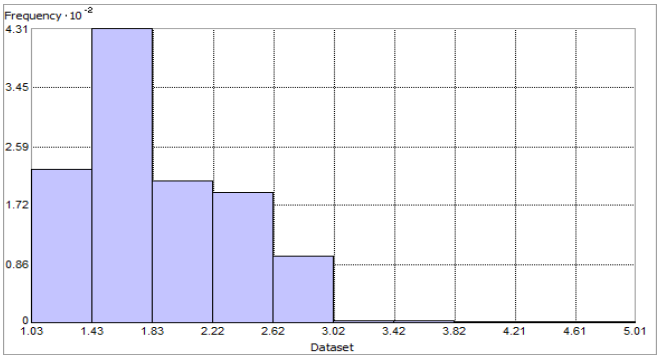

Fig. 141. Distribution of Surface Salinity Average Range. Histogram was illustrated using 10 bins. Y axis is shown at 10^{-2}.

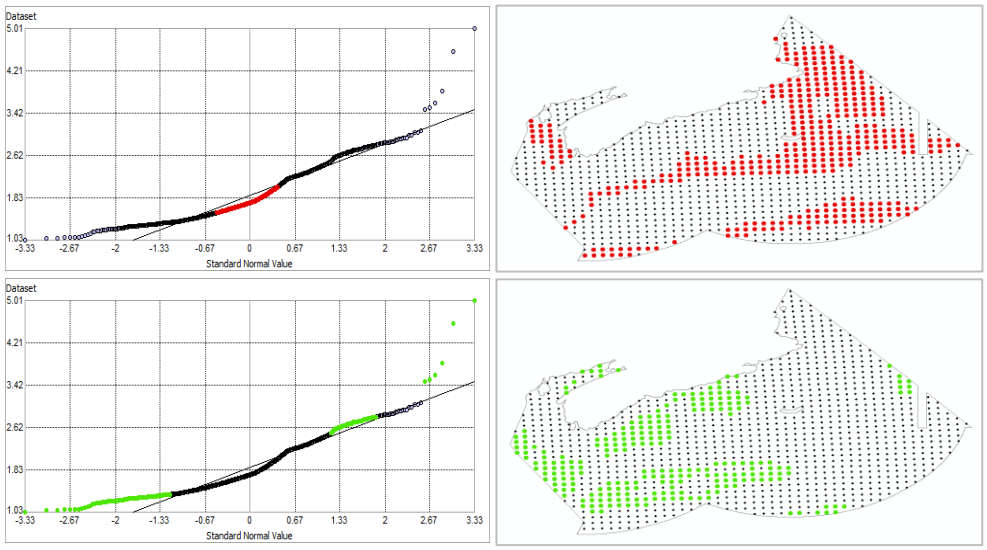

Fig. 142. Normal Q-Q plot for data values of Surface Salinity Average Range. Points falling under (upper panel) and over (bottom panel) the reference line are mapped.

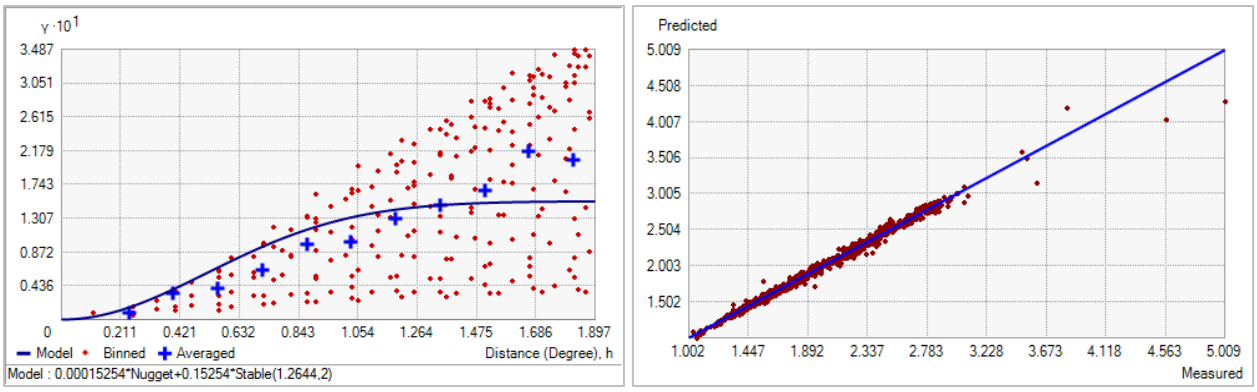

Fig. 143. Left panel: Semivariogram of Surface Salinity Average Range. Binned values are shown as red dots; average points are shown as blue crosses; the model fit to the averaged values is shown as a blue line. Lag size: 0.168 degrees; number of lags: 12; Parameter: 2; Range: 1.264 degrees; Partial Sill: 0.153. Right panel: Scatterplot of predicted values versus observed values for the model of Surface Salinity Average Range.

Table 58. Results of cross-validation of the kriged model for Surface Salinity Average Range.

Prediction error	**Value**
Number of Observations	1160
Overall Mean Error	-7.544×10^{-4}
Root Mean Square Prediction Error	0.048
Standardized Mean	7.539×10^{-3}
Standardized Root Mean Square Prediction Error	2.108
Average Standard Error	0.020

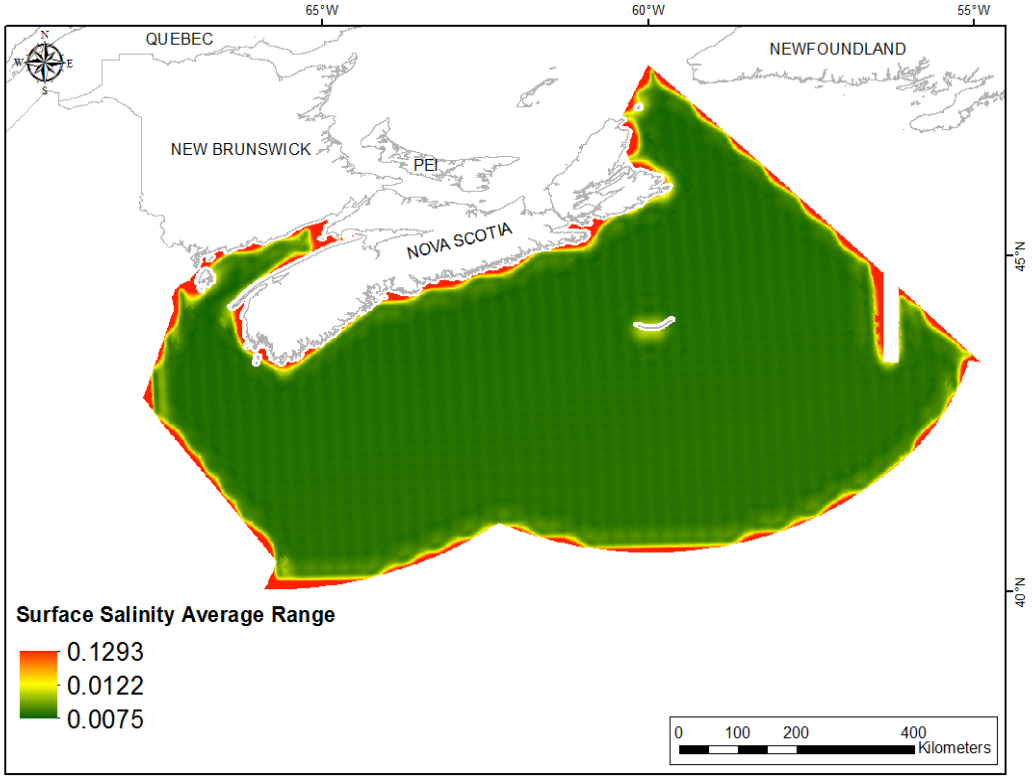

Fig. 144. Prediction standard error surface of Surface Salinity Average Range.

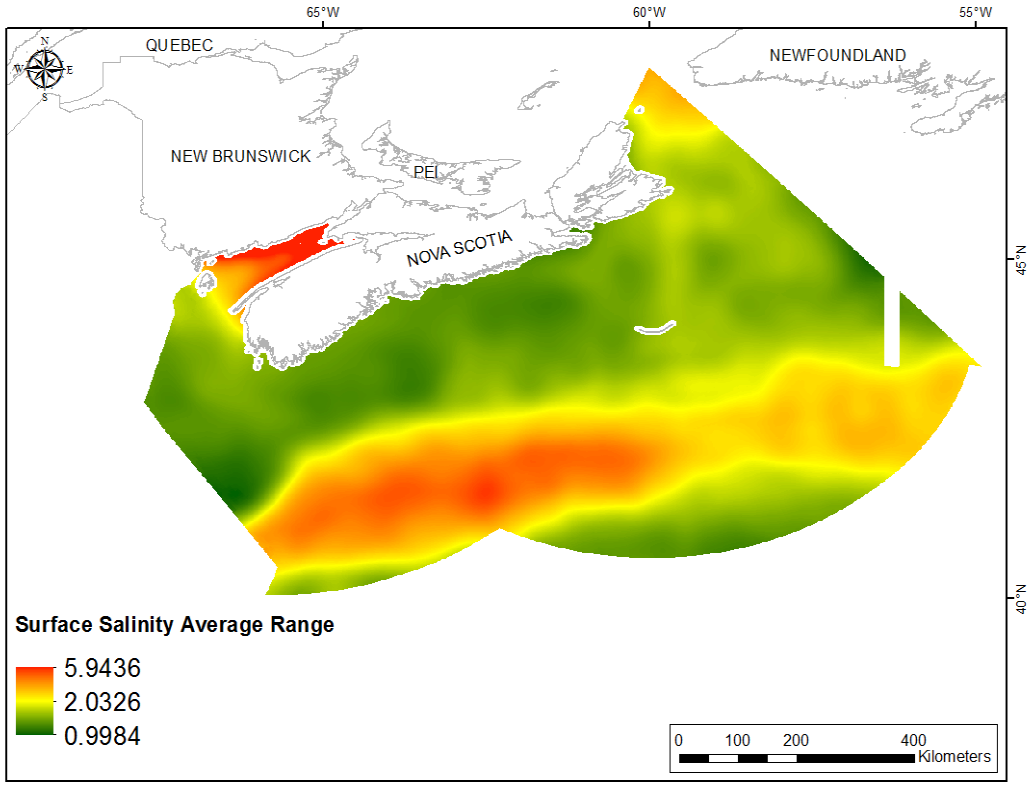

Fig. 145. Interpolated prediction surface of Surface Salinity Average Range.

Current Speed

Currents move water and heat around in the world's oceans and influence the chemical composition of the water column. Upwelling and downwelling currents strongly influence the distribution and abundance of marine life. Similarly, current speed determines the rate at which food particles reach benthic species through both vertical and horizontal transmission and consequently influences the distribution of filter-feeding species. Upwelling currents enhance productivity in the water column, while downwelling currents bring food and oxygen to the sea floor. Organisms also use currents for active and passive transport for migration and dispersal. Current speed can influence morphology, especially of marine macrophytes.

Bottom Current Mean

This variable displayed a right-skewed, leptokurtic distribution prior to interpolation (Table 59, Fig. 146). The data were higher than predicted by a normal distribution at both tails (Fig. 147). Mid-range values were lower than the reference line. The areas of over- and under-prediction showed little spatial pattern with both error types distributed throughout the study extent (Fig. 147).

The semivariogram showed moderate autocorrelation present in the data (Fig. 148). There was a fair fit between measured and predicted values (Fig. 148), and the model showed good cross-validation statistics (Table 60) indicating that it was good at prediction. The error map showed high error along the edges of the study extent (Fig. 149). The kriged surface is presented in Fig. 150.

Table 59. Distributional properties of Bottom Current Mean (m s^{-1}).

Property	Value
Number of Observations	1143
Minimum	0.002
Maximum	0.135
Mean	0.026
Median	0.020
Standard Deviation	0.021
Skewness	2.337
Kurtosis	9.179

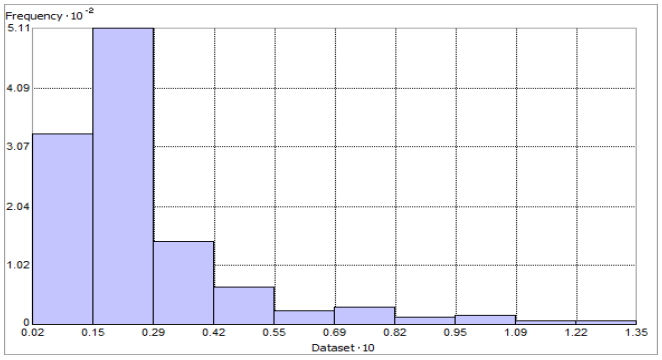

Fig. 146. Distribution of Bottom Current Mean (m s^{-1}). Histogram was illustrated using 10 bins. X axis is shown at 10; Y axis is shown at 10^{-2}.

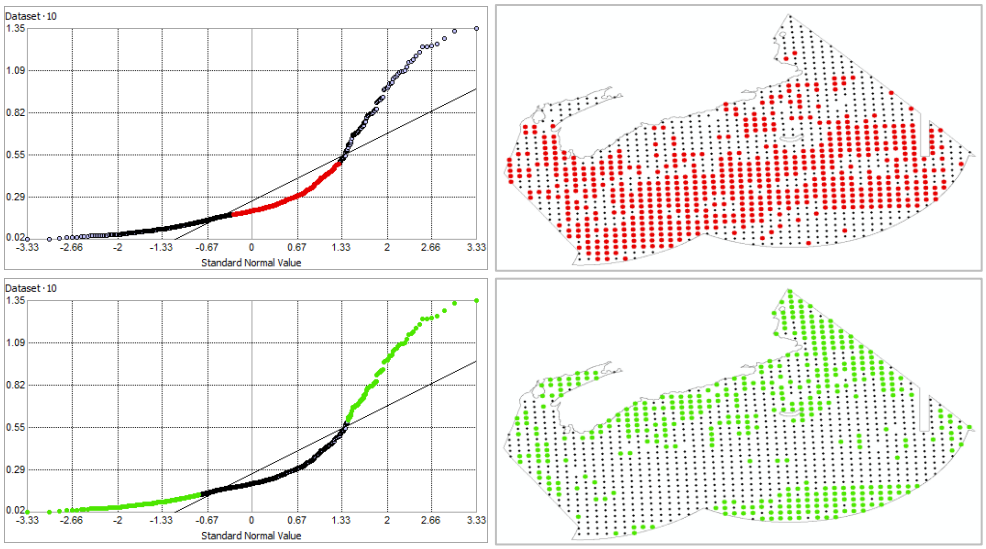

Fig. 147. Normal Q-Q plot for data values of Bottom Current Mean (m s^{-1}). Points falling under (upper panel) and over (bottom panel) the reference line are mapped.

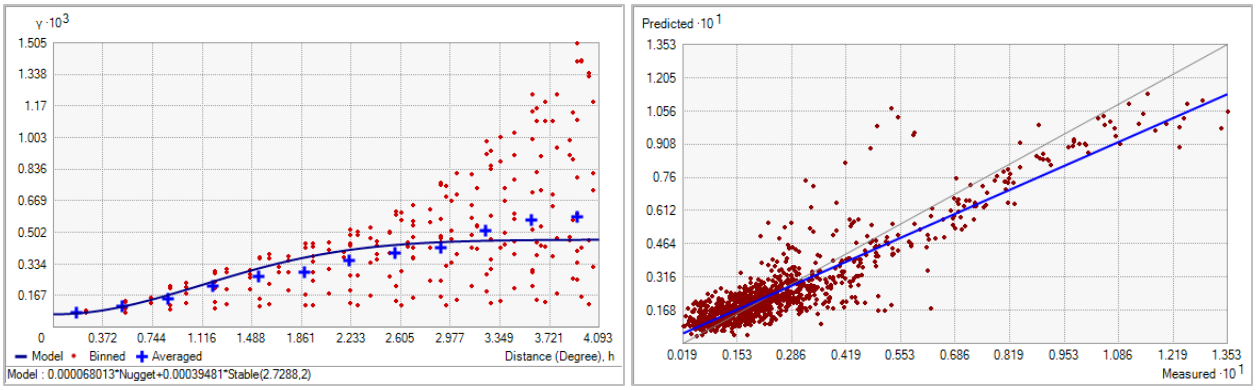

Fig. 148. Left panel: Semivariogram of Bottom Current Mean (m s^{-1}). Binned values are shown as red dots; average points are shown as blue crosses; the model fit to the averaged values is shown as a blue line. Lag size: 0.341 degrees; number of lags: 12; Parameter: 2; Range: 2.729 degrees; Partial Sill: 3.948 x 10^{-4}. Right panel: Scatterplot of predicted values versus observed values for the model of Bottom Current Mean (m s^{-1}).

Table 60. Results of cross-validation of the kriged model for Bottom Current Mean (m s^{-1}).

Prediction error	**Value**
Number of Observations	1143
Overall Mean Error	9.819 x 10^{-5}
Root Mean Square Prediction Error	8.853 x 10^{-3}
Standardized Mean	0.013
Standardized Root Mean Square Prediction Error	1.019
Average Standard Error	8.659 x 10^{-3}

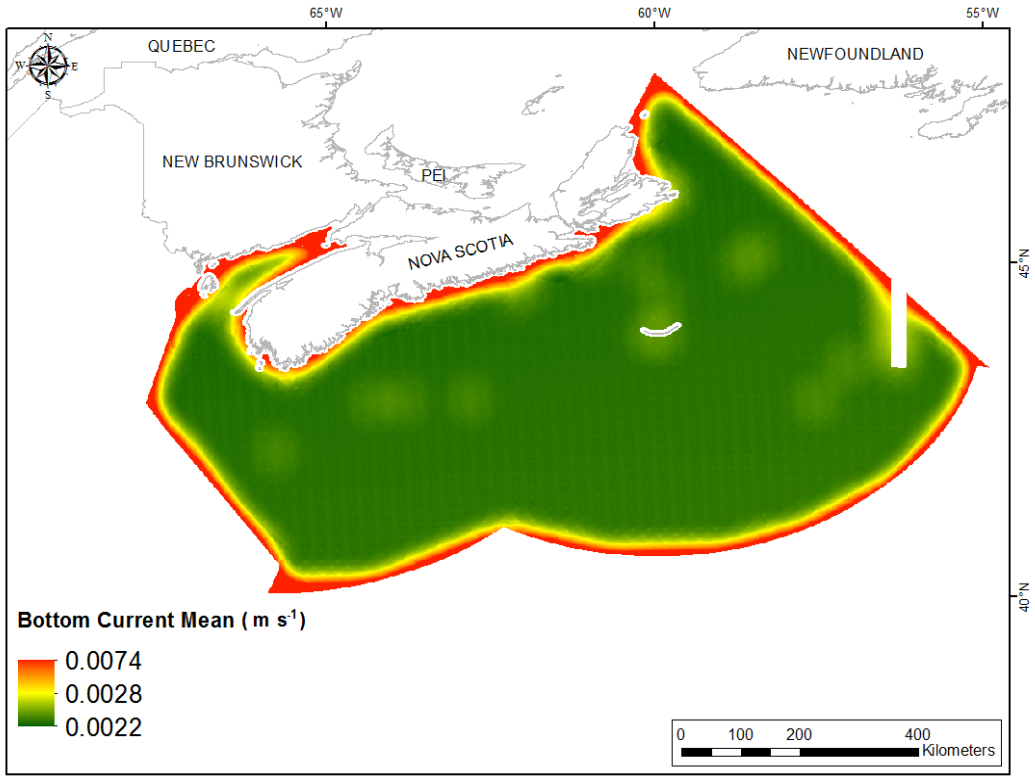

Fig. 149. Prediction standard error surface of Bottom Current Mean (m s^{-1}).

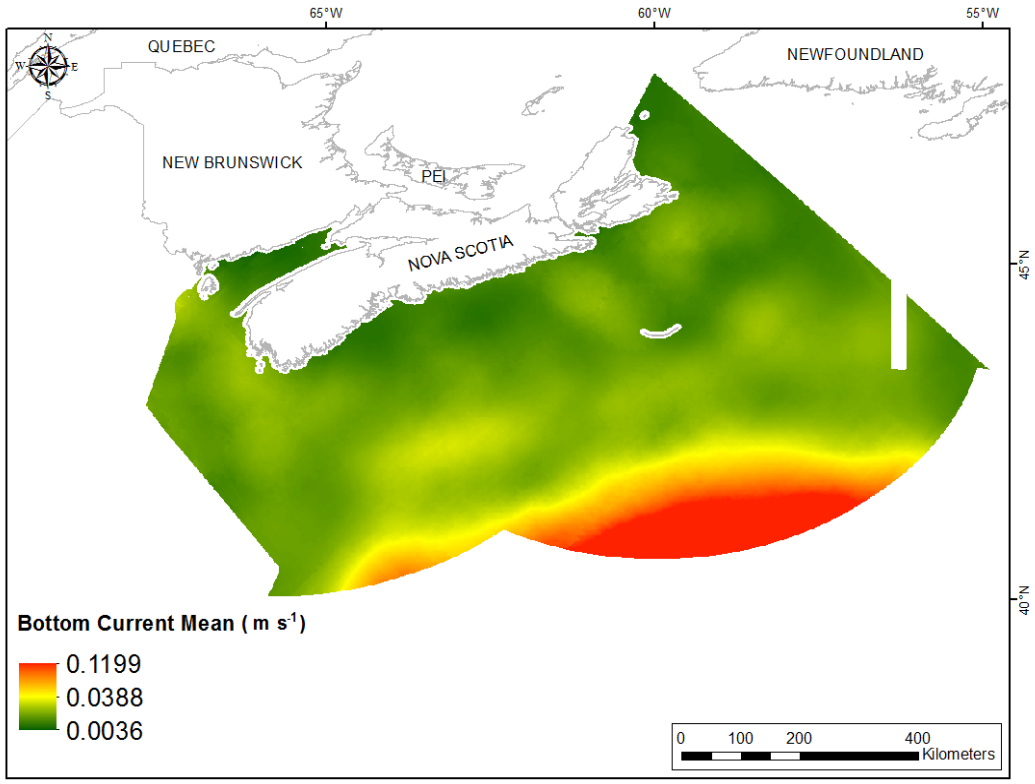

Fig. 150. Interpolated prediction surface of Bottom Current Mean (m s^{-1}).

Bottom Current Minimum

This variable displayed a right-skewed, highly leptokurtic distribution and outlying data in the upper range (Table 61, Fig. 151). The data were higher than predicted by a normal distribution at both tails and lower than predicted at mid-range values (Fig. 152). The areas of over- and under-prediction did not show a strong spatial pattern with both error types distributed throughout the study extent (Fig. 152).

The semivariogram showed weak autocorrelation present in the data (Fig. 153). The fit between measured and predicted values was very poor (Fig. 153). Nevertheless, the model showed good cross-validation statistics (Table 62) indicating that it was good at prediction. The error map showed high error along the edges of the study extent (Fig. 154). The kriged surface is presented in Fig. 155.

Table 61. Distributional properties of Bottom Current Minimum (m s^{-1}).

Property	Value
Number of Observations	1143
Minimum	1.000 x 10^{-6}
Maximum	0.015
Mean	8.296 x 10^{-4}
Median	3.073 x 10^{-4}
Standard Deviation	1.482 x 10^{-3}
Skewness	4.273
Kurtosis	27.666

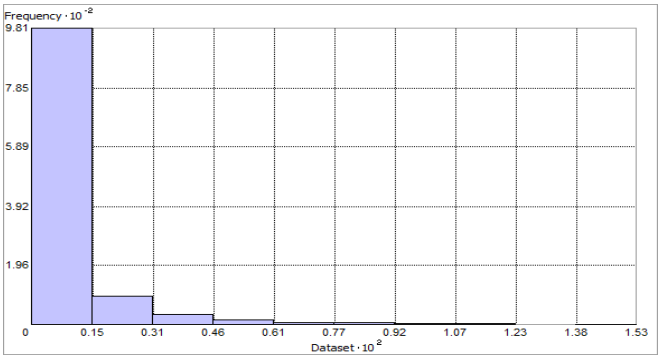

Fig. 151. Distribution of Bottom Current Minimum (m s^{-1}). Histogram was illustrated using 10 bins. X axis shown at 10^{2}; Y axis is shown at 10^{-2}.

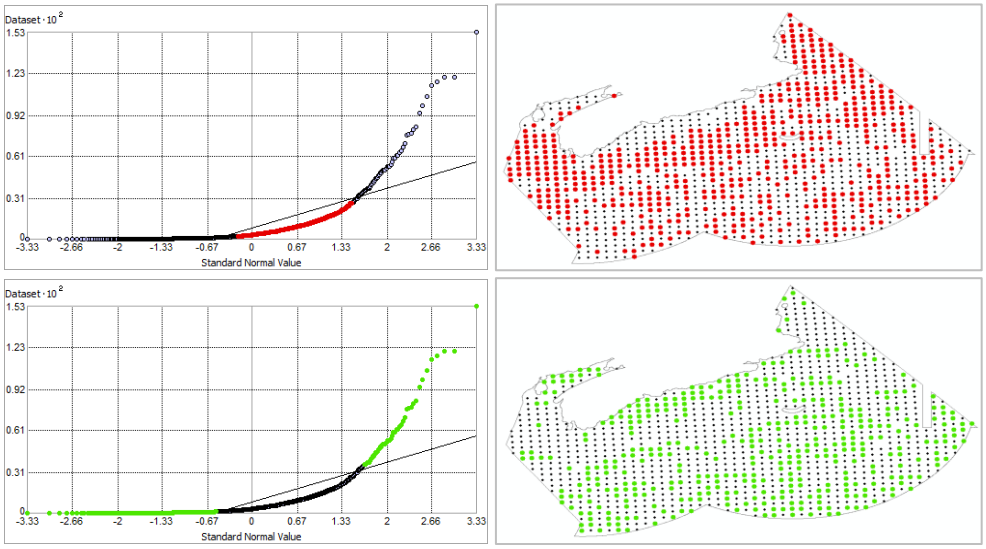

Fig. 152. Normal Q-Q plot for data values of Bottom Current Minimum (m s^{-1}). Points falling under (upper panel) and over (bottom panel) the reference line are mapped.

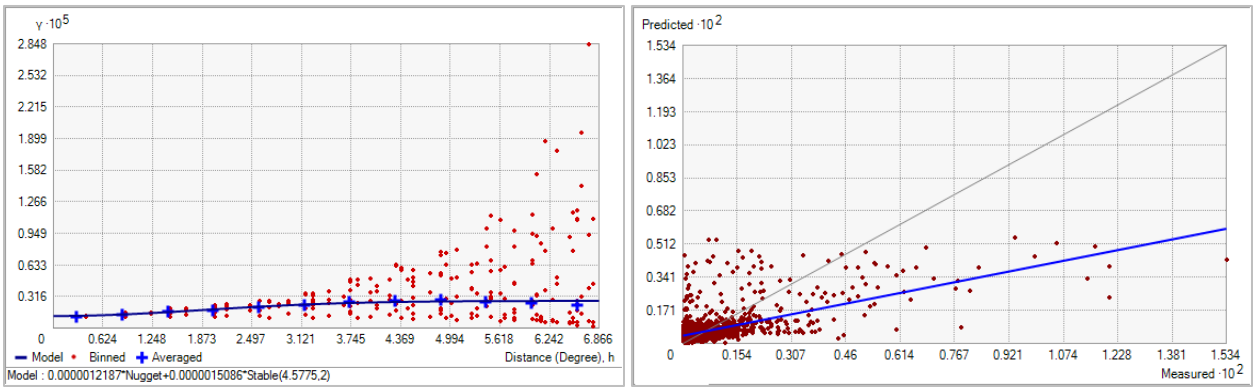

Fig. 153. Left panel: Semivariogram of Bottom Current Minimum (m s^{-1}). Binned values are shown as red dots; average points are shown as blue crosses; the model fit to the averaged values is shown as a blue line. Lag size: 0.572 degrees; number of lags: 12; Parameter: 2; Range: 4.577 degrees; Partial Sill: 1.509 x 10^{-6}. Right panel: Scatterplot of predicted values versus observed values for the model of Bottom Current Minimum (m s^{-1}).

Table 62. Results of cross-validation of the kriged model for Bottom Current Minimum (m s^{-1}).

Prediction error	**Value**
Number of Observations	1143
Overall Mean Error	-7.284 x 10^{-6}
Root Mean Square Prediction Error	1.170 x 10^{-3}
Standardized Mean	-6.106 x 10^{-3}
Standardized Root Mean Square Prediction Error	1.027
Average Standard Error	1.135 x 10^{-3}

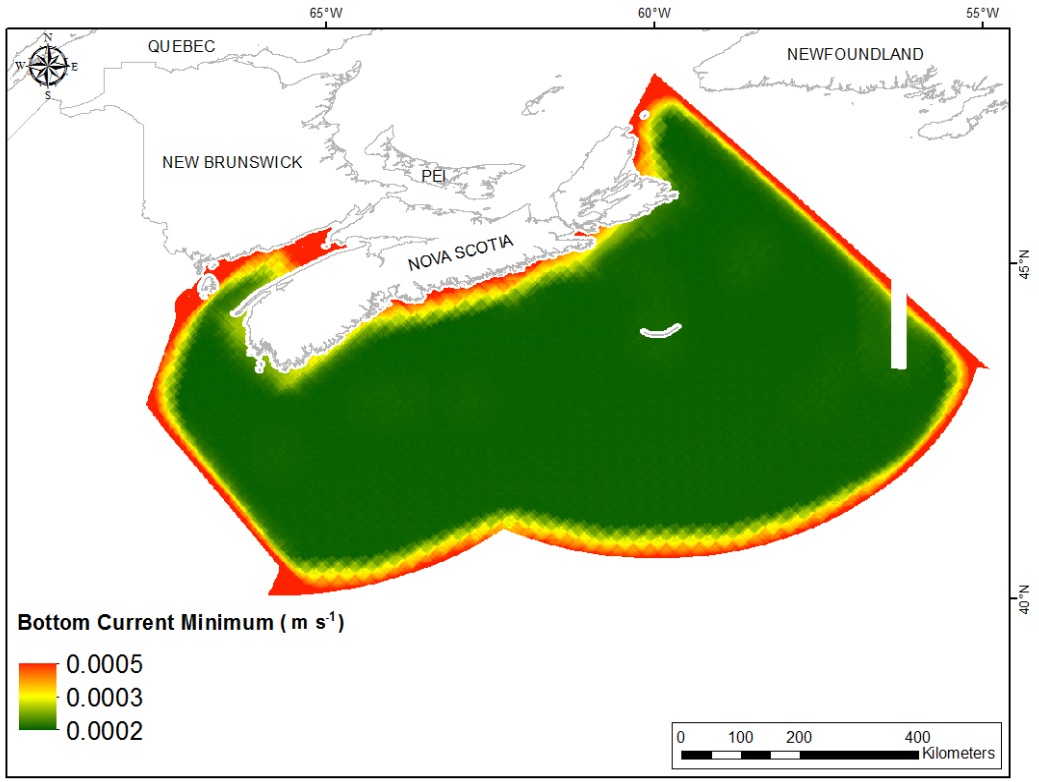

Fig. 154. Prediction standard error surface of Bottom Current Minimum (m s^{-1}).

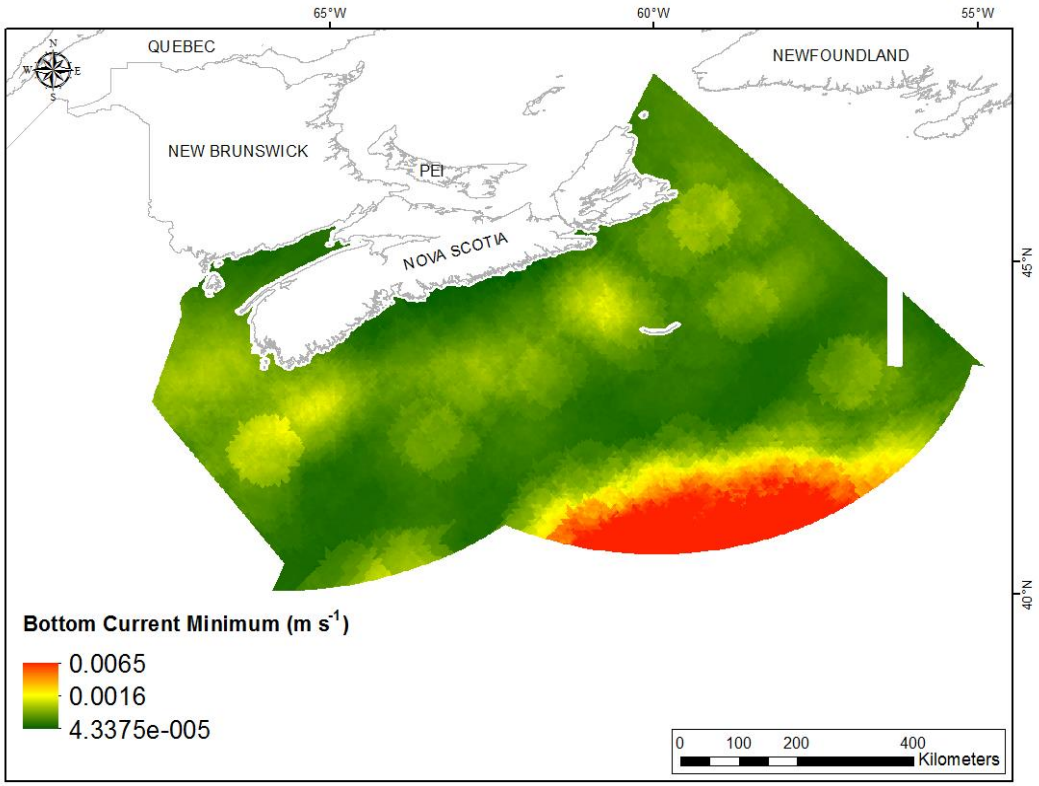

Fig. 155. Interpolated prediction surface of Bottom Current Minimum (m s^{-1}).

Bottom Current Maximum

This variable displayed a right-skewed, leptokurtic distribution prior to interpolation (Table 63, Fig. 156). The data were higher than predicted by a normal distribution at both tails, with mid-range values located below the reference line (Fig. 157). The areas of over- and under-prediction did not show a strong spatial pattern with both error types distributed through the study extent (Fig. 157).

The semivariogram showed moderate autocorrelation present in the data (Fig. 158). There was a poor fit between the measured and predicted values (Fig. 158). Nevertheless, the model showed good cross-validation statistics (Table 64) indicating that it was good at prediction. The error map showed high error along the edges of the study extent (Fig. 159). The kriged surface is presented in Fig. 160.

Table 63. Distributional properties of Bottom Current Maximum (m s^{-1}).

Property	Value
Number of Observations	1143
Minimum	0.006
Maximum	0.440
Mean	0.088
Median	0.066
Standard Deviation	0.071
Skewness	2.106
Kurtosis	7.480

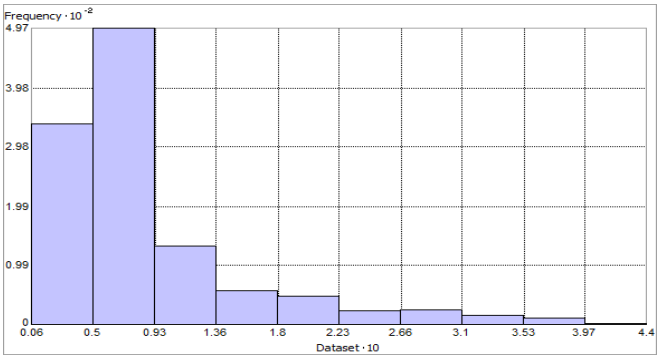

Fig. 156. Distribution of Bottom Current Maximum (m s^{-1}). Histogram was illustrated using 10 bins. X axis is shown at 10; Y axis is shown at 10^{-2}.

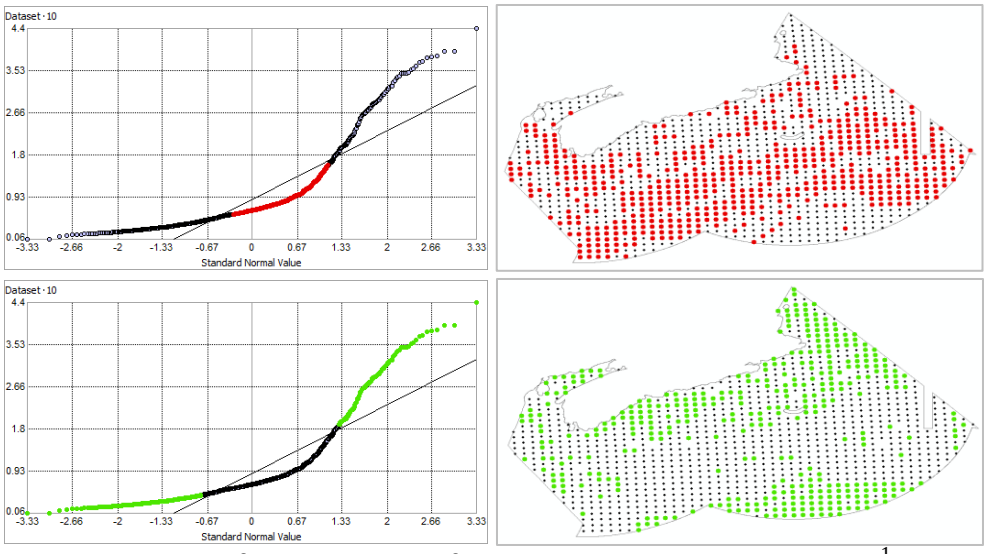

Fig. 157. Normal Q-Q plot for data values of Bottom Current Maximum (m s^{-1}). Points falling under (upper panel) and over (bottom panel) the reference line are mapped.

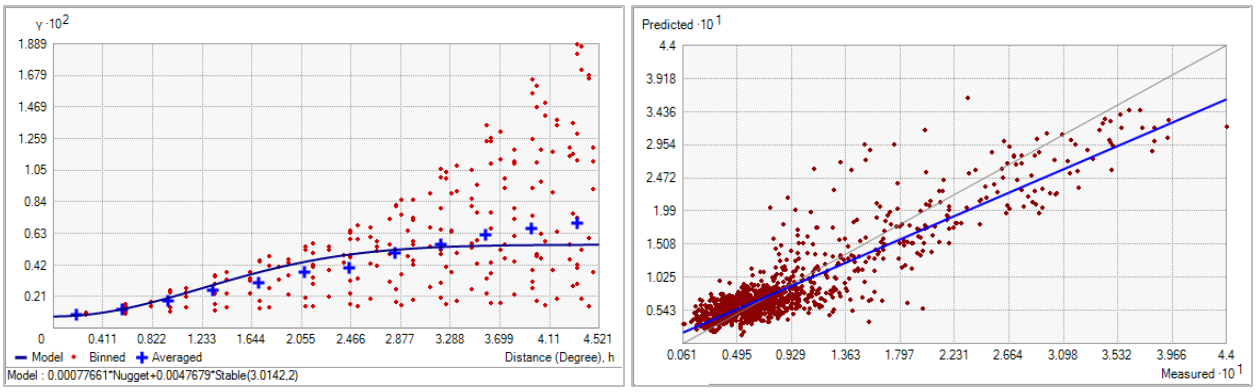

Fig. 158. Left panel: Semivariogram of Bottom Current Maximum (m s^{-1}). Binned values are shown as red dots; average points are shown as blue crosses; the model fit to the averaged values is shown as a blue line. Lag size: 0.377 degrees; number of lags: 12; Parameter: 2; Range: 3.014 degrees; Partial Sill: 0.005. Right panel: Scatterplot of predicted values versus observed values for the model of Bottom Current Maximum (m s^{-1}).

Table 64. Results of cross-validation of the kriged model for Bottom Current Maximum (m s^{-1}).

Prediction error	**Value**
Number of Observations	1143
Overall Mean Error	3.073×10^{-4}
Root Mean Square Prediction Error	0.030
Standardized Mean	0.012
Standardized Root Mean Square Prediction Error	1.032
Average Standard Error	0.029

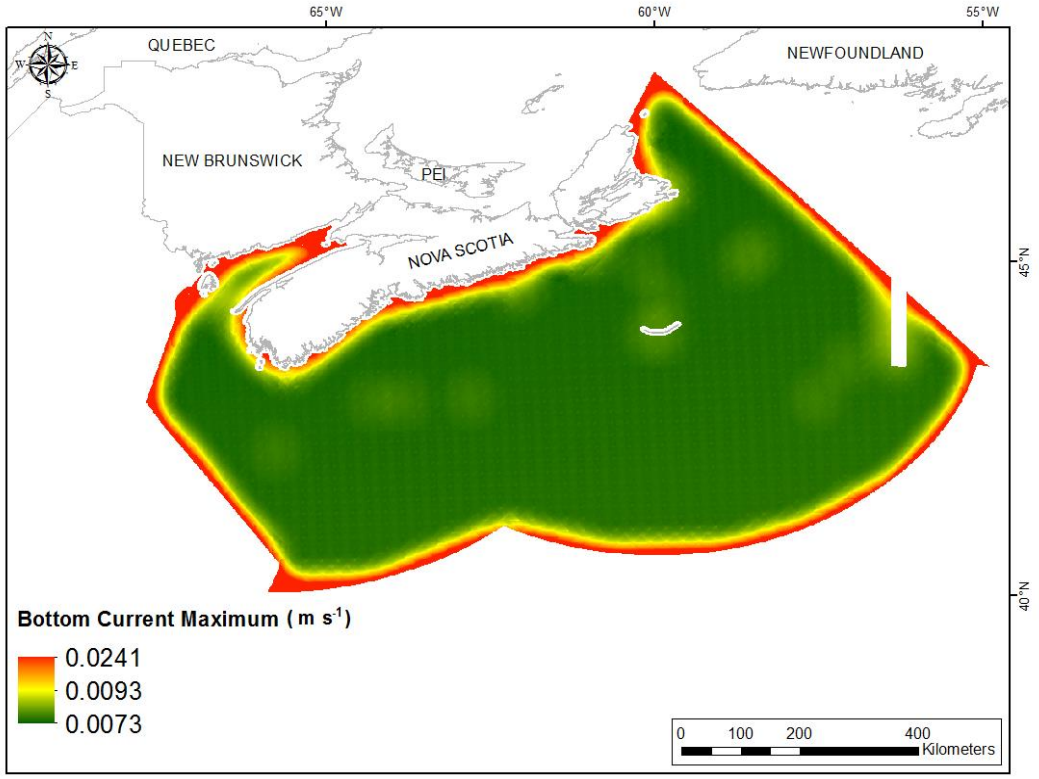

Fig. 159. Prediction standard error surface of Bottom Current Maximum (m s^{-1}).

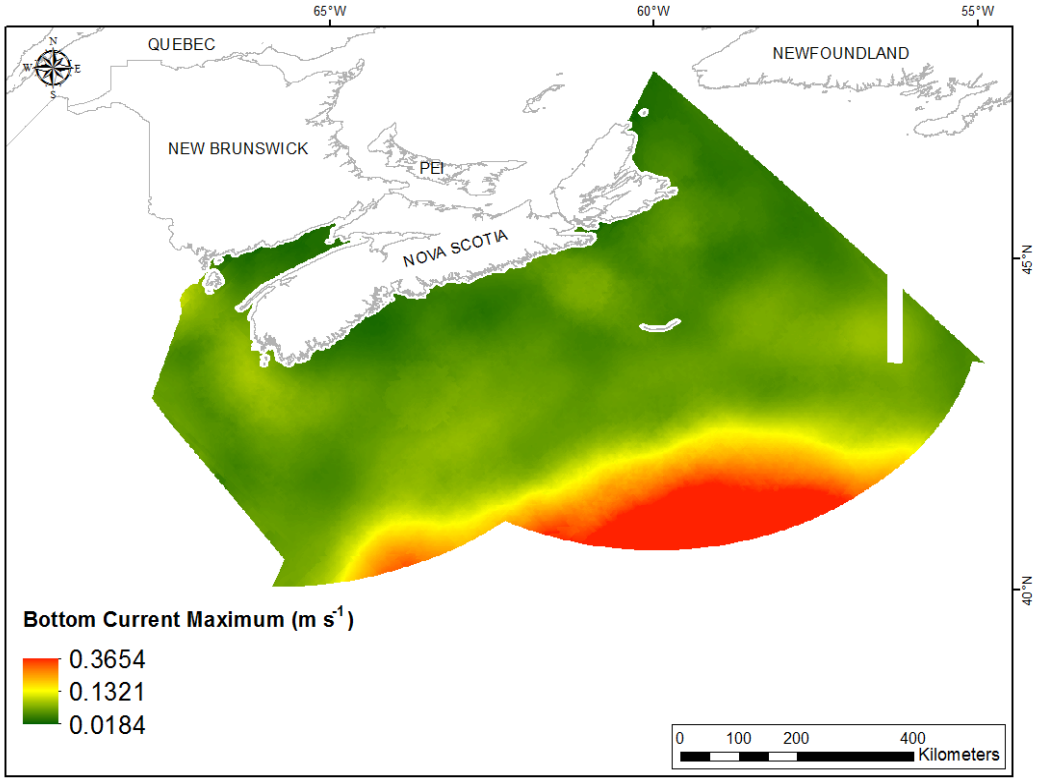

Fig. 160. Interpolated prediction surface of Bottom Current Maximum (m s^{-1}).

Bottom Current Range

This variable displayed a right-skewed, leptokurtic distribution prior to interpolation (Table 65, Fig. 161). The data were higher than predicted by a normal distribution at both tails, with mid-range values located below the reference line (Fig. 162). The areas of over- and under-prediction did not show a strong spatial pattern with both error types distributed through the study extent (Fig. 162).

The semivariogram showed little autocorrelation present in the data (Fig. 163). There was a poor fit between the measured and predicted values. Nevertheless, the model showed good cross-validation statistics (Table 66) indicating that it was good at prediction. The error map showed high error along the edges of the study extent (Fig. 164). The kriged surface is presented in Fig. 165.

Table 65. Distributional properties of Bottom Current Range (m s^{-1}).

Property	Value
Number of Observations	1143
Minimum	0.006
Maximum	0.439
Mean	0.087
Median	0.065
Standard Deviation	0.070
Skewness	2.089
Kurtosis	7.400

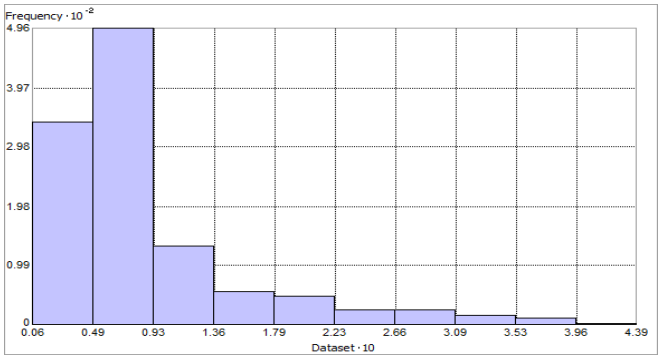

Fig. 161. Distribution of Bottom Current Range (m s^{-1}). Histogram was illustrated using 10 bins. X axis is shown at 10; Y axis is shown at 10^{-2}.

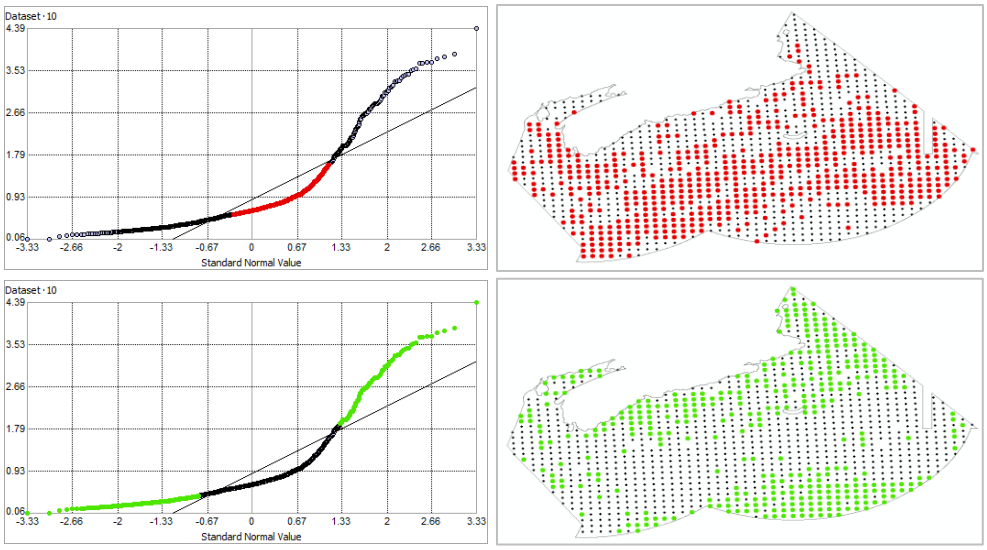

Fig. 162. Normal Q-Q plot for data values of Bottom Current Range (m s^{-1}). Points falling under (upper panel) and over (bottom panel) the reference line are mapped.

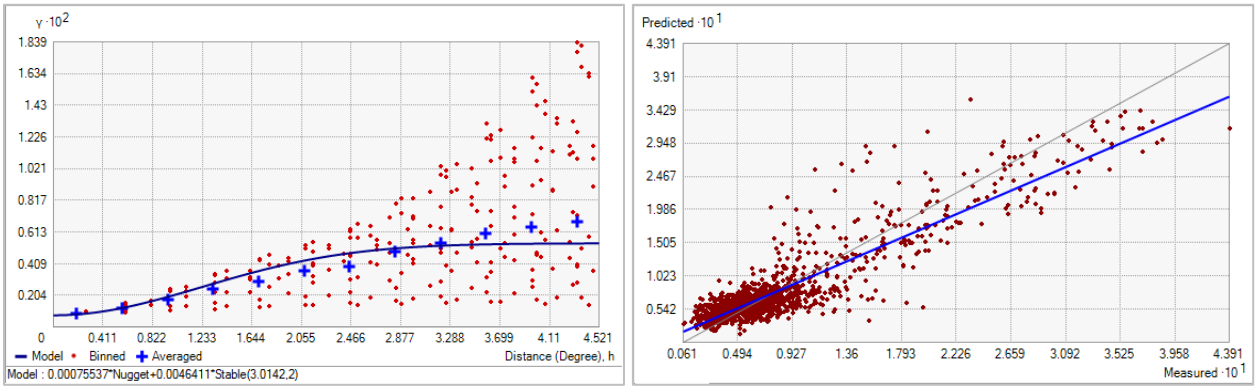

Fig. 163. Left panel: Semivariogram of Bottom Current Range (m s^{-1}). Binned values are shown as red dots; average points are shown as blue crosses; the model fit to the averaged values is shown as a blue line. Lag size: 0.377 degrees; number of lags: 12; Parameter: 2; Range: 3.014 degrees; Partial Sill: 0.005. Right panel: Scatterplot of predicted values versus observed values for the model of Bottom Current Range (m s^{-1}).

Table 66. Results of cross-validation of the kriged model for Bottom Current Range (m s^{-1}).

Prediction error	**Value**
Number of Observations	1143
Overall Mean Error	3.040×10^{-4}
Root Mean Square Prediction Error	0.030
Standardized Mean	0.012
Standardized Root Mean Square Prediction Error	1.033
Average Standard Error	0.029

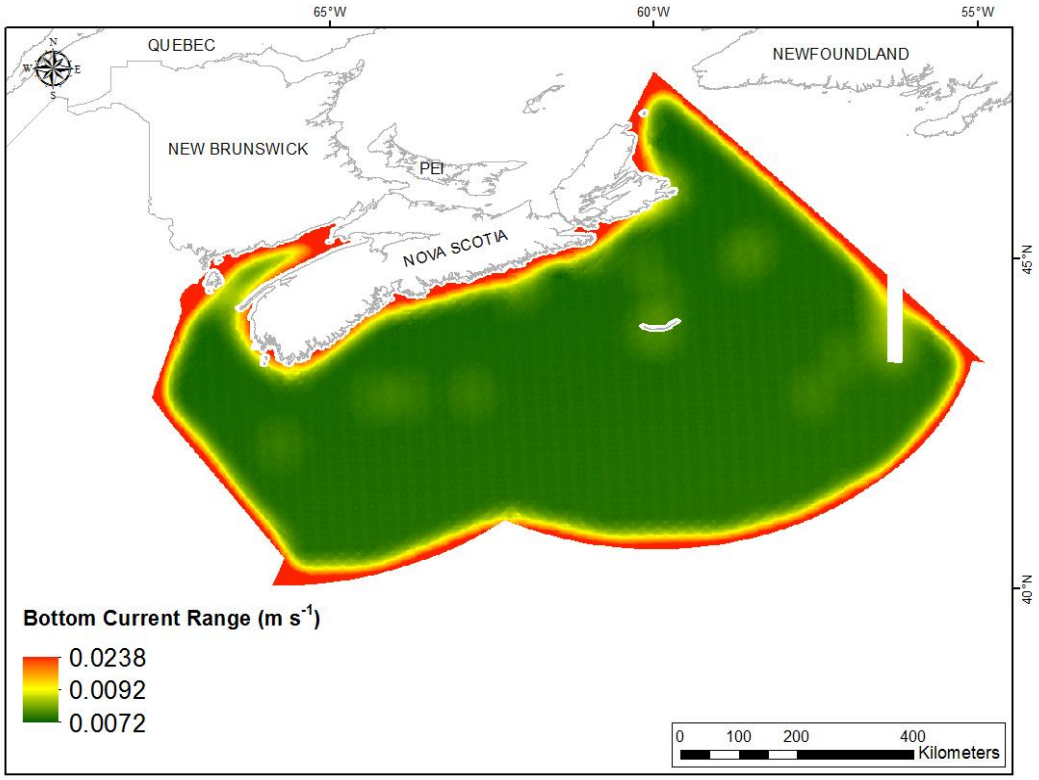

Fig. 164. Prediction standard error surface of Bottom Current Range (m s^{-1}).

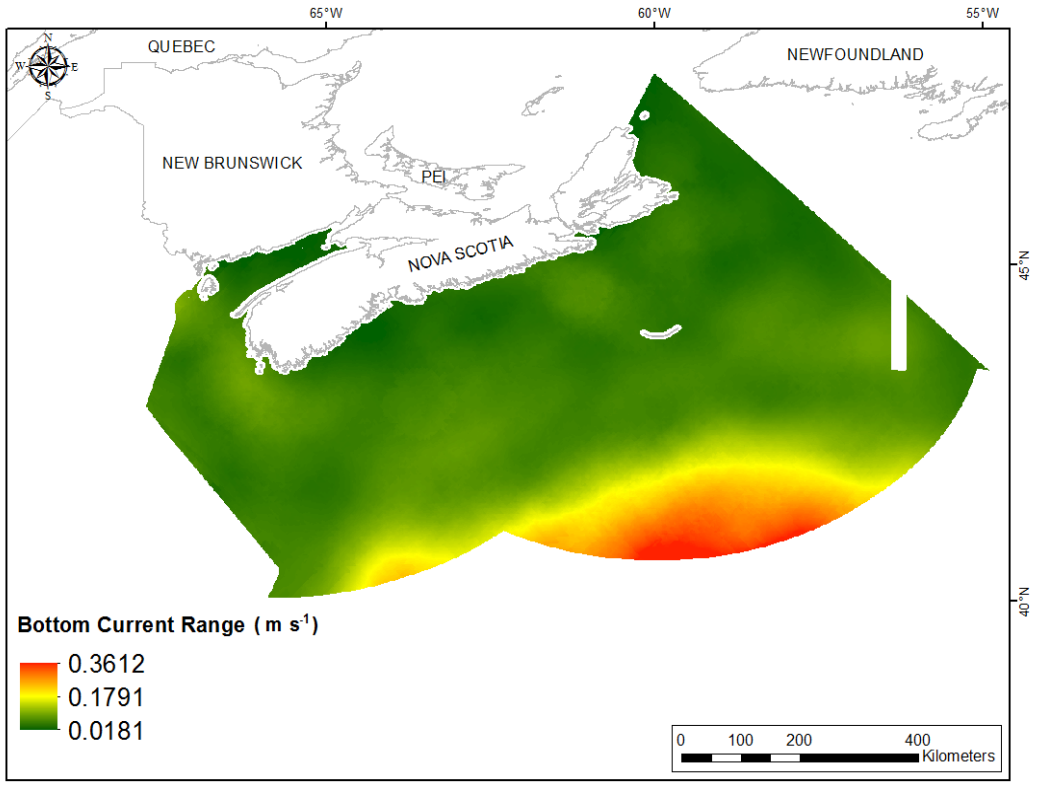

Fig. 165. Interpolated prediction surface of Bottom Current Range (m s^{-1}).

Bottom Current Average Minimum

This variable displayed a right-skewed, leptokurtic distribution prior to interpolation (Table 67, Fig. 166). The data were higher than predicted by a normal distribution at both tails with mid-range values located below the reference line (Fig. 167). The areas of over- and under-prediction did not show a strong spatial pattern with both error types distributed across the study extent (Fig. 167).

The semivariogram showed little autocorrelation present in the data and the model showed poor fit between measured and predicted values (Fig. 168). Nevertheless, the model showed good cross-validation statistics (Table 68) indicating that it was good at prediction. The error map showed high error along the edges of the study extent (Fig. 169). The kriged surface is presented in Fig. 170.

Table 67. Distributional properties of Bottom Current Average Minimum (m s^{-1}).

Property	Value
Number of Observations	1143
Minimum	2.300×10^{-4}
Maximum	0.043
Mean	5.477×10^{-3}
Median	3.841×10^{-3}
Standard Deviation	5.319×10^{-3}
Skewness	2.670
Kurtosis	12.276

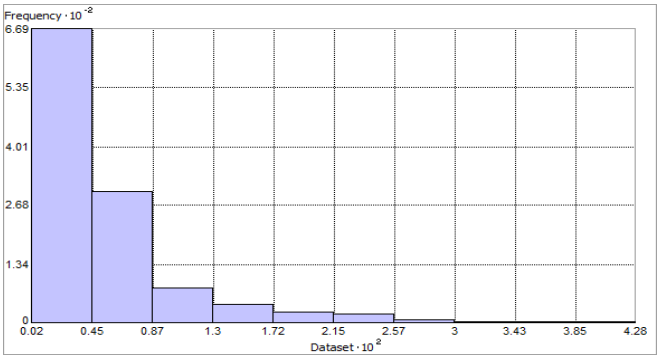

Fig. 166. Distribution of Bottom Current Average Minimum (m s^{-1}). Histogram was illustrated using 10 bins. X axis is shown at 10^2; Y axis is shown at 10^{-2}.

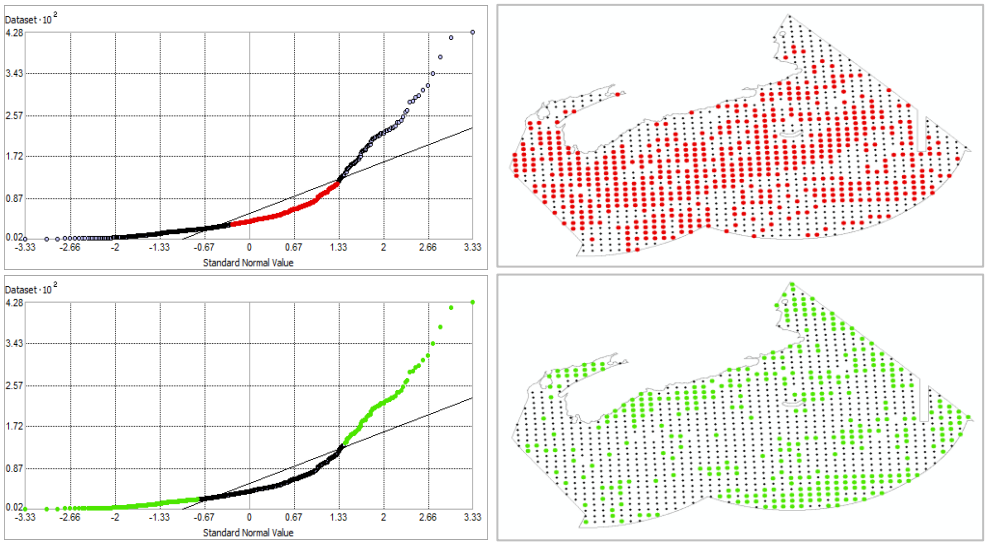

Fig. 167. Normal Q-Q plot for data values of Bottom Current Average Minimum (m s^{-1}). Points falling under (upper panel) and over (bottom panel) the reference line are mapped.

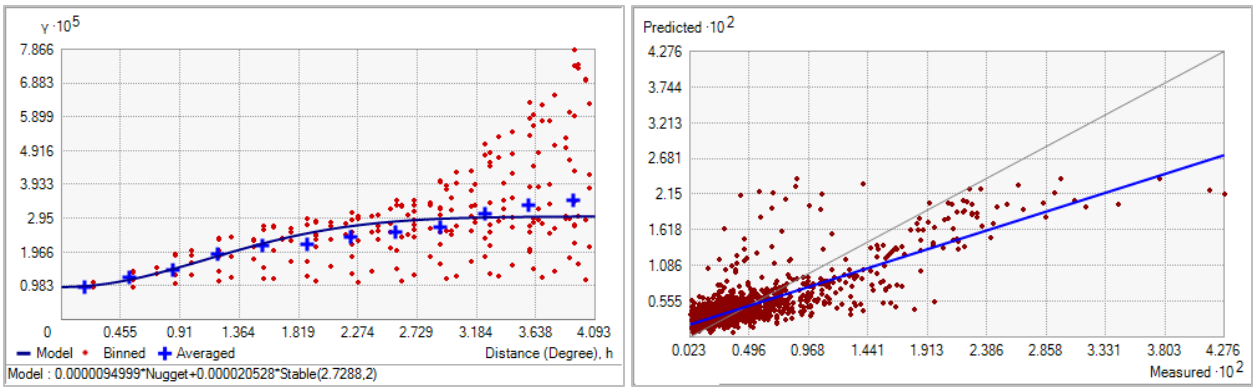

Fig. 168. Left panel: Semivariogram of Bottom Current Average Minimum (m s^{-1}). Binned values are shown as red dots; average points are shown as blue crosses; the model fit to the averaged values is shown as a blue line. Lag size: 0.341 degrees; number of lags: 12; Parameter: 2; Range: 2.729 degrees; Partial Sill: 2.053 x 10^{-5}. Right panel: Scatterplot of predicted values versus observed values for the model of Bottom Current Average Minimum (m s^{-1}).

Table 68. Results of cross-validation of the kriged model for Bottom Current Average Minimum (m s^{-1}).

Prediction error	**Value**
Number of Observations	1143
Overall Mean Error	-3.809 x 10^{-6}
Root Mean Square Prediction Error	3.258 x 10^{-3}
Standardized Mean	-2.347 x 10^{-4}
Standardized Root Mean Square Prediction Error	1.014
Average Standard Error	3.198 x 10^{-3}

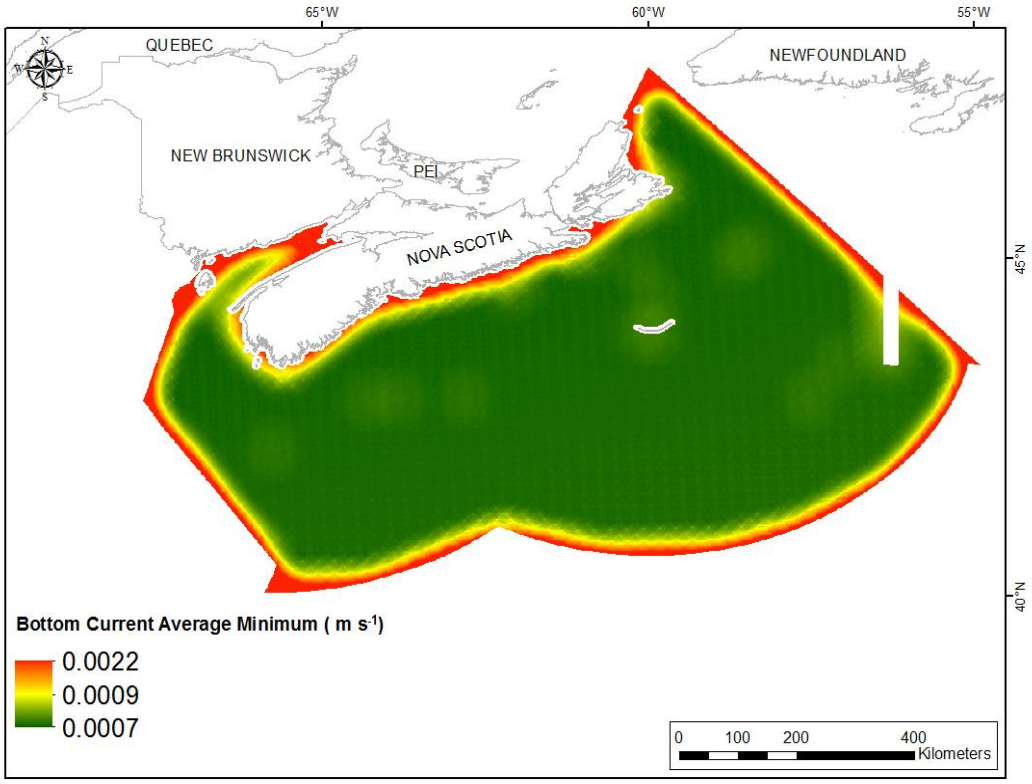

Fig. 169. Prediction standard error surface of Bottom Current Average Minimum (m s^{-1}).

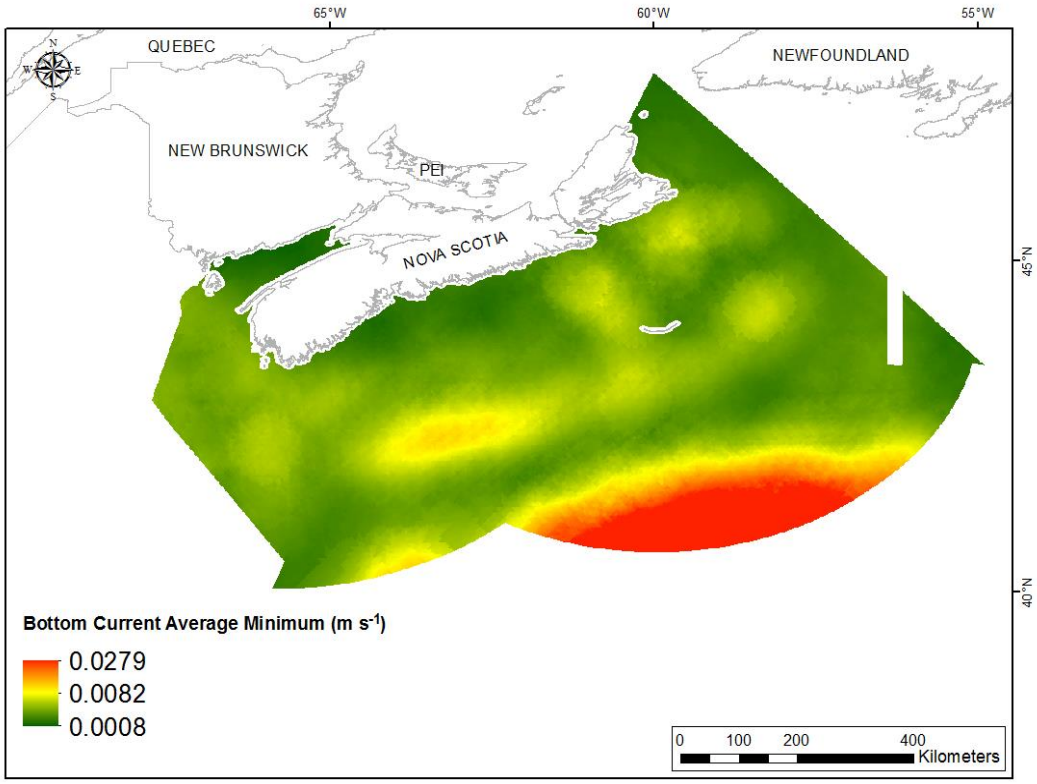

Fig. 170. Interpolated prediction surface of Bottom Current Average Minimum (m s^{-1}).

Bottom Current Average Maximum

This variable displayed a right-skewed, leptokurtic distribution prior to interpolation (Table 69, Fig. 171). The data were higher than predicted by a normal distribution at both tails and lower at mid-range values (Fig. 172). The areas of over- and under-prediction did not show a strong spatial pattern with both error types distributed across the study extent (Fig. 172).

The semivariogram showed little autocorrelation present in the data and the model showed poor fit between measured and predicted values (Fig. 173). Nevertheless, the model showed good cross-validation statistics (Table 70) indicating that it was good at prediction. The error map showed high error along the edges of the study extent (Fig. 174). The kriged surface is presented in Fig. 175.

Table 69. Distributional properties of Bottom Current Average Maximum (m s^{-1}).

Property	Value
Number of Observations	1143
Minimum	0.004
Maximum	0.267
Mean	0.056
Median	0.042
Standard Deviation	0.046
Skewness	2.188
Kurtosis	7.983

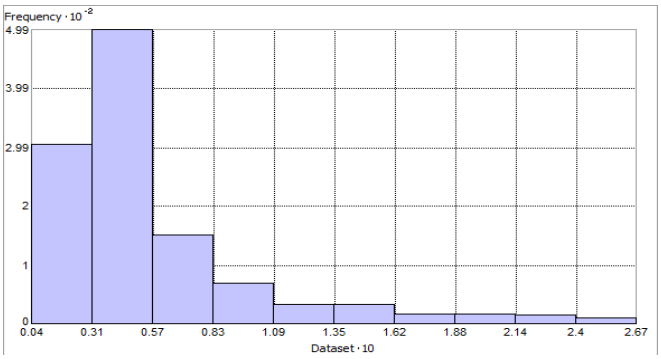

Fig. 171. Distribution of Bottom Current Average Maximum (m s^{-1}). Histogram was illustrated using 10 bins. X axis is shown at 10; Y axis is shown at 10^{-2}.

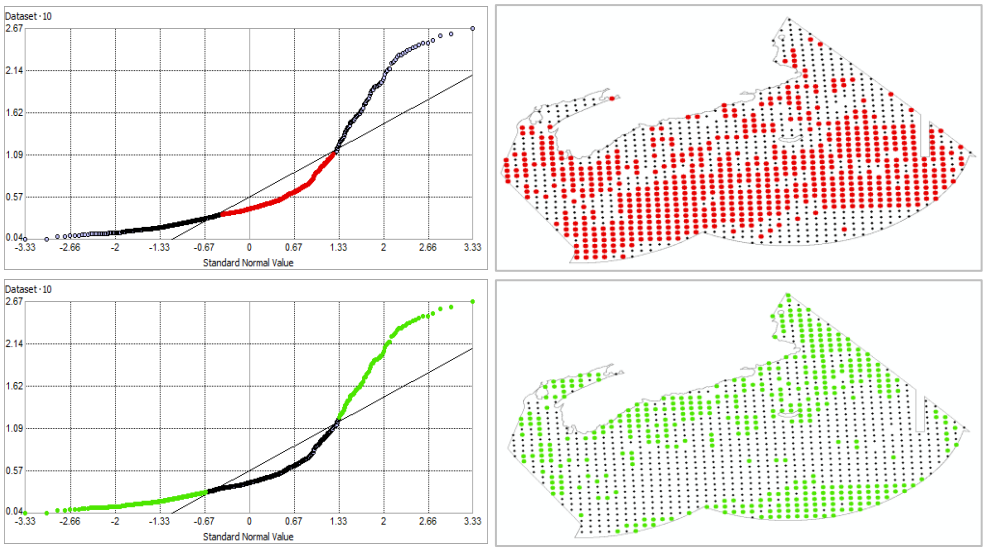

Fig. 172. Normal Q-Q plot for data values of Bottom Current Average Maximum (m s^{-1}). Points falling under (upper panel) and over (bottom panel) the reference line are mapped.

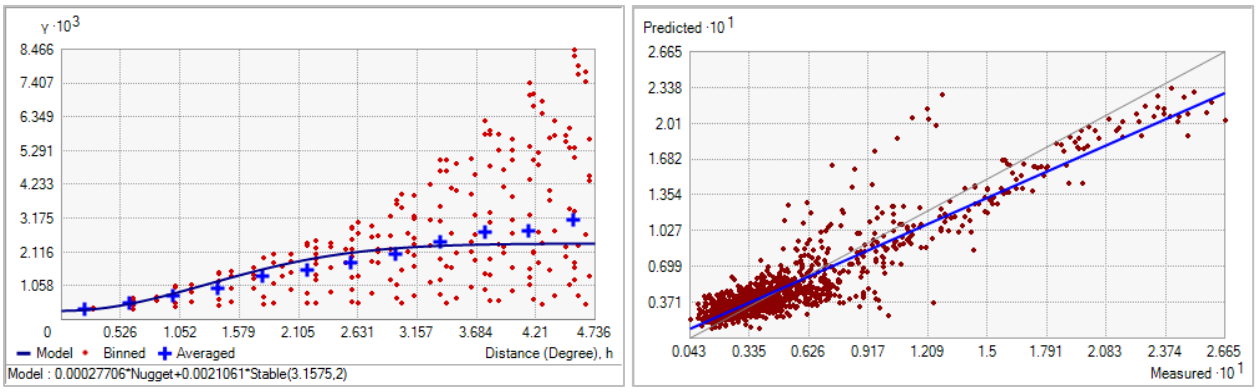

Fig. 173. Left panel: Semivariogram of Bottom Current Average Maximum (m s^{-1}). Binned values are shown as red dots; average points are shown as blue crosses; the model fit to the averaged values is shown as a blue line. Lag size: 0.395 degrees; number of lags: 12; Parameter: 1.831; Range: 3.157 degrees; Partial Sill: 2.106 x 10^{-3}. Right panel: Scatterplot of predicted values versus observed values for the model of Bottom Current Average Maximum (m s^{-1}).

Table 70. Results of cross-validation of the kriged model for Bottom Current Average Maximum (m s^{-1}).

Prediction error	**Value**
Number of Observations	1143
Overall Mean Error	2.587 x 10^{-4}
Root Mean Square Prediction Error	0.018
Standardized Mean	0.017
Standardized Root Mean Square Prediction Error	1.022
Average Standard Error	0.017

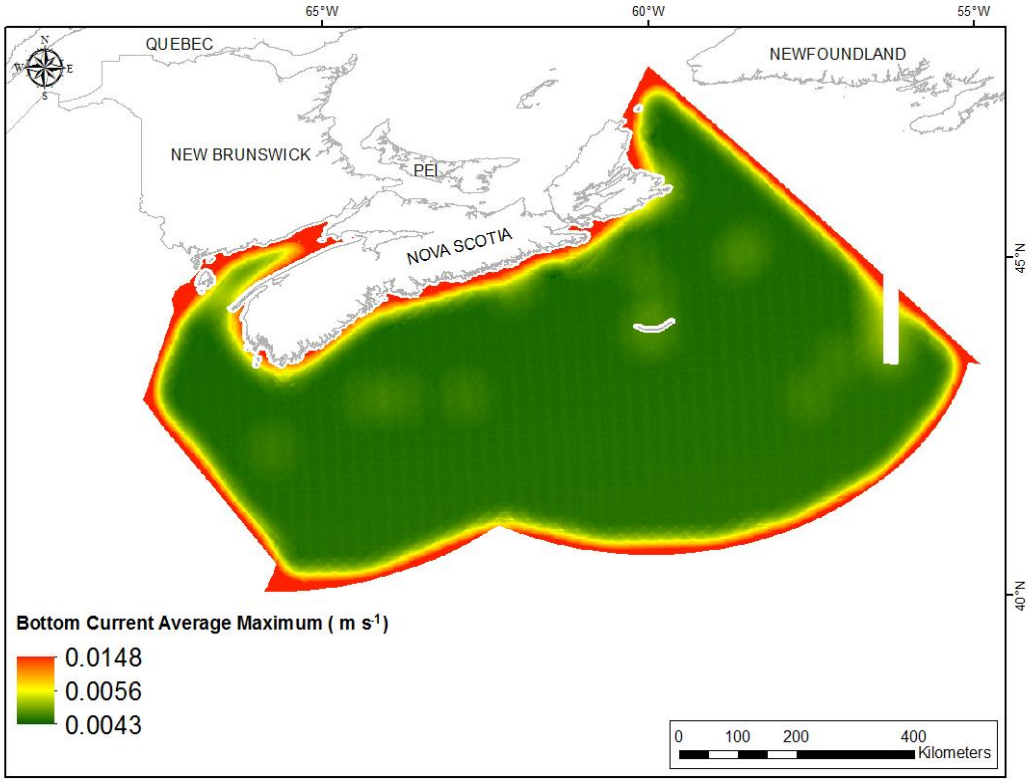

Fig. 174. Prediction standard error surface of Bottom Current Average Maximum (m s^{-1}).

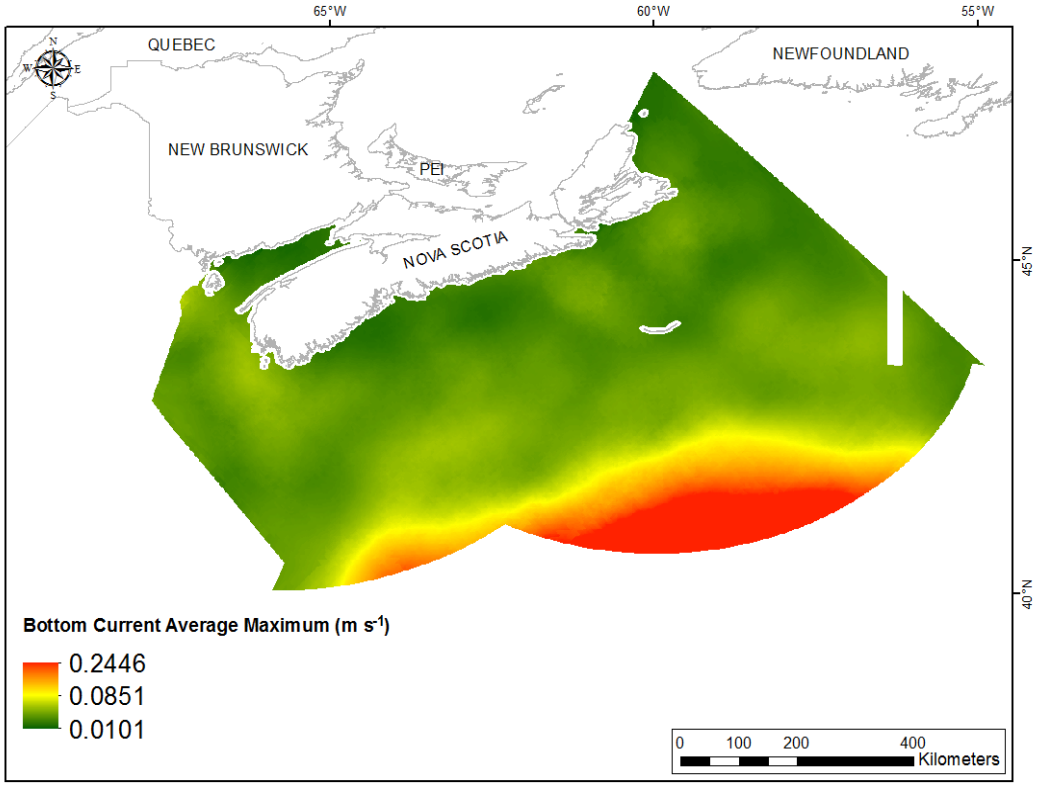

Fig. 175. Interpolated prediction surface of Bottom Current Average Maximum (m s^{-1}).

Bottom Current Average Range

This variable displayed a right-skewed, leptokurtic distribution prior to interpolation (Table 71, Fig. 176). The data were higher than predicted by a normal distribution at both tails, with mid-range values located below the reference line (Fig. 177). The areas of over- and under-prediction did not show a strong spatial pattern with both error types distributed across the study extent (Fig. 177).

The semivariogram showed weak autocorrelation present in the data and the model showed poor fit between measured and predicted values (Fig. 178). Nevertheless, the model showed good cross-validation statistics (Table 72) indicating that it was good at prediction. The error map showed high error along the edges of the study extent (Fig. 179). The kriged surface is presented in Fig. 180.

Table 71. Distributional properties of Bottom Current Average Range (m s^{-1}).

Property	Value
Number of Observations	1143
Minimum	0.004
Maximum	0.236
Mean	0.051
Median	0.037
Standard Deviation	0.041
Skewness	2.126
Kurtosis	7.629

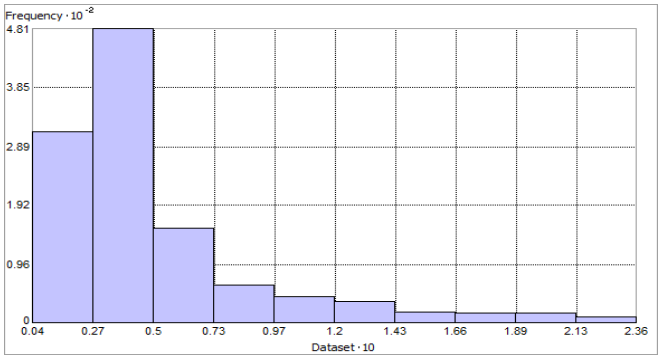

Fig. 176. Distribution of Bottom Current Average Range (m s^{-1}). Histogram was illustrated using 10 bins. X axis is shown at 10; Y axis is shown at 10^{-2}.

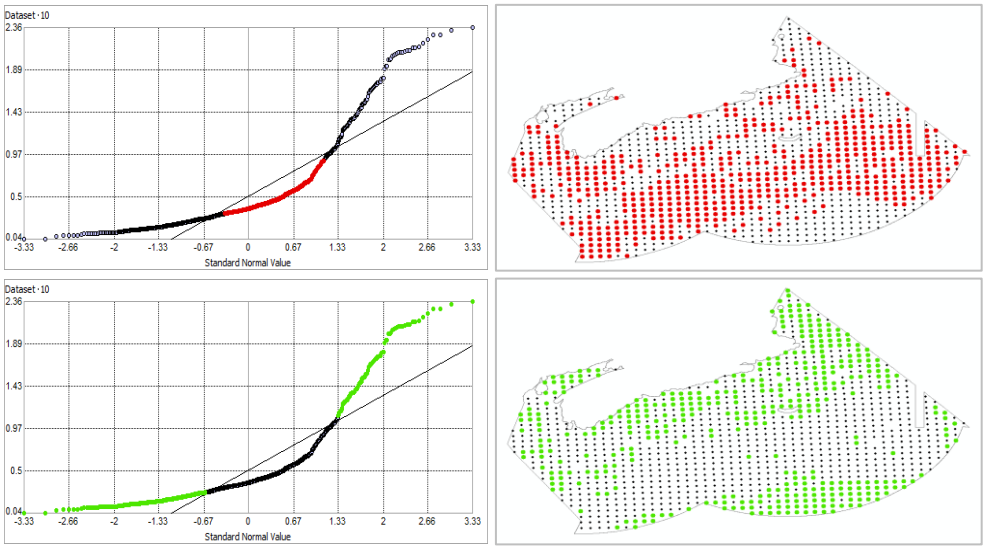

Fig. 177. Normal Q-Q plot for data values of Bottom Current Average Range (m s^{-1}). Points falling under (upper panel) and over (bottom panel) the reference line are mapped.

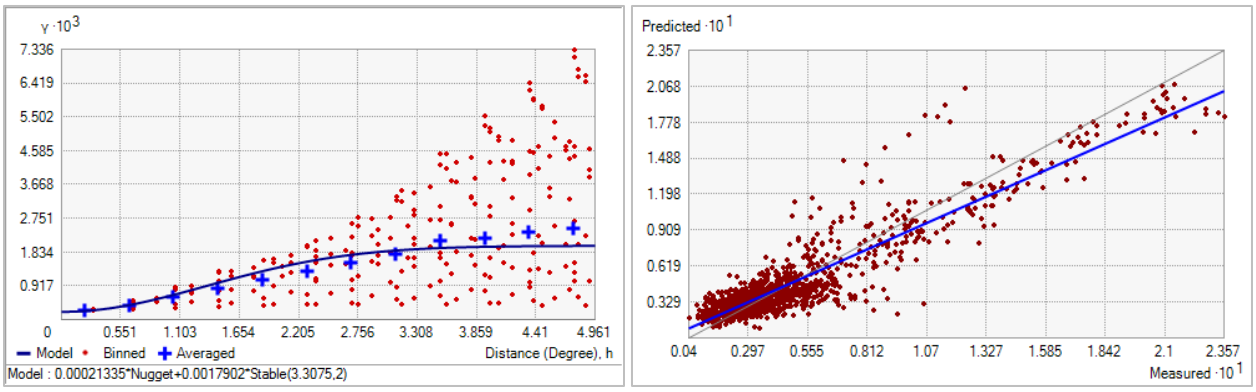

Fig. 178. Left panel: Semivariogram of Bottom Current Average Range (m s^{-1}). Binned values are shown as red dots; average points are shown as blue crosses; the model fit to the averaged values is shown as a blue line. Lag size: 0.413 degrees; number of lags: 12; Parameter: 2; Range: 3.307 degrees; Partial Sill: 1.790 x 10^{-3}. Right panel: Scatterplot of predicted values versus observed values for the model of Bottom Current Average Range (m s^{-1}).

Table 72. Results of cross-validation of the kriged model for Bottom Current Average Range (m s^{-1}).

Prediction error	**Value**
Number of Observations	1143
Overall Mean Error	2.515 x 10^{-4}
Root Mean Square Prediction Error	0.016
Standardized Mean	0.018
Standardized Root Mean Square Prediction Error	1.023
Average Standard Error	0.015

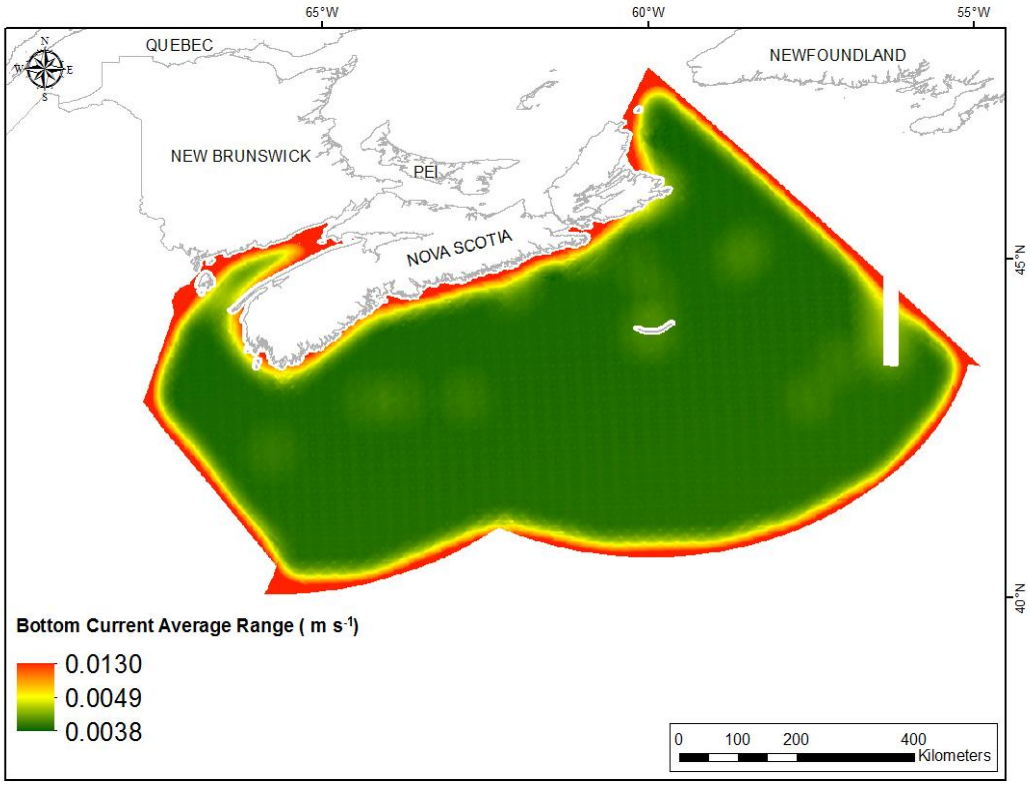

Fig. 179. Prediction standard error surface of Bottom Current Average Range (m s^{-1}).

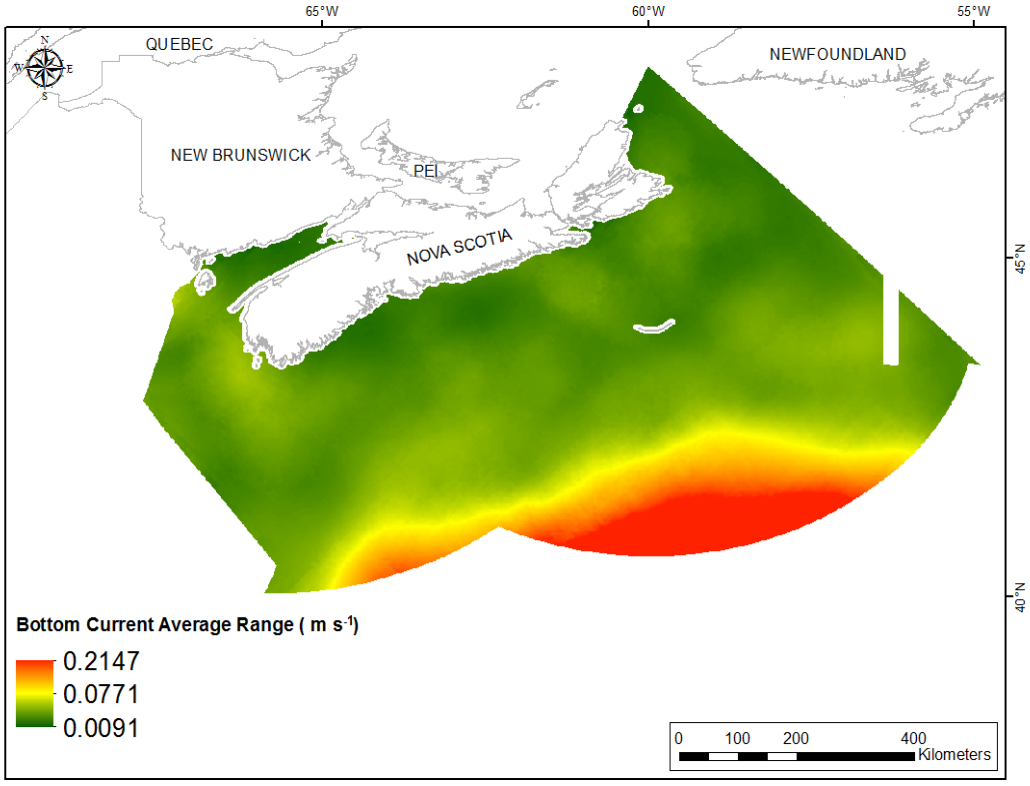

Fig. 180. Interpolated prediction surface of Bottom Current Average Range (m s^{-1}).

Surface Current Mean

This variable displayed a right-skewed, leptokurtic distribution prior to interpolation (Table 73, Fig. 181). The data were higher than predicted by a normal distribution at both tails, with mid-range values located below the reference line (Fig. 182). The areas of over- and under-prediction showed spatial cohesion across the study extent (Fig. 182).

The semivariogram showed weak autocorrelation present in the data (Fig. 183). There was an excellent fit between measured and predicted values (Fig. 183). The cross-validation statistics were fair (Table 74). The error map showed a 'bullseye' pattern with error increasing with distance from data points (Fig. 184). The kriged surface is presented in Fig. 185.

Table 73. Distributional properties of Surface Current Mean (m s^{-1}).

Property	Value
Number of Observations	1152
Minimum	0.016
Maximum	0.349
Mean	0.118
Median	0.098
Standard Deviation	0.066
Skewness	1.123
Kurtosis	3.603

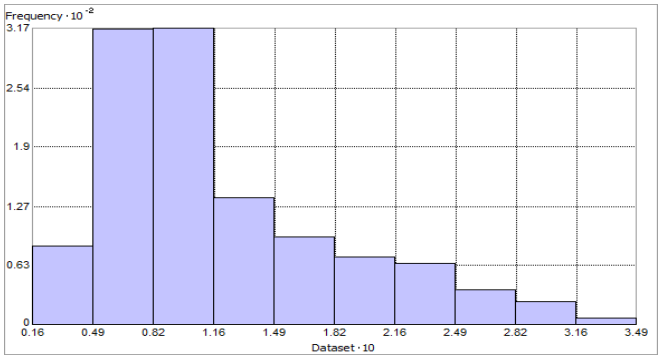

Fig. 181. Distribution of Surface Current Mean (m s^{-1}). Histogram was illustrated using 10 bins. X axis is shown at 10; Y axis is shown at 10^{-2}.

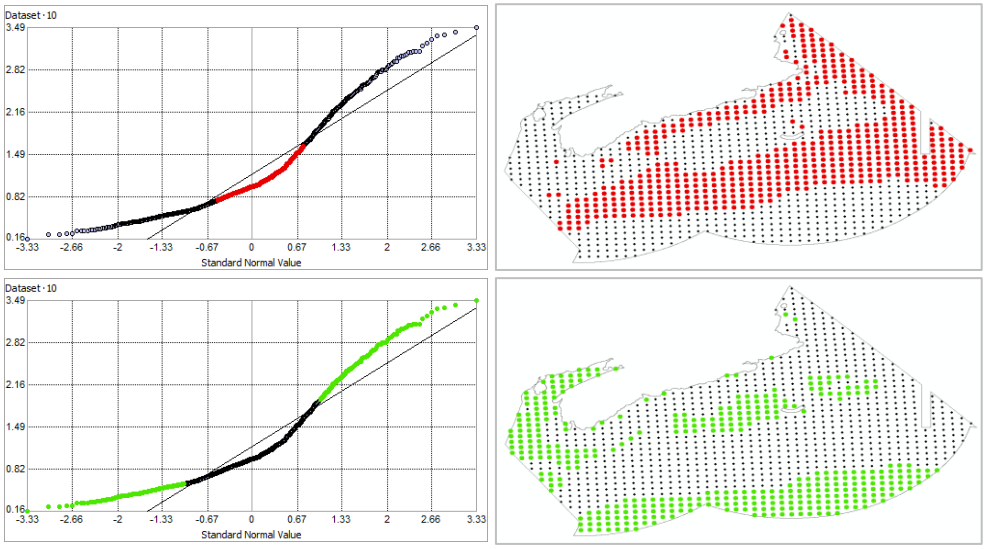

Fig. 182. Normal Q-Q plot for data values of Surface Current Mean (m s^{-1}). Points falling under (upper panel) and over (bottom panel) the reference line are mapped.

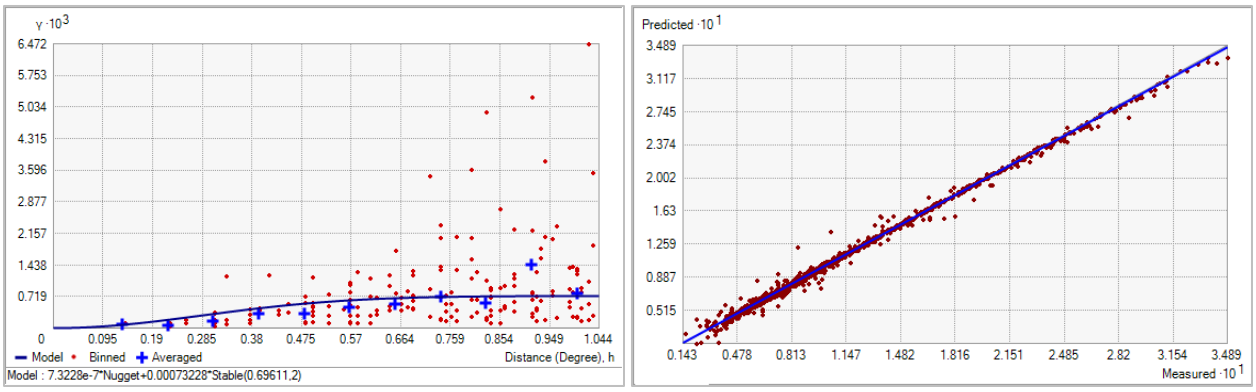

Fig. 183. Left panel: Semivariogram of Surface Current Mean (m s^{-1}). Binned values are shown as red dots; average points are shown as blue crosses; the model fit to the averaged values is shown as a blue line. Lag size: 0.087 degrees; number of lags: 12; Parameter: 2; Range: 0.696 degrees; Partial Sill: 7.323 x 10^{-4}. Right panel: Scatterplot of predicted values versus observed values for the model of Surface Current Mean (m s^{-1}).

Table 74. Results of cross-validation of the kriged model for Surface Current Mean (m s^{-1}).

Prediction error	**Value**
Number of Observations	1152
Overall Mean Error	-5.01 x 10^{-5}
Root Mean Square Prediction Error	4.128 x 10^{-3}
Standardized Mean	4.624 x 10^{-3}
Standardized Root Mean Square Prediction Error	1.435
Average Standard Error	3.097 x 10^{-3}

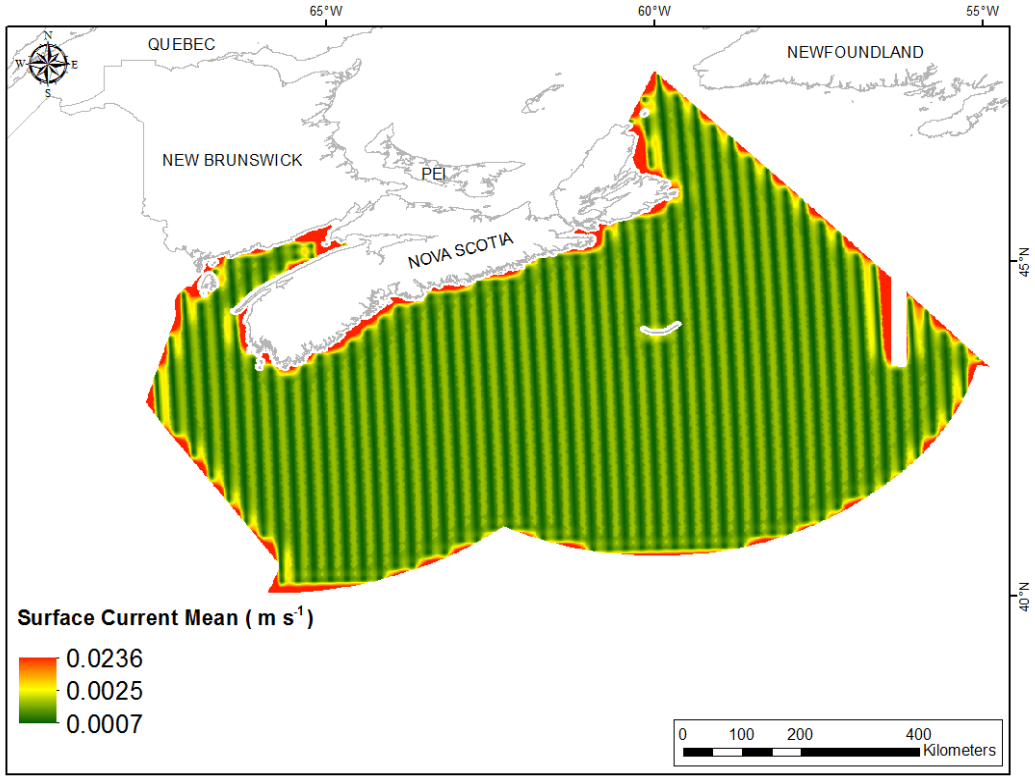

Fig. 184. Prediction standard error surface of Surface Current Mean (m s^{-1}).

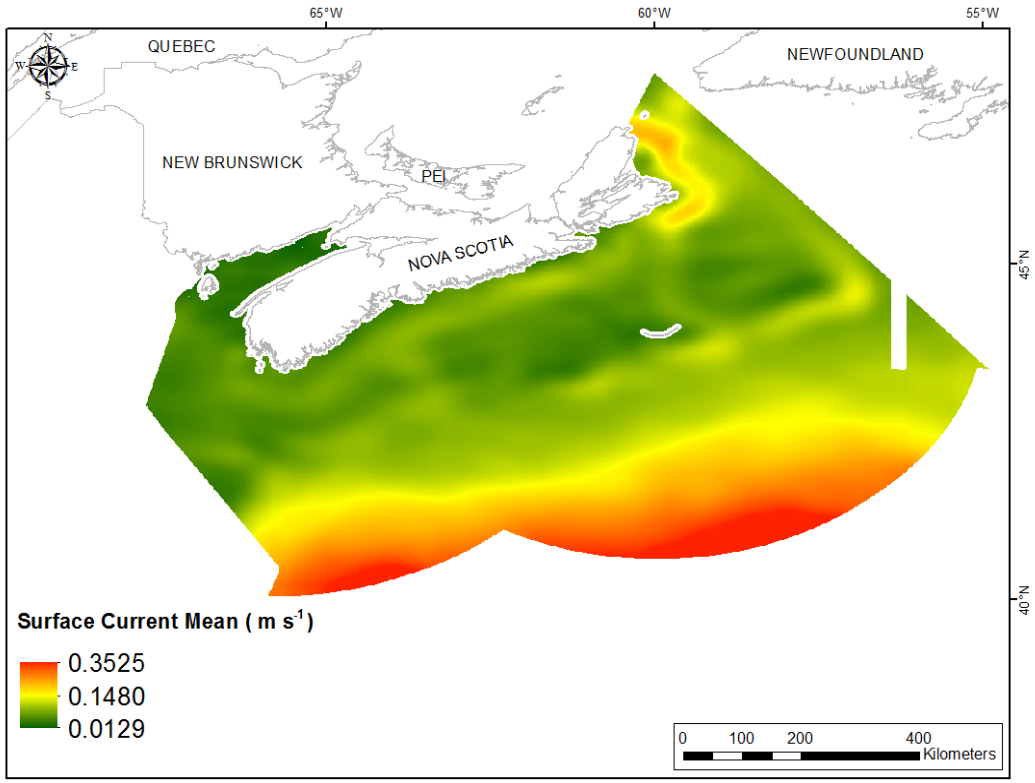

Fig. 185. Interpolated prediction surface of Surface Current Mean (m s^{-1}).

Surface Current Minimum

This variable displayed a right-skewed, leptokurtic distribution prior to interpolation (Table 75, Fig. 186). The data were higher than predicted by a normal distribution at both tails, with mid-range values located below the reference line (Fig. 187). The areas of over- and under-prediction showed little spatial pattern with both error types distributed randomly across the study extent (Fig. 187).

The semivariogram showed weak autocorrelation present in the data, with a poor fit between measured and predicted values (Fig. 188). Nevertheless, good performance of the model was indicated by the good cross-validation statistics (Table 76). The error map showed a 'bullseye' pattern with error increasing with distance from data points (Fig. 189). The kriged surface is presented in Fig. 190.

Table 75. Distributional properties of Surface Current Minimum (m s^{-1}).

Property	Value
Number of Observations	1152
Minimum	3.805×10^{-5}
Maximum	0.033
Mean	7.478×10^{-3}
Median	6.251×10^{-3}
Standard Deviation	5.326×10^{-3}
Skewness	1.282
Kurtosis	5.173

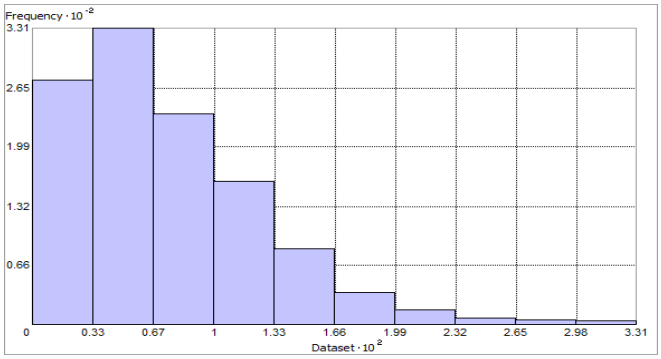

Fig. 186. Distribution of Surface Current Minimum (m s^{-1}). Histogram was illustrated using 10 bins. X axis shown at 10^{2}; Y axis shown at 10^{-2}.

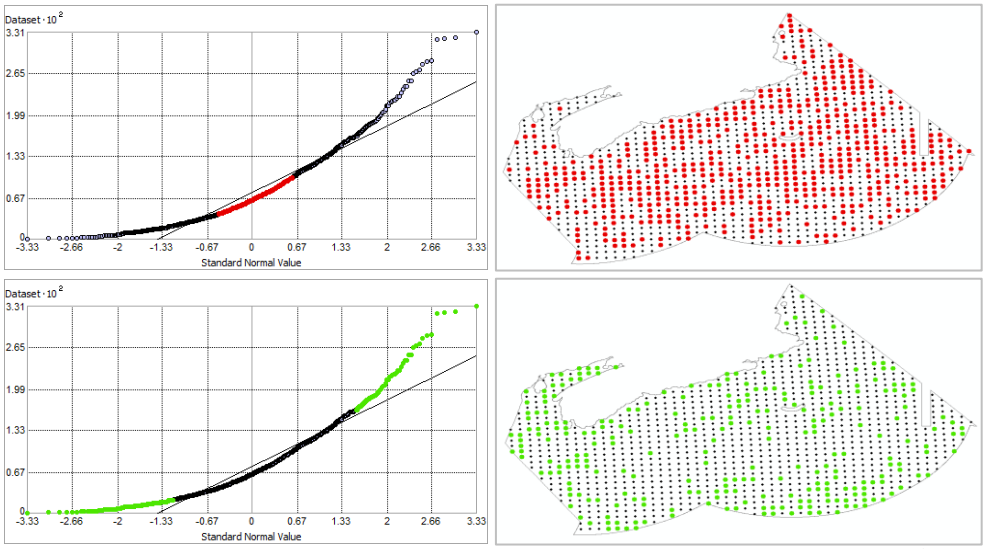

Fig. 187. Normal Q-Q plot for data values of Surface Current Minimum (m s^{-1}). Points falling under (upper panel) and over (bottom panel) the reference line are mapped.

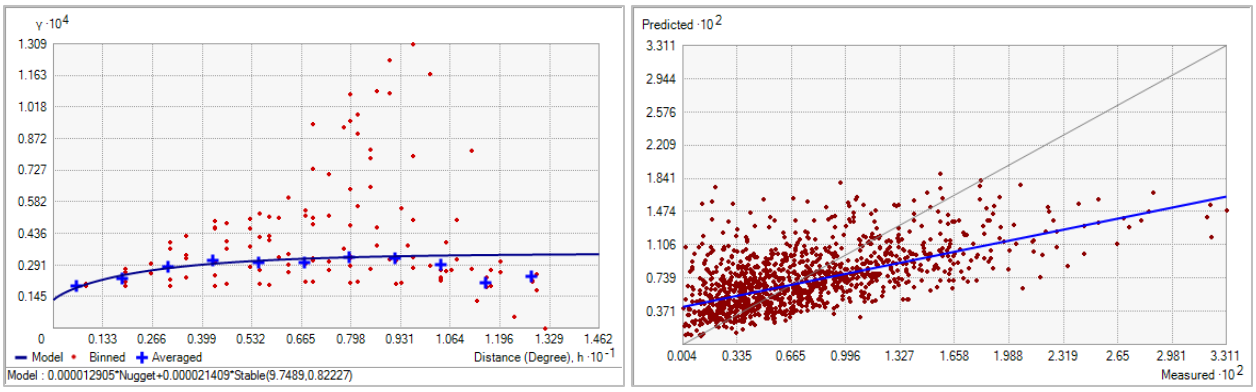

Fig. 188. Left panel: Semivariogram of Surface Current Minimum (m s^{-1}). Binned values are shown as red dots; average points are shown as blue crosses; the model fit to the averaged values is shown as a blue line. Lag size: 1.219 degrees; number of lags: 12; Parameter: 0.822; Range: 9.749 degrees; Partial Sill: 2.141 x 10^{-5}. Right panel: Scatterplot of predicted values versus observed values for the model of Surface Current Minimum (m s^{-1}).

Table 76. Results of cross-validation of the kriged model for Surface Current Minimum (m s^{-1}).

Prediction error	**Value**
Number of Observations	1152
Overall Mean Error	-3.170 x 10^{-6}
Root Mean Square Prediction Error	4.304 x 10^{-3}
Standardized Mean	-8.852 x 10^{-4}
Standardized Root Mean Square Prediction Error	1.054
Average Standard Error	4.080 x 10^{-3}

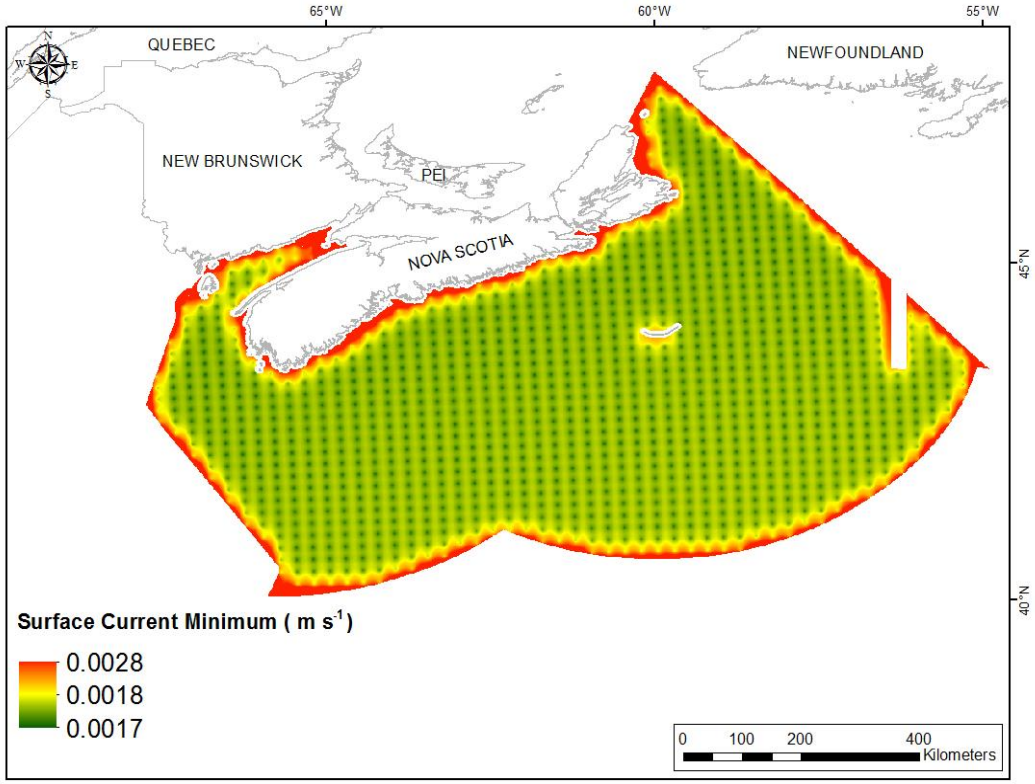

Fig. 189. Prediction standard error surface of Surface Current Minimum (m s^{-1}).

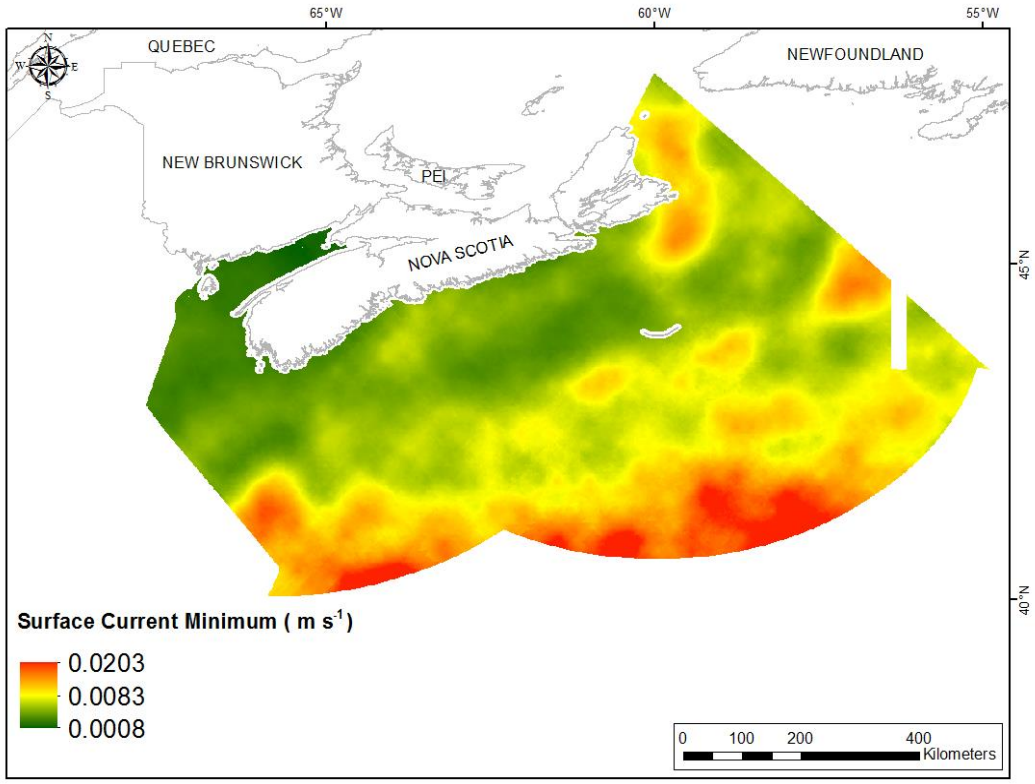

Fig. 190. Interpolated prediction surface of Surface Current Minimum (m s^{-1}).

Surface Current Maximum

This variable displayed a right-skewed, platykurtic distribution prior to interpolation (Table 77, Fig. 191). The data were higher than predicted by a normal distribution at both tails, with mid-range values located below the reference line (Fig. 192). The areas of over- and under-prediction showed spatial pattern (Fig. 192).

The semivariogram showed weak autocorrelation present in the data and the model (Fig. 193). However, there was a good fit between measured and predicted values, and the model showed good cross-validation statistics (Table 78). The error map showed a 'bullseye' pattern with error increasing with distance from data points (Fig. 194). The kriged surface is presented in Fig. 195.

Table 77. Distributional properties of Surface Current Maximum (m s^{-1}).

Property	Value
Number of Observations	1152
Minimum	0.067
Maximum	1.248
Mean	0.419
Median	0.325
Standard Deviation	0.271
Skewness	0.872
Kurtosis	2.708

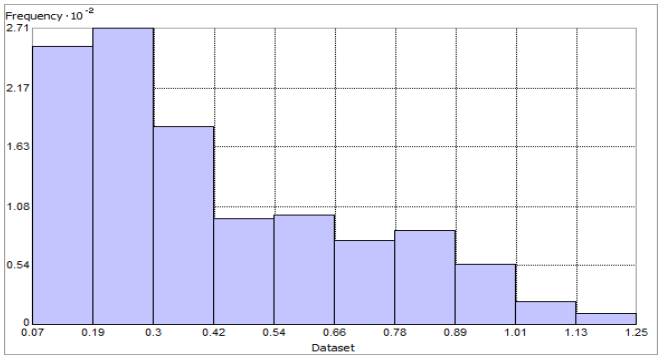

Fig. 191. Distribution of Surface Current Maximum (m s^{-1}). Histogram was illustrated using 10 bins. Y axis is shown at 10^{-2}.

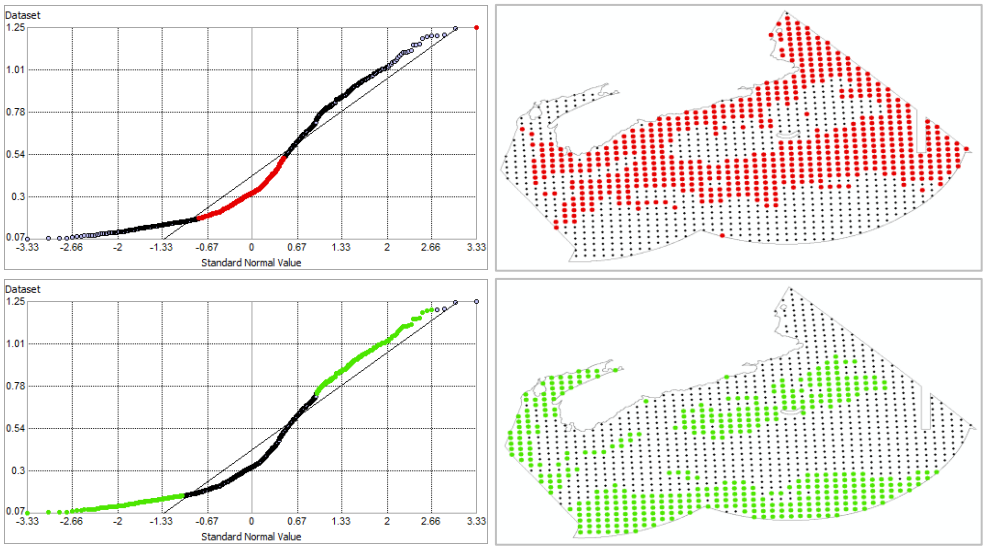

Fig. 192. Normal Q-Q plot for data values of Surface Current Maximum (m s^{-1}). Points falling under (upper panel) and over (bottom panel) the reference line are mapped.

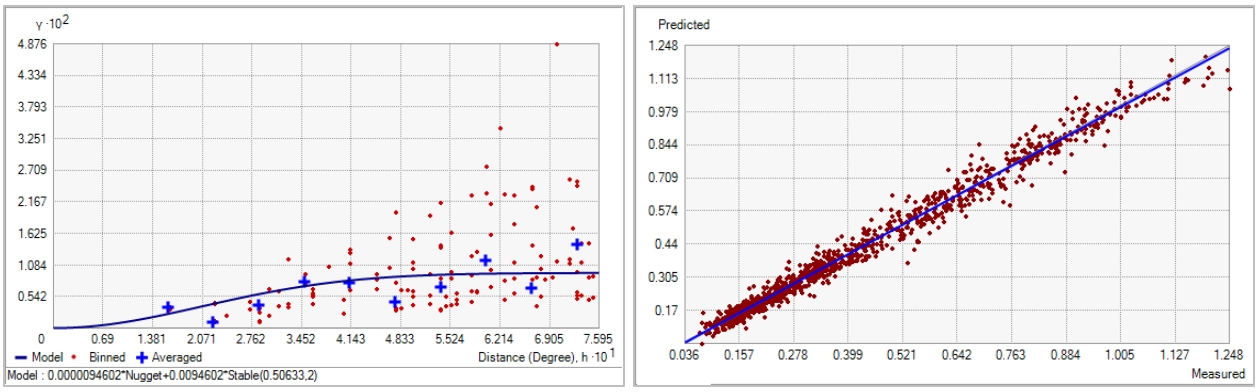

Fig. 193. Left panel: Semivariogram of Surface Current Maximum (m s^{-1}). Binned values are shown as red dots; average points are shown as blue crosses; the model fit to the averaged values is shown as a blue line. Lag size: 0.063 degrees; number of lags: 12; Parameter: 2; Range: 0.506 degrees; Partial Sill: 9.460 x 10^{-3}. Right panel: Scatterplot of predicted values versus observed values for the model of Surface Current Maximum (m s^{-1}).

Table 78. Results of cross-validation of the kriged model for Surface Current Maximum (m s^{-1}).

Prediction error	**Value**
Number of Observations	1152
Overall Mean Error	4.032 x 10^{-4}
Root Mean Square Prediction Error	0.036
Standardized Mean	5.351 x 10^{-3}
Standardized Root Mean Square Prediction Error	1.289
Average Standard Error	0.028

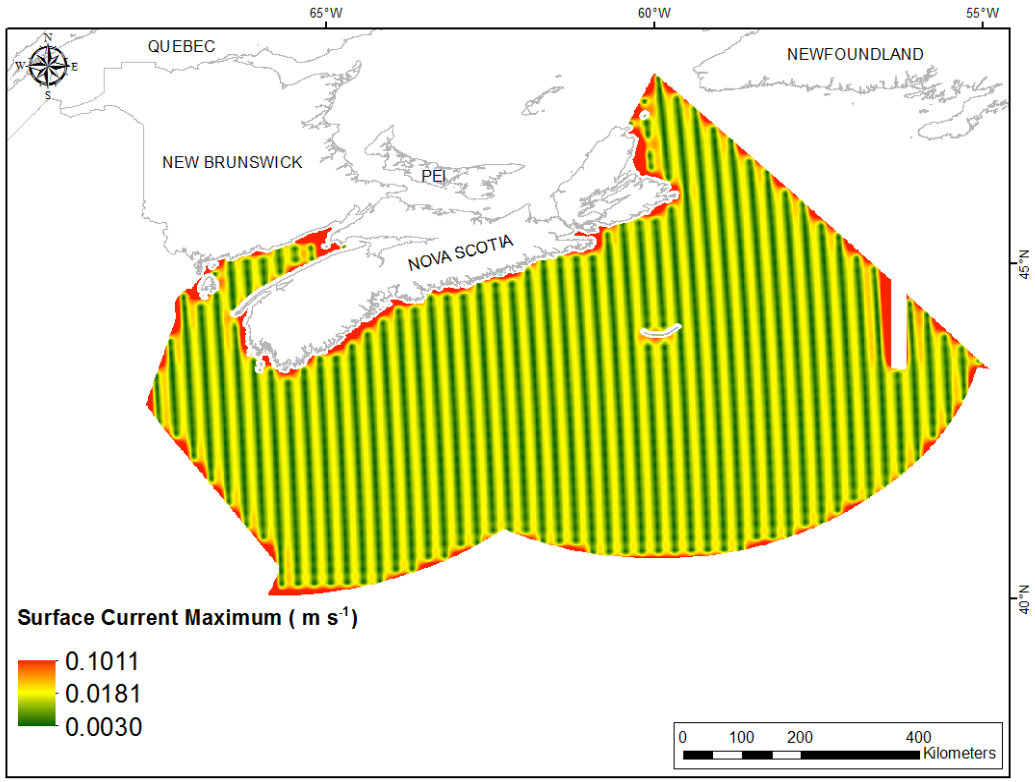

Fig. 194. Prediction standard error surface of Surface Current Maximum (m s^{-1}).

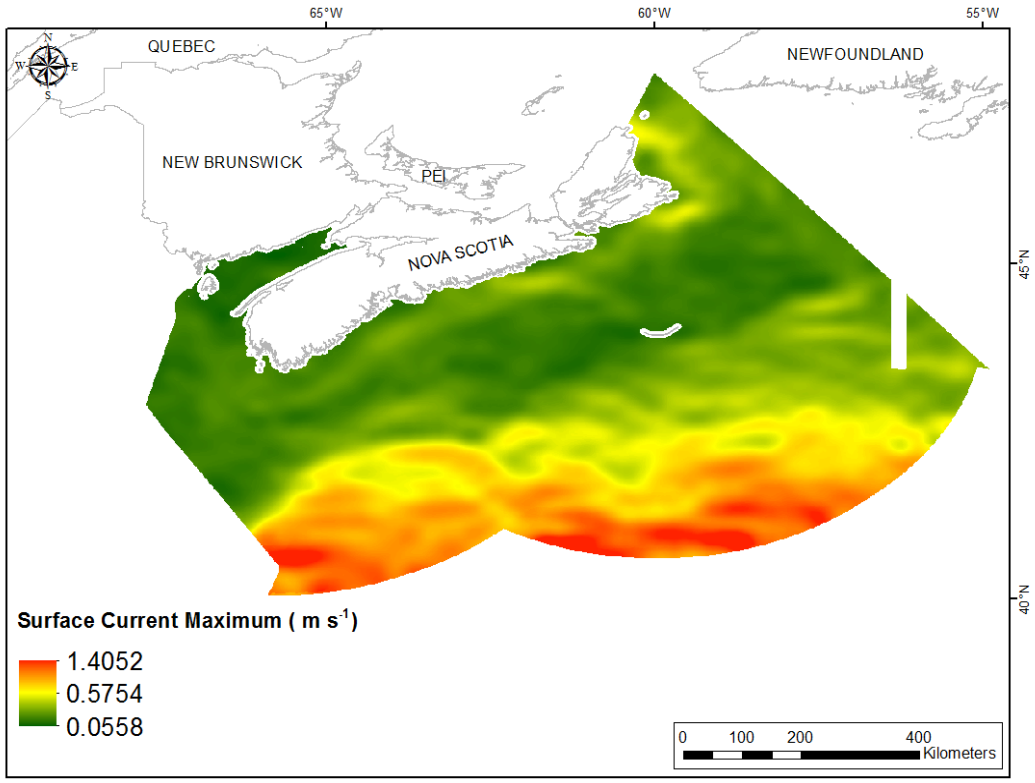

Fig. 195. Interpolated prediction surface of Surface Current Maximum (m s^{-1}).

Surface Current Range

This variable displayed a right-skewed, platykurtic distribution prior to interpolation (Table 79, Fig. 196). The data were higher than predicted by a normal distribution at both tails, with mid-range values located below the reference line (Fig. 197). The areas of over- and under-prediction showed spatial pattern (Fig. 197).

The semivariogram showed weak autocorrelation present in the data and the model (Fig. 198). However, there was a good fit between measured and predicted values (Fig. 198), and the model showed good cross-validation statistics (Table 80). The error map showed a 'bullseye' pattern with error increasing with distance from data points (Fig. 199). The kriged surface is presented in Fig. 200.

Table 79. Distributional properties of Surface Current Range (m s^{-1}).

Property	Value
Number of Observations	1152
Minimum	0.067
Maximum	1.231
Mean	0.412
Median	0.137
Standard Deviation	0.268
Skewness	0.873
Kurtosis	2.703

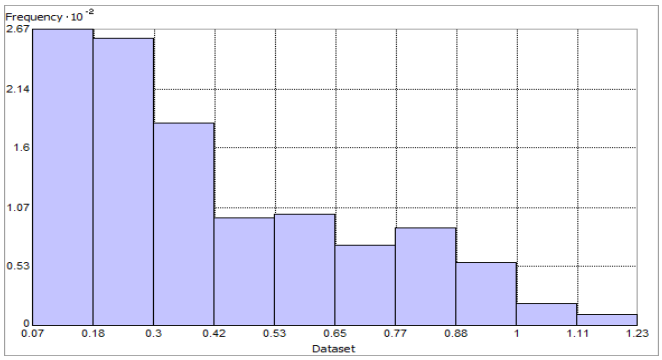

Fig. 196. Distribution of Surface Current Range (m s^{-1}). Histogram was illustrated using 10 bins. Y axis is shown at 10^{-2}.

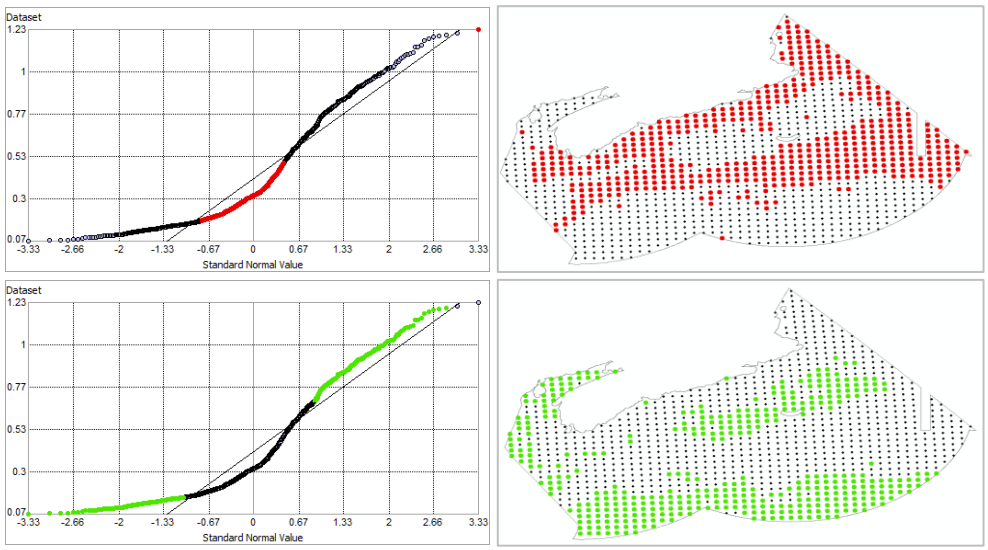

Fig. 197. Normal Q-Q plot for data values of Surface Current Range (m s^{-1}). Points falling under (upper panel) and over (bottom panel) the reference line are mapped.

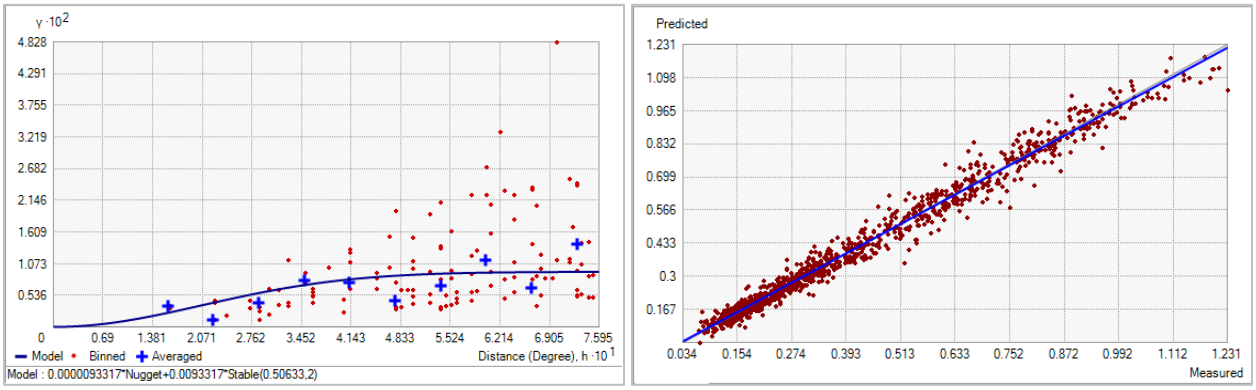

Fig. 198. Left panel: Semivariogram of Surface Current Range (m s^{-1}). Binned values are shown as red dots; average points are shown as blue crosses; the model fit to the averaged values is shown as a blue line. Lag size: 0.063 degrees; number of lags: 12; Parameter: 2; Range: 0.506 degrees; Partial Sill: 9.332 x 10^{-3}. Right panel: Scatterplot of predicted values versus observed values for the model of Surface Current Range (m s^{-1}).

Table 80. Results of cross-validation of the kriged model for Surface Current Range (m s^{-1}).

Prediction error	**Value**
Number of Observations	1152
Overall Mean Error	4.181 x 10^{-4}
Root Mean Square Prediction Error	0.037
Standardized Mean	5.681 x 10^{-3}
Standardized Root Mean Square Prediction Error	1.339
Average Standard Error	0.029

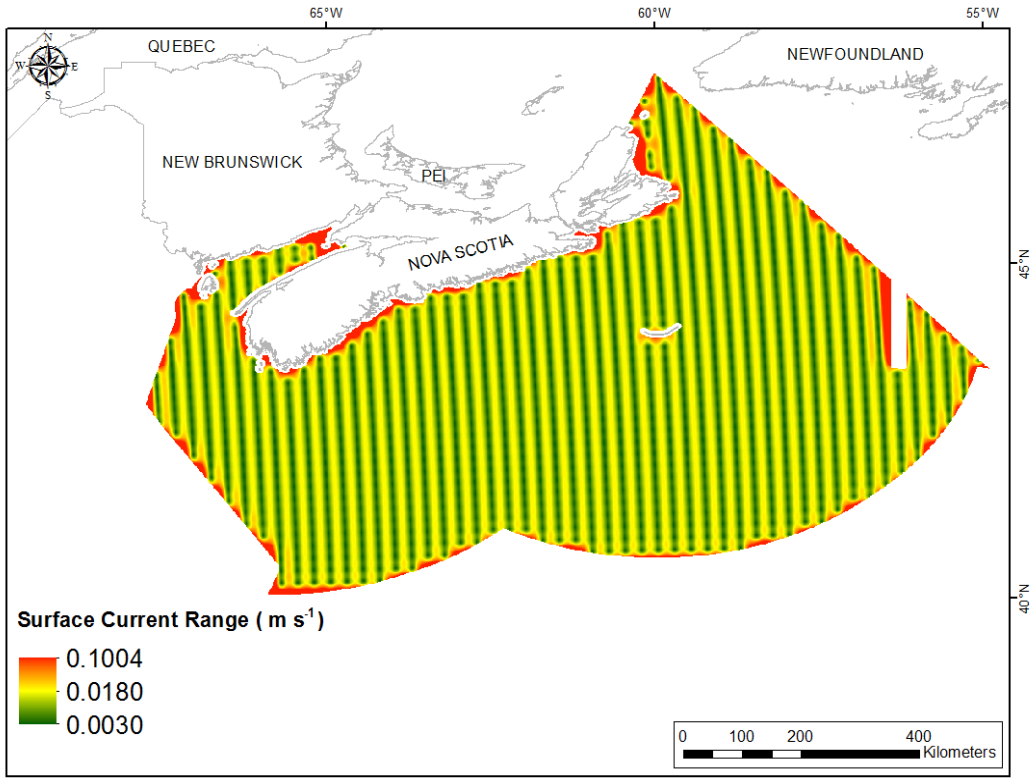

Fig. 199. Prediction standard error surface of Surface Current Range (m s^{-1}).

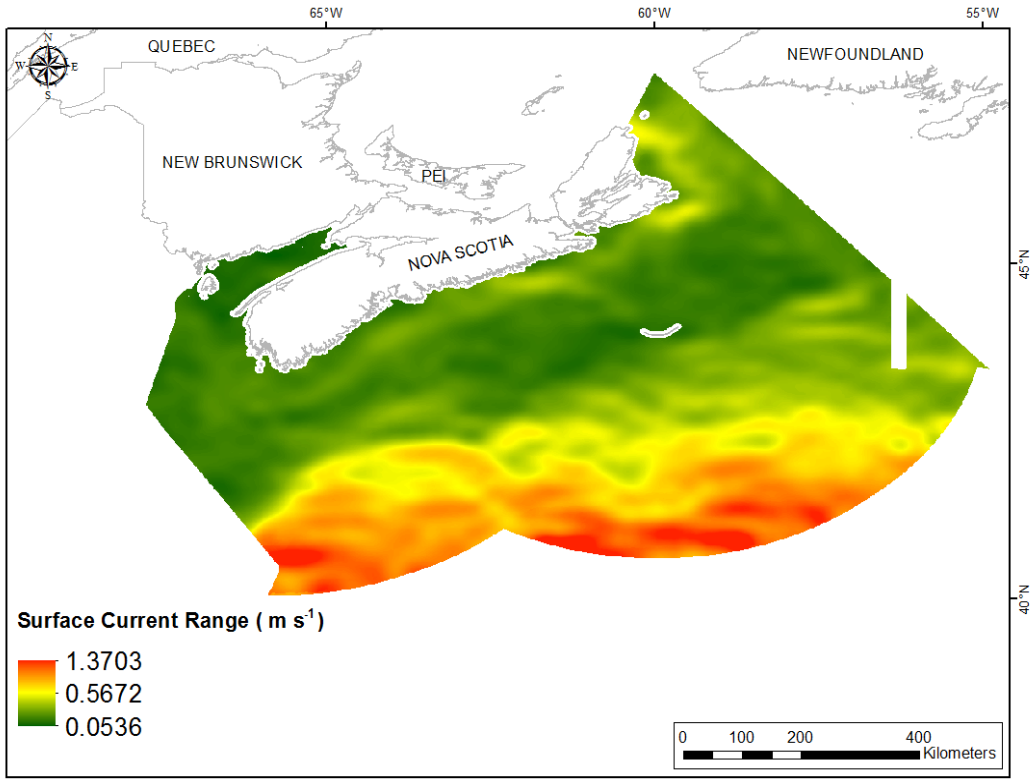

Fig. 200. Interpolated prediction surface of Surface Current Range (m s^{-1}).

Surface Current Average Minimum

This variable displayed slight positive skew and leptokurtosis prior to interpolation (Table 81, Fig. 201). The data were higher than predicted by a normal distribution at both tails, with mid-range values located below the reference line (Fig. 202). The areas of over- and under-prediction showed a slight spatial pattern (Fig. 202).

The semivariogram showed moderate autocorrelation present in the data and the model showed fair fit between measured and predicted values (Fig. 203). Nevertheless, the model showed good cross-validation statistics (Table 82) indicating that it was good at prediction. The error map showed low error and no strong spatial pattern over the study extent although error was highest along the coast and in deep waters (Fig. 204). The kriged surface is presented in Fig. 205.

Table 81. Distributional properties of Surface Current Average Minimum (m s^{-1}).

Property	Value
Number of Observations	1152
Minimum	1.739 x 10^{-3}
Maximum	0.089
Mean	0.032
Median	0.030
Standard Deviation	0.015
Skewness	0.739
Kurtosis	3.327

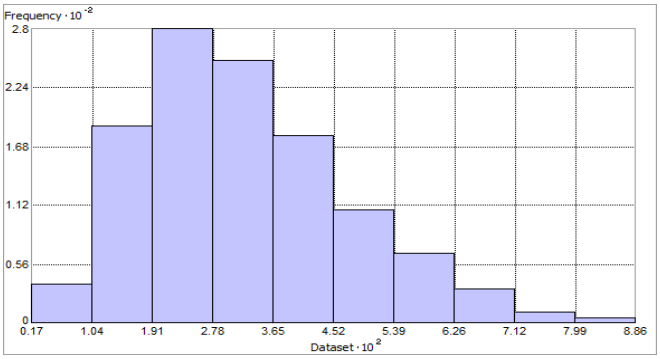

Fig. 201. Distribution of Surface Current Average Minimum (m s^{-1}). Histogram was illustrated using 10 bins. X axis shown at 10^{2}; Y axis shown at 10^{-2}.

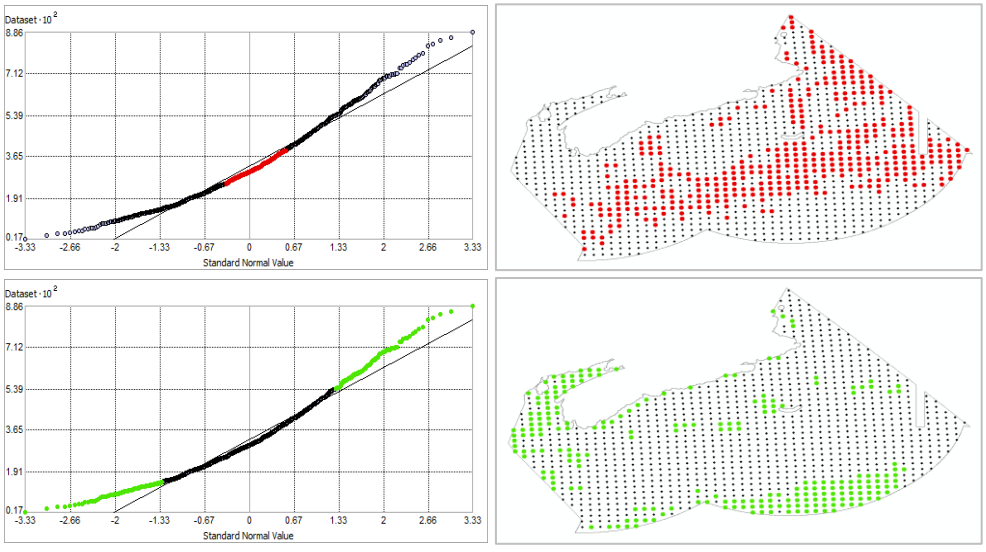

Fig. 202. Normal Q-Q plot for data values of Surface Current Average Minimum (m s^{-1}). Points falling under (upper panel) and over (bottom panel) the reference line are mapped.

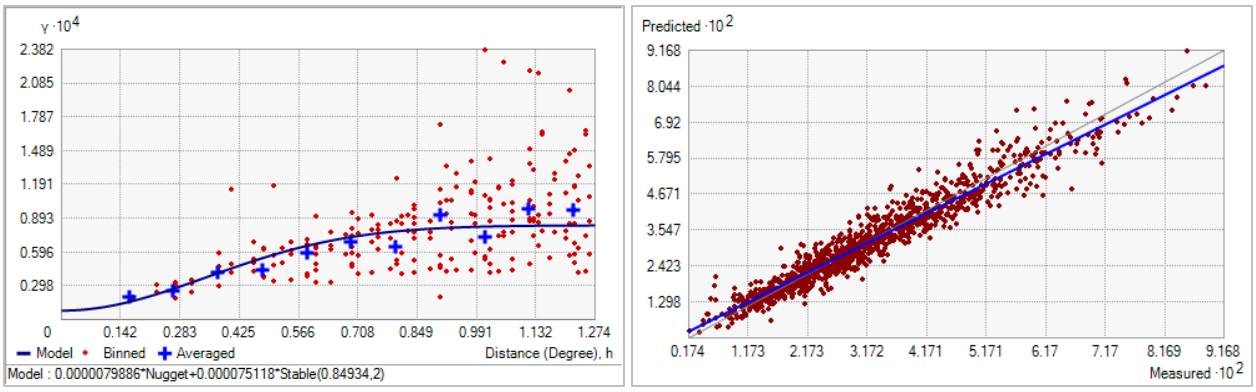

Fig. 203. Left panel: Semivariogram of Surface Current Average Minimum (m s^{-1}). Binned values are shown as red dots; average points are shown as blue crosses; the model fit to the averaged values is shown as a blue line. Lag size: 0.106 degrees; number of lags: 12; Parameter: 2; Range: 0.849 degrees; Partial Sill: 7.512 x 10^{-5}. Right panel: Scatterplot of predicted values versus observed values for the model of Surface Current Average Minimum (m s^{-1}).

Table 82. Results of cross-validation of the kriged model for Surface Current Average Minimum (m s^{-1}).

Prediction error	**Value**
Number of Observations	1152
Overall Mean Error	3.537 x 10^{-5}
Root Mean Square Prediction Error	3.949 x 10^{-3}
Standardized Mean	4.886 x 10^{-3}
Standardized Root Mean Square Prediction Error	1.102
Average Standard Error	3.531 x 10^{-3}

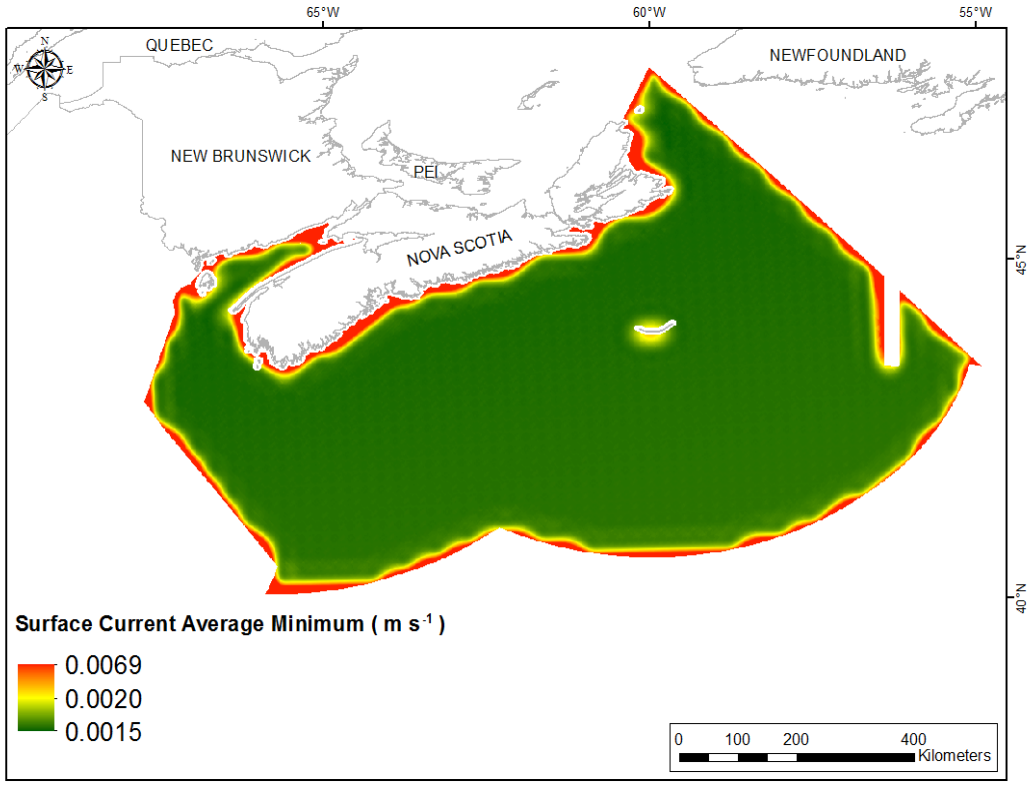

Fig. 204. Prediction standard error surface of Surface Current Average Minimum (m s^{-1}).

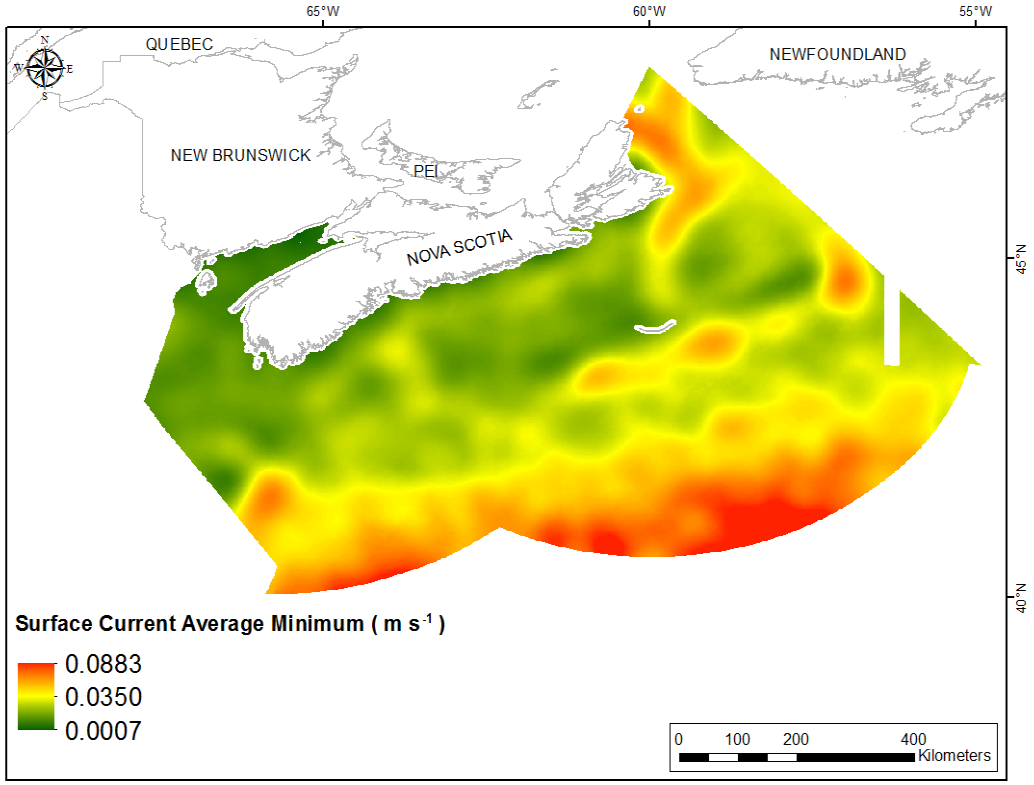

Fig. 205. Interpolated prediction surface of Surface Current Average Minimum (m s^{-1}).

Surface Current Average Maximum

This variable displayed a slightly right-skewed distribution prior to interpolation (Table 83, Fig. 206). The data were higher than predicted by a normal distribution at both tails, with mid-range values located below the reference line (Fig. 207). The areas of over- and under-prediction showed a strong spatial pattern (Fig. 207).

The semivariogram showed weak autocorrelation present in the data (Fig. 208). The model showed excellent fit between measured and predicted values (Fig. 208), but poor performance was indicated by the cross-validation statistics (Table 84). The Standardized Root-Mean-Square Prediction Error was less than 1, indicating that variability in the predictions has been overestimated. The error map showed a 'bullseye' pattern with error increasing with distance from data points (Fig. 209). The kriged surface is presented in Fig. 210.

Table 83. Distributional properties of Surface Current Average Maximum (m s^{-1}).

Property	Value
Number of Observations	1152
Minimum	0.040
Maximum	0.718
Mean	0.255
Median	0.198
Standard Deviation	0.160
Skewness	1.061
Kurtosis	3.068

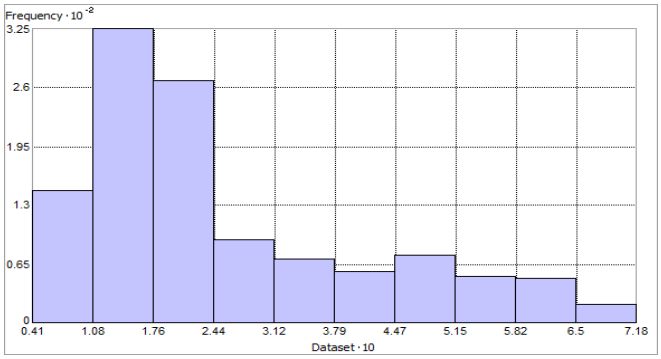

Fig. 206. Distribution of Surface Current Average Maximum (m s^{-1}). Histogram was illustrated using 10 bins. X axis shown at 10; Y axis shown at 10^{-2}.

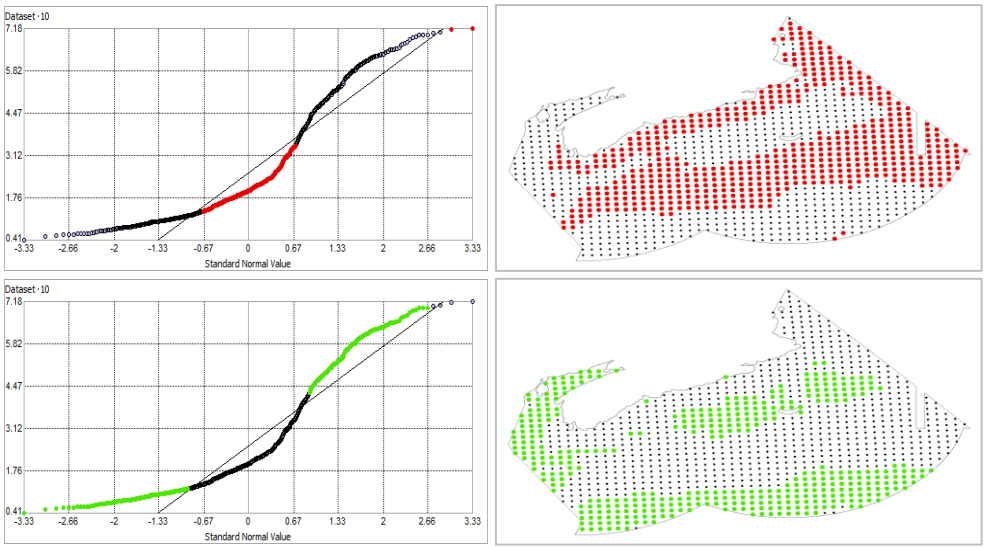

Fig. 207. Normal Q-Q plot for data values of Surface Current Average Maximum (m s^{-1}). Points falling under (upper panel) and over (bottom panel) the reference line are mapped.

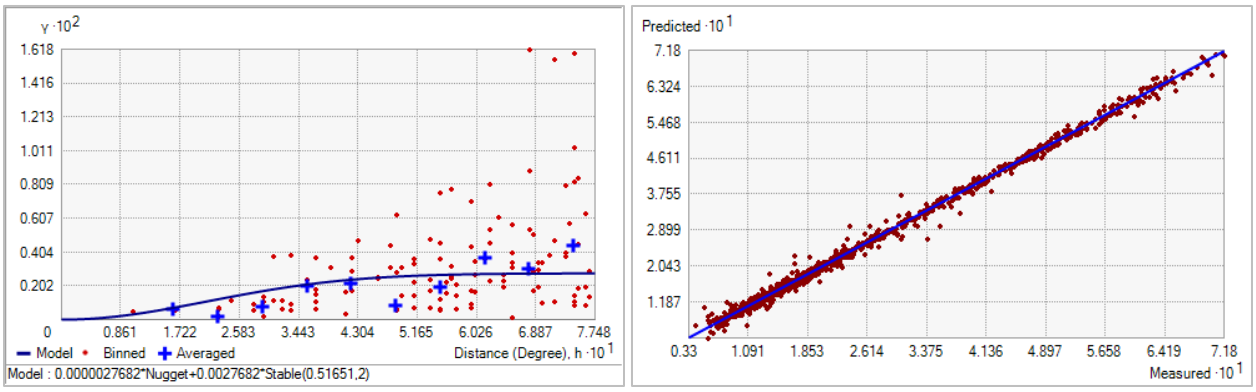

Fig. 208. Left panel: Semivariogram of Surface Current Average Maximum (m s^{-1}). Binned values are shown as red dots; average points are shown as blue crosses; the model fit to the averaged values is shown as a blue line. Lag size: 0.065 degrees; number of lags: 12; Parameter: 2; Range: 0.517 degrees; Partial Sill: 2.768 x 10^{-3}. Right panel: Scatterplot of predicted values versus observed values for the model of Surface Current Average Maximum (m s^{-1}).

Table 84. Results of cross-validation of the kriged model for Surface Current Average Maximum (m s^{-1}).

Prediction error	**Value**
Number of Observations	1152
Overall Mean Error	5.851 x 10^{-5}
Root Mean Square Prediction Error	0.010
Standardized Mean	-9.394 x 10^{-4}
Standardized Root Mean Square Prediction Error	0.672
Average Standard Error	0.014

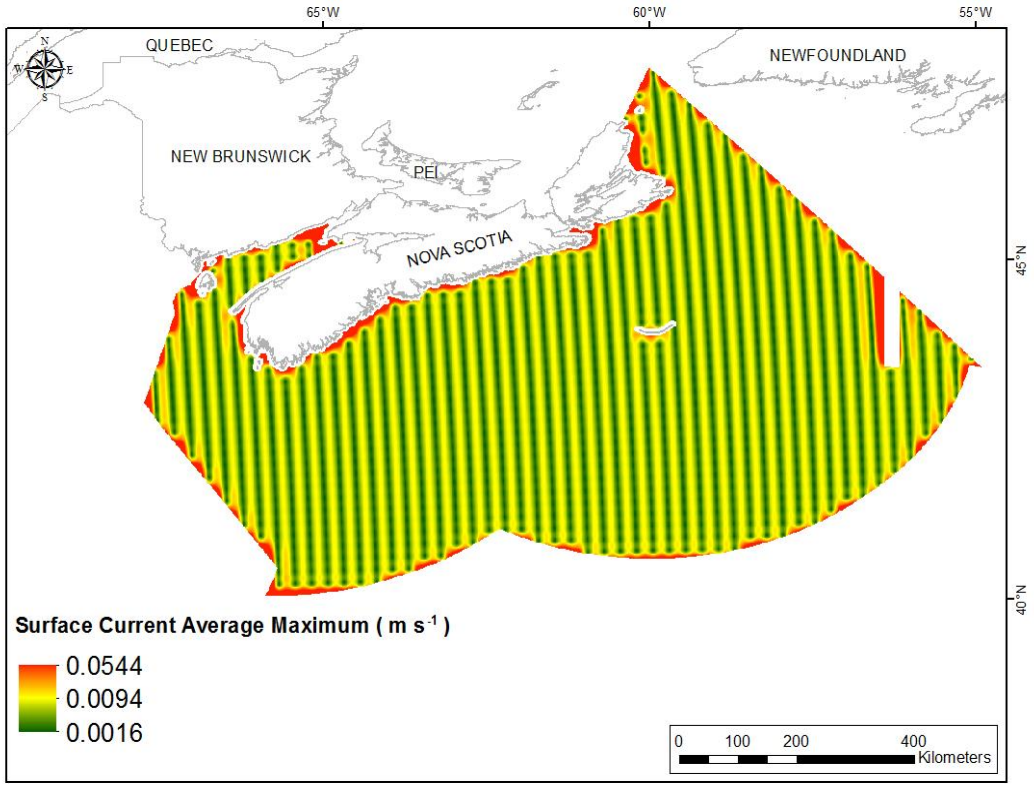

Fig. 209. Prediction standard error surface of Surface Current Average Maximum (m s^{-1}).

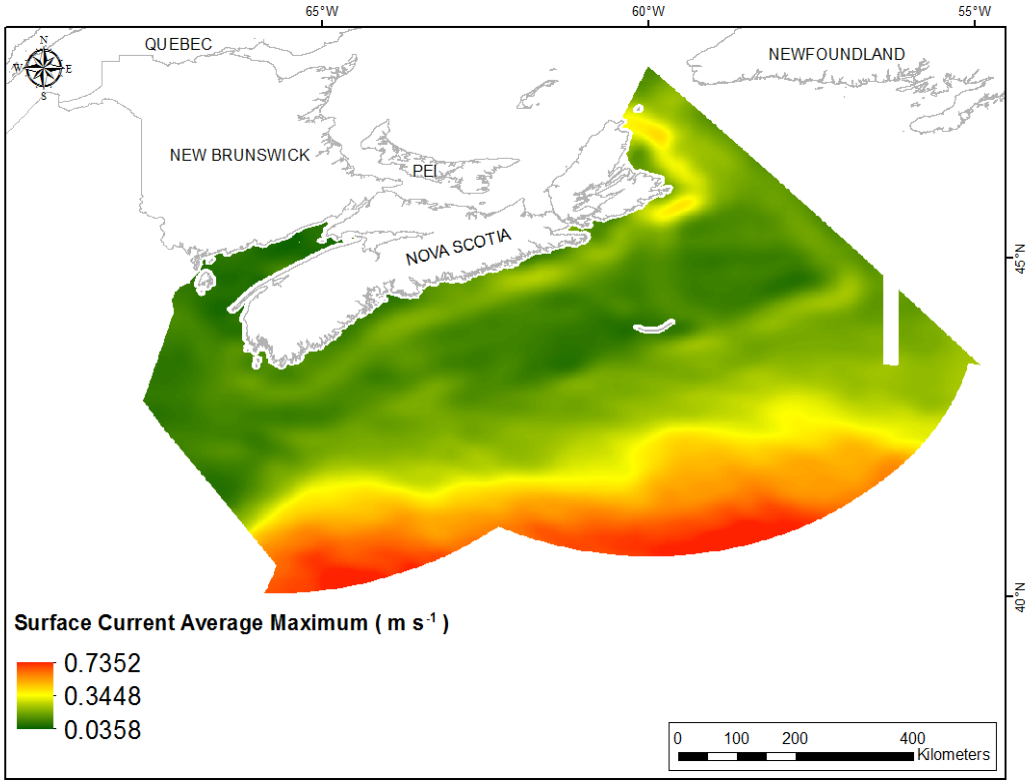

Fig. 210. Interpolated prediction surface of Surface Current Average Maximum (m s^{-1}).

Surface Current Average Range

This variable displayed a slightly right-skewed distribution prior to interpolation (Table 85, Fig. 211). The data were higher than predicted by a normal distribution at both tails, with mid-range values located below the reference line (Fig. 212). The areas of over- and under-prediction showed a strong spatial pattern (Fig. 212).

The semivariogram showed weak autocorrelation present in the data (Fig. 213). The model showed excellent fit between measured and predicted values (Fig. 213), and good performance was indicated by the cross-validation statistics (Table 86). The error map showed a 'bullseye' pattern with error increasing with distance from data points (Fig. 214). The kriged surface is presented in Fig. 215.

Table 85. Distributional properties of Surface Current Average Range (m s^{-1}).

Property	Value
Number of Observations	1152
Minimum	0.039
Maximum	0.641
Mean	0.223
Median	0.168
Standard Deviation	0.147
Skewness	1.084
Kurtosis	3.071

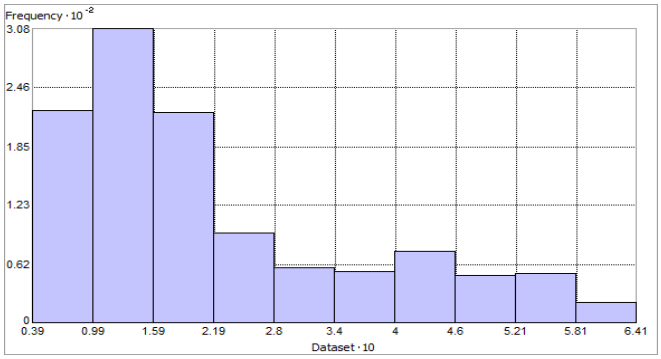

Fig. 211. Distribution of Surface Current Average Range (m s^{-1}). Histogram was illustrated using 10 bins. X axis shown at 10; Y axis shown at 10^{-2}.

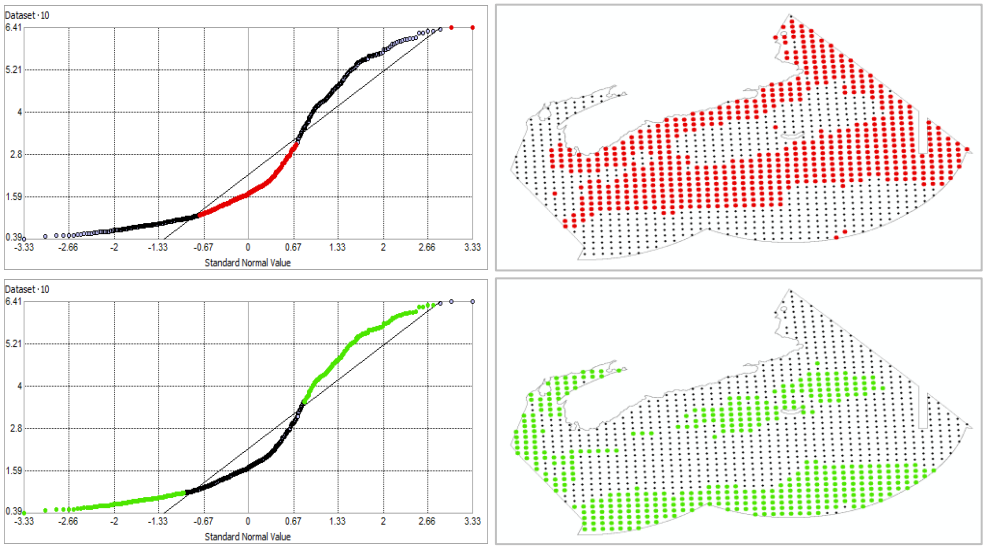

Fig. 212. Normal Q-Q plot for data values of Surface Current Average Range (m s^{-1}). Points falling under (upper panel) and over (bottom panel) the reference line are mapped.

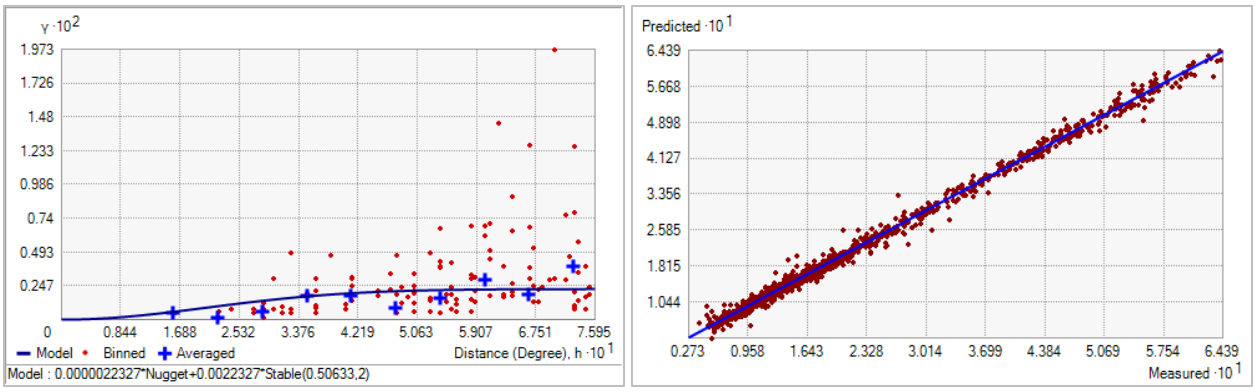

Fig. 213. Left panel: Semivariogram of Surface Current Average Range (m s^{-1}). Binned values are shown as red dots; average points are shown as blue crosses; the model fit to the averaged values is shown as a blue line. Lag size: 0.063 degrees; number of lags: 12; Parameter: 2; Range: 0.506 degrees; Partial Sill: 2.232 x 10^{-3}. Right panel: Scatterplot of predicted values versus observed values for the model of Surface Current Average Range (m s^{-1}).

Table 86. Results of cross-validation of the kriged model for Surface Current Average Range (m s^{-1}).

Prediction error	**Value**
Number of Observations	1152
Overall Mean Error	1.244 x 10^{-4}
Root Mean Square Prediction Error	0.011
Standardized Mean	3.765 x 10^{-3}
Standardized Root Mean Square Prediction Error	0.749
Average Standard Error	0.014

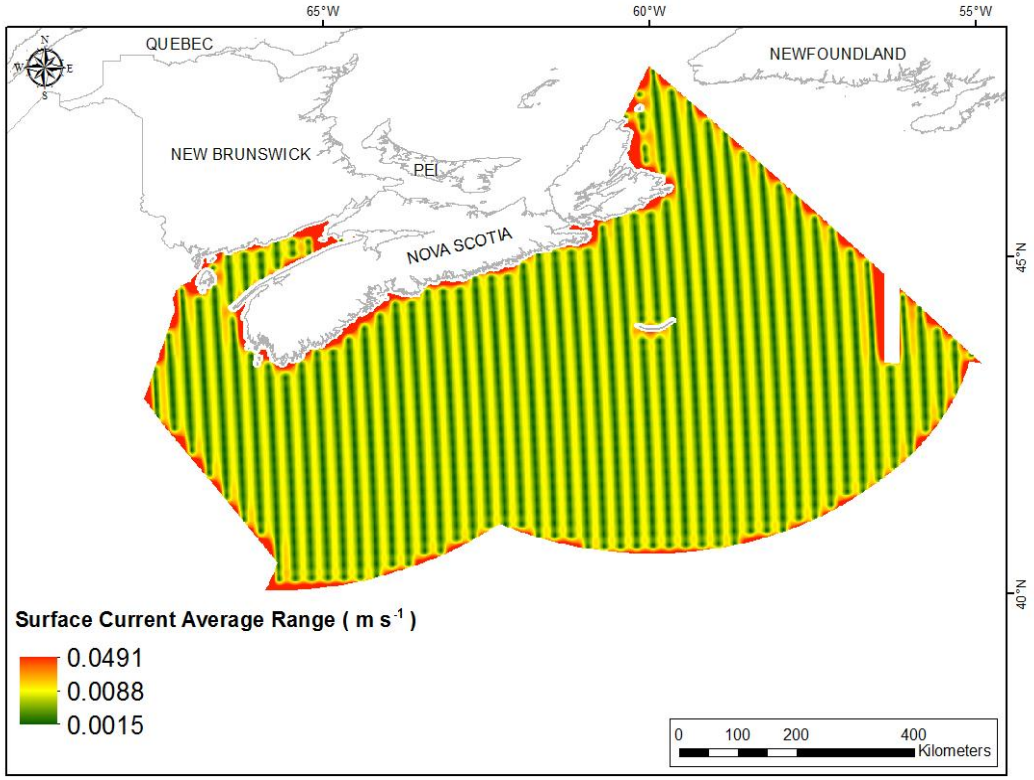

Fig. 214. Prediction standard error surface of Surface Current Average Range (m s^{-1}).

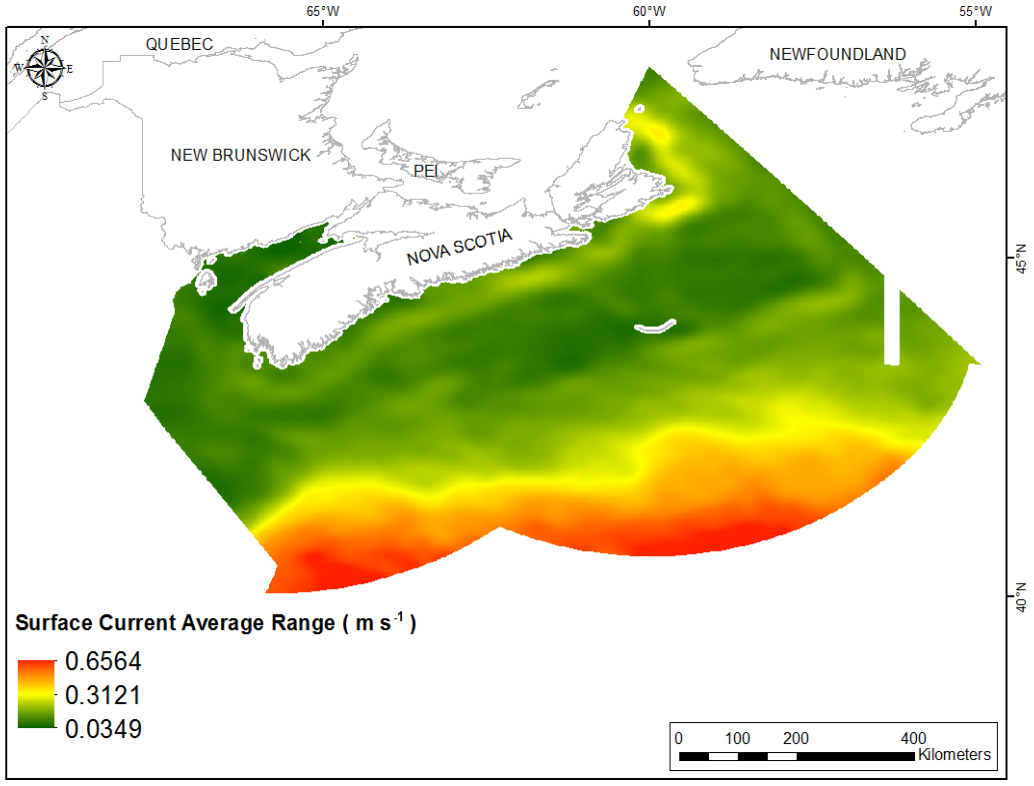

Fig. 215. Interpolated prediction surface of Surface Current Average Range (m s^{-1}).

Maximum Seasonal Mixed Layer Depth

Maximum mixed layer depth, or, the depth at which surface vertical mixing dissipates, is a near-universal feature of the open ocean (de Boyer Montégut et al., 2004). Within this mixed layer, salinity, temperature, or density are nearly uniform, a phenomenon caused by surface forcing, lateral advection, and internal wave processes that vary on diurnal, intra-seasonal, seasonal, and inter-annual scales (de Boyer Montégut et al., 2004). The depth of this mixed zone can show large spatial variability, ranging from less than 20 m in the summer hemisphere, to more than 500 m in the winter hemisphere at subpolar latitudes (de Boyer Montégut et al., 2004). The mixed layer depth has a significant influence on primary production in the surface waters. As the mixed layer depth increases it entrains nutrients from deeper waters below, supplying additional nutrients for primary production (Polovina et al., 1995; Carstensen et al., 2002).

Maximum Spring Mixed Layer Depth

This variable displayed a right-skewed distribution prior to interpolation (Table 87, Fig. 216). The data were higher than predicted by a normal distribution at both tails, with mid-range values located below the reference line (Fig. 217). The areas of over- and under-prediction showed no strong spatial pattern (Fig. 217).

The semivariogram showed weak autocorrelation present in the data (Fig. 218). The model showed a good fit between measured and predicted values (Fig. 218), but only fair performance as indicated by the cross validation statistics (Table 88). The error map showed a 'bullseye' pattern with error increasing with distance from data points (Fig. 219). The kriged surface is presented in Fig. 220.

Table 87. Distributional properties of Maximum Spring Mixed Layer Depth (m).

Property	Value
Number of Observations	1160
Minimum	11.762
Maximum	282.250
Mean	61.667
Median	33.134
Standard Deviation	55.948
Skewness	1.545
Kurtosis	4.352

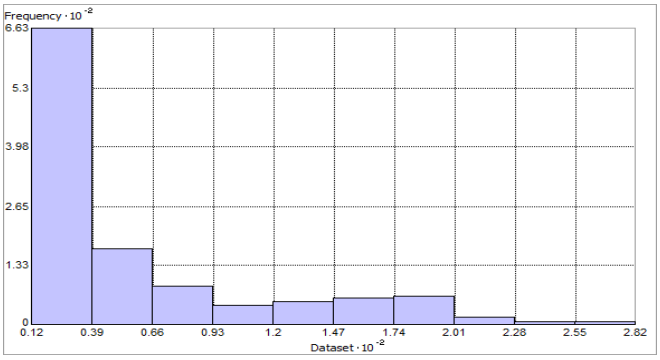

Fig. 216. Distribution of Maximum Spring Mixed Layer Depth (m). Histogram was illustrated using 10 bins. X axis is shown at 10^{-2}; Y axis is shown at 10^{-2}.

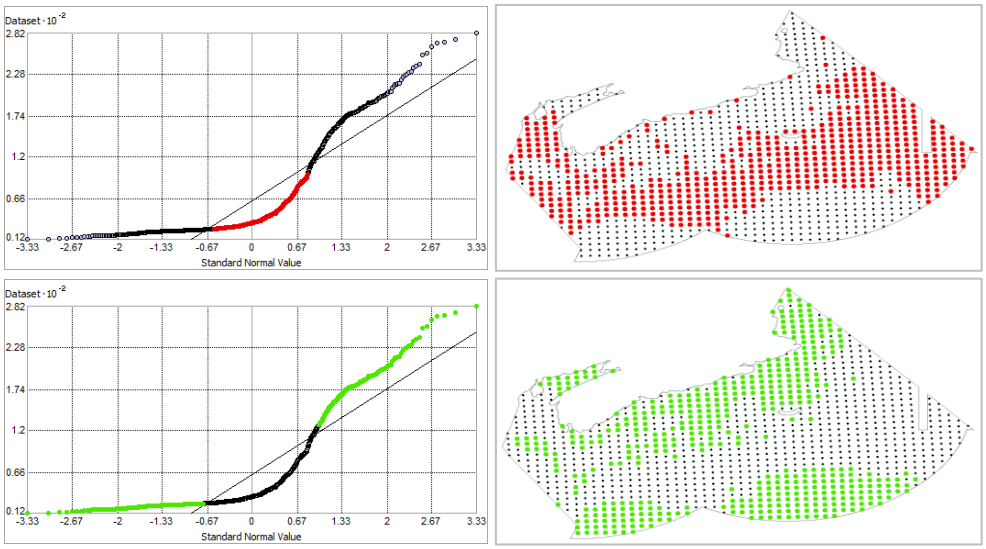

Fig. 217. Normal Q-Q plot for data values of Maximum Spring Mixed Layer Depth (m). Points falling under (upper panel) and over (bottom panel) the reference line are mapped.

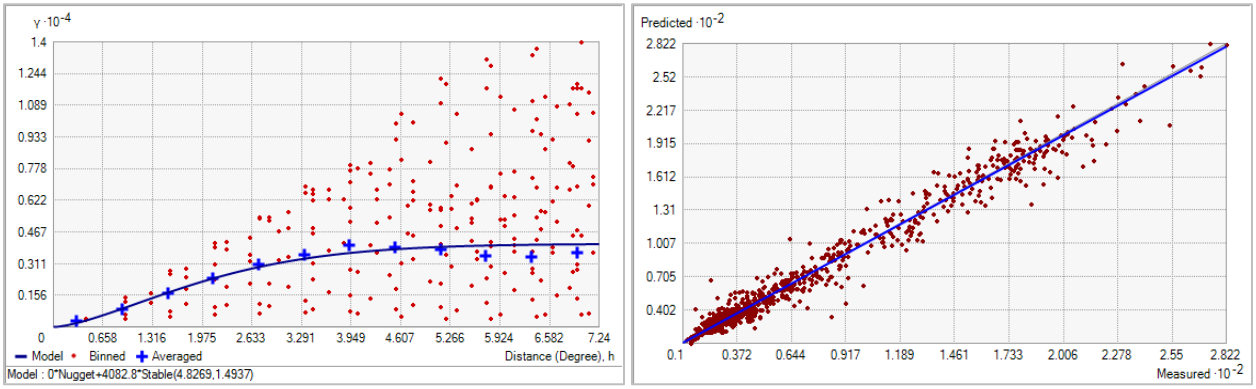

Fig. 218. Left panel: Semivariogram of Maximum Spring Mixed Layer Depth (m). Binned values are shown as red dots; average points are shown as blue crosses; the model fit to the averaged values is shown as a blue line. Lag size: 0.603 degrees; number of lags: 12; Parameter: 1.494; Range: 4.827 degrees; Partial Sill: 4082.815. Right panel: Scatterplot of predicted values versus observed values for the model of Maximum Spring Mixed Layer Depth (m).

Table 88. Results of cross-validation of the kriged model for Maximum Spring Mixed Layer Depth (m).

Prediction error	**Value**
Number of Observations	1160
Overall Mean Error	0.026
Root Mean Square Prediction Error	8.664
Standardized Mean	1.889×10^{-3}
Standardized Root Mean Square Prediction Error	1.243
Average Standard Error	6.869

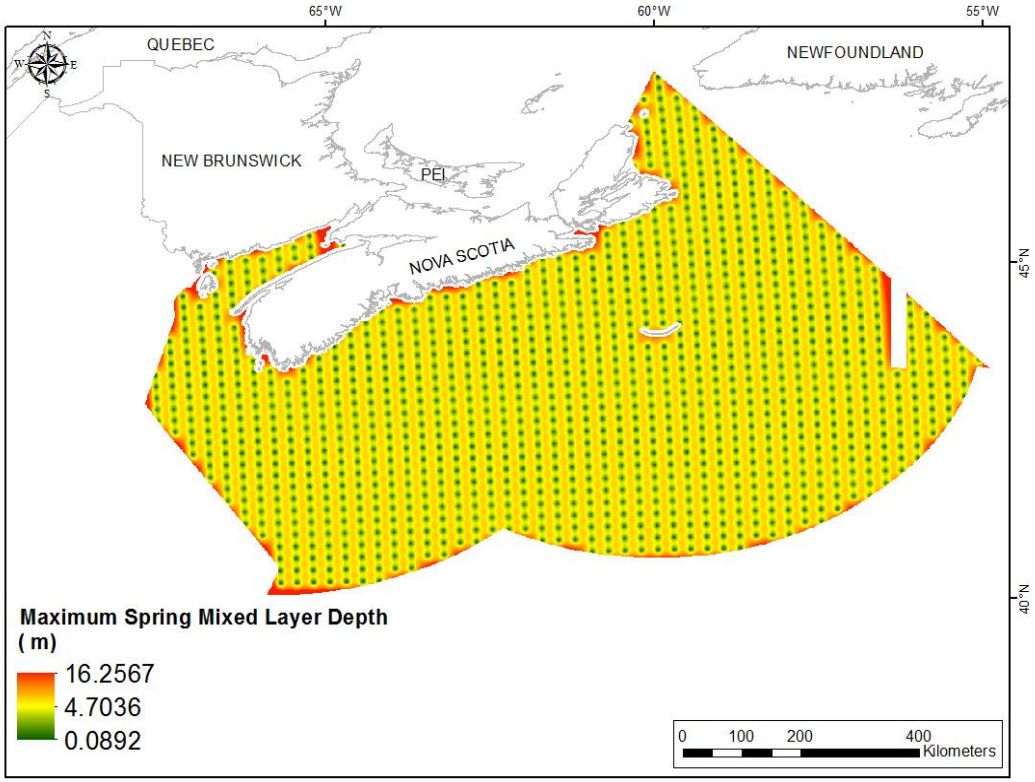

Fig. 219. Prediction standard error surface of Maximum Spring Mixed Layer Depth (m).

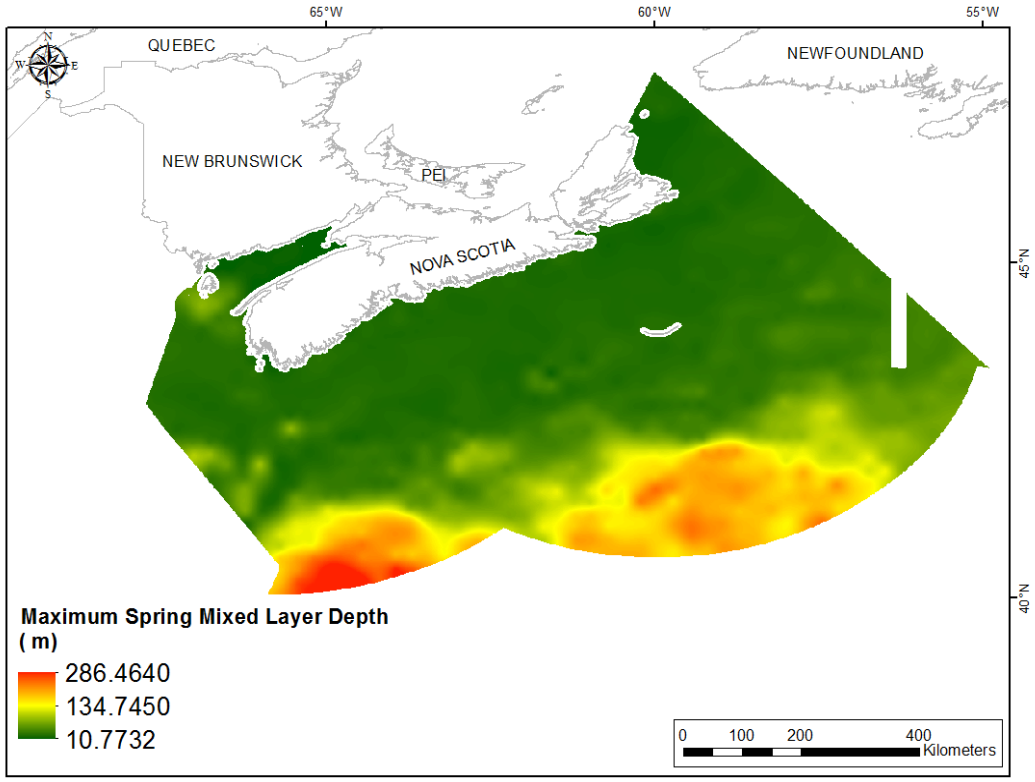

Fig. 220. Interpolated prediction surface of Maximum Spring Mixed Layer Depth (m).

Maximum Summer Mixed Layer Depth

This variable displayed a right-skewed distribution and slight bimodality prior to interpolation (Table 89, Fig. 221). The data were higher than predicted by a normal distribution at both tails, with mid-range values located below the reference line (Fig. 222). The areas of over- and under-prediction showed a spatial pattern (Fig. 222).

The semivariogram showed weak autocorrelation present in the data (Fig. 223). The model showed a good fit between measured and predicted values (Fig. 223), but only fair performance as indicated by the cross validation statistics (Table 90). The error map showed a 'bullseye' pattern with error increasing with distance from data points (Fig. 224). The kriged surface is presented in Fig. 225.

Table 89. Distributional properties of Maximum Summer Mixed Layer Depth (m).

Property	Value
Number of Observations	1160
Minimum	10.794
Maximum	44.340
Mean	21.990
Median	19.212
Standard Deviation	7.857
Skewness	0.957
Kurtosis	2.910

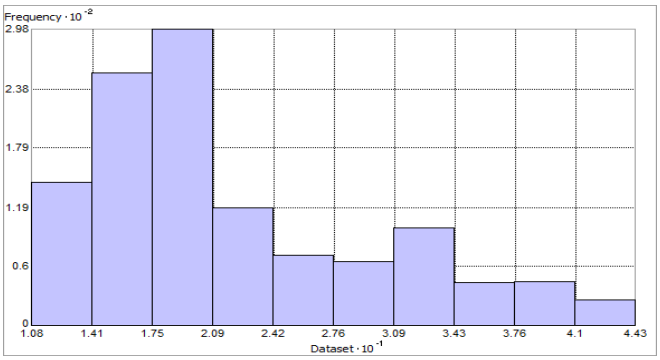

Fig. 221. Distribution of Maximum Summer Mixed Layer Depth (m). Histogram was illustrated using 10 bins. X axis is shown at 10^{-1}; Y axis is shown at 10^{-2}.

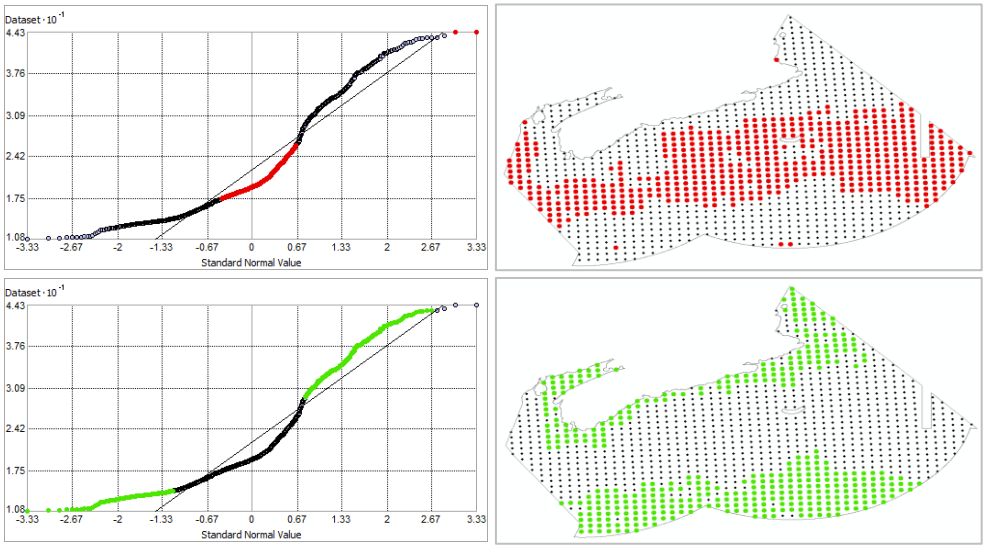

Fig. 222. Normal Q-Q plot for data values of Maximum Summer Mixed Layer Depth (m). Points falling under (upper panel) and over (bottom panel) the reference line are mapped.

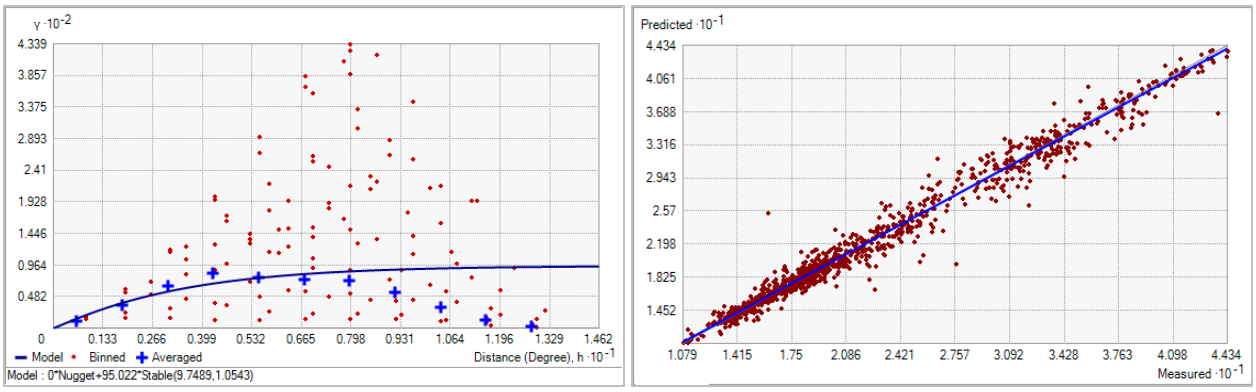

Fig. 223. Left panel: Semivariogram of Maximum Summer Mixed Layer Depth (m). Binned values are shown as red dots; average points are shown as blue crosses; the model fit to the averaged values is shown as a blue line. Lag size: 1.219 degrees; number of lags: 12; Parameter: 1.054; Range: 9.749 degrees; Partial Sill: 95.022. Right panel: Scatterplot of predicted values versus observed values for the model of Maximum Summer Mixed Layer Depth (m).

Table 90. Results of cross-validation of the kriged model for Maximum Summer Mixed Layer Depth (m).

Prediction error	**Value**
Number of Observations	1160
Overall Mean Error	-6.465×10^{-3}
Root Mean Square Prediction Error	1.183
Standardized Mean	-1.250×10^{-3}
Standardized Root Mean Square Prediction Error	0.618
Average Standard Error	1.916

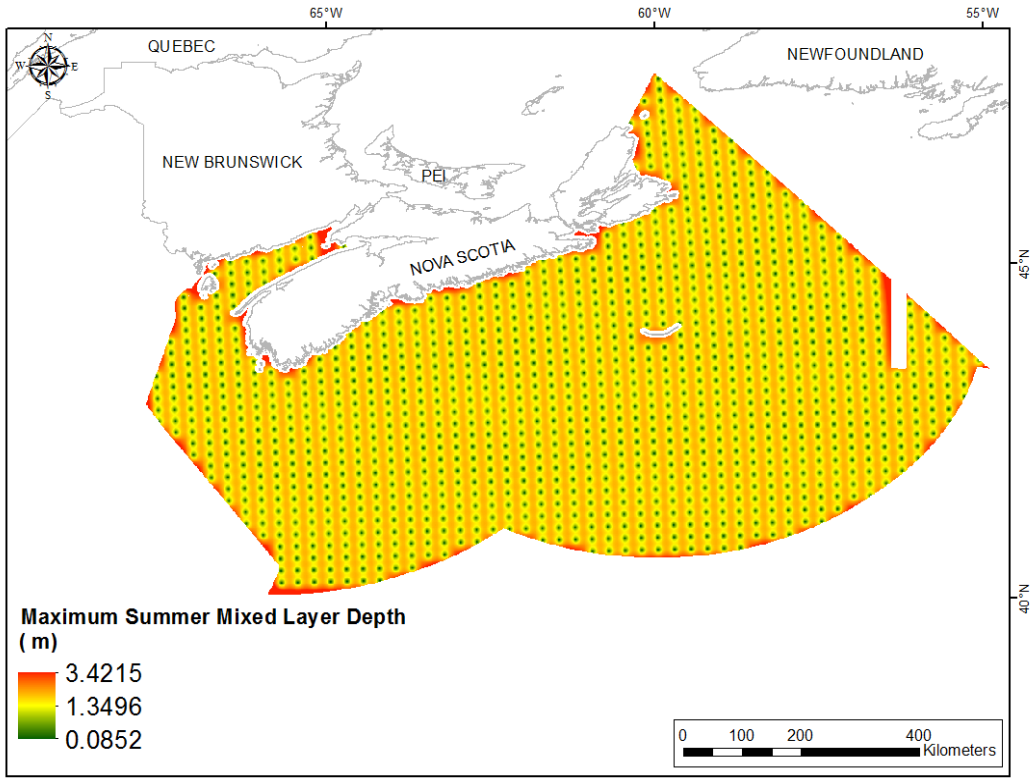

Fig. 224. Prediction standard error surface of Maximum Summer Mixed Layer Depth (m).

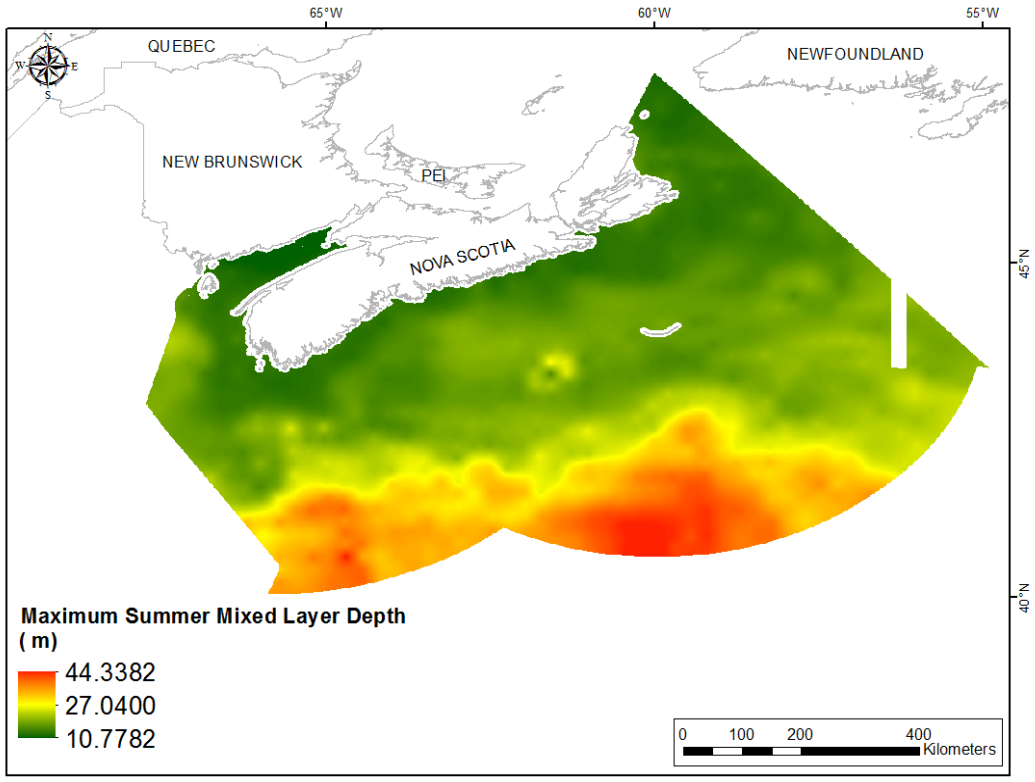

Fig. 225. Interpolated prediction surface of Maximum Summer Mixed Layer Depth (m).

Maximum Fall Mixed Layer Depth

This variable displayed a right-skewed, leptokurtic distribution prior to interpolation (Table 91, Fig. 226). The data were higher than predicted by a normal distribution at both tails, with mid-range values located below the reference line (Fig. 227). The areas of over- and under-prediction showed spatial pattern (Fig. 227).

The semivariogram showed weak autocorrelation present in the data (Fig. 228). The model showed a good fit between measured and predicted values (Fig. 228), and good performance as indicated by the cross validation statistics (Table 92). The error map showed a 'bullseye' pattern with error increasing with distance from data points (Fig. 229). The kriged surface is presented in Fig. 230.

Table 91. Distributional properties of Maximum Fall Mixed Layer Depth (m).

Property	Value
Number of Observations	1160
Minimum	11.985
Maximum	215.33
Mean	64.812
Median	51.220
Standard Deviation	35.349
Skewness	1.279
Kurtosis	4.415

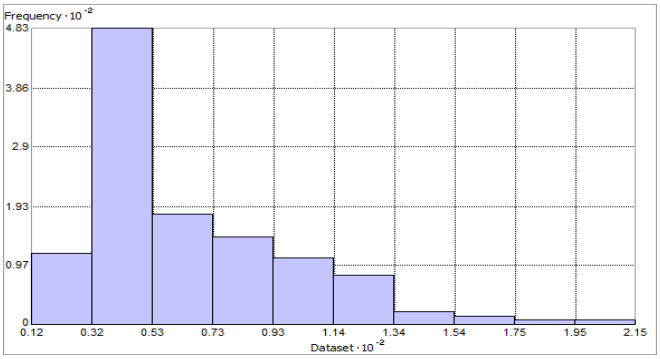

Fig. 226. Distribution of Maximum Fall Mixed Layer Depth (m). Histogram was illustrated using 10 bins. X and Y axes shown at 10^{-2}.

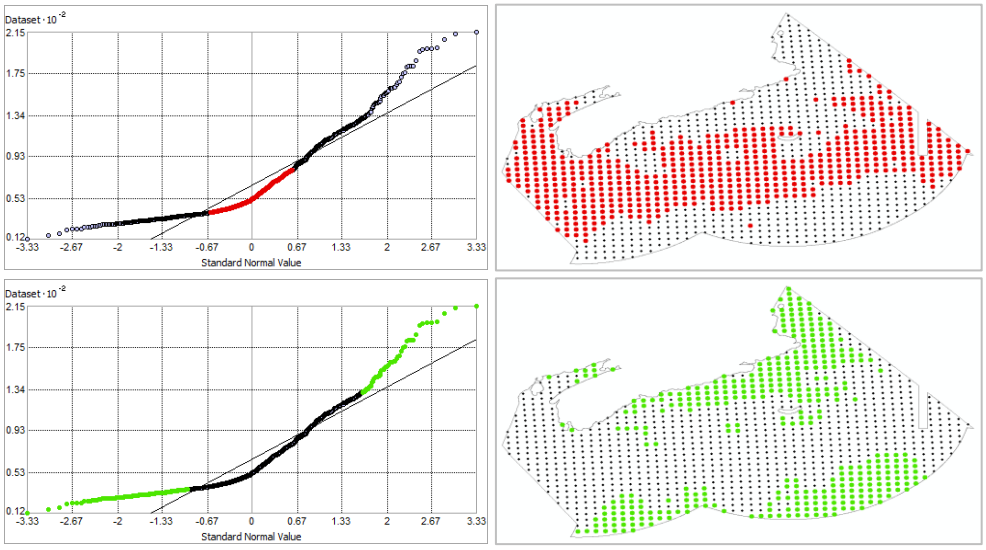

Fig. 227. Normal Q-Q plot for data values of Maximum Fall Mixed Layer Depth (m). Points falling under (upper panel) and over (bottom panel) the reference line are mapped.

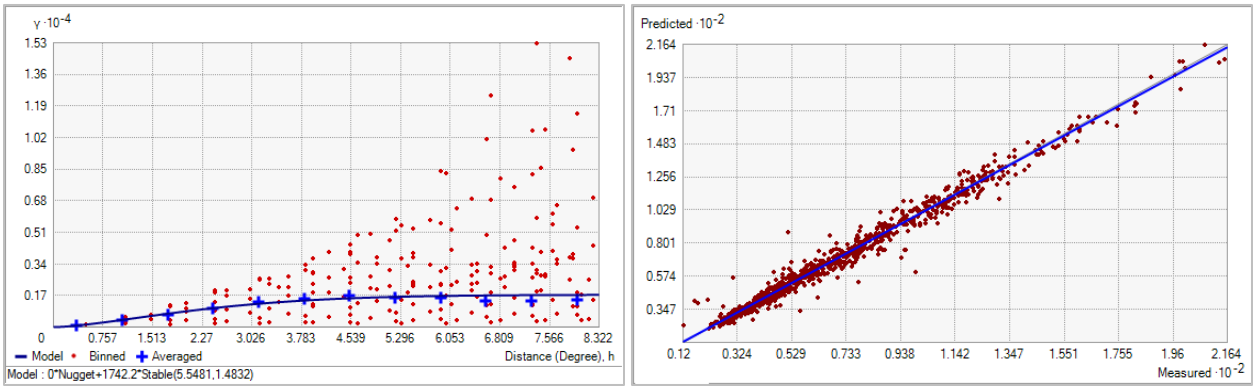

Fig. 228. Left panel: Semivariogram of Maximum Fall Mixed Layer Depth (m). Binned values are shown as red dots; average points are shown as blue crosses; the model fit to the averaged values is shown as a blue line. Lag size: 0.694 degrees; number of lags: 12; Parameter: 1.483; Range: 5.548 degrees; Partial Sill: 1742.209. Right panel: Scatterplot of predicted values versus observed values for the model of Maximum Fall Mixed Layer Depth (m).

Table 92. Results of cross-validation of the kriged model for Maximum Fall Mixed Layer Depth (m).

Prediction error	**Value**
Number of Observations	1160
Overall Mean Error	0.030
Root Mean Square Prediction Error	4.671
Standardized Mean	3.257×10^{-3}
Standardized Root Mean Square Prediction Error	1.102
Average Standard Error	4.148

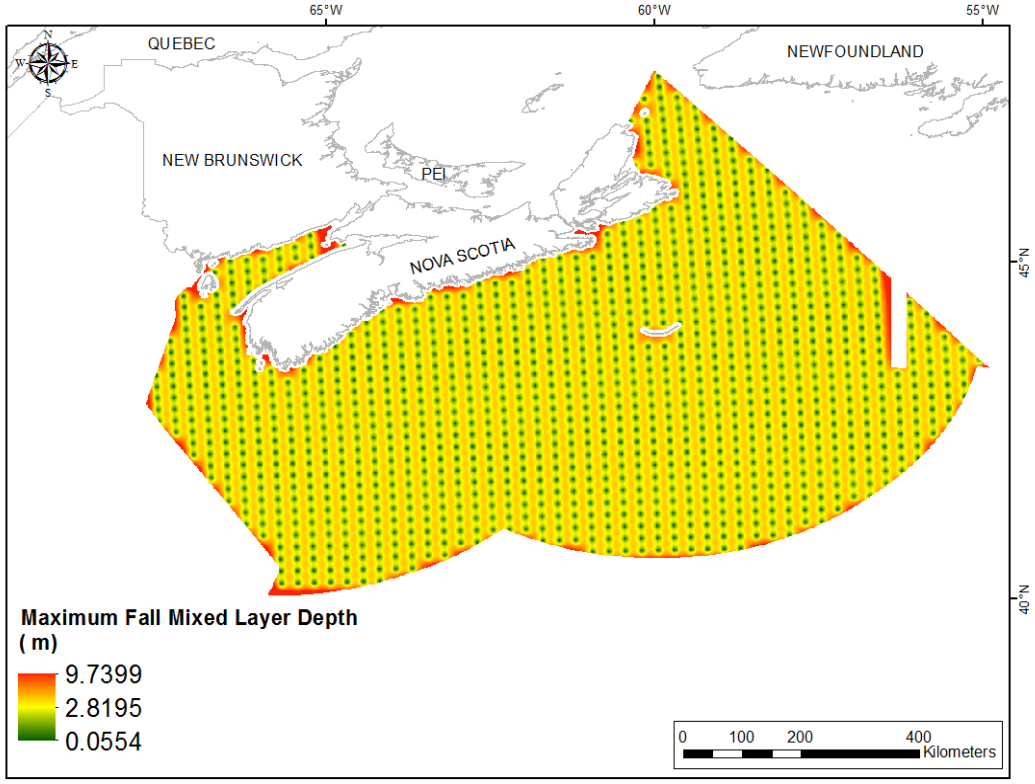

Fig. 229. Prediction standard error surface of Maximum Fall Mixed Layer Depth (m).

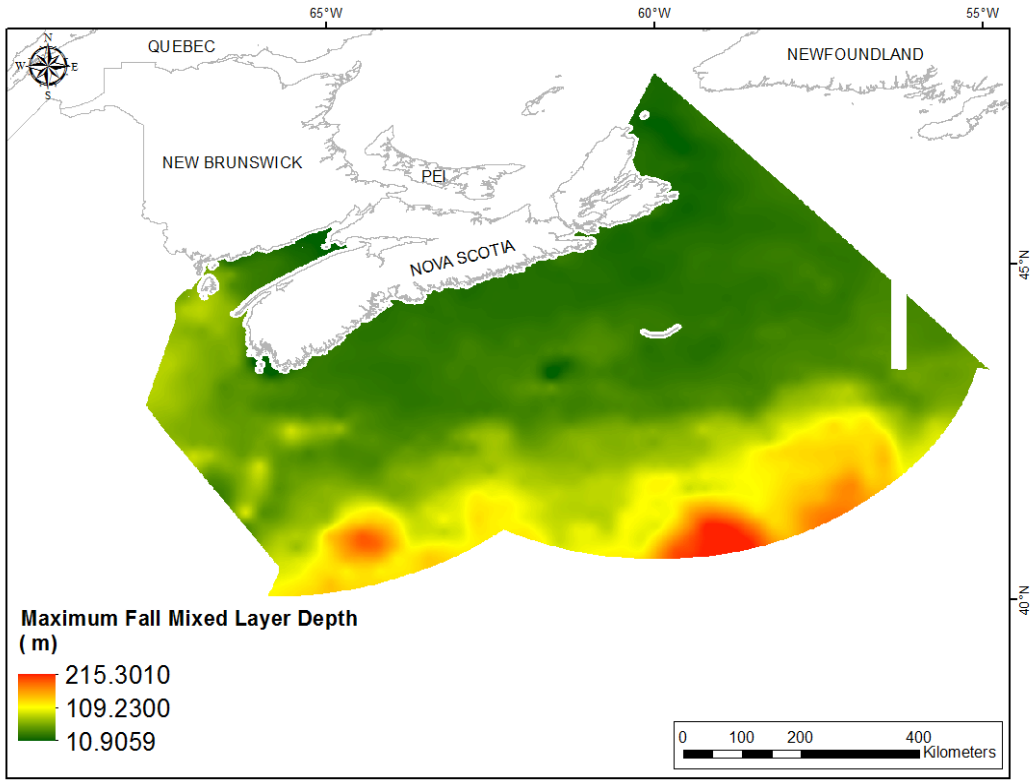

Fig. 230. Interpolated prediction surface of Maximum Fall Mixed Layer Depth (m).

Maximum Winter Mixed Layer Depth

This variable displayed a right-skewed distribution and kurtosis (Table 93, Fig. 231). The data were higher than predicted by a normal distribution at both tails, with mid-range values located below the reference line (Fig. 232). The areas of over- and under-prediction showed a strong spatial pattern (Fig. 232).

The semivariogram showed little to no autocorrelation present in the data (Fig. 233). The model showed a good fit between measured and predicted values (Fig. 233), and good performance was indicated by the cross-validation statistics (Table 94). The error map showed a 'bullseye' pattern with error increasing with distance from data points (Fig. 234). The kriged surface is presented in Fig. 235.

Table 93. Distributional properties of Maximum Winter Mixed Layer Depth (m).

Property	Value
Number of Observations	1160
Minimum	11.982
Maximum	356.520
Mean	99.387
Median	64.985
Standard Deviation	75.870
Skewness	1.165
Kurtosis	3.257

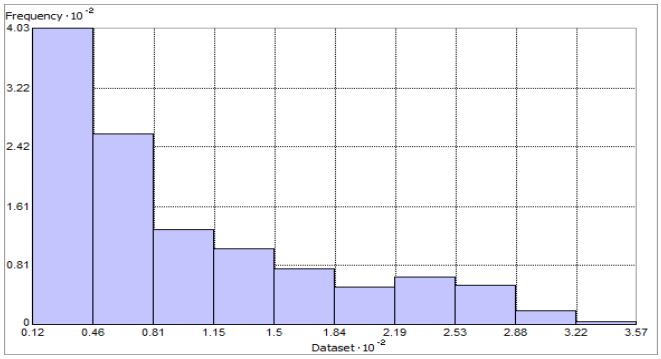

Fig. 231. Distribution of Maximum Winter Mixed Layer Depth (m). Histogram was illustrated using 10 bins. X and Y axes are shown at 10^{-2}.

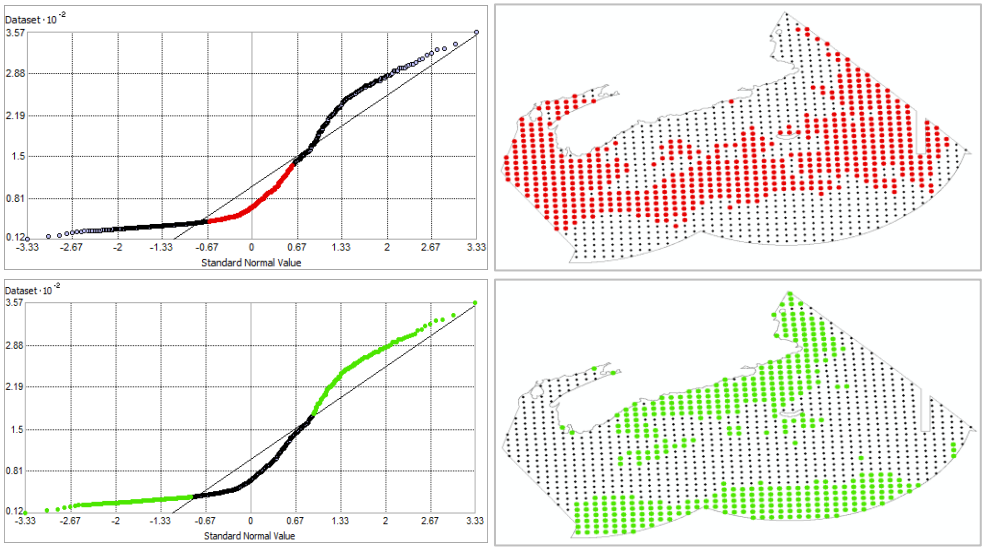

Fig. 232. Normal Q-Q plot for data values of Maximum Winter Mixed Layer Depth (m). Points falling under (upper panel) and over (bottom panel) the reference line are mapped.

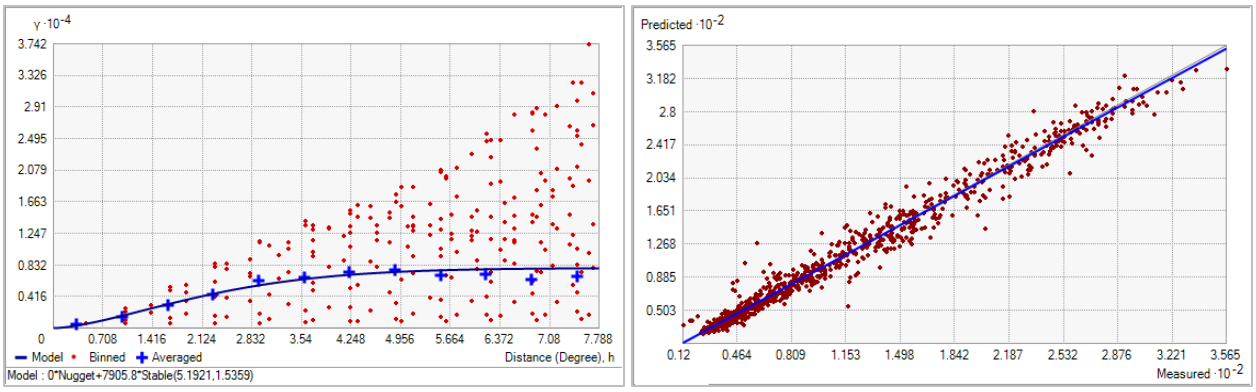

Fig. 233. Left panel: Semivariogram of Maximum Winter Mixed Layer Depth (m). Binned values are shown as red dots; average points are shown as blue crosses; the model fit to the averaged values is shown as a blue line. Lag size: 0.649 degrees; number of lags: 12; Parameter: 1.536; Range: 5.192 degrees; Partial Sill: 7905.802. Right panel: Scatterplot of predicted values versus observed values for the model of Maximum Winter Mixed Layer Depth (m).

Table 94. Results of cross-validation of the kriged model for Maximum Winter Mixed Layer Depth (m).

Prediction error	**Value**
Number of Observations	1160
Overall Mean Error	0.075
Root Mean Square Prediction Error	10.383
Standardized Mean	4.062×10^{-3}
Standardized Root Mean Square Prediction Error	1.256
Average Standard Error	8.092

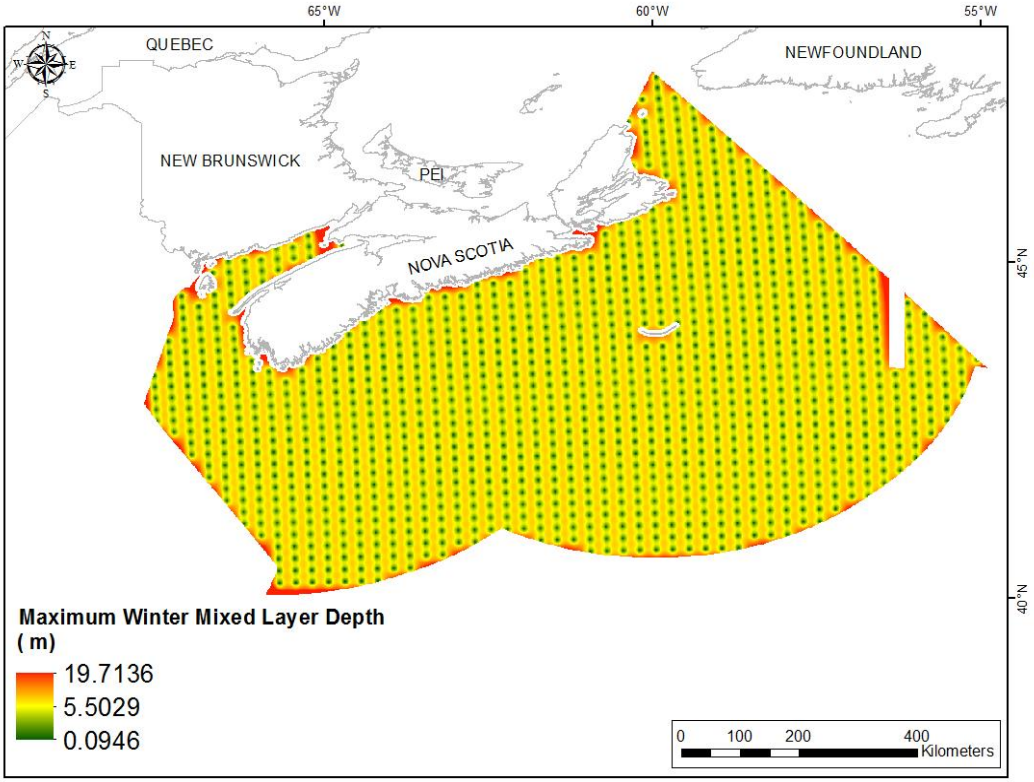

Fig. 234. Prediction standard error surface of Maximum Winter Mixed Layer Depth (m).

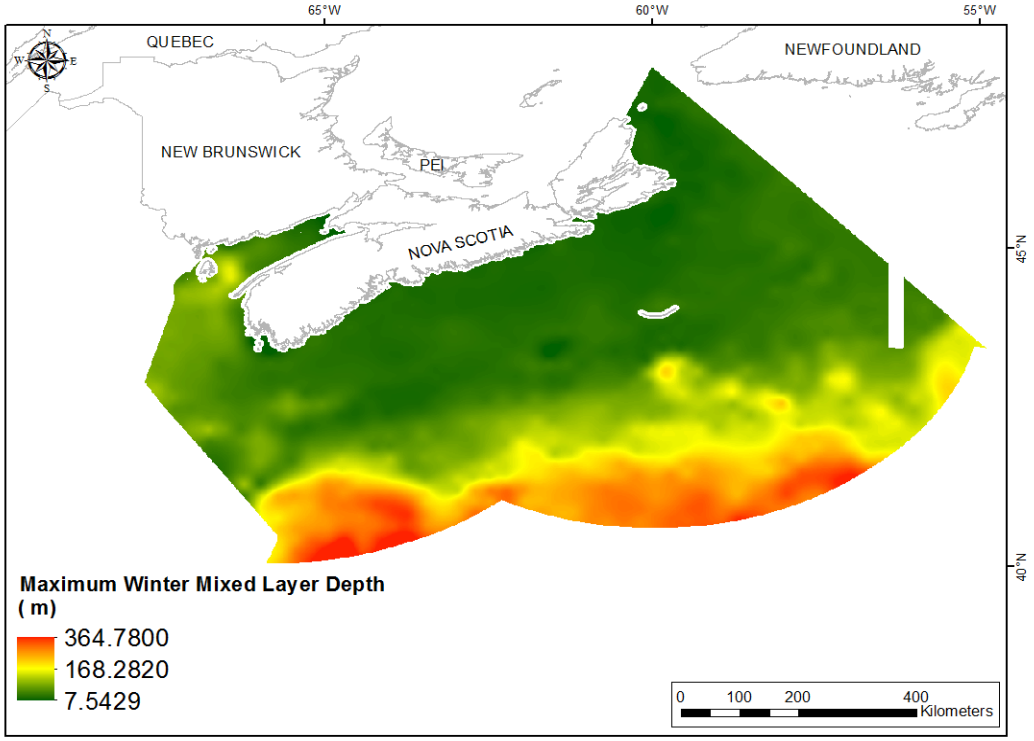

Fig. 235. Interpolated prediction surface of Maximum Winter Mixed Layer Depth (m).

Maximum Average Spring Mixed Layer Depth

This variable displayed a right-skewed, leptokurtic distribution prior to interpolation (Table 95, Fig. 236). The data were higher than predicted by a normal distribution at both tails, with mid-range values located below the reference line (Fig. 237). The areas of over- and under-prediction showed spatial pattern (Fig. 237).

The semivariogram showed weak autocorrelation present in the data (Fig. 238). The model showed a good fit between measured and predicted values (Fig. 238), but poor performance was indicated by the poor cross-validation statistics (Table 96). The Standardized Root-Mean-Square Prediction Error was greater than 1 indicating that variability in the predictions has been underestimated. The error map showed high error along the edges of the study extent (Fig. 239). The kriged surface is presented in Fig. 240.

Table 95. Distributional properties of Maximum Average Spring Mixed Layer Depth (m).

Property	Value
Number of Observations	1160
Minimum	11.022
Maximum	87.219
Mean	29.830
Median	21.428
Standard Deviation	18.376
Skewness	1.509
Kurtosis	4.043

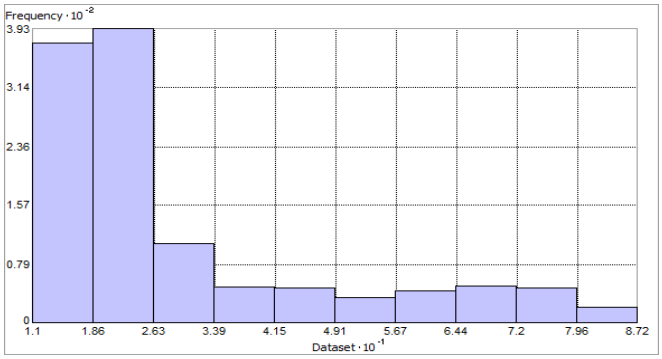

Fig. 236. Distribution of Maximum Average Spring Mixed Layer Depth (m). Histogram was illustrated using 10 bins. X axis is shown at 10^{-1}; Y axis is shown at 10^{-2}.

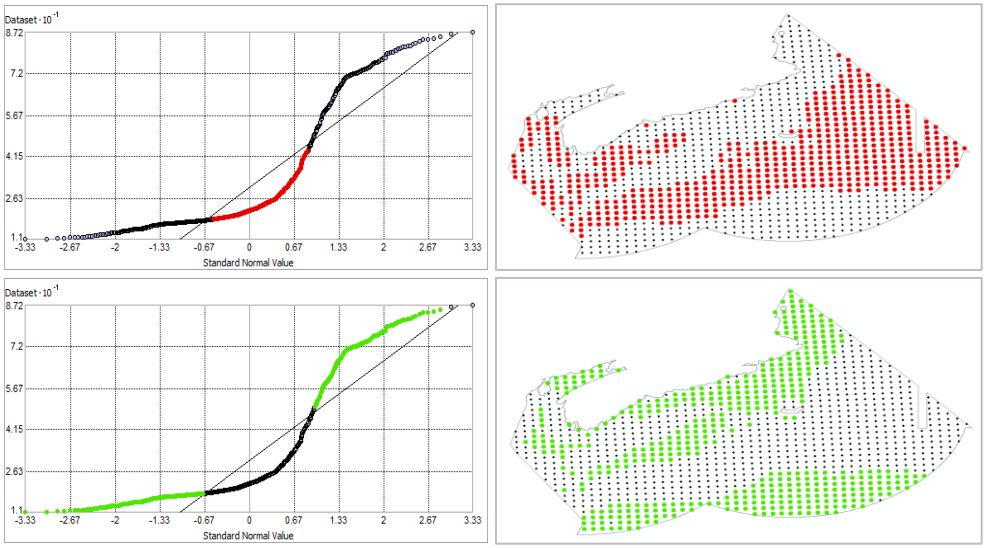

Fig. 237. Normal Q-Q plot for data values of Maximum Average Spring Mixed Layer Depth (m). Points falling under (upper panel) and over (bottom panel) the reference line are mapped.

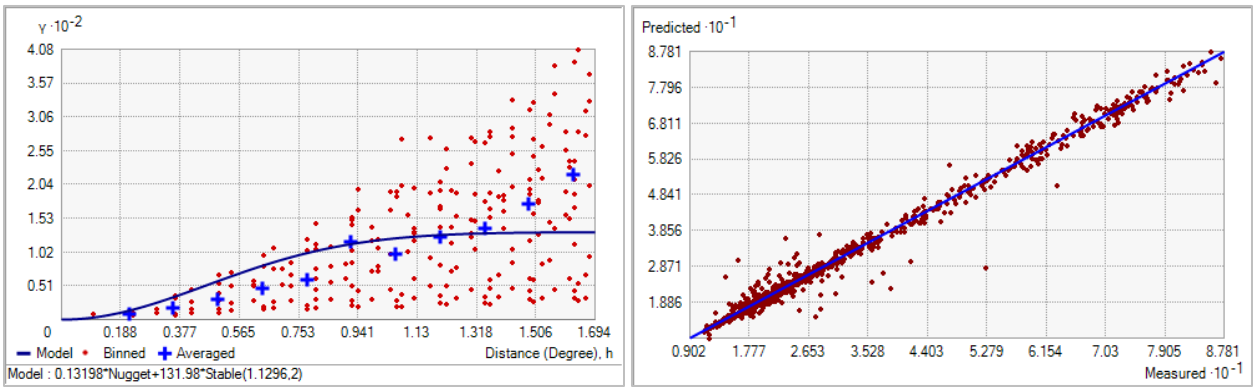

Fig. 238. Left panel: Semivariogram of Maximum Average Spring Mixed Layer Depth (m). Binned values are shown as red dots; average points are shown as blue crosses; the model fit to the averaged values is shown as a blue line. Lag size: 0.141 degrees; number of lags: 12; Parameter: 2; Range: 1.130 degrees; Partial Sill: 131.982. Right panel: Scatterplot of predicted values versus observed values for the model of Maximum Average Spring Mixed Layer Depth (m).

Table 96. Results of cross-validation of the kriged model for Maximum Average Spring Mixed Layer Depth (m).

Prediction error	**Value**
Number of Observations	1160
Overall Mean Error	3.935×10^{-3}
Root Mean Square Prediction Error	2.000
Standardized Mean	-1.155×10^{-3}
Standardized Root Mean Square Prediction Error	3.524
Average Standard Error	0.671

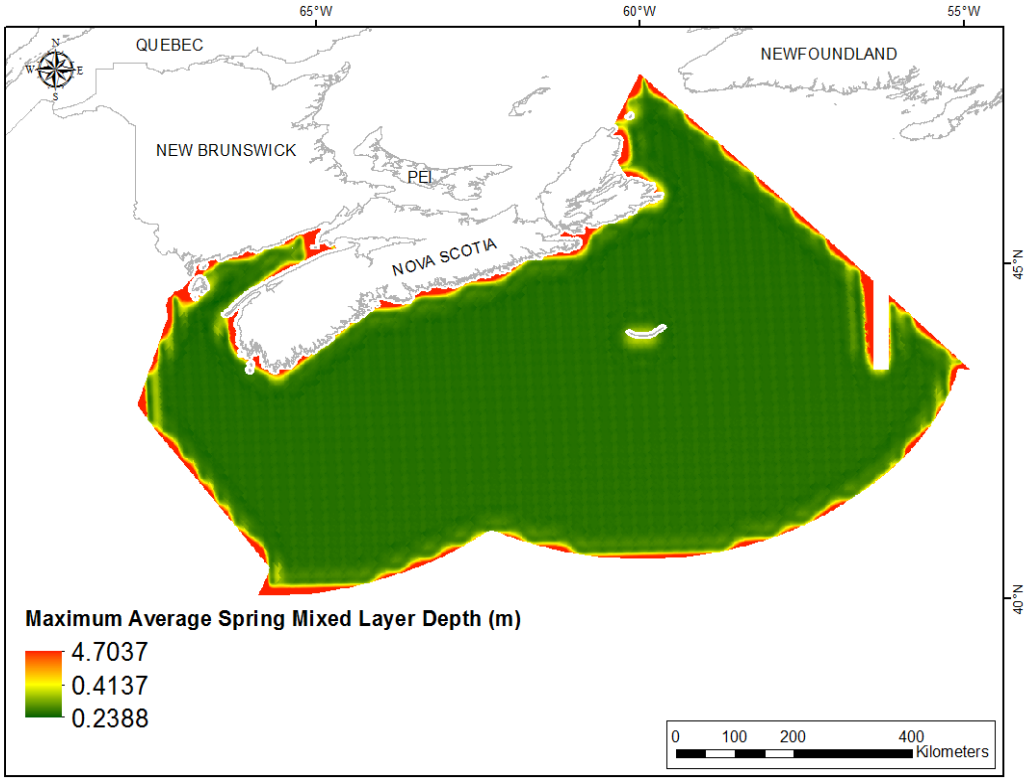

Fig. 239. Prediction standard error surface of Maximum Average Spring Mixed Layer Depth (m).

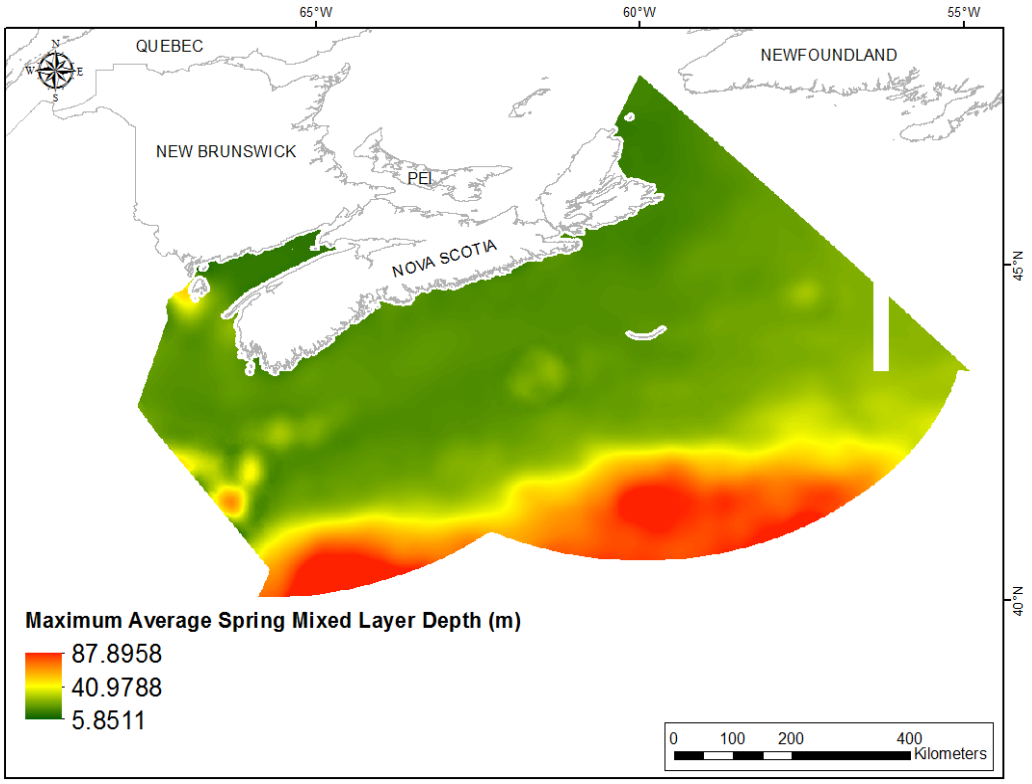

Fig. 240. Interpolated prediction surface of Maximum Average Spring Mixed Layer Depth (m).

Maximum Average Summer Mixed Layer Depth

This variable displayed a right-skewed, leptokurtic distribution prior to interpolation (Table 97, Fig. 241). The data were higher than predicted by a normal distribution at both tails, with mid-range values located below the reference line (Fig. 242). The areas of over- and under-prediction showed spatial pattern (Fig. 242).

The semivariogram showed weak autocorrelation present in the data (Fig. 243). The model showed an excellent fit between measured and predicted values (Fig. 243), with fair performance indicated by the cross-validation statistics (Table 98). The error map showed a 'bullseye' pattern with error increasing with distance from data points (Fig. 244). The kriged surface is presented in Fig. 245.

Table 97. Distributional properties of Maximum Average Summer Mixed Layer Depth (m).

Property	Value
Number of Observations	1160
Minimum	10.771
Maximum	28.408
Mean	15.879
Median	14.501
Standard Deviation	4.1007
Skewness	1.217
Kurtosis	3.528

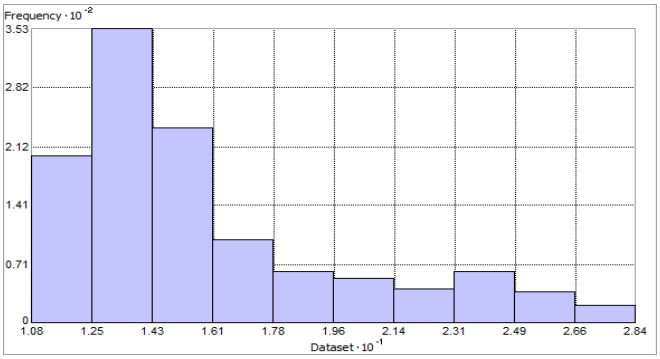

Fig. 241. Distribution of Maximum Average Summer Mixed Layer Depth (m). Histogram was illustrated using 10 bins. X axis shown at 10^{-1}; Y axis is shown at 10^{-2}.

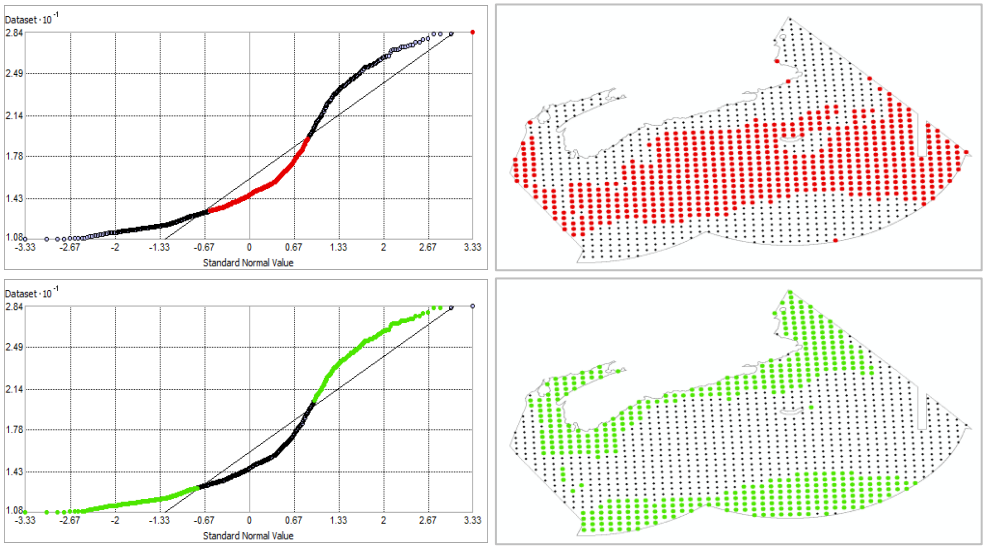

Fig. 242. Normal Q-Q plot for data values of Maximum Average Summer Mixed Layer Depth (m). Points falling under (upper panel) and over (bottom panel) the reference line are mapped.

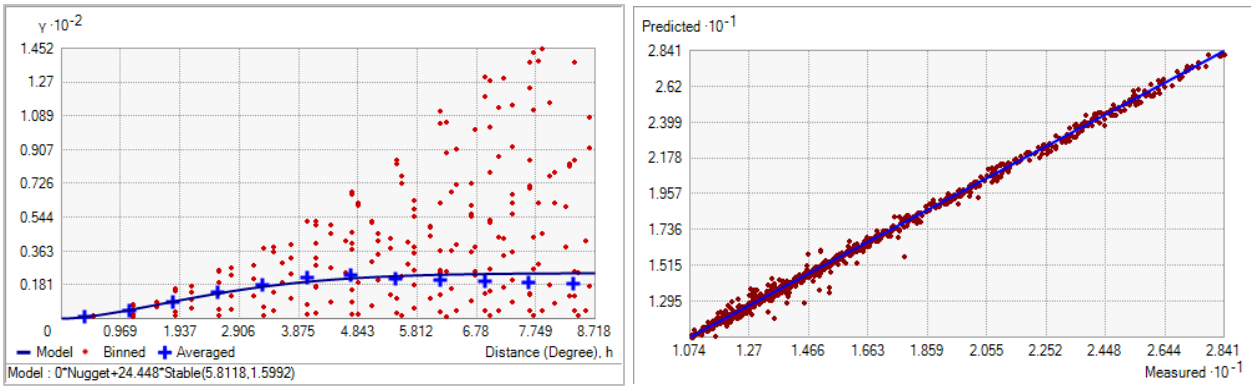

Fig. 243. Left panel: Semivariogram of Maximum Average Summer Mixed Layer Depth (m). Binned values are shown as red dots; average points are shown as blue crosses; the model fit to the averaged values is shown as a blue line. Lag size: 0.726 degrees; number of lags: 12; Parameter: 1.599; Range: 5.812 degrees; Partial Sill: 24.448. Right panel: Scatterplot of predicted values versus observed values for the model of Maximum Average Summer Mixed Layer Depth (m).

Table 98. Results of cross-validation of the kriged model for Maximum Average Summer Mixed Layer Depth (m).

Prediction error	**Value**
Number of Observations	1160
Overall Mean Error	-1.503×10^{-3}
Root Mean Square Prediction Error	0.248
Standardized Mean	-9.168×10^{-4}
Standardized Root Mean Square Prediction Error	0.714
Average Standard Error	0.345

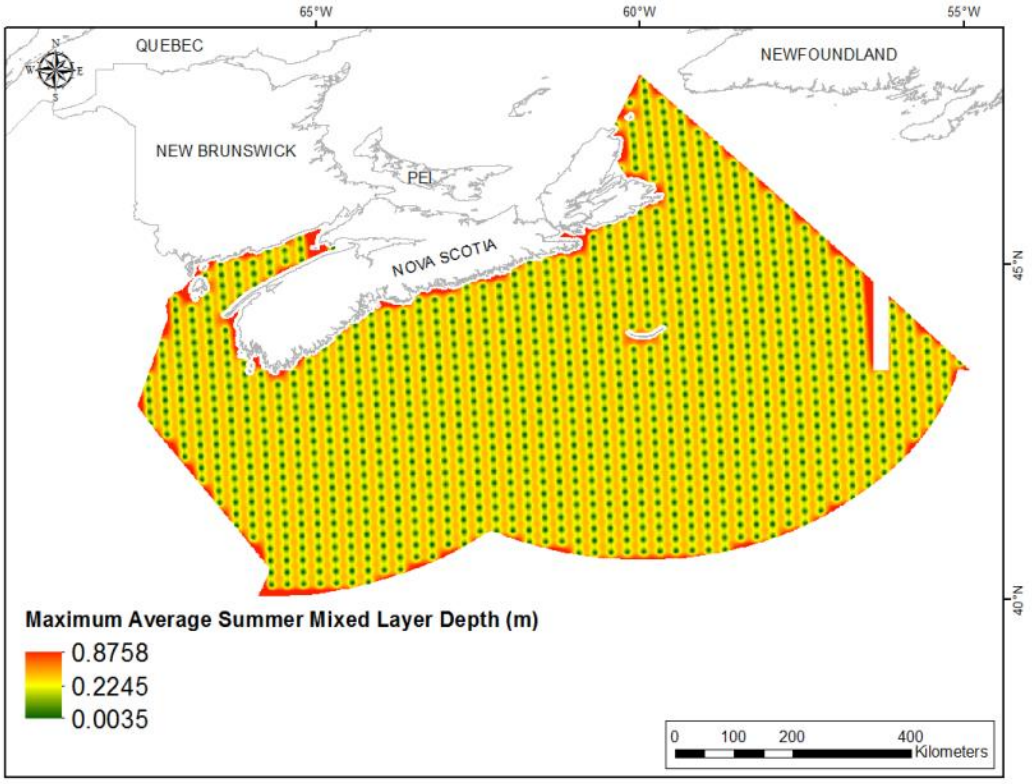

Fig. 244. Prediction standard error surface of Maximum Average Summer Mixed Layer Depth (m).

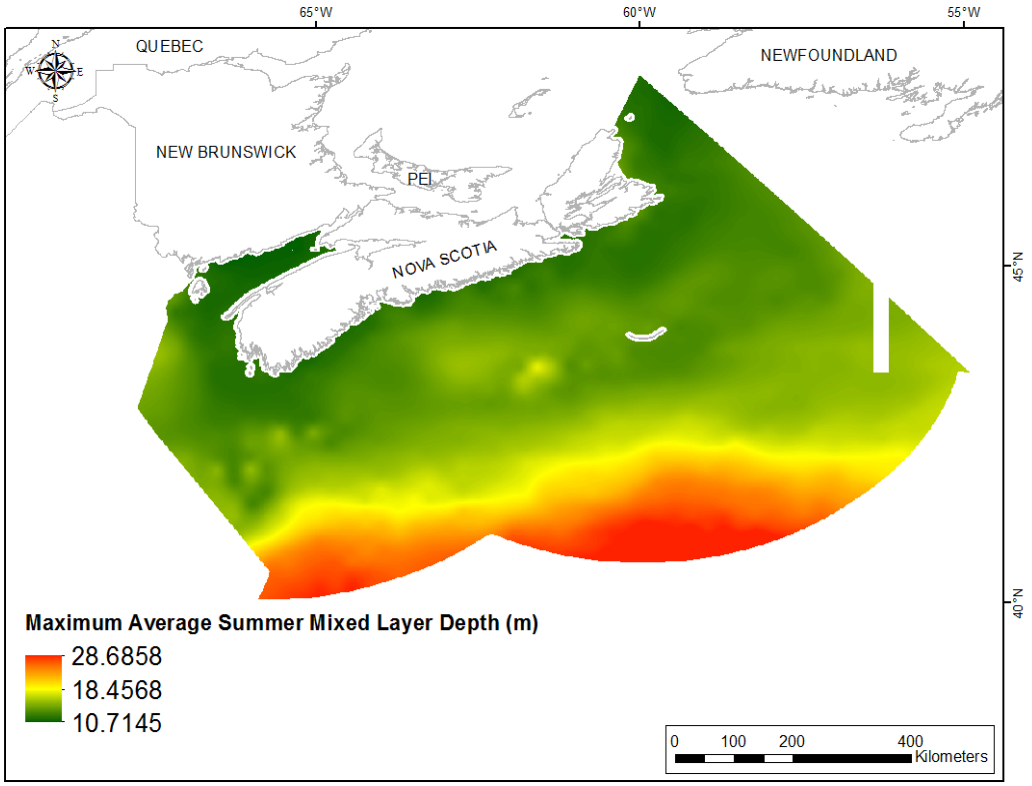

Fig. 245. Interpolated prediction surface of Maximum Average Summer Mixed Layer Depth (m).

Maximum Average Fall Mixed Layer Depth

This variable displayed a right-skewed, slightly bimodal distribution prior to interpolation (Table 99, Fig. 246). The data were higher than predicted by a normal distribution at low and high values, with mid-range and the highest values located below the reference line (Fig. 247). The areas of over- and under-prediction showed spatial pattern (Fig. 247).

The semivariogram showed weak autocorrelation present in the data (Fig. 248). The model showed an excellent fit between measured and predicted values (Fig. 248), but poor performance was indicated by the cross-validation statistics (Table 100). The Standardized Root-Mean-Square Prediction Error was greater than 1 indicating that variability in the predictions has been underestimated. The error map showed a 'bullseye' pattern with error increasing with distance from data points (Fig. 249). The kriged surface is presented in Fig. 250.

Table 99. Distributional properties of Maximum Average Fall Mixed Layer Depth (m).

Property	Value
Number of Observations	1160
Minimum	11.907
Maximum	97.178
Mean	42.796
Median	36.894
Standard Deviation	17.850
Skewness	0.977
Kurtosis	3.002

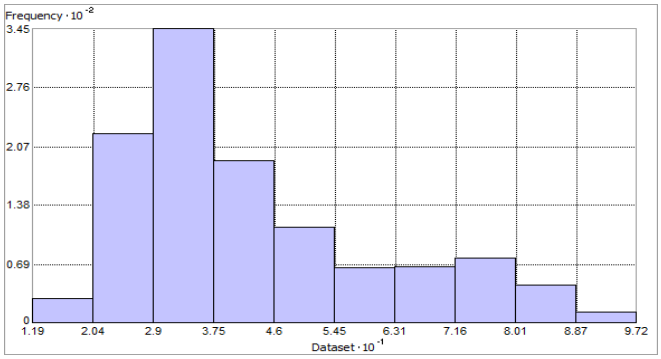

Fig. 246. Distribution of Maximum Average Fall Mixed Layer Depth (m). Histogram was illustrated using 10 bins. X axis is shown at 10^{-1}; Y axis is shown at 10^{-2}.

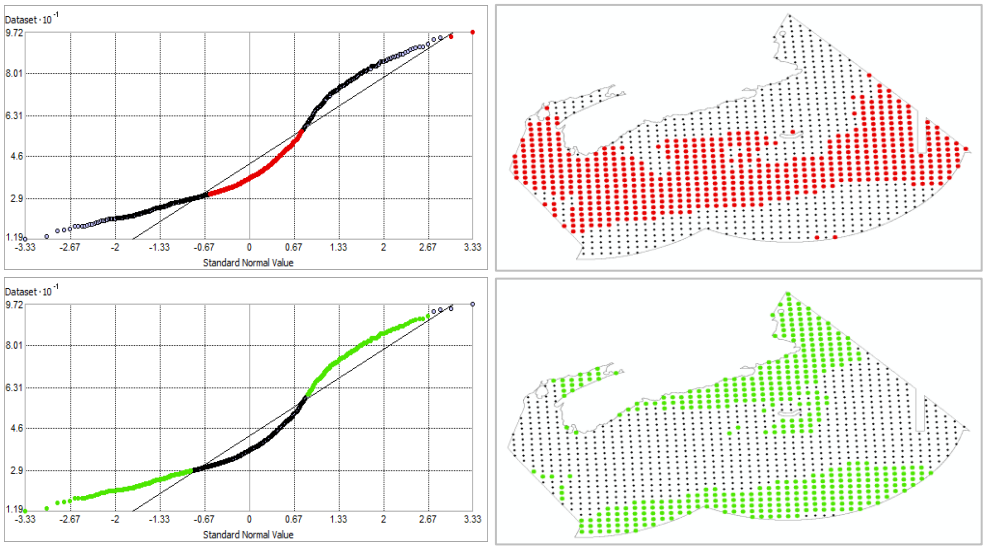

Fig. 247. Normal Q-Q plot for data values of Maximum Average Fall Mixed Layer Depth (m). Points falling under (upper panel) and over (bottom panel) the reference line are mapped.

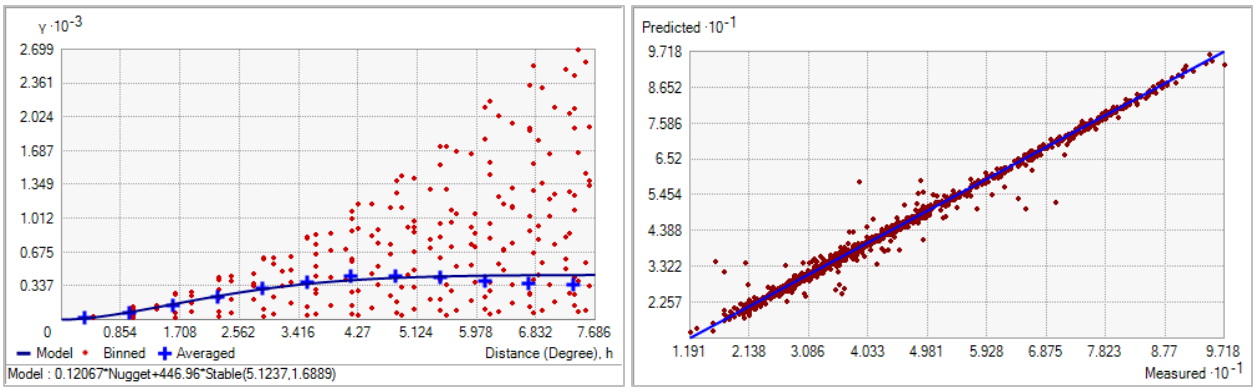

Fig. 248. Left panel: Semivariogram of Maximum Average Fall Mixed Layer Depth (m). Binned values are shown as red dots; average points are shown as blue crosses; the model fit to the averaged values is shown as a blue line. Lag size: 0.640 degrees; number of lags: 12; Parameter: 1.689; Range: 5.124 degrees; Partial Sill: 446.962. Right panel: Scatterplot of predicted values versus observed values for the model of Maximum Average Fall Mixed Layer Depth (m).

Table 100. Results of cross-validation of the kriged model for Maximum Average Fall Mixed Layer Depth (m).

Prediction error	**Value**
Number of Observations	1160
Overall Mean Error	0.019
Root Mean Square Prediction Error	1.868
Standardized Mean	6.525×10^{-3}
Standardized Root Mean Square Prediction Error	1.369
Average Standard Error	1.319

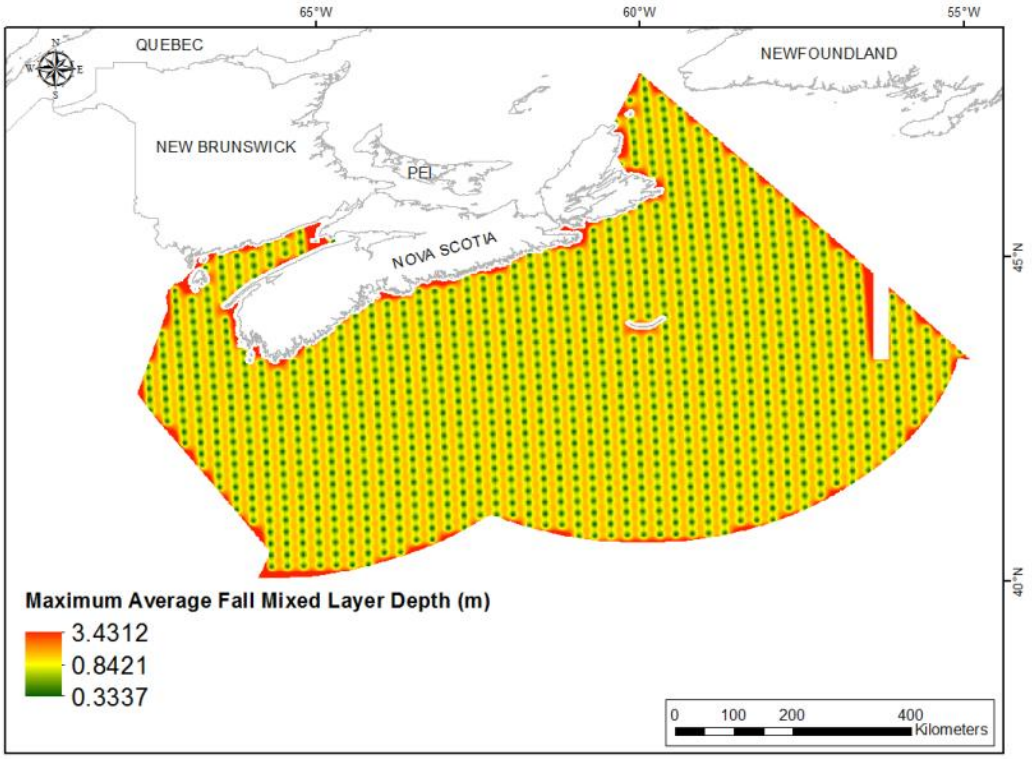

Fig. 249. Prediction standard error surface of Maximum Average Fall Mixed Layer Depth (m).

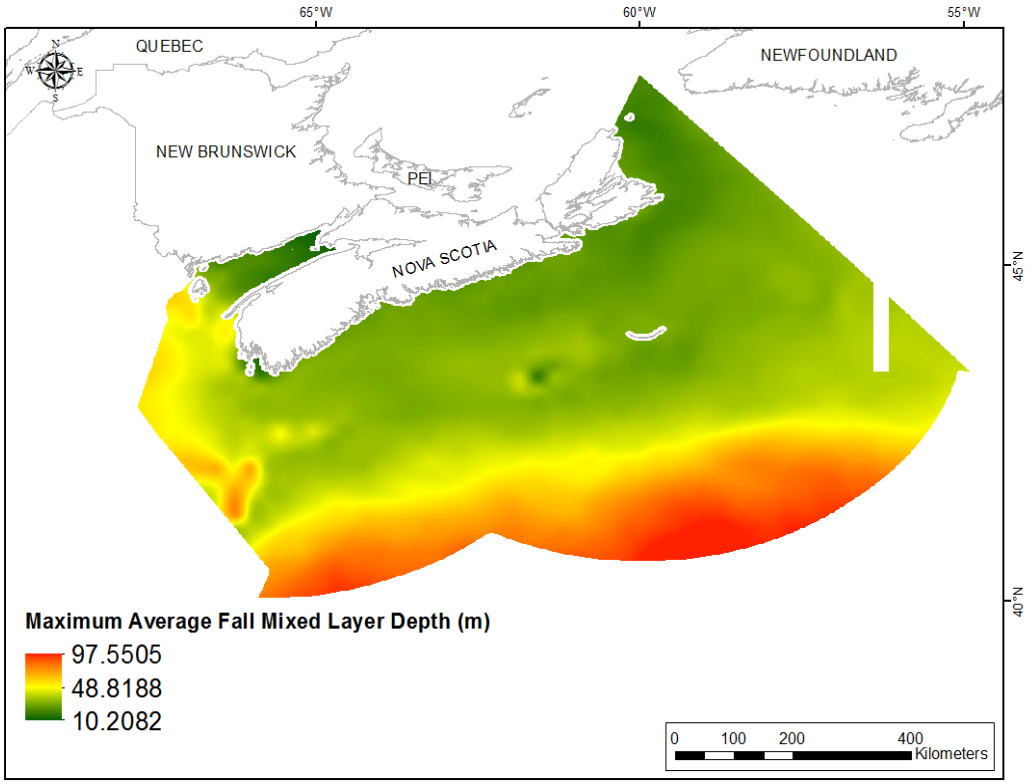

Fig. 250. Interpolated prediction surface of Maximum Average Fall Mixed Layer Depth (m).

Maximum Average Winter Mixed Layer Depth

This variable displayed a right-skewed, leptokurtic distribution prior to interpolation (Table 101, Fig. 251). The data were higher than predicted by a normal distribution at low and high values, with the highest and mid-range values located below the reference line (Fig. 252). The areas of over- and under-prediction showed spatial pattern (Fig. 252).

The semivariogram showed weak autocorrelation present in the data (Fig. 253). The model showed an excellent fit between measured and predicted values (Fig. 253), and good performance was indicated by the cross-validation statistics (Table 102). The error map showed a 'bullseye' pattern with error increasing with distance from data points (Fig. 254). The kriged surface is presented in Fig. 255.

Table 101. Distributional properties of Maximum Average Winter Mixed Layer Depth (m).

Property	Value
Number of Observations	1160
Minimum	11.848
Maximum	186.070
Mean	59.243
Median	41.835
Standard Deviation	40.216
Skewness	1.439
Kurtosis	3.919

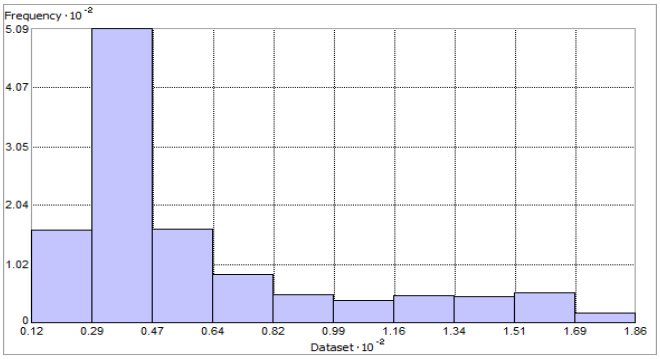

Fig. 251. Distribution of Maximum Average Winter Mixed Layer Depth (m). Histogram was illustrated using 10 bins. X and Y axes shown at 10^{-2}.

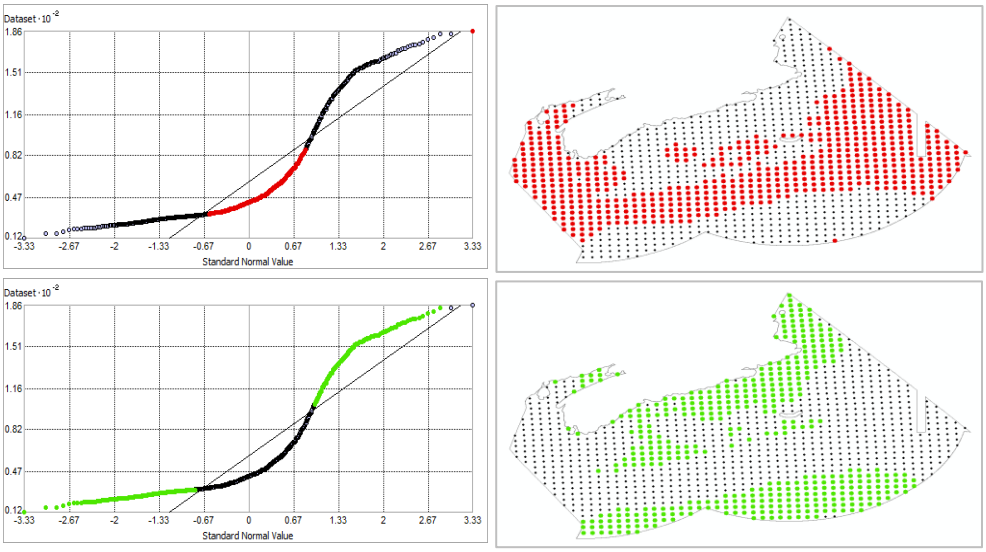

Fig. 252. Normal Q-Q plot for data values of Maximum Average Winter Mixed Layer Depth (m). Points falling under (upper panel) and over (bottom panel) the reference line are mapped.

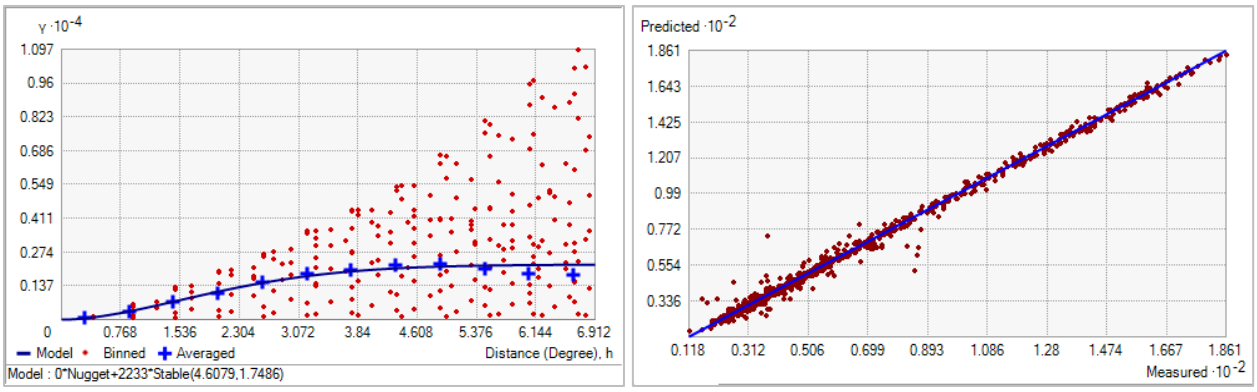

Fig. 253. Left panel: Semivariogram of Maximum Average Winter Mixed Layer Depth (m). Binned values are shown as red dots; average points are shown as blue crosses; the model fit to the averaged values is shown as a blue line. Lag size: 0.576 degrees; number of lags: 12; Parameter: 1.749; Range: 4.608 degrees; Partial Sill: 2233.046. Right panel: Scatterplot of predicted values versus observed values for the model of Maximum Average Winter Mixed Layer Depth (m).

Table 102. Results of cross-validation of the kriged model for Maximum Average Winter Mixed Layer Depth (m).

Prediction error	**Value**
Number of Observations	1160
Overall Mean Error	0.045
Root Mean Square Prediction Error	2.955
Standardized Mean	7.662×10^{-3}
Standardized Root Mean Square Prediction Error	1.128
Average Standard Error	2.496

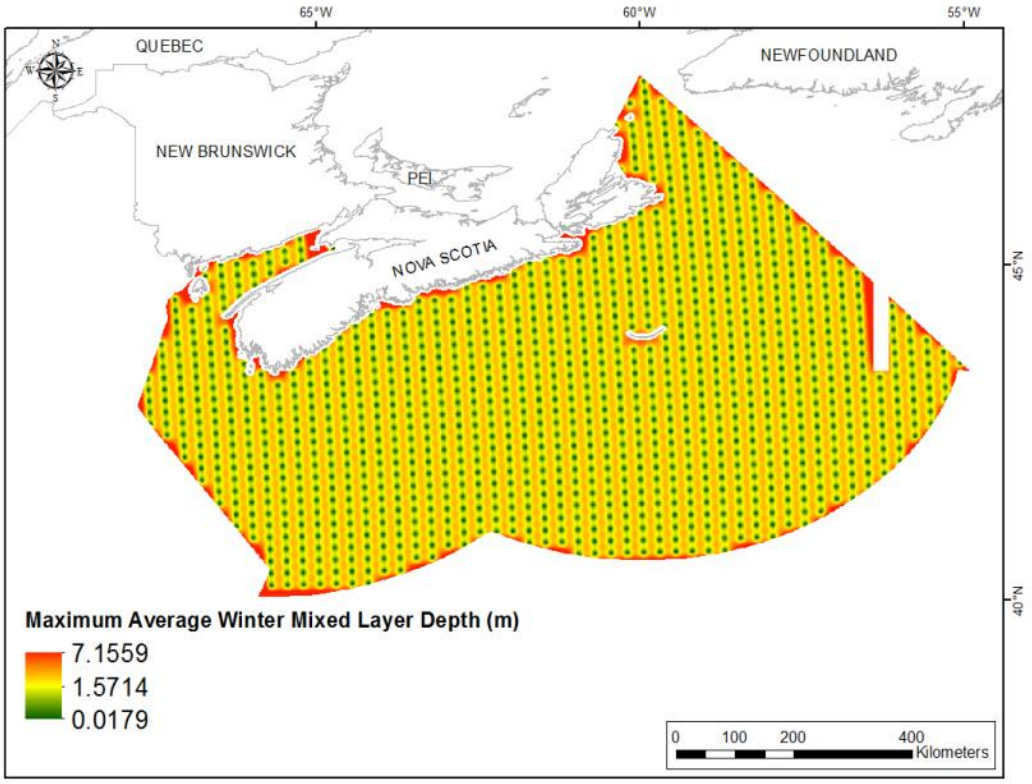

Fig. 254. Prediction standard error surface of Maximum Average Winter Mixed Layer Depth (m).

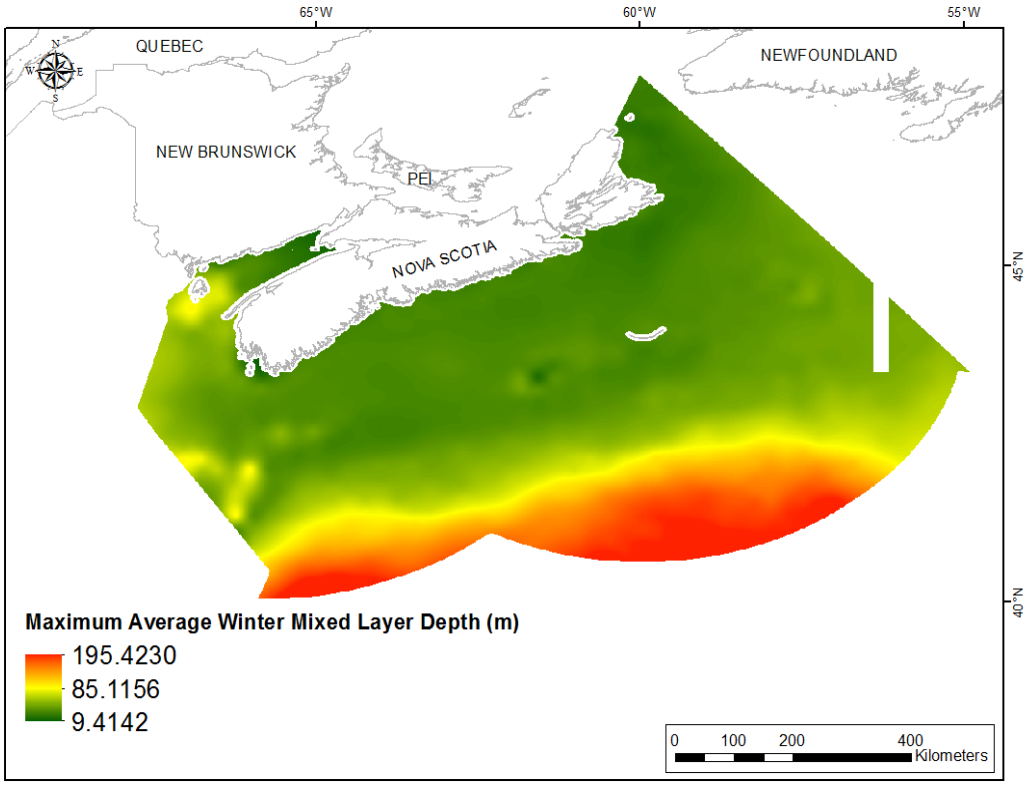

Fig. 255. Interpolated prediction surface of Maximum Average Winter Mixed Layer Depth (m).

Bottom Shear

Bottom shear stress is a function of the maximum predicted tidal current and reflects friction pressure on the seabed. Its unit is Pa or pascal, which is equivalent to one newton (1 N) of force over one meter squared. Shear stress near the seabed causes sediment erosion and affects vertical mixing and conditions conducive to sediment deposition (Cheng et al., 1999).

Bottom Shear Mean

This variable displayed a right-skewed distribution and extreme leptokurtosis prior to interpolation (Table 103, Fig. 256). The data were higher than predicted by a normal distribution at both tails, with mid-range values located below the reference line (Fig. 257). The areas of over- and under-prediction showed a weak spatial pattern (Fig. 257).

The semivariogram showed weak autocorrelation present in the data (Fig. 258). The model showed fair fit between measured and predicted values (Fig. 258), and good performance was indicated by the cross-validation statistics (Table 104). The error map showed high error along the edges of the study extent (Fig. 259). The kriged surface is presented in Fig. 260.

Table 103. Distributional properties of Bottom Shear Mean (Pa).

Property	Value
Number of Observations	1143
Minimum	6.912×10^{-4}
Maximum	0.099
Mean	0.012
Median	7.421×10^{-3}
Standard Deviation	0.013
Skewness	3.317
Kurtosis	15.592

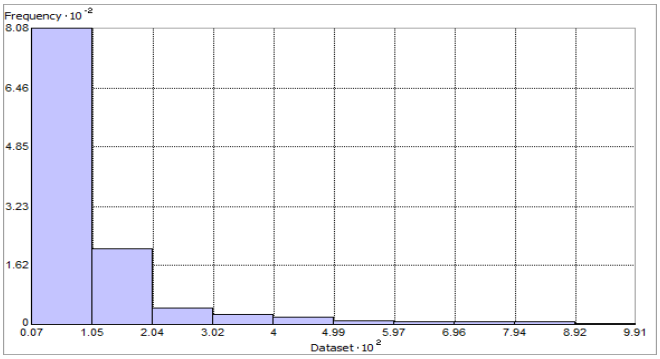

Fig. 256. Distribution of Bottom Shear Mean (Pa). Histogram was illustrated using 10 bins. X and Y axes are shown at 10^{2} and 10^{-2}, respectively.

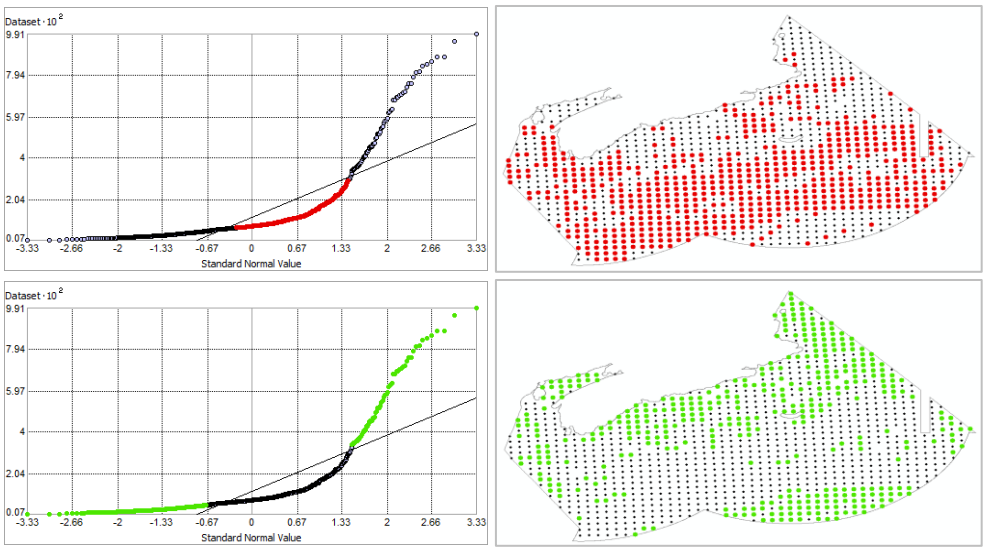

Fig. 257. Normal Q-Q plot for data values of Bottom Shear Mean (Pa). Points falling under (upper panel) and over (bottom panel) the reference line are mapped.

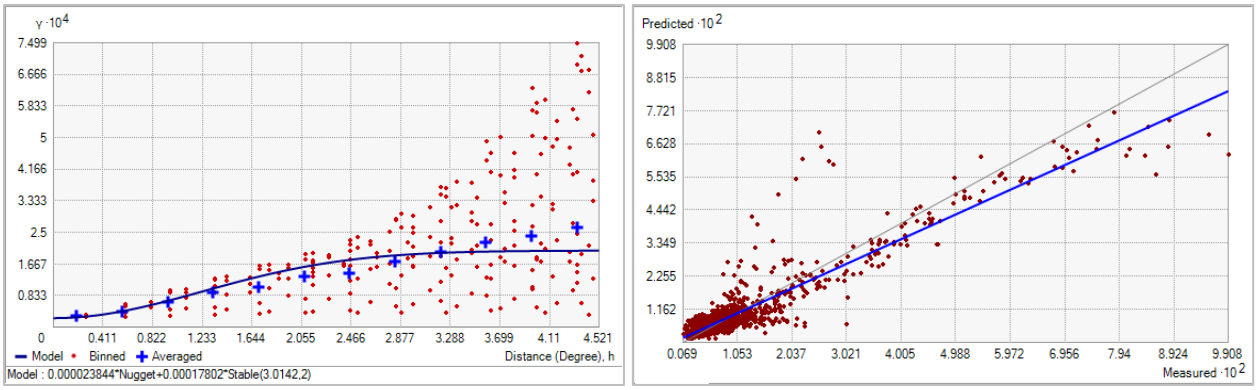

Fig. 258. Left panel: Semivariogram of Bottom Shear Mean (Pa). Binned values are shown as red dots; average points are shown as blue crosses; the model fit to the averaged values is shown as a blue line. Lag size: 0.377 degrees; number of lags: 12; Parameter: 2; Range: 3.014 degrees; Partial Sill: 1.780 x 10^{-4}. Right panel: Scatterplot of predicted values versus observed values for the model of Bottom Shear Mean (Pa).

Table 104. Results of cross-validation of the kriged model for Bottom Shear Mean (Pa).

Prediction error	**Value**
Number of Observations	1143
Overall Mean Error	9.675 x 10^{-5}
Root Mean Square Prediction Error	5.262 x 10^{-3}
Standardized Mean	0.021
Standardized Root Mean Square Prediction Error	1.018
Average Standard Error	5.119 x 10^{-3}

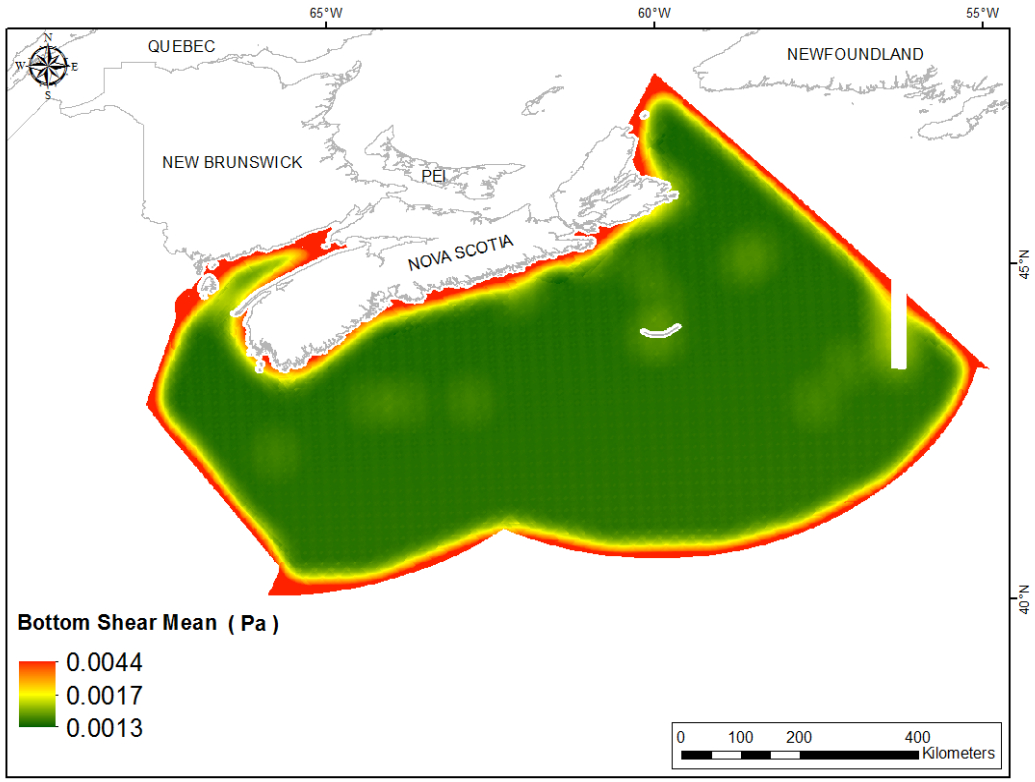

Fig. 259. Prediction standard error surface of Bottom Shear Mean (Pa).

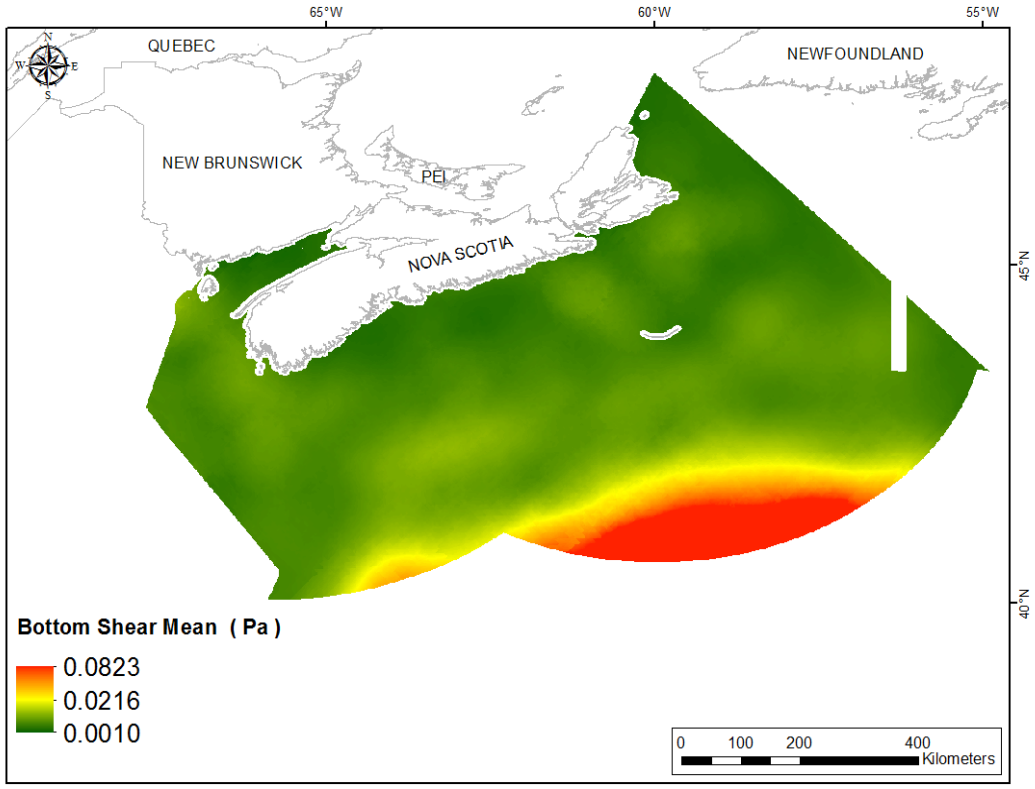

Fig, 260. Interpolated prediction surface of Bottom Shear Mean (Pa).

Bottom Shear Minimum

This variable displayed a right-skewed distribution with extreme leptokurtosis and outlying data in the upper range (Table 105, Fig. 261). The data were higher than predicted by a normal distribution at both tails, with mid-range values located below the reference line (Fig. 262). The areas of over- and under-prediction showed no spatial pattern (Fig. 262).

The semivariogram showed weak autocorrelation present in the data and the model showed very poor fit between measured and predicted values (Fig. 263). Nevertheless, good performance was indicated by the cross-validation statistics (Table 106). The error map showed high error along the edges of the study extent (Fig. 264). The kriged surface is presented in Fig. 265.

Table 105. Distributional properties of Bottom Shear Minimum (Pa).

Property	Value
Number of Observations	1143
Minimum	1.000×10^{-6}
Maximum	5.504×10^{-3}
Mean	2.948×10^{-4}
Median	1.100×10^{-4}
Standard Deviation	5.274×10^{-4}
Skewness	4.305
Kurtosis	28.095

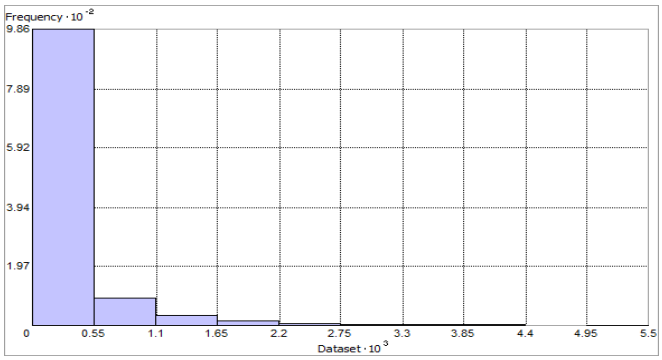

Fig. 261. Distribution of Bottom Shear Minimum (Pa). Histogram was illustrated using 10 bins. X axis is shown at 10^3; Y axis is shown at 10^{-2}.

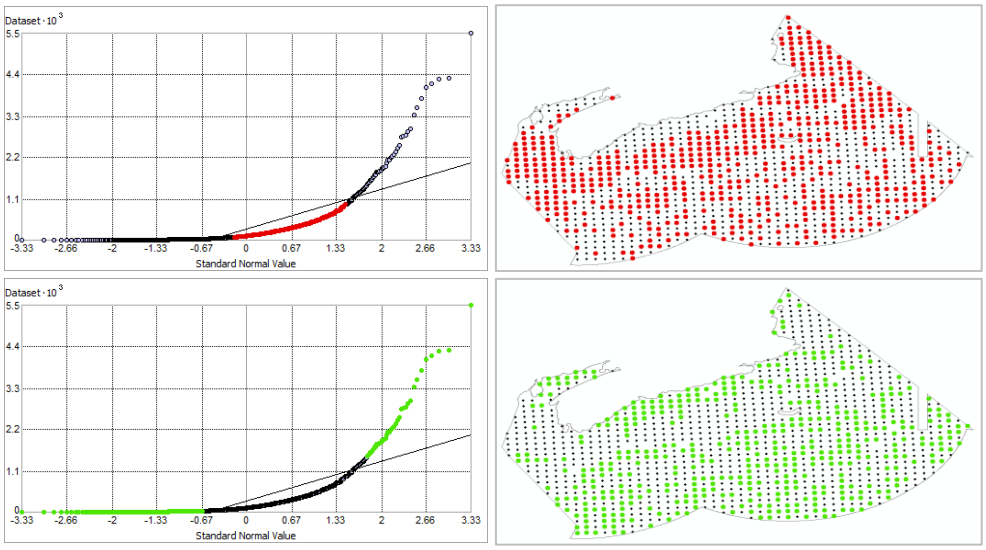

Fig. 262. Normal Q-Q plot for data values of Bottom Shear Minimum (Pa). Points falling under (upper panel) and over (bottom panel) the reference line are mapped.

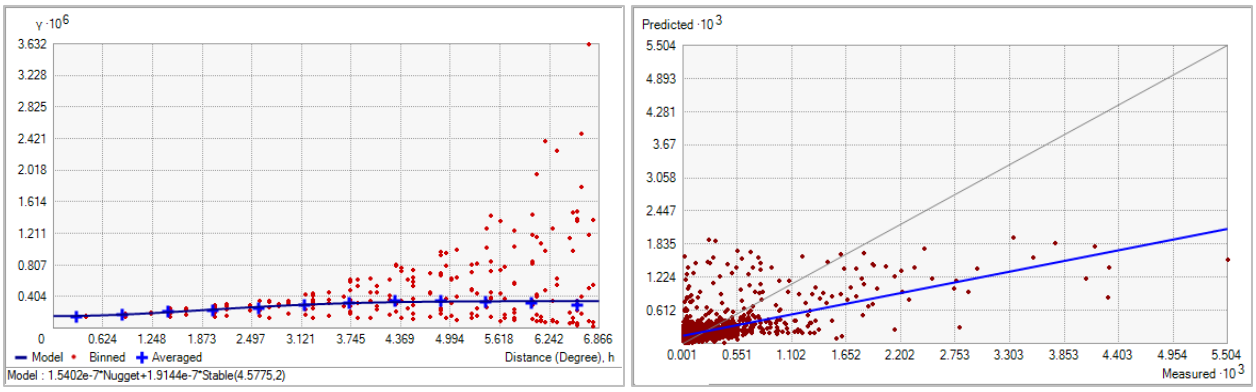

Fig. 263. Left panel: Semivariogram of Bottom Shear Minimum (Pa). Binned values are shown as red dots; average points are shown as blue crosses; the model fit to the averaged values is shown as a blue line. Lag size: 0.572 degrees; number of lags: 12; Parameter: 2; Range: 4.577 degrees; Partial Sill: 1.914 x 10^{-7}. Right panel: Scatterplot of predicted values versus observed values for the model of Bottom Shear Minimum (Pa).

Table 106. Results of cross-validation of the kriged model for Bottom Shear Minimum (Pa).

Prediction error	**Value**
Number of Observations	1143
Overall Mean Error	-2.601 x 10^{-6}
Root Mean Square Prediction Error	4.165 x 10^{-4}
Standardized Mean	-6.134 x 10^{-3}
Standardized Root Mean Square Prediction Error	1.029
Average Standard Error	4.035 x 10^{-4}

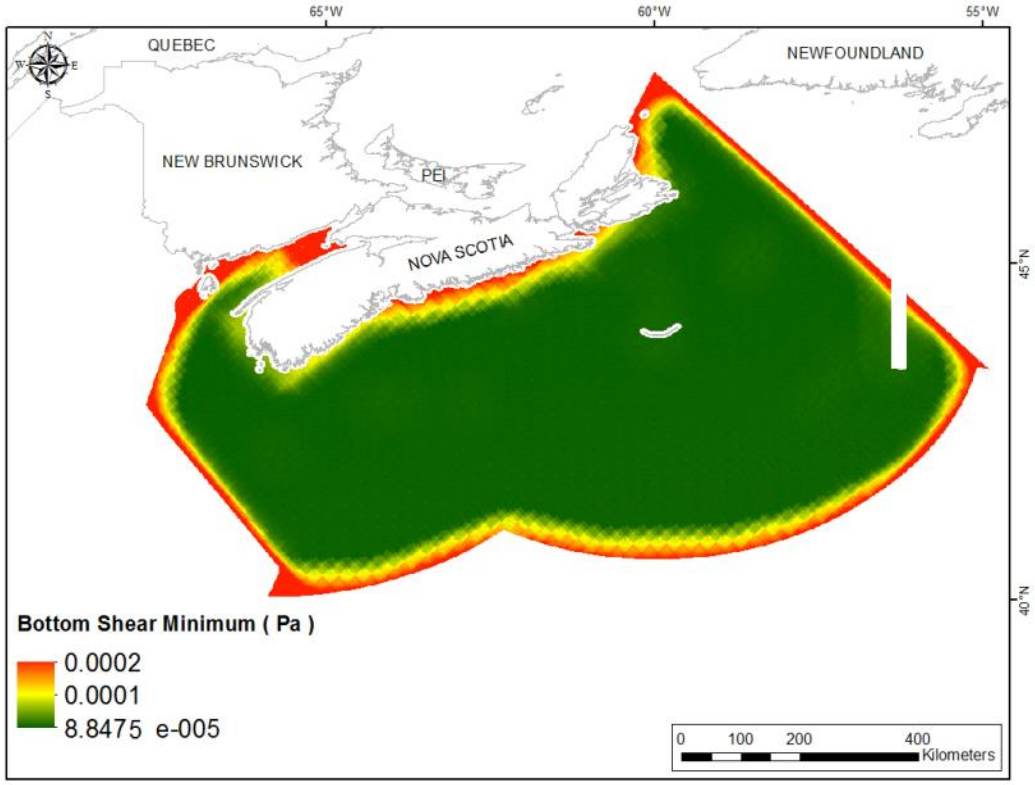

Fig. 264. Prediction standard error surface of Bottom Shear Minimum (Pa).

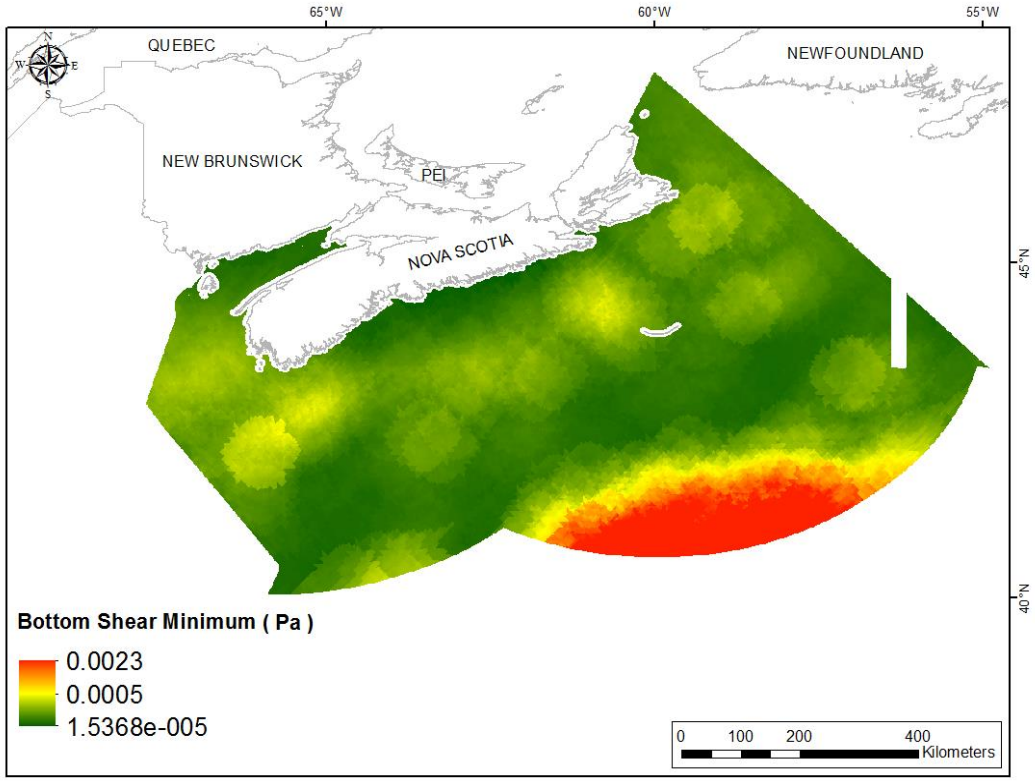

Fig. 265. Interpolated prediction surface of Bottom Shear Minimum (Pa).

Bottom Shear Maximum

This variable displayed a right-skewed, highly leptokurtic distribution prior to interpolation (Table 107, Fig. 266). The data were higher than predicted by a normal distribution at both tails, with mid-range values located below the reference line (Fig. 267). The areas of over- and under-prediction showed no strong spatial pattern (Fig. 267).

The semivariogram showed weak autocorrelation present in the data and the model showed a fair fit between measured and predicted values (Fig. 268). Nevertheless, good performance of the model was indicated by the cross-validation statistics (Table 108). The error map showed high error along the edges of the study extent (Fig. 269). The kriged surface is presented in Fig. 270.

Table 107. Distributional properties of Bottom Shear Maximum (Pa).

Property	Value
Number of Observations	1143
Minimum	2.178 x 10^{-3}
Maximum	0.704
Mean	0.057
Median	0.028
Standard Deviation	0.087
Skewness	3.400
Kurtosis	15.926

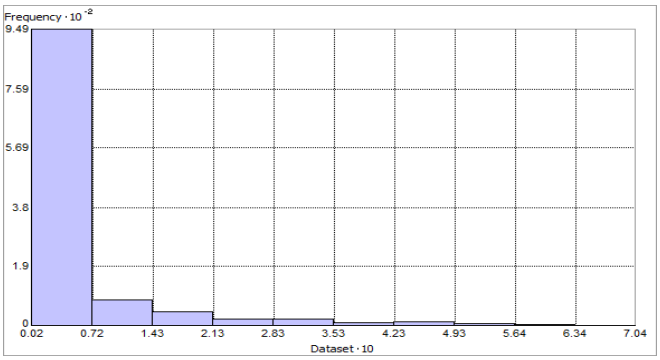

Fig. 266. Distribution of Bottom Shear Maximum (Pa). Histogram was illustrated using 10 bins.X axis is shown at 10; Y axis is shown at 10^{-2}.

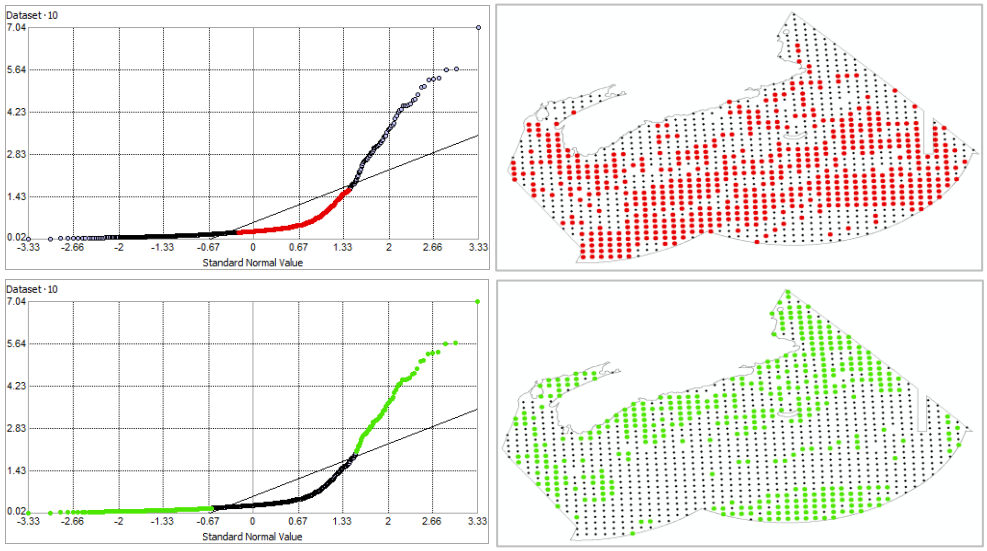

Fig. 267. Normal Q-Q plot for data values of Bottom Shear Maximum (Pa). Points falling under (upper panel) and over (bottom panel) the reference line are mapped.

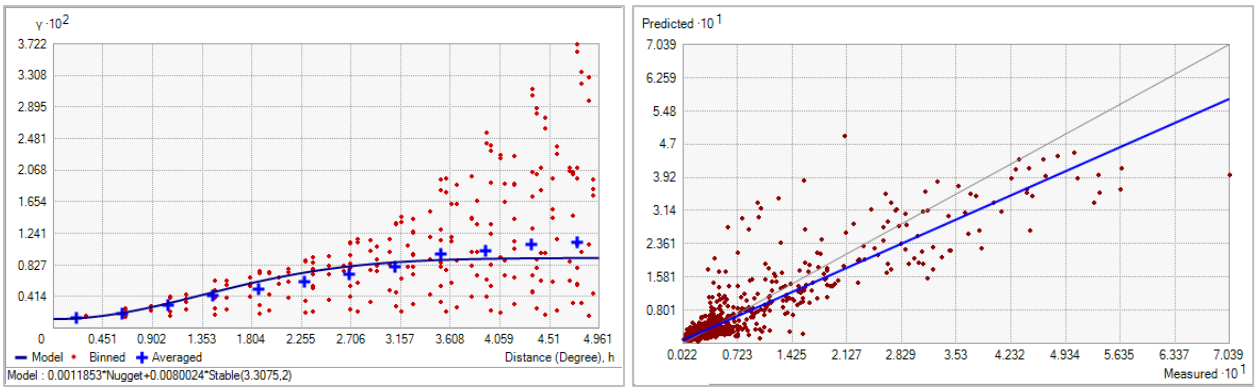

Fig. 268. Left panel: Semivariogram of Bottom Shear Maximum (Pa). Binned values are shown as red dots; average points are shown as blue crosses; the model fit to the averaged values is shown as a blue line. Lag size: 0.413 degrees; number of lags: 12; Parameter: 2; Range: 3.308 degrees; Partial Sill: 8.002 x 10^{-3}. Right panel: Scatterplot of predicted values versus observed values for the model of Bottom Shear Maximum (Pa).

Table 108. Results of cross-validation of the kriged model for Bottom Shear Maximum (Pa).

Prediction error	**Value**
Number of Observations	1143
Overall Mean Error	5.532 x 10^{-4}
Root Mean Square Prediction Error	0.038
Standardized Mean	0.017
Standardized Root Mean Square Prediction Error	1.041
Average Standard Error	0.036

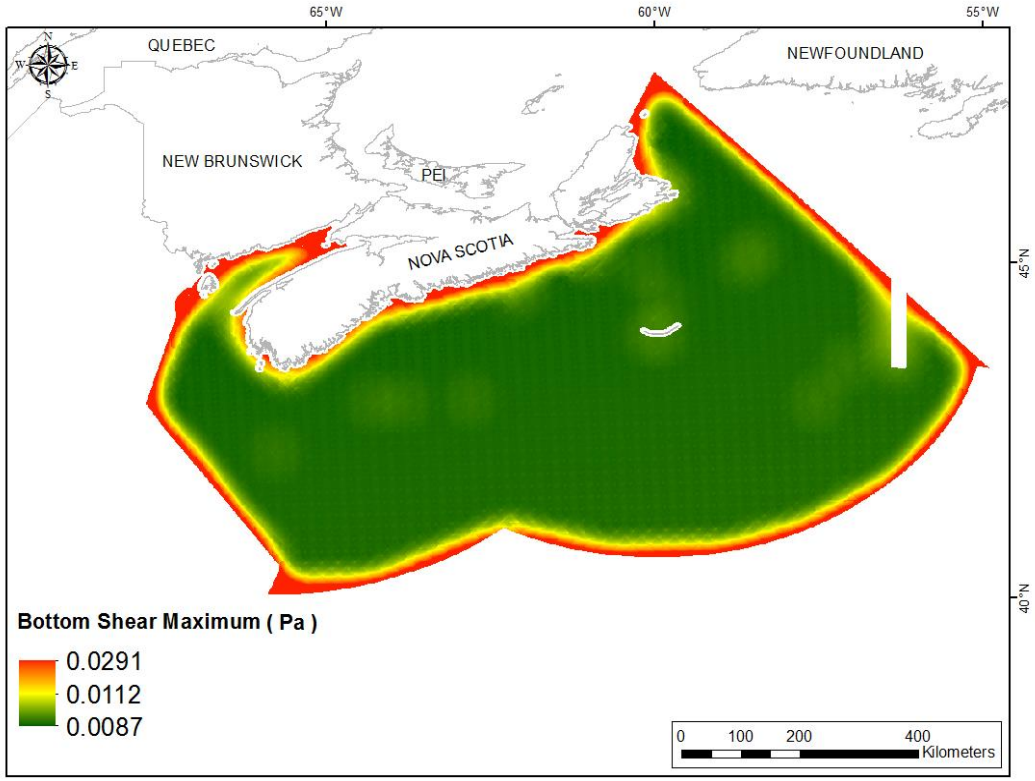

Fig. 269. Prediction standard error surface of Bottom Shear Maximum (Pa).

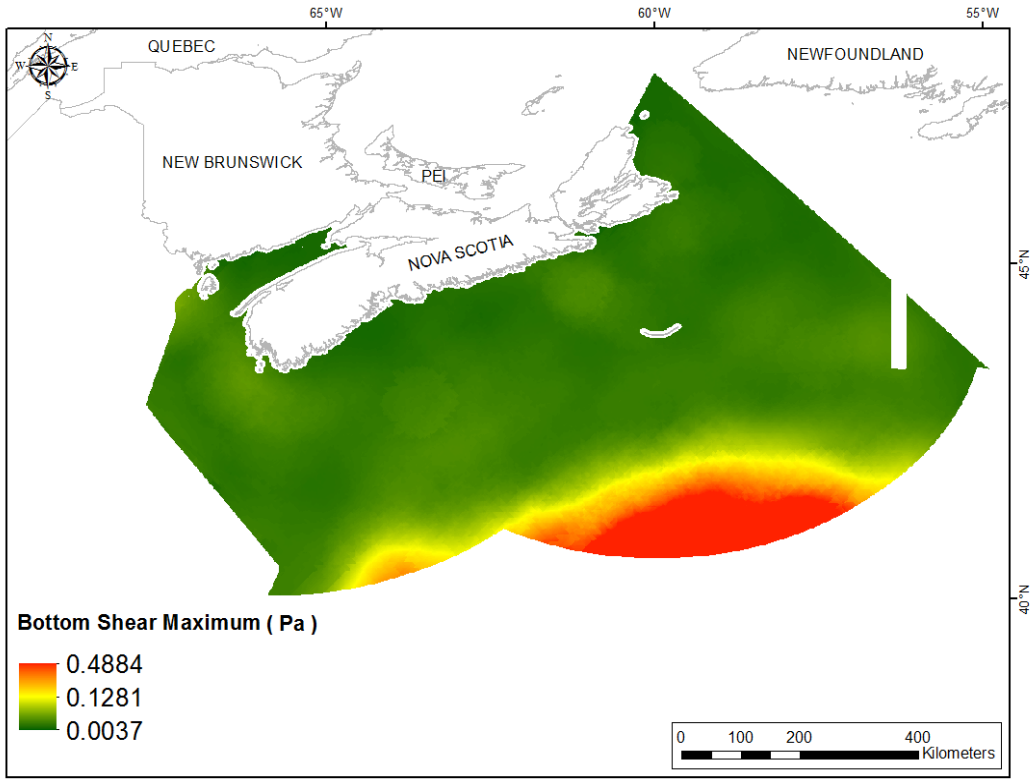

Fig. 270. Interpolated prediction surface of Bottom Shear Maximum (Pa).

Bottom Shear Range

This variable displayed a right-skewed, highly leptokurtic distribution with outlying data in the upper range (Table 109, Fig. 271). The data were higher than predicted by a normal distribution at both tails, with mid-range values located lower than the reference line (Fig. 272). The areas of over- and under-prediction showed no spatial pattern (Fig. 272).

The semivariogram showed weak autocorrelation present in the data and the model showed a fair fit between measured and predicted values (Fig. 273). Nevertheless, good performance of the model was indicated by the good cross-validation statistics (Table 110). The error map showed high error along the edges of the study extent (Fig. 274). The kriged surface is presented in Fig. 275.

Table 109. Distributional properties of Bottom Shear Range (Pa).

Property	Value
Number of Observations	1143
Minimum	2.172 x 10^{-3}
Maximum	0.704
Mean	0.057
Median	0.028
Standard Deviation	0.086
Skewness	3.401
Kurtosis	15.943

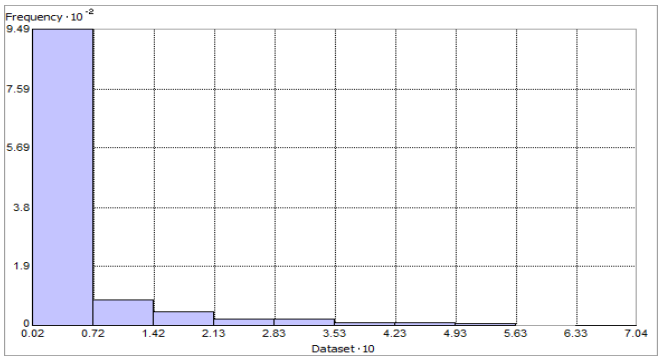

Fig. 271. Distribution of Bottom Shear Range (Pa). Histogram was illustrated using 10 bins. X axis is shown at 10; Y axis is shown at 10^{-2}.

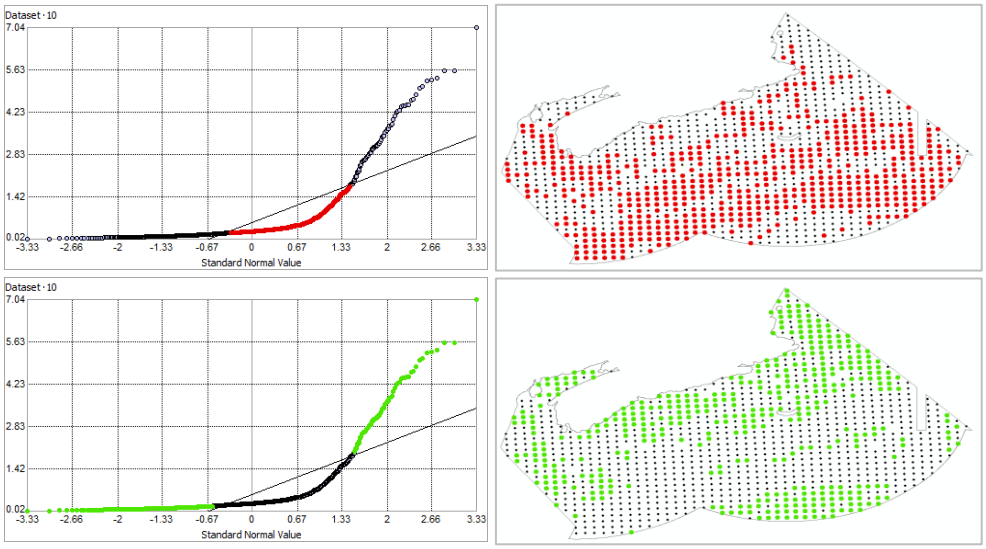

Fig. 272. Normal Q-Q plot for data values of Bottom Shear Range (Pa). Points falling under (upper panel) and over (bottom panel) the reference line are mapped.

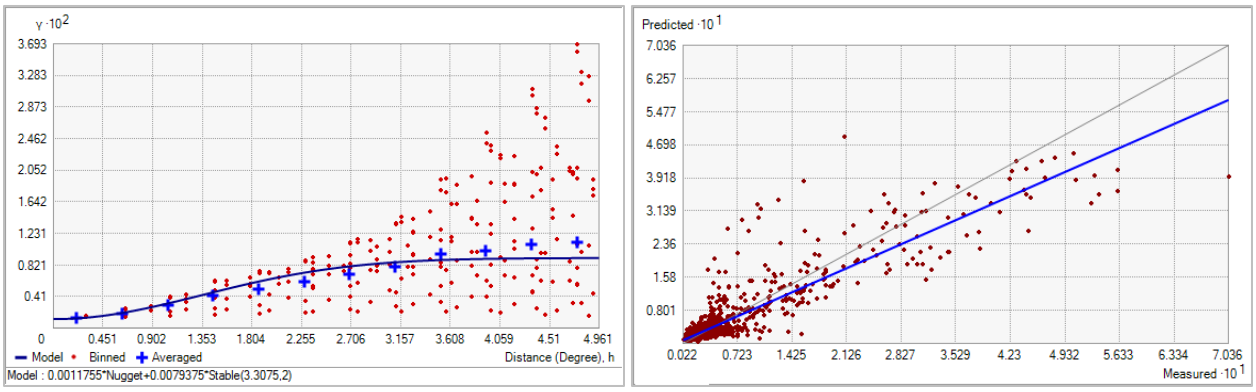

Fig. 273. Left panel: Semivariogram of Bottom Shear Range (Pa). Binned values are shown as red dots; average points are shown as blue crosses; the model fit to the averaged values is shown as a blue line. Lag size: 0.413 degrees; number of lags: 12; Parameter: 2; Range: 3.308 degrees; Partial Sill: 7.938 x 10^{-3}. Right panel: Scatterplot of predicted values versus observed values for the model of Bottom Shear Range (Pa).

Table 110. Results of cross-validation of the kriged model for Bottom Shear Range (Pa).

Prediction error	**Value**
Number of Observations	1143
Overall Mean Error	5.519 x 10^{-4}
Root Mean Square Prediction Error	0.037
Standardized Mean	0.017
Standardized Root Mean Square Prediction Error	1.041
Average Standard Error	0.036

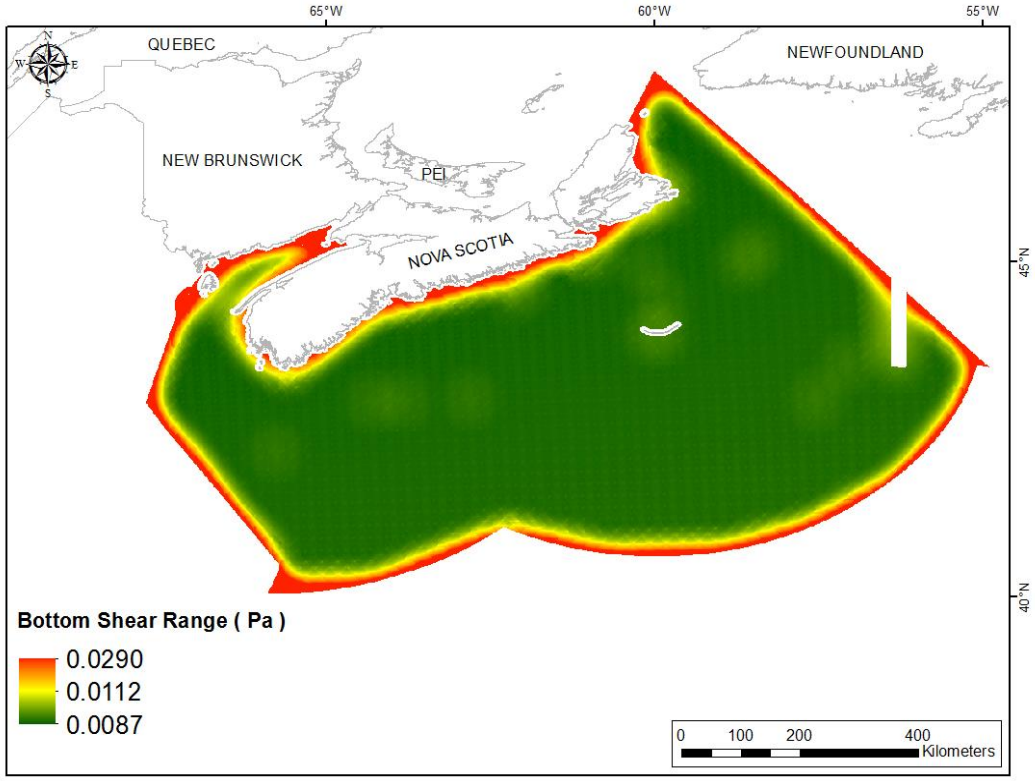

Fig. 274. Prediction standard error surface of Bottom Shear Range (Pa).

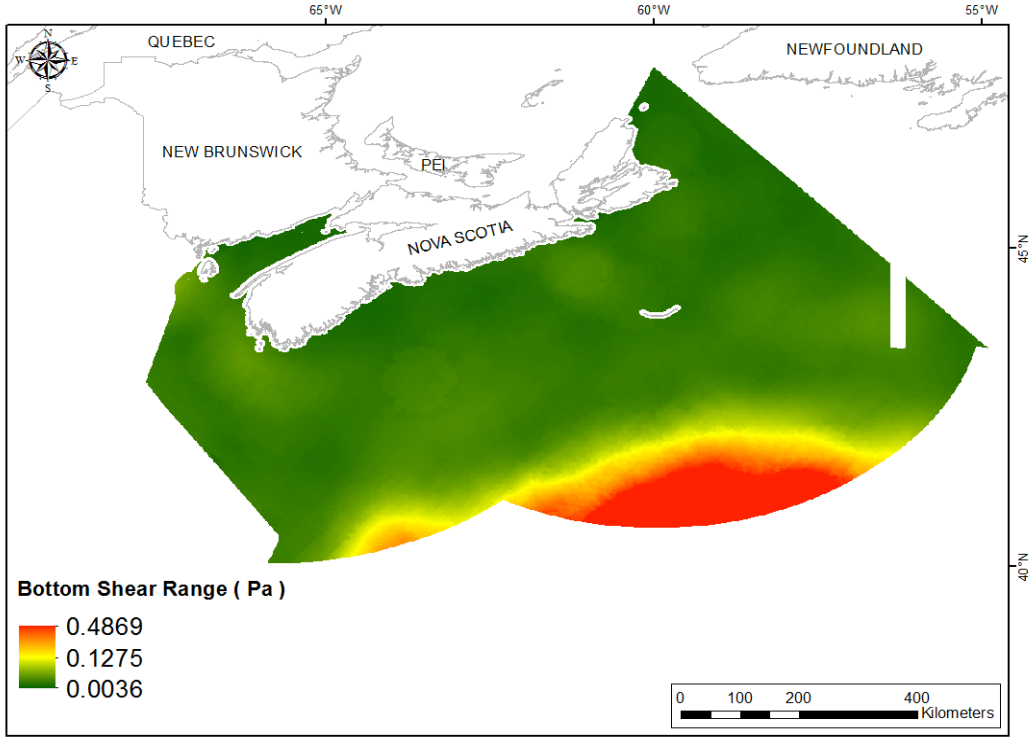

Fig. 275. Interpolated prediction surface of Bottom Shear Range (Pa).

Bottom Shear Average Minimum

This variable displayed a right-skewed, highly leptokurtic distribution with outlying data in the upper range (Table 111, Fig. 276). The data were higher than predicted by a normal distribution at both tails, with mid-range values located below the reference line (Fig. 277). The areas of over- and under-prediction showed no strong spatial pattern (Fig. 277).

The semivariogram showed weak autocorrelation present in the data and the model showed a poor fit between measured and predicted values (Fig. 278). Nevertheless, good performance was indicated by the good cross-validation statistics (Table 112). The error map showed high error along the edges of the study extent (Fig. 279). The kriged surface is presented in Fig. 280.

Table 111. Distributional properties of Bottom Shear Average Minimum (Pa).

Property	Value
Number of Observations	1143
Minimum	8.200×10^{-5}
Maximum	0.017
Mean	1.980×10^{-3}
Median	1.374×10^{-3}
Standard Deviation	2.002×10^{-3}
Skewness	2.913
Kurtosis	14.500

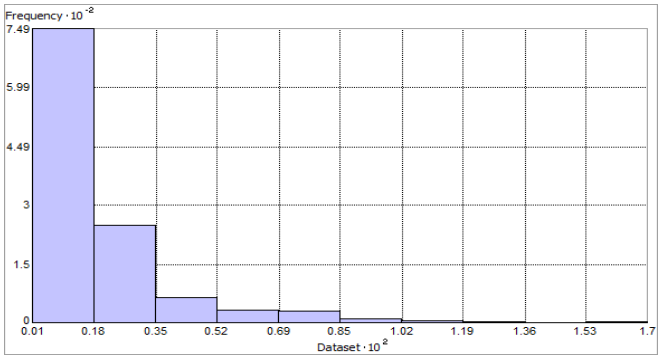

Fig. 276. Distribution of Bottom Shear Average Minimum (Pa). Histogram was illustrated using 10 bins. X axis is shown at 10^{2}; Y axis is shown at 10^{-2}.

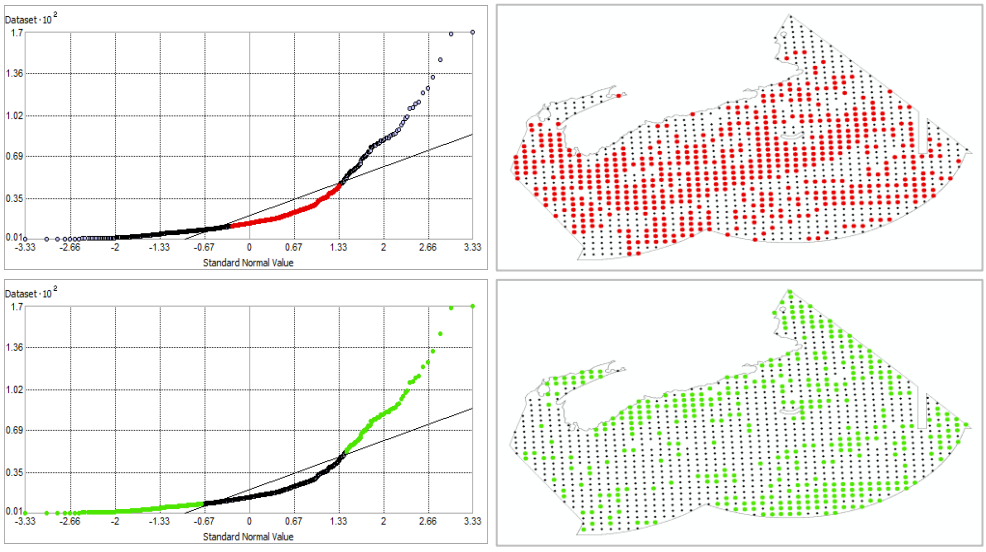

Fig. 277. Normal Q-Q plot for data values of Bottom Shear Average Minimum (Pa). Points falling under (upper panel) and over (bottom panel) the reference line are mapped.

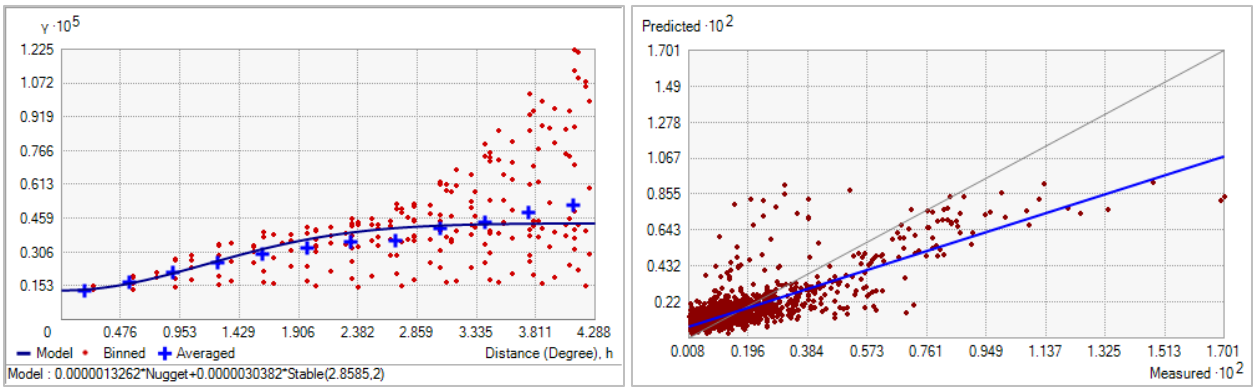

Fig. 278. Left panel: Semivariogram of Bottom Shear Average Minimum (Pa). Binned values are shown as red dots; average points are shown as blue crosses; the model fit to the averaged values is shown as a blue line. Lag size: 0.357 degrees; number of lags: 12; Parameter: 2; Range: 2.859 degrees; Partial Sill: 3.038 x 10^{-6}. Right panel: Scatterplot of predicted values versus observed values for the model of Bottom Shear Average Minimum (Pa).

Table 112. Results of cross-validation of the kriged model for Bottom Shear Average Minimum (Pa).

Prediction error	**Value**
Number of Observations	1143
Overall Mean Error	-1.428 x 10^{-6}
Root Mean Square Prediction Error	1.226 x 10^{-3}
Standardized Mean	-1.793 x 10^{-4}
Standardized Root Mean Square Prediction Error	1.021
Average Standard Error	1.194 x 10^{-3}

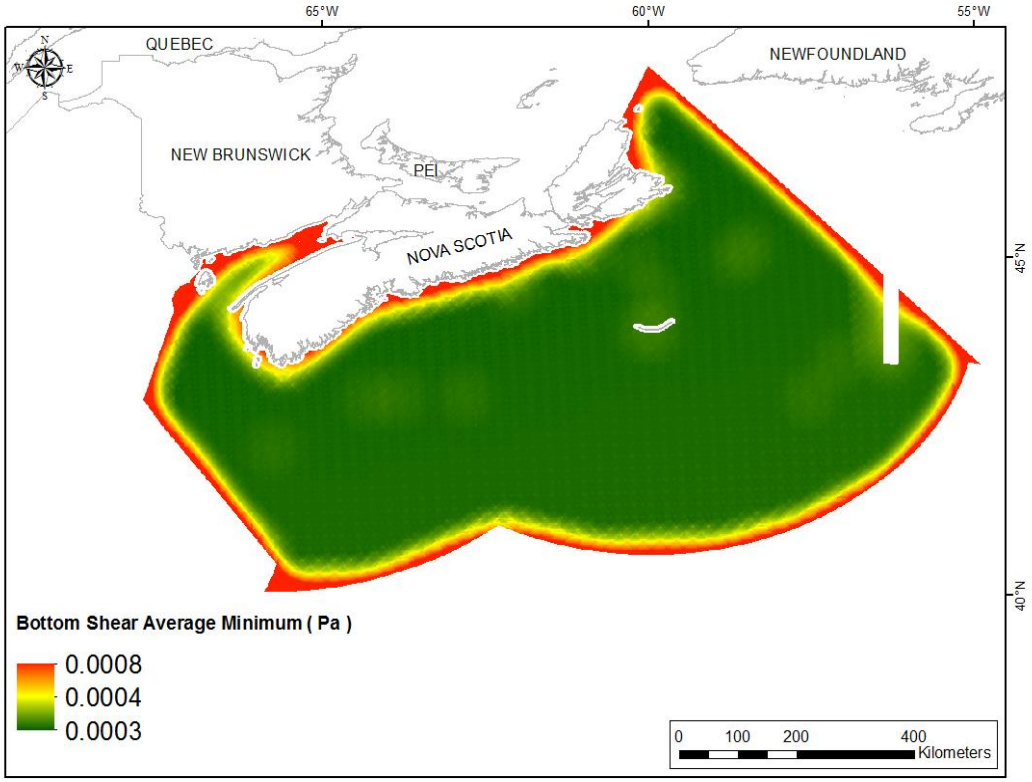

Fig. 279. Prediction standard error surface of Bottom Shear Average Minimum (Pa).

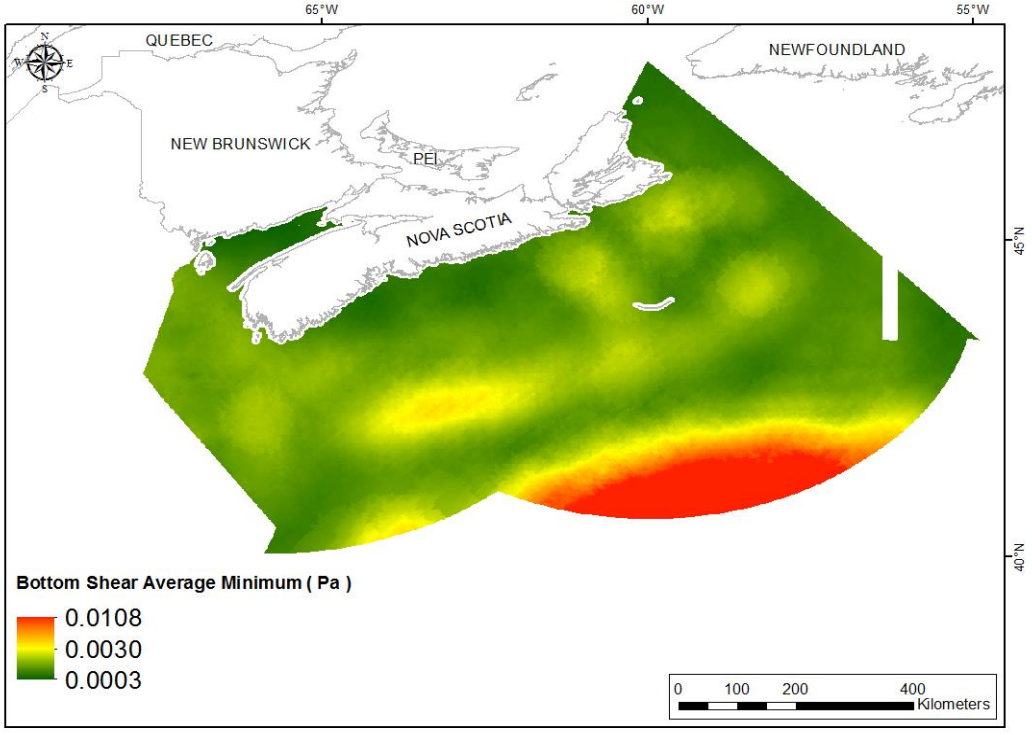

Fig. 280. Interpolated prediction surface of Bottom Shear Average Minimum (Pa).

Bottom Shear Average Maximum

This variable displayed a right-skewed, highly leptokurtic distribution prior to interpolation (Table 113, Fig. 281). The data were higher than predicted by a normal distribution at both tails, with mid-range values located below the reference line (Fig. 282). The areas of over- and under-prediction showed no strong spatial pattern (Fig. 282).

The semivariogram showed weak autocorrelation present in the data and the model showed a fair fit between measured and predicted values (Fig. 283). Nevertheless, good performance of the model was indicated by the good cross-validation statistics (Table 114). The error map showed high error along the edges of the study extent (Fig. 284). The kriged surface is presented in Fig. 285.

Table 113. Distributional properties of Bottom Shear Average Maximum (Pa).

Property	Value
Number of Observations	1143
Minimum	1.536 x 10^{-3}
Maximum	0.276
Mean	0.030
Median	0.016
Standard Deviation	0.040
Skewness	3.324
Kurtosis	15.053

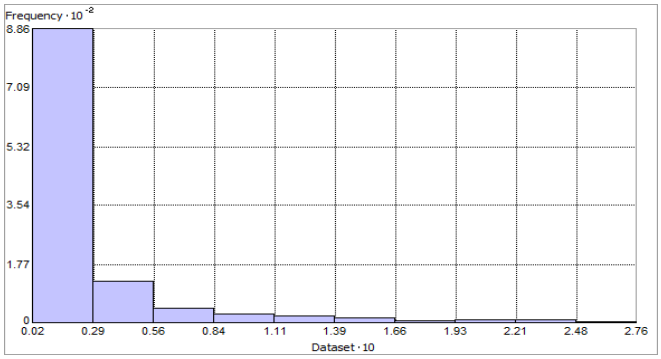

Fig. 281. Distribution of Bottom Shear Average Maximum (Pa). Histogram was illustrated using 10 bins. X axis is shown at 10; Y axis is shown at 10^{-2}.

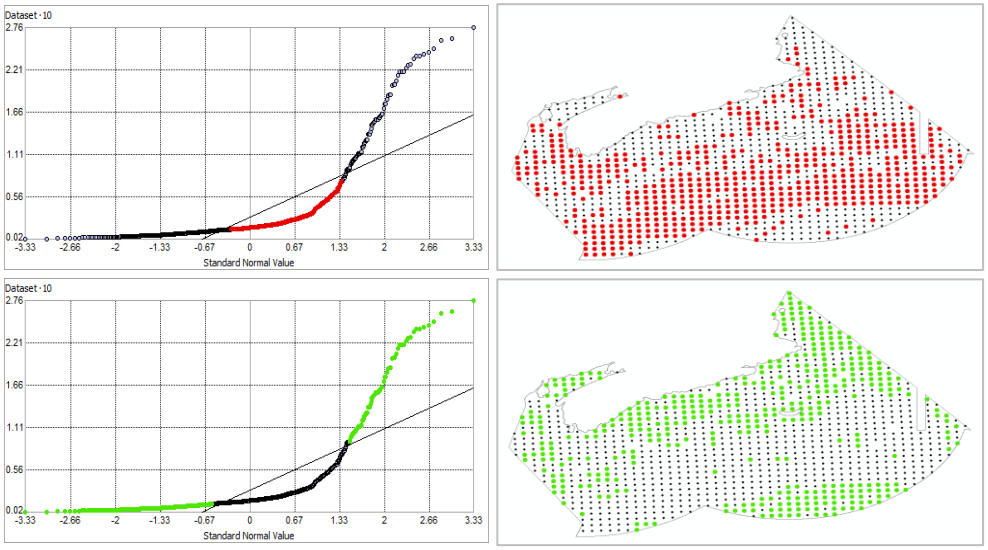

Fig. 282. Normal Q-Q plot for data values of Bottom Shear Average Maximum (Pa). Points falling under (upper panel) and over (bottom panel) the reference line are mapped.

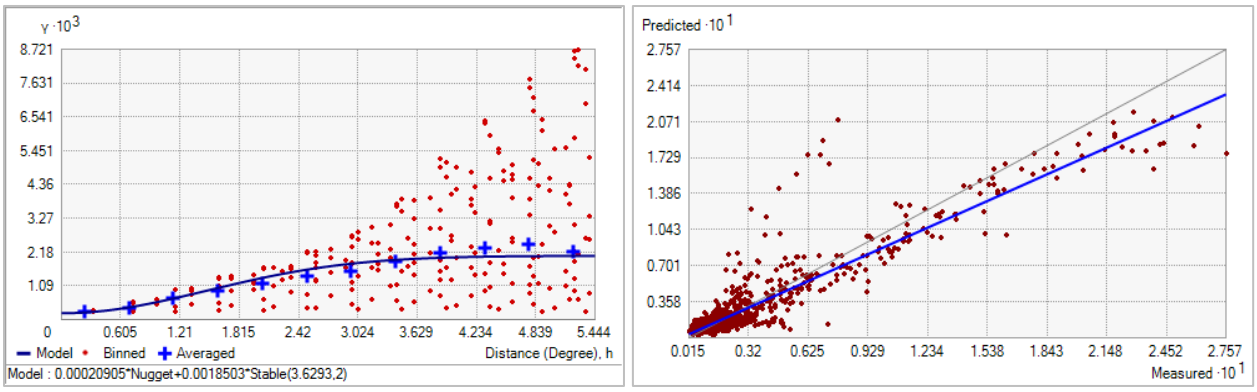

Fig. 283. Left panel: Semivariogram of Bottom Shear Average Maximum (Pa). Binned values are shown as red dots; average points are shown as blue crosses; the model fit to the averaged values is shown as a blue line. Lag size: 0.454 degrees; number of lags: 12; Parameter: 2; Range: 3.629 degrees; Partial Sill: 1.850 x 10^{-3}. Right panel: Scatterplot of predicted values versus observed values for the model of Bottom Shear Average Maximum (Pa).

Table 114. Results of cross-validation of the kriged model for Bottom Shear Average Maximum (Pa).

Prediction error	**Value**
Number of Observations	1143
Overall Mean Error	3.183 x 10^{-4}
Root Mean Square Prediction Error	0.015
Standardized Mean	0.023
Standardized Root Mean Square Prediction Error	0.997
Average Standard Error	0.015

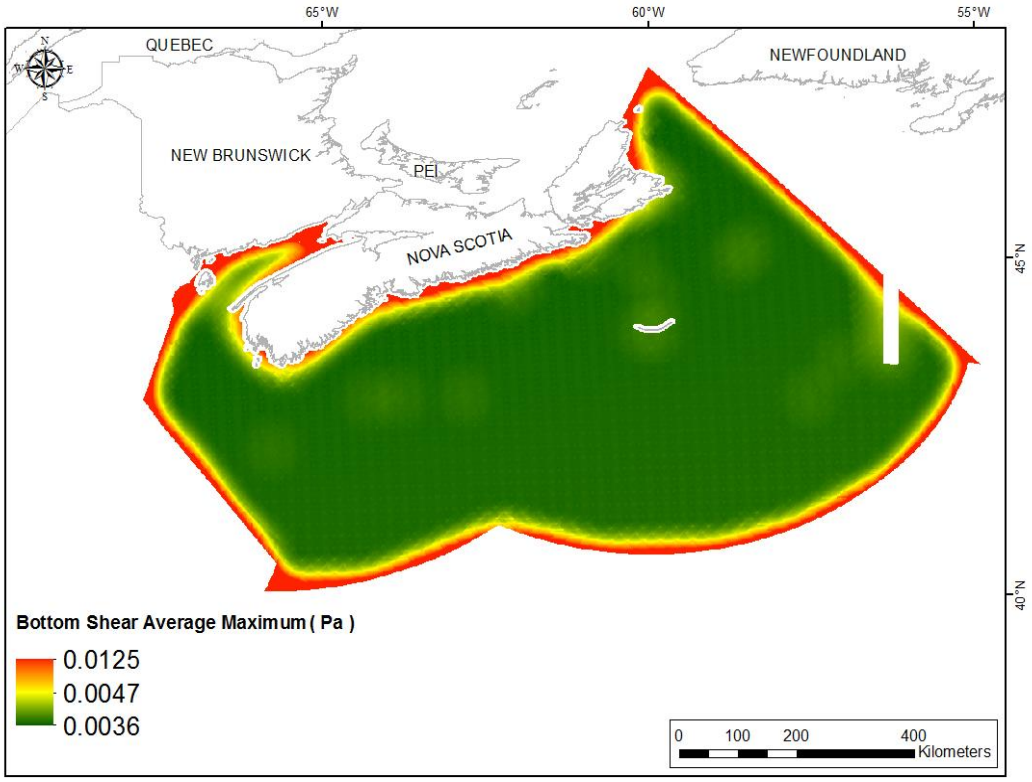

Fig. 284. Prediction standard error surface of Bottom Shear Average Maximum (Pa).

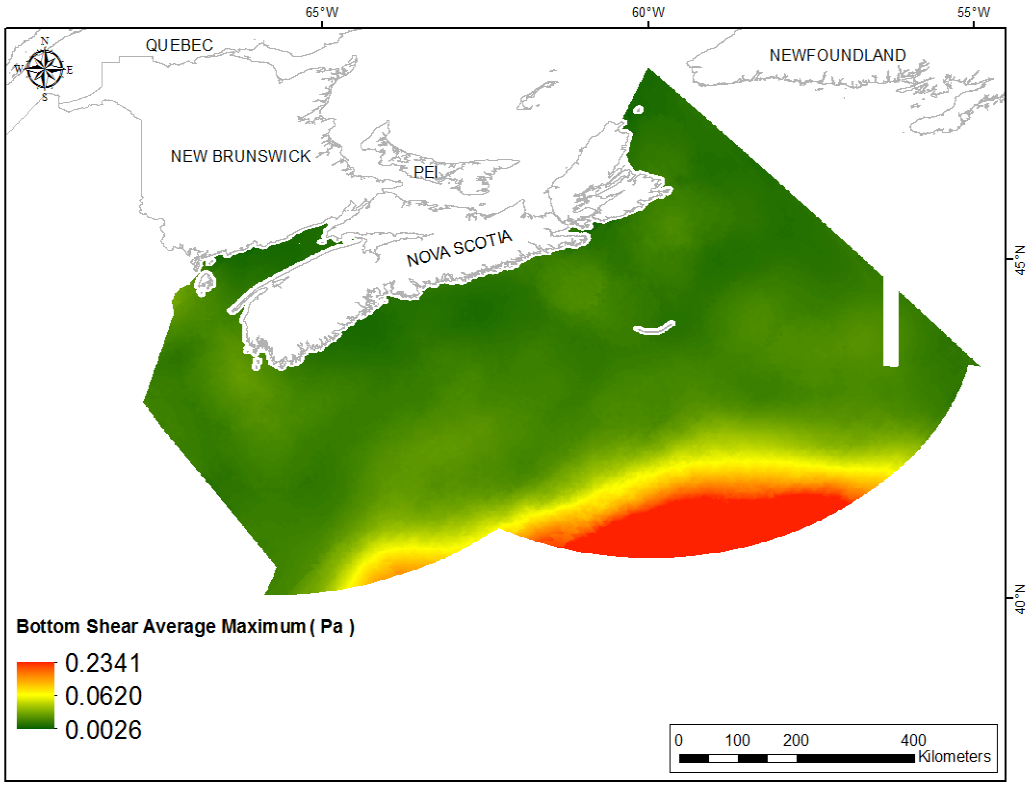

Fig. 285. Interpolated prediction surface of Bottom Shear Average Maximum (Pa).

Bottom Shear Average Range

This variable displayed a right-skewed, highly leptokurtic distribution prior to interpolation (Table 115, Fig. 286). The data were higher than predicted by a normal distribution at both tails, with mid-range values located below the reference line (Fig. 287). The areas of over- and under-prediction showed no strong spatial pattern (Fig. 287).

The semivariogram showed weak autocorrelation present in the data and the model showed a fair fit between measured and predicted values (Fig. 288). Nevertheless, good performance of the model was indicated by the good cross-validation statistics (Table 116). The error map showed high error along the edges of the study extent (Fig. 289). The kriged surface is presented in Fig. 290.

Table 115. Distributional properties of Bottom Shear Average Range (Pa).

Property	Value
Number of Observations	1143
Minimum	1.410×10^{-3}
Maximum	0.264
Mean	0.028
Median	0.015
Standard Deviation	0.038
Skewness	3.334
Kurtosis	15.101

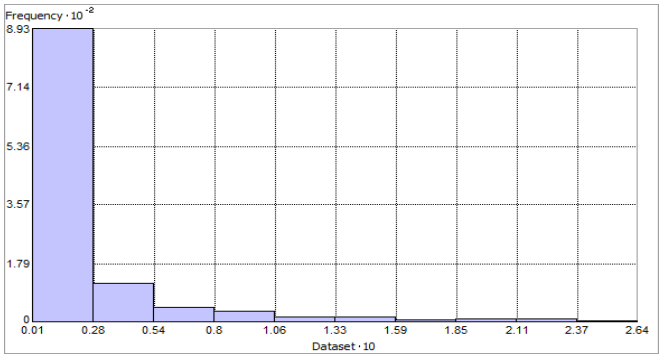

Fig. 286. Distribution of Bottom Shear Average Range (Pa). Histogram was illustrated using 10 bins. X axis is shown at 10; Y axis is shown at 10^{-2}.

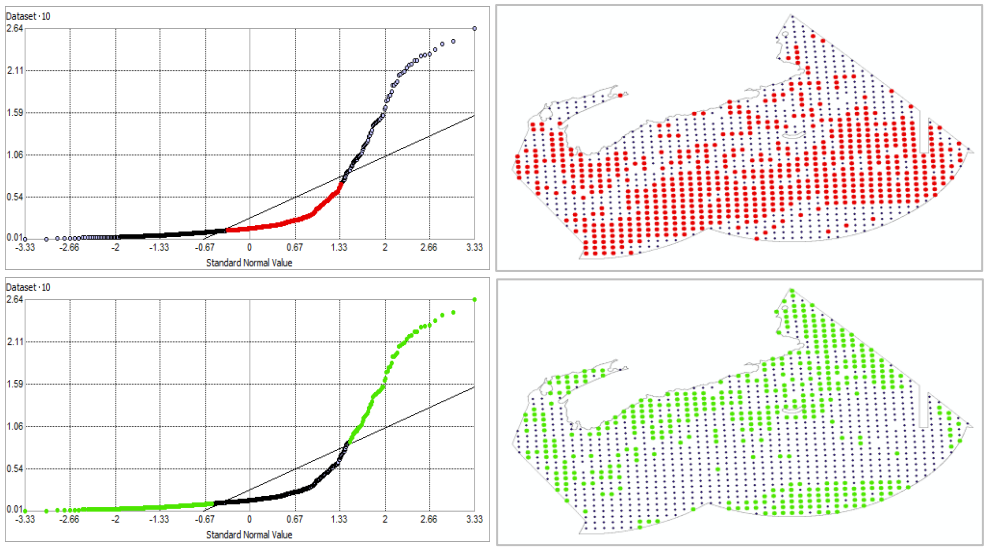

Fig. 287. Normal Q-Q plot for data values of Bottom Shear Average Range (Pa). Points falling under (upper panel) and over (bottom panel) the reference line are mapped.

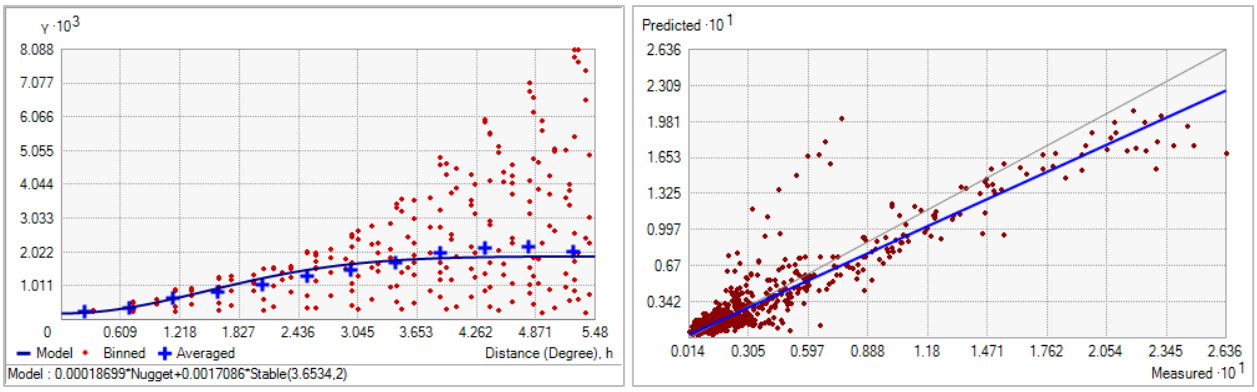

Fig. 288. Left panel: Semivariogram of Bottom Shear Average Range (Pa). Binned values are shown as red dots; average points are shown as blue crosses; the model fit to the averaged values is shown as a blue line. Lag size: 0.457 degrees; number of lags: 12; Parameter: 2; Range: 3.653 degrees; Partial Sill: 1.709 x 10^{-3}. Right panel: Scatterplot of predicted values versus observed values for the model of Bottom Shear Average Range (Pa).

Table 116. Results of cross-validation of the kriged model for Bottom Shear Average Range (Pa).

Prediction error	**Value**
Number of Observations	1143
Overall Mean Error	3.163 x 10^{-4}
Root Mean Square Prediction Error	0.014
Standardized Mean	0.024
Standardized Root Mean Square Prediction Error	0.996
Average Standard Error	0.014

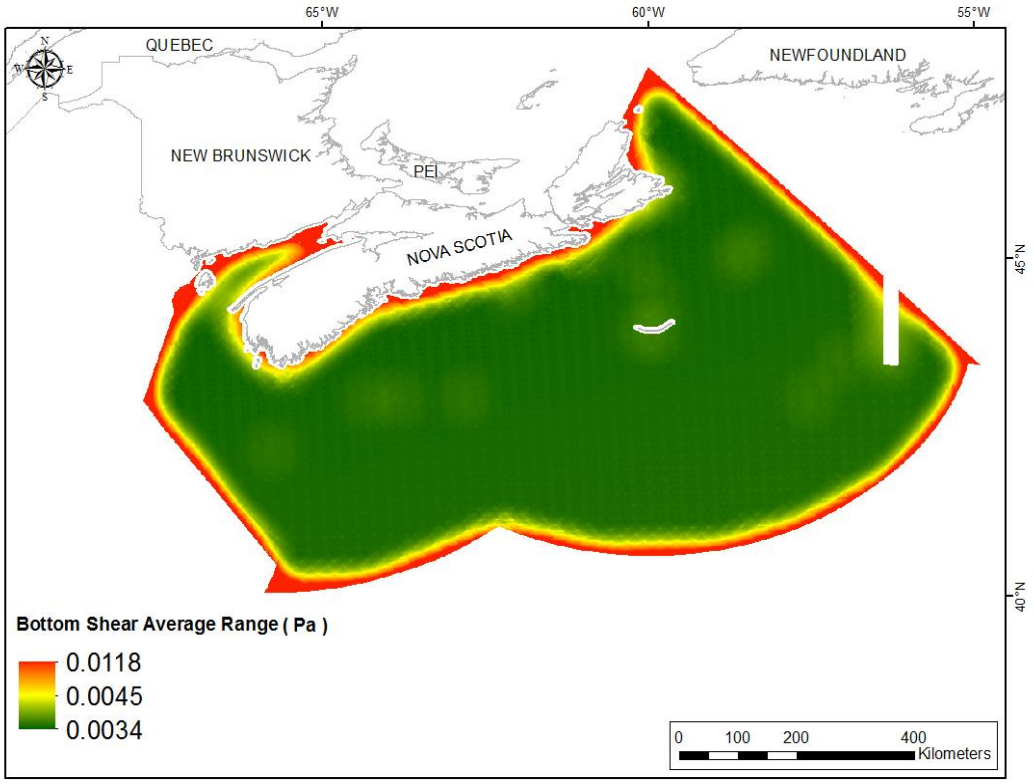

Fig. 289. Prediction standard error surface of Bottom Shear Average Range (Pa).

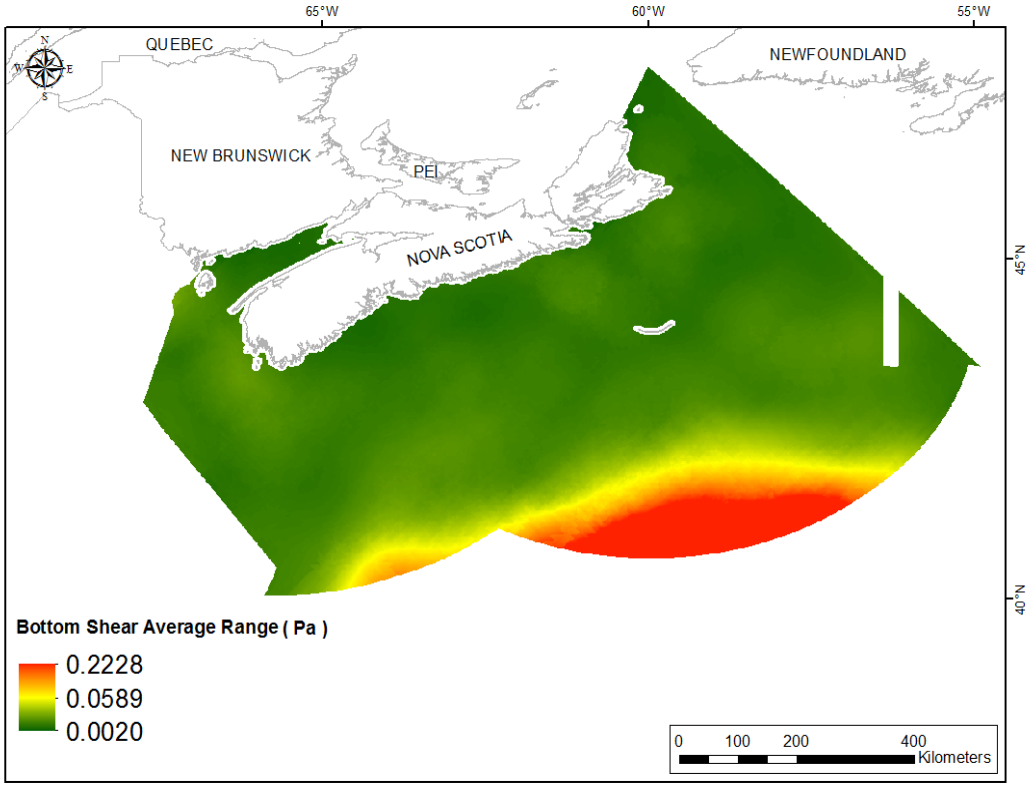

Fig. 290. Interpolated prediction surface of Bottom Shear Average Range (Pa).

Sea Surface Chlorophyll *a*

Sea surface chlorophyll *a* concentration is a proxy for phytoplankton biomass and is therefore related to the vertical flux of particulate organic carbon and food supply to the seafloor (Lutz et al., 2007). Gradients in food supply have often been identified as the main factor in controlling changes in benthic biomass, diversity, distribution, and zonation in the deep sea (Levin et al., 2001; Carney, 2005; Soltwedel et al., 2009; MacDonald et al., 2010; Papiol et al., 2012). In the northwest Atlantic, surface chlorophyll *a* has shown to be an important determinant in generalized linear models of megafaunal abundance and richness (Beazley et al. 2013) and was an important variable in random forest models predicting the presence of *Geodia* sponge and sponge grounds (Knudby et al., 2013). The spring phytoplankton bloom is thought to be a controlling factor in the reproductive cycles of several deep-sea corals (Sun et al., 2010a; 2010b; 2011; Mercier and Hamel, 2011) and sponges (Spetland et al., 2007) in the North Atlantic. Therefore, we expect that seasonal rather than annual measures of chlorophyll *a* will be more important in species distribution models.

Spring Chlorophyll *a* Mean

This variable displayed a right-skewed distribution with extreme leptokurtosis prior to interpolation (Table 117, Fig. 291). The data were higher than predicted by a normal distribution at both tails and lower than predicted at mid-values (Fig. 292). The areas of under- and over-prediction showed spatial pattern over the study extent (Fig. 292).

The semivariogram showed weak autocorrelation present in the data and the model showed a very good fit between measured and predicted values (Fig. 293). Nevertheless, poor performance of the model was indicated by the poor cross-validation statistics (Table 118). The Standardized Root-Mean-Square Prediction Error was greater than 1 indicating that variability in the predictions has been underestimated. The error map showed low error across the study extent (Fig. 294). The kriged surface is presented in Fig. 295.

Table 117. Distributional properties of Spring Chlorophyll *a* Mean (mg m^{-3}).

Property	Value
Number of Observations	157201
Minimum	0.428
Maximum	10.930
Mean	1.026
Median	0.869
Standard Deviation	0.563
Skewness	4.757
Kurtosis	42.236

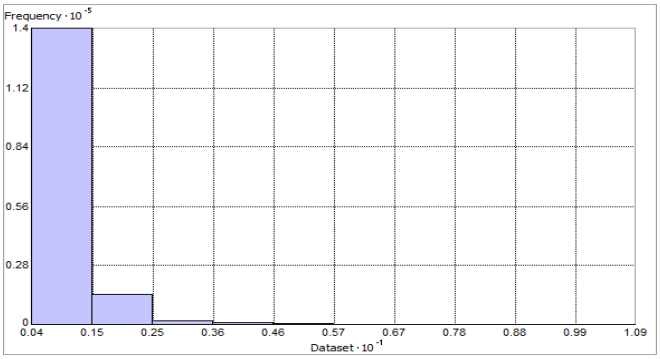

Fig. 291. Distribution of Spring Chlorophyll *a* Mean (mg m^{-3}). Histogram was illustrated using 10 bins. X and Y axes are shown at 10^{-1} and 10^{-5} respectively.

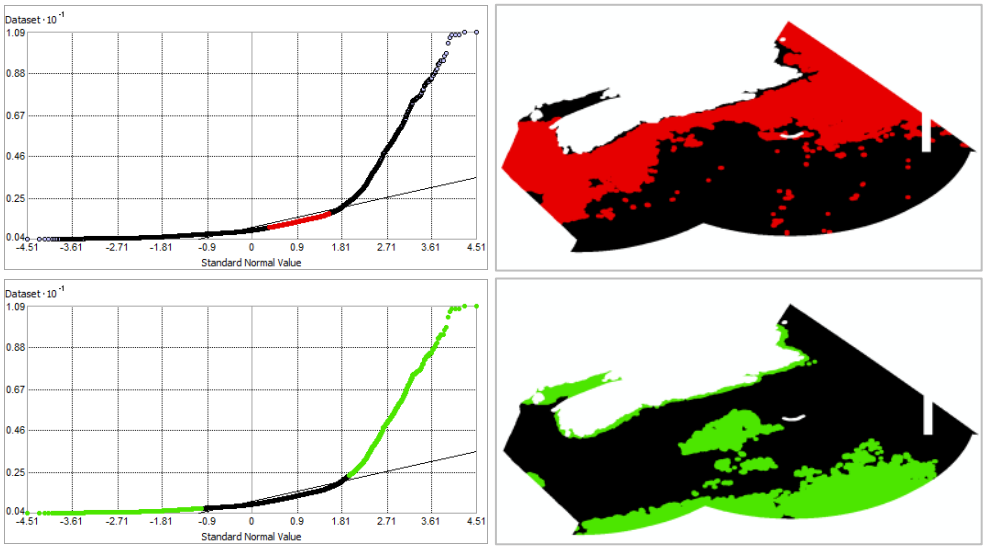

Fig. 292. Normal Q-Q plot for data values of Spring Chlorophyll *a* Mean (mg m^{-3}). Points falling under (upper panel) and over (bottom panel) the reference line are mapped.

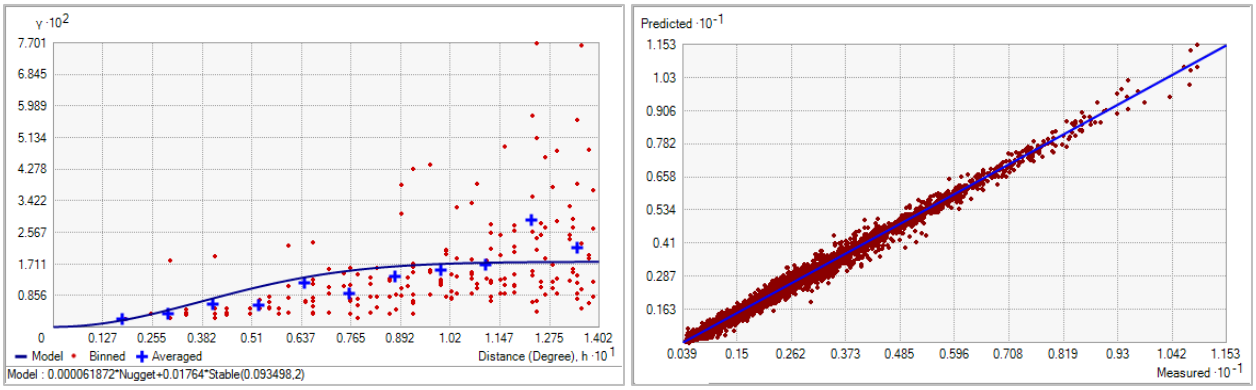

Fig. 293. Left panel: Semivariogram of Spring Chlorophyll *a* Mean (mg m^{-3}). Binned values are shown as red dots; average points are shown as blue crosses; the model fit to the averaged values is shown as a blue line. Lag size: 0.012 degrees; number of lags: 12; Parameter: 2; Range: 0.093 degrees; Partial Sill: 0.018. Right panel: Scatterplot of predicted values versus observed values for the model of Spring Chlorophyll *a* Mean (mg m^{-3}).

Table 118. Results of cross-validation of the kriged model for Spring Chlorophyll *a* Mean (mg m^{-3}).

Prediction error	**Value**
Number of Observations	157201
Overall Mean Error	-1.278×10^{-4}
Root Mean Square Prediction Error	0.041
Standardized Mean	-8.116×10^{-3}
Standardized Root Mean Square Prediction Error	3.762
Average Standard Error	0.011

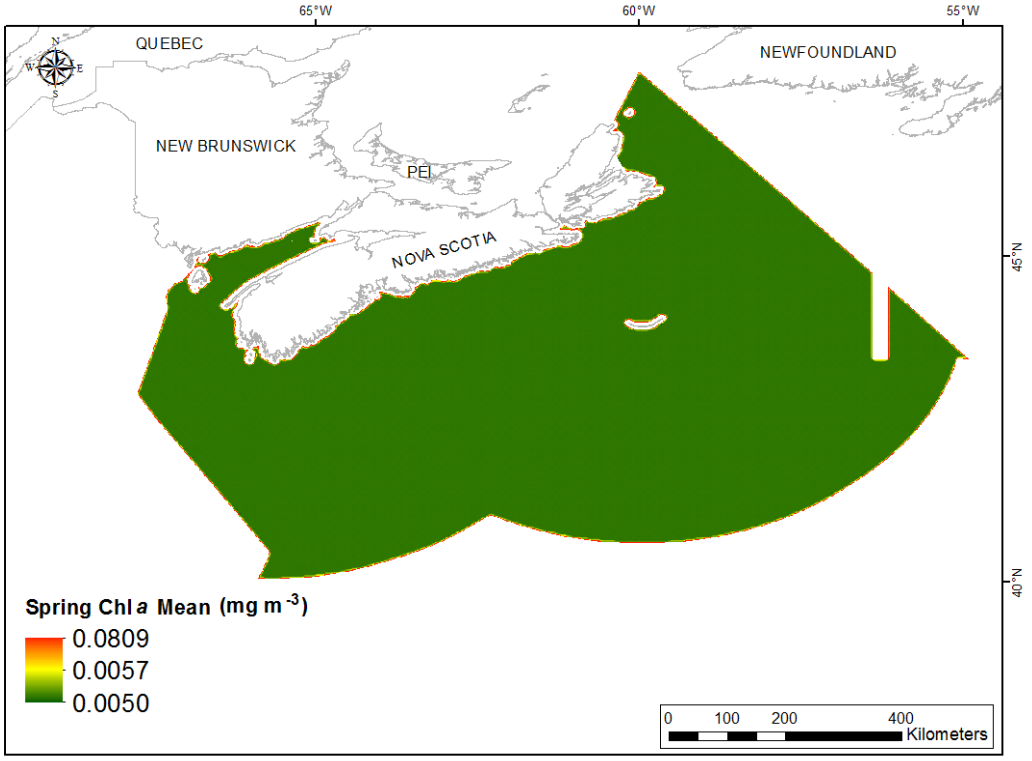

Fig. 294. Prediction standard error surface of Spring Chlorophyll *a* Mean (mg m^{-3}).

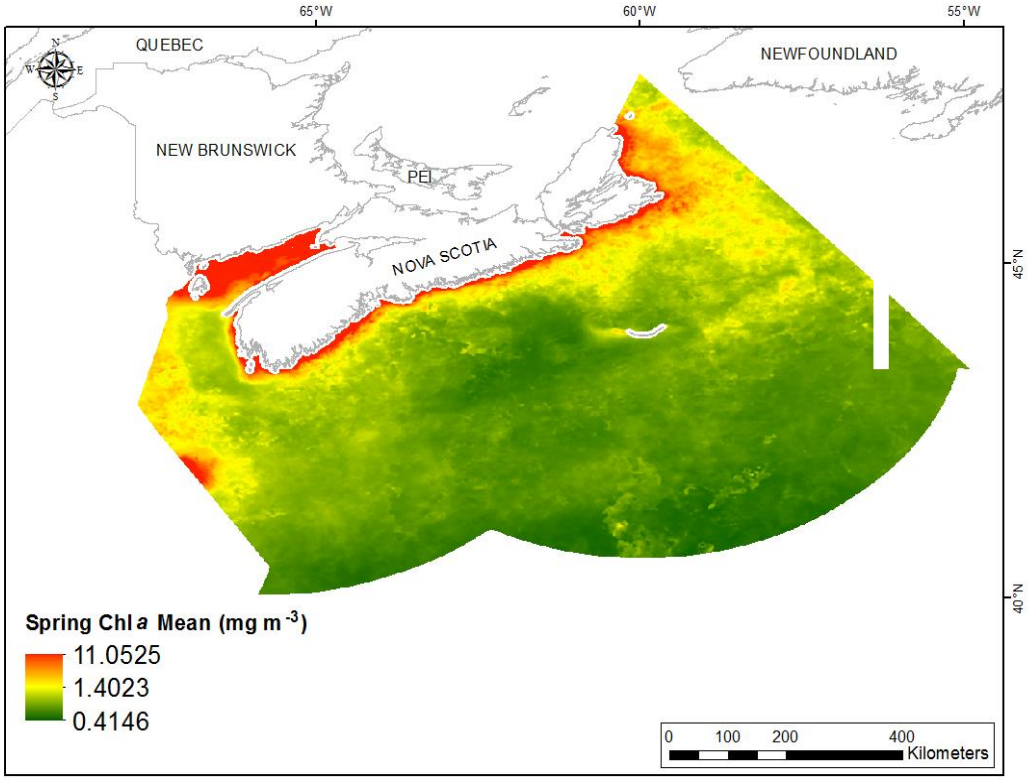

Fig. 295. Interpolated prediction surface of Spring Chlorophyll *a* Mean (mg m^{-3}).

Spring Chlorophyll *a* Minimum

This variable displayed a right-skewed, extremely leptokurtic distribution prior to interpolation (Table 119, Fig. 296). The data were higher than predicted by a normal distribution at both tails and lower than predicted at mid-values (Fig. 297). The areas of under- and over-prediction showed a spatial pattern over the study extent (Fig. 297).

The semivariogram showed weak autocorrelation present in the data and the model showed a very good fit between measured and predicted values (Fig. 298). Good performance of the model was indicated by the good cross-validation statistics (Table 120). The error map showed low error across the study extent (Fig. 299). The kriged surface is presented in Fig. 300.

Table 119. Distributional properties of Spring Chlorophyll *a* Minimum (mg m^{-3}).

Property	Value
Number of Observations	157201
Minimum	0.171
Maximum	8.264
Mean	0.627
Median	0.550
Standard Deviation	0.398
Skewness	6.775
Kurtosis	71.759

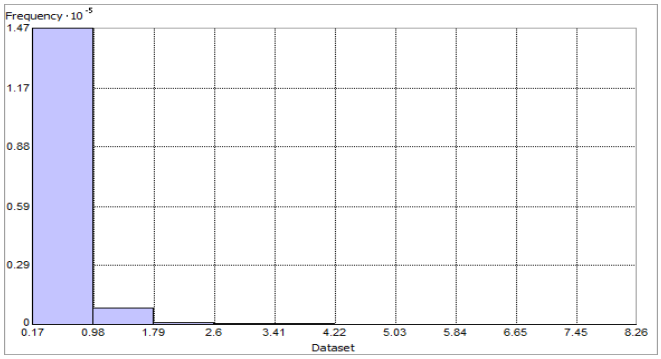

Fig. 296. Distribution of Spring Chlorophyll *a* Minimum (mg m^{-3}). Histogram was illustrated using 10 bins. Y axis is shown at 10^{-5}.

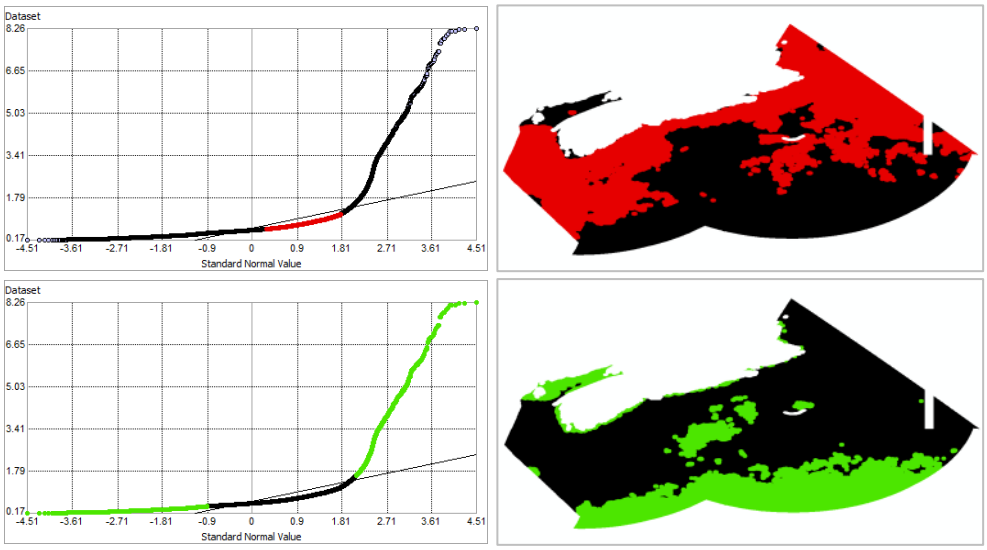

Fig. 297. Normal Q-Q plot for data values of Spring Chlorophyll *a* Minimum (mg m^{-3}). Points falling under (upper panel) and over (bottom panel) the reference line are mapped.

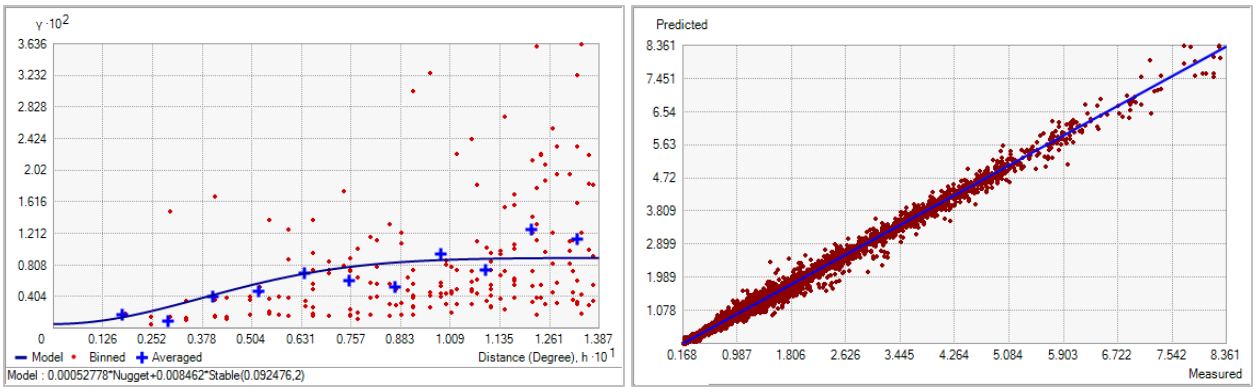

Fig. 298. Left panel: Semivariogram of Spring Chlorophyll *a* Minimum (mg m^{-3}). Binned values are shown as red dots; average points are shown as blue crosses; the model fit to the averaged values is shown as a blue line. Lag size: 0.012 degrees; number of lags: 12; Parameter: 2; Range: 0.092 degrees; Partial Sill: 8.462 x 10^{-3}. Right panel: Scatterplot of predicted values versus observed values for the variable Spring Chlorophyll *a* Minimum.

Table 120. Results of cross-validation of the kriged model for Spring Chlorophyll *a* Minimum (mg m^{-3}).

Prediction error	**Value**
Number of Observations	157201
Overall Mean Error	-3.457 x 10^{-5}
Root Mean Square Prediction Error	0.028
Standardized Mean	-4.478 x 10^{-4}
Standardized Root Mean Square Prediction Error	1.006
Average Standard Error	0.027

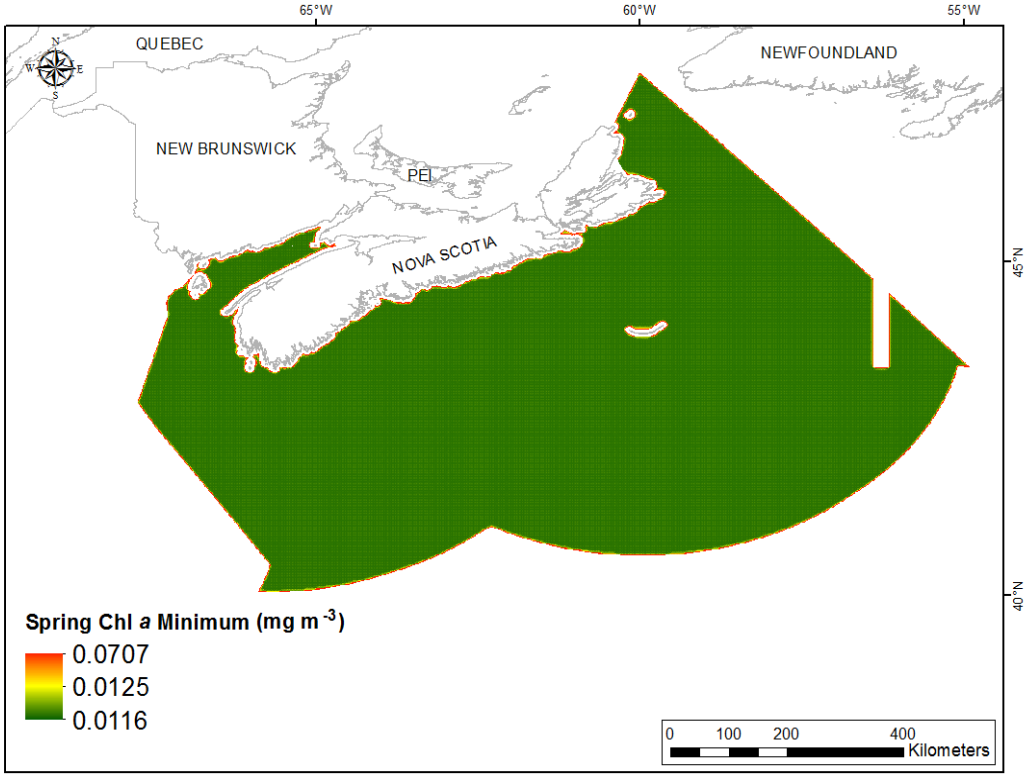

Fig. 299. Prediction standard error surface of Spring Chlorophyll *a* Minimum (mg m^{-3}).

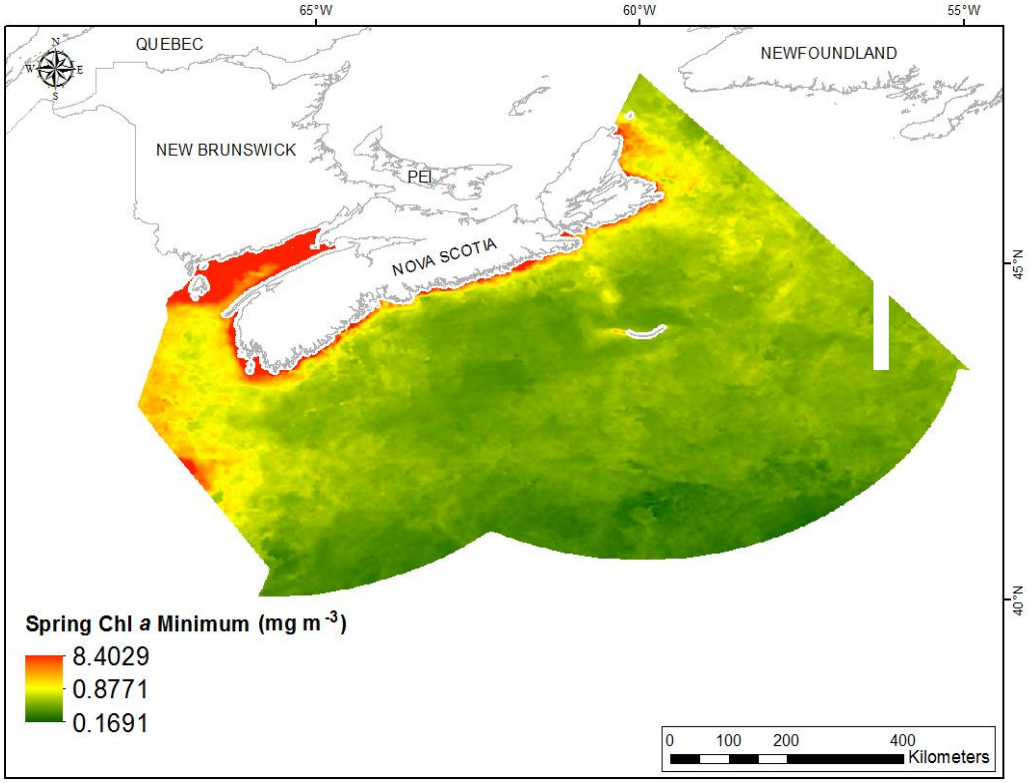

Fig. 300. Interpolated prediction surface of Spring Chlorophyll *a* Minimum (mg m^{-3}).

Spring Chlorophyll *a* Maximum

This variable displayed a right-skewed, highly leptokurtic distribution prior to interpolation (Table 121, Fig. 301). The data were higher than predicted by a normal distribution at both tails and lower than predicted at mid-values (Fig. 302). The areas of under- and over-prediction showed no strong spatial pattern over the study extent (Fig. 302).

The semivariogram showed autocorrelation present in the data and the model showed a good fit between measured and predicted values (Fig. 303). Fair performance was indicated by the cross-validation statistics (Table 122). The Standardized Root-Mean-Square Prediction Error was higher than 1 indicating that variability in the predictions has been underestimated. The error map showed medium error in a grid-like pattern over the study extent (Fig. 304). The kriged surface is presented in Fig. 305.

Table 121. Distributional properties of Spring Chlorophyll *a* Maximum (mg m^{-3}).

Property	Value
Number of Observations	157201
Minimum	0.521
Maximum	18.400
Mean	1.811
Median	1.502
Standard Deviation	1.023
Skewness	2.578
Kurtosis	15.548

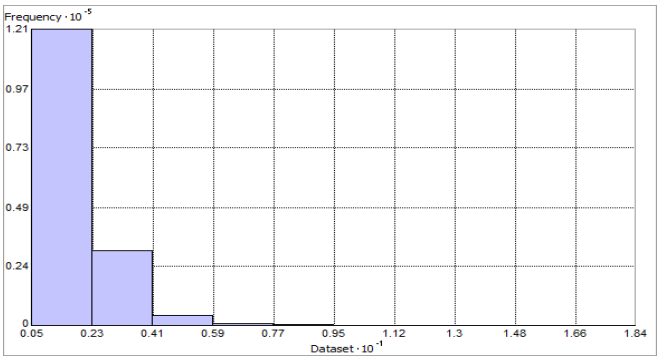

Fig. 301. Distribution of Spring Chlorophyll *a* Maximum (mg m^{-3}). Histogram was illustrated using 10 bins. X and Y axes are shown at 10^{-1} and 10^{-5} respectively.

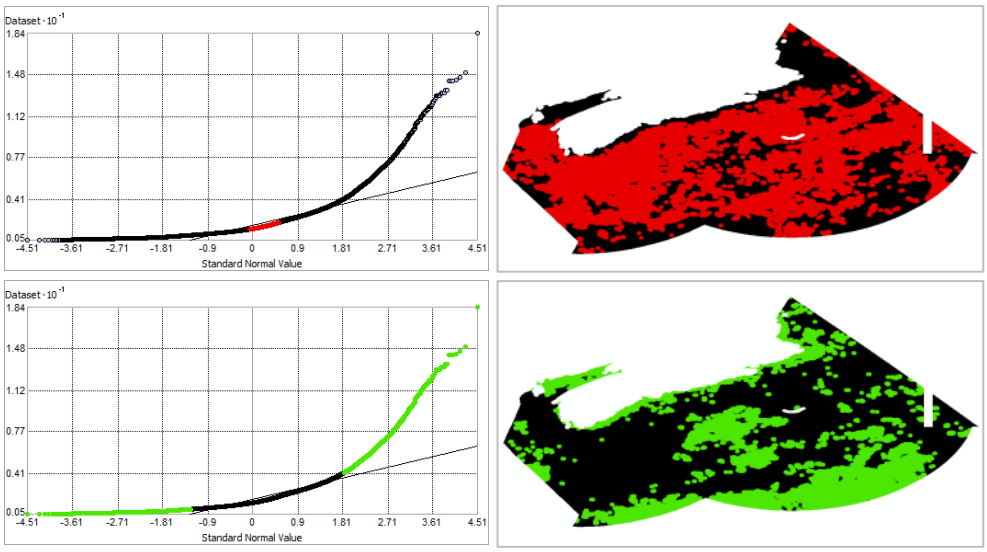

Fig. 302. Normal Q-Q plot for data values of Spring Chlorophyll *a* Maximum (mg m^{-3}). Points falling under (upper panel) and over (lower panel) the reference line are mapped.

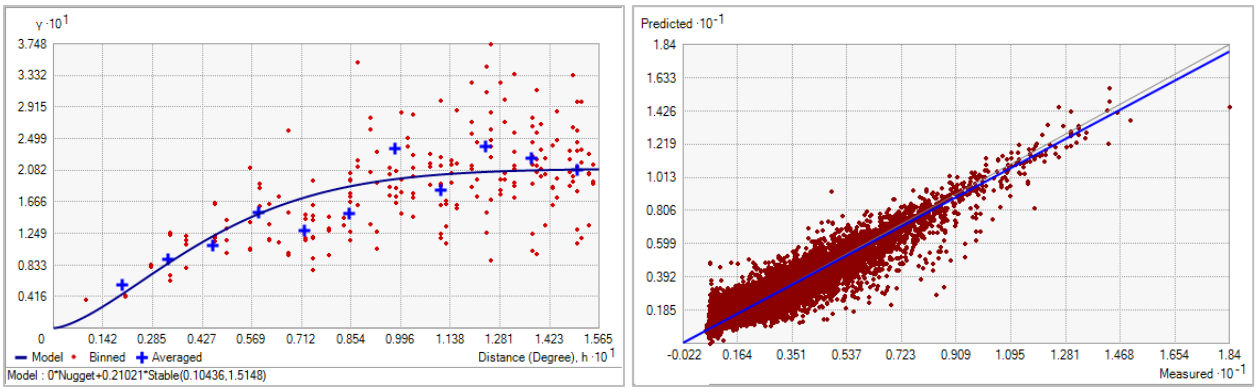

Fig. 303. Left panel: Semivariogram of Spring Chlorophyll *a* Maximum (mg m^{-3}). Binned values are shown as red dots; average points are shown as blue crosses; the model fit to the averaged values is shown as a blue line. Lag size: 0.013 degrees; number of lags: 12; Parameter: 1.515; Range: 0.104 degrees; Partial Sill: 0.210. Right panel: Scatterplot of predicted values versus observed values for the variable Spring Chlorophyll *a* Maximum (mg m^{-3}).

Table 122. Results of cross-validation of the kriged model for Spring Chlorophyll *a* Maximum (mg m^{-3}).

Prediction error	**Value**
Number of Observations	157201
Overall Mean Error	-2.146×10^{-4}
Root Mean Square Prediction Error	0.235
Standardized Mean	-8.448×10^{-4}
Standardized Root Mean Square Prediction Error	1.636
Average Standard Error	0.142

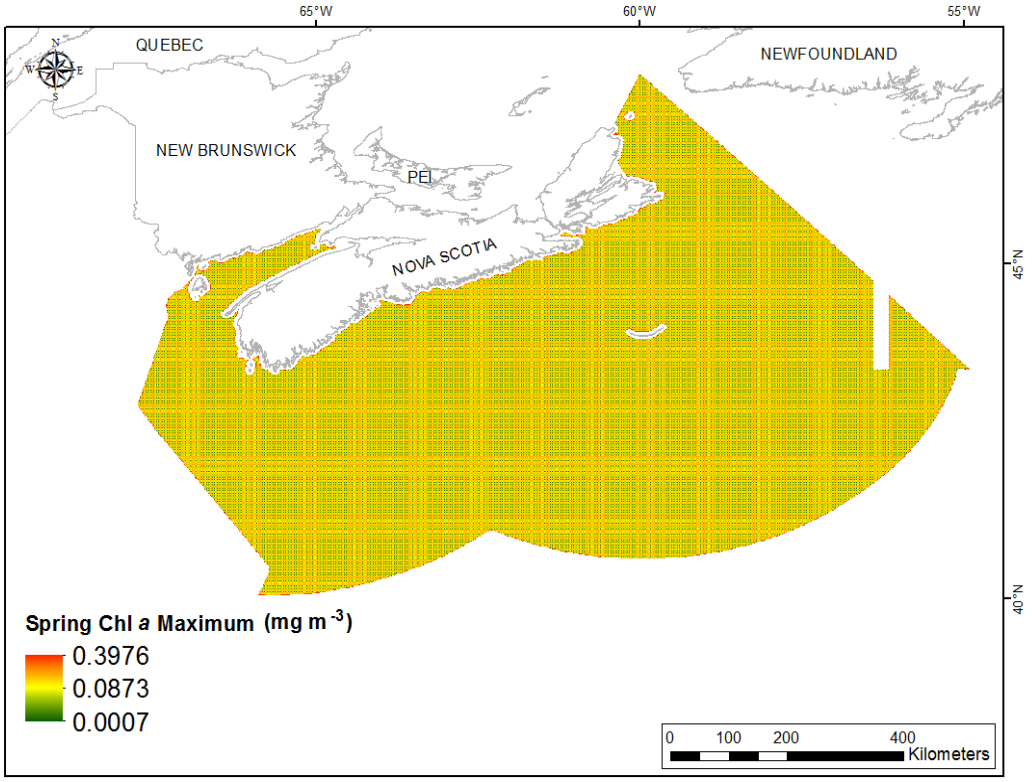

Fig. 304. Prediction standard error surface of Spring Chlorophyll *a* Maximum (mg m^{-3}).

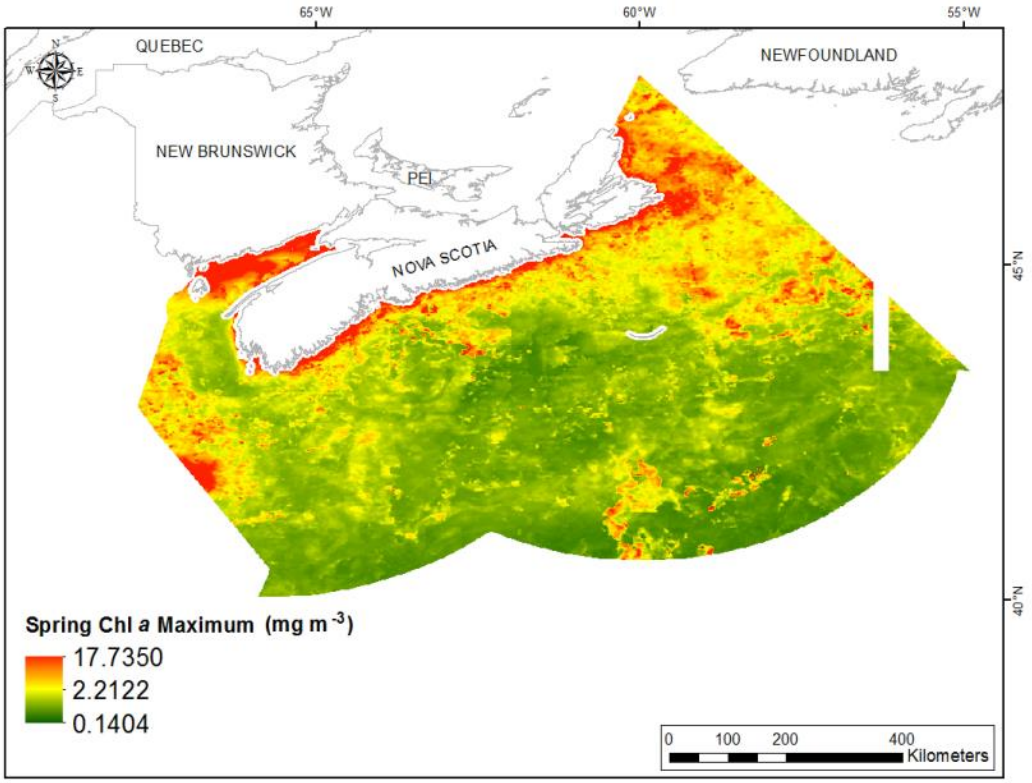

Fig. 305. Interpolated prediction surface of Spring Chlorophyll *a* Maximum (mg m^{-3}).

Spring Chlorophyll *a* Range

This variable displayed a right-skewed, highly leptokurtic distribution prior to interpolation (Table 123, Fig. 306). The data were higher than predicted by a normal distribution at both tails and lower than predicted at mid-values (Fig. 307). The areas of under- and over-prediction showed no spatial pattern over the study extent (Fig. 307).

The semivariogram showed moderate autocorrelation present in the data and the model showed good fit between measured and predicted values (Fig. 308). Fair performance was indicated by the cross-validation statistics (Table 124). The error map showed medium error in a grid-like pattern over the study extent (Fig. 309). The kriged surface is presented in Fig. 310. Negative values resulted from the right-skewed nature of the raw data (Fig. 306). Of the 326,283 raster cells in the study extent, only 2 contained negative values (see Table A1). These were located together near the southern edge of the study extent above the abyssal plan (Fig. A5).

Table 123. Distributional properties of Spring Chlorophyll *a* Range (mg m^{-3}).

Property	Value
Number of Observations	157201
Minimum	0.127
Maximum	13.101
Mean	1.184
Median	0.929
Standard Deviation	0.797
Skewness	2.011
Kurtosis	9.684

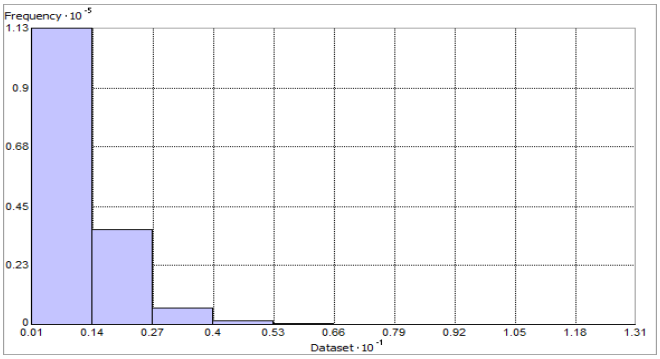

Fig. 306. Distribution of Spring Chlorophyll *a* Range (mg m^{-3}). Histogram was illustrated using 10 bins. X and Y axes are shown at 10^{-1} and 10^{-5} respectively.

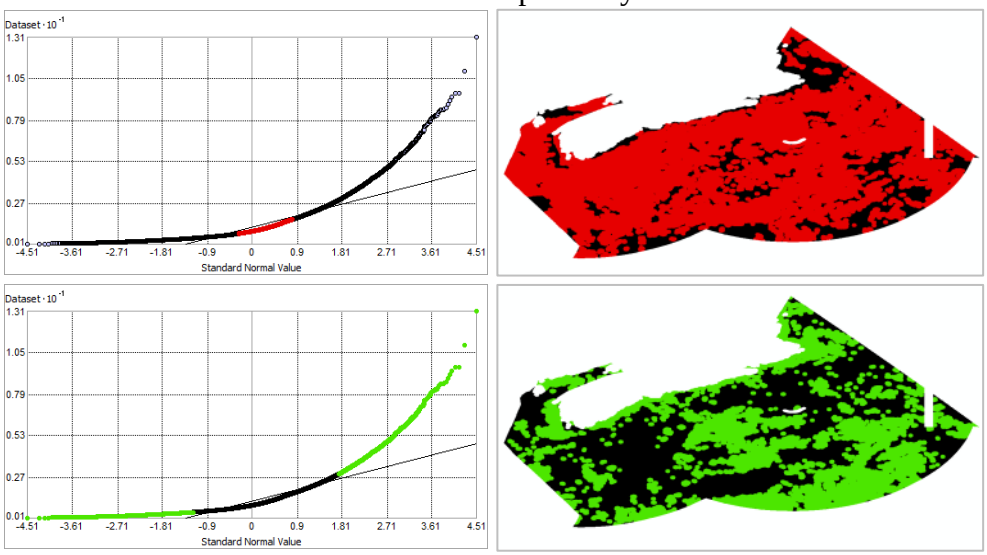

Fig. 307. Normal Q-Q plot for data values of Spring Chlorophyll *a* Range (mg m^{-3}). Points falling under (upper panel) and over (bottom panel) the reference line are mapped.

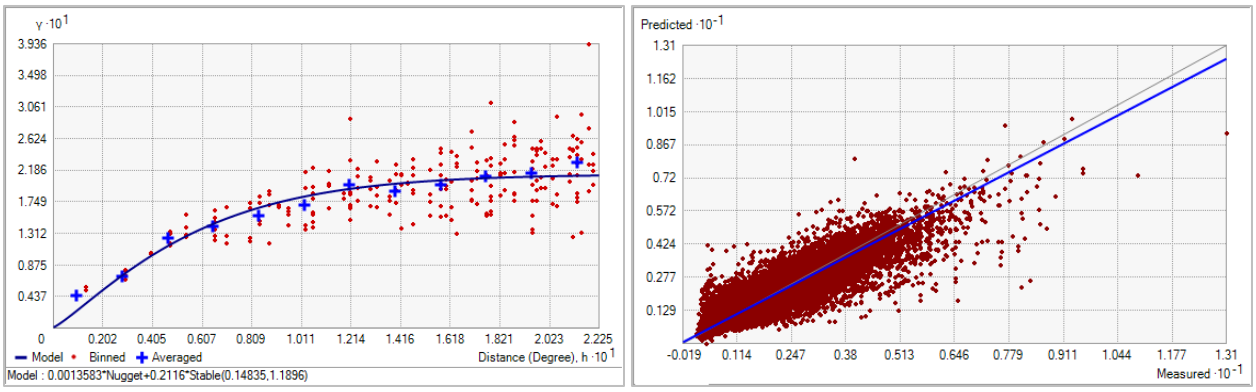

Fig. 308. Left panel: Semivariogram of Spring Chlorophyll *a* Range (mg m^{-3}). Binned values are shown as red dots; average points are shown as blue crosses; the model fit to the averaged values is shown as a blue line. Lag size: 0.019 degrees; number of lags: 12; Parameter: 1.190; Range: 0.148 degrees; Partial Sill: 0.212. Right panel: Scatterplot of predicted values versus observed values for the variable Spring Chlorophyll *a* Range (mg m^{-3}).

Table 124. Results of cross-validation of the kriged model for Spring Chlorophyll *a* Range (mg m^{-3}).

Prediction error	**Value**
Number of Observations	157201
Overall Mean Error	-1.363×10^{-4}
Root Mean Square Prediction Error	0.232
Standardized Mean	-3.953×10^{-4}
Standardized Root Mean Square Prediction Error	1.206
Average Standard Error	0.191

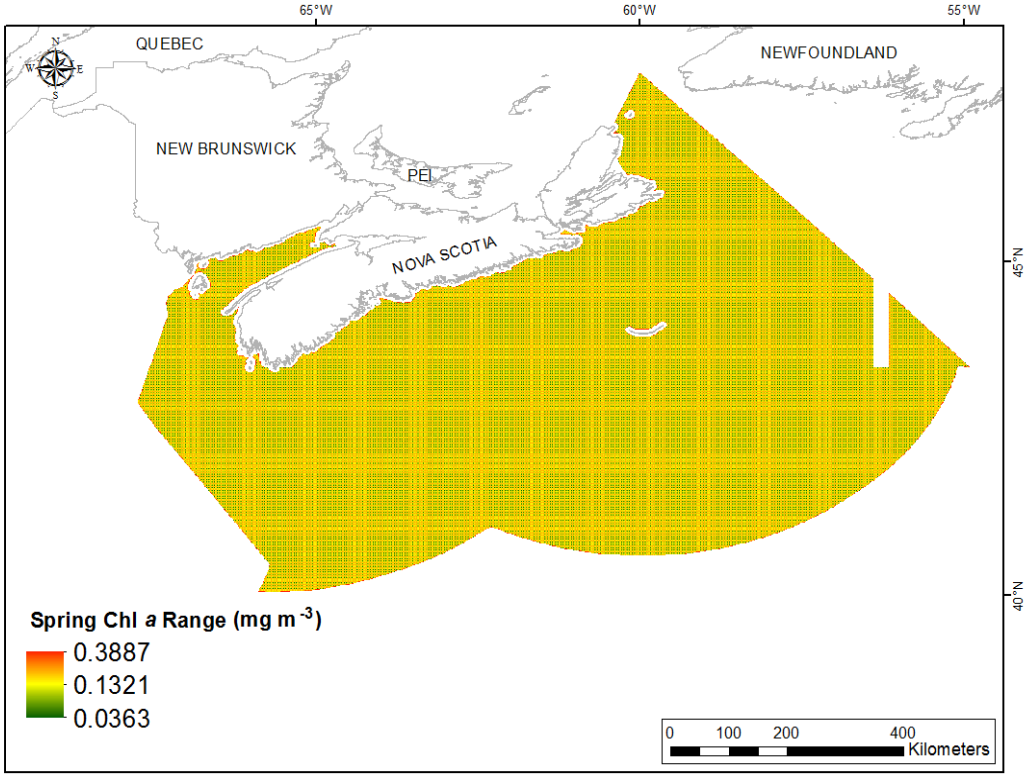

Fig. 309. Prediction standard error surface of Spring Chlorophyll *a* Range (mg m^{-3}).

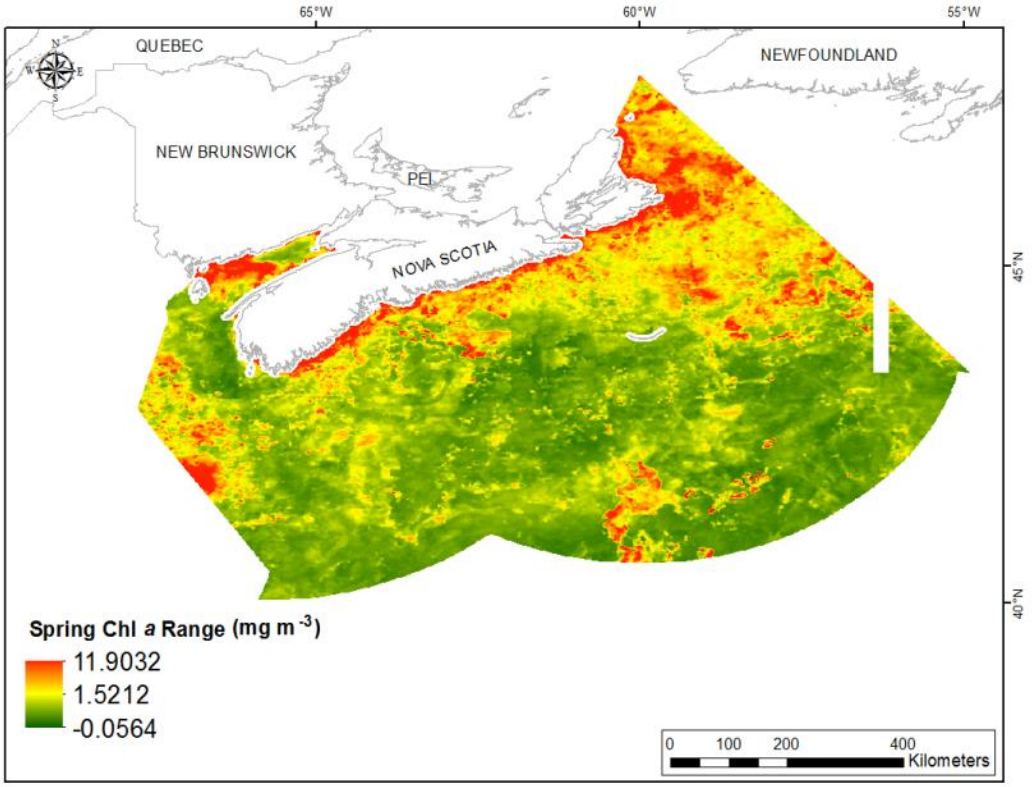

Fig. 310. Interpolated prediction surface of Spring Chlorophyll *a* Range (mg m^{-3}).

Summer Chlorophyll *a* Mean

This variable displayed a right-skewed, extremely leptokurtic distribution prior to interpolation (Table 125, Fig. 311). The data were higher than predicted by a normal distribution at both tails and lower than predicted at mid-values (Fig. 312). The areas of under- and over-prediction showed a very strong spatial pattern over the study extent (Fig. 312).

The semivariogram showed weak autocorrelation present in the data and the model showed a very good fit between measured and predicted values (Fig. 313). Fair performance was indicated by the cross-validation statistics (Table 126). The Standardized Root-Mean-Square Prediction Error was less than 1 indicating that variability in the predictions has been overestimated. The error map showed low to medium error over the study extent (Fig. 314). The kriged surface is presented in Fig. 315.

Table 125. Distributional properties of Summer Chlorophyll *a* Mean (mg m^{-3}).

Property	Value
Number of Observations	157201
Minimum	0.140
Maximum	8.655
Mean	0.565
Median	0.398
Standard Deviation	0.525
Skewness	3.845
Kurtosis	30.224

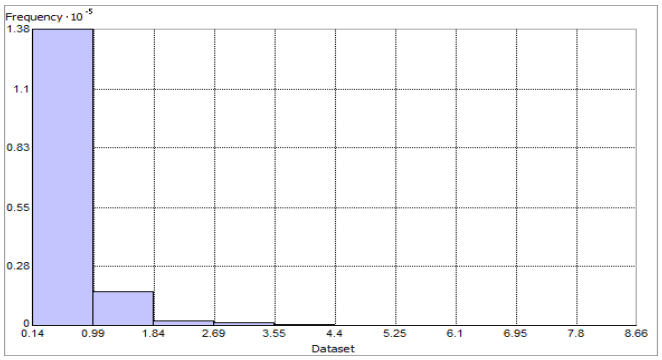

Fig. 311. Distribution of Summer Chlorophyll *a* Mean (mg m^{-3}). Histogram was illustrated using 10 bins. Y axis is shown at 10^{-5}.

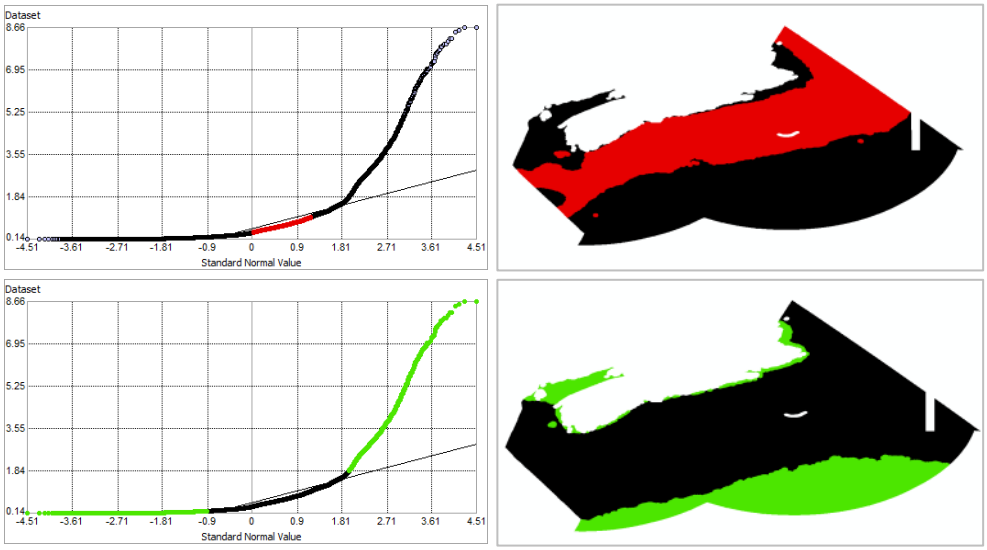

Fig. 312. Normal Q-Q plot for data values of Summer Chlorophyll *a* Mean (mg m^{-3}). Points falling under (upper panel) and over (bottom panel) the reference line are mapped.

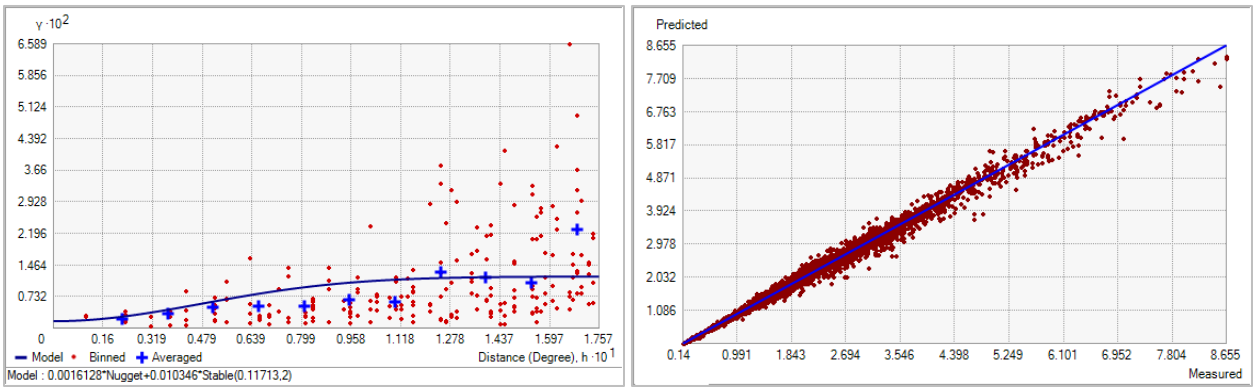

Fig. 313. Left panel: Semivariogram of Summer Chlorophyll *a* Mean (mg m^{-3}). Binned values are shown as red dots; average points are shown as blue crosses; the model fit to the averaged values is shown as a blue line. Lag size: 0.015 degrees; number of lags: 12; Parameter: 2; Range: 0.117 degrees; Partial Sill: 0.010. Right panel: Scatterplot of predicted values versus observed values for the variable Summer Chlorophyll *a* Mean (mg m^{-3}).

Table 126. Results of cross-validation of the kriged model for Summer Chlorophyll *a* Mean (mg m^{-3}).

Prediction error	**Value**
Number of Observations	157201
Overall Mean Error	7.438×10^{-5}
Root Mean Square Prediction Error	0.024
Standardized Mean	2.758×10^{-3}
Standardized Root Mean Square Prediction Error	0.506
Average Standard Error	0.044

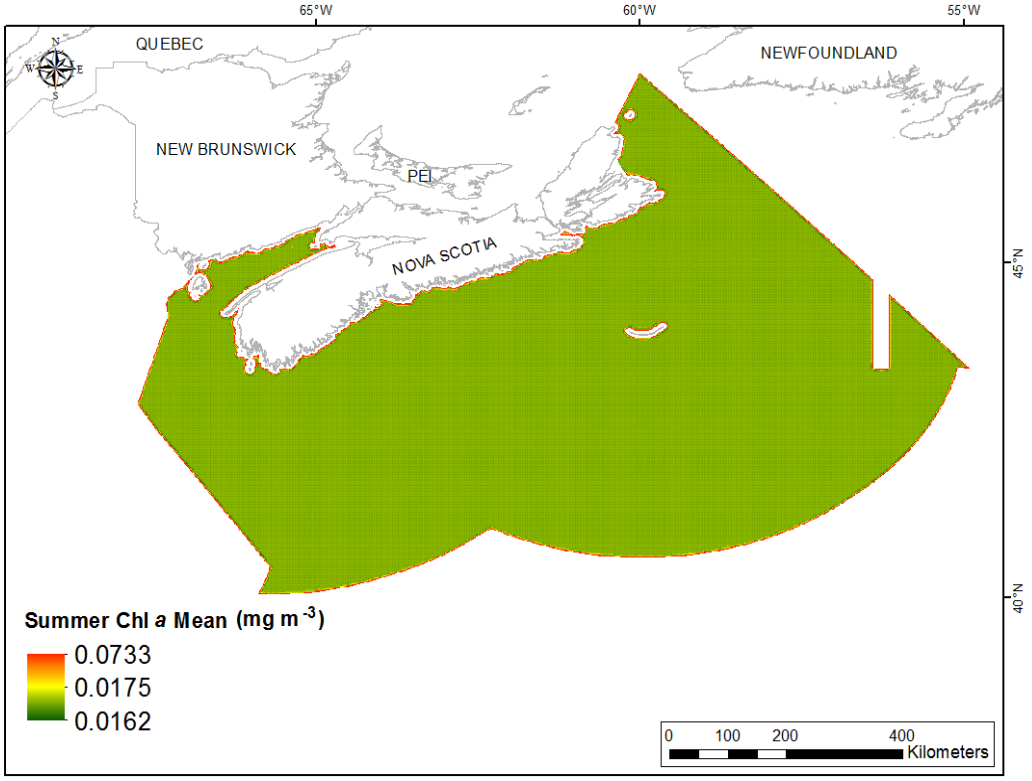

Fig. 314. Prediction standard error surface of Summer Chlorophyll *a* Mean (mg m^{-3}).

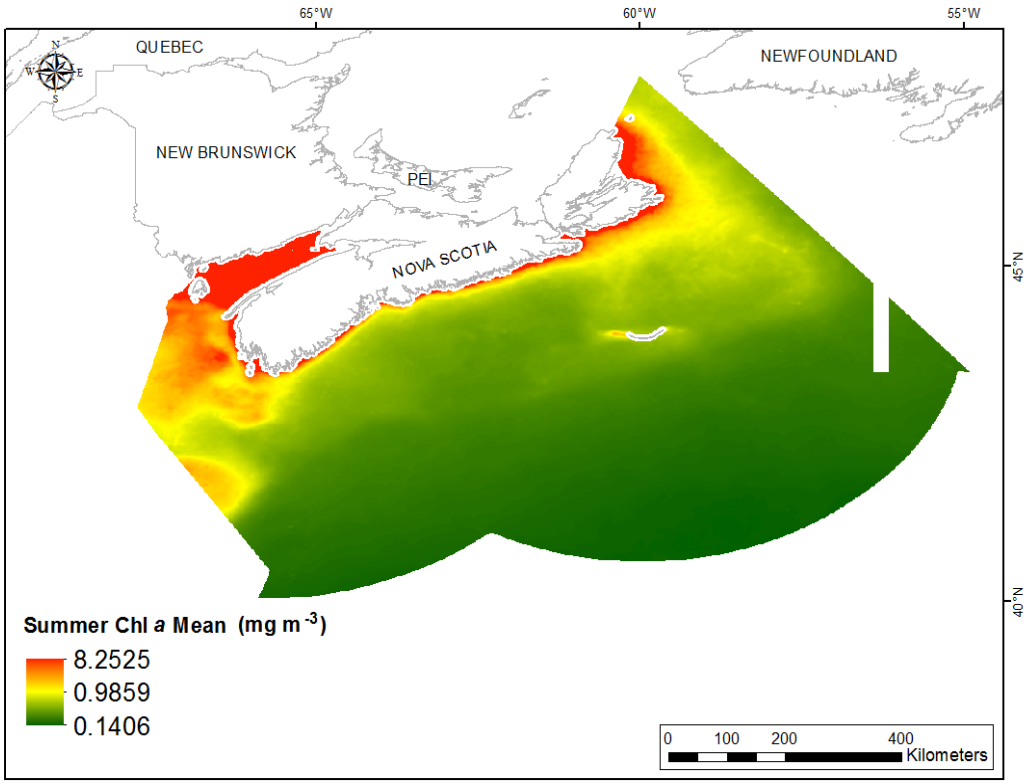

Fig. 315. Interpolated prediction surface of Summer Chlorophyll *a* Mean (mg m^{-3}).

Summer Chlorophyll *a* Minimum

This variable displayed a right-skewed, extremely leptokurtic distribution prior to interpolation (Table 127, Fig. 316). The data were higher than predicted by a normal distribution at both tails and only slightly lower than predicted at mid-values (Fig. 317). The areas of under- and over-prediction showed a very strong spatial pattern over the study extent (Fig. 317).

The semivariogram showed weak autocorrelation present in the data and the model showed a good fit between measured and predicted values (Fig. 318). Fair performance was indicated by the cross-validation statistics (Table 128). The Standardized Root-Mean-Square Prediction Error was less than 1 indicating that variability in the predictions has been overestimated. The error map showed low to medium error over the study extent (Fig. 319). The kriged surface is presented in Fig. 320.

Table 127. Distributional properties of Summer Chlorophyll *a* Minimum (mg m^{-3}).

Property	Value
Number of Observations	157201
Minimum	0.099
Maximum	7.130
Mean	0.421
Median	0.310
Standard Deviation	0.372
Skewness	3.888
Kurtosis	32.782

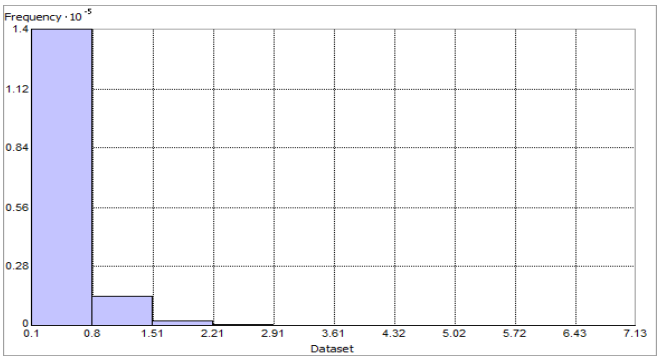

Fig. 316. Distribution of Summer Chlorophyll *a* Minimum (mg m^{-3}). Histogram was illustrated using 10 bins. Y axis is shown at 10^{-5}.

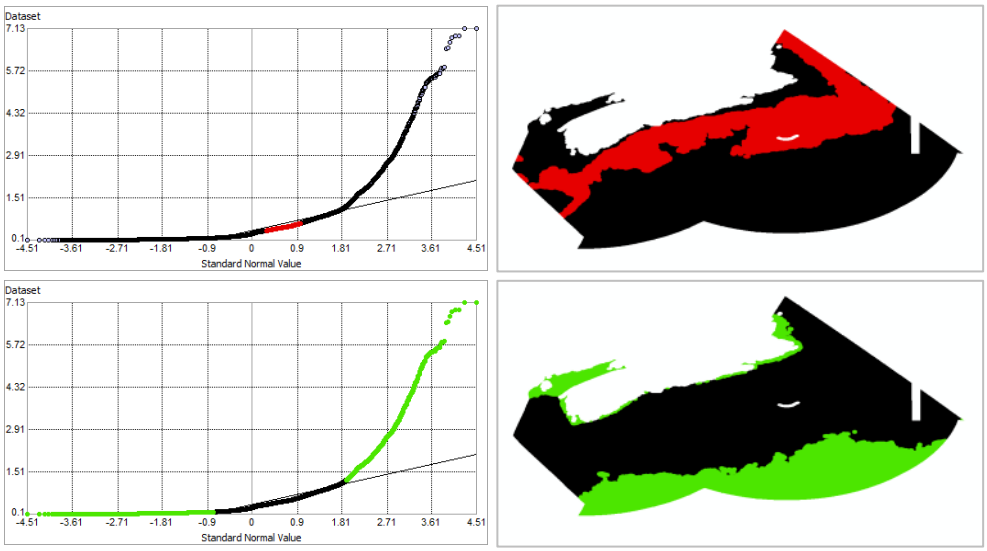

Fig. 317. Normal Q-Q plot for data values of Summer Chlorophyll *a* Minimum (mg m^{-3}). Points falling under (upper panel) and over (bottom panel) the reference line are mapped.

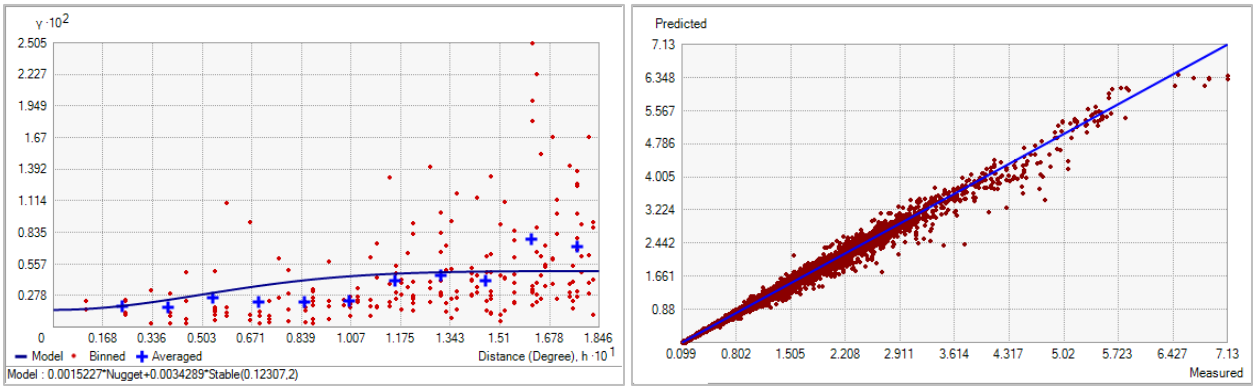

Fig. 318. Left panel: Semivariogram of Summer Chlorophyll *a* Minimum (mg m^{-3}). Binned values are shown as red dots; average points are shown as blue crosses; the model fit to the averaged values is shown as a blue line. Lag size: 0.015 degrees; number of lags: 12; Parameter: 2; Range: 0.123 degrees; Partial Sill: 3.429 x 10^{-3}. Right panel: Scatterplot of predicted values versus observed values for the variable Summer Chlorophyll *a* Minimum (mg m^{-3}).

Table 128. Results of cross-validation of the kriged model for Summer Chlorophyll *a* Minimum (mg m^{-3}).

Prediction error	**Value**
Number of Observations	157201
Overall Mean Error	4.779 x 10^{-5}
Root Mean Square Prediction Error	0.022
Standardized Mean	1.921 x 10^{-3}
Standardized Root Mean Square Prediction Error	0.512
Average Standard Error	0.042

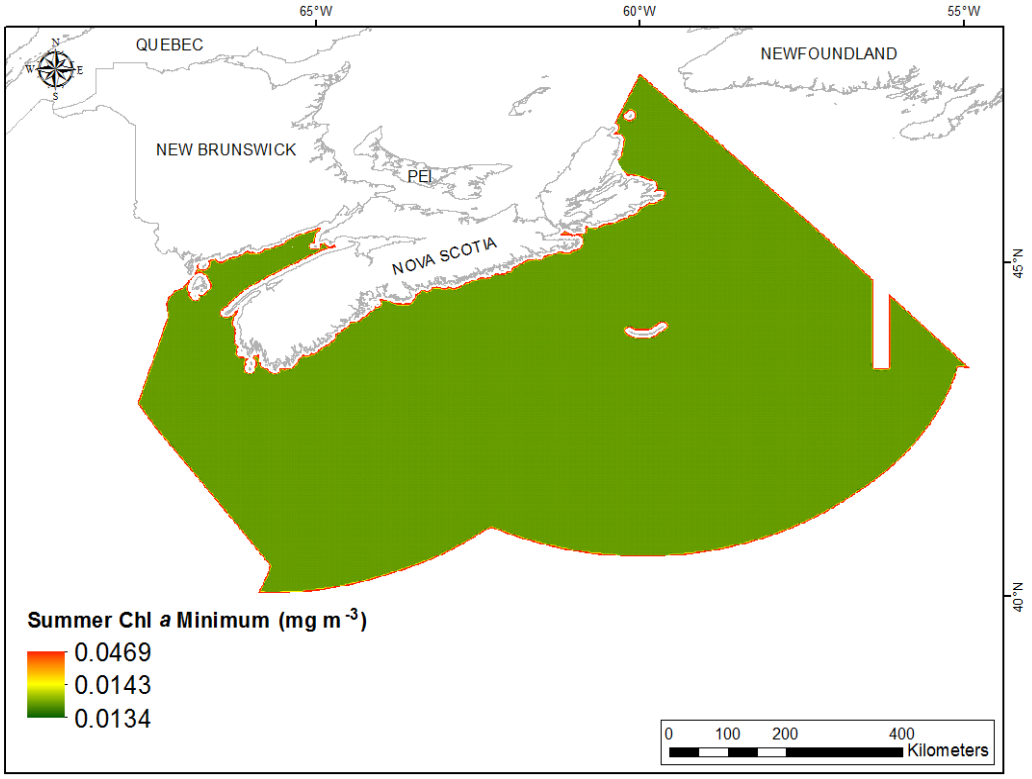

Fig. 319. Prediction standard error surface of Summer Chlorophyll *a* Minimum (mg m^{-3}).

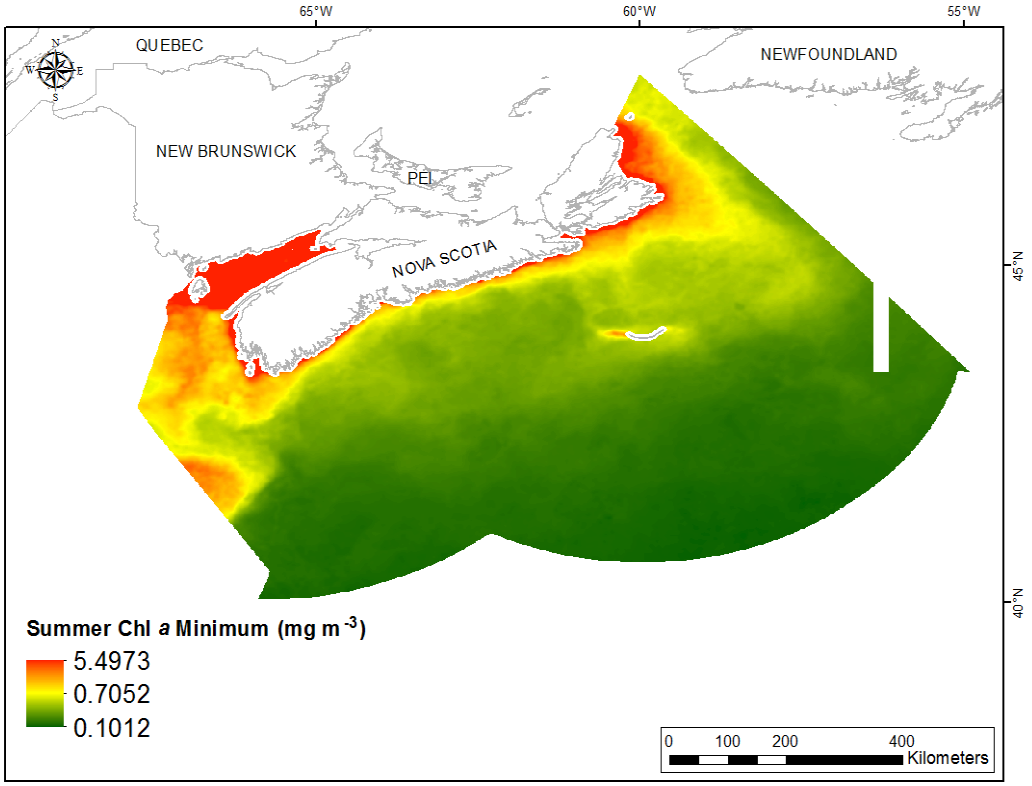

Fig. 320. Interpolated prediction surface of Summer Chlorophyll *a* Minimum (mg m^{-3}).

Summer Chlorophyll *a* Maximum

This variable displayed a right-skewed, extremely leptokurtic distribution prior to interpolation (Table 129, Fig. 321). The data were higher than predicted by a normal distribution at both tails and slightly lower than predicted at mid-values (Fig. 322). The areas of under- and over-prediction showed a strong spatial pattern over the study extent (Fig. 322).

The semivariogram showed weak autocorrelation present in the data and the model showed a very good fit between measured and predicted values (Fig. 323). However, poor performance was indicated by poor cross-validation results (Table 130). The Standardized Root-Mean-Square Prediction Error was greater than 1 indicating that variability in the predictions has been underestimated. The error map showed low to medium error over the study extent (Fig. 324). The kriged surface is presented in Fig. 325.

Table 129. Distributional properties of Summer Chlorophyll *a* Maximum (mg m^{-3}).

Property	Value
Number of Observations	157201
Minimum	0.156
Maximum	13.202
Mean	0.769
Median	0.499
Standard Deviation	0.810
Skewness	4.370
Kurtosis	33.846

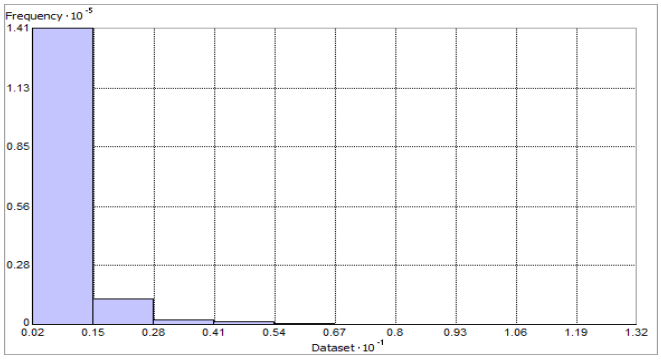

Fig. 321. Distribution of Summer Chlorophyll *a* Maximum (mg m^{-3}). Histogram was illustrated using 10 bins. X and Y axes are shown at 10^{-1} and 10^{-5} respectively.

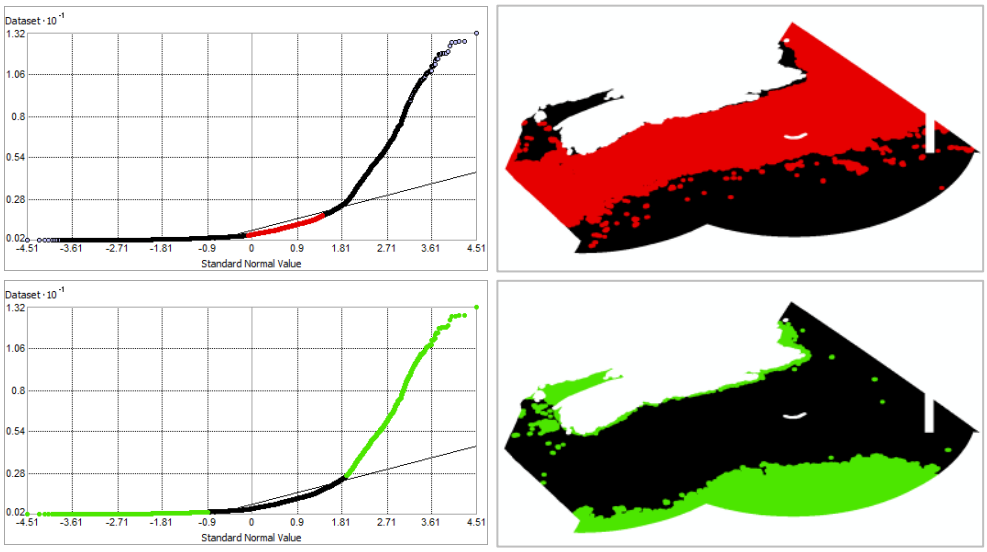

Fig. 322. Normal Q-Q plot for data values of Summer Chlorophyll *a* Maximum (mg m^{-3}). Points falling under (upper panel) and over (bottom panel) the reference line are mapped.

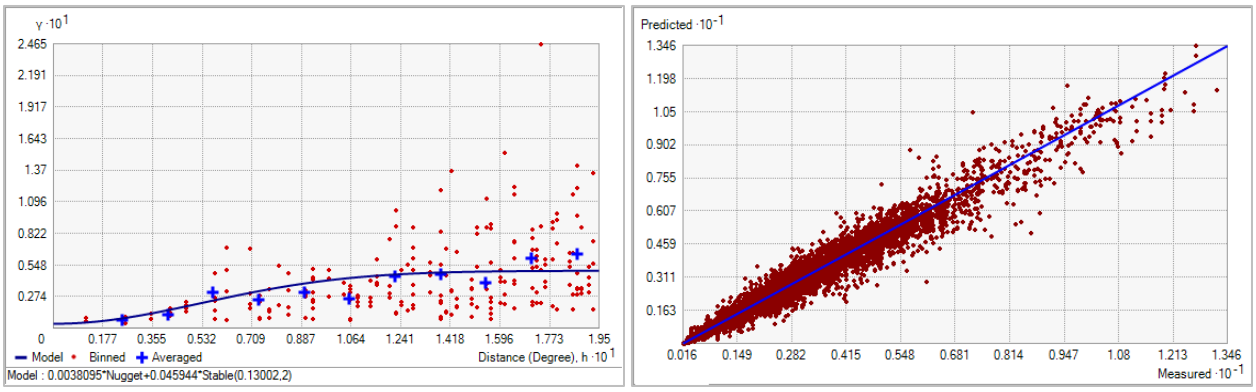

Fig. 323. Left panel: Semivariogram of Summer Chlorophyll *a* Maximum (mg m^{-3}). Binned values are shown as red dots; average points are shown as blue crosses; the model fit to the averaged values is shown as a blue line. Lag size: 0.016 degrees; number of lags: 12; Parameter: 2; Range: 0.130 degrees; Partial Sill: 0.046. Right panel: Scatterplot of predicted values versus observed values for the variable Summer Chlorophyll *a* Maximum (mg m^{-3}).

Table 130. Results of cross-validation of the kriged model for Summer Chlorophyll *a* Maximum (mg m^{-3}).

Prediction error	**Value**
Number of Observations	157201
Overall Mean Error	1.891×10^{-4}
Root Mean Square Prediction Error	0.096
Standardized Mean	3.690×10^{-3}
Standardized Root Mean Square Prediction Error	1.369
Average Standard Error	0.069

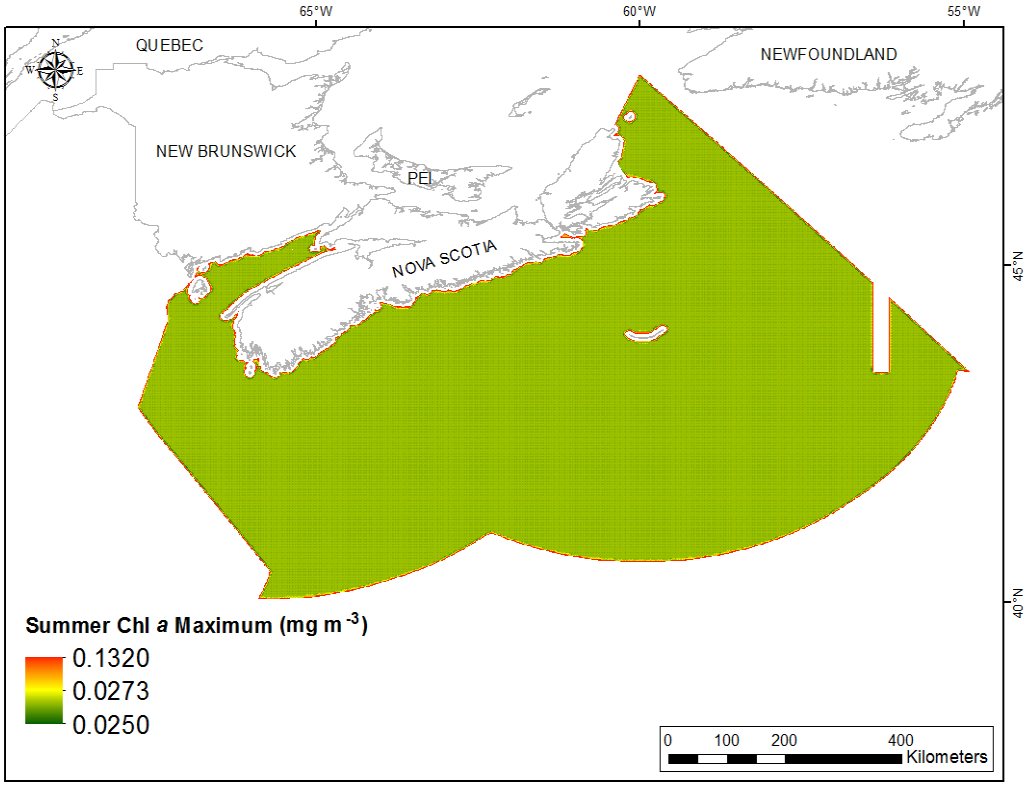

Fig. 324. Prediction standard error surface of Summer Chlorophyll *a* Maximum (mg m^{-3}).

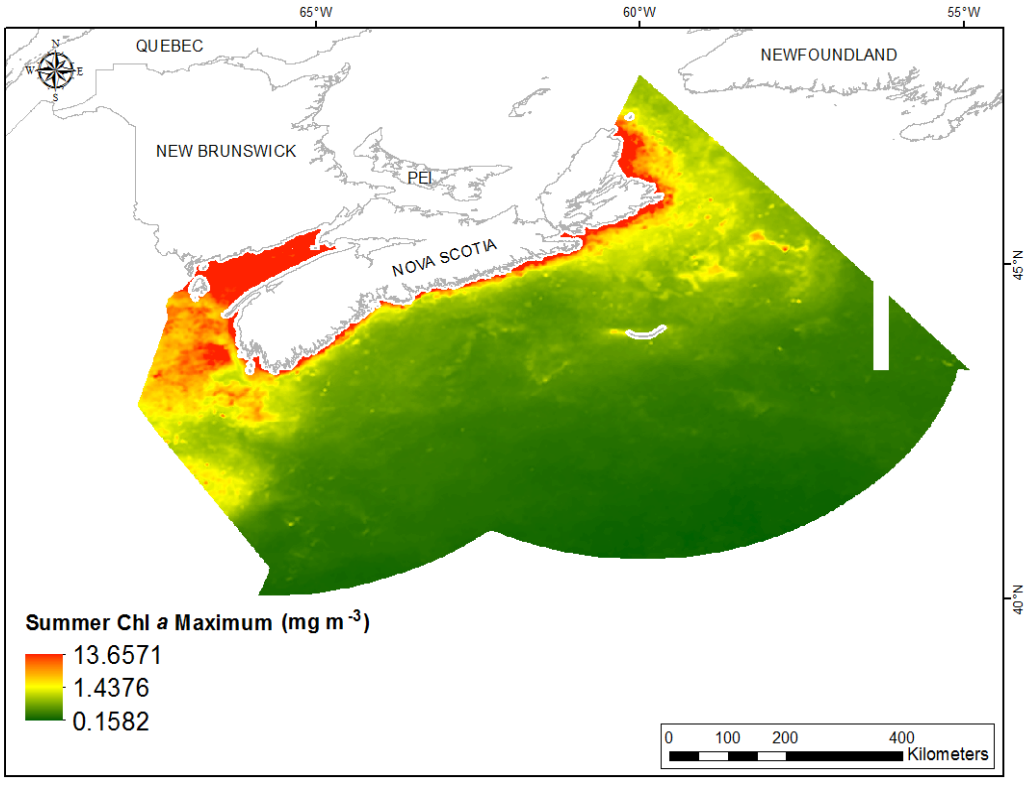

Fig. 325. Interpolated prediction surface of Summer Chlorophyll *a* Maximum (mg m^{-3}).

Summer Chlorophyll *a* Range

This variable displayed a right-skewed, extremely leptokurtic distribution prior to interpolation (Table 131, Fig. 326). The data were higher than predicted by a normal distribution at both tails and lower than predicted at mid-values (Fig. 327). The areas of under- and over-prediction showed a strong spatial pattern over the study extent (Fig. 327).

The semivariogram showed moderate autocorrelation present in the data and the model showed good fit between measured and predicted values (Fig. 328). The model showed fair cross-validation statistics (Table 132). The error map showed medium to high error in a grid-like pattern over the study extent (Fig. 329). The kriged surface is presented in Fig. 330.

Table 131. Distributional properties of Summer Chlorophyll *a* Range (mg m^{-3}).

Property	Value
Number of Observations	157201
Minimum	0.035
Maximum	9.341
Mean	0.348
Median	0.193
Standard Deviation	0.471
Skewness	5.240
Kurtosis	45.549

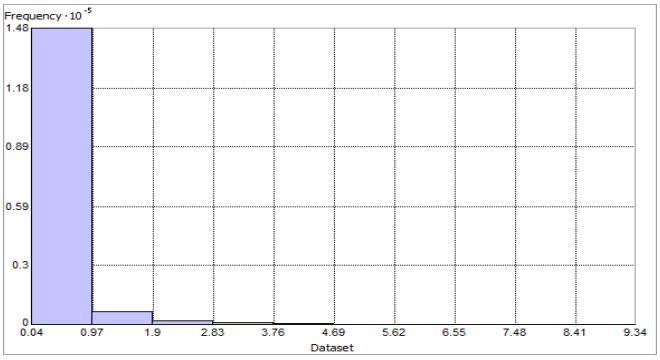

Fig. 326. Distribution of Summer Chlorophyll *a* Range (mg m^{-3}). Histogram was illustrated using 10 bins. Y axis is shown at 10^{-5}.

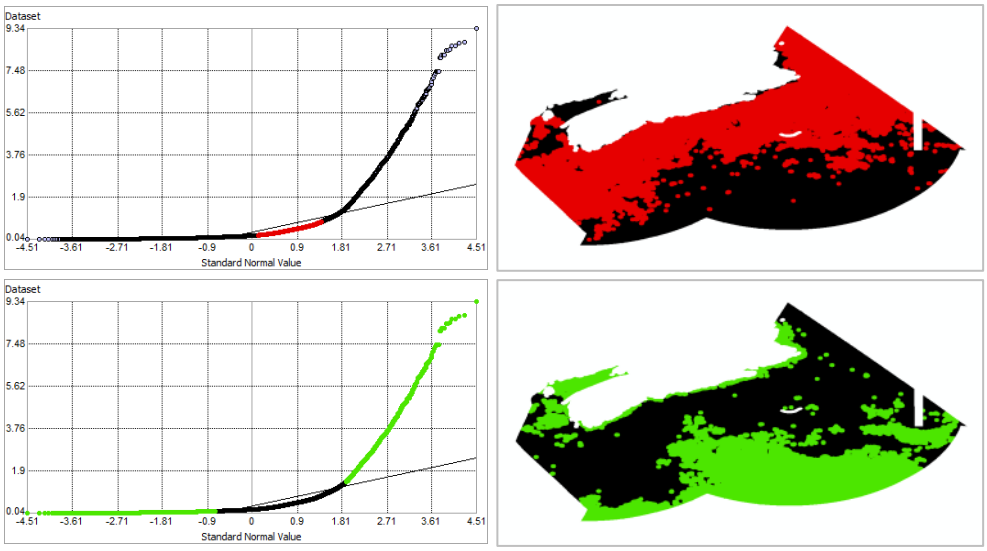

Fig. 327. Normal Q-Q plot for data values of Summer Chlorophyll *a* Range (mg m^{-3}). Points falling under (upper panel) and over (bottom panel) the reference line are mapped.

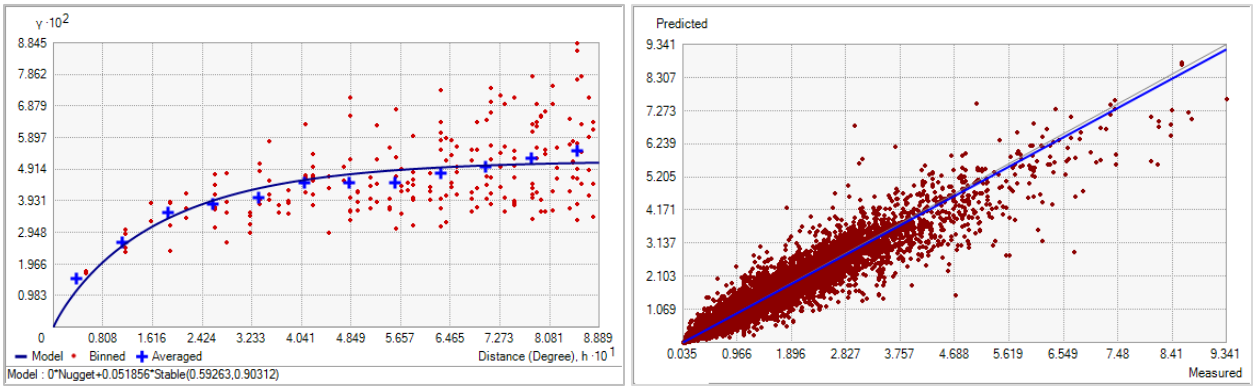

Fig. 328. Left panel: Semivariogram of Summer Chlorophyll *a* Range (mg m^{-3}). Binned values are shown as red dots; average points are shown as blue crosses; the model fit to the averaged values is shown as a blue line. Lag size: 0.074 degrees; number of lags: 12; Parameter: 0.903; Range: 0.593 degrees; Partial Sill: 0.052. Right panel: Scatterplot of predicted values versus observed values for the variable Summer Chlorophyll *a* Range (mg m^{-3}).

Table 132. Results of cross-validation of the kriged model for Summer Chlorophyll *a* Range (mg m^{-3}).

Prediction error	**Value**
Number of Observations	157201
Overall Mean Error	-1.108×10^{-4}
Root Mean Square Prediction Error	0.093
Standardized Mean	-6.054×10^{-4}
Standardized Root Mean Square Prediction Error	1.231
Average Standard Error	0.074

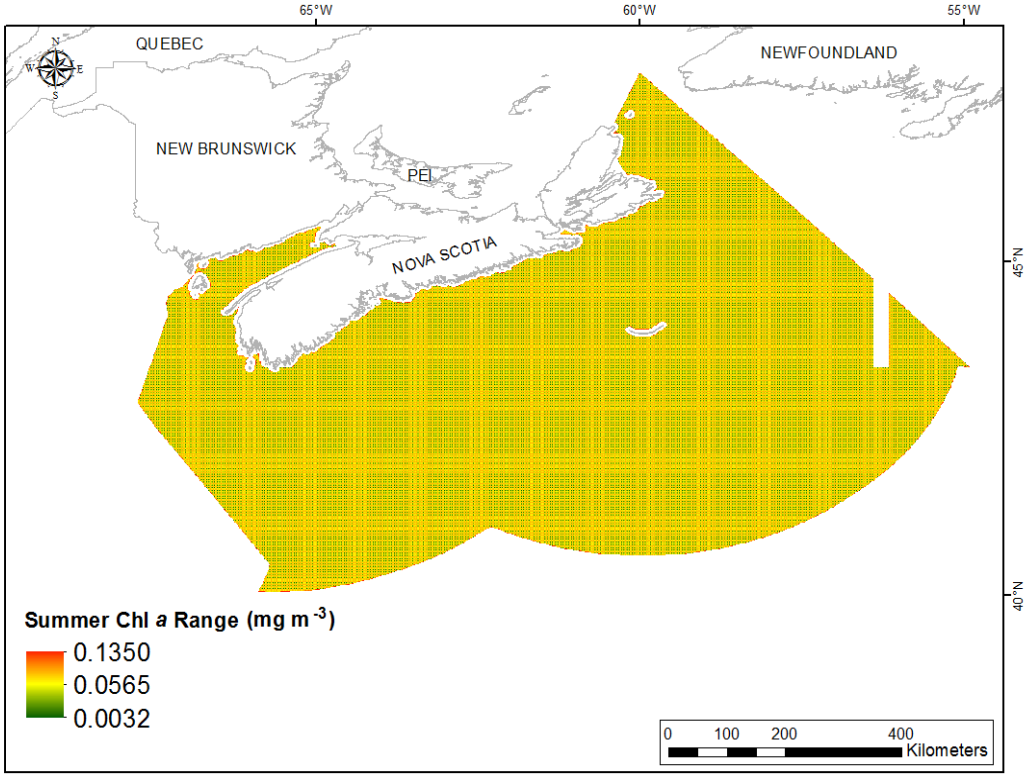

Fig. 329. Prediction standard error surface of Summer Chlorophyll *a* Range (mg m^{-3}).

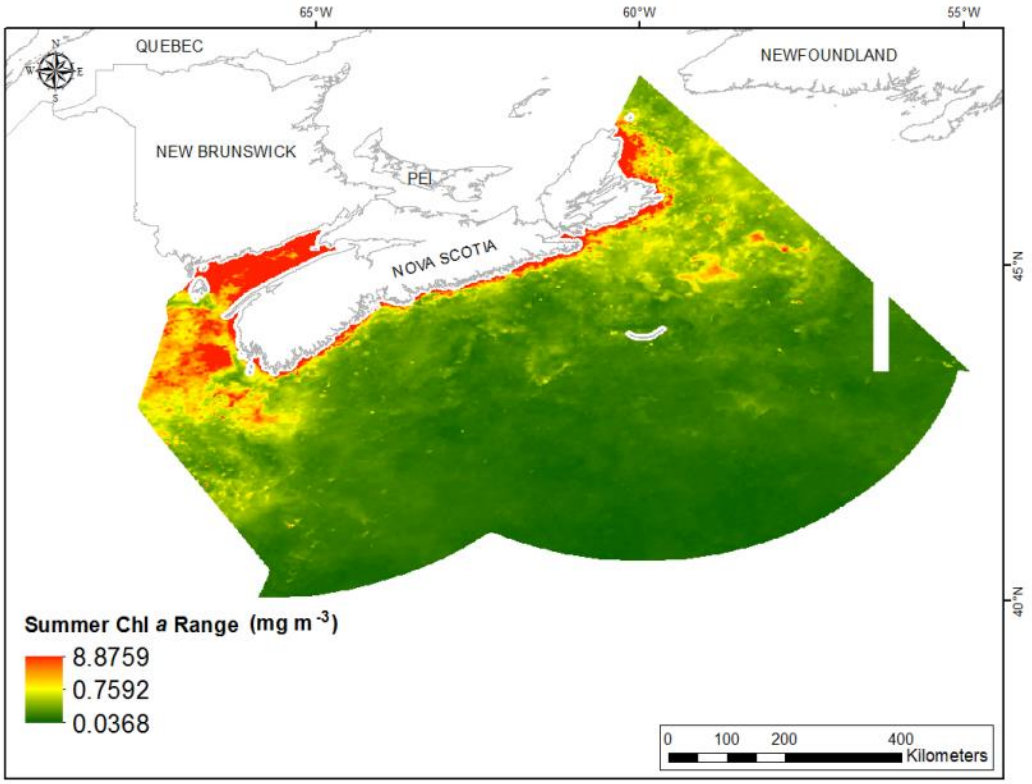

Fig. 330. Interpolated prediction surface of Summer Chlorophyll *a* Range (mg m^{-3}).

Fall Chlorophyll *a* Mean

This variable displayed a right-skewed, highly leptokurtic distribution prior to interpolation (Table 133, Fig. 331). The data were higher than predicted by a normal distribution at both tails and slightly lower than predicted at mid-values (Fig. 332). The areas of under- and over-prediction showed a very strong spatial pattern over the study extent (Fig. 332).

The semivariogram showed weak autocorrelation present in the data and the model showed good fit between measured and predicted values (Fig. 333). However, poor performance was indicated by the cross-validation statistics (Table 134), with a standardized root mean square greater than 1 indicating that variability in the predictions has been underestimated. The error map showed low error over the study extent (Fig. 334). The kriged surface is presented in Fig. 335.

Table 133. Distributional properties of Fall Chlorophyll *a* Mean (mg m^{-3}).

Property	Value
Number of Observations	157201
Minimum	0.240
Maximum	7.287
Mean	0.755
Median	0.646
Standard Deviation	0.497
Skewness	3.130
Kurtosis	20.684

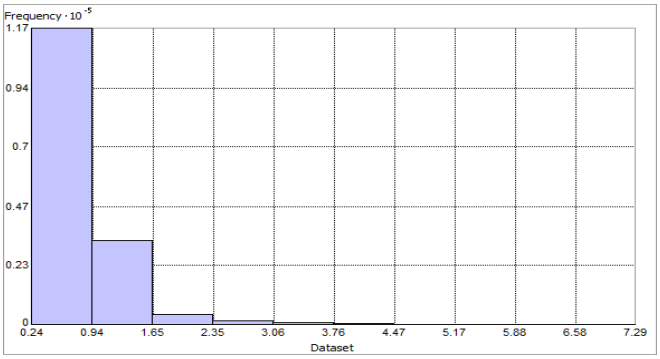

Fig. 331. Distribution of Fall Chlorophyll *a* Mean (mg m^{-3}). Histogram was illustrated using 10 bins. Y axis is shown at 10^{-5}.

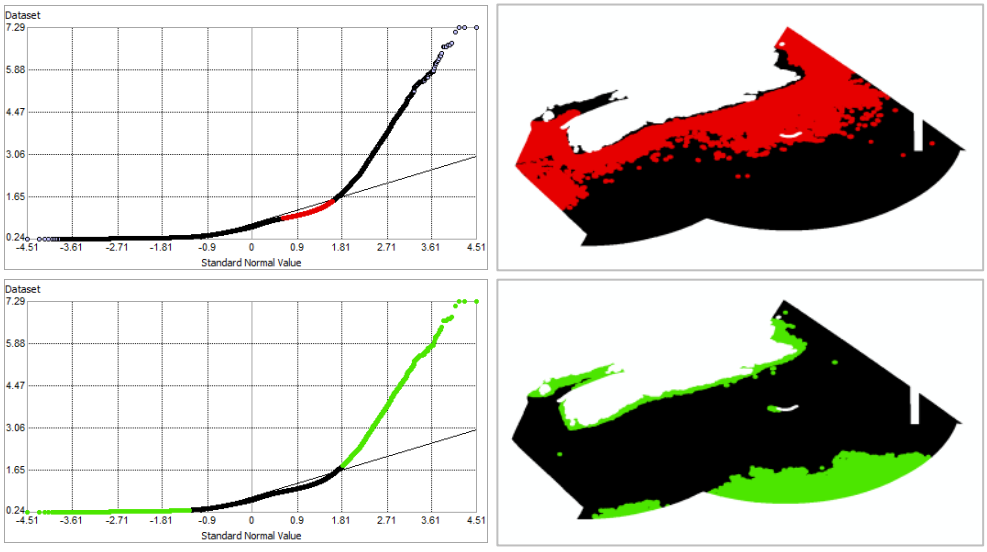

Fig. 332. Normal Q-Q plot for data values of Fall Chlorophyll *a* Mean (mg m^{-3}). Points falling under (upper panel) and over (bottom panel) the reference line are mapped.

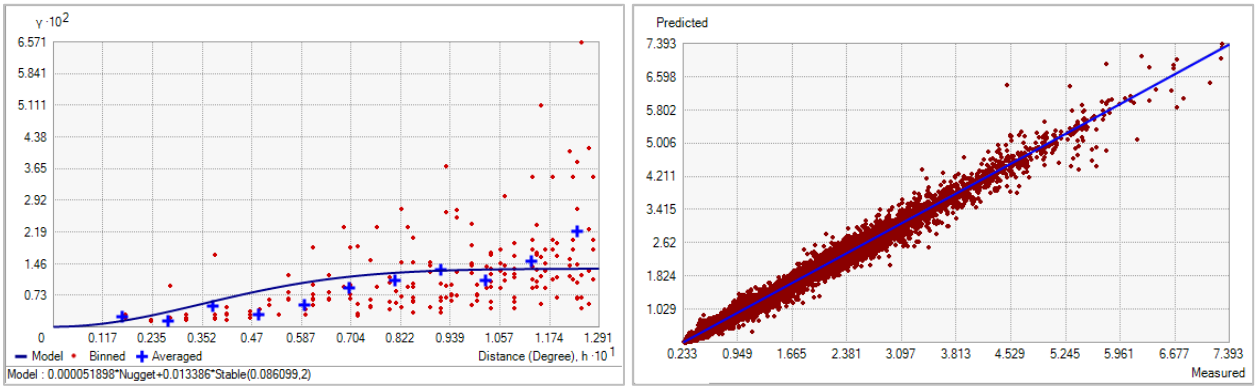

Fig. 333. Left panel: Semivariogram of Fall Chlorophyll *a* Mean (mg m^{-3}). Binned values are shown as red dots; average points are shown as blue crosses; the model fit to the averaged values is shown as a blue line. Lag size: 0.011 degrees; number of lags: 12; Parameter: 2; Range: 0.086 degrees; Partial Sill: 0.013. Right panel: Scatterplot of predicted values versus observed values for the variable Fall Chlorophyll *a* Mean (mg m^{-3}).

Table 134. Results of cross-validation of the kriged model for Fall Chlorophyll *a* Mean (mg m^{-3}).

Prediction error	**Value**
Number of Observations	157201
Overall Mean Error	-9.322×10^{-5}
Root Mean Square Prediction Error	0.043
Standardized Mean	-6.695×10^{-3}
Standardized Root Mean Square Prediction Error	4.048
Average Standard Error	0.010

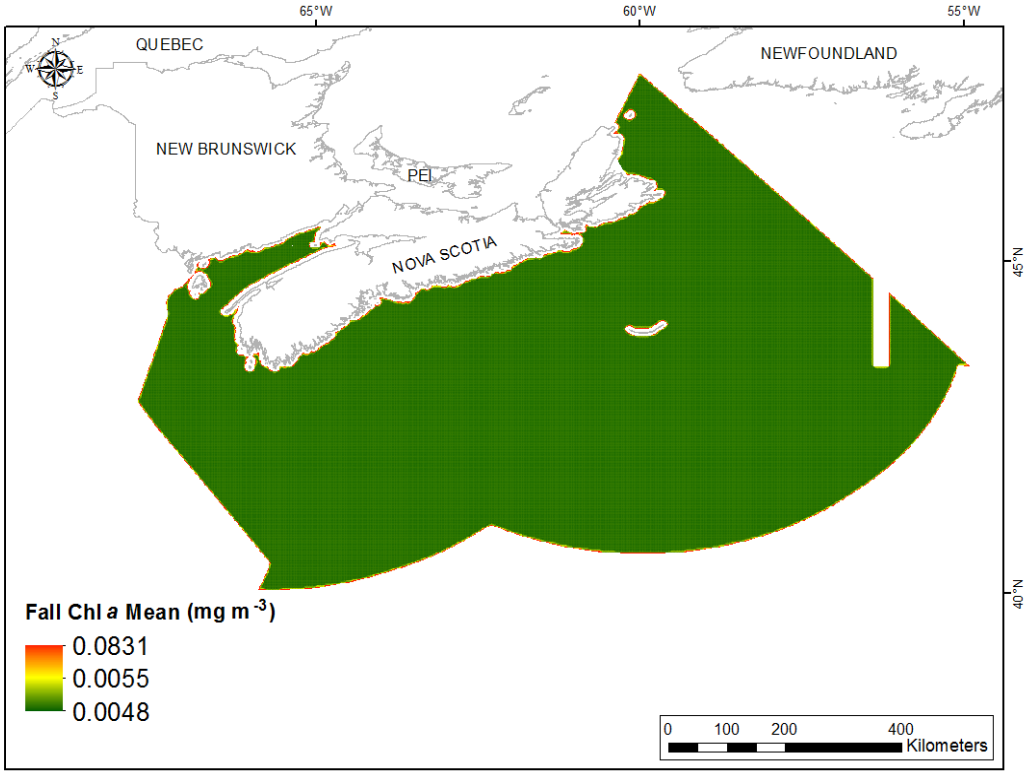

Fig. 334. Prediction standard error surface of Fall Chlorophyll *a* Mean (mg m^{-3}).

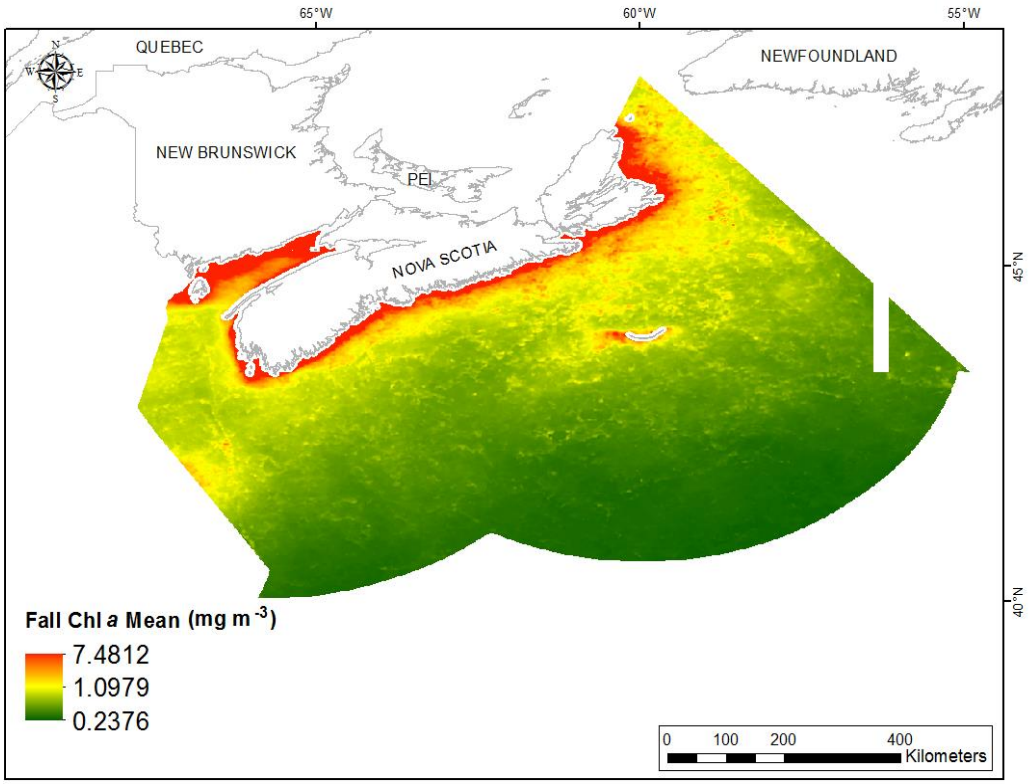

Fig. 335. Interpolated prediction surface of Fall Chlorophyll *a* Mean (mg m^{-3}).

Fall Chlorophyll *a* Minimum

This variable displayed a right-skewed, highly leptokurtic distribution prior to interpolation (Table 135, Fig. 336). The data were higher than predicted by a normal distribution at the upper range and slightly lower than predicted at mid-values (Fig. 337). The areas of under- and over-prediction showed a strong spatial pattern over the study extent (Fig. 337).

The semivariogram showed weak autocorrelation present in the data (Fig. 338). There was a very good fit between measured and predicted values (Fig. 338). Fair performance was indicated by the cross-validation results (Table 136), although the Standardized Root-Mean-Square Prediction Error was greater than 1 indicating that variability in the predictions has been underestimated. The error map showed low error over the study extent with high error in areas without data points (Fig. 339). The kriged surface is presented in Fig. 340.

Table 135. Distributional properties of Fall Chlorophyll *a* Minimum (mg m^{-3}).

Property	Value
Number of Observations	157169
Minimum	0.058
Maximum	5.361
Mean	0.487
Median	0.412
Standard Deviation	0.331
Skewness	3.928
Kurtosis	32.511

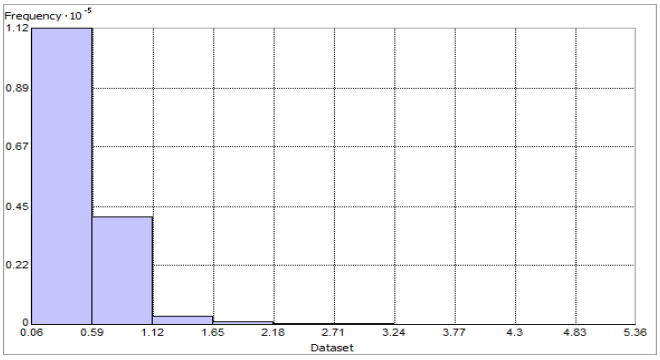

Fig. 336. Distribution of Fall Chlorophyll *a* Minimum (mg m^{-3}). Histogram was illustrated using 10 bins Y axis is shown at 10^{-5}.

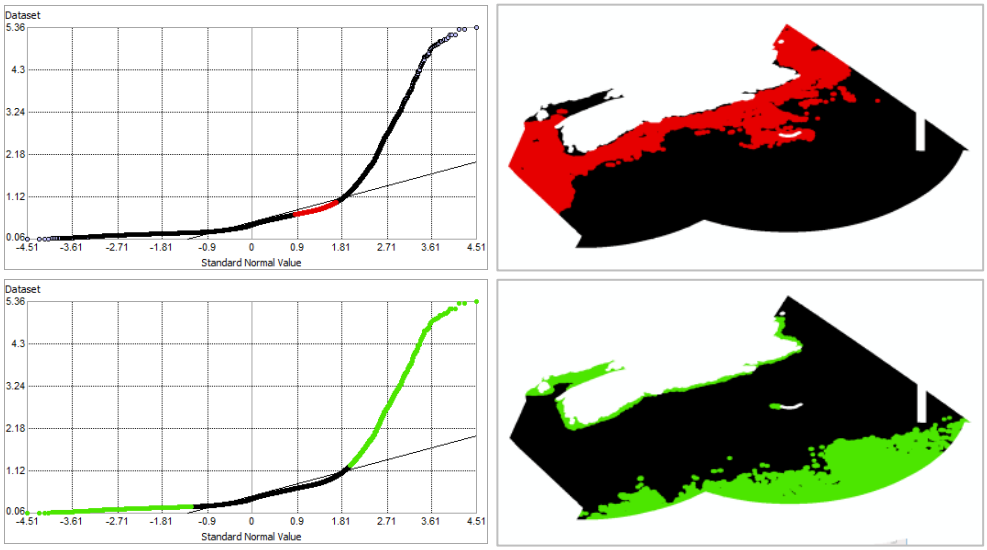

Fig. 337. Normal Q-Q plot for data values of Fall Chlorophyll *a* Minimum (mg m^{-3}). Points falling under (upper panel) and over (bottom panel) the reference line are mapped.

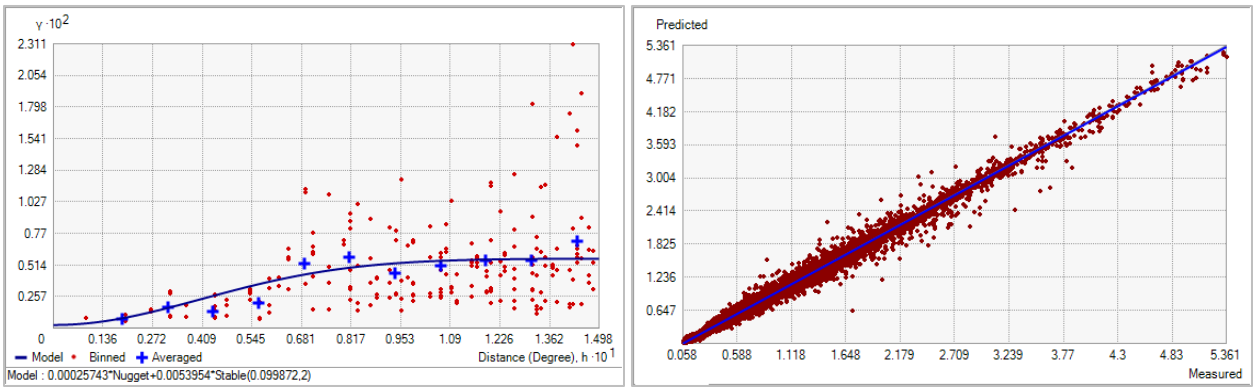

Fig. 338. Left panel: Semivariogram of Fall Chlorophyll *a* Minimum (mg m^{-3}). Binned values are shown as red dots; average points are shown as blue crosses; the model fit to the averaged values is shown as a blue line. Lag size: 0.012 degrees; number of lags: 12; Parameter: 1.657; Range: 0.100 degrees; Partial Sill: 5.395 x 10^{-3}. Right panel: Scatterplot of predicted values versus observed values for the variable Fall Chlorophyll *a* Minimum (mg m^{-3}).

Table 136. Results of cross-validation of the kriged model for Fall Chlorophyll *a* Minimum (mg m^{-3}).

Prediction error	**Value**
Number of Observations	157169
Overall Mean Error	-2.678 x 10^{-5}
Root Mean Square Prediction Error	0.028
Standardized Mean	-2.998 x 10^{-4}
Standardized Root Mean Square Prediction Error	1.474
Average Standard Error	0.019

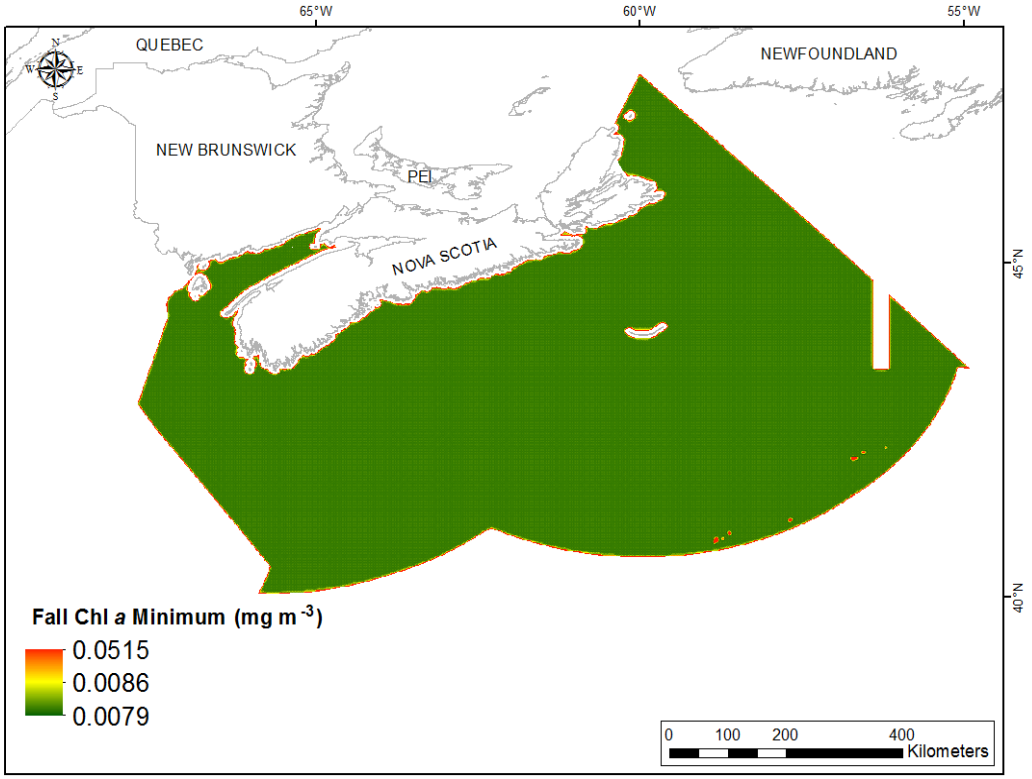

Fig. 339. Prediction standard error surface of Fall Chlorophyll *a* Minimum (mg m^{-3}).

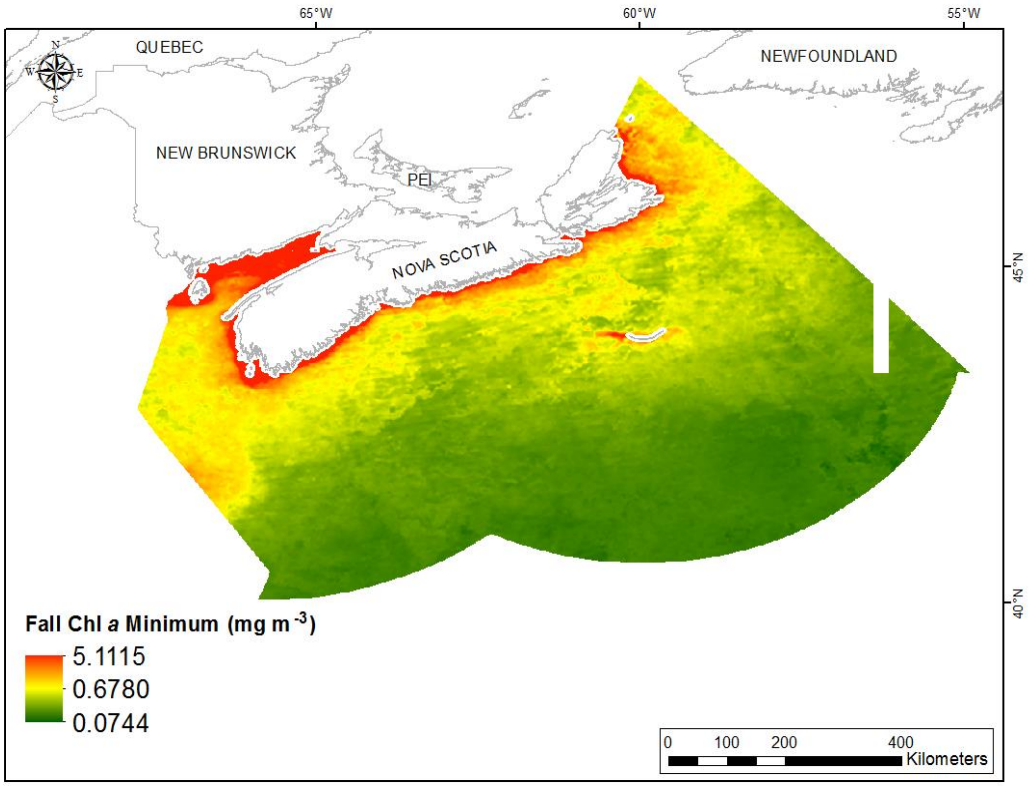

Fig. 340. Interpolated prediction surface of Fall Chlorophyll *a* Minimum (mg m^{-3}).

Fall Chlorophyll *a* Maximum

This variable displayed a right-skewed, highly leptokurtic distribution prior to interpolation (Table 137, Fig. 341). The data were higher than predicted by a normal distribution at both tails and slightly lower than predicted at mid-values (Fig. 342). The areas of under- and over-prediction showed some spatial pattern over the study extent (Fig. 342).

The semivariogram showed moderate autocorrelation present in the data and the model showed fair fit between measured and predicted values (Fig. 343). Good performance of the model was indicated by the good cross-validation results (Table 138). The error map showed medium to high error in a grid-like pattern over the study extent (Fig. 344). The kriged surface is presented in Fig. 345.

Table 137. Distributional properties of Fall Chlorophyll *a* Maximum (mg m^{-3}).

Property	Value
Number of Observations	157201
Minimum	0.280
Maximum	17.178
Mean	1.298
Median	1.054
Standard Deviation	1.009
Skewness	2.968
Kurtosis	18.946

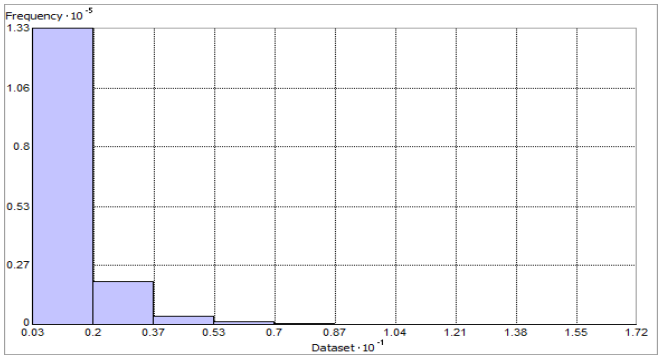

Fig. 341. Distribution of Fall Chlorophyll *a* Maximum (mg m^{-3}). Histogram was illustrated using 10 bins. X and Y axes are shown at 10^{-1} and 10^{-5} respectively.

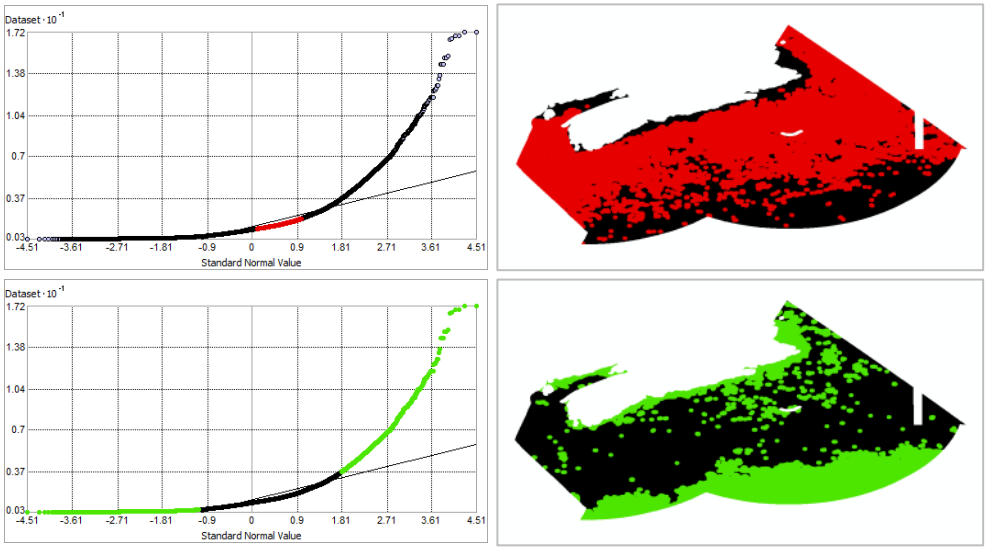

Fig. 342. Normal Q-Q plot for data values of Fall Chlorophyll *a* Maximum (mg m^{-3}). Points falling under (upper panel) and over (bottom panel) the reference line are mapped.

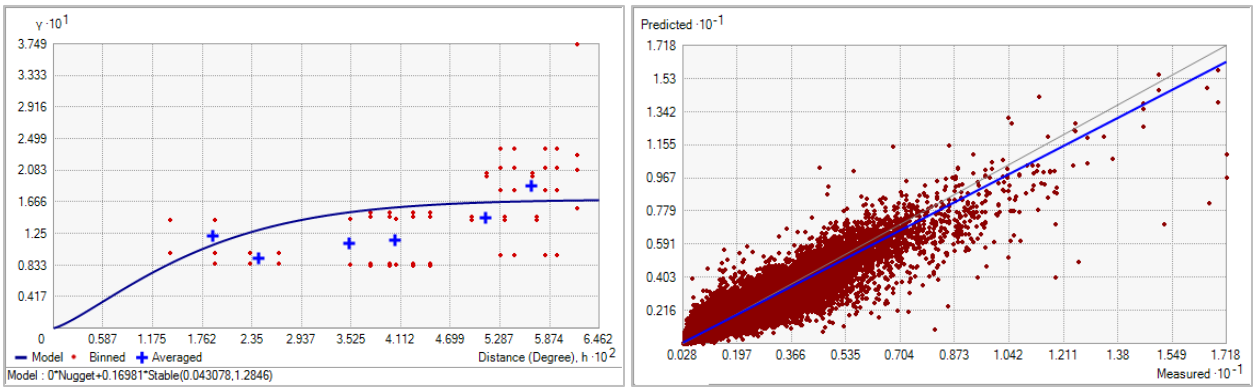

Fig. 343. Left panel: Semivariogram of Fall Chlorophyll *a* Maximum (mg m^{-3}). Binned values are shown as red dots; average points are shown as blue crosses; the model fit to the averaged values is shown as a blue line. Lag size: 5.385 x 10^{-3} degrees; number of lags: 12; Parameter: 1.285; Range: 0.043 degrees; Partial Sill: 0.170. Right panel: Scatterplot of predicted values versus observed values for the variable Fall Chlorophyll *a* Maximum (mg m^{-3}).

Table 138. Results of cross-validation of the kriged model for Fall Chlorophyll *a* Maximum (mg m^{-3}).

Prediction error	**Value**
Number of Observations	157201
Overall Mean Error	-3.664 x 10^{-4}
Root Mean Square Prediction Error	0.292
Standardized Mean	-8.759 x 10^{-4}
Standardized Root Mean Square Prediction Error	0.892
Average Standard Error	0.326

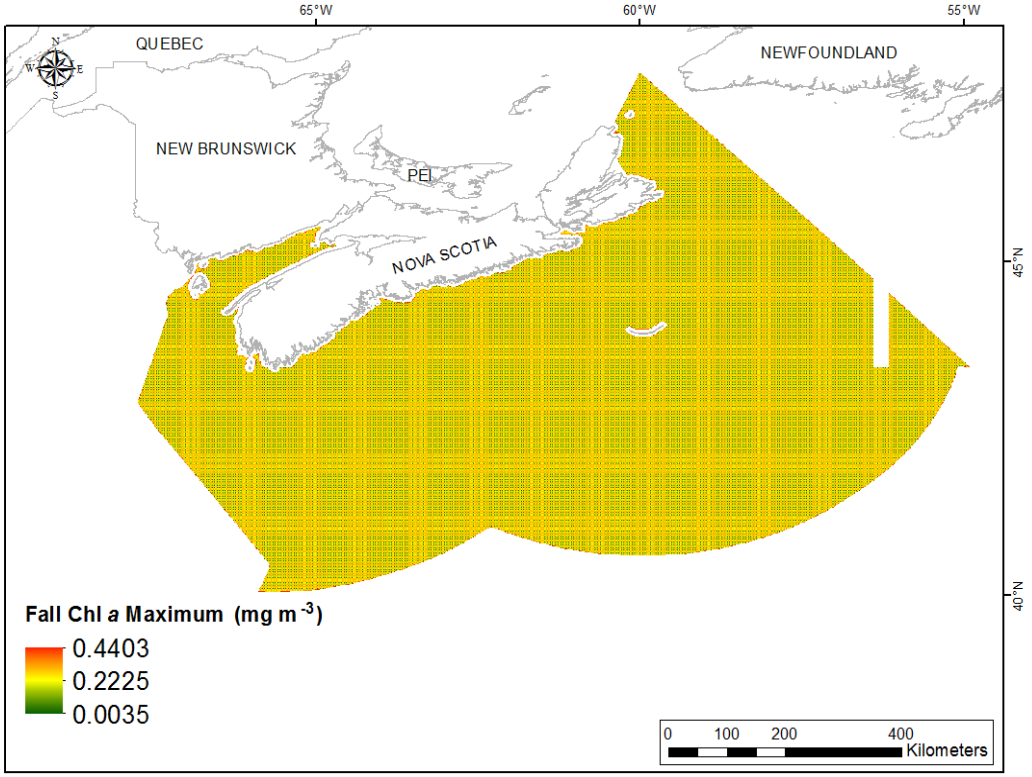

Fig. 344. Prediction standard error surface of Fall Chlorophyll *a* Maximum (mg m^{-3}).

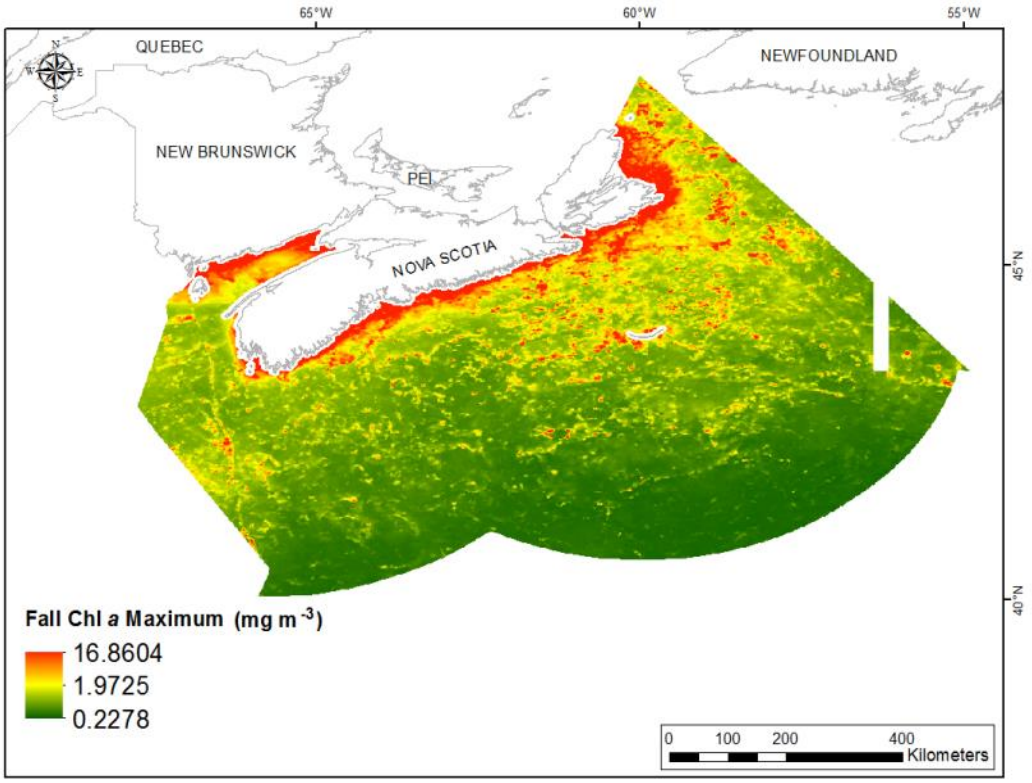

Fig. 345. Interpolated prediction surface of Fall Chlorophyll *a* Maximum (mg m^{-3}).

Fall Chlorophyll *a* Range

This variable displayed a right-skewed, highly leptokurtic distribution prior to interpolation (Table 139, Fig. 346). The data were higher than predicted by a normal distribution at both tails and slightly lower than predicted at mid-values (Fig. 347). The areas of under- and over-prediction showed some spatial pattern over the study extent (Fig. 347).

The semivariogram showed autocorrelation present in the data and the model showed fair fit between measured and predicted values (Fig. 348). Good performance of the model was indicated by the good cross-validation results (Table 140). The error map showed medium to high error in a grid-like pattern over the study extent (Fig. 349). The kriged surface is presented in Fig. 350.

Table 139. Distributional properties of Fall Chlorophyll *a* Range (mg m^{-3}).

Property	Value
Number of Observations	157201
Minimum	0.060
Maximum	15.782
Mean	0.811
Median	0.566
Standard Deviation	0.800
Skewness	3.508
Kurtosis	25.154

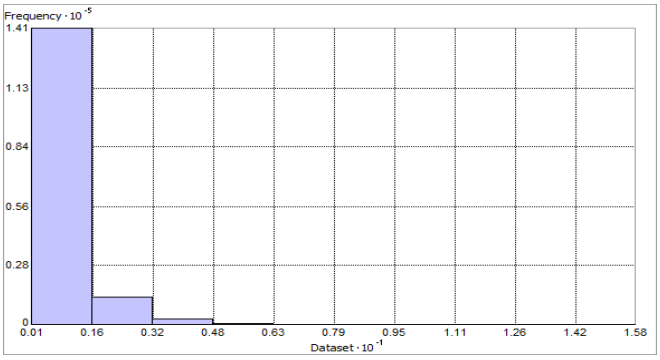

Fig. 346. Distribution of Fall Chlorophyll *a* Range (mg m^{-3}). Histogram was illustrated using 10 bins. X and Y axes are shown at 10^{-1} and 10^{-5} respectively.

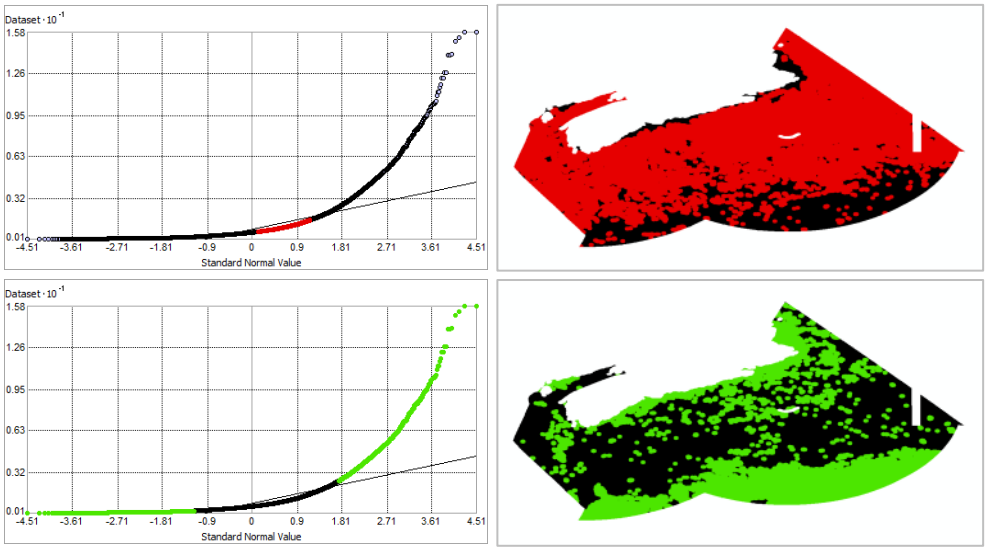

Fig. 347. Normal Q-Q plot for data values of Fall Chlorophyll *a* Range (mg m^{-3}). Points falling under (upper panel) and over (bottom panel) the reference line are mapped.

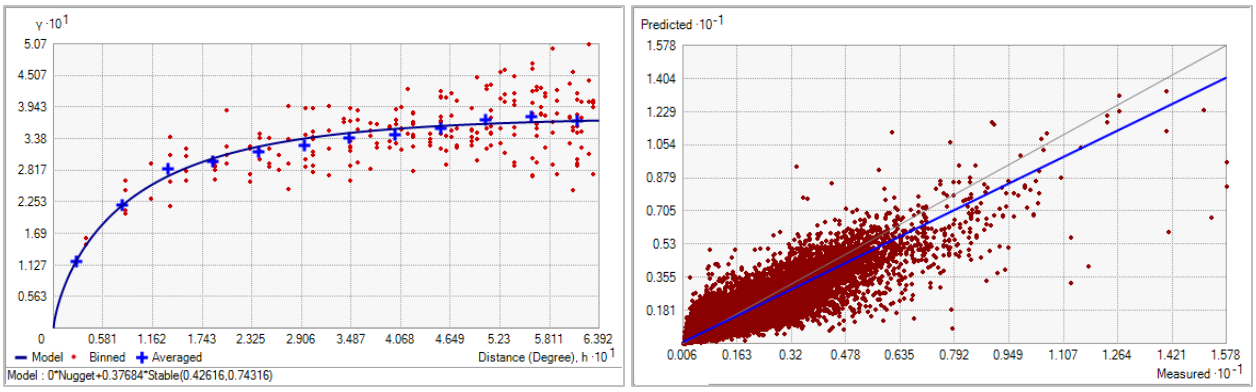

Fig. 348. Left panel: Semivariogram of Fall Chlorophyll *a* Range (mg m^{-3}). Binned values are shown as red dots; average points are shown as blue crosses; the model fit to the averaged values is shown as a blue line. Lag size: 0.053 degrees; number of lags: 12; Parameter: 0.743; Range: 0.426 degrees; Partial Sill: 0.377. Right panel: Scatterplot of predicted values versus observed values for the variable Fall Chlorophyll *a* Range (mg m^{-3}).

Table 140. Results of cross-validation of the kriged model for Fall Chlorophyll *a* Range.

Prediction error	**Value**
Number of Observations	157201
Overall Mean Error	5.399×10^{-5}
Root Mean Square Prediction Error	0.294
Standardized Mean	2.522×10^{-4}
Standardized Root Mean Square Prediction Error	0.966
Average Standard Error	0.303

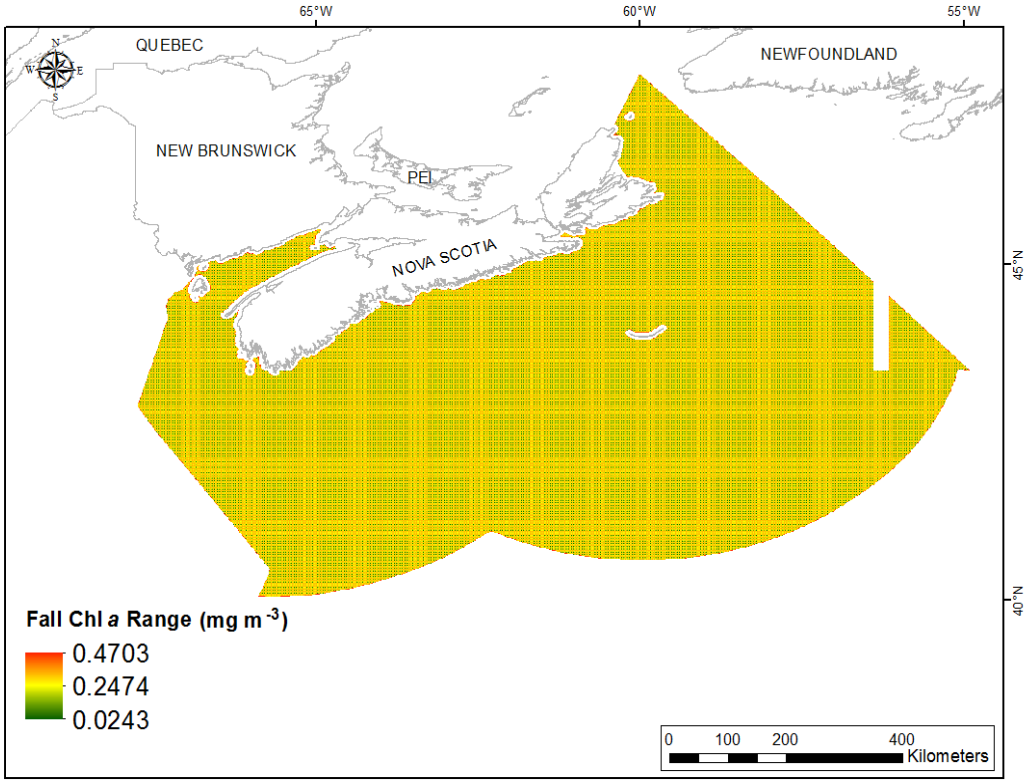

Fig. 349. Prediction standard error surface of Fall Chlorophyll *a* Range (mg m^{-3}).

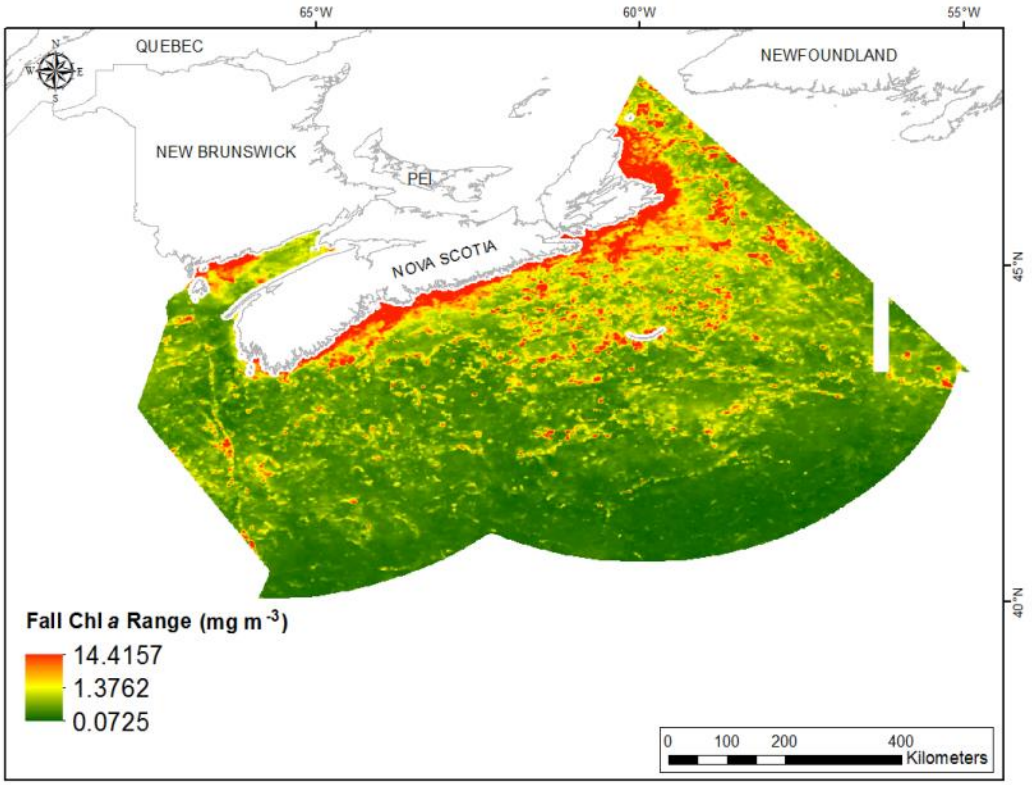

Fig. 350. Interpolated prediction surface of Fall Chlorophyll *a* Range (mg m^{-3}).

Annual Chlorophyll *a* Mean

This variable displayed a right-skewed, highly leptokurtic distribution prior to interpolation (Table 141, Fig. 351). The data were higher than predicted by a normal distribution at both tails and lower than predicted at mid-values (Fig. 352). The areas of under- and over-prediction showed a very strong spatial pattern over the study extent (Fig. 352).

The semivariogram showed weak autocorrelation present in the data and the model showed a very good fit between measured and predicted values (Fig. 353). Nevertheless, poor performance of the model was indicated by the cross-validation results (Table 142). The error map showed low error over the study extent (Fig. 354). The kriged surface is presented in Fig. 355.

Table 141. Distributional properties of Annual Chlorophyll *a* Mean (mg m^{-3}).

Property	Value
Number of Observations	157201
Minimum	0.262
Maximum	7.711
Mean	0.799
Median	0.686
Standard Deviation	0.491
Skewness	3.614
Kurtosis	26.529

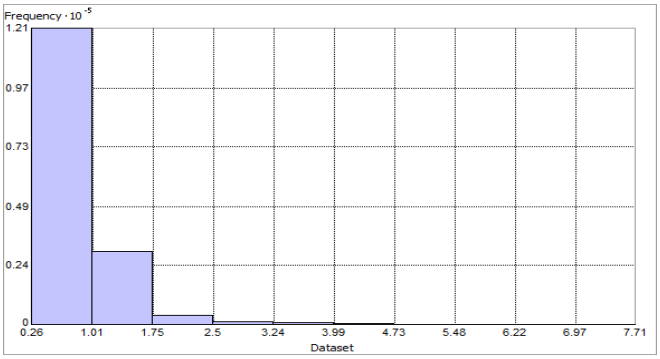

Fig. 351. Distribution of Annual Chlorophyll *a* Mean (mg m^{-3}). Histogram was illustrated using 10 bins. Y axis is shown at 10^{-5}.

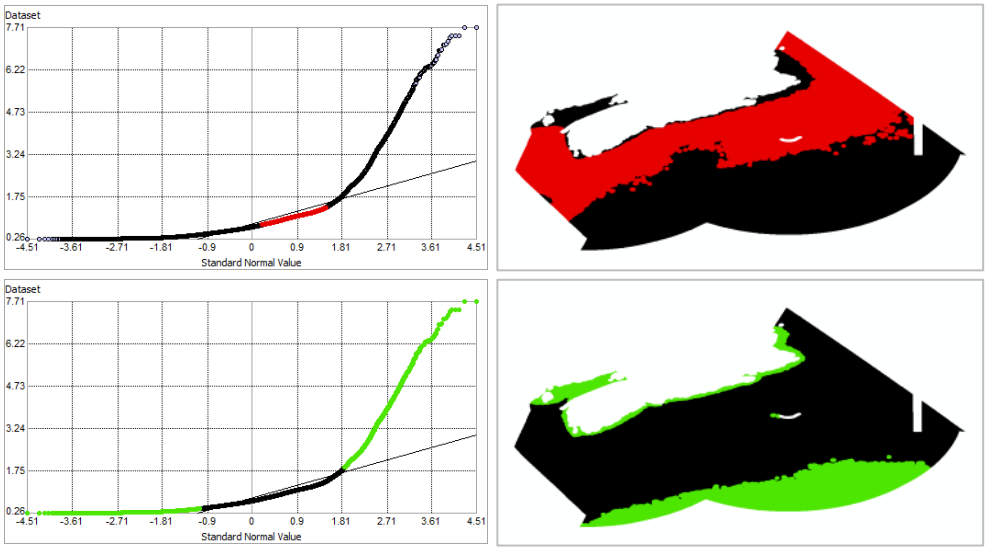

Fig. 352. Normal Q-Q plot for data values of Annual Chlorophyll *a* Mean (mg m^{-3}). Points falling under (upper panel) and over (bottom panel) the reference line are mapped.

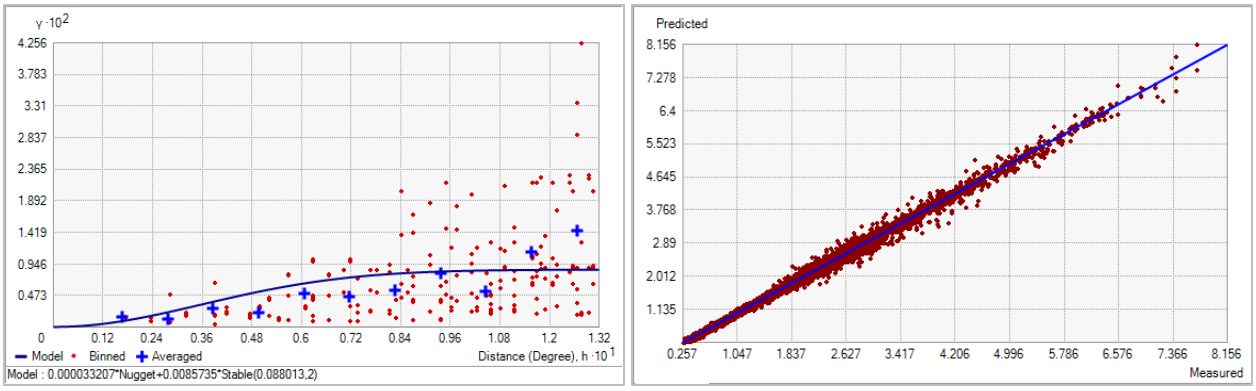

Fig. 353. Left panel: Semivariogram of Annual Chlorophyll *a* Mean (mg m^{-3}). Binned values are shown as red dots; average points are shown as blue crosses; the model fit to the averaged values is shown as a blue line. Lag size: 0.011 degrees; number of lags: 12; Parameter: 2; Range: 0.088 degrees; Partial Sill: 8.573 x 10^{-3}. Right panel: Scatterplot of predicted values versus observed values for the variable Annual Chlorophyll *a* Mean (mg m^{-3}).

Table 142. Results of cross-validation of the kriged model for Annual Chlorophyll *a* Mean (mg m^{-3}).

Prediction error	**Value**
Number of Observations	157201
Overall Mean Error	-1.091 x 10^{-4}
Root Mean Square Prediction Error	0.023
Standardized Mean	-9.262 x 10^{-3}
Standardized Root Mean Square Prediction Error	2.612
Average Standard Error	8.001 x 10^{-3}

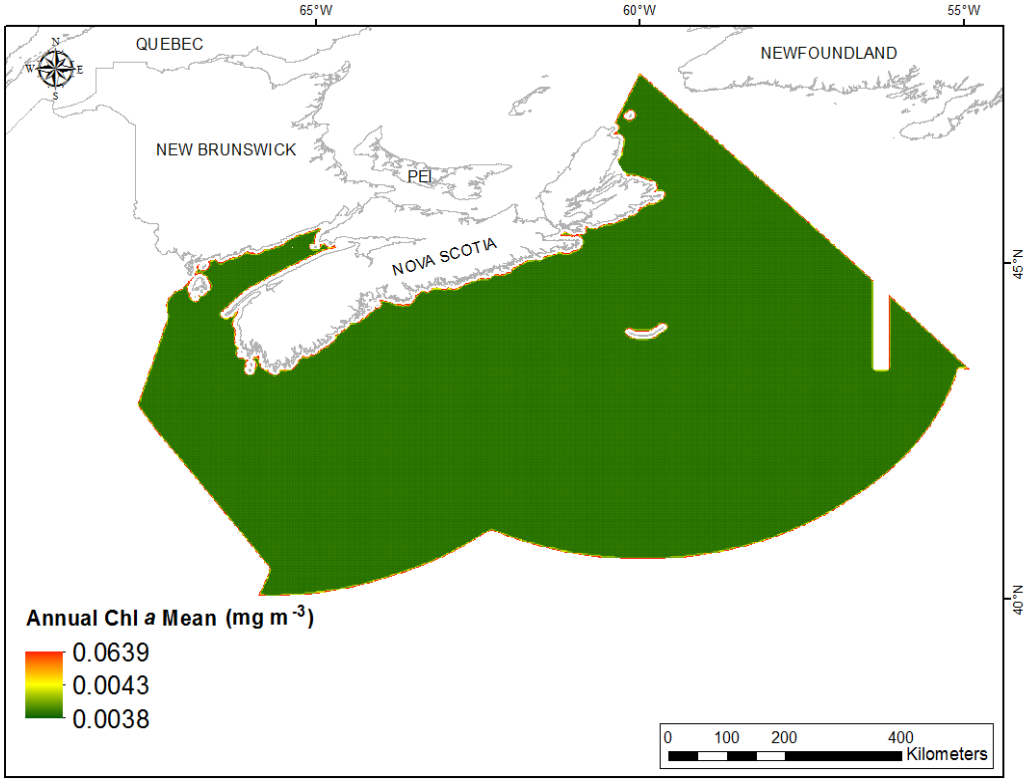

Fig. 354. Prediction standard error surface of Annual Chlorophyll *a* Mean (mg m^{-3}).

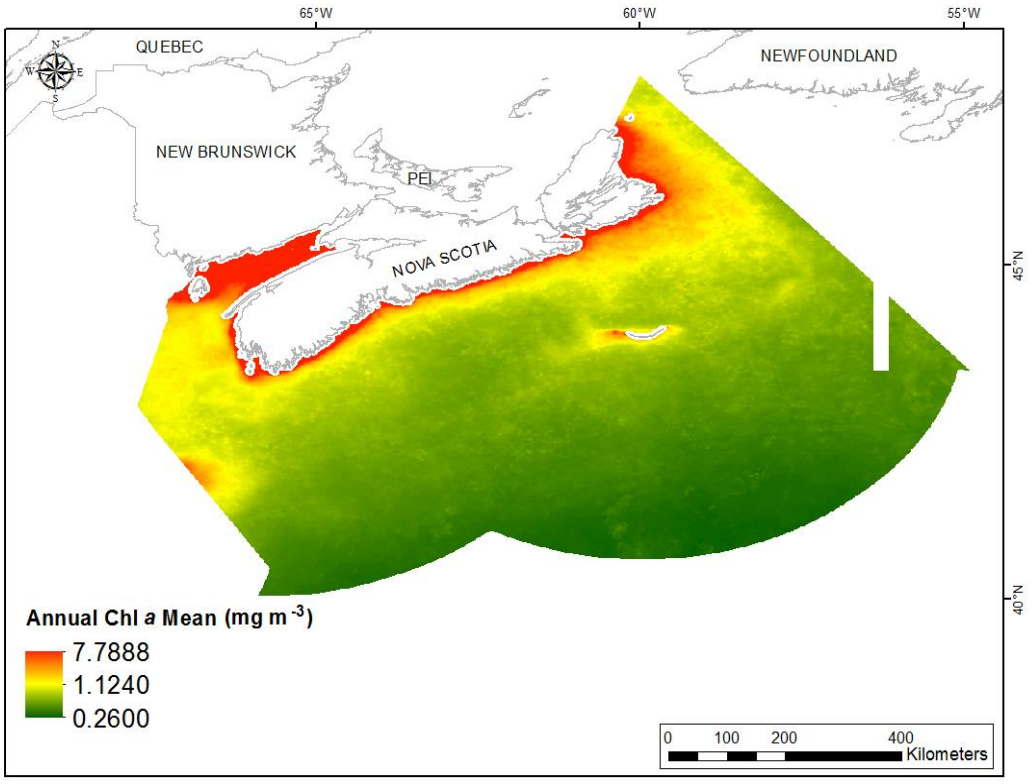

Fig. 355. Interpolated prediction surface of Annual Chlorophyll *a* Mean (mg m^{-3}).

Annual Chlorophyll *a* Minimum

This variable displayed a right-skewed, highly leptokurtic prior to interpolation (Table 143, Fig. 356). The data were higher than predicted by a normal distribution at both tails and lower than predicted at mid-values (Fig. 357). The areas of under- and over-prediction showed a very strong spatial pattern over the study extent (Fig. 357).

The semivariogram showed weak autocorrelation present in the data and the model showed a very good fit between measured and predicted values (Fig. 358). However, poor model performance was indicated by the cross-validation results (Table 144). The Standardized Root-Mean-Square Prediction Error was greater than 1 indicating that variability in the predictions has been underestimated. The error map showed low error over the study extent (Fig. 359). The kriged surface is presented in Fig. 360.

Table 143. Distributional properties of Annual Chlorophyll *a* Minimum (mg m^{-3}).

Property	Value
Number of Observations	157201
Minimum	0.110
Maximum	6.642
Mean	0.532
Median	0.423
Standard Deviation	0.415
Skewness	3.550
Kurtosis	27.101

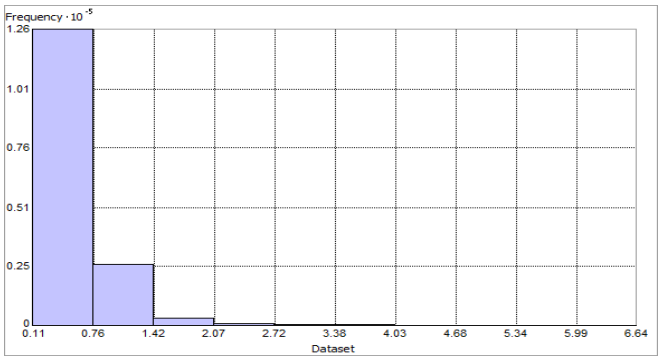

Fig. 356. Distribution of Annual Chlorophyll *a* Minimum (mg m^{-3}). Histogram was illustrated using 10 bins. Y axis is shown at 10^{-5}.

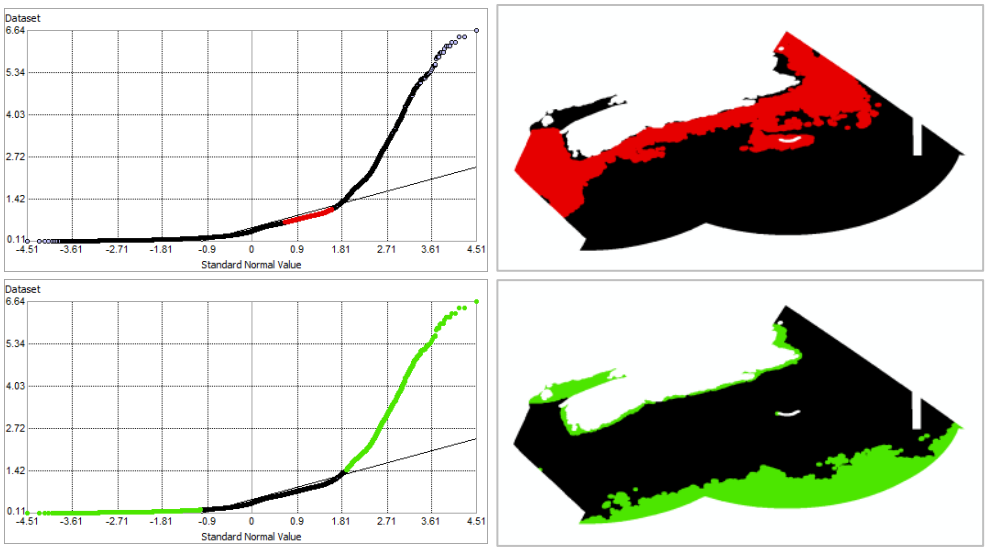

Fig. 357. Normal Q-Q plot for data values of Annual Chlorophyll *a* Minimum (mg m^{-3}). Points falling under (upper panel) and over (bottom panel) the reference line are mapped.

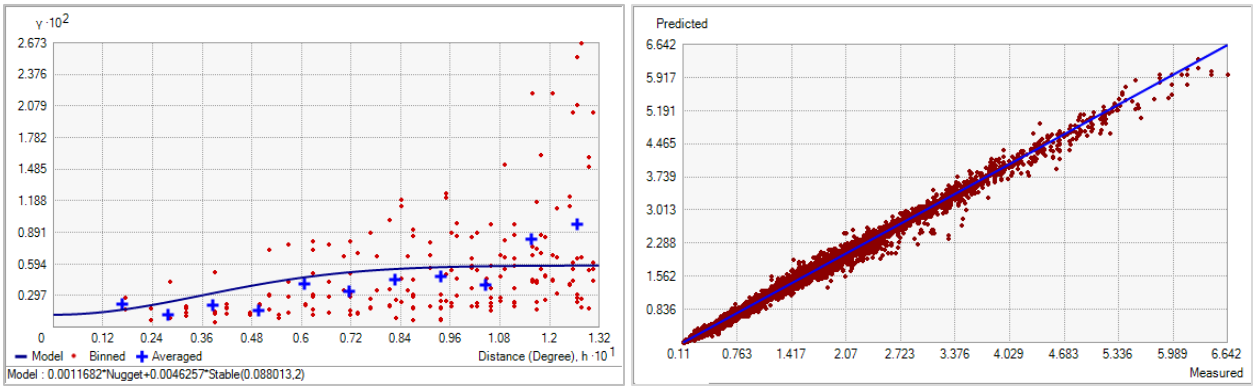

Fig. 358. Left panel: Semivariogram of Annual Chlorophyll *a* Minimum (mg m^{-3}). Binned values are shown as red dots; average points are shown as blue crosses; the model fit to the averaged values is shown as a blue line. Lag size: 0.011 degrees; number of lags: 12; Parameter: 2; Range: 0.088 degrees; Partial Sill: 4.626 x 10^{-3}. Right panel: Scatterplot of predicted values versus observed values for the variable Annual Chlorophyll *a* Minimum (mg m^{-3}).

Table 144. Results of cross-validation of the kriged model for Annual Chlorophyll *a* Minimum (mg m^{-3}).

Prediction error	**Value**
Number of Observations	157201
Overall Mean Error	-5.680 x 10^{-5}
Root Mean Square Prediction Error	0.023
Standardized Mean	-4.044 x 10^{-4}
Standardized Root Mean Square Prediction Error	5.831
Average Standard Error	0.039

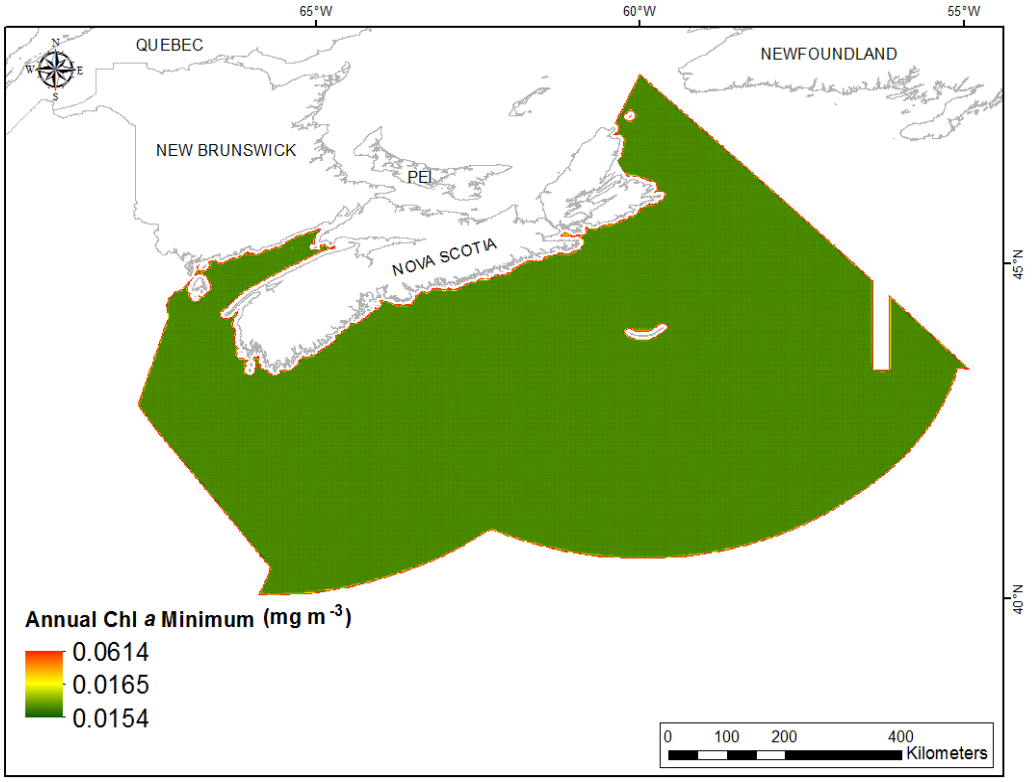

Fig. 359. Prediction standard error surface of Annual Chlorophyll *a* Minimum (mg m^{-3}).

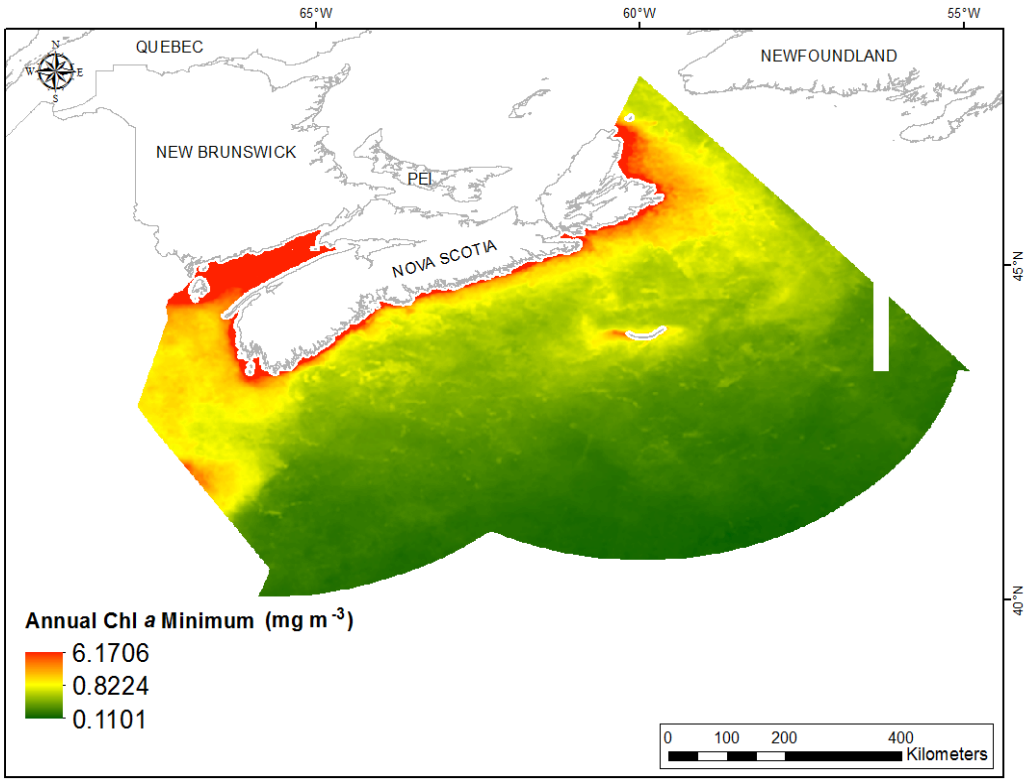

Fig. 360. Interpolated prediction surface of Annual Chlorophyll *a* Minimum (mg m^{-3}).

Annual Chlorophyll *a* Maximum

This variable displayed a right-skewed, highly leptokurtic distribution prior to interpolation (Table 145, Fig. 361). The data were higher than predicted by a normal distribution at both tails and slightly lower than predicted at mid-values (Fig. 362). The areas of under- and over-prediction showed some spatial pattern over the study extent (Fig. 362).

The semivariogram showed moderate autocorrelation present in the data and the model showed good fit between measured and predicted values (Fig. 363). However, poor model performance was indicated by the cross-validation results (Table 146). The Standardized Root-Mean-Square Prediction Error was greater than 1 indicating that variability in the predictions has been underestimated. The error map showed low error over the study extent (Fig. 364). The kriged surface is presented in Fig. 365.

Table 145. Distributional properties of Annual Chlorophyll *a* Maximum (mg m^{-3}).

Property	Value
Number of Observations	157201
Minimum	0.317
Maximum	10.412
Mean	1.127
Median	0.988
Standard Deviation	0.641
Skewness	2.963
Kurtosis	19.666

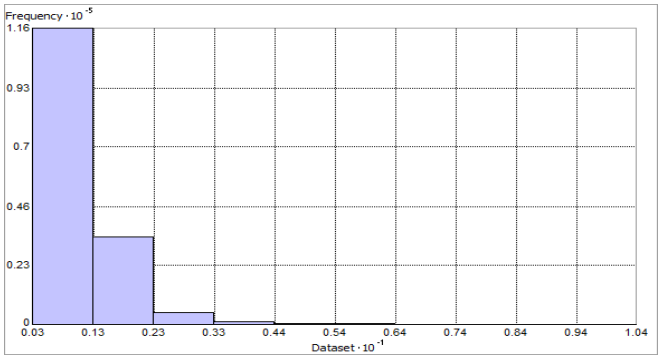

Fig. 361. Distribution of Annual Chlorophyll *a* Maximum (mg m^{-3}). Histogram was illustrated using 10 bins. X and Y axes are shown at 10^{-1} and 10^{-5} respectively.

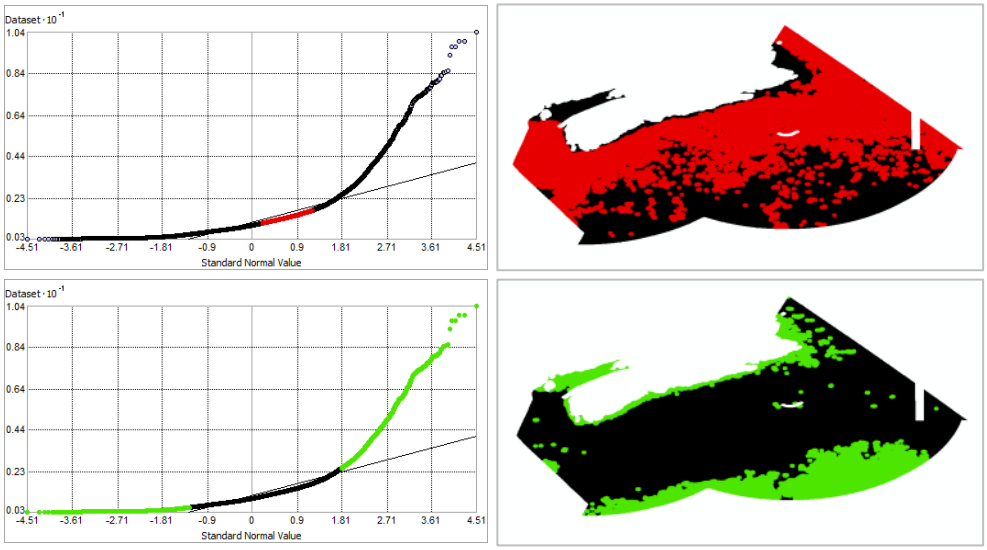

Fig. 362. Normal Q-Q plot for data values of Annual Chlorophyll *a* Maximum (mg m^{-3}). Points falling under (upper panel) and over (bottom panel) the reference line are mapped.

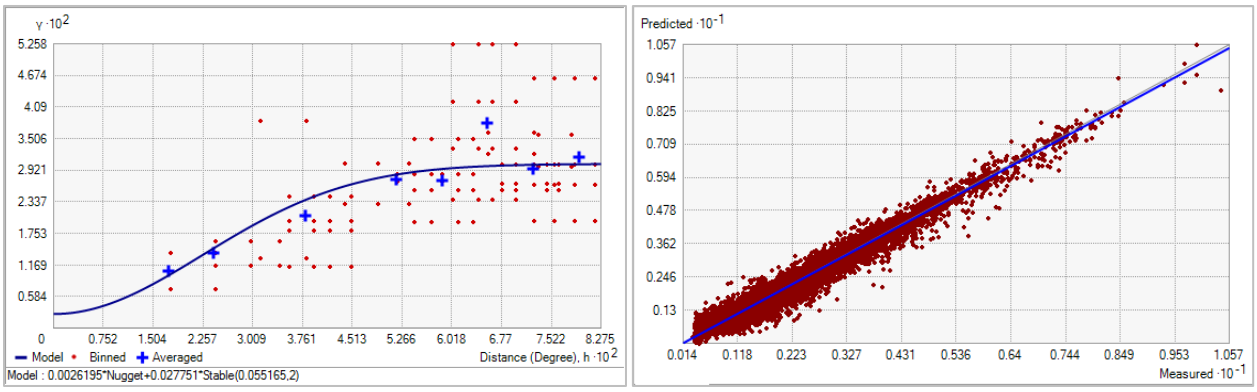

Fig. 363. Left panel: Semivariogram of Annual Chlorophyll *a* Maximum (mg m^{-3}). Binned values are shown as red dots; average points are shown as blue crosses; the model fit to the averaged values is shown as a blue line. Lag size: 6.900 x 10^{-3} degrees; number of lags: 12; Parameter: 2; Range: 0.055 degrees; Partial Sill: 0.028. Right panel: Scatterplot of predicted values versus observed values for the variable Annual Chlorophyll *a* Maximum (mg m^{-3}).

Table 146. Results of cross-validation of the kriged model for Annual Chlorophyll *a* Maximum (mg m^{-3}).

Prediction error	**Value**
Number of Observations	157201
Overall Mean Error	-1.961 x 10^{-4}
Root Mean Square Prediction Error	0.099
Standardized Mean	-1.500 x 10^{-3}
Standardized Root Mean Square Prediction Error	1.357
Average Standard Error	0.072

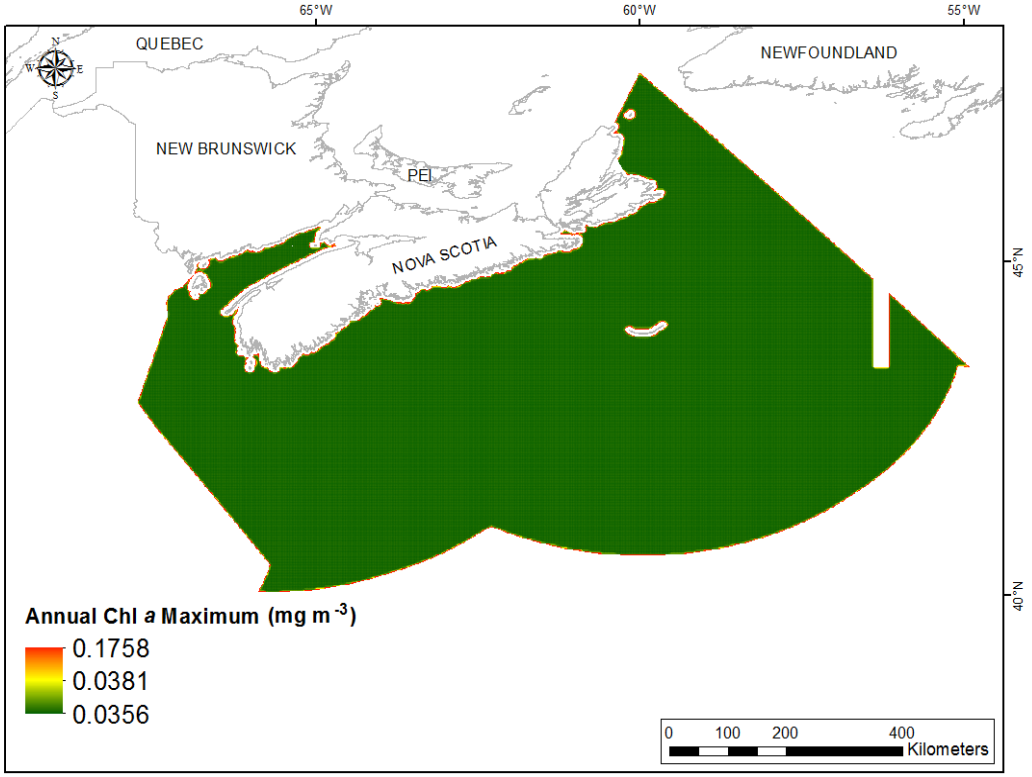

Fig. 364. Prediction standard error surface of Annual Chlorophyll *a* Maximum (mg m^{-3}).

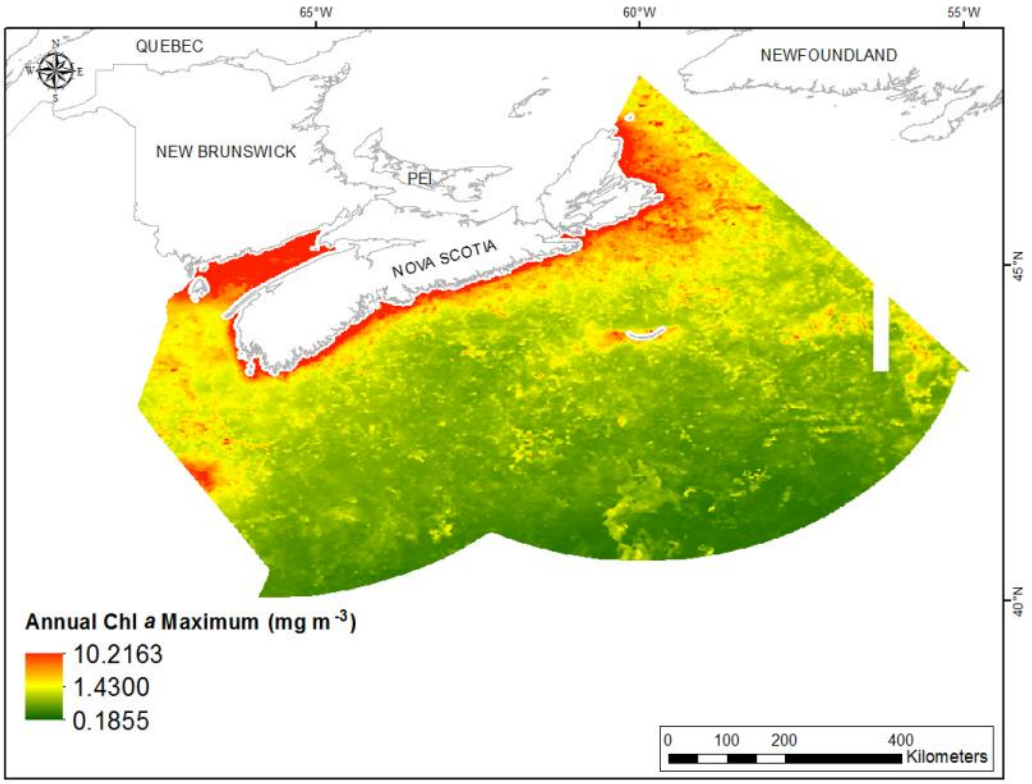

Fig. 365. Interpolated prediction surface of Annual Chlorophyll *a* Maximum (mg m^{-3}).

Annual Chlorophyll *a* Range

This variable displayed a right-skewed, highly leptokurtic distribution prior to interpolation (Table 147, Fig. 366). The data were higher than predicted by a normal distribution at both tails and slightly lower than predicted at mid-values (Fig. 367). The areas of under- and over-prediction showed no spatial pattern over the study extent (Fig. 367).

The semivariogram showed moderate autocorrelation present in the data and the model showed good fit between measured and predicted values (Fig. 368). However, poor model performance was indicated by the cross-validation results (Table 148). The Standardized Root-Mean-Square Prediction Error was greater than 1 indicating that variability in the predictions has been underestimated. The error map showed low error over the study extent (Fig. 369). The kriged surface is presented in Fig. 370. Negative values resulted from the right-skewed nature of the raw data (Fig. 366). Of the 326,283 raster cells in the study extent, only 1 was negative (see Table A1). This was located near the southern edge of the study extent above the abyssal plain (Fig. A6).

Table 147. Distributional properties of Annual Chlorophyll *a* Range (mg m^{-3}).

Property	Value
Number of Observations	157201
Minimum	0.128
Maximum	4.877
Mean	0.595
Median	0.516
Standard Deviation	0.305
Skewness	2.237
Kurtosis	11.932

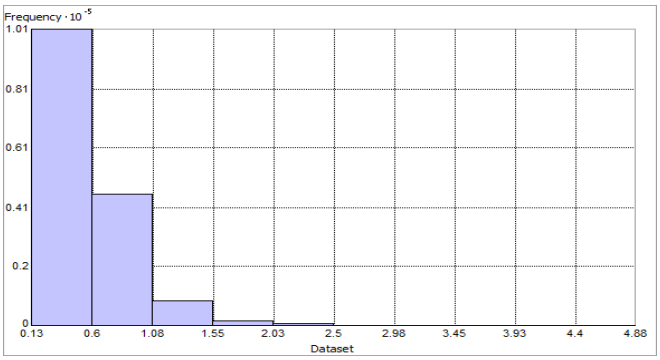

Fig. 366. Distribution of Annual Chlorophyll *a* Range (mg m^{-3}). Histogram was illustrated using 10 bins. Y axis is shown at 10^{-5}.

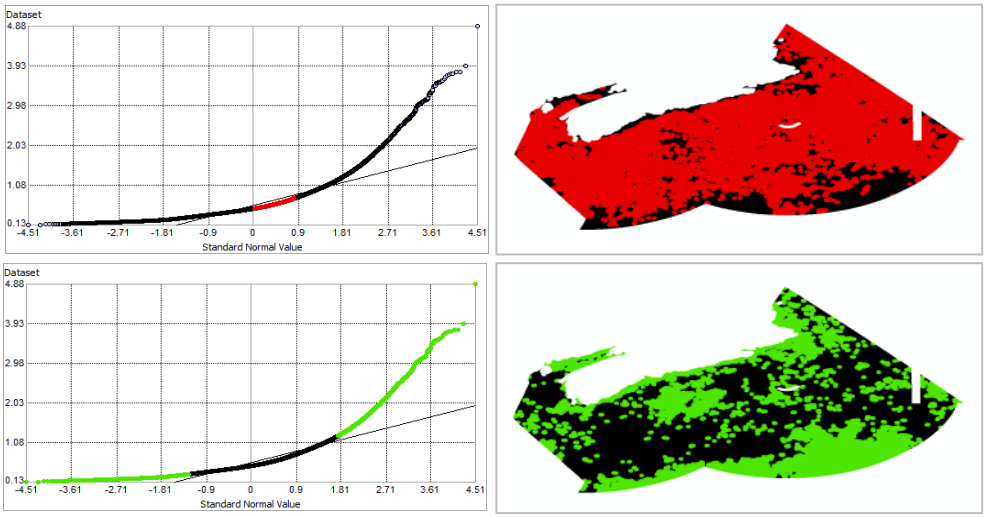

Fig. 367. Normal Q-Q plot for data values of Annual Chlorophyll *a* Range (mg m^{-3}). Points falling under (upper panel) and over (bottom panel) the reference line are mapped.

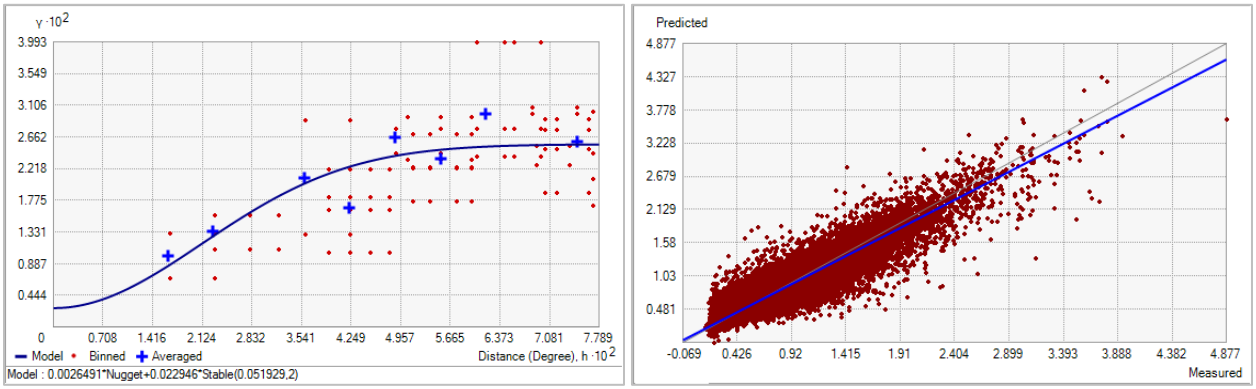

Fig. 368. Left panel: Semivariogram of Annual Chlorophyll *a* Range (mg m^{-3}). Binned values are shown as red dots; average points are shown as blue crosses; the model fit to the averaged values is shown as a blue line. Lag size: 6.491 x 10^{-3} degrees; number of lags: 12; Parameter: 1.325; Range: 0.052 degrees; Partial Sill: 0.023. Right panel: Scatterplot of predicted values versus observed values for the variable Annual Chlorophyll *a* Range (mg m^{-3}).

Table 148. Results of cross-validation of the kriged model for Annual Chlorophyll *a* Range (mg m^{-3}).

Prediction error	**Value**
Number of Observations	157201
Overall Mean Error	-7.161 x 10^{-5}
Root Mean Square Prediction Error	0.099
Standardized Mean	-5.353 x 10^{-4}
Standardized Root Mean Square Prediction Error	1.326
Average Standard Error	0.074

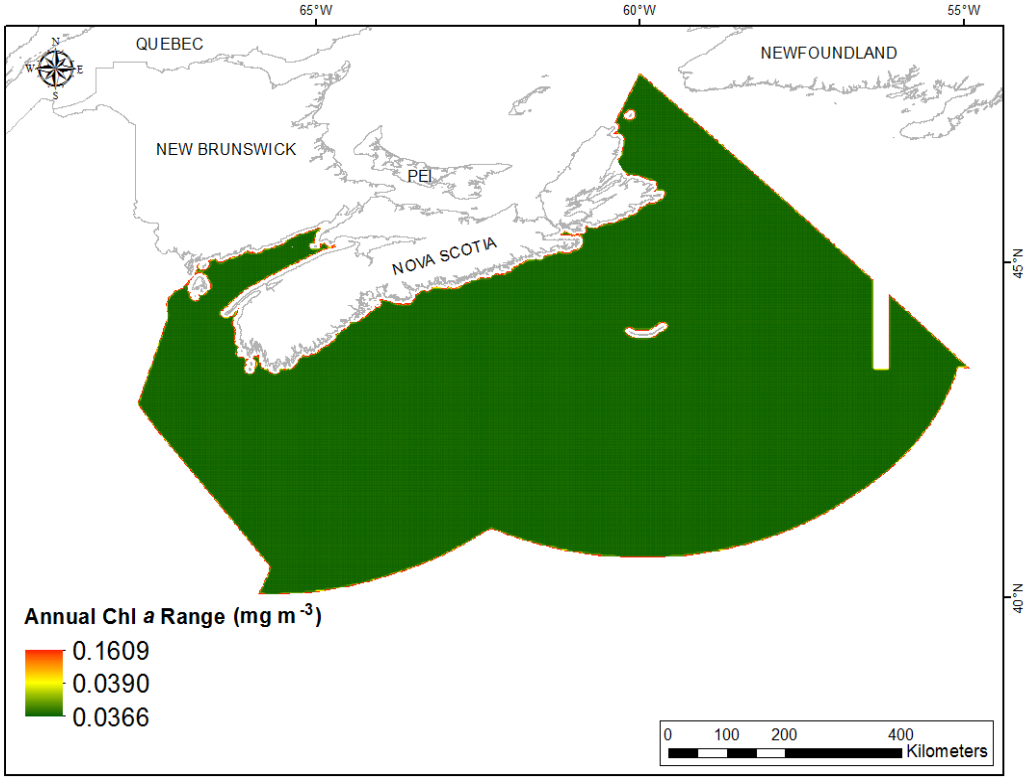

Fig. 369. Prediction standard error surface of Annual Chlorophyll *a* Range (mg m^{-3}).

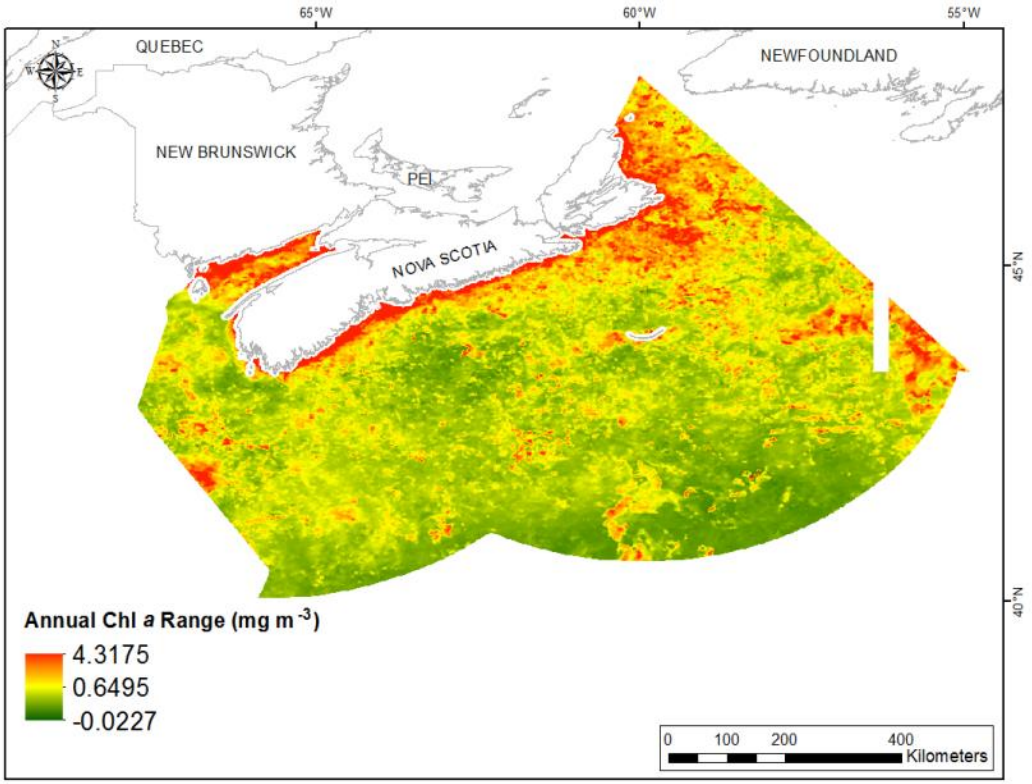

Fig. 370. Interpolated prediction surface of Annual Chlorophyll *a* Range (mg m^{-3}).

Primary Production

Primary production measures the rate at which atmospheric or aqueous carbon dioxide is converted to organic carbon by autotrophs (Bender et al., 1987) and relates more directly to the flux of particulate organic carbon and food supply to the seafloor than sea surface chlorophyll *a* concentration. However, as satellite-derived chlorophyll *a* is a main source of data used in the calculation of the primary production variables in this report, we expect these variables to be highly correlated.

Spring Primary Production Mean

This variable displayed a near-normal distribution prior to interpolation (Table 149, Fig. 371). The data were higher than predicted by a normal distribution at the lower range and lower than predicted at the highest and the lowest values (Fig. 372). The areas of under- and over-prediction showed no spatial pattern over the study extent (Fig. 372).

The semivariogram showed moderate autocorrelation present in the data and the model showed fair fit between measured and predicted values (Fig. 373). Good performance of the model was indicated by the cross-validation results (Table 150). The error map showed high error along the edges of the study extent (Fig. 374). The kriged surface is presented in Fig. 375.

Table 149. Distributional properties of Spring Primary Production Mean (mg C m^{-2} day^{-1}).

Property	Value
Number of Observations	5321
Minimum	306.670
Maximum	1224.400
Mean	868.350
Median	868.420
Standard Deviation	101.610
Skewness	3.418 x 10^{-3}
Kurtosis	3.065

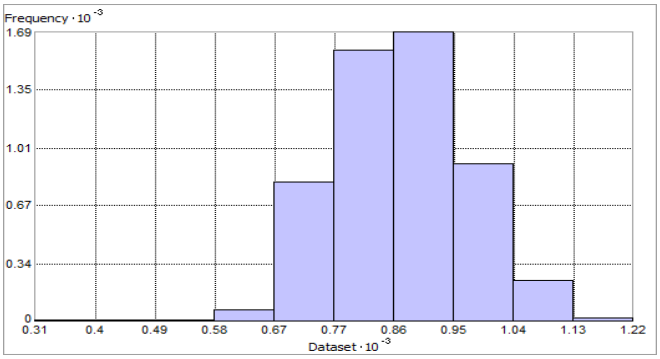

Fig. 371. Distribution of Spring Primary Production Mean (mg C m^{-2} day^{-1}). Histogram was illustrated using 10 bins. X and Y axes are shown at 10^{-3}.

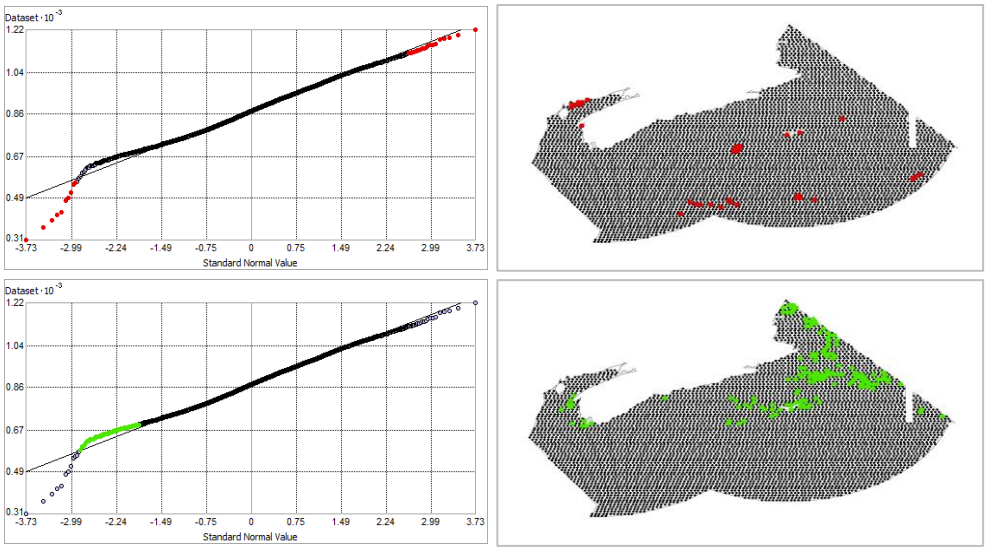

Fig. 372. Normal Q-Q plot for data values of Spring Primary Production Mean (mg C m^{-2} day^{-1}). Points falling under (upper panel) and over (bottom panel) the reference line are mapped.

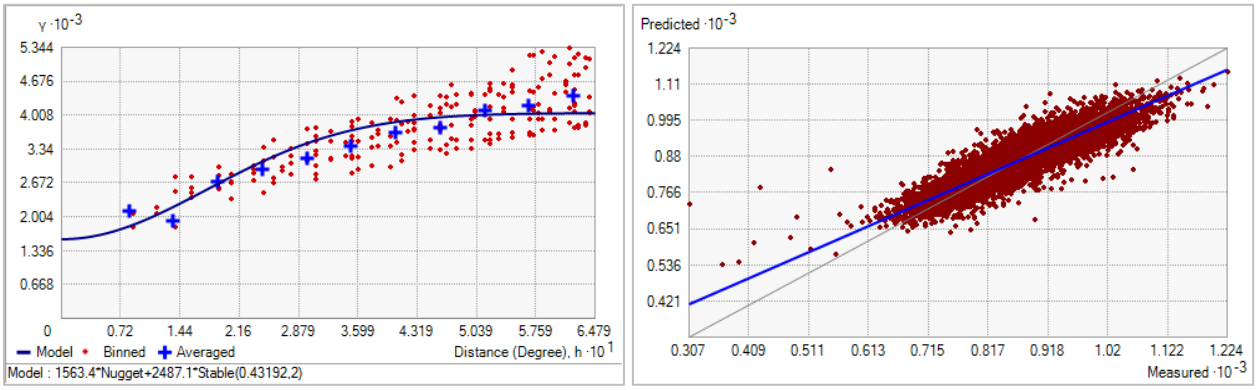

Fig. 373. Left panel: Semivariogram of Spring Primary Production Mean (mg C m^{-2} day^{-1}). Binned values are shown as red dots; average points are shown as blue crosses; the model fit to the averaged values is shown as a blue line. Lag size: 0.054 degrees; number of lags: 12; Parameter: 2; Range: 0.432 degrees; Partial Sill: 2487.116. Right panel: Scatterplot of predicted values versus observed values for the variable Spring Primary Production Mean (mg C m^{-2} day^{-1}).

Table 150. Results of cross-validation of the kriged model for Spring Primary Production Mean (mg C m^{-2} day^{-1}).

Prediction error	**Value**
Number of Observations	5321
Overall Mean Error	-0.042
Root Mean Square Prediction Error	46.1725
Standardized Mean	-1.195×10^{-3}
Standardized Root Mean Square Prediction Error	1.045
Average Standard Error	44.023

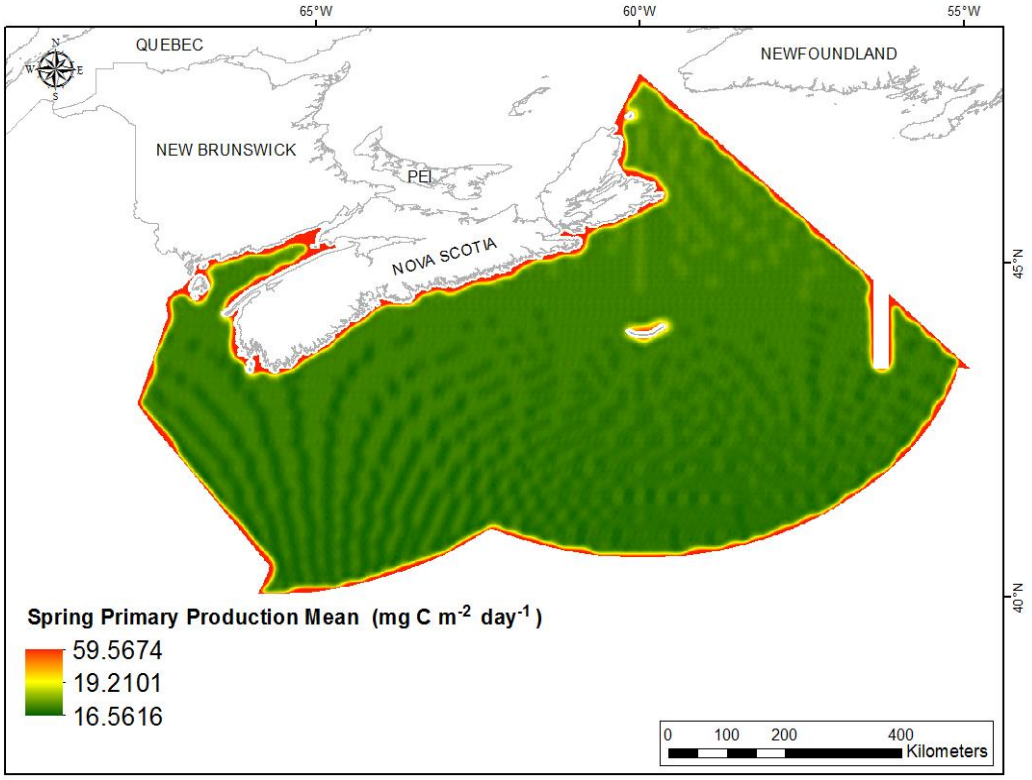

Fig. 374. Prediction standard error surface of Spring Primary Production Mean (mg C m^{-2} day^{-1}).

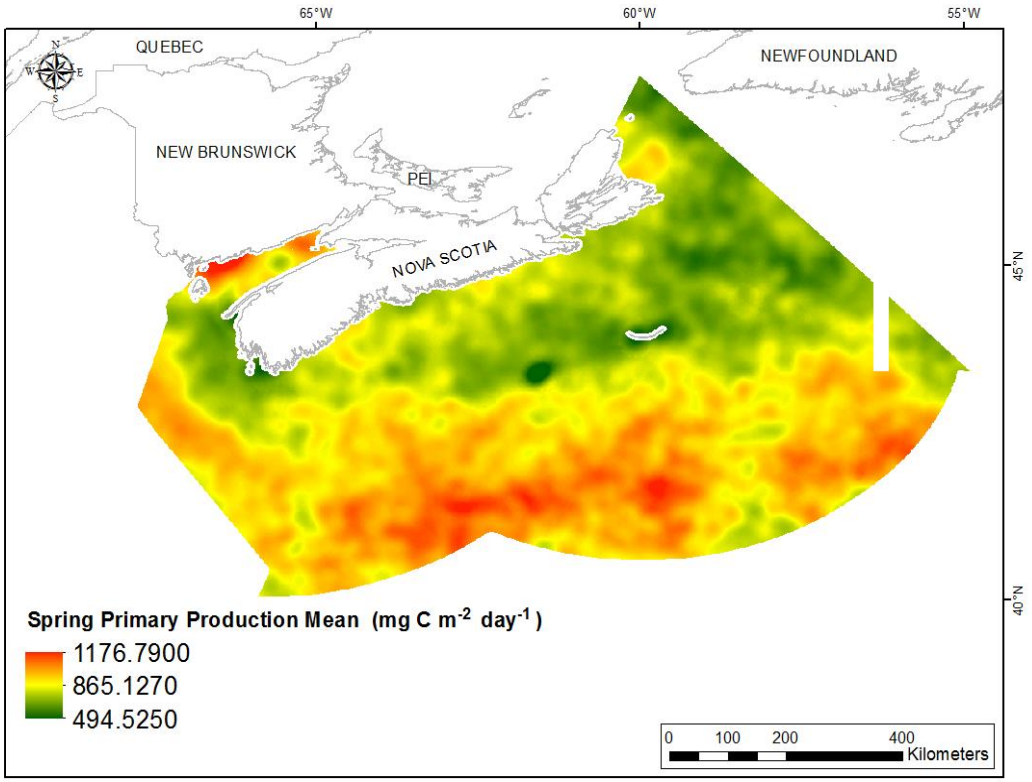

Fig. 375. Interpolated prediction surface of Spring Primary Production Mean (mg C m^{-2} day^{-1}).

Spring Primary Production Minimum

This variable displayed a near-normal distribution with light leptokurtosis prior to interpolation (Table 151, Fig. 376). The data were higher than predicted by a normal distribution at both tails and slightly lower than predicted at mid-values (Fig. 377). The areas of under- and over-prediction showed no spatial pattern over the study extent (Fig. 377).

The semivariogram showed moderate autocorrelation present in the data (Fig. 378). The fit between measured and predicted values was fair (Fig. 378), with under-prediction of large values and over-prediction of small values, a property inherent to the kriging method. Good performance of the model was indicated by the cross-validation results (Table 152). The error map showed moderate error over the study extent (Fig. 379). The kriged surface is presented in Fig. 380.

Table 151. Distributional properties of Spring Primary Production Minimum (mg C m^{-2} day^{-1}).

Property	Value
Number of Observations	5321
Minimum	170.120
Maximum	896.290
Mean	486.430
Median	471.840
Standard Deviation	83.675
Skewness	0.730
Kurtosis	3.703

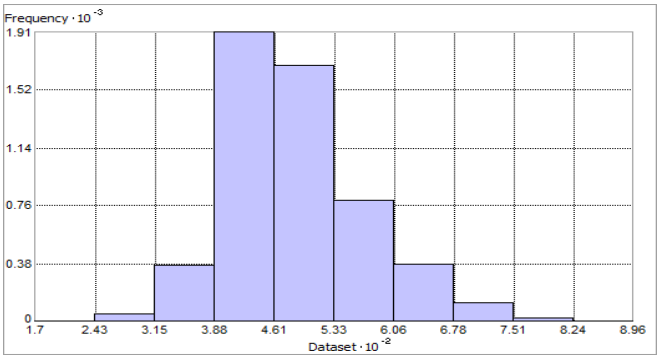

Fig. 376. Distribution of Spring Primary Production Minimum (mg C m^{-2} day^{-1}). Histogram was illustrated using 10 bins. X axis is shown at 10^{-2}; Y axis is shown at 10^{-3}.

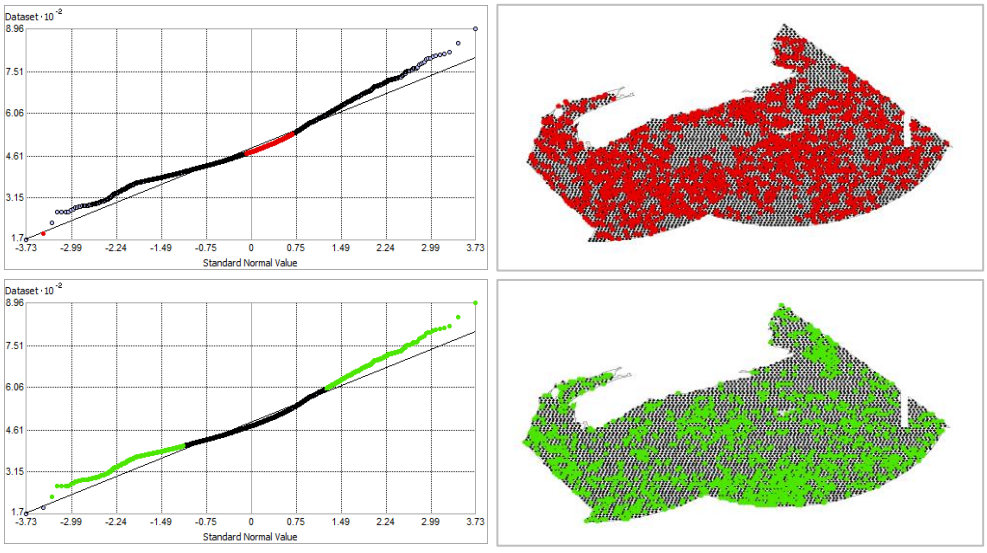

Fig. 377. Normal Q-Q plot for data values of Spring Primary Production Minimum (mg C m^{-2} day^{-1}). Points falling under (upper panel) and over (bottom panel) the reference line are mapped.

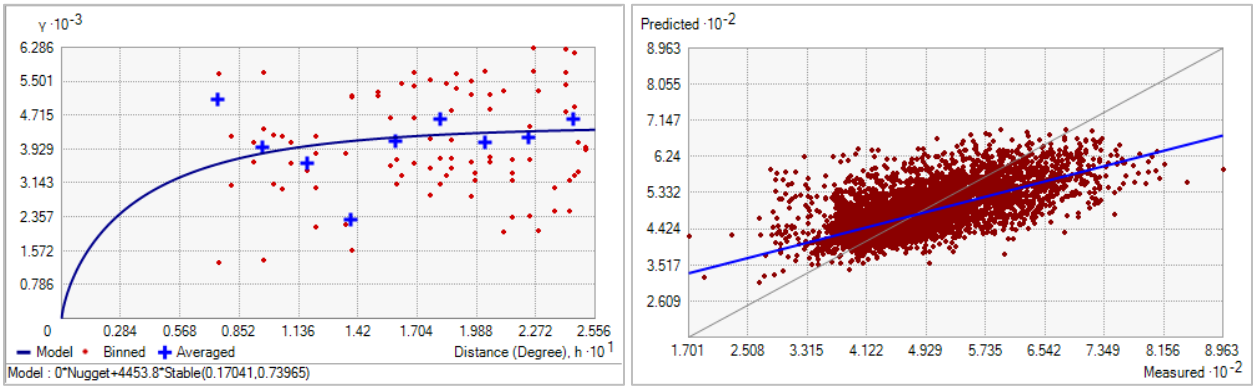

Fig. 378. Left panel: Semivariogram of Spring Primary Production Minimum (mg C m^{-2} day^{-1}). Binned values are shown as red dots; average points are shown as blue crosses; the model fit to the averaged values is shown as a blue line. Lag size: 0.021 degrees; number of lags: 12; Parameter: 0.740; Range: 0.170 degrees; Partial Sill: 4453.784. Right panel: Scatterplot of predicted values versus observed values for the variable Spring Primary Production Minimum (mg C m^{-2} day^{-1}).

Table 152. Results of cross-validation of the kriged model for Spring Primary Production Minimum (mg C m^{-2} day^{-1}).

Prediction error	**Value**
Number of Observations	5321
Overall Mean Error	-0.083
Root Mean Square Prediction Error	64.050
Standardized Mean	-1.252×10^{-3}
Standardized Root Mean Square Prediction Error	0.978
Average Standard Error	65.492

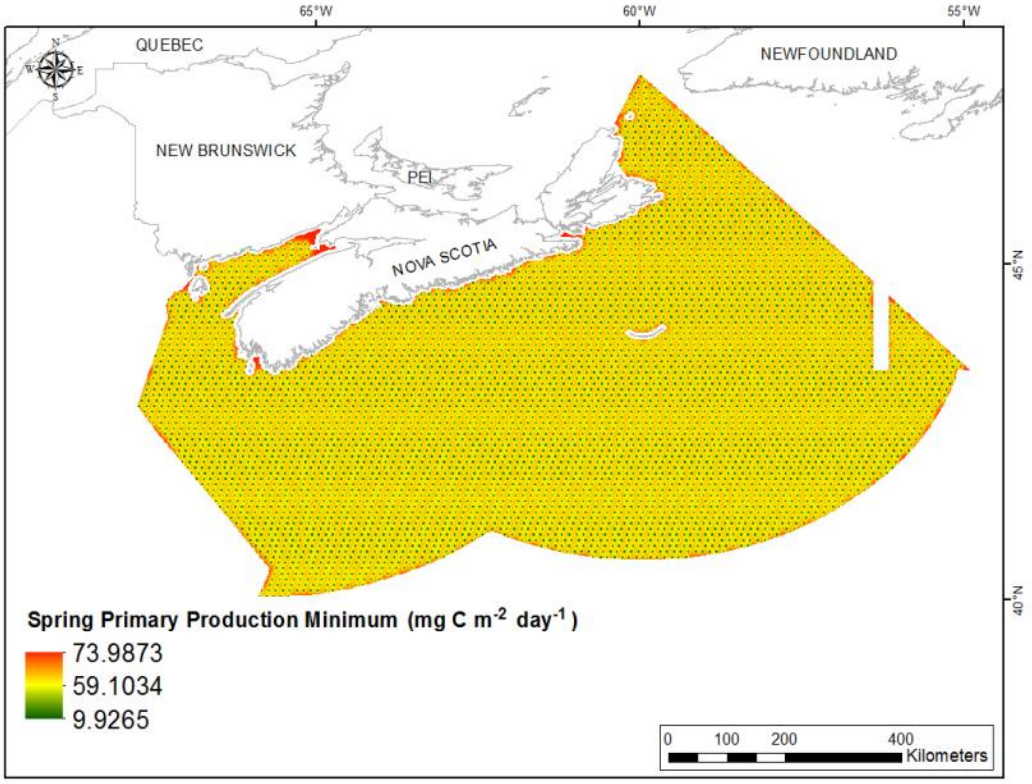

Fig. 379. Prediction standard error surface of Spring Primary Production Minimum (mg C m^{-2} day^{-1}).

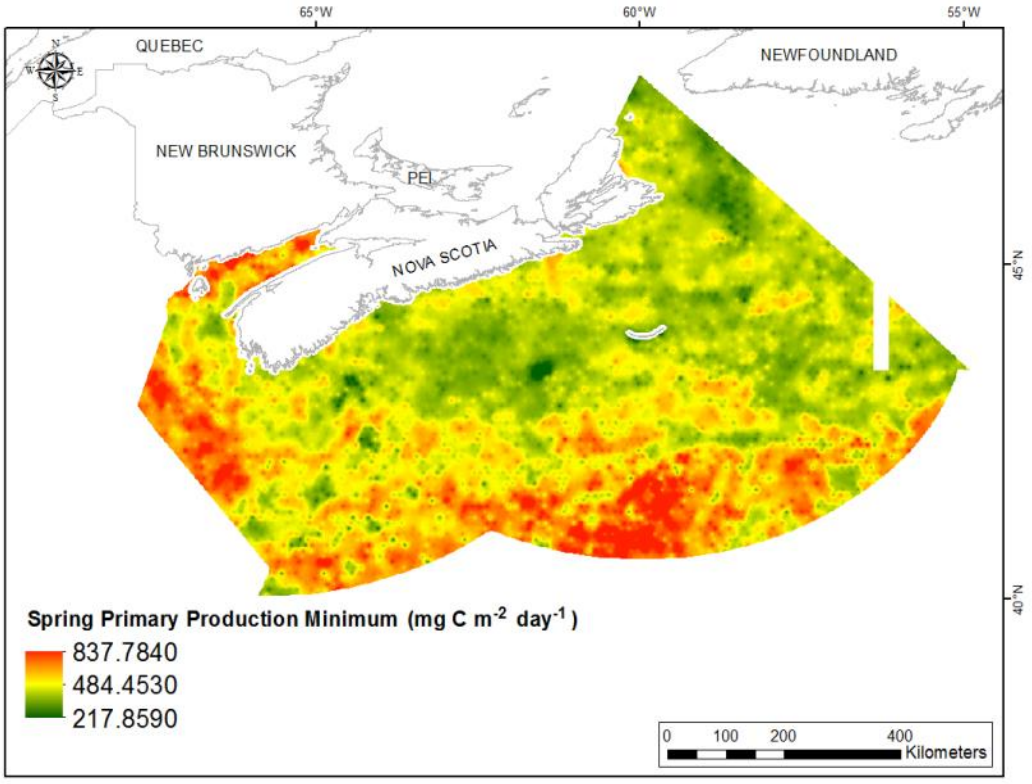

Fig. 380. Interpolated prediction surface of Spring Primary Production Minimum (mg C m^{-2} day^{-1}).

Spring Primary Production Maximum

This variable displayed a negatively skewed, leptokurtic distribution with outlying data in the upper range (Table 153, Fig. 381). The data followed the 1:1 reference line in the Q-Q plot (Fig. 382) except at the extreme tails where the data were higher than predicted at the upper range and lower than predicted at the lower range. The areas of under- and over-prediction showed no spatial pattern over the study extent (Fig. 382).

The semivariogram showed moderate autocorrelation present in the data (Fig. 383). The fit between measured and predicted values was fair (Fig. 383), with under-prediction of large values and over-prediction of small values, a property inherent to the kriging method. The single large outlier was poorly predicted. Good performance of the model was indicated by the cross-validation results (Table 154). The error map showed high error along the edges of the study extent (Fig. 384). The kriged surface is presented in Fig. 385.

Table 153. Distributional properties of Spring Primary Production Maximum (mg C m^{-2} day^{-1}).

Property	Value
Number of Observations	5321
Minimum	509.550
Maximum	2980.700
Mean	1385.400
Median	1406.500
Standard Deviation	175.240
Skewness	-0.318
Kurtosis	4.525

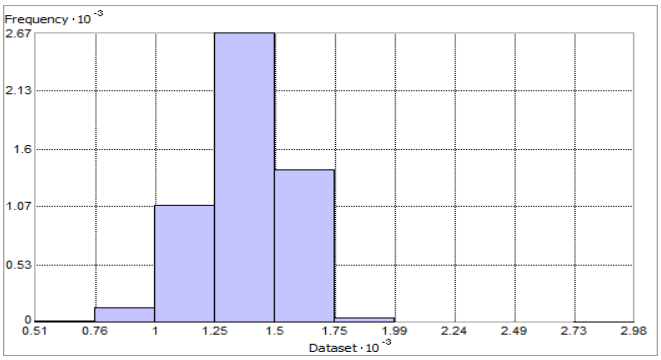

Fig. 381. Distribution of Spring Primary Production Maximum (mg C m^{-2} day^{-1}). Histogram was illustrated using 10 bins. X and Y axes are shown at 10^{-3}.

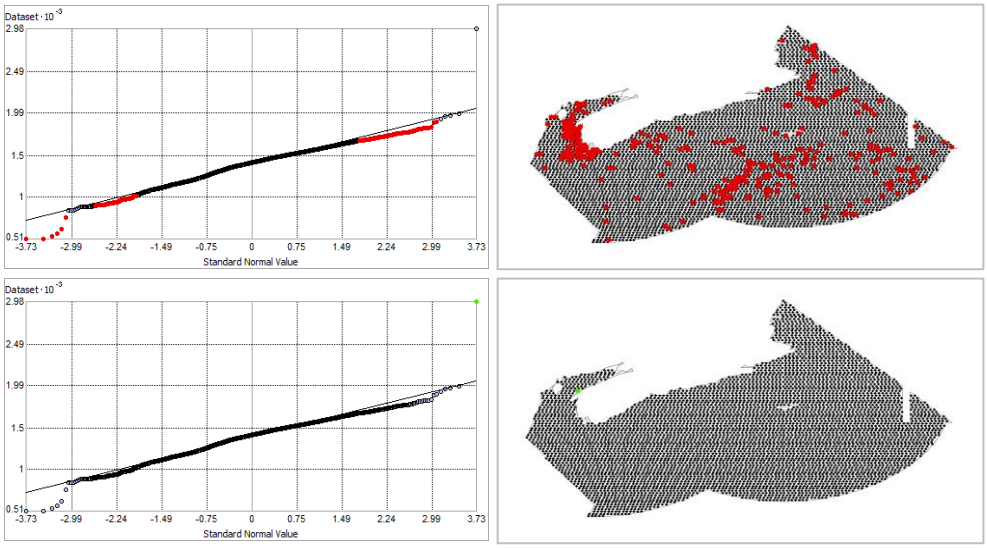

Fig. 382. Normal Q-Q plot for data values of Spring Primary Production Maximum (mg C m^{-2} day^{-1}). Points falling under (upper panel) and over (bottom panel) the reference line are mapped.

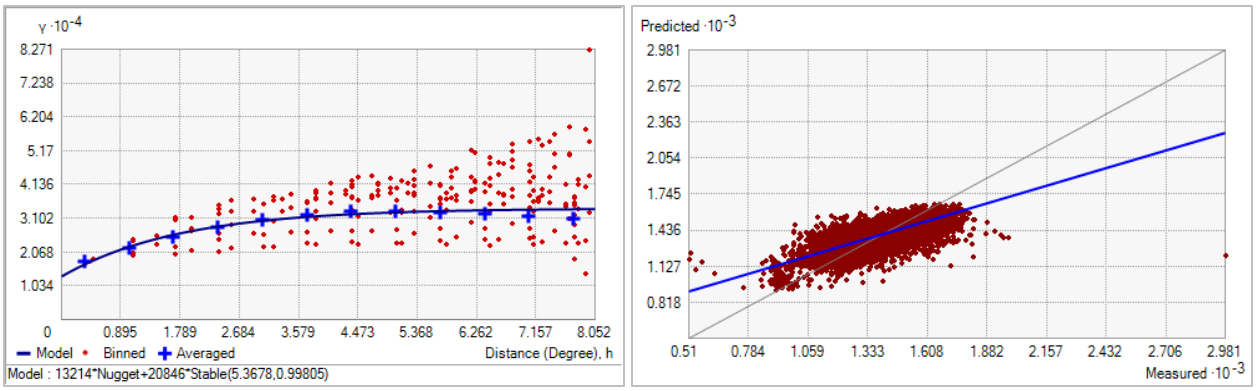

Fig. 383. Left panel: Semivariogram of Spring Primary Production Maximum (mg C m^{-2} day^{-1}). Binned values are shown as red dots; average points are shown as blue crosses; the model fit to the averaged values is shown as a blue line. Lag size: 0.671 degrees; number of lags: 12; Parameter: 0.998; Range: 5.368 degrees; Partial Sill: 20845.870. Right panel: Scatterplot of predicted values versus observed values for the variable Spring Primary Production Maximum (mg C m^{-2} day^{-1}).

Table 154. Results of cross-validation of the kriged model for Spring Primary Production Maximum (mg C m^{-2} day^{-1}).

Prediction error	**Value**
Number of Observations	5321
Overall Mean Error	-7492×10^{-3}
Root Mean Square Prediction Error	123.168
Standardized Mean	-8.158×10^{-5}
Standardized Root Mean Square Prediction Error	0.996
Average Standard Error	123.462

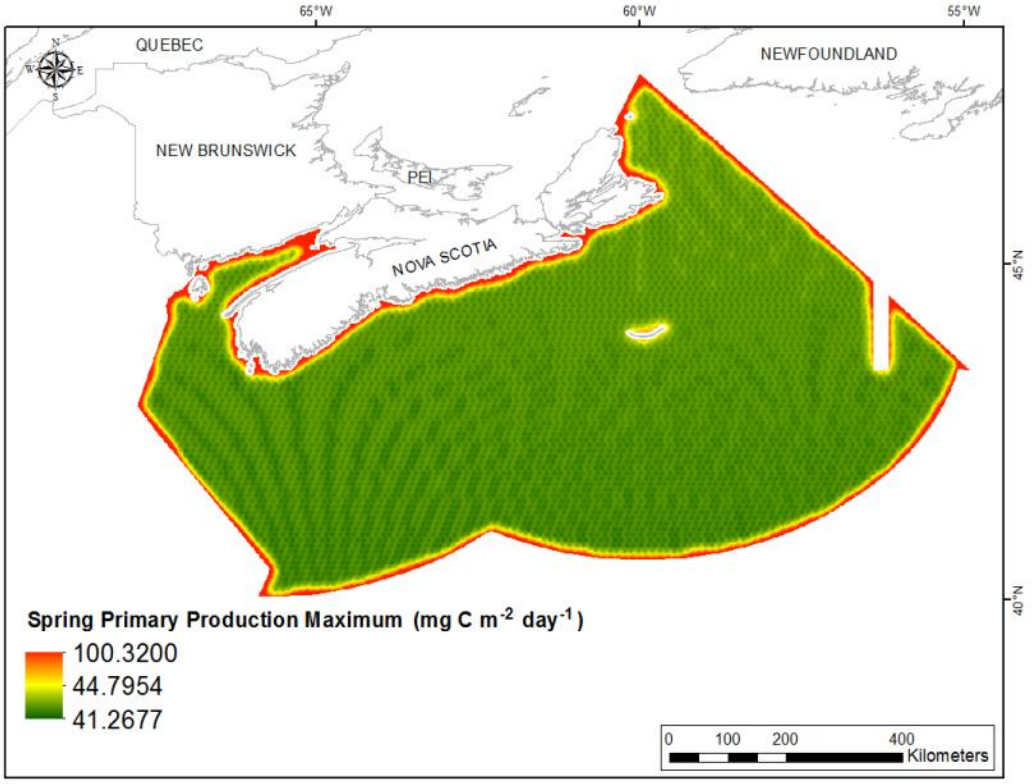

Fig. 384. Prediction standard error surface of Spring Primary Production Maximum (mg C m^{-2} day^{-1}).

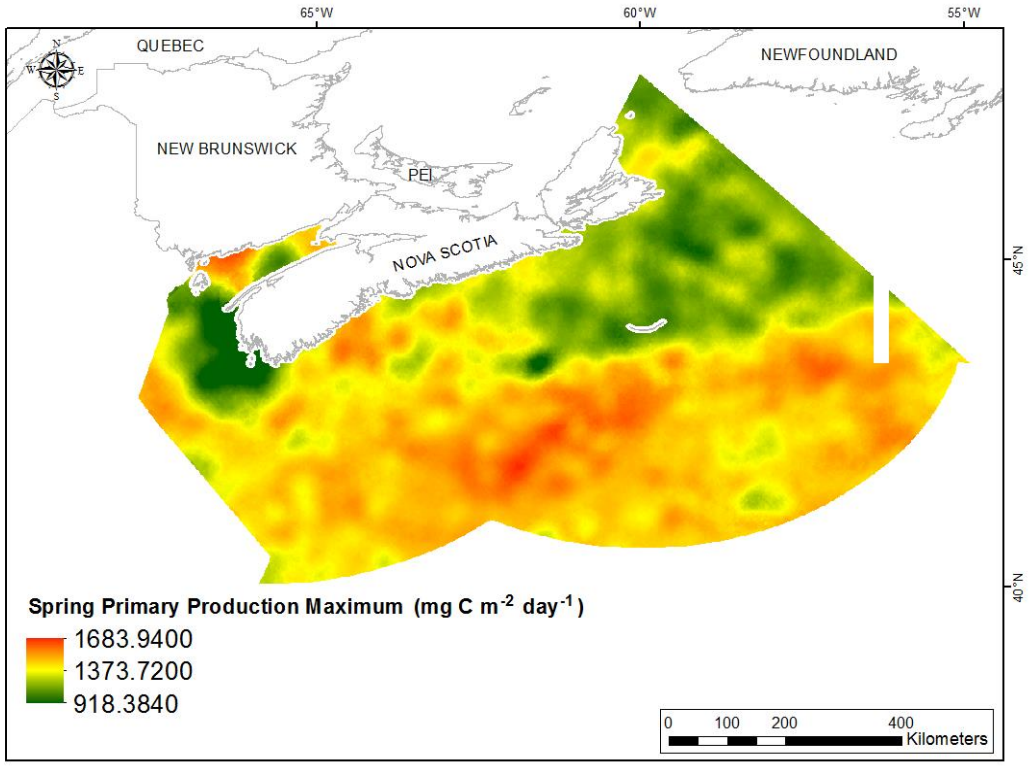

Fig. 385. Interpolated prediction surface of Spring Primary Production Maximum (mg C m^{-2} day^{-1}).

Spring Primary Production Range

This variable displayed a negatively skewed, leptokurtic distribution with outlying data in the upper range (Table 155, Fig. 386). The data followed the 1:1 reference line in the Q-Q plot (Fig. 387) except at the extreme tails where the data were higher than predicted at the upper range and lower than predicted at the lower range. The areas of under- and over-prediction showed no spatial pattern over the study extent (Fig. 387).

The semivariogram showed moderate autocorrelation present in the data (Fig. 388). The fit between measured and predicted values was fair (Fig. 388), with under-prediction of large values and over-prediction of small values. The single large outlier was poorly predicted. Good performance of the model was indicated by the cross-validation results (Table 156). The error map showed high error along the edges of the study extent (Fig. 389). The kriged surface is presented in Fig. 390.

Table 155. Distributional properties of Spring Primary Production Range (mg C m^{-2} day^{-1}).

Property	Value
Number of Observations	5321
Minimum	154.360
Maximum	2384.300
Mean	898.960
Median	908.250
Standard Deviation	179.010
Skewness	-0.107
Kurtosis	3.864

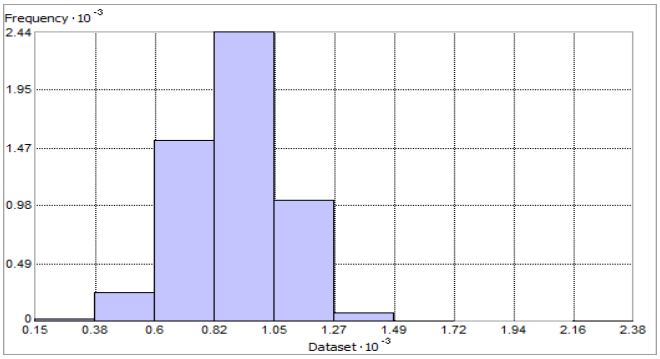

Fig. 386. Distribution of Spring Primary Production Range (mg C m^{-2} day^{-1}). Histogram was illustrated using 10 bins. X and Y axes are shown at 10^{-3}.

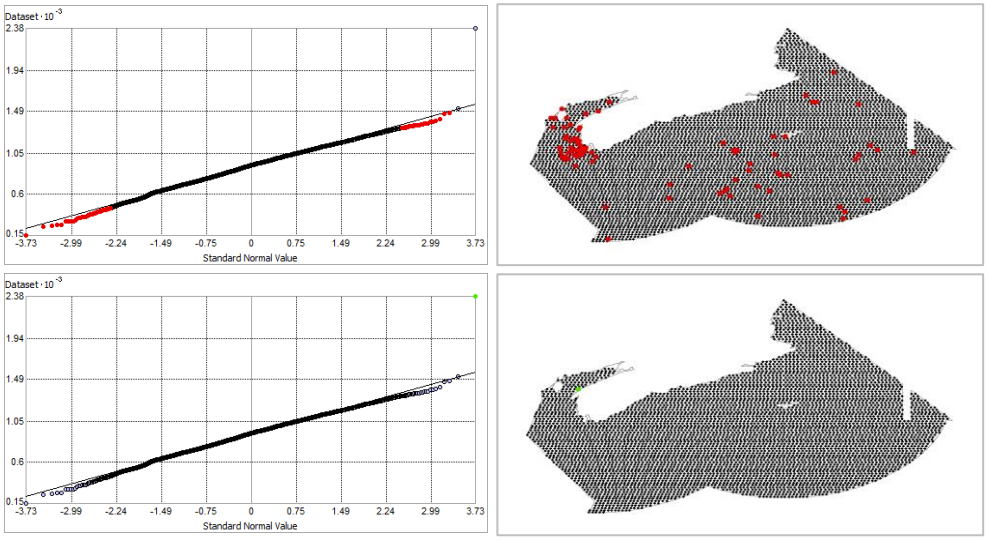

Fig. 387. Normal Q-Q plot for data values of Spring Primary Production Range (mg C m^{-2} day^{-1}). Points falling under (upper panel) and over (bottom panel) the reference line are mapped.

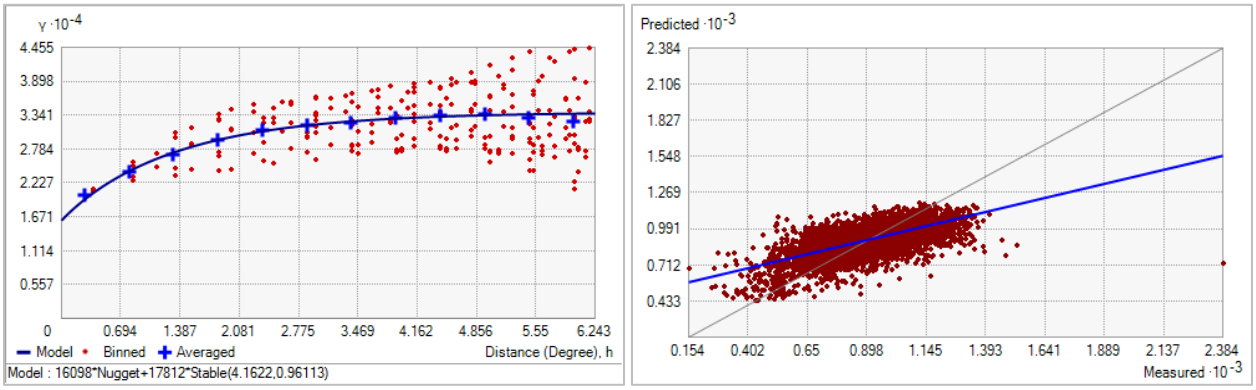

Fig. 388. Left panel: Semivariogram of Spring Primary Production Range (mg C m^{-2} day^{-1}). Binned values are shown as red dots; average points are shown as blue crosses; the model fit to the averaged values is shown as a blue line. Lag size: 0.520 degrees; number of lags: 12; Parameter: 0.961; Range: 4.162 degrees; Partial Sill: 17811.780. Right panel: Scatterplot of predicted values versus observed values for the variable Spring Primary Production Range (mg C m^{-2} day^{-1}).

Table 156. Results of cross-validation of the kriged model for Spring Primary Production Range (mg C m^{-2} day^{-1}).

Prediction error	**Value**
Number of Observations	5321
Overall Mean Error	0.044
Root Mean Square Prediction Error	136.497
Standardized Mean	2.917×10^{-4}
Standardized Root Mean Square Prediction Error	0.999
Average Standard Error	136.465

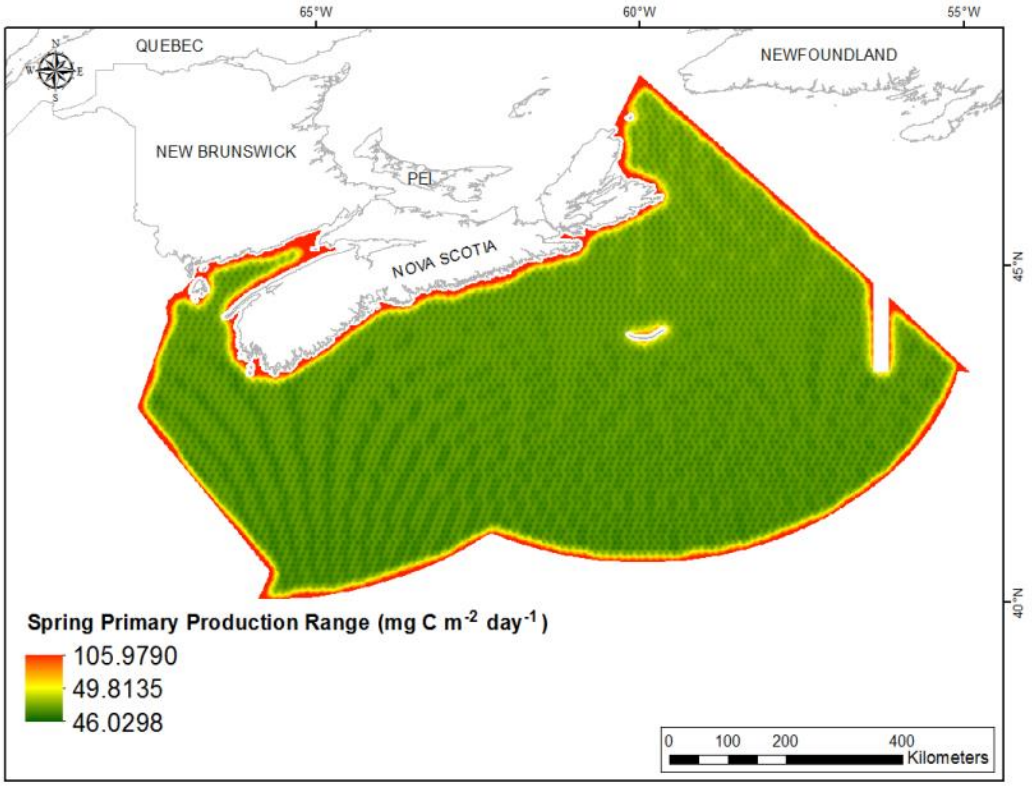

Fig. 389. Prediction standard error surface of Spring Primary Production Range (mg C m^{-2} day^{-1}).

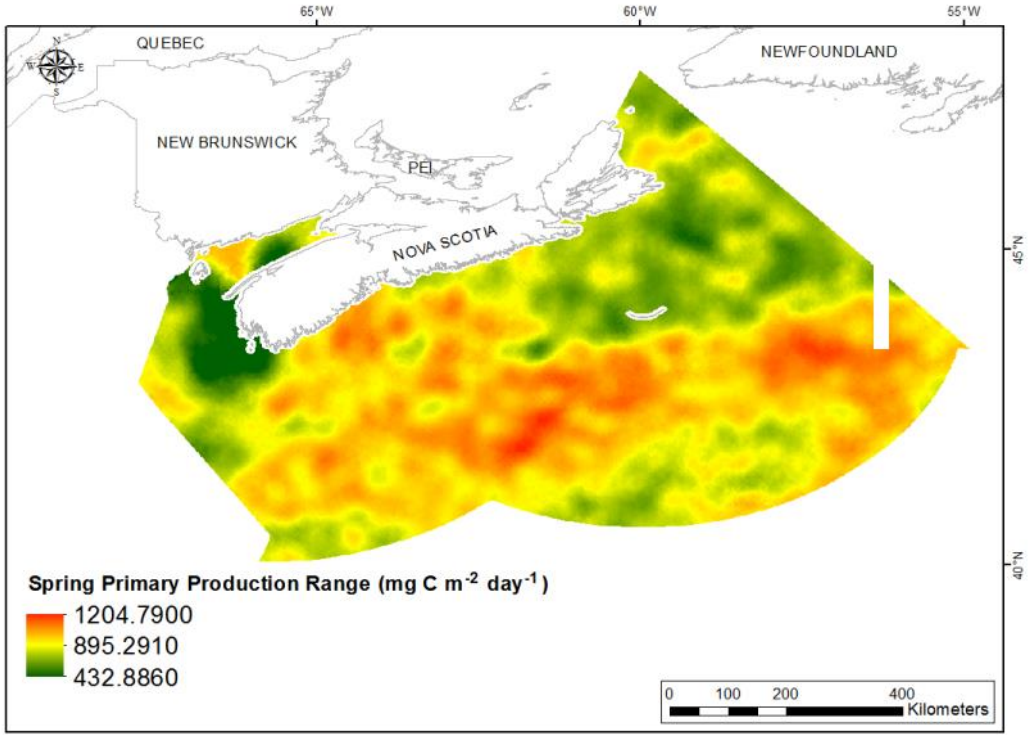

Fig. 390. Interpolated prediction surface of Spring Primary Production Range (mg C m^{-2} day^{-1}).

Spring Primary Production Average Minimum

This variable displayed a near-normal distribution prior to interpolation (Table 157, Fig. 391). The data were higher than predicted by a normal distribution at low and high values however the mid-region was very well-predicted (Fig. 392). The areas of over- and under-prediction showed no spatial pattern over the study extent (Fig. 292).

The semivariogram showed weak autocorrelation present in the data (Fig. 393). The fit between measured and predicted values was fair (Fig. 393), with under-prediction of large values and over-prediction of small values. Good performance of the model was indicated by the cross-validation results (Table 158). Moderate error was predicted over the study extent (Fig. 394). The kriged surface is presented in Fig. 395.

Table 157. Distributional properties of Spring Primary Production Average Minimum (mg C m^{-2} day^{-1}).

Property	Value
Number of Observations	5321
Minimum	235.750
Maximum	1059
Mean	638.970
Median	627.33
Standard Deviation	97.470
Skewness	0.514
Kurtosis	3.206

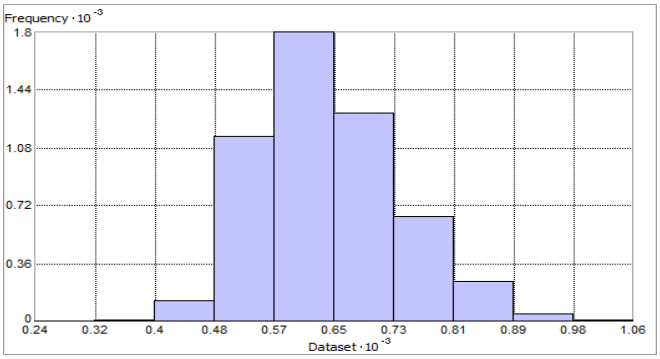

Fig. 391. Distribution of Spring Primary Production Average Minimum (mg C m^{-2} day^{-1}). Histogram was illustrated using 10 bins. X and Y axes are shown at 10^{-3}.

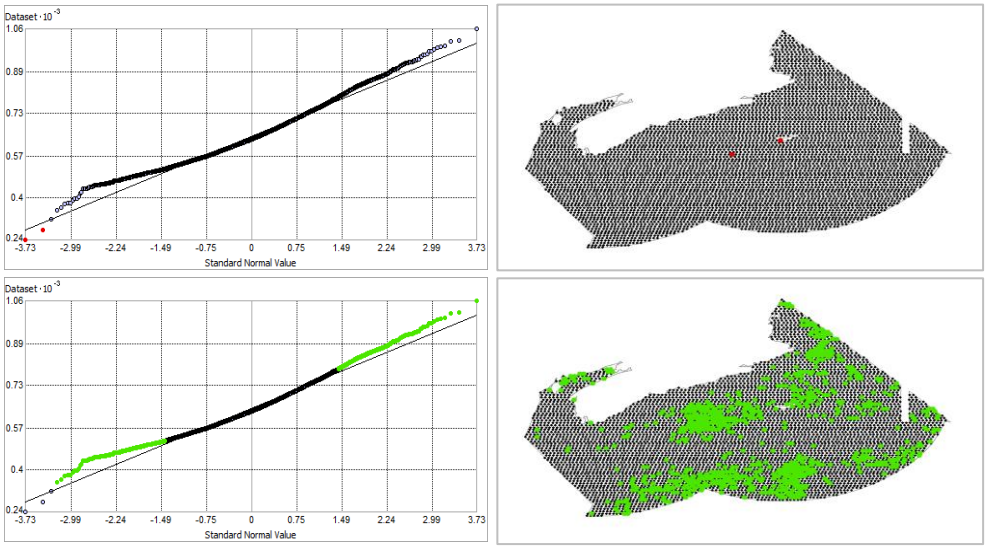

Fig. 392. Normal Q-Q plot for data values of Spring Primary Production Average Minimum (mg C m^{-2} day^{-1}). Points falling under (upper panel) and over (bottom panel) the reference line are mapped.

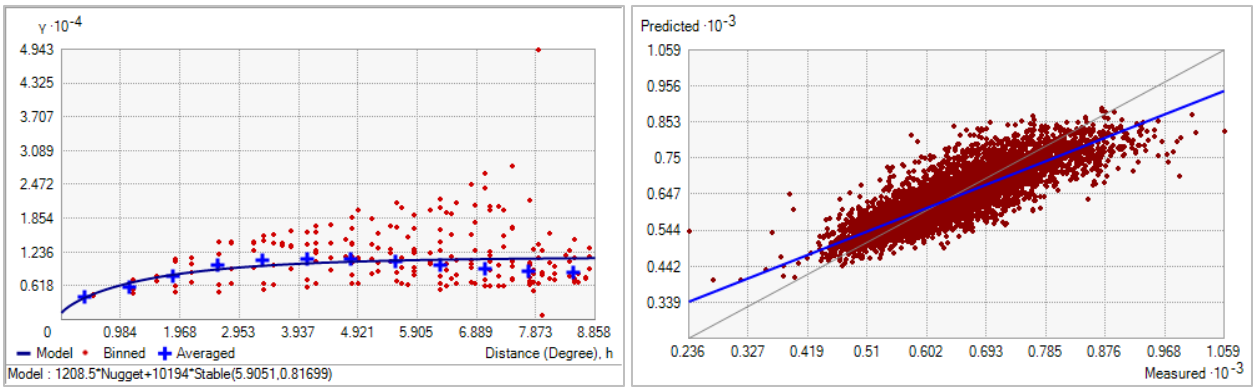

Fig. 393. Left panel: Semivariogram of Spring Primary Production Average Minimum (mg C m^{-2} day^{-1}). Binned values are shown as red dots; average points are shown as blue crosses; the model fit to the averaged values is shown as a blue line. Lag size: 0.738 degrees; number of lags: 12; Parameter: 0.87; Range: 5.905 degrees; Partial Sill: 10193.75. Right panel: Scatterplot of predicted values versus observed values for the model of Spring Primary Production Average Minimum (mg C m^{-2} day^{-1}).

Table 158. Results of cross-validation of the kriged model for Spring Primary Production Average Minimum (mg C m^{-2} day^{-1}).

Prediction error	**Value**
Number of Observations	5321
Overall Mean Error	-3.548×10^{-3}
Root Mean Square Prediction Error	52.599
Standardized Mean	1.059×10^{-4}
Standardized Root Mean Square Prediction Error	1.087
Average Standard Error	48.365

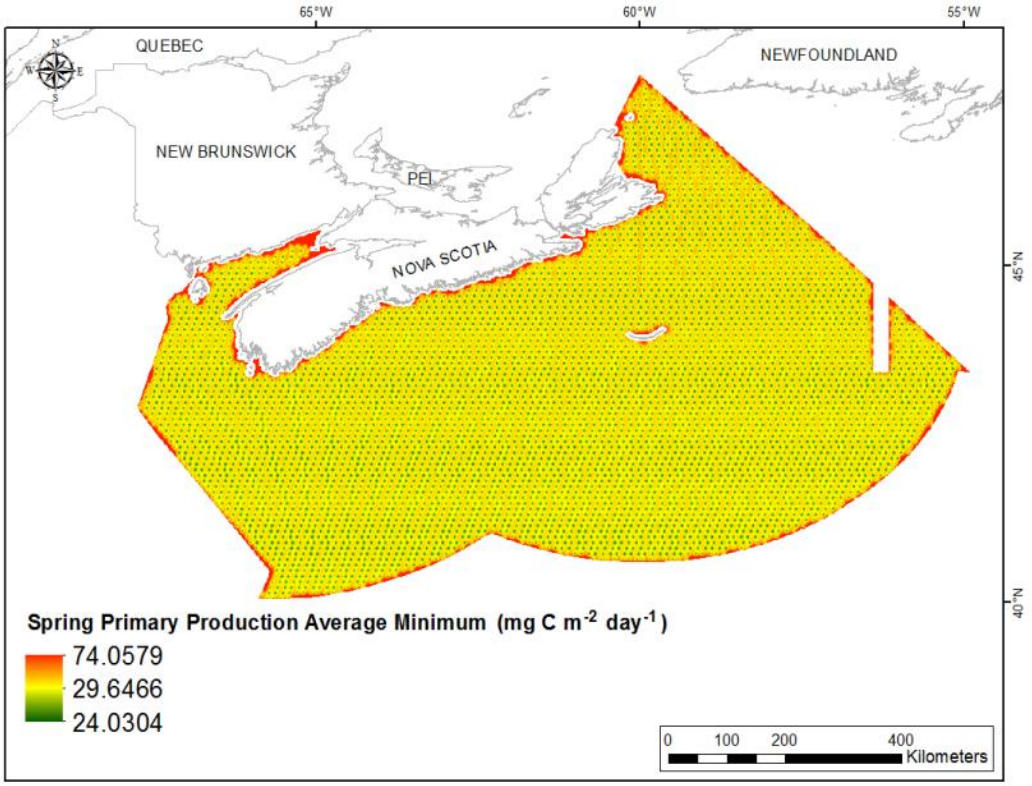

Fig. 394. Prediction standard error surface of Spring Primary Production Average Minimum (mg C m^{-2} day^{-1}).

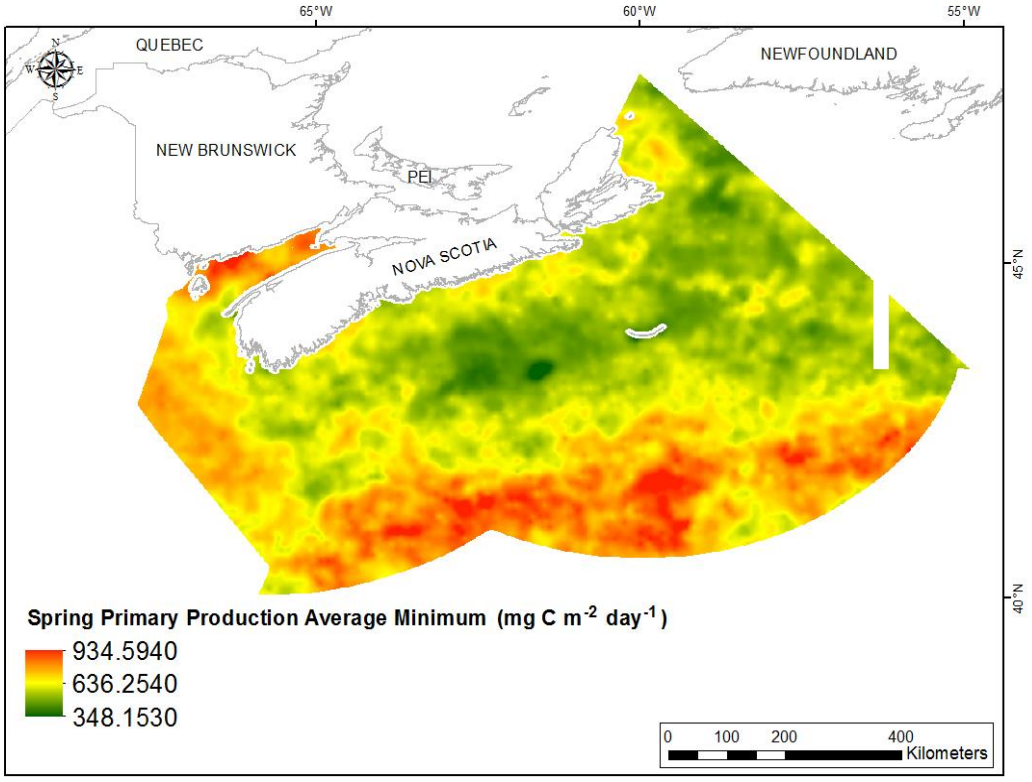

Fig. 395. Interpolated prediction surface of Spring Primary Production Average Minimum (mg C m^{-2} day^{-1}).

Spring Primary Production Average Maximum

This variable displayed a slightly left-skewed, playkurtic distribution prior to interpolation (Table 159, Fig. 396). The data were lower than predicted by a normal distribution at both tails and slightly higher than predicted at lower mid-range values (Fig. 397). The areas of over-prediction showed no spatial pattern over the study extent (Fig. 397).

The semivariogram showed weak autocorrelation present in the data (Fig. 398). The fit between measured and predicted values was fair (Fig. 398), with under-prediction of large values and over-prediction of small values. Good performance of the model was indicated by the cross-validation results (Table 160). Moderate error was predicted over the study extent (Fig. 399). The kriged surface is presented in Fig. 400.

Table 159. Distributional properties of Spring Primary Production Average Maximum (mg C m^{-2} day^{-1}).

Property	Value
Number of Observations	5321
Minimum	371.450
Maximum	1511.200
Mean	1121.300
Median	1132.100
Standard Deviation	144.300
Skewness	-0.270
Kurtosis	2.814

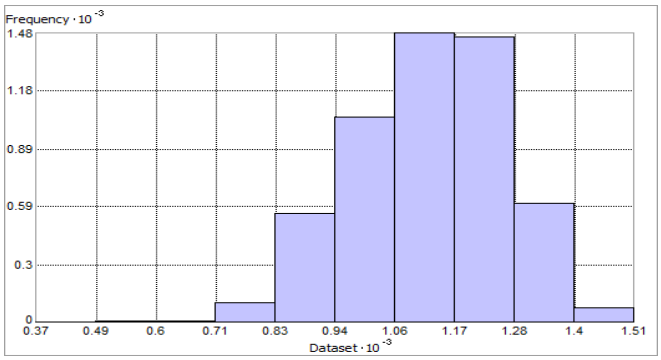

Fig. 396. Distribution of Spring Primary Production Average Maximum (mg C m^{-2} day^{-1}). Histogram was illustrated using 10 bins. X and Y axes are shown at 10^{-3}.

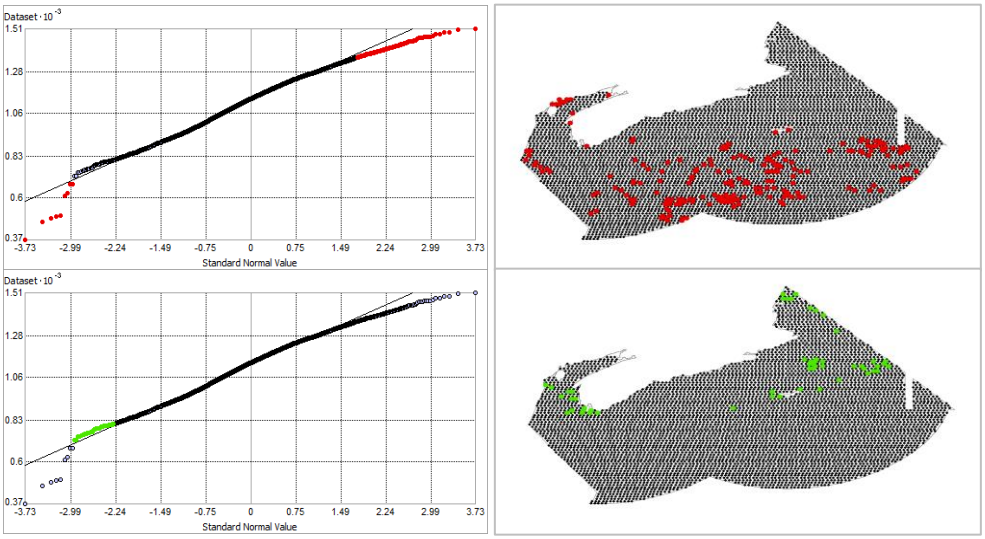

Fig. 397. Normal Q-Q plot for data values of Spring Primary Production Average Maximum (mg C m^{-2} day^{-1}). Points falling under (upper panel) and over (bottom panel) the reference line are mapped.

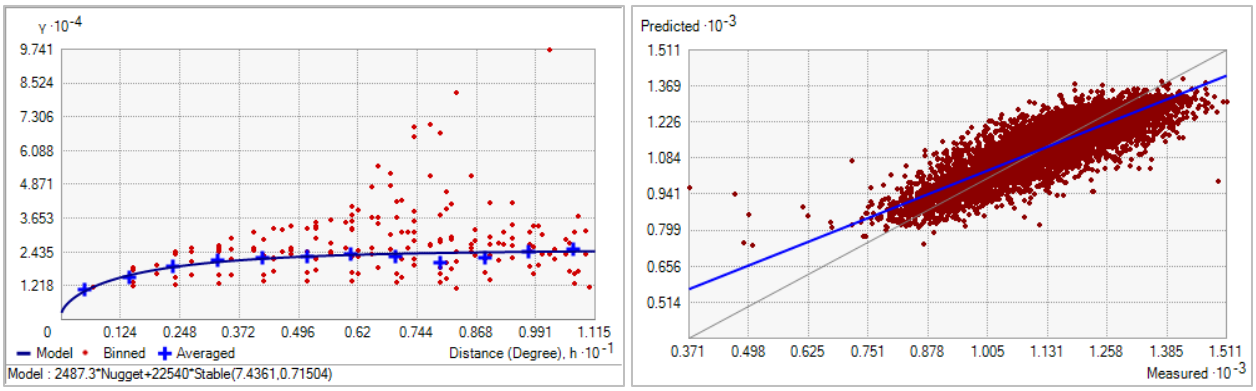

Fig 398. Left panel: Semivariogram of Spring Primary Production Average Maximum (mg C m^{-2} day^{-1}). Binned values are shown as red dots; average points are shown as blue crosses; the model fit to the averaged values is shown as a blue line. Lag size: 0.930 degrees; number of lags: 12; Parameter: 0.715; Range: 7.436 degrees; Partial Sill: 22540.080. Right panel: Scatterplot of predicted values versus observed values for the model of Spring Primary Production Average Maximum (mg C m^{-2} day^{-1}).

Table 160. Results of cross-validation of the kriged model for Spring Primary Production Average Maximum (mg C m^{-2} day^{-1}).

Prediction error	**Value**
Number of Observations	5321
Overall Mean Error	0.028
Root Mean Square Prediction Error	77.765
Standardized Mean	2.460×10^{-5}
Standardized Root Mean Square Prediction Error	1.033
Average Standard Error	75.115

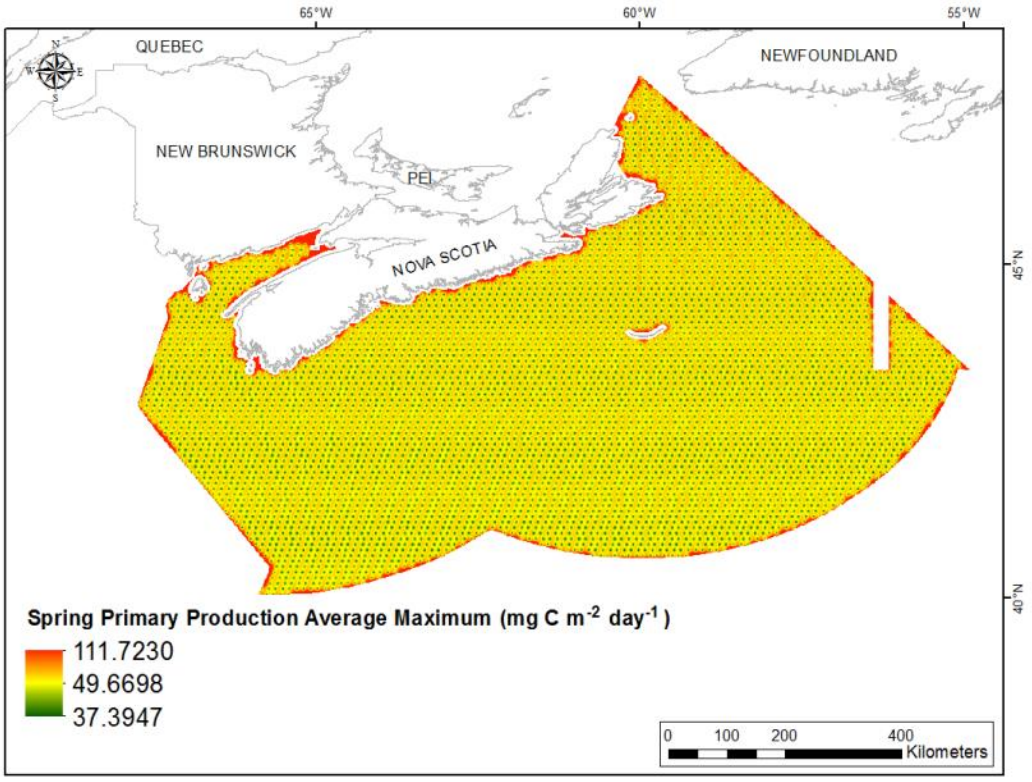

Fig. 399. Prediction standard error surface of Spring Primary Production Average Maximum (mg C m^{-2} day^{-1}).

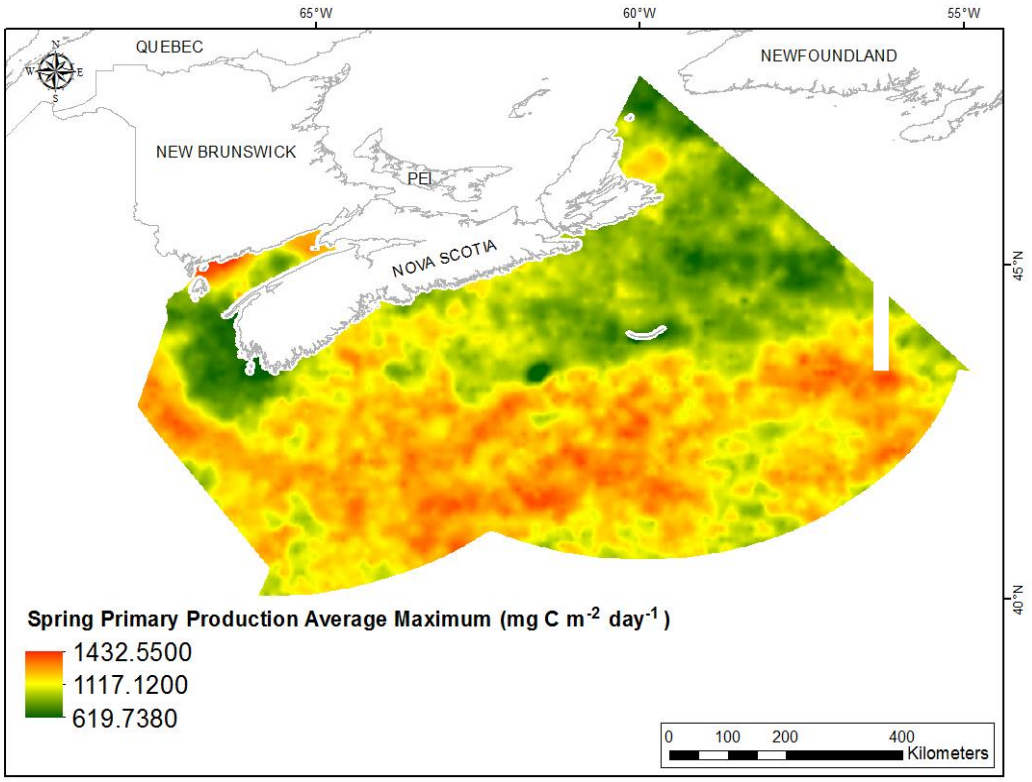

Fig. 400. Interpolated prediction surface of Spring Primary Production Average Maximum (mg C m^{-2} day^{-1}).

Spring Primary Production Average Range

This variable displayed a near normal distribution prior to interpolation (Table 161, Fig. 401). The data were higher than predicted by a normal distribution at the lowest values and lower than predicted at the highest values (Fig. 402). However, the mid-region was very well-predicted (Fig. 402). The areas of over-prediction showed no spatial pattern over the study extent (Fig. 402).

The semivariogram showed moderate autocorrelation present in the data (Fig. 403). The fit between measured and predicted values was fair (Fig. 403), with under-prediction of large values and over-prediction of small values. Good performance of the model was indicated by the cross-validation results (Table 162). Moderate error was predicted over the study extent (Fig. 404). The kriged surface is presented in Fig. 405.

Table 161. Distributional properties of Spring Primary Production Average Range (mg C m^{-2} day^{-1}).

Property	Value
Number of Observations	5321
Minimum	79.020
Maximum	914.100
Mean	482.350
Median	481.680
Standard Deviation	134.060
Skewness	0.066
Kurtosis	2.770

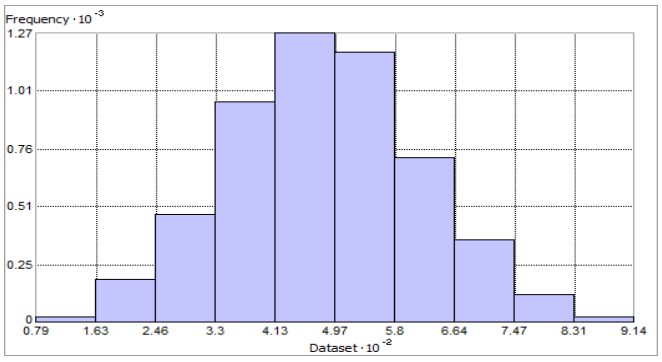

Fig. 401. Distribution of Spring Primary Production Average Range (mg C m^{-2} day^{-1}). Histogram was illustrated using 10 bins. X axis is shown at 10^{-2}; Y axis is shown at 10^{-3}.

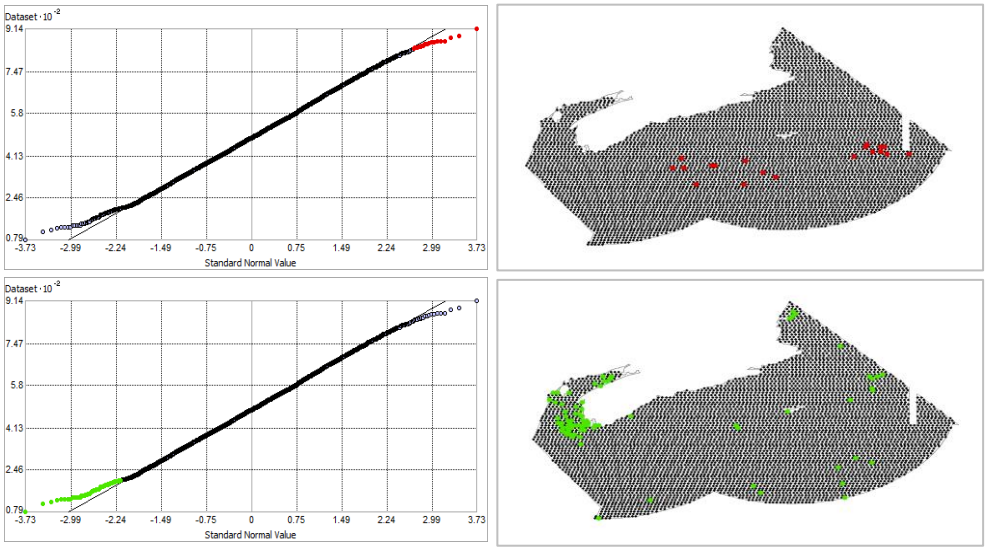

Fig. 402. Normal Q-Q plot for data values of Spring Primary Production Average Range (mg C m^{-2} day^{-1}). Points falling over the reference line are mapped; no points fall under the reference line.

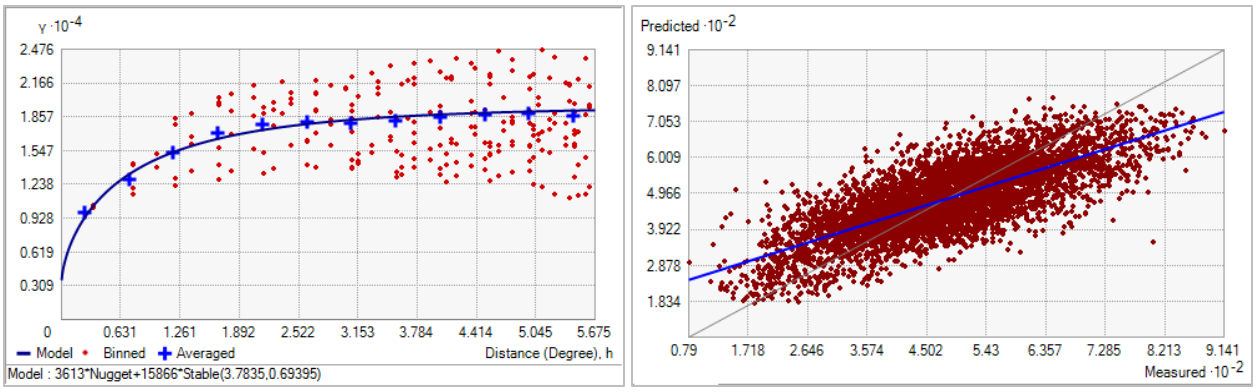

Fig 403. Left panel: Semivariogram of Spring Primary Production Average Range (mg C m^{-2} day^{-1}). Binned values are shown as red dots; average points are shown as blue crosses; the model fit to the averaged values is shown as a blue line. Lag size: 0.473 degrees; number of lags: 12; Parameter: 0.694; Range: 3.784 degrees; Partial Sill: 15865.82. Right panel: Scatterplot of predicted values versus observed values for the model of Spring Primary Production Average Range (mg C m^{-2} day^{-1}).

Table 162. Results of cross-validation of the kriged model for Spring Primary Production Average Range (mg C m^{-2} day^{-1}).

Prediction error	**Value**
Number of Observations	5321
Overall Mean Error	0.040
Root Mean Square Prediction Error	87.858
Standardized Mean	2.218×10^{-4}
Standardized Root Mean Square Prediction Error	1.017
Average Standard Error	86.306

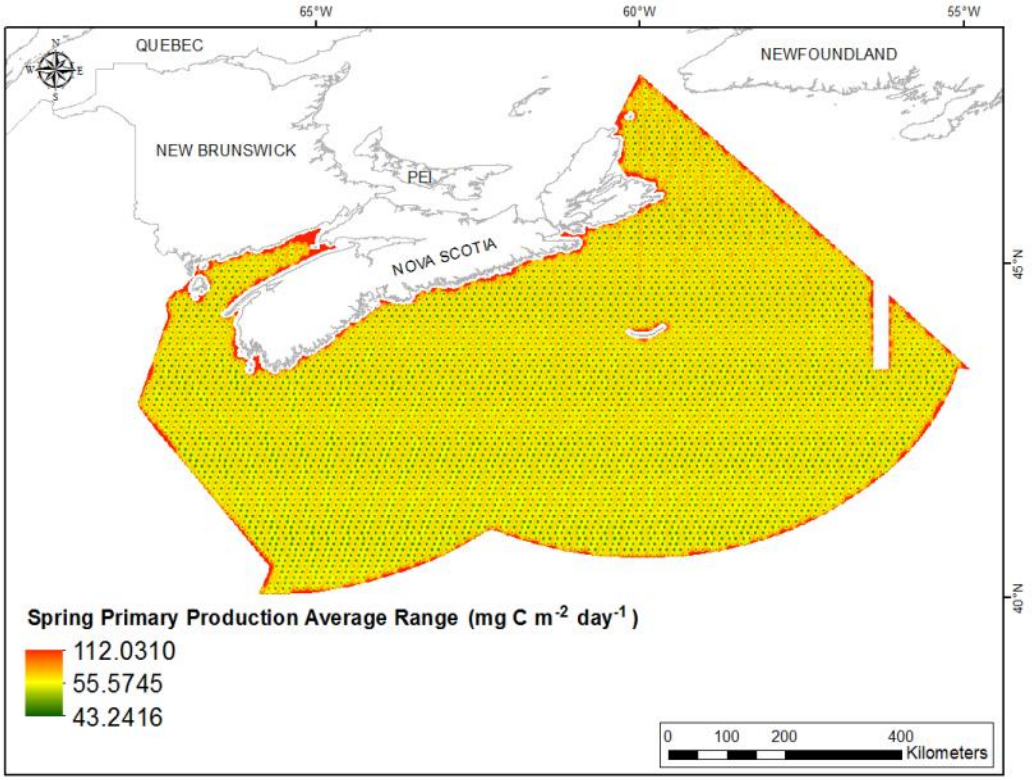

Fig. 404. Prediction standard error surface of Spring Primary Production Average Range (mg C m^{-2} day^{-1}).

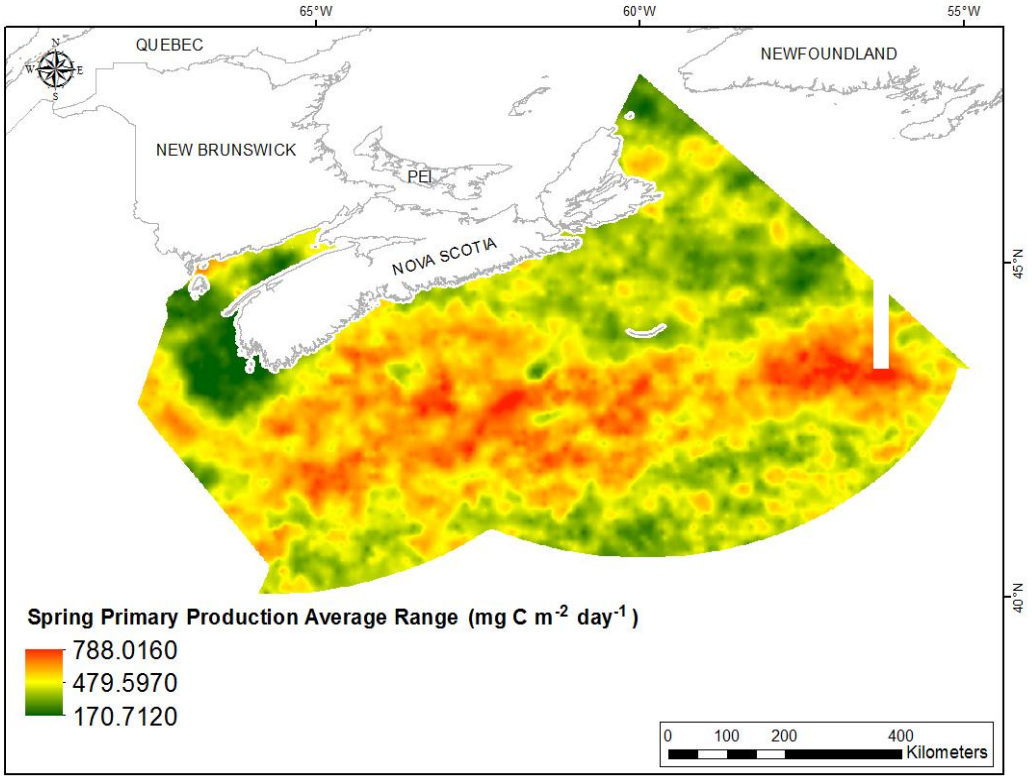

Fig. 405. Interpolated prediction surface of Spring Primary Production Average Range (mg C m^{-2} day^{-1}).

Summer Primary Production Mean

This variable displayed a bimodal distribution prior to interpolation (Table 163, Fig. 406). The data were higher than predicted by a normal distribution at mid- and the lowest range values and lower than predicted at low and the highest range values (Fig. 407). The areas of under- and over-prediction showed a spatial pattern over the study extent (Fig. 407).

The semivariogram showed moderate autocorrelation present in the data and the model showed a good fit between measured and predicted values (Fig. 408). Good performance of the model was indicated by the cross-validation results (Table 164). The error map showed moderate error across the study extent except at the exact location of data points where it was low (Fig. 409). The kriged surface is presented in Fig. 410.

Table 163. Distributional properties of Summer Primary Production Mean (mg C m^{-2} day^{-1}).

Property	Value
Number of Observations	5329
Minimum	415.900
Maximum	1239.700
Mean	791.130
Median	821.080
Standard Deviation	148.100
Skewness	-0.485
Kurtosis	2.486

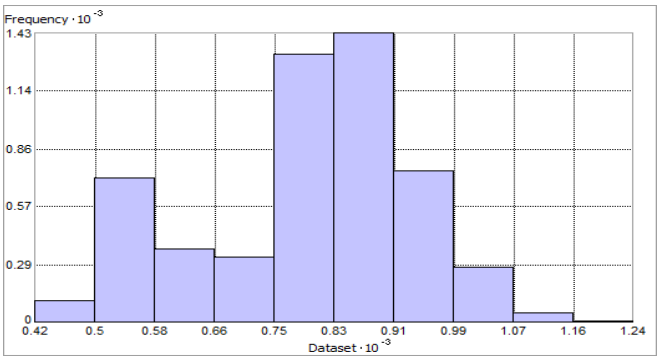

Fig. 406. Distribution of Summer Primary Production Mean (mg C m^{-2} day^{-1}). Histogram was illustrated using 10 bins. X and Y axes are shown at 10^{-3}.

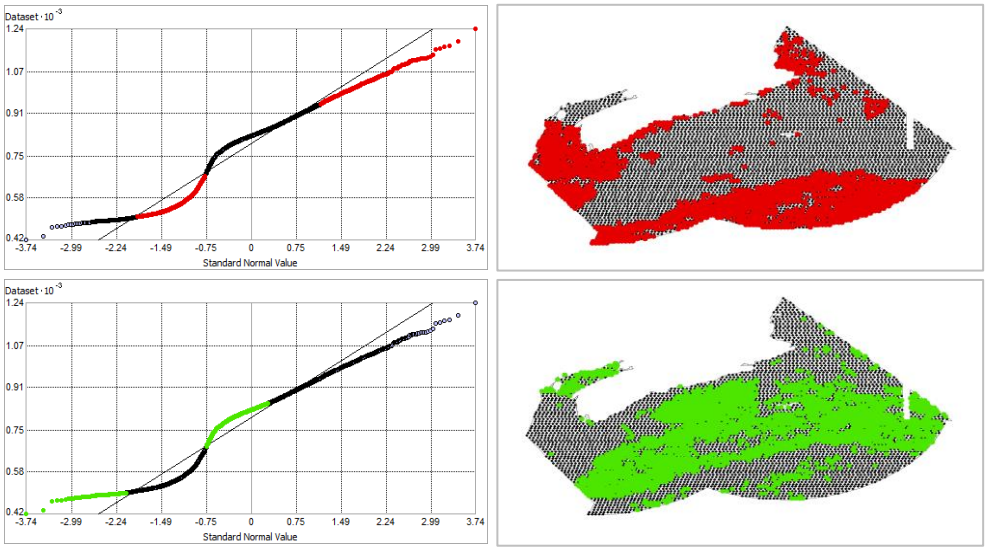

Fig. 407. Normal Q-Q plot for data values of Summer Primary Production Mean (mg C m^{-2} day^{-1}). Points falling under (upper panel) and over (bottom panel) the reference line are mapped.

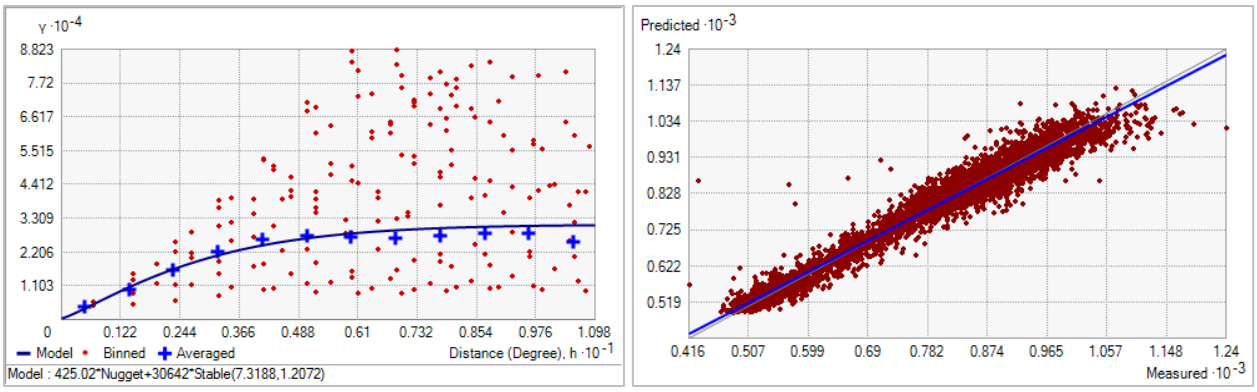

Fig. 408. Left panel: Semivariogram of Summer Primary Production Mean (mg C m^{-2} day^{-1}). Binned values are shown as red dots; average points are shown as blue crosses; the model fit to the averaged values is shown as a blue line. Lag size: 0.915 degrees; number of lags: 12; Parameter: 1.207; Range: 7.319 degrees; Partial Sill: 30641.890. Right panel: Scatterplot of predicted values versus observed values for the variable Summer Primary Production Mean (mg C m^{-2} day^{-1}).

Table 164. Results of cross-validation of the kriged model for Summer Primary Production Mean (mg C m^{-2} day^{-1}).

Prediction Error	**Value**
Number of Observations	5329
Overall Mean Error	-2.377×10^{-3}
Root Mean Square Prediction Error	32.427
Standardized Mean	-2.152×10^{-4}
Standardized Root Mean Square Prediction Error	1.105
Average Standard Error	29.153

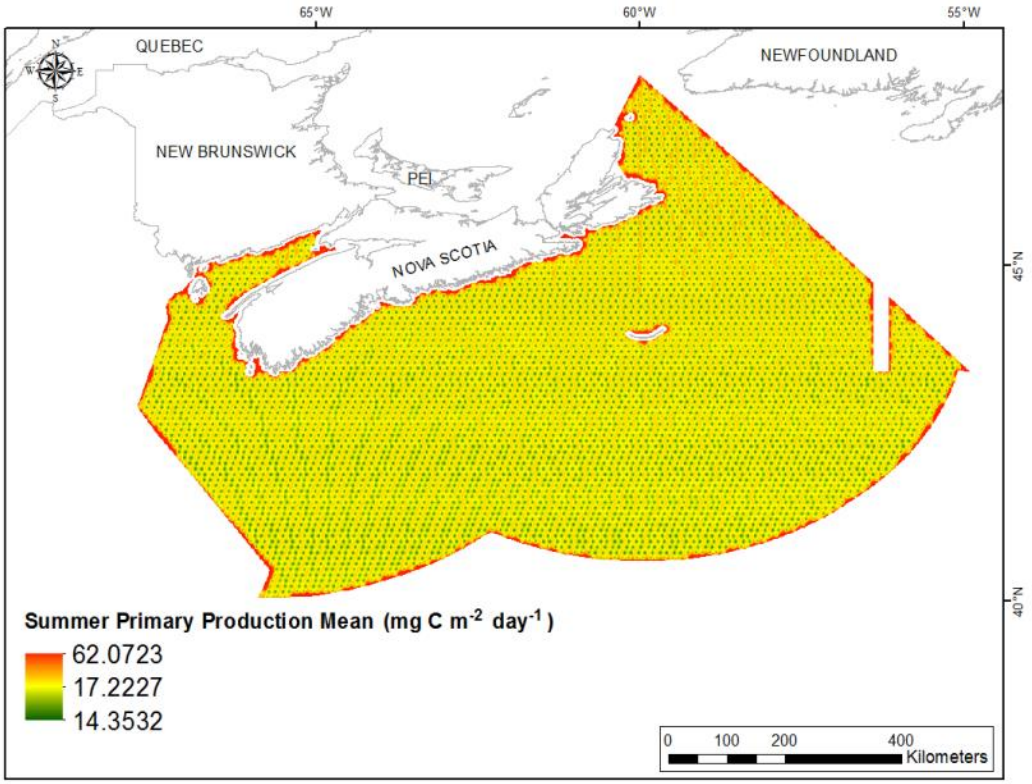

Fig. 409. Prediction standard error surface of Summer Primary Production Mean (mg C m^{-2} day^{-1}).

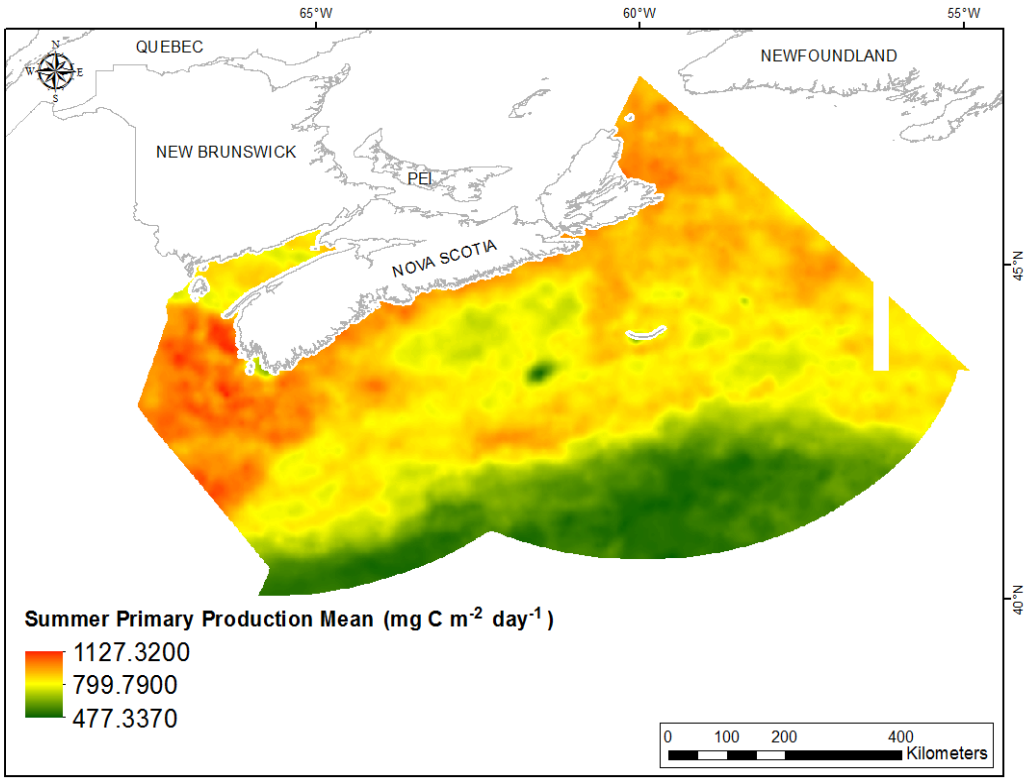

Fig. 410. Interpolated prediction surface of Summer Primary Production Mean (mg C m^{-2} day^{-1}).

Summer Primary Production Minimum

This variable displayed a platykurtic distribution prior to interpolation (Table 165, Fig. 411). The data were higher than predicted by a normal distribution at low and upper-mid range values and lower than predicted at mid and high values (Fig. 412). The areas of under- and over-prediction showed some spatial pattern over the study extent (Fig. 412).

The semivariogram showed moderate autocorrelation present in the data and the model showed good fit between measured and predicted values (Fig. 413). Good performance was indicated by the cross-validation results (Table 166). The error map showed high error along the edges of the study extent (Fig. 414). The kriged surface is presented in Fig. 415.

Table 165. Distributional properties of Summer Primary Production Minimum (mg C m^{-2} day^{-1}).

Property	Value
Number of Observations	5329
Minimum	174.090
Maximum	885.170
Mean	557.880
Median	571.680
Standard Deviation	118.250
Skewness	0.015
Kurtosis	1.889

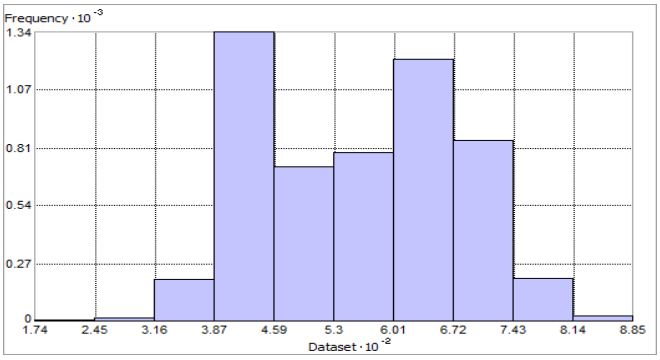

Fig. 411. Distribution of Summer Primary Production Minimum (mg C m^{-2} day^{-1}). Histogram was illustrated using 10 bins. X axis is shown at 10^{-2}; Y axis is shown at 10^{-3}.

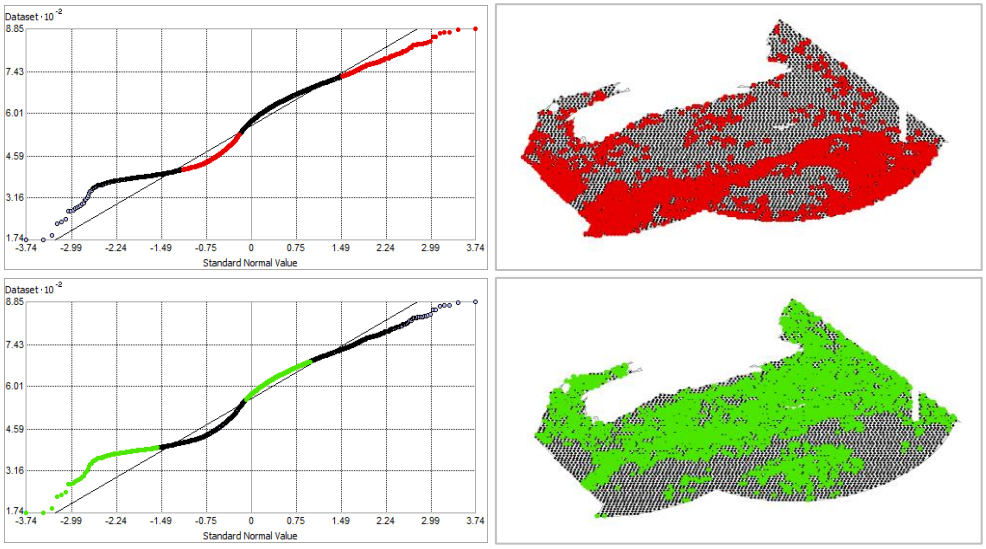

Fig. 412. Normal Q-Q plot for data values of Summer Primary Production Minimum (mg C m^{-2} day^{-1}). Points falling under (upper panel) and over (bottom panel) the reference line are mapped.

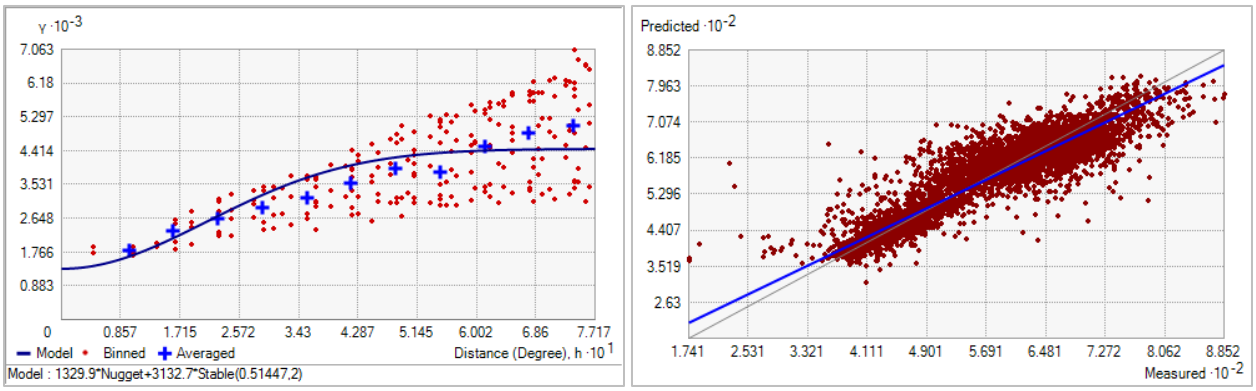

Fig. 413. Left panel: Semivariogram of Summer Primary Production Minimum (mg C m^{-2} day^{-1}). Binned values are shown as red dots; average points are shown as blue crosses; the model fit to the averaged values is shown as a blue line. Lag size: 0.064 degrees; number of lags: 12; Parameter: 2; Range: 0.514 degrees; Partial Sill: 3132.746. Right panel: Scatterplot of predicted values versus observed values for the variable Summer Primary Production Minimum (mg C m^{-2} day^{-1}).

Table 166. Results of cross-validation of the kriged model for Summer Primary Production Minimum (mg C m^{-2} day^{-1}).

Prediction error	**Value**
Number of Observations	5329
Overall Mean Error	0.070 x 10^{-6}
Root Mean Square Prediction Error	43.931
Standardized Mean	1.687 x 10^{-3}
Standardized Root Mean Square Prediction Error	1.089
Average Standard Error	40.254

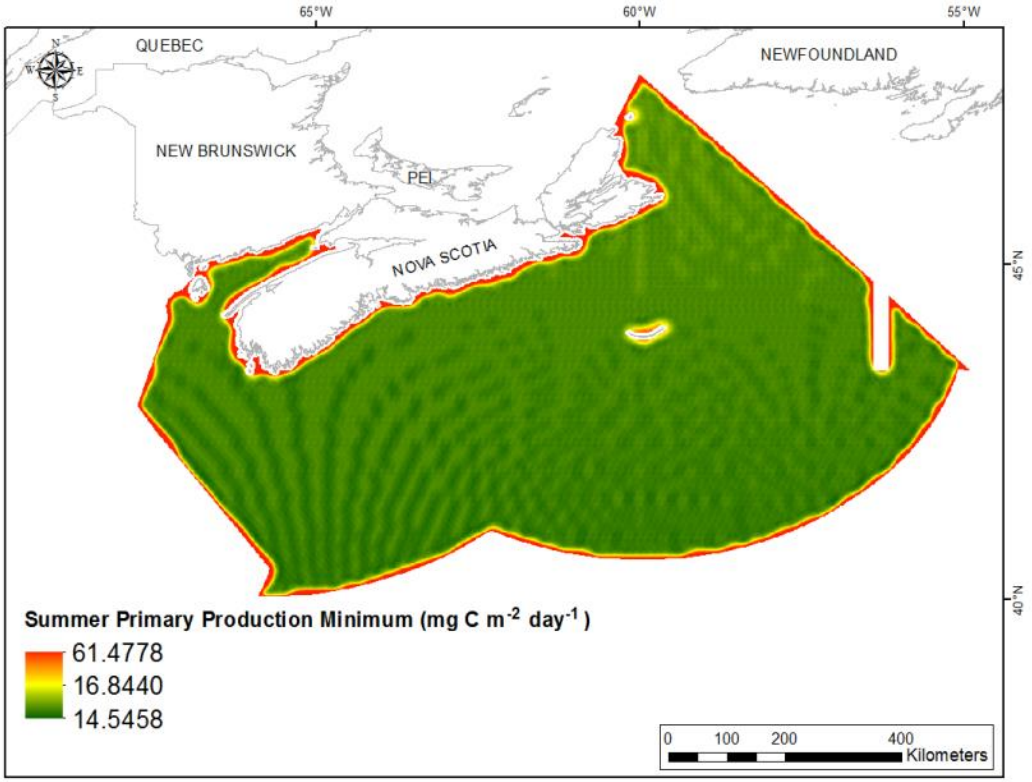

Fig. 414. Prediction standard error surface of Summer Primary Production Minimum (mg C m^{-2} day^{-1}).

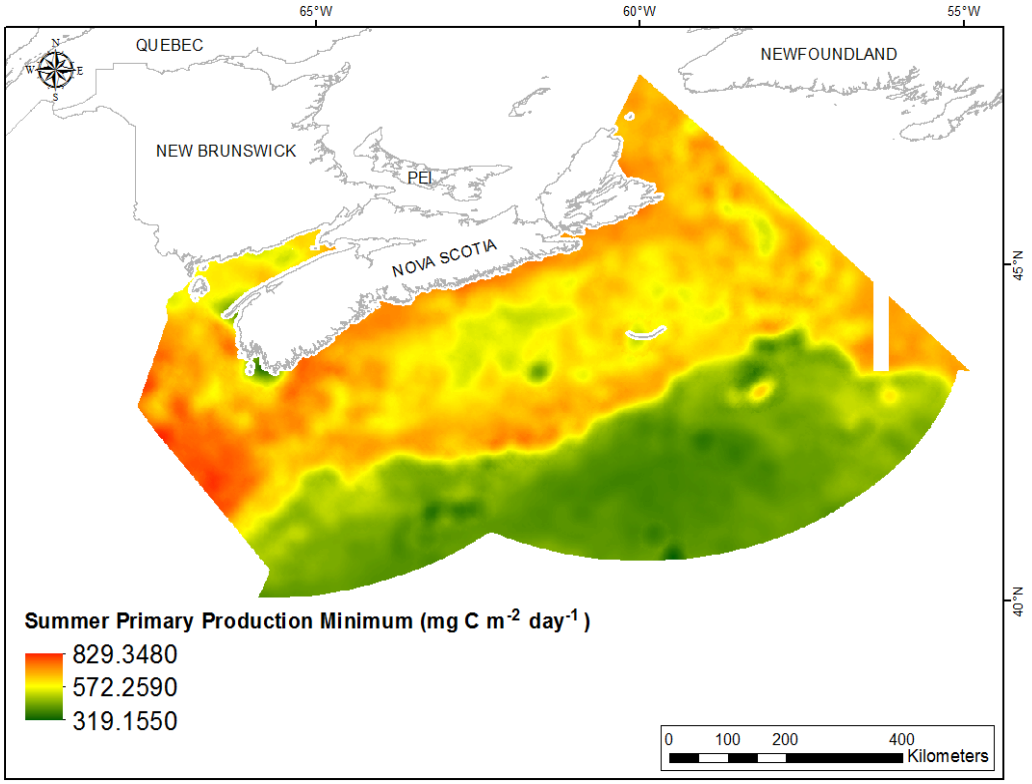

Fig. 415. Interpolated prediction surface of Summer Primary Production Minimum (mg C m^{-2} day^{-1}).

Summer Primary Production Maximum

This variable displayed a near-normal, but slightly platykurtic distribution prior to interpolation (Table 167, Fig. 416). The data were higher than predicted by a normal distribution at lower and upper-mid ranges and lower than predicted at high values (Fig. 417). The areas of under- and over-prediction showed no spatial pattern over the study extent (Fig. 417).

The semivariogram showed moderate autocorrelation present in the data (Fig. 418). The fit between measured and predicted values was fair (Fig. 418), with under-prediction of large values and over-prediction of small values. Good performance of the model was indicated by the cross-validation results (Table 168). The error map showed high error along the edges of the study extent (Fig. 419). The kriged surface is presented in Fig. 420.

Table 167. Distributional properties of Summer Primary Production Maximum (mg C m^{-2} day^{-1}).

Property	Value
Number of Observations	5329
Minimum	499.520
Maximum	1944.800
Mean	1187
Median	1175.800
Standard Deviation	273.140
Skewness	-0.010
Kurtosis	2.526

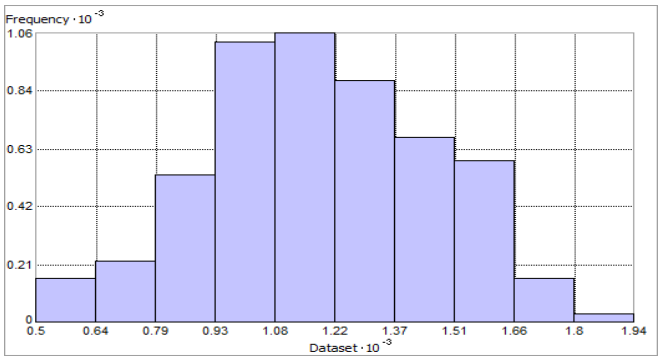

Fig. 416. Distribution of Summer Primary Production Maximum (mg C m^{-2} day^{-1}). Histogram was illustrated using 10 bins. X and Y axes are shown at 10^{-3}.

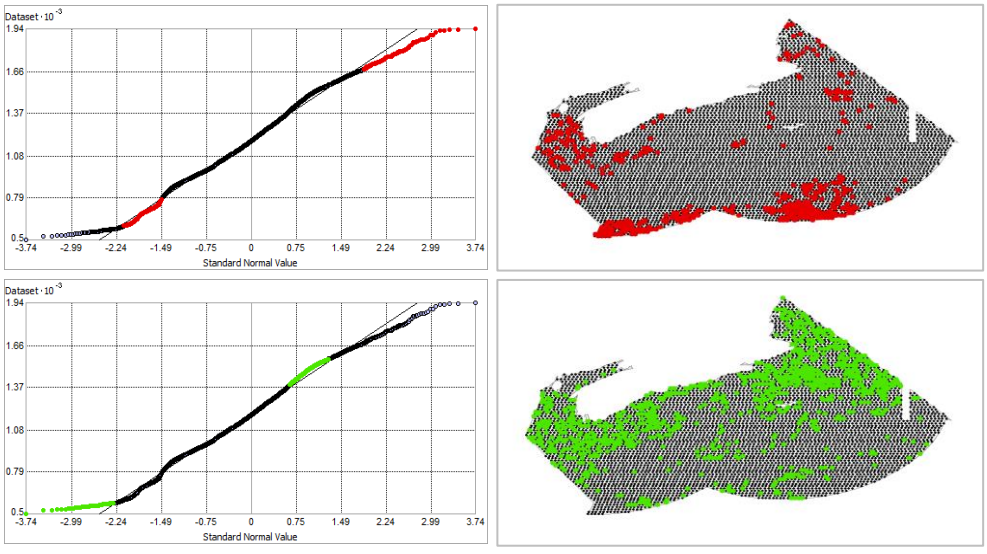

Fig. 417. Normal Q-Q plot for data values of Summer Primary Production Maximum (mg C m^{-2} day^{-1}). Points falling under (upper panel) and over (bottom panel) the reference line are mapped.

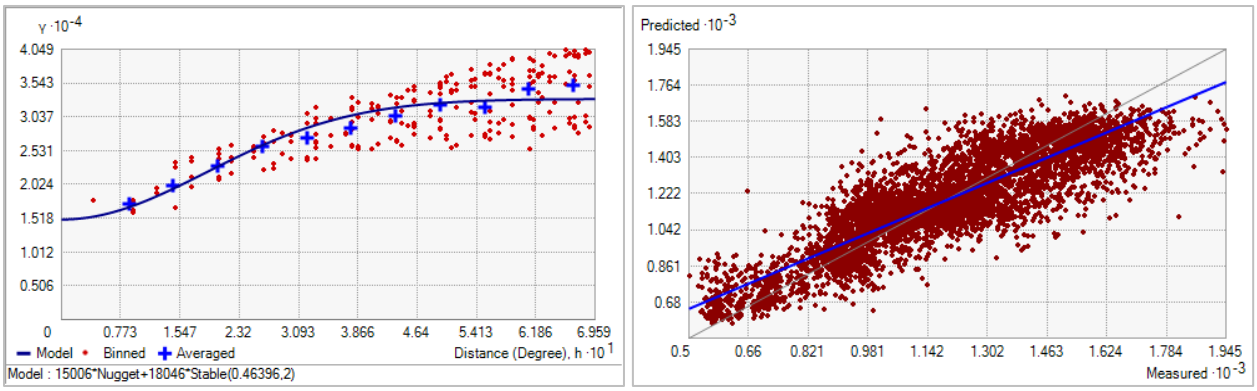

Fig. 418. Left panel: Semivariogram of Summer Primary Production Maximum (mg C m^{-2} day^{-1}). Binned values are shown as red dots; average points are shown as blue crosses; the model fit to the averaged values is shown as a blue line. Lag size: 0.058 degrees; number of lags: 12; Parameter: 2; Range: 0.464 degrees; Partial Sill: 18045.730. Right panel: Scatterplot of predicted values versus observed values for the variable Summer Primary Production Maximum (mg C m^{-2} day^{-1}).

Table 168. Results of cross-validation of the kriged model for Summer Primary Production Maximum (mg C m^{-2} day^{-1}).

Prediction error	**Value**
Number of Observations	5329
Overall Mean Error	0.016
Root Mean Square Prediction Error	137.618
Standardized Mean	-9.482×10^{-5}
Standardized Root Mean Square Prediction Error	1.027
Average Standard Error	133.835

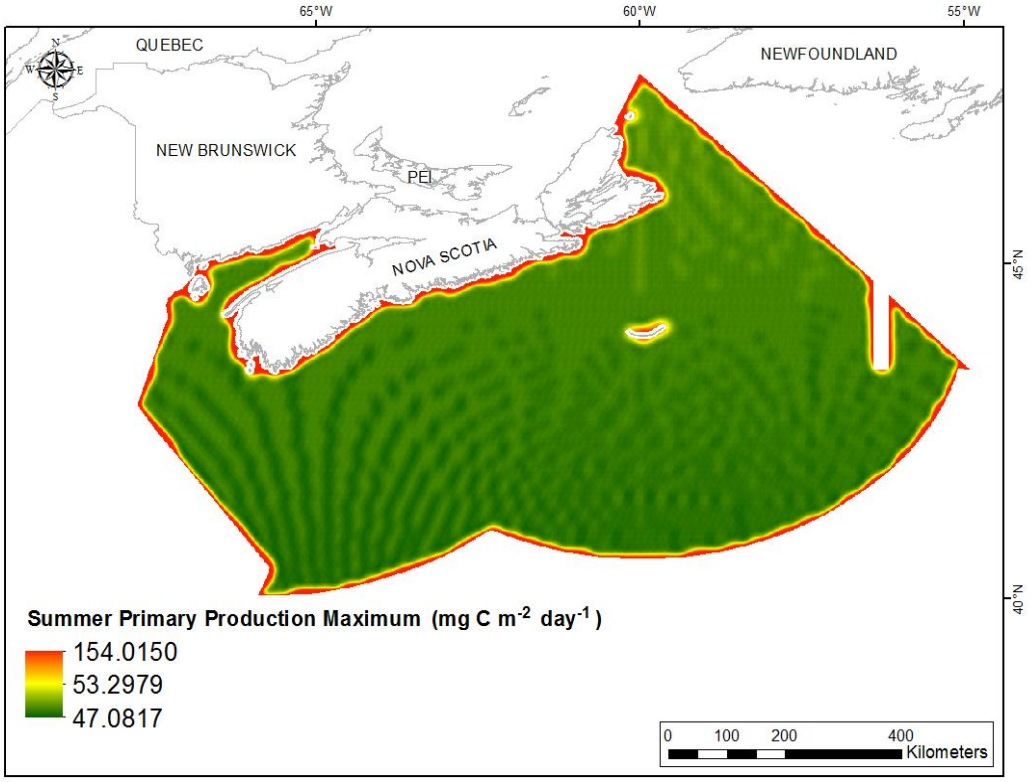

Fig. 419. Prediction standard error surface of Summer Primary Production Maximum (mg C m^{-2} day^{-1}).

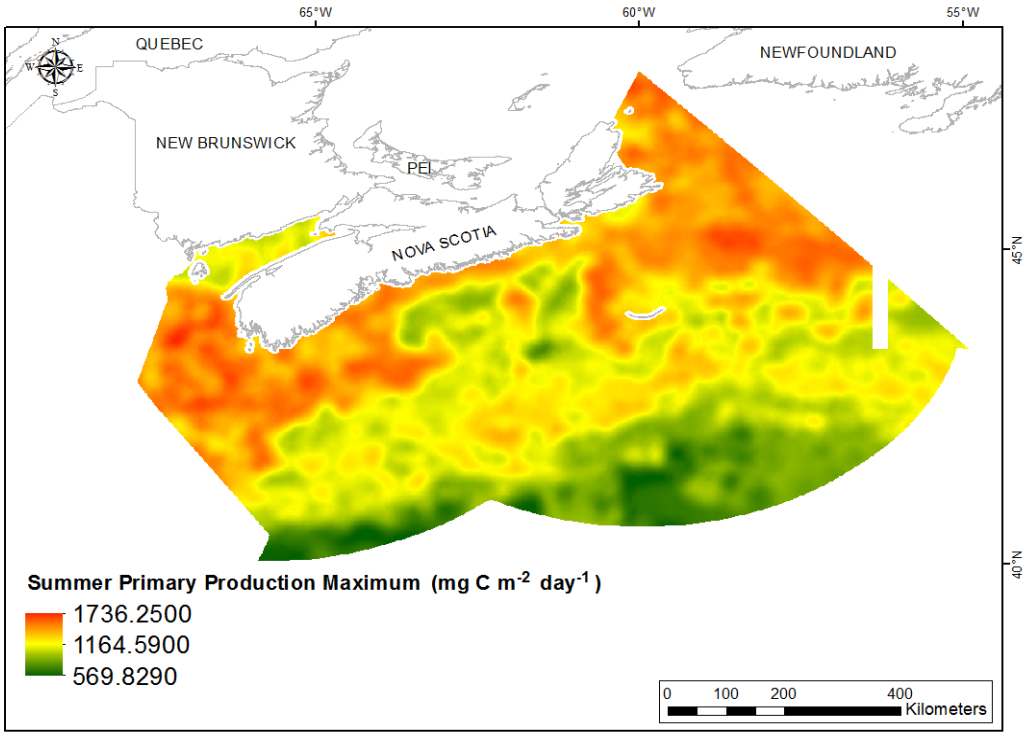

Fig. 420. Interpolated prediction surface of Summer Primary Production Maximum (mg C m^{-2} day^{-1}).

Summer Primary Production Range

This variable displayed a near-normal, but slightly platykurtic distribution prior to interpolation (Table 169, Fig. 421). The data were higher than predicted by a normal distribution at the lowest values and slightly lower than predicted at the highest values (Fig. 422). The areas of under- and over-prediction showed some spatial pattern over the study extent (Fig. 422).

The semivariogram showed autocorrelation present in the data (Fig. 423). The fit between measured and predicted values was fair (Fig. 423), with under-prediction of large values and over-prediction of small values. Excellent performance of the model was indicated by the cross-validation results (Table 170). The error map showed moderate error over the study extent (Fig. 424). The kriged surface is presented in Fig. 425.

Table 169. Distributional properties of Summer Primary Production Range (mg C m^{-2} day^{-1}).

Property	Value
Number of Observations	5329
Minimum	105.300
Maximum	1430.700
Mean	629.090
Median	611.830
Standard Deviation	224.440
Skewness	0.143
Kurtosis	2.517

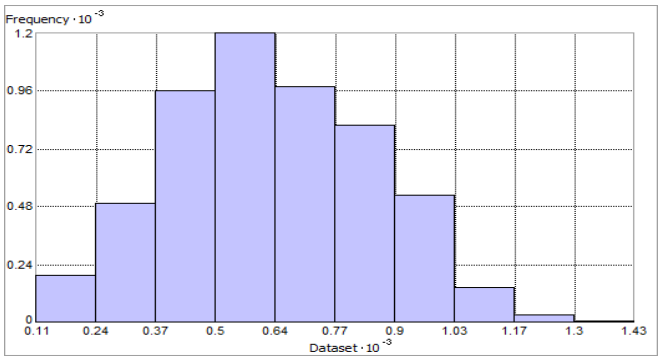

Fig. 421. Distribution of Summer Primary Production Range (mg C m^{-2} day^{-1}). Histogram was illustrated using 10 bins. X and Y axes are shown at 10^{-3}.

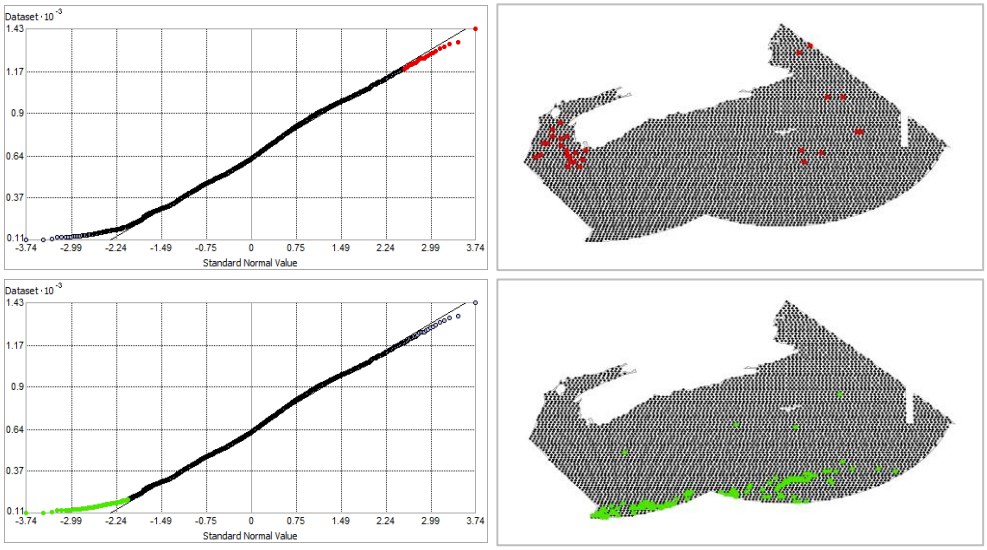

Fig. 422. Normal Q-Q plot for data values of Summer Primary Production Range (mg C m^{-2} day^{-1}). Points falling under (upper panel) and over (bottom panel) the reference line are mapped.

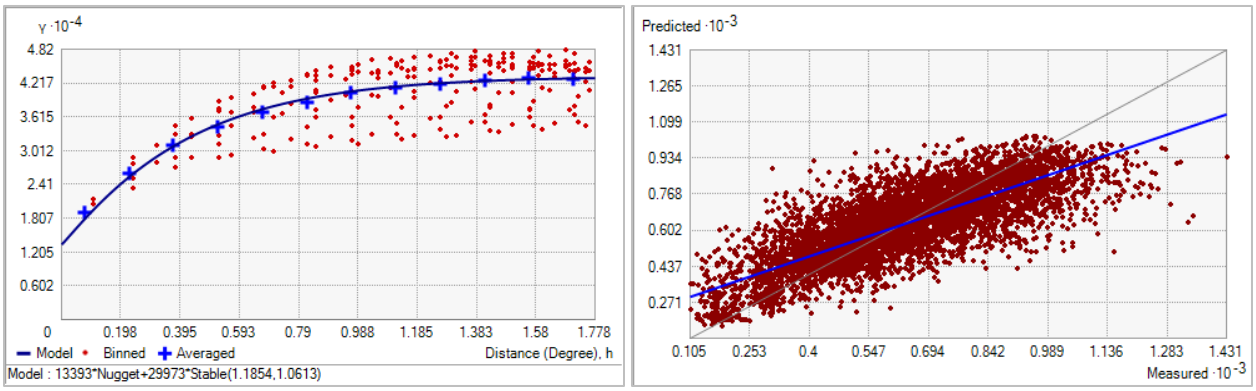

Fig. 423. Left panel: Semivariogram of Summer Primary Production Range (mg C m^{-2} day^{-1}). Binned values are shown as red dots; average points are shown as blue crosses; the model fit to the averaged values is shown as a blue line. Lag size: 0.148 degrees; number of lags: 12; Parameter: 1.061; Range: 1.185 degrees; Partial Sill: 29972.610. Right panel: Scatterplot of predicted values versus observed values for the variable Summer Primary Production Range (mg C m^{-2} day^{-1}).

Table 170. Results of cross-validation of the kriged model for Summer Primary Production Range (mg C m^{-2} day^{-1}).

Prediction error	**Value**
Number of Observations	5329
Overall Mean Error	0.082
Root Mean Square Prediction Error	142.571
Standardized Mean	3.990×10^{-4}
Standardized Root Mean Square Prediction Error	1.000
Average Standard Error	142.549

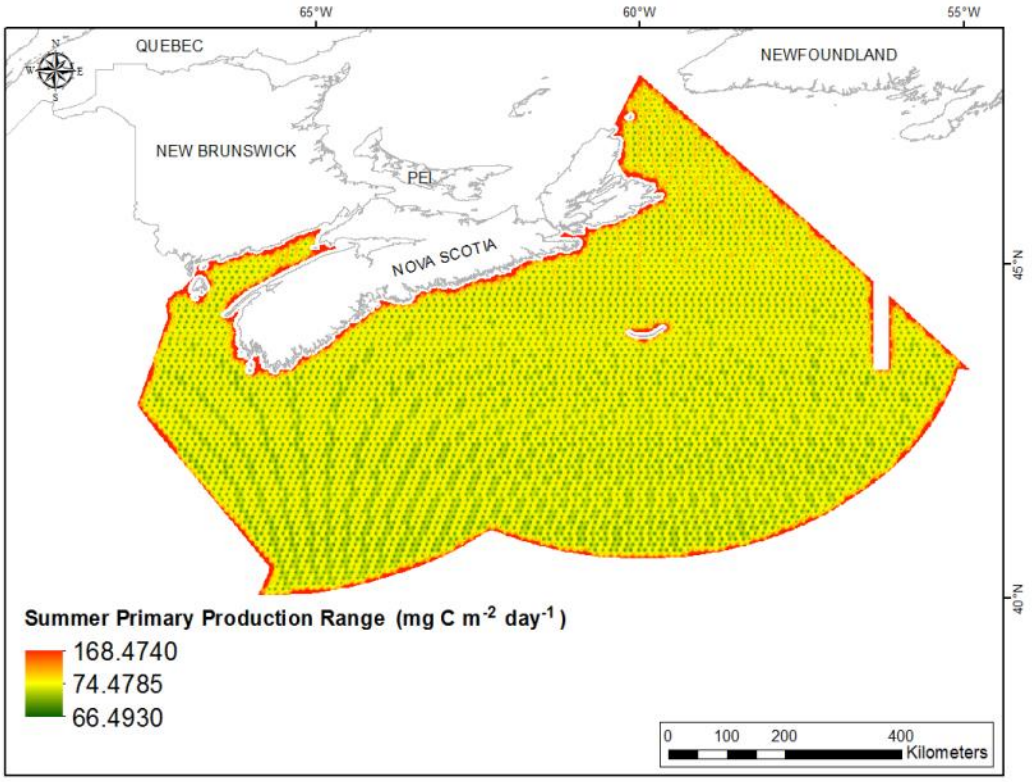

Fig. 424. Prediction standard error surface of Summer Primary Production Range (mg C m^{-2} day^{-1}).

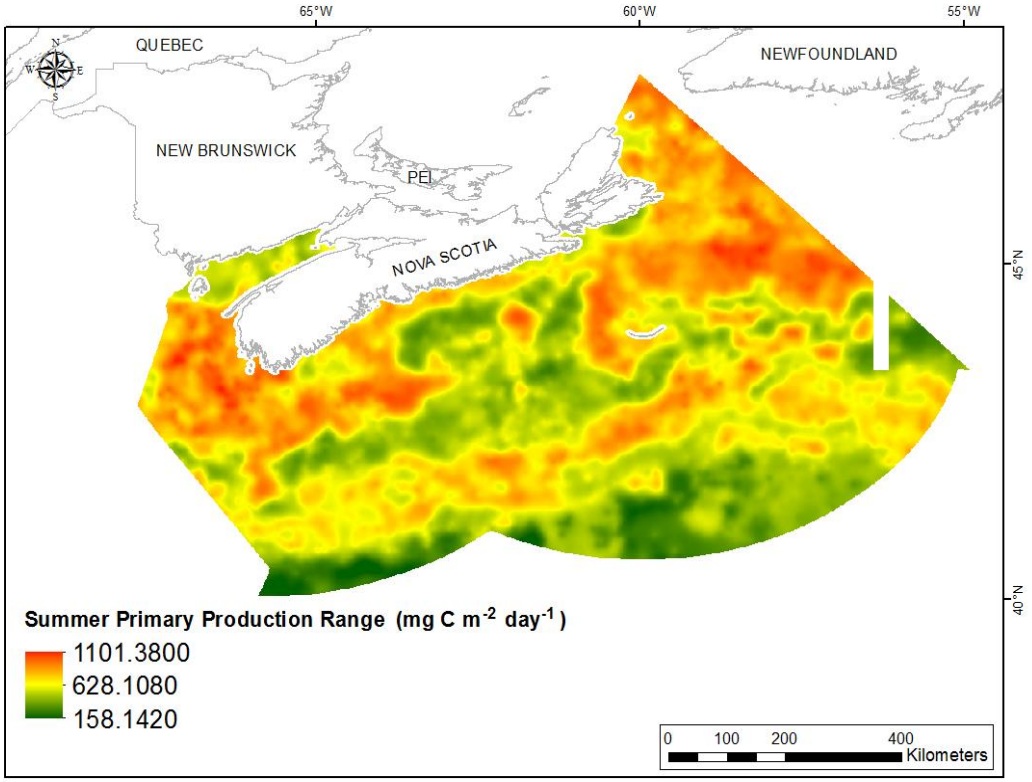

Fig. 425. Interpolated prediction surface of Summer Primary Production Range (mg C m^{-2} day^{-1}).

Summer Primary Production Average Minimum

This variable displayed a left-skewed, bimodal distribution prior to interpolation (Table 171, Fig. 426). The data were lower than predicted by a normal distribution at high and mid-values, and higher than predicted at low and upper mid-range values (Fig. 427). The areas of under- and over-prediction showed some spatial pattern over the study extent (Fig. 427).

The semivariogram showed moderate autocorrelation present in the data and the model showed a good fit between measured and predicted values (Fig. 428). Good performance of the model was indicated by the cross-validation results (Table 172). The error map showed moderate error across the study extent (Fig. 429). The kriged surface is presented in Fig. 430.

Table 171. Distributional properties of Summer Primary Production Average Minimum (mg C m^{-2} day^{-1}).

Property	Value
Number of Observations	5329
Minimum	312.630
Maximum	1086.200
Mean	667.350
Median	700.870
Standard Deviation	125.040
Skewness	-0.436
Kurtosis	2.260

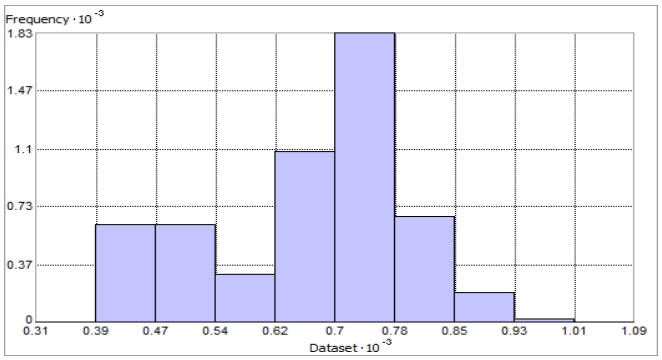

Fig. 426. Distribution of Summer Primary Production Average Minimum (mg C m^{-2} day^{-1}). Histogram was illustrated using 10 bins. X and Y axes are shown at 10^{-3}.

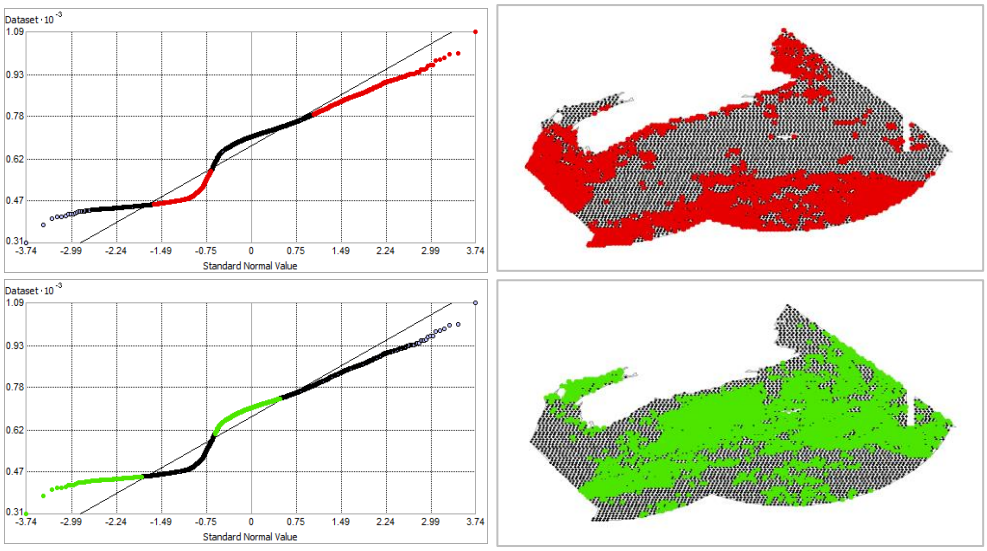

Fig. 427. Normal Q-Q plot for data values of Summer Primary Production Average Minimum (mg C m^{-2} day^{-1}). Points falling under (upper panel) and over (bottom panel) the reference line are mapped.

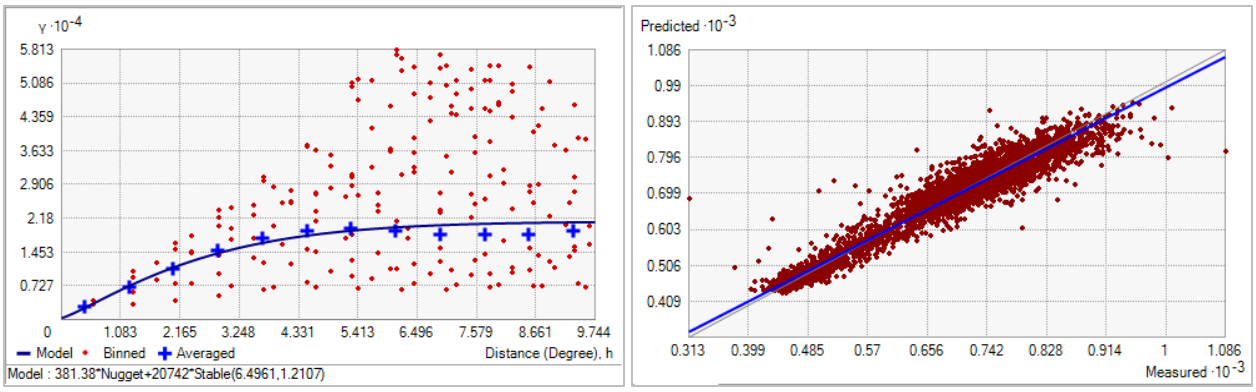

Fig. 428. Left panel: Semivariogram of Summer Primary Production Average Minimum (mg C m^{-2} day^{-1}). Binned values are shown as red dots; average points are shown as blue crosses; the model fit to the averaged values is shown as a blue line. Lag size: 0.812 degrees; number of lags: 12; Parameter: 1.211; Range: 6.496 degrees; Partial Sill: 20741.640. Right panel: Scatterplot of predicted values versus observed values for the model of Summer Primary Production Average Minimum (mg C m^{-2} day^{-1}).

Table 172. Results of cross-validation of the kriged model for Summer Primary Production Average Minimum (mg C m^{-2} day^{-1}).

Prediction error	**Value**
Number of Observations	5329
Overall Mean Error	-0.014
Root Mean Square Prediction Error	29.697
Standardized Mean	-4.849×10^{-4}
Standardized Root Mean Square Prediction Error	1.100
Average Standard Error	26.785

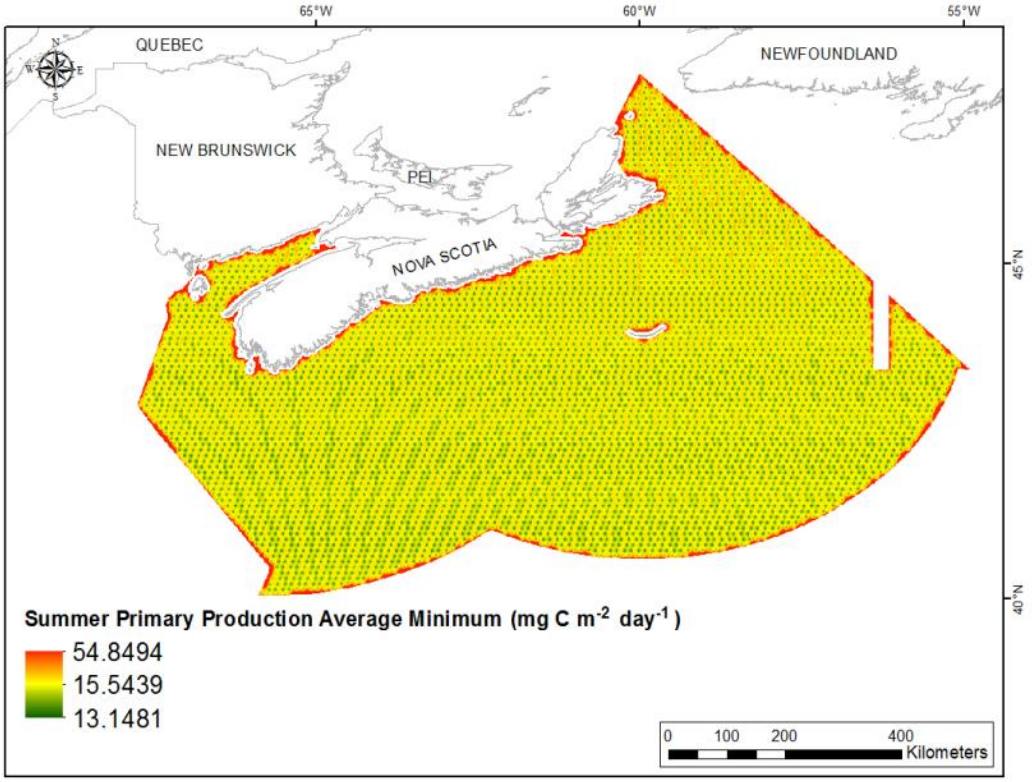

Fig. 429. Prediction standard error surface of Summer Primary Production Average Minimum (mg C m^{-2} day^{-1}).

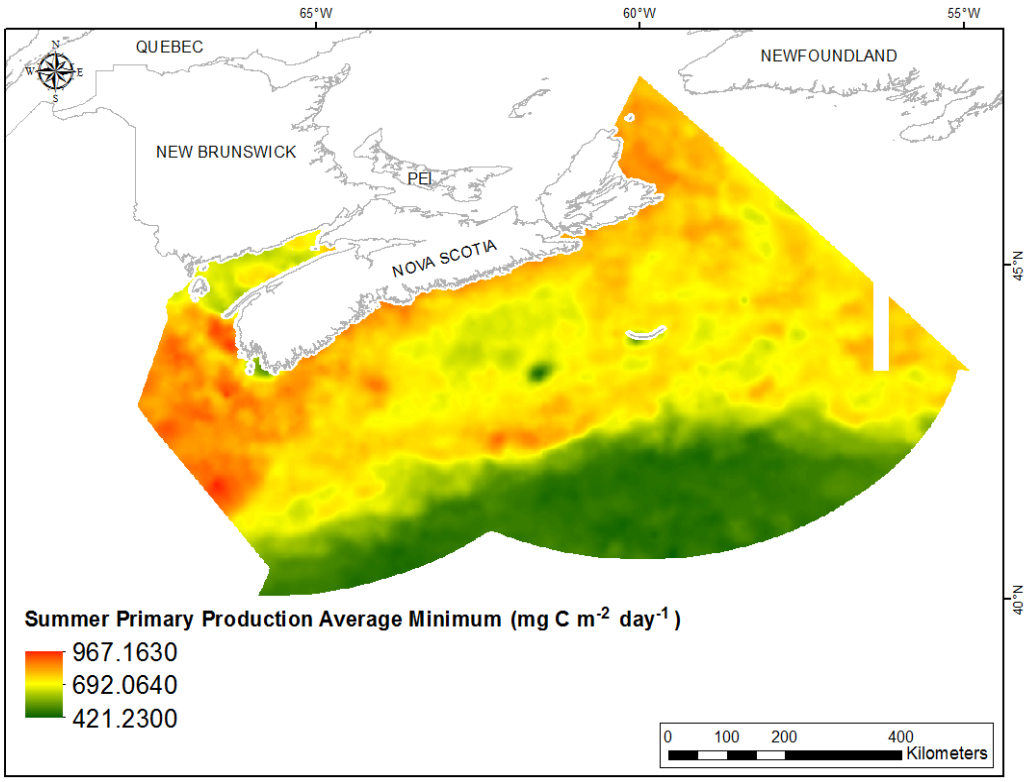

Fig. 430. Interpolated prediction surface of Summer Primary Production Average Minimum (mg C m^{-2} day^{-1}).

Summer Primary Production Average Maximum

This variable displayed a slightly left-skewed, platykurtic distribution prior to interpolation (Table 173, Fig. 431). The data were higher than predicted by a normal distribution at low and upper mid-range values and lower than predicted at high and mid-range values (Fig. 432). The areas of under- and over-prediction showed some spatial pattern over the study extent (Fig. 432).

The semivariogram showed weak autocorrelation present in the data and the model showed a good fit between measured and predicted values (Fig. 433). Good performance of the model was indicated by the cross-validation results (Table 174). The error map showed moderate error across the study extent (Fig. 434). The kriged surface is presented in Fig. 435.

Table 173. Distributional properties of Summer Primary Production Average Maximum (mg C m^{-2} day^{-1}).

Property	Value
Number of Observations	5329
Minimum	449.760
Maximum	1562.700
Mean	931.720
Median	948.430
Standard Deviation	189.100
Skewness	-0.310
Kurtosis	2.678

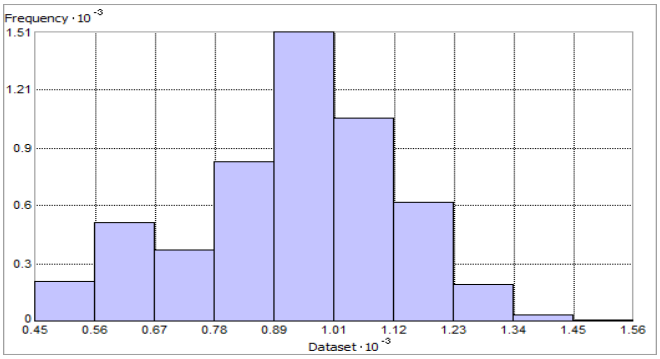

Fig. 431. Distribution of Summer Primary Production Average Maximum (mg C m^{-2} day^{-1}). Histogram was illustrated using 10 bins. X and Y axes are shown at 10^{-3}.

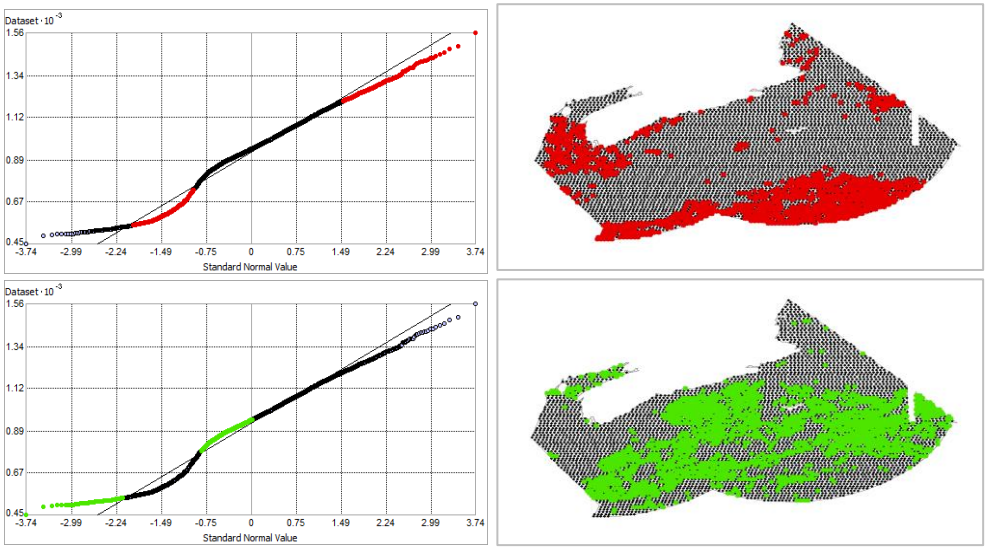

Fig. 432. Normal Q-Q plot for data values of Summer Primary Production Average Maximum (mg C m^{-2} day^{-1}). Points falling under (upper panel) and over (bottom panel) the reference line are mapped.

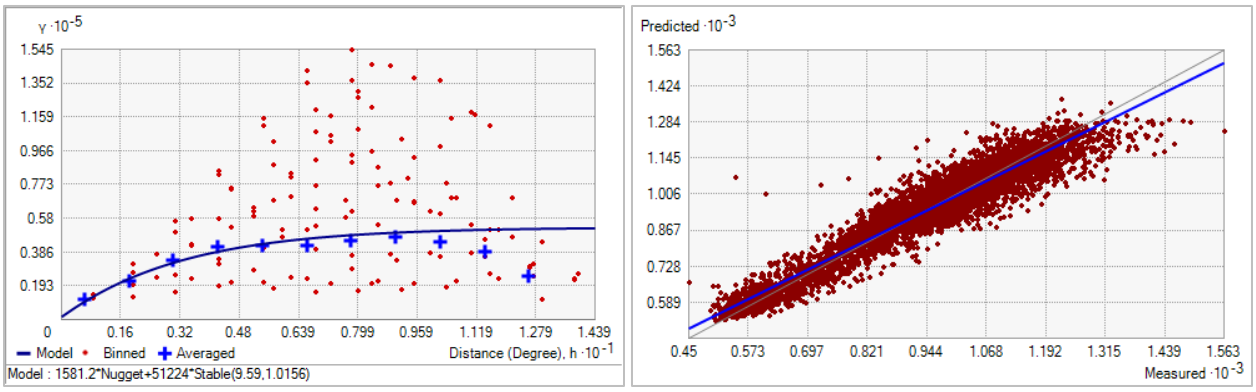

Fig. 433. Left panel: Semivariogram of Summer Primary Production Average Maximum (mg C m^{-2} day^{-1}). Binned values are shown as red dots; average points are shown as blue crosses; the model fit to the averaged values is shown as a blue line. Lag size: 1.199 degrees; number of lags: 12; Parameter: 1.016; Range: 9.590 degrees; Partial Sill: 51223.870. Right panel: Scatterplot of predicted values versus observed values for the model of Summer Primary Production Average Maximum (mg C m^{-2} day^{-1}).

Table 174. Results of cross-validation of the kriged model for Summer Primary Production Average Maximum (mg C m^{-2} day^{-1}).

Prediction error	**Value**
Number of Observations	5329
Overall Mean Error	0.011
Root Mean Square Prediction Error	59.528
Standardized Mean	1.635×10^{-5}
Standardized Root Mean Square Prediction Error	1.079
Average Standard Error	54.985

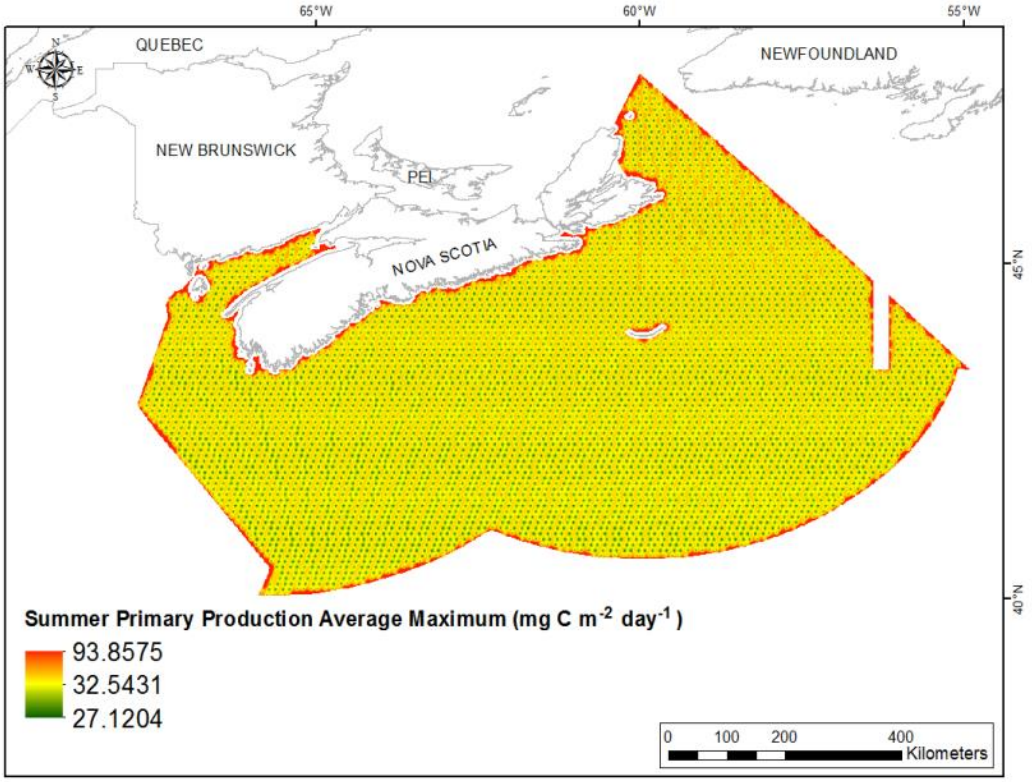

Fig. 434. Prediction standard error surface of Summer Primary Production Average Maximum (mg C m^{-2} day^{-1}).

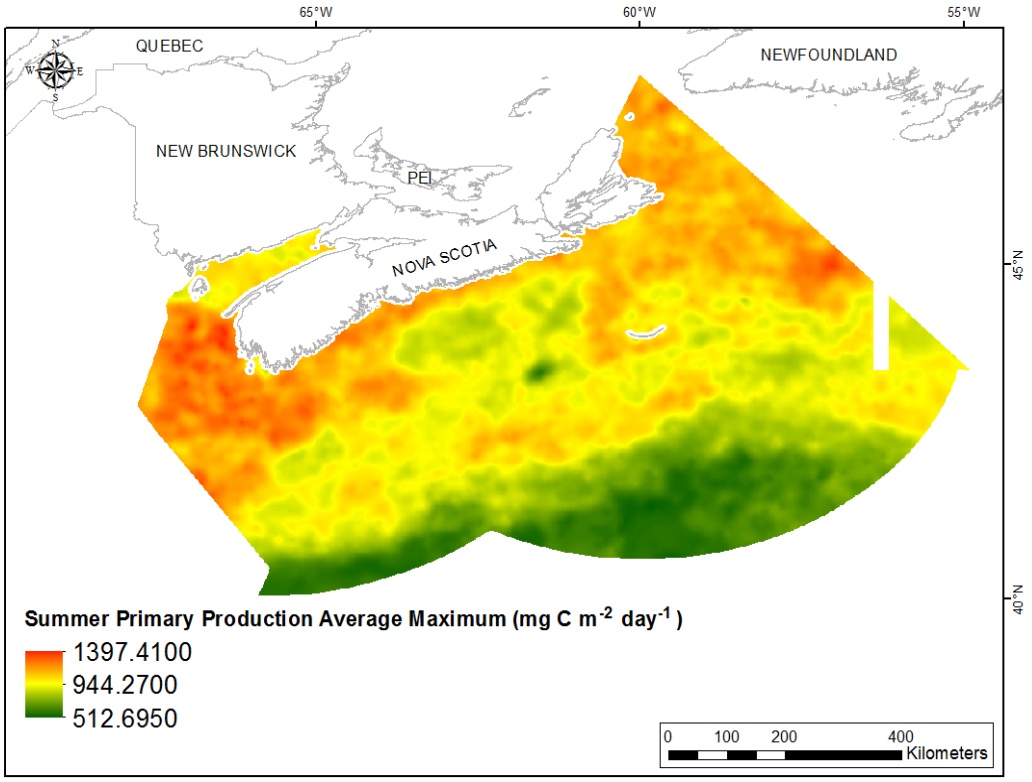

Fig. 435. Interpolated prediction surface of Summer Primary Production Average Maximum (mg C m^{-2} day^{-1}).

Summer Primary Production Average Range

This variable displayed a right-skewed distribution prior to interpolation (Table 175, Fig. 436). The data were higher than predicted by a normal distribution at both tails (Fig. 437). No data points fell below the reference line. The areas of over-prediction showed no strong spatial pattern over the study extent (Fig. 437).

The semivariogram showed weak autocorrelation present in the data (Fig. 438). The fit between measured and predicted values was fair (Fig. 438), with under-prediction of large values and over-prediction of small values. Good performance of the model was indicated by the cross-validation statistics (Table 176). The error map showed moderate error across the study extent (Fig. 439). The kriged surface is presented in Fig. 440.

Table 175. Distributional properties of Summer Primary Production Average Range (mg C m^{-2} day^{-1}).

Property	Value
Number of Observations	5329
Minimum	31.300
Maximum	784.230
Mean	264.37
Median	255.880
Standard Deviation	105.03
Skewness	0.441
Kurtosis	3.061

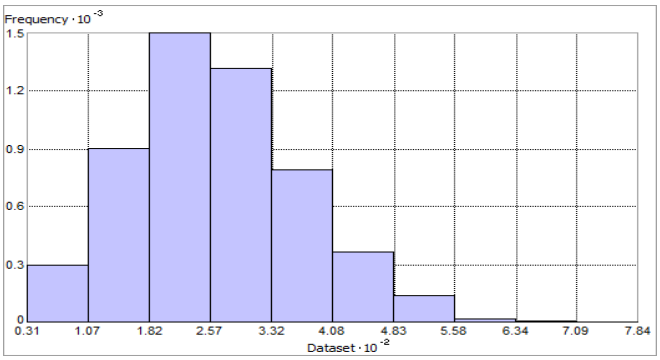

Fig. 436. Distribution of Summer Primary Production Average Range (mg C m^{-2} day^{-1}). Histogram was illustrated using 10 bins. X axis is shown at 10^{-2}; Y axis is shown at 10^{-3}.

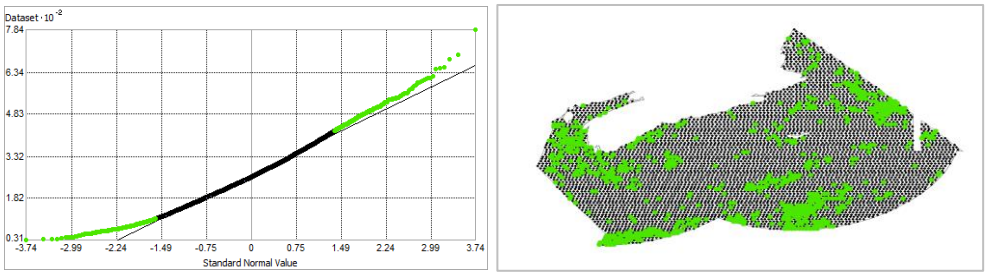

Fig. 437. Normal Q-Q plot for data values of Summer Primary Production Average Range (mg C m^{-2} day^{-1}). Points falling over (bottom panel) the reference line are mapped; no points fall under the reference line.

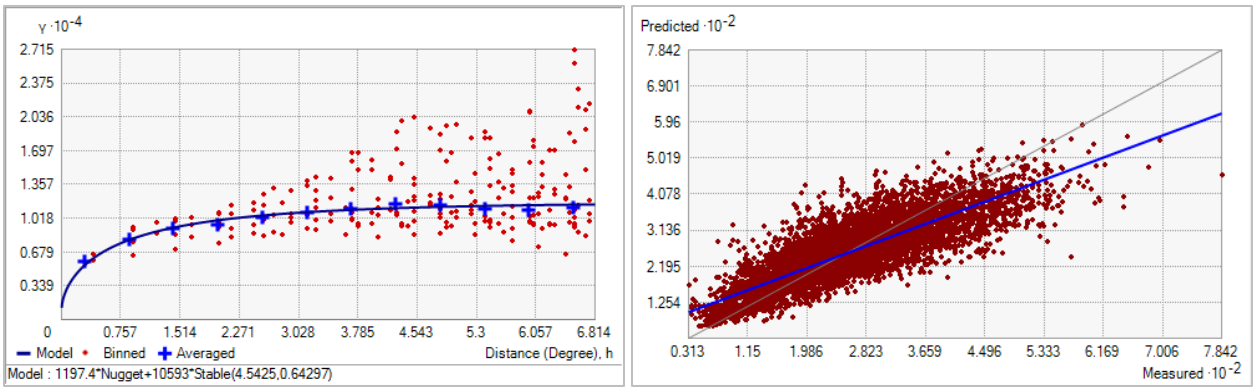

Fig. 438. Left panel: Semivariogram of Summer Primary Production Average Range (mg C m^{-2} day^{-1}). Binned values are shown as red dots; average points are shown as blue crosses; the model fit to the averaged values is shown as a blue line. Lag size: 0.568 degrees; number of lags: 12; Parameter: 0.643; Range: 4.543 degrees; Partial Sill: 10593.400. Right panel: Scatterplot of predicted values versus observed values for the model of Summer Primary Production Average Range (mg C m^{-2} day^{-1}).

Table 176. Results of cross-validation of the kriged model for Summer Primary Production Average Range (mg C m^{-2} day^{-1}).

Prediction error	**Value**
Number of Observations	5329
Overall Mean Error	0.027
Root Mean Square Prediction Error	60.608
Standardized Mean	3.176×10^{-4}
Standardized Root Mean Square Prediction Error	0.983
Average Standard Error	61.560

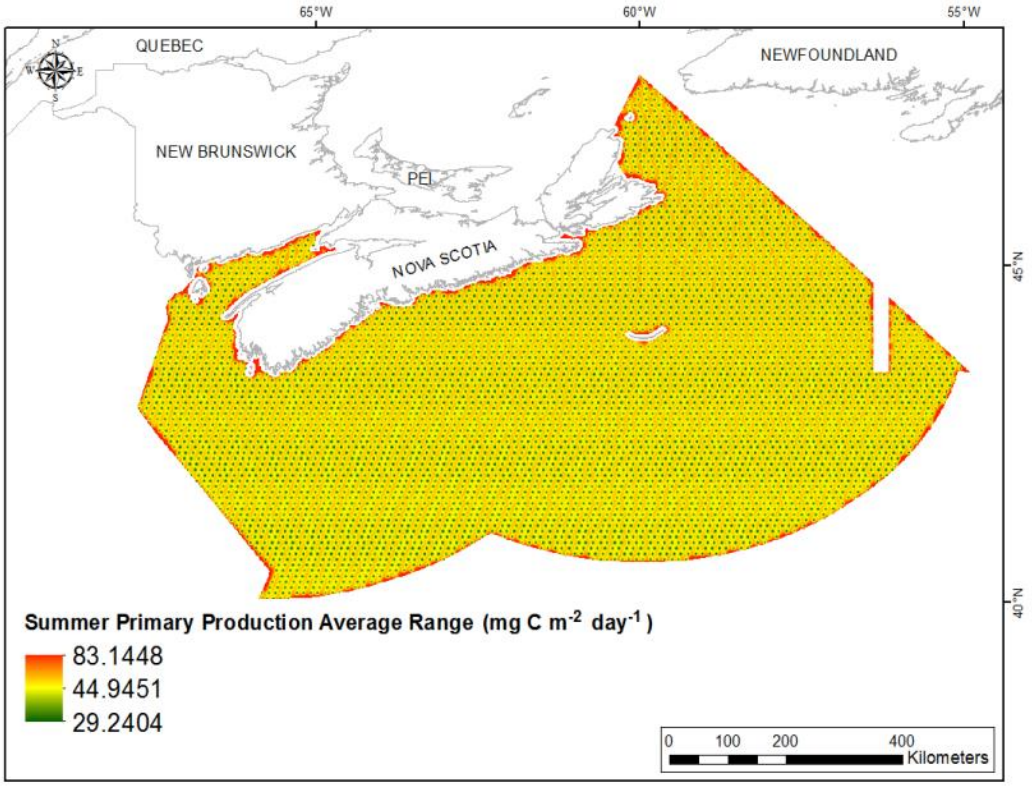

Fig. 439. Prediction standard error surface of Summer Primary Production Average Range (mg C m^{-2} day^{-1}).

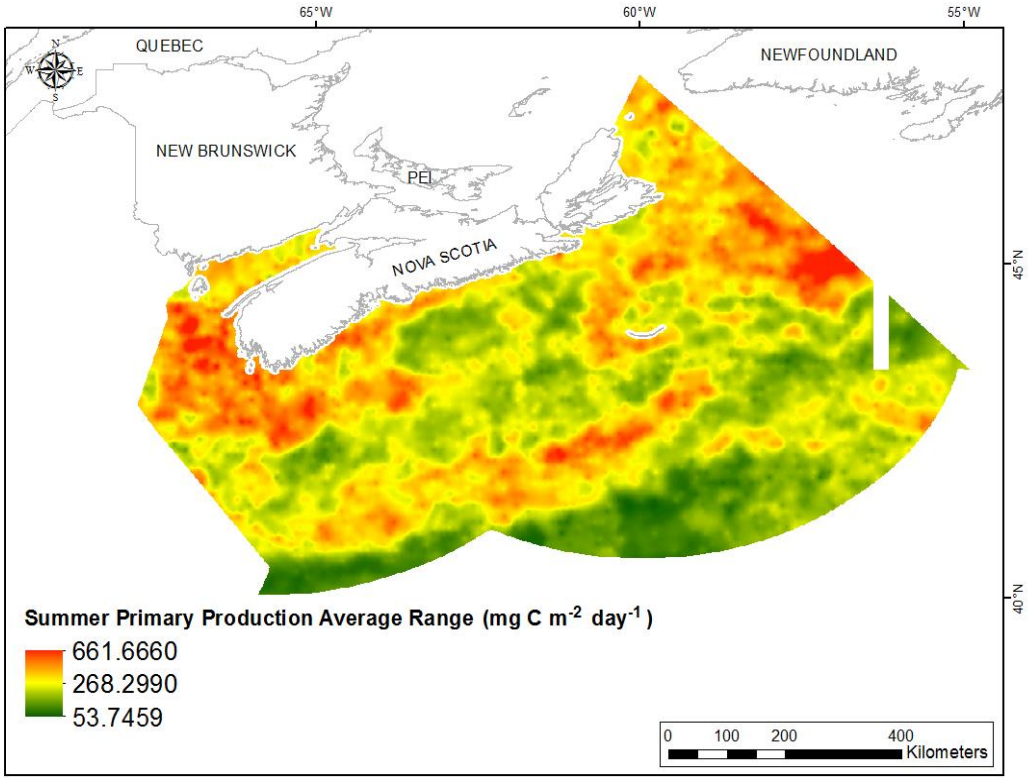

Fig. 440. Interpolated prediction surface of Summer Primary Production Average Range (mg C m^{-2} day^{-1}).

Fall Primary Production Mean

There was incomplete coverage of this variable across the study extent. Prior to interpolation, this variable displayed a slightly right-skewed, leptokurtic distribution (Table 177, Fig. 441). The data were higher than predicted by a normal distribution at mid-range and high values and slightly lower than predicted at low values (Fig. 442). The areas of under- and over-prediction showed no spatial pattern over the study extent (Fig. 442).

The semivariogram showed moderate autocorrelation present in the data (Fig. 443). The fit between measured and predicted values was fair (Fig. 443), with under-prediction of large values and over-prediction of small values. Good performance of the model was indicated by the cross-validation statistics (Table 178). The error map showed patches of high error across the study extent, particularly off Cape Breton (Fig. 444). The kriged surface is presented in Fig. 445.

Table 177. Distributional properties of Fall Primary Production Mean (mg C m^{-2} day^{-1}).

Property	Value
Number of Observations	4426
Minimum	269.910
Maximum	861.300
Mean	521.420
Median	515.960
Standard Deviation	64.683
Skewness	0.305
Kurtosis	4.020

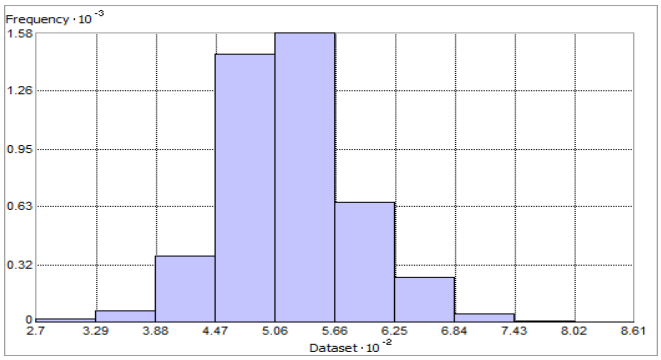

Fig. 441. Distribution of Fall Primary Production Mean (mg C m^{-2} day^{-1}). Histogram was illustrated using 10 bins. X axis is shown at 10^{-2}; Y axis is shown at 10^{-3}.

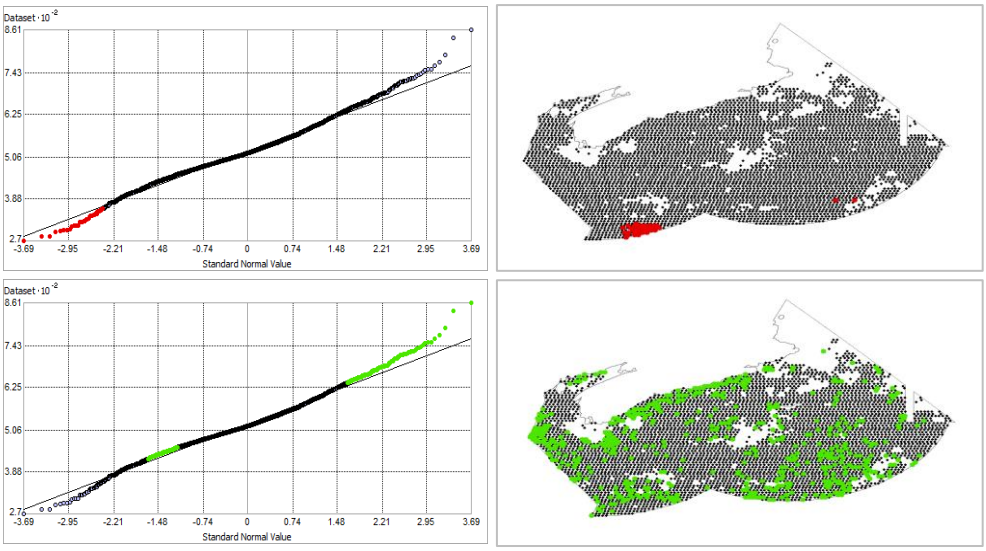

Fig. 442. Normal Q-Q plot for data values of Fall Primary Production Mean (mg C m^{-2} day^{-1}). Points falling under (upper panel) and over (bottom panel) the reference line are mapped.

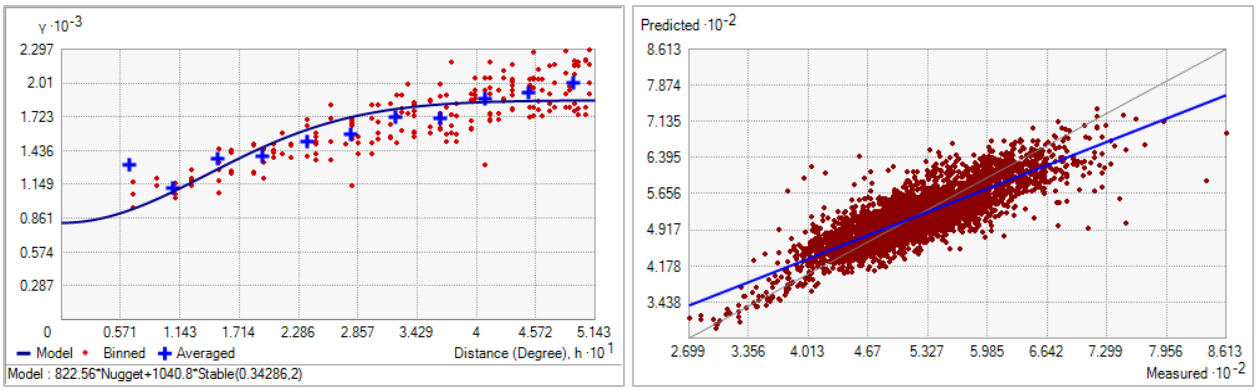

Fig. 443. Left panel: Semivariogram of Fall Primary Production Mean (mg C m^{-2} day^{-1}). Binned values are shown as red dots; average points are shown as blue crosses; the model fit to the averaged values is shown as a blue line. Lag size: 0.043 degrees; number of lags: 12; Parameter: 2; Range: 0.343 degrees; Partial Sill: 1040.843. Right panel: Scatterplot of predicted values versus observed values for the variable Fall Primary Production Mean (mg C m^{-2} day^{-1}).

Table 178. Results of cross-validation of the kriged model for Fall Primary Production Mean (mg C m^{-2} day^{-1}).

Prediction error	**Value**
Number of Observations	4426
Overall Mean Error	0.078
Root Mean Square Prediction Error	35.523
Standardized Mean	1.717×10^{-3}
Standardized Root Mean Square Prediction Error	1.068
Average Standard Error	33.019

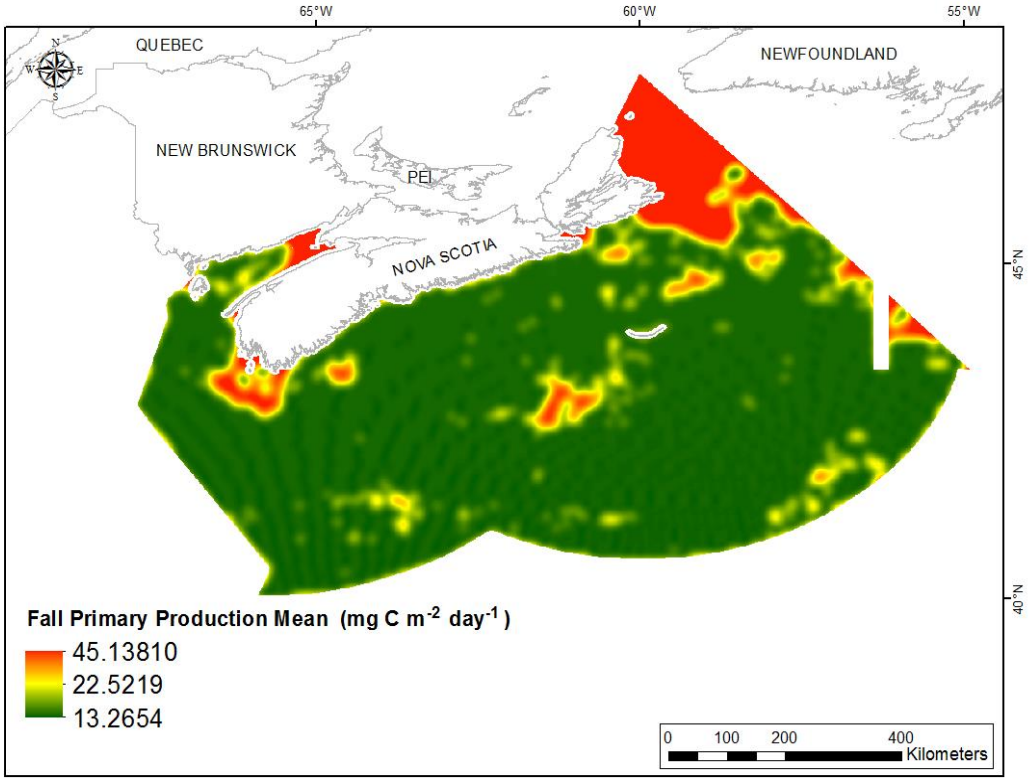

Fig. 444. Prediction standard error surface of Fall Primary Production Mean (mg C m^{-2} day^{-1}).

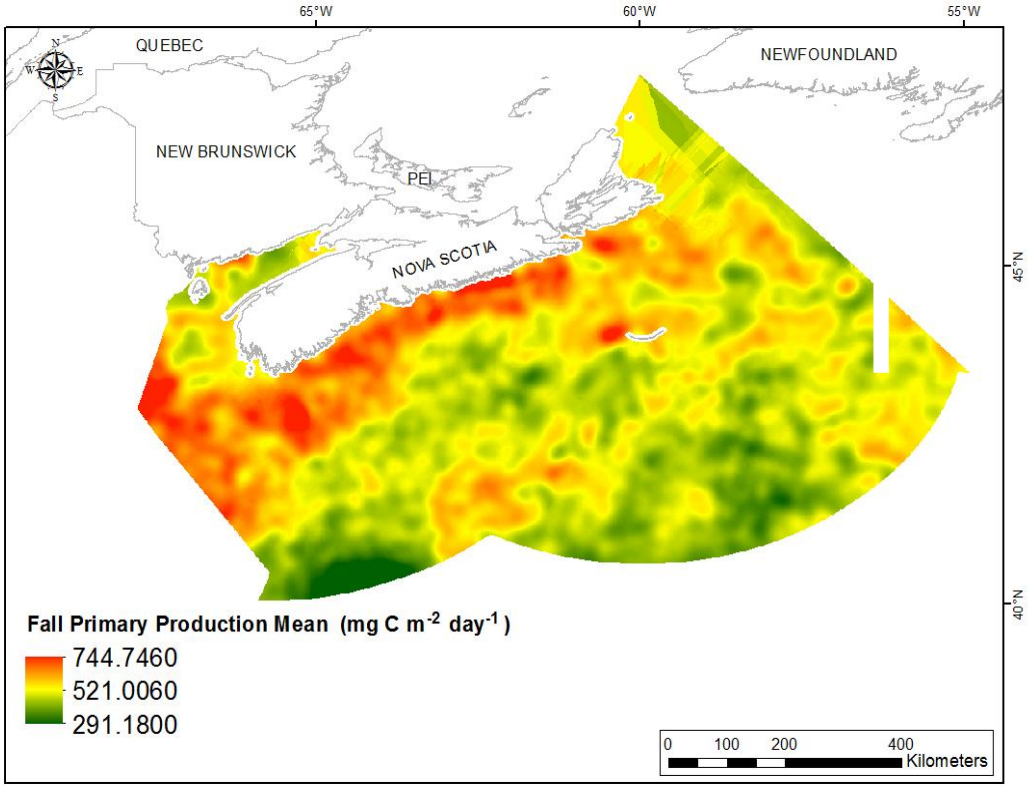

Fig. 445. Interpolated prediction surface of Fall Primary Production Mean (mg C m^{-2} day^{-1}).

Fall Primary Production Minimum

There was incomplete coverage of this variable across the study extent. Prior to interpolation, this variable displayed a slightly left-skewed, platykurtic distribution (Table 179, Fig. 446). The data were slightly lower than predicted by a normal distribution at lower mid-range and high values and slightly higher than predicted at low values (Fig. 447). The areas of under- and over-prediction showed no spatial pattern over the study extent (Fig. 447).

The semivariogram showed moderate autocorrelation present in the data (Fig. 448). The fit between measured and predicted values was fair (Fig. 448), with under-prediction of large values and over-prediction of small values. Good performance of the model was indicated by the cross-validation statistics (Table 180). The error map showed patches of high error across the study extent, particularly off Cape Breton (Fig. 449). The kriged surface is presented in Fig. 450.

Table 179. Distributional properties of Fall Primary Production Minimum (mg C m^{-2} day^{-1}).

Property	Value
Number of Observations	4426
Minimum	86.590
Maximum	625.340
Mean	336.280
Median	372.320
Standard Deviation	85.143
Skewness	-0.289
Kurtosis	2.612

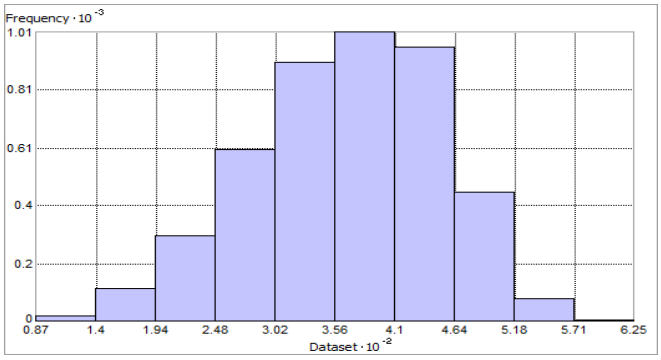

Fig. 446. Distribution of Fall Primary Production Minimum (mg C m^{-2} day^{-1}). Histogram was illustrated using 10 bins. X axis is shown at 10^{-2}; Y axis is shown at 10^{-3}.

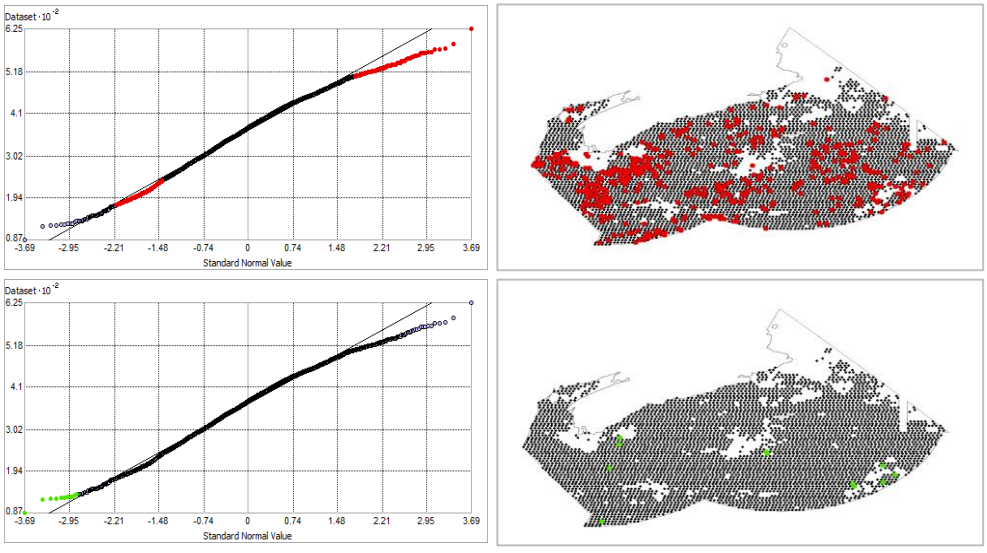

Fig. 447. Normal Q-Q plot for data values of Fall Primary Production Minimum (mg C m^{-2} day^{-1}). Points falling under (upper panel) and over (bottom panel) the reference line are mapped.

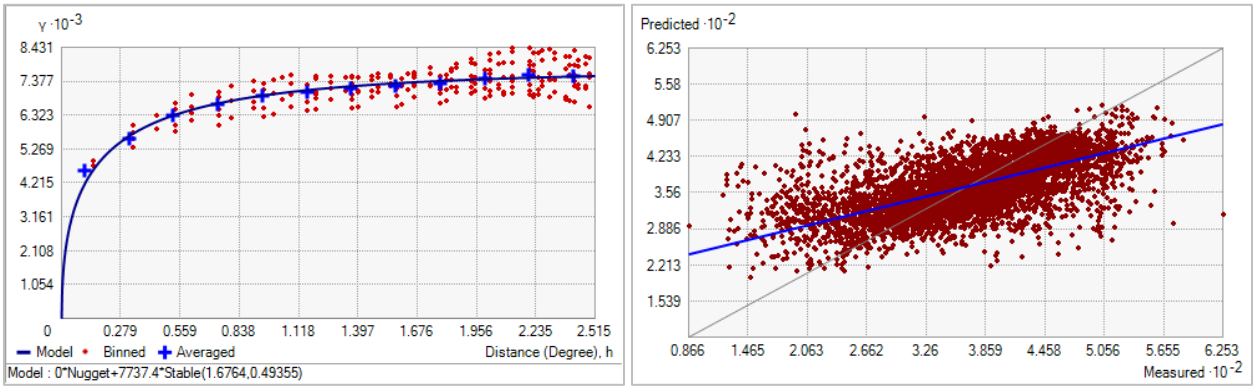

Fig. 448. Left panel: Semivariogram of Fall Primary Production Minimum (mg C m^{-2} day^{-1}). Binned values are shown as red dots; average points are shown as blue crosses; the model fit to the averaged values is shown as a blue line. Lag size: 0.210 degrees; number of lags: 12; Parameter: 0.494; Range: 1.676 degrees; Partial Sill: 7737.392. Right panel: Scatterplot of predicted values versus observed values for the variable Fall Primary Production Minimum (mg C m^{-2} day^{-1}).

Table 180. Results of cross-validation of the kriged model for Fall Primary Production Minimum (mg C m^{-2} day^{-1}).

Prediction error	**Value**
Number of Observations	4426
Overall Mean Error	0.081
Root Mean Square Prediction Error	67.953
Standardized Mean	8.344×10^{-4}
Standardized Root Mean Square Prediction Error	1.025
Average Standard Error	66.284

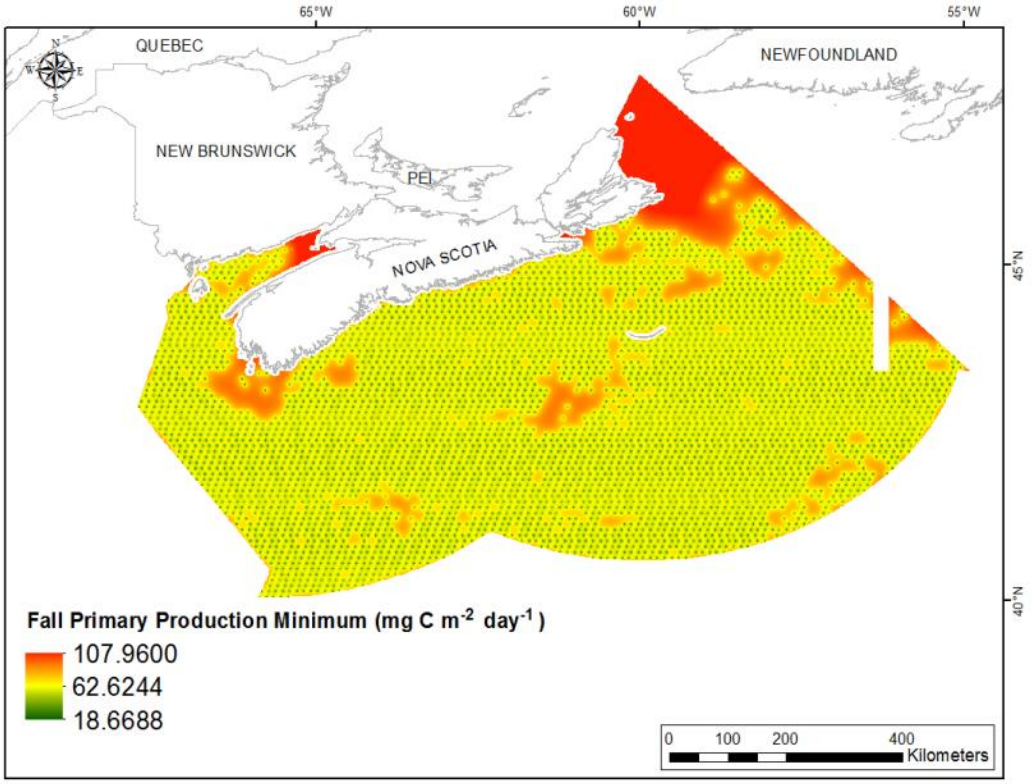

Fig. 449. Prediction standard error surface of Fall Primary Production Minimum (mg C m^{-2} day^{-1}).

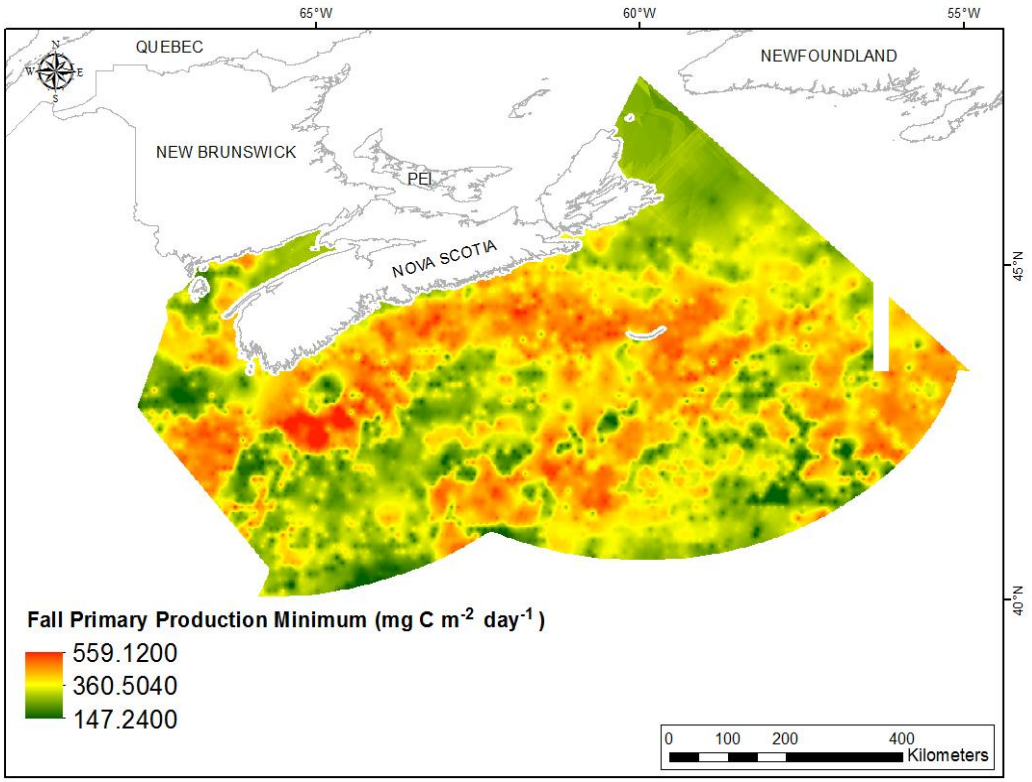

Fig. 450. Interpolated prediction surface of Fall Primary Production Minimum (mg C m^{-2} day^{-1}).

Fall Primary Production Maximum

There was incomplete coverage of this variable across the study extent. Prior to interpolation, this variable displayed a slightly right-skewed, leptokurtic distribution (Table 181, Fig. 451). The data were lower than predicted by a normal distribution at mid-range values and higher than predicted at both tails (Fig. 452). The areas of under- and over-prediction showed no spatial pattern over the study extent (Fig. 452).

The semivariogram showed moderate autocorrelation present in the data (Fig. 453). The fit between measured and predicted values was fair (Fig. 453), with under-prediction of large values. Good performance of the model was indicated by the cross-validation statistics (Table 182). The error map showed patches of high error across the study extent, particularly off Cape Breton (Fig. 454). The kriged surface is presented in Fig. 455.

Table 181. Distributional properties of Fall Primary Production Maximum (mg C m^{-2} day^{-1}).

Property	Value
Number of Observations	4426
Minimum	326.470
Maximum	1481.500
Mean	677.710
Median	644.870
Standard Deviation	133.940
Skewness	1.237
Kurtosis	4.660

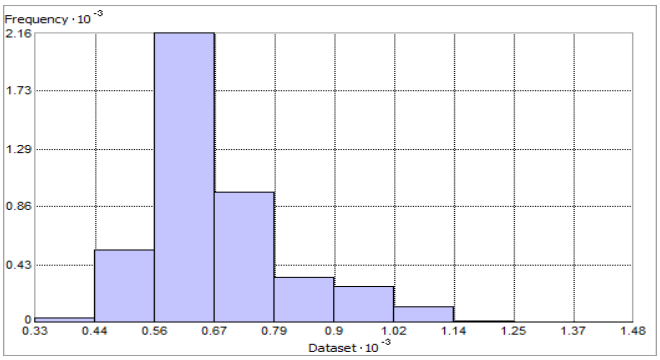

Fig. 451. Distribution of Fall Primary Production Maximum (mg C m^{-2} day^{-1}). Histogram was illustrated using 10 bins. X and Y axes are shown at 10^{-3}.

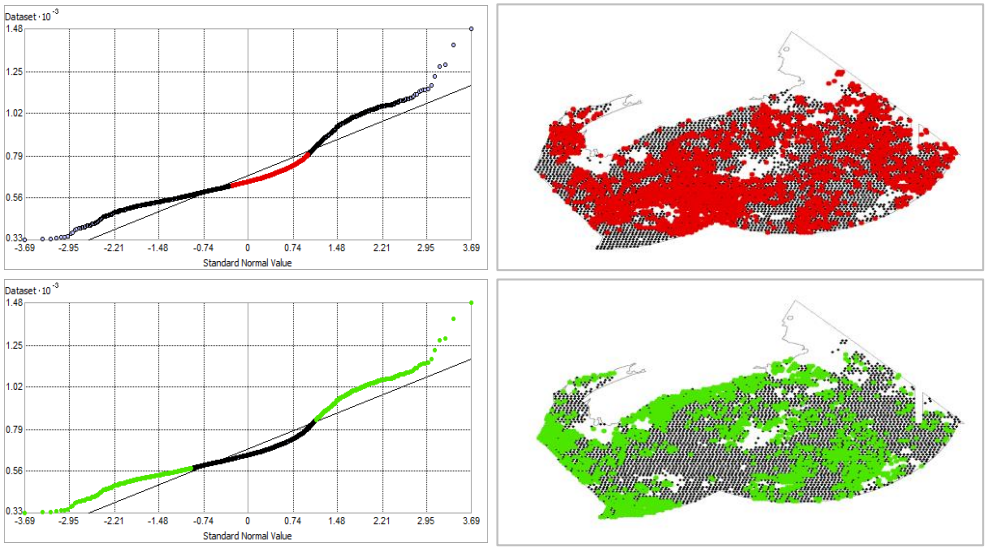

Fig. 452. Normal Q-Q plot for data values of Fall Primary Production Maximum (mg C m^{-2} day^{-1}). Points falling under (upper panel) and over (bottom panel) the reference line are mapped.

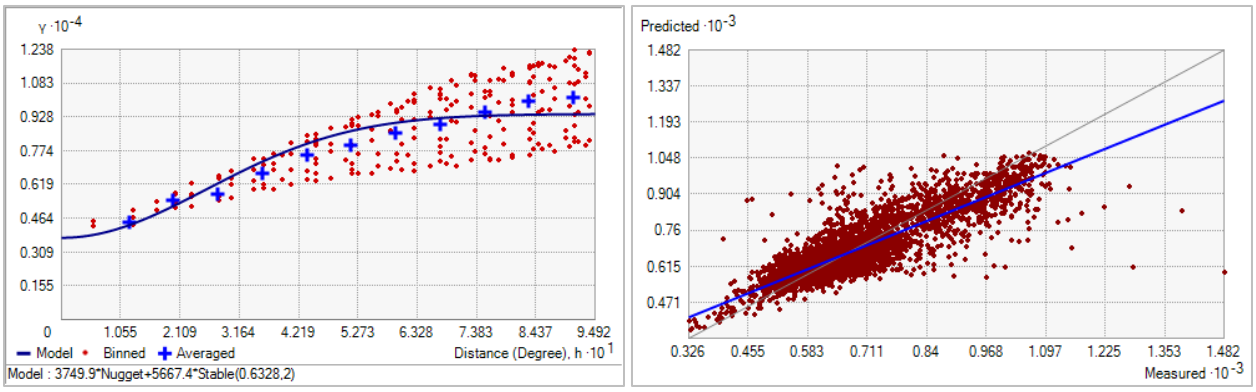

Fig. 453. Left panel: Semivariogram of Fall Primary Production Maximum (mg C m^{-2} day^{-1}). Binned values are shown as red dots; average points are shown as blue crosses; the model fit to the averaged values is shown as a blue line. Lag size: 0.079 degrees; number of lags: 12; Parameter: 2; Range: 0.633 degrees; Partial Sill: 5667.416. Right panel: Scatterplot of predicted values versus observed values for the variable Fall Primary Production Maximum (mg C m^{-2} day^{-1}).

Table 182. Results of cross-validation of the kriged model for Fall Primary Production Maximum (mg C m^{-2} day^{-1}).

Prediction error	**Value**
Number of Observations	4426
Overall Mean Error	6.161×10^{-3}
Root Mean Square Prediction Error	70.713
Standardized Mean	-3.351×10^{-4}
Standardized Root Mean Square Prediction Error	1.071
Average Standard Error	65.625

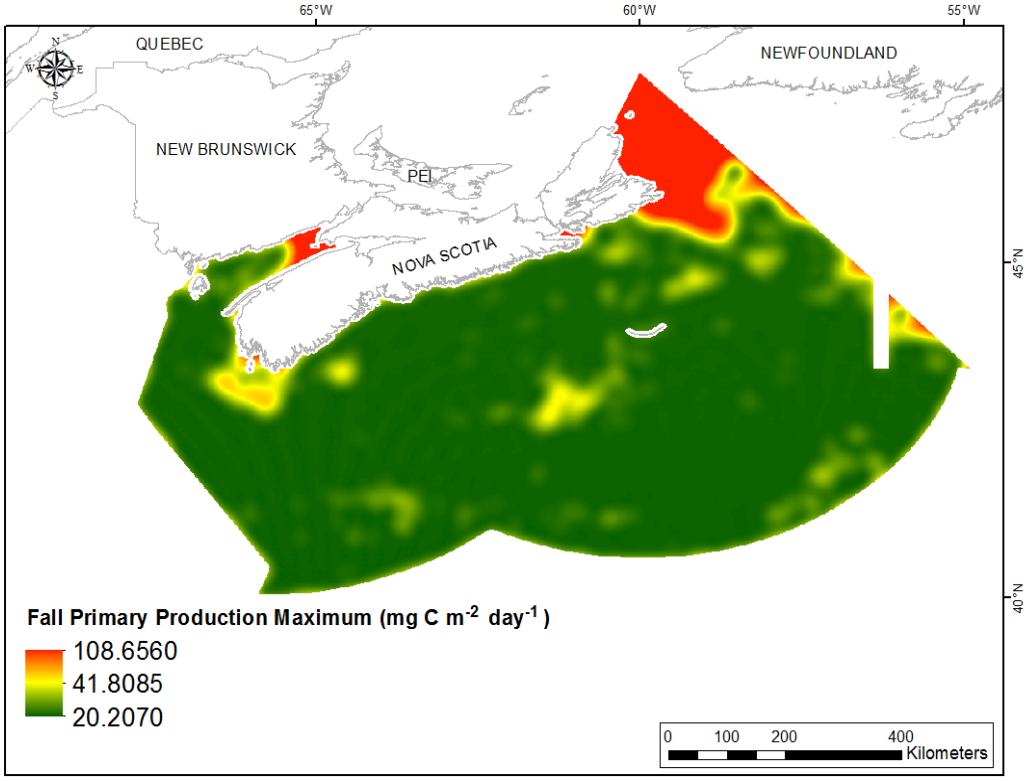

Fig. 454. Prediction standard error surface of Fall Primary Production Maximum (mg C m^{-2} day^{-1}).

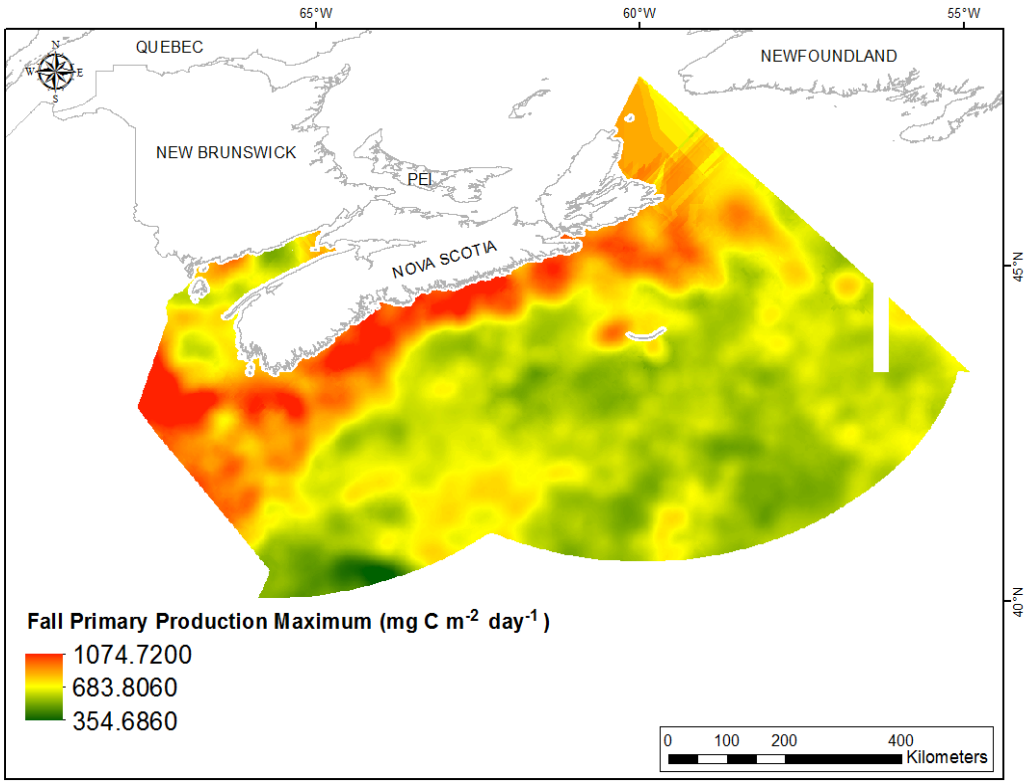

Fig. 455. Interpolated prediction surface of Fall Primary Production Maximum (mg C m^{-2} day^{-1}).

Fall Primary Production Range

There was incomplete coverage of this variable across the study extent. Prior to interpolation, this variable displayed a slightly right-skewed, leptokurtic distribution (Table 183, Fig. 456). The data were higher than predicted by a normal distribution at both tails, and slightly lower than predicted at mid-range values (Fig. 457). The areas of under- and over-prediction showed no spatial pattern over the study extent (Fig. 457).

The semivariogram showed moderate autocorrelation present in the data (Fig. 458). The fit between measured and predicted values was fair (Fig. 458), with under-prediction of large values and over-prediction of small values. Good performance of the model was indicated by the cross-validation statistics (Table 184). The error map showed patches of high error across the study extent, particularly off Cape Breton (Fig. 459). The kriged surface is presented in Fig. 460.

Table 183. Distributional properties of Fall Primary Production Range (mg C m^{-2} day^{-1}).

Property	Value
Number of Observations	4426
Minimum	19.090
Maximum	1025
Mean	311.43
Median	284.69
Standard Deviation	151.440
Skewness	1.004
Kurtosis	4.125

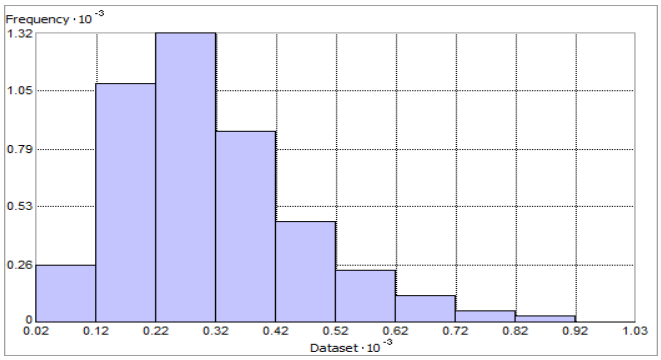

Fig. 456. Distribution of Fall Primary Production Range (mg C m^{-2} day^{-1}). Histogram was illustrated using 10 bins. X and Y axes are shown at 10^{-3}.

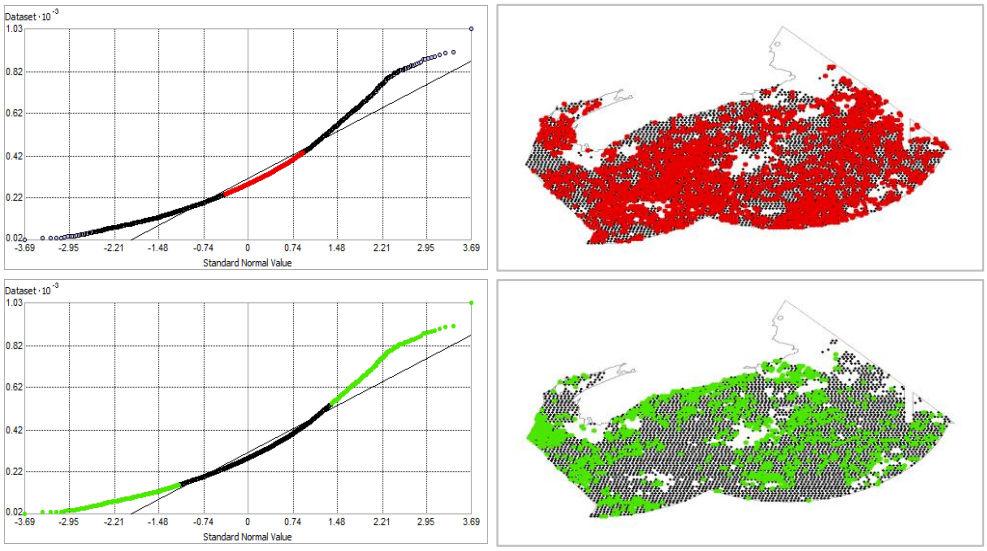

Fig. 457. Normal Q-Q plot for data values of Fall Primary Production Range (mg C m^{-2} day^{-1}). Points falling under (upper panel) and over (bottom panel) the reference line are mapped.

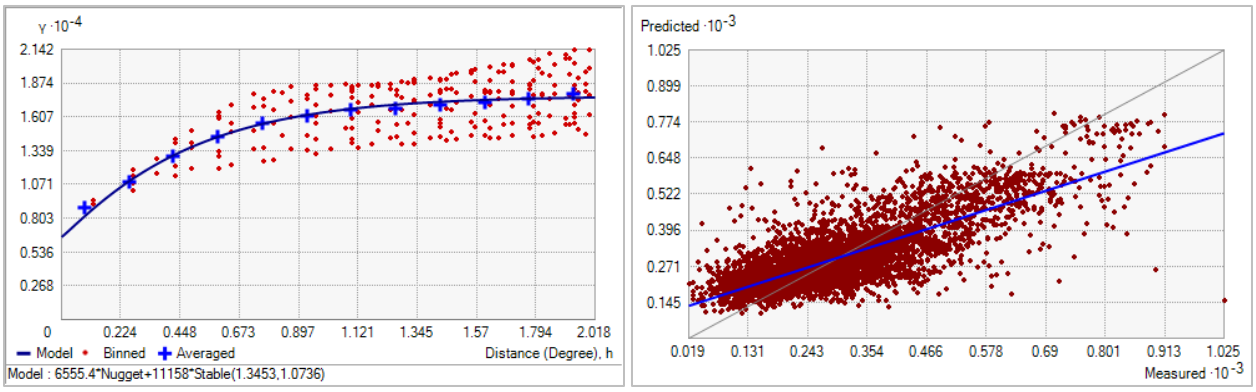

Fig. 458. Left panel: Semivariogram of Fall Primary Production Range (mg C m^{-2} day^{-1}). Binned values are shown as red dots; average points are shown as blue crosses; the model fit to the averaged values is shown as a blue line. Lag size: 0.168 degrees; number of lags: 12; Parameter: 1.074; Range: 1.345 degrees; Partial Sill: 11158.190. Right panel: Scatterplot of predicted values versus observed values for the variable Fall Primary Production Range (mg C m^{-2} day^{-1}).

Table 184. Results of cross-validation of the kriged model for Fall Primary Production Range (mg C m^{-2} day^{-1}).

Prediction error	**Value**
Number of Observations	4426
Overall Mean Error	2.878×10^{-3}
Root Mean Square Prediction Error	97.123
Standardized Mean	4.264×10^{-5}
Standardized Root Mean Square Prediction Error	1.020
Average Standard Error	95.020

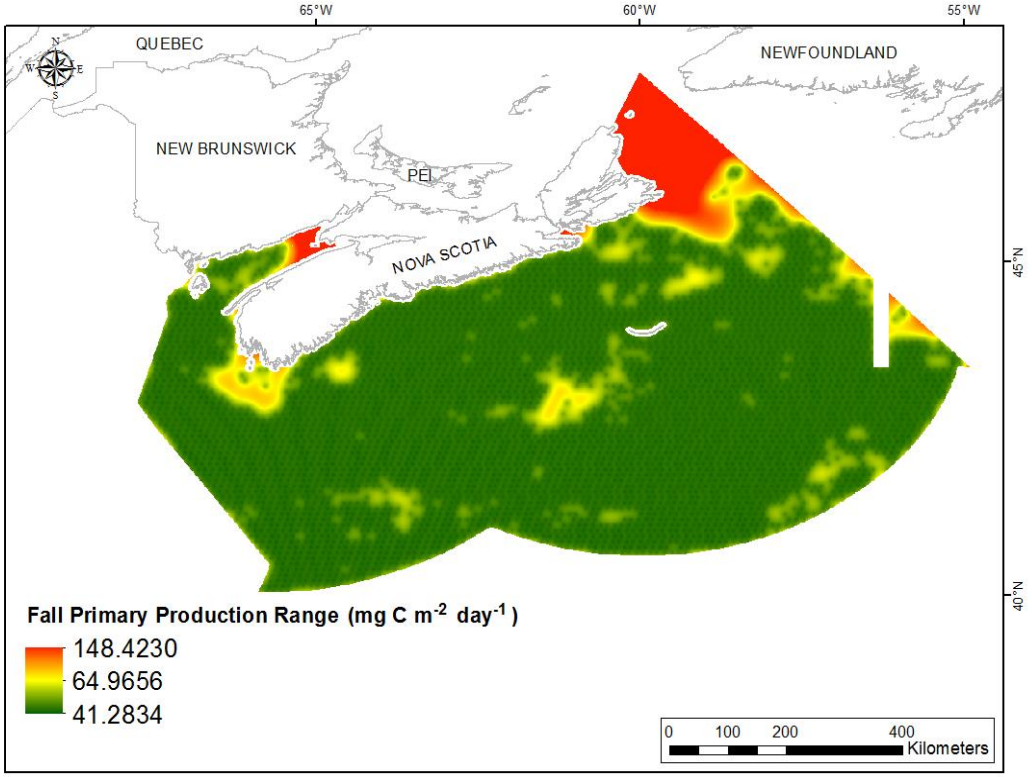

Fig. 459. Prediction standard error surface of Fall Primary Production Range (mg C m^{-2} day^{-1}).

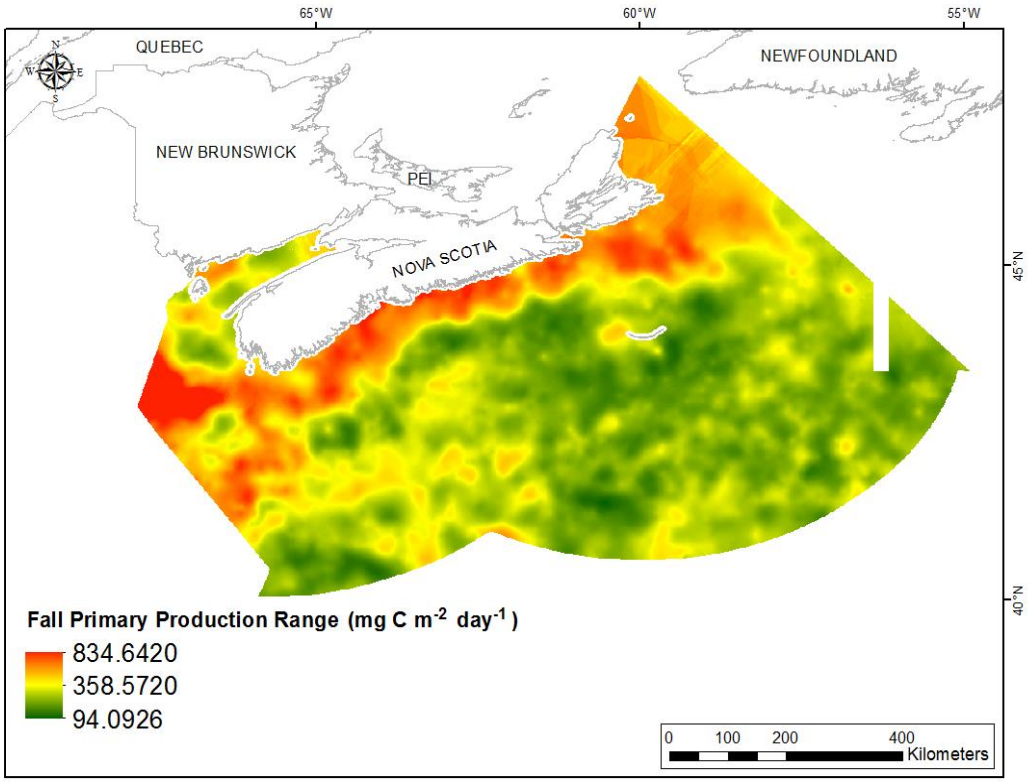

Fig. 460. Interpolated prediction surface of Fall Primary Production Range (mg C m^{-2} day^{-1}).

Fall Primary Production Average Minimum

There was incomplete coverage of this variable across the study extent. This variable displayed a near-normal distribution with negative skew (Table 185, Fig. 461). The data were higher than predicted by a normal distribution at both tails and lower than predicted at lower and upper mid-range values (Fig. 462). Mid-range values were well predicted. The areas of under- and over-prediction showed no spatial pattern over the study extent (Fig. 462).

The semivariogram showed weak autocorrelation present in the data (Fig. 463). The fit between measured and predicted values was fair (Fig. 463), with under-prediction of large values and over-prediction of small values. Good performance of the model was indicated by the cross-validation statistics (Table 186). The error map showed patches of high error across the study extent, particularly off Cape Breton (Fig. 464). The kriged surface is presented in Fig. 465.

Table 185. Distributional properties of Fall Primary Production Average Minimum (mg C m^{-2} day^{-1}).

Property	Value
Number of Observations	4426
Minimum	222.310
Maximum	686.050
Mean	430.630
Median	434.840
Standard Deviation	63.630
Skewness	-0.242
Kurtosis	2.986

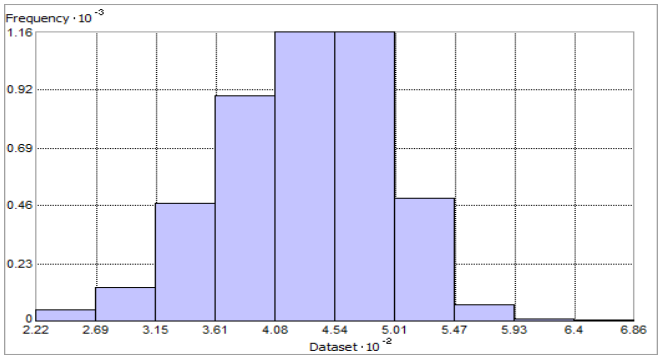

Fig. 461. Distribution of Fall Primary Production Average Minimum (mg C m^{-2} day^{-1}). Histogram was illustrated using 10 bins. X axis is shown at 10^{-2}; Y axis is shown at 10^{-3}.

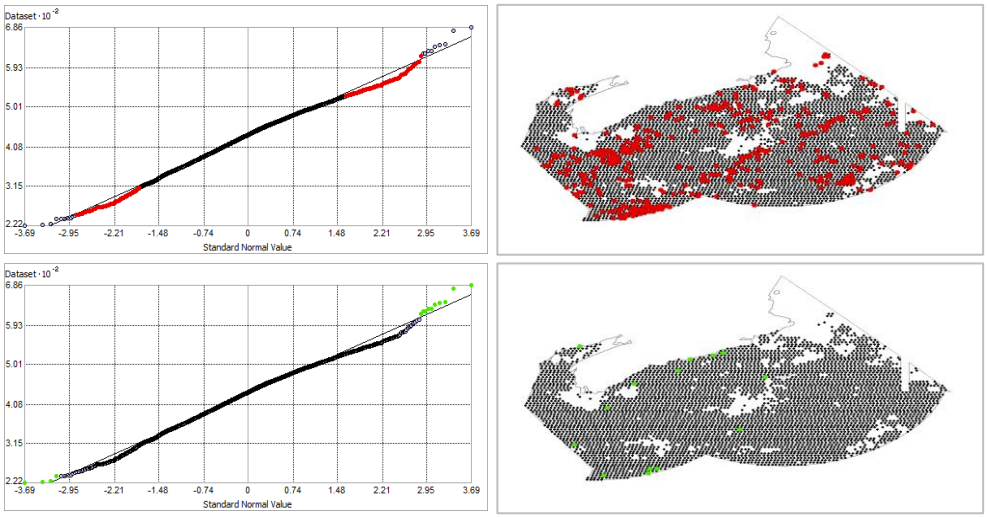

Fig. 462. Normal Q-Q plot for data values of Fall Primary Production Average Minimum (mg C m^{-2} day^{-1}). Points falling under (upper panel) and over (bottom panel) the reference line are mapped.

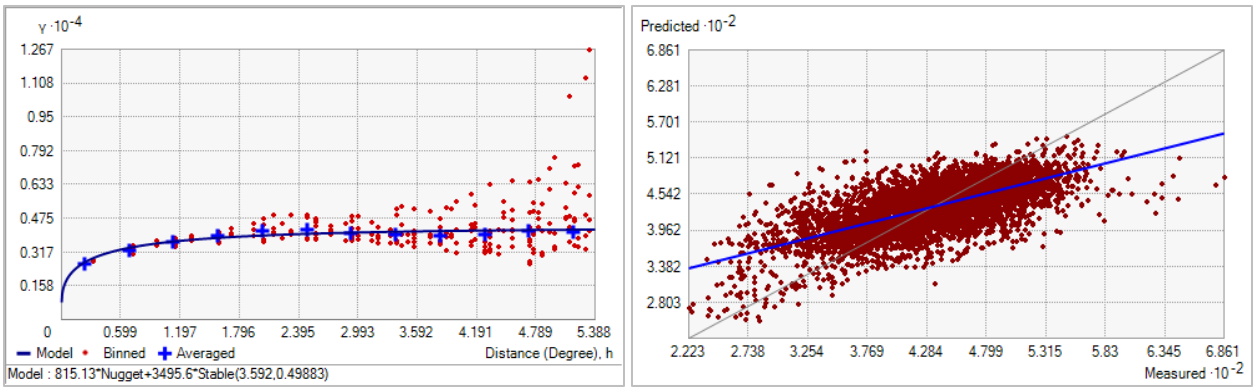

Fig. 463. Left panel: Semivariogram of Fall Primary Production Average Minimum (mg C m^{-2} day^{-1}). Binned values are shown as red dots; average points are shown as blue crosses; the model fit to the averaged values is shown as a blue line. Lag size: 0.449 degrees; number of lags: 12; Parameter: 0.499; Range: 3.592 degrees; Partial Sill: 3495.583. Right panel: Scatterplot of predicted values versus observed values for the variable Fall Primary Production Average Minimum (mg C m^{-2} day^{-1}).

Table 186. Results of cross-validation of the kriged model for Fall Primary Production Average Minimum (mg C m^{-2} day^{-1}).

Prediction error	**Value**
Number of Observations	4426
Overall Mean Error	0.050
Root Mean Square Prediction Error	46.765
Standardized Mean	7.044×10^{-4}
Standardized Root Mean Square Prediction Error	0.958
Average Standard Error	48.759

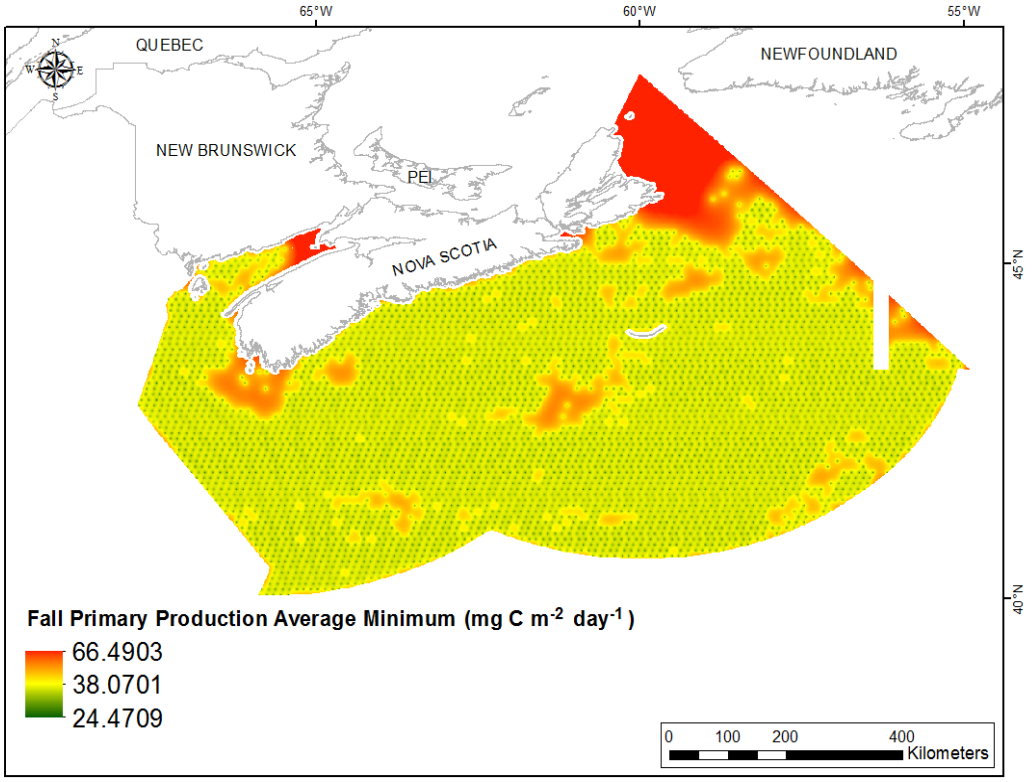

Fig. 464. Prediction standard error surface of Fall Primary Production Average Minimum (mg C m^{-2} day^{-1}).

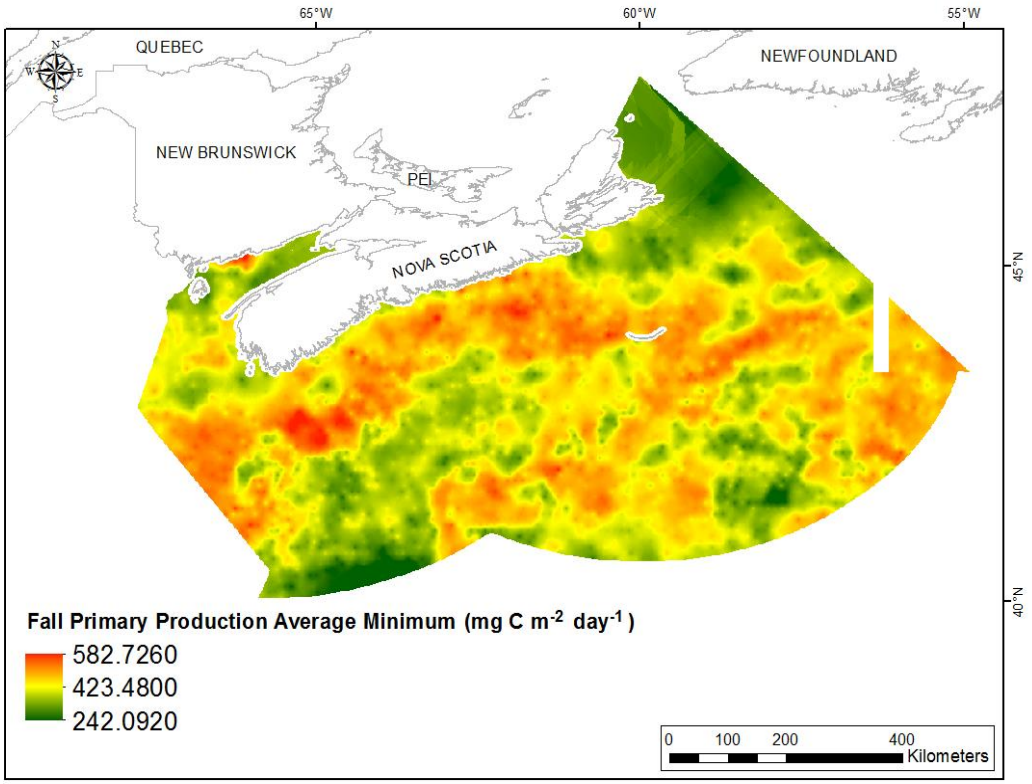

Fig. 465. Interpolated prediction surface of Fall Primary Production Average Minimum (mg C m^{-2} day^{-1}).

Fall Primary Production Average Maximum

There was incomplete coverage of this variable across the study extent. Prior to interpolation, this variable displayed slightly right-skewed, leptokurtic distribution (Table 187, Fig. 466). The data were lower than predicted by a normal distribution at mid-range values and higher than predicted at both tails (Fig. 467). The areas of under- and over-prediction showed no spatial pattern over the study extent (Fig. 467).

The semivariogram showed moderate autocorrelation present in the data (Fig. 468). The fit between measured and predicted values was fair (Fig. 468), with under-prediction of large values and over-prediction of small values. Good performance of the model was indicated by the cross-validation statistics (Table 188). The error map showed patches of high error across the study extent, particularly off Cape Breton (Fig. 469). The kriged surface is presented in Fig. 470.

Table 187. Distributional properties of Fall Primary Production Average Maximum (mg C m^{-2} day^{-1}).

Property	Value
Number of Observations	4426
Minimum	317.51
Maximum	1082
Mean	612.23
Median	594.510
Standard Deviation	98.649
Skewness	0.976
Kurtosis	4.596

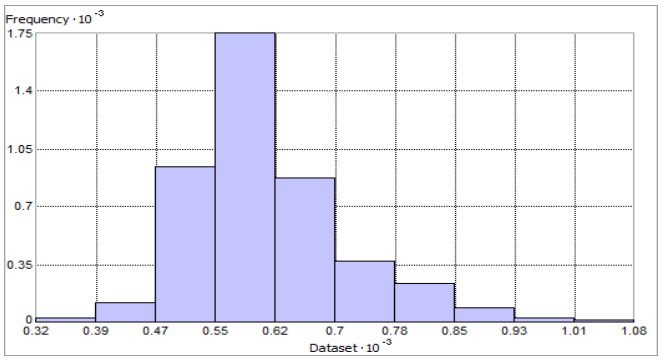

Fig. 466. Distribution of Fall Primary Production Average Maximum (mg C m^{-2} day^{-1}). Histogram was illustrated using 10 bins. X and Y axes are shown at 10^{-3}.

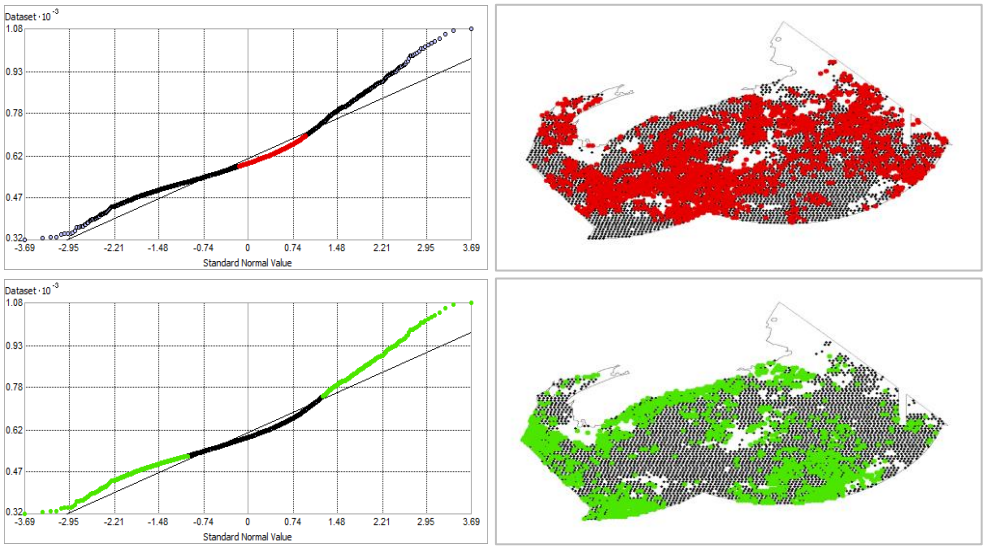

Fig. 467. Normal Q-Q plot for data values of Fall Primary Production Average Maximum (mg C m^{-2} day^{-1}). Points falling under (upper panel) and over (bottom panel) the reference line are mapped.

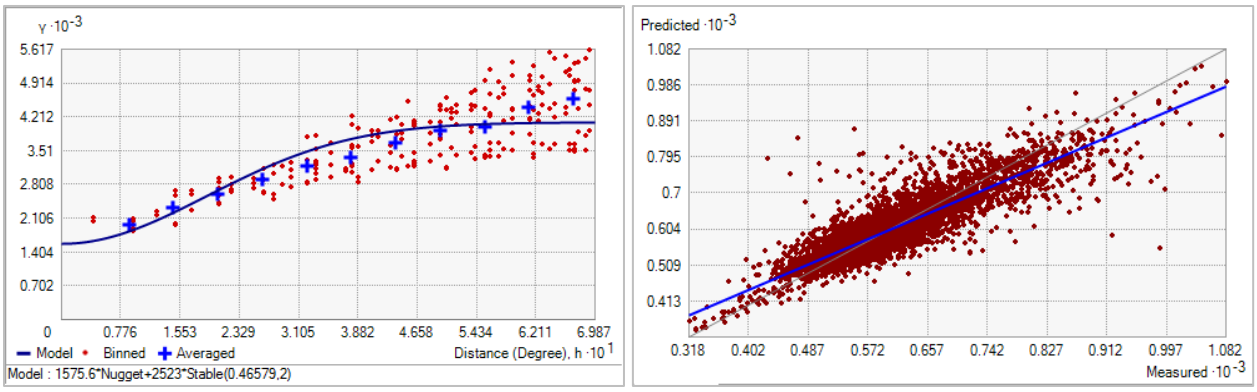

Fig. 468. Left panel: Semivariogram of Fall Primary Production Average Maximum (mg C m^{-2} day^{-1}). Binned values are shown as red dots; average points are shown as blue crosses; the model fit to the averaged values is shown as a blue line. Lag size: 0.058 degrees; number of lags: 12; Parameter: 2; Range: 0.466 degrees; Partial Sill: 2523.029. Right panel: Scatterplot of predicted values versus observed values for the variable Fall Primary Production Average Maximum (mg C m^{-2} day^{-1}).

Table 188. Results of cross-validation of the kriged model for Fall Primary Production Average Maximum (mg C m^{-2} day^{-1}).

Prediction error	**Value**
Number of Observations	4426
Overall Mean Error	0.037
Root Mean Square Prediction Error	48.520
Standardized Mean	1.590×10^{-4}
Standardized Root Mean Square Prediction Error	1.092
Average Standard Error	44.035

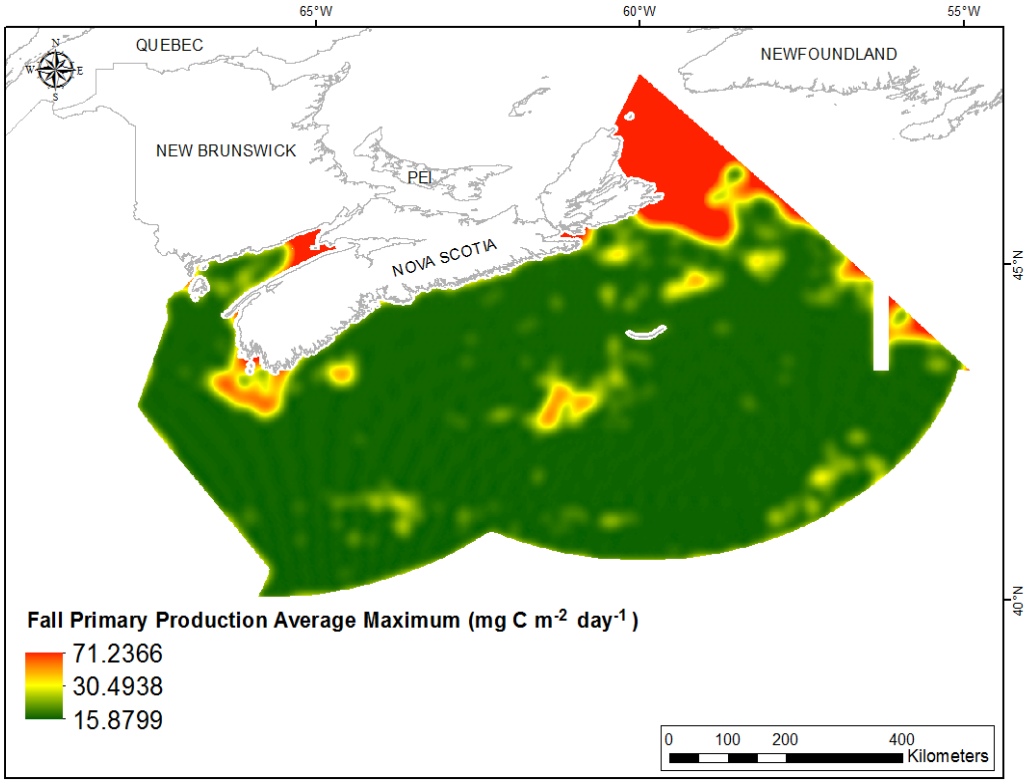

Fig. 469. Prediction standard error surface of Fall Primary Production Average Maximum (mg C m^{-2} day^{-1}).

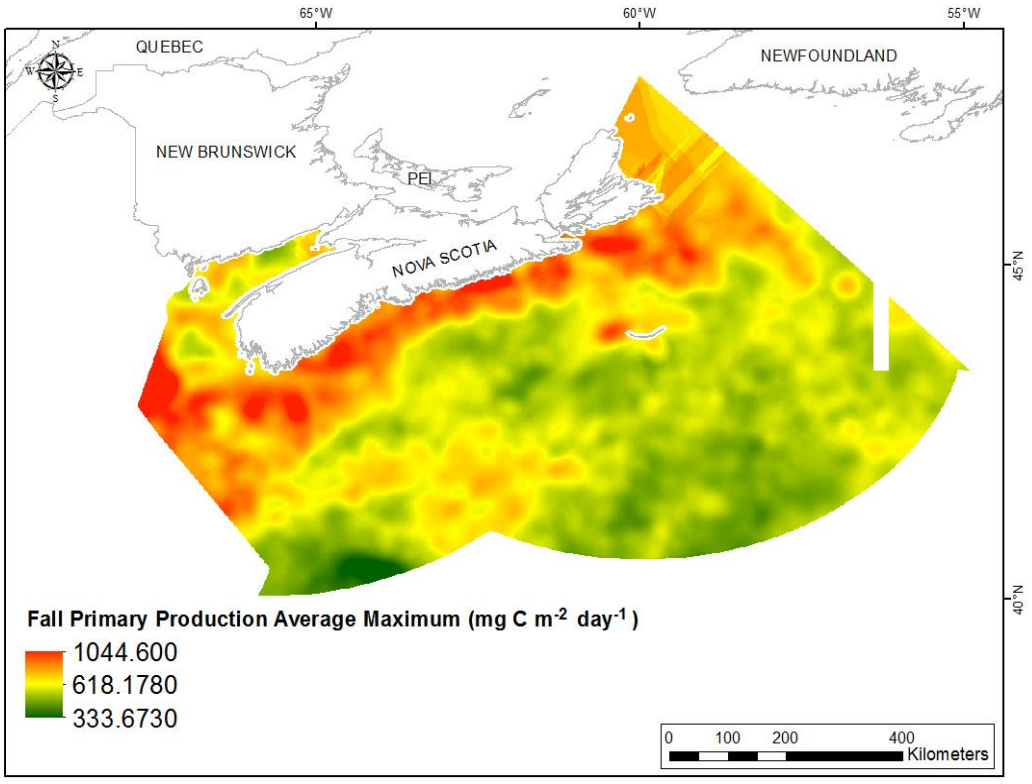

Fig. 470. Interpolated prediction surface of Fall Primary Production Average Maximum (mg C m^{-2} day^{-1}).

Fall Primary Production Average Range

There was incomplete coverage of this variable across the study extent. Prior to interpolation, this variable displayed right-skewed, leptokurtic distribution (Table 189, Fig. 471). The data were lower than predicted by a normal distribution at mid-range values and higher than predicted at both tails (Fig. 472). The areas of under- and over-prediction showed no spatial pattern over the study extent (Fig. 472).

The semivariogram showed moderate autocorrelation present in the data (Fig. 473). The fit between measured and predicted values was fair (Fig. 473), with under-prediction of large values and over-prediction of small values. Good performance of the model was indicated by the cross-validation statistics (Table 190). The error map showed patches of high error across the study extent, particularly off Cape Breton (Fig. 474). The kriged surface is presented in Fig. 475.

Table 189. Distributional properties of Fall Primary Production Average Range (mg C m^{-2} day^{-1}).

Property	Value
Number of Observations	4426
Minimum	5.030
Maximum	642.120
Mean	181.600
Median	161.310
Standard Deviation	103.180
Skewness	1.014
Kurtosis	4.133

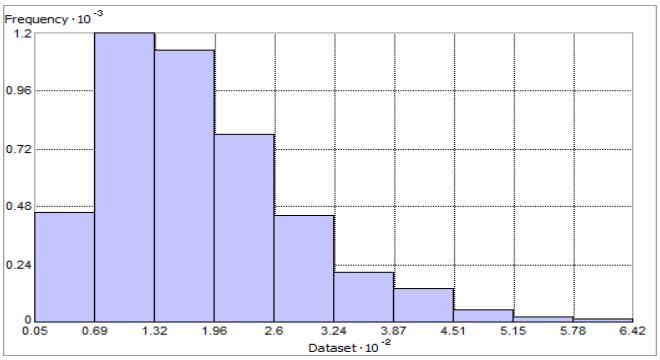

Fig. 471. Distribution of Fall Primary Production Average Range (mg C m^{-2} day^{-1}). Histogram was illustrated using 10 bins. X axis is shown at 10^{-2}; Y axis is shown at 10^{-3}.

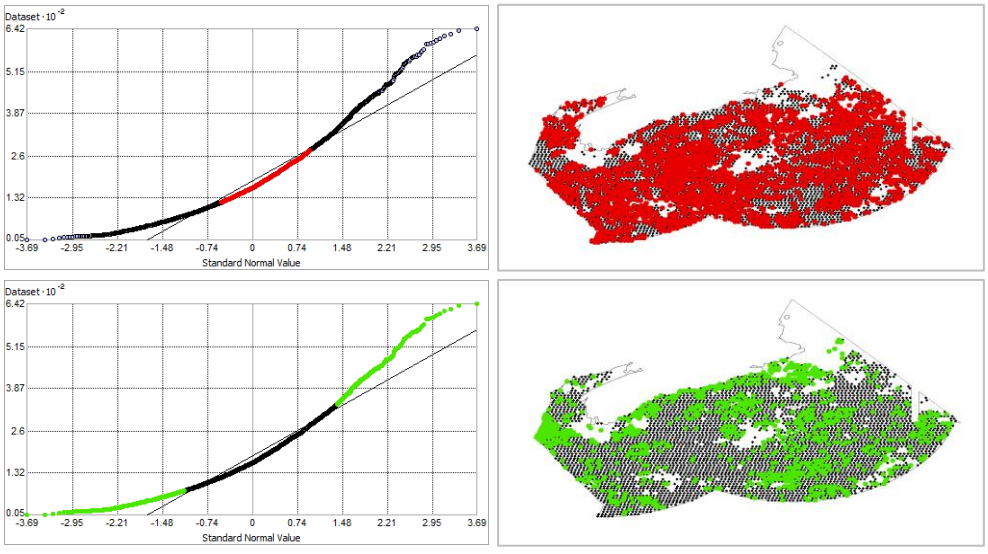

Fig. 472. Normal Q-Q plot for data values of Fall Primary Production Average Range (mg C m^{-2} day^{-1}). Points falling under (upper panel) and over (bottom panel) the reference line are mapped.

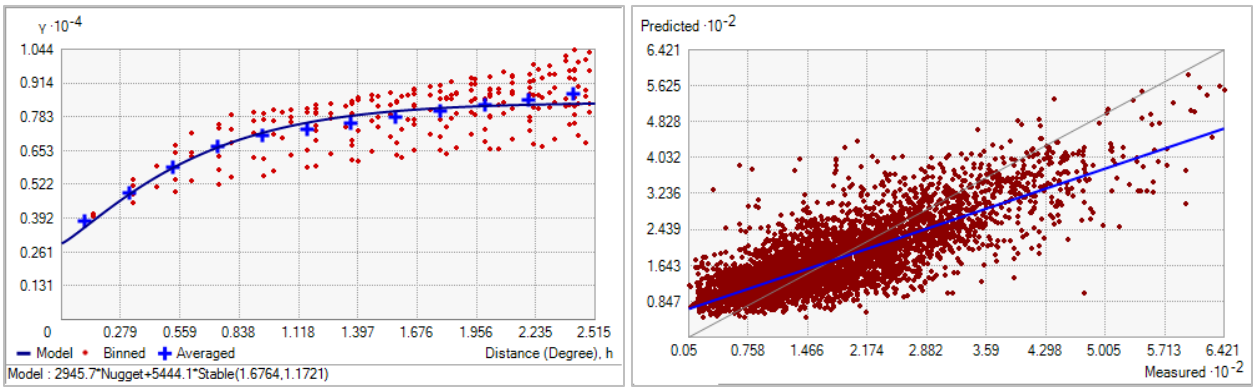

Fig. 473. Left panel: Semivariogram of Fall Primary Production Average Range (mg C m^{-2} day^{-1}). Binned values are shown as red dots; average points are shown as blue crosses; the model fit to the averaged values is shown as a blue line. Lag size: 0.209 degrees; number of lags: 12; Parameter: 1.172; Range: 1.676 degrees; Partial Sill: 5444.139. Right panel: Scatterplot of predicted values versus observed values for the variable Fall Primary Production Average Range (mg C m^{-2} day^{-1}).

Table 190. Results of cross-validation of the kriged model for Fall Primary Production Average Range (mg C m^{-2} day^{-1}).

Prediction error	**Value**
Number of Observations	4426
Overall Mean Error	0.029
Root Mean Square Prediction Error	62.574
Standardized Mean	4.162×10^{-4}
Standardized Root Mean Square Prediction Error	1.019
Average Standard Error	61.216

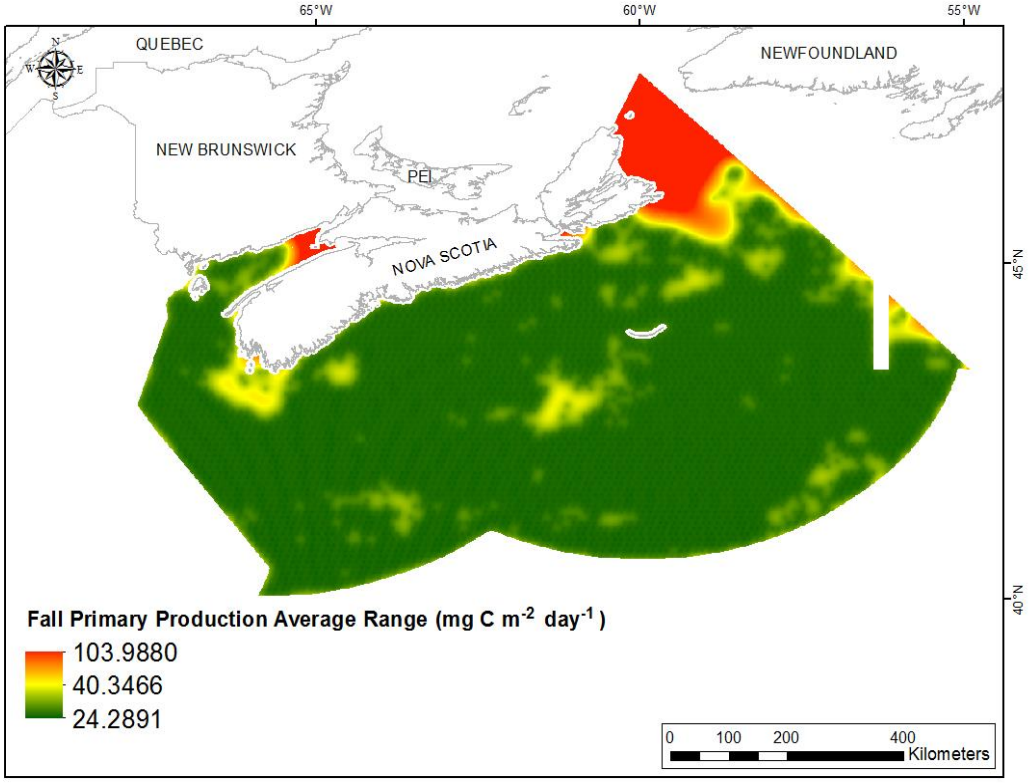

Fig. 474. Prediction standard error surface of Fall Primary Production Average Range (mg C m^{-2} day^{-1}).

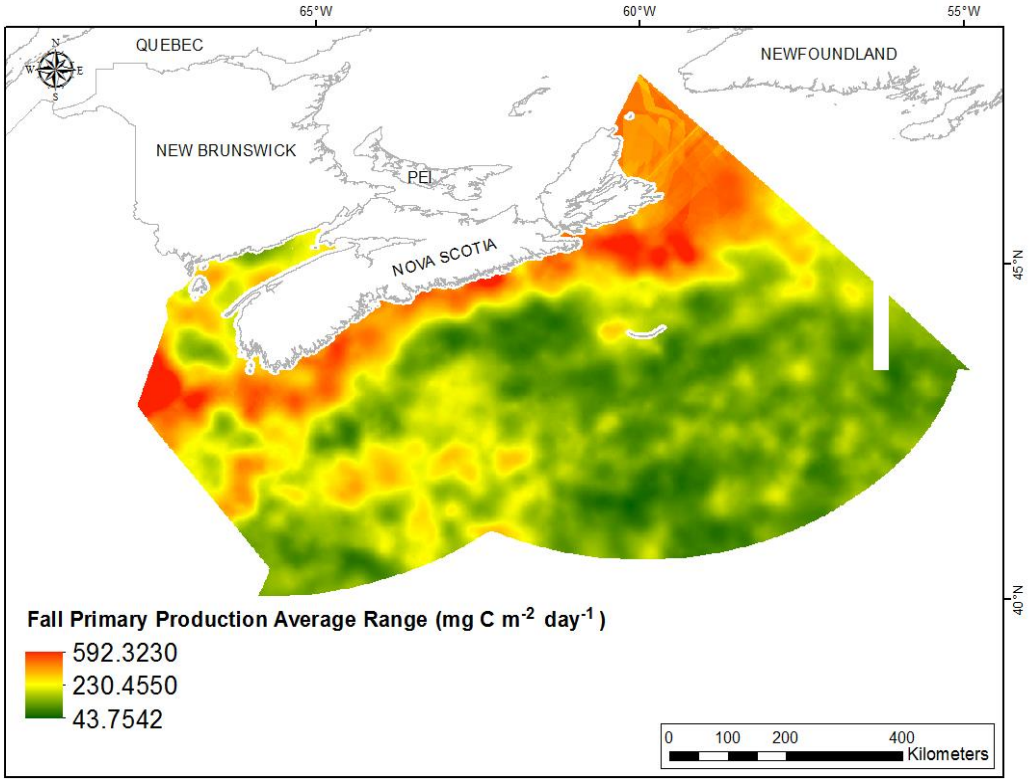

Fig. 475. Interpolated prediction surface of Fall Primary Production Average Range (mg C m^{-2} day^{-1}).

Annual Primary Production Mean

This variable displayed a right-skewed, leptokurtic distribution prior to interpolation (Table 191, Fig. 476). The data were higher than predicted by a normal distribution at high values and lower than predicted at low values however the mid-region was well-predicted (Fig. 477). The areas of under- and over-prediction showed no spatial pattern over the study extent (Fig. 477).

The semivariogram showed moderate autocorrelation present in the data (Fig. 478). The fit between measured and predicted values was fair (Fig. 478), with under-prediction of large values and over-prediction of small values. Good performance of the model was indicated by the cross-validation results (Table 192). The error map showed high error along the edges of the study extent (Fig. 479). The kriged surface is presented in Fig. 480.

Table 191. Distributional properties of Annual Primary Production Mean (mg C m^{-2} day^{-1}).

Property	Value
Number of Observations	5330
Minimum	375.130
Maximum	988.290
Mean	700.480
Median	699.740
Standard Deviation	47.576
Skewness	0.106
Kurtosis	5.555

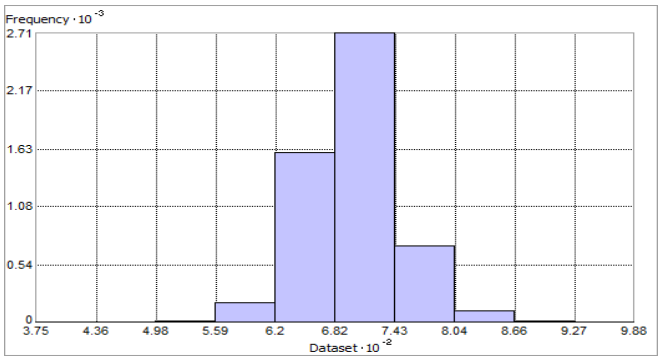

Fig. 476. Distribution of Annual Primary Production Mean (mg C m^{-2} day^{-1}). Histogram was illustrated using 10 bins. X axis is shown at 10^{-2}; Y axis is shown at 10^{-3}.

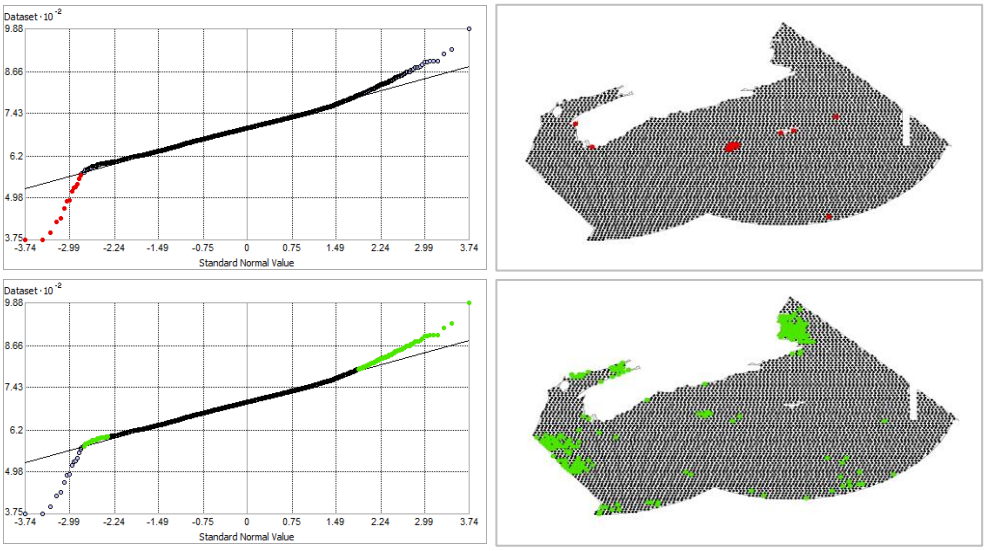

Fig. 477. Normal Q-Q plot for data values Annual Primary Production Mean (mg C m^{-2} day^{-1}). Points falling under (upper panel) and over (bottom panel) the reference line are mapped.

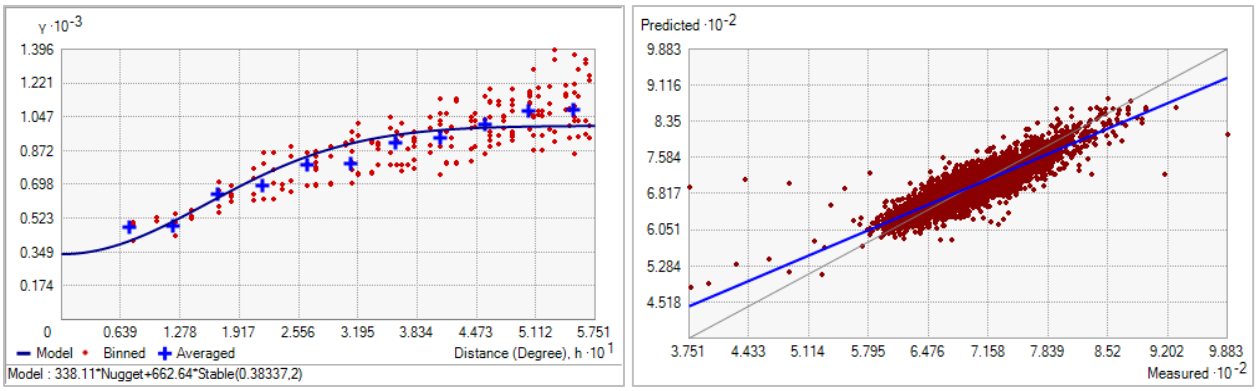

Fig. 478. Left panel: Semivariogram of Annual Primary Production Mean (mg C m^{-2} day^{-1}). Binned values are shown as red dots; average points are shown as blue crosses; the model fit to the averaged values is shown as a blue line. Lag size: 0.048 degrees; number of lags: 12; Parameter: 2; Range: 0.383 degrees; Partial Sill: 662.644. Right panel: Scatterplot of predicted values versus observed values for the variable Annual Primary Production Mean (mg C m^{-2} day^{-1}).

Table 192. Results of cross-validation of the kriged model for Annual Primary Production Mean (mg C m^{-2} day^{-1}).

Prediction error	**Value**
Number of Observations	5330
Overall Mean Error	-0.038
Root Mean Square Prediction Error	23.352
Standardized Mean	-1.407×10^{-3}
Standardized Root Mean Square Prediction Error	1.095
Average Standard Error	21.048

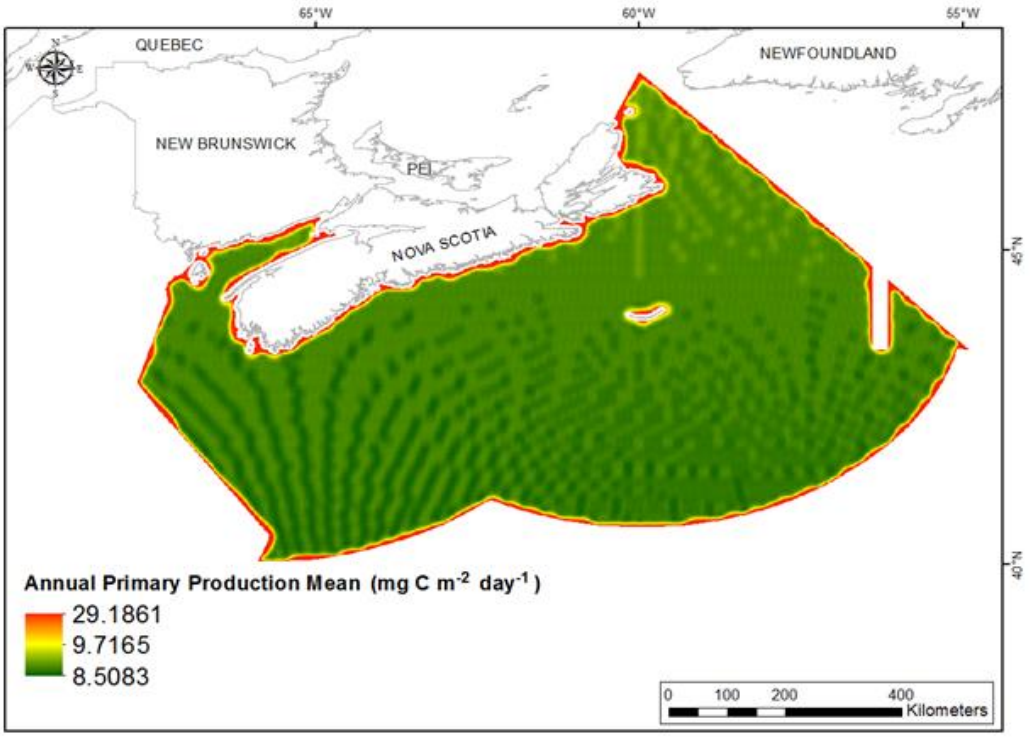

Fig. 479. Prediction standard error surface of Annual Primary Production Mean (mg C m^{-2} day^{-1}).

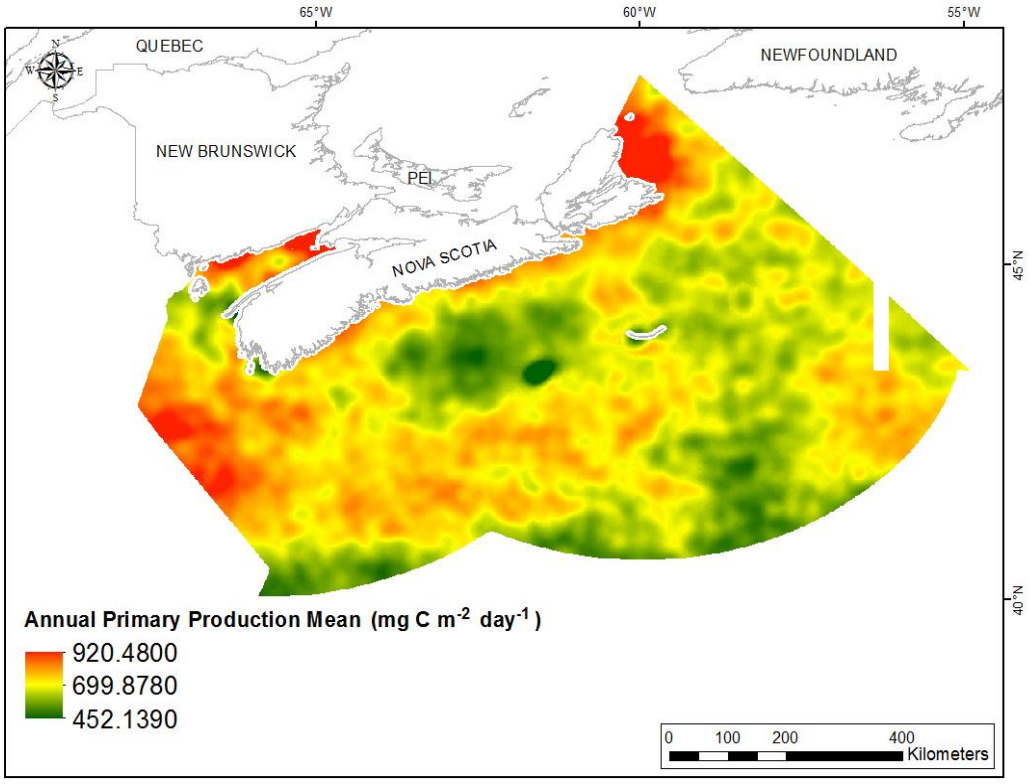

Fig. 480. Interpolated prediction surface of Annual Primary Production Mean (mg C m^{-2} day^{-1}).

Annual Primary Production Minimum

This variable displayed a right-skewed, slightly platykurtic distribution prior to interpolation (Table 193, Fig. 481). The data were higher than predicted by a normal distribution at low and high values and slightly lower than predicted at mid-values (Fig. 482). The areas of under- and over-prediction showed no spatial pattern over the study extent (Fig. 482).

The semivariogram showed moderate autocorrelation present in the data (Fig. 483). The fit between measured and predicted values was fair (Fig. 483), with under-prediction of large values and over-prediction of small values. Good performance of the model was indicated by the cross-validation results (Table 194). The error map showed high error along the edges of the study extent (Fig. 484). The kriged surface is presented in Fig. 485.

Table 193. Distributional properties of Annual Primary Production Minimum (mg C m^{-2} day^{-1}).

Property	Value
Number of Observations	5330
Minimum	77.590
Maximum	502.980
Mean	215.990
Median	207.840
Standard Deviation	60.209
Skewness	0.540
Kurtosis	2.778

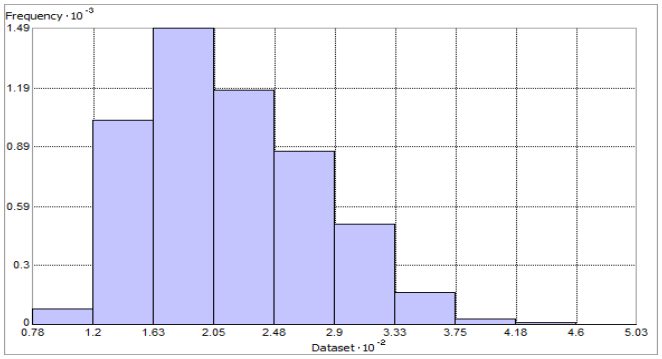

Fig. 481. Distribution of Annual Primary Production Minimum (mg C m^{-2} day^{-1}). Histogram was illustrated using 10 bins. X axis is shown at 10^{-2}; Y axis is shown at 10^{-3}.

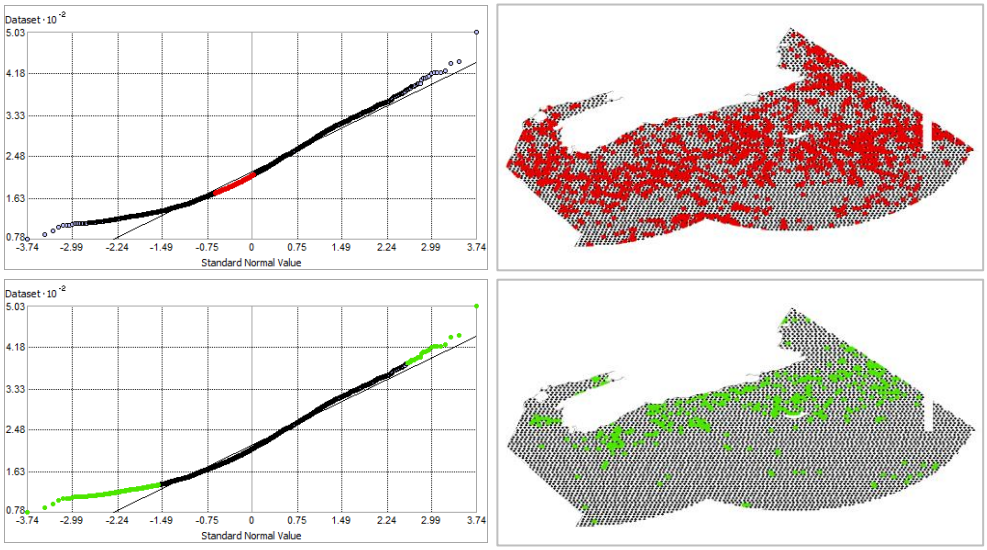

Fig. 482. Normal Q-Q plot for data values of Annual Primary Production Minimum (mg C m^{-2} day^{-1}). Points falling under (upper panel) and over (bottom panel) the reference line are mapped.

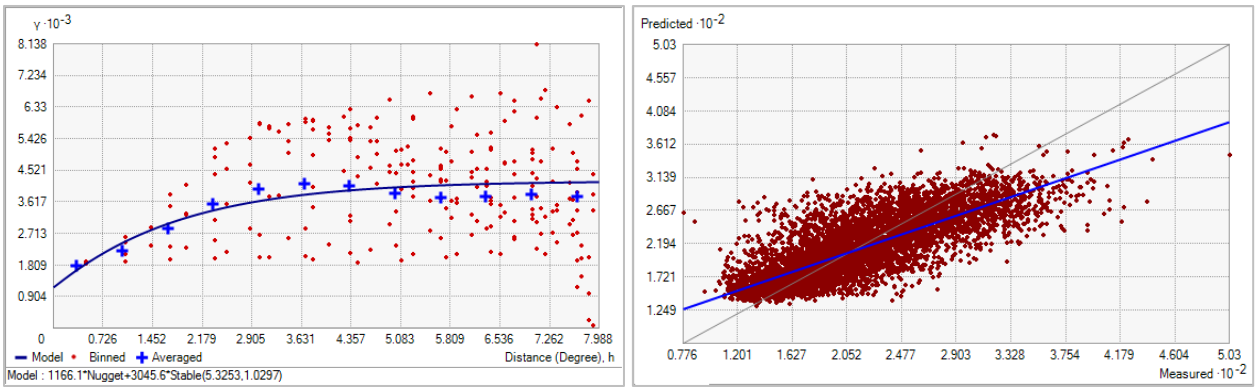

Fig. 483. Left panel: Semivariogram of Annual Primary Production Minimum (mg C m^{-2} day^{-1}). Binned values are shown as red dots; average points are shown as blue crosses; the model fit to the averaged values is shown as a blue line. Lag size: 0.666 degrees; number of lags: 12; Parameter: 1.030; Range: 5.325 degrees; Partial Sill: 3045.595. Right panel: Scatterplot of predicted values versus observed values for the variable Annual Primary Production Minimum (mg C m^{-2} day^{-1}).

Table 194. Results of cross-validation of the kriged model for Annual Primary Production Minimum (mg C m^{-2} day^{-1}).

Prediction error	**Value**
Number of Observations	5330
Overall Mean Error	-0.070
Root Mean Square Prediction Error	38.998
Standardized Mean	-1.633×10^{-3}
Standardized Root Mean Square Prediction Error	1.043
Average Standard Error	37.367

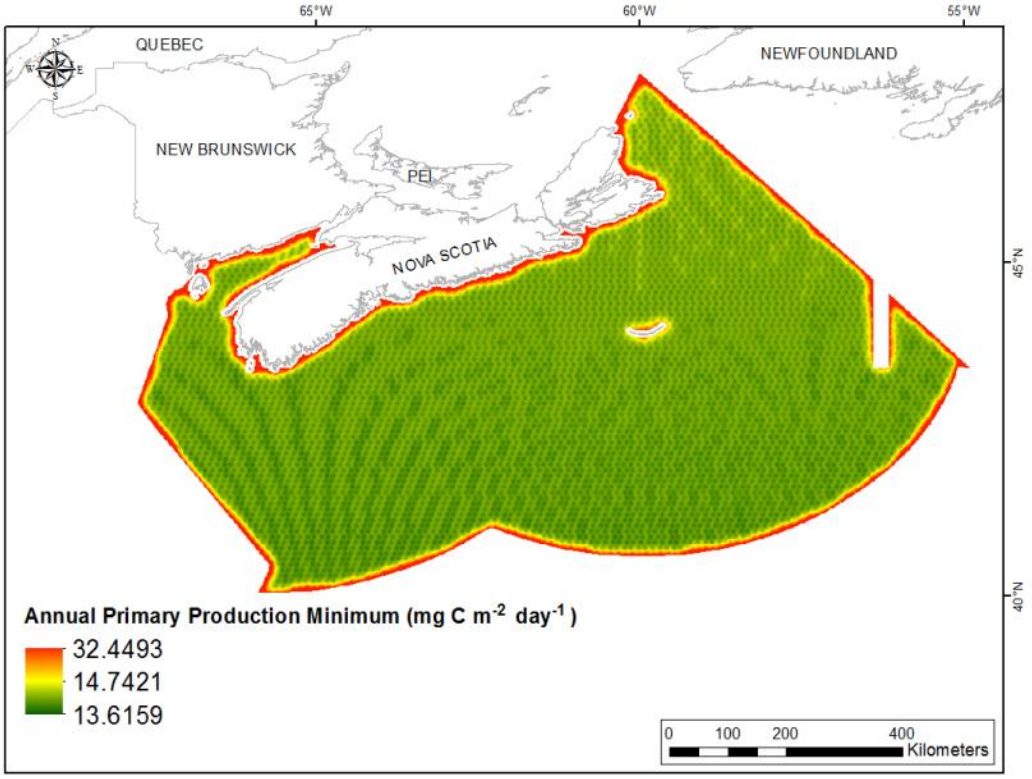

Fig. 484. Prediction standard error surface of Annual Primary Production Minimum (mg C m^{-2} day^{-1}).

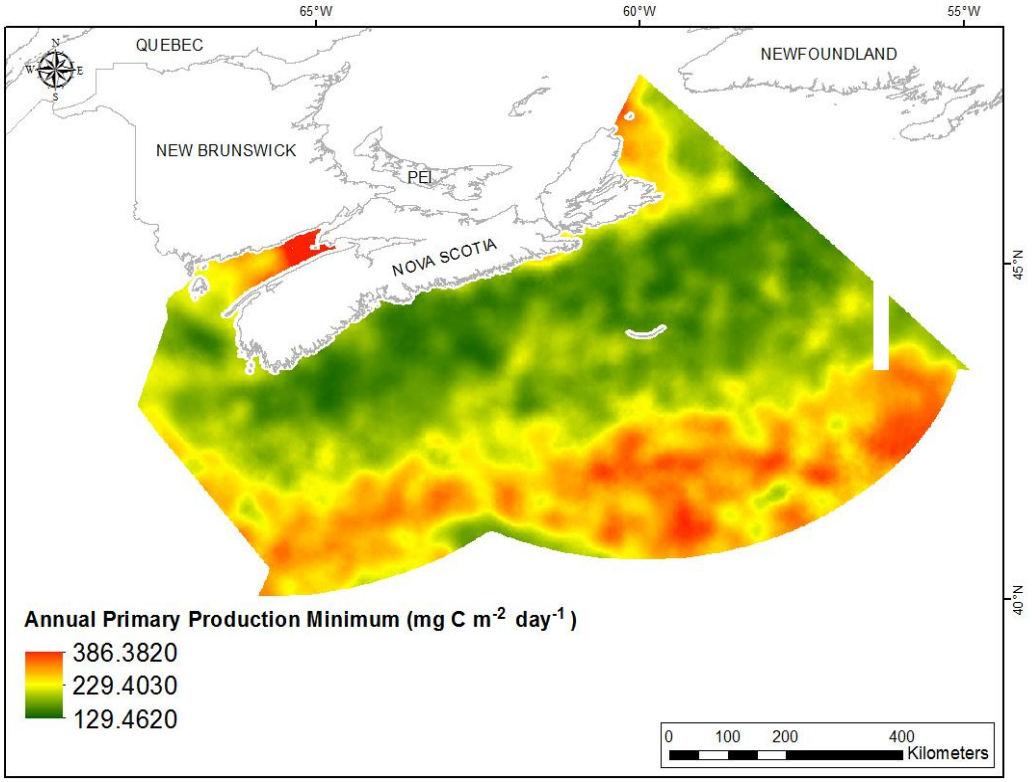

Fig. 485. Interpolated prediction surface of Annual Primary Production Minimum (mg C m^{-2} day^{-1}).

Annual Primary Production Maximum

This variable displayed a left-skewed, leptokurtic distribution with outlying data in the upper range (Table 195, Fig. 486). The data were higher than predicted by a normal distribution at the highest values and lower than predicted at the lowest values (Fig. 487) with good prediction of mid-range values (Fig. 487). The areas of under- and over-prediction showed no spatial pattern over the study extent (Fig. 487).

The semivariogram showed weak to moderate autocorrelation present in the data (Fig. 488). The fit between measured and predicted values was poor (Fig. 488), with under-prediction of large values and over-prediction of small values. The single large outlier was poorly predicted. Nonetheless good performance of the model was indicated by the cross-validation results (Table 196). The error map showed high error along the edges of the study extent (Fig. 489). The kriged surface is presented in Fig. 490.

Table 195. Distributional properties of Annual Primary Production Maximum (mg C m^{-2} day^{-1}).

Property	Value
Number of Observations	5330
Minimum	775.150
Maximum	2980.700
Mean	1461.200
Median	1467.300
Standard Deviation	144.720
Skewness	-0.019
Kurtosis	5.714

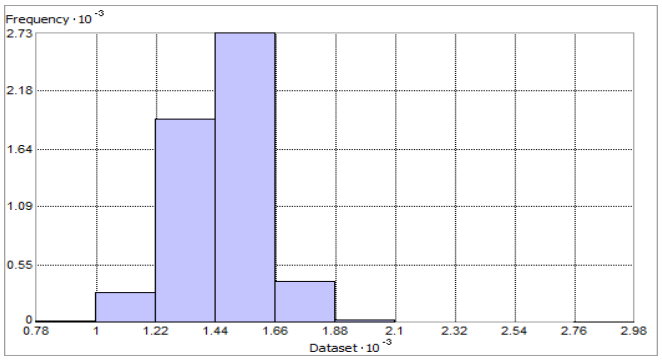

Fig. 486. Distribution of Annual Primary Production Maximum (mg C m^{-2} day^{-1}). Histogram was illustrated using 10 bins. X and Y axes are shown at 10^{-3}.

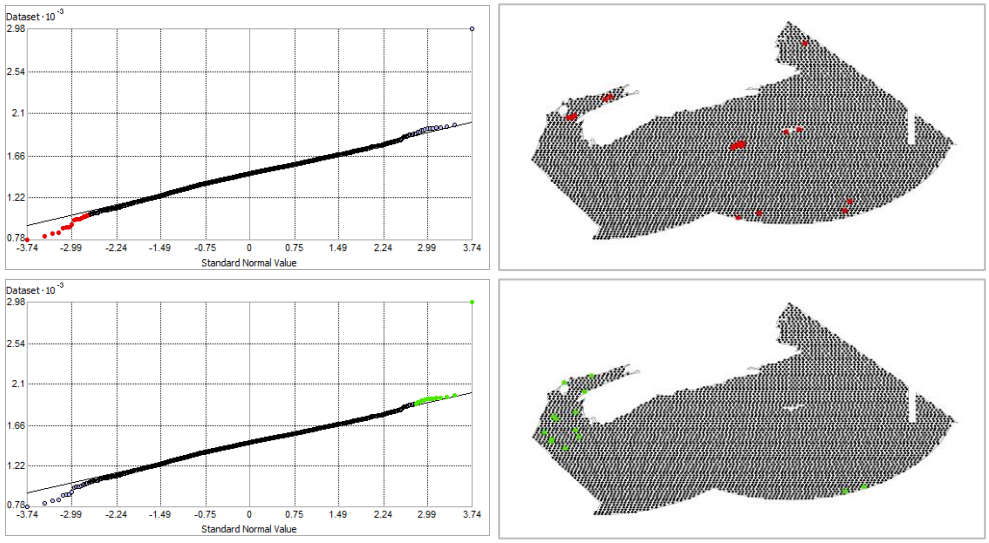

Fig. 487. Normal Q-Q plot for data values of Annual Primary Production Maximum (mg C m^{-2} day^{-1}). Points falling under (upper panel) and over (bottom panel) the reference line are mapped.

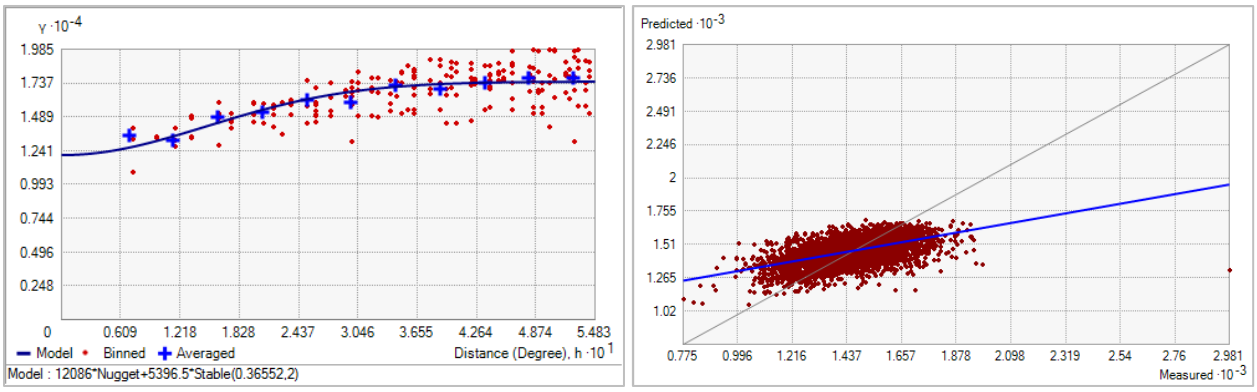

Fig. 488. Left panel: Semivariogram of Annual Primary Production Maximum (mg C m^{-2} day^{-1}). Binned values are shown as red dots; average points are shown as blue crosses; the model fit to the averaged values is shown as a blue line. Lag size: 0.046 degrees; number of lags: 12; Parameter: 2; Range: 0.366 degrees; Partial Sill: 5396.508. Right panel: Scatterplot of predicted values versus observed values for the variable Annual Primary Production Maximum (mg C m^{-2} day^{-1}).

Table 196. Results of cross-validation of the kriged model for Annual Primary Production Maximum (mg C m^{-2} day^{-1}).

Prediction error	**Value**
Number of Observations	5330
Overall Mean Error	0.077
Root Mean Square Prediction Error	122.062
Standardized Mean	6.112×10^{-4}
Standardized Root Mean Square Prediction Error	1.024
Average Standard Error	118.877

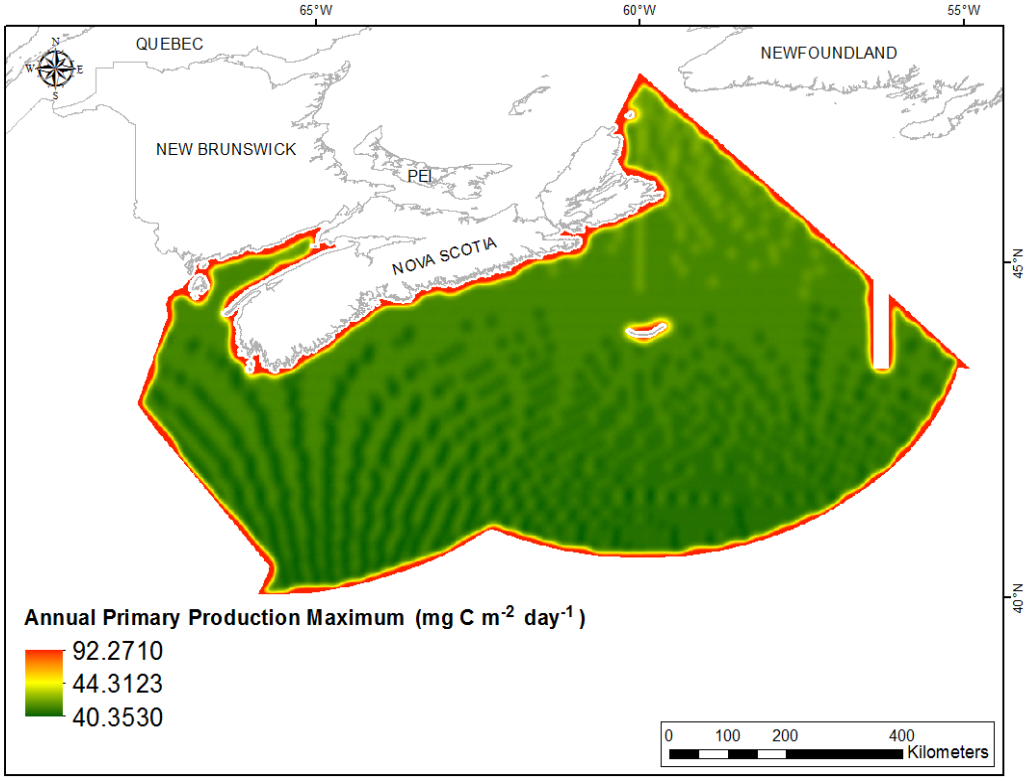

Fig. 489. Prediction standard error surface of Annual Primary Production Maximum (mg C m^{-2} day^{-1}).

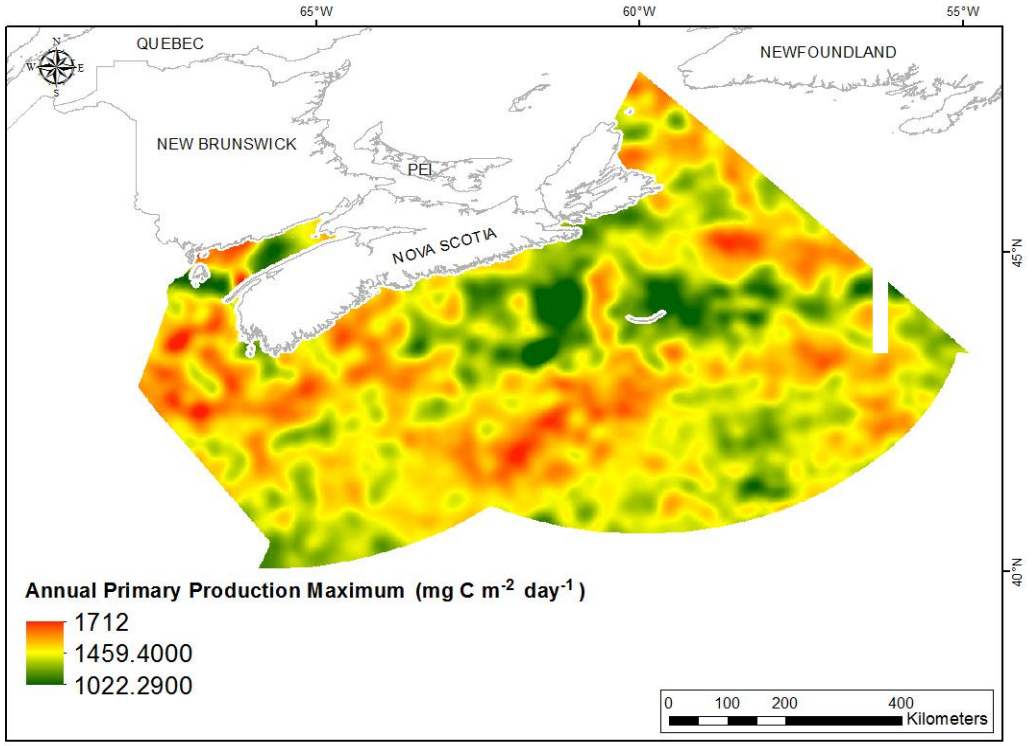

Fig. 490. Interpolated prediction surface of Annual Primary Production Maximum (mg C m^{-2} day^{-1}).

Annual Primary Production Range

This variable displayed a leptokurtic distribution with outlying data in the upper range prior to interpolation (Table 197, Fig. 591). The data were higher than predicted by a normal distribution at the highest value and lower than predicted at the lowest values (Fig. 492). However, the mid-region was well-predicted. The areas of under- and over-prediction showed no spatial pattern over the study extent (Fig. 492).

The semivariogram showed weak autocorrelation present in the data and the model showed poor fit between measured and predicted values (Fig. 493). The fit between measured and predicted values was poor (Fig. 493), with under-prediction of large values and over-prediction of small values. The single large outlier was poorly predicted. Nonetheless good performance of the model was indicated by the cross-validation results (Table 198). The error map showed high error along the edges of the study extent (Fig. 494). The kriged surface is presented in Fig. 495.

Table 197. Distributional properties of Annual Primary Production Range (mg C m^{-2} day^{-1}).

Property	Value
Number of Observations	5330
Minimum	615.040
Maximum	2697.700
Mean	1245.200
Median	1244.600
Standard Deviation	155.38
Skewness	0.059
Kurtosis	4.530

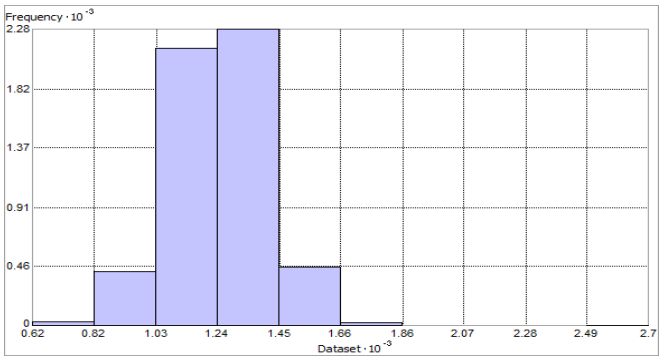

Fig. 491. Distribution of Annual Primary Production Range (mg C m^{-2} day^{-1}). Histogram was illustrated using 10 bins. X and Y axes are shown at 10^{-3}.

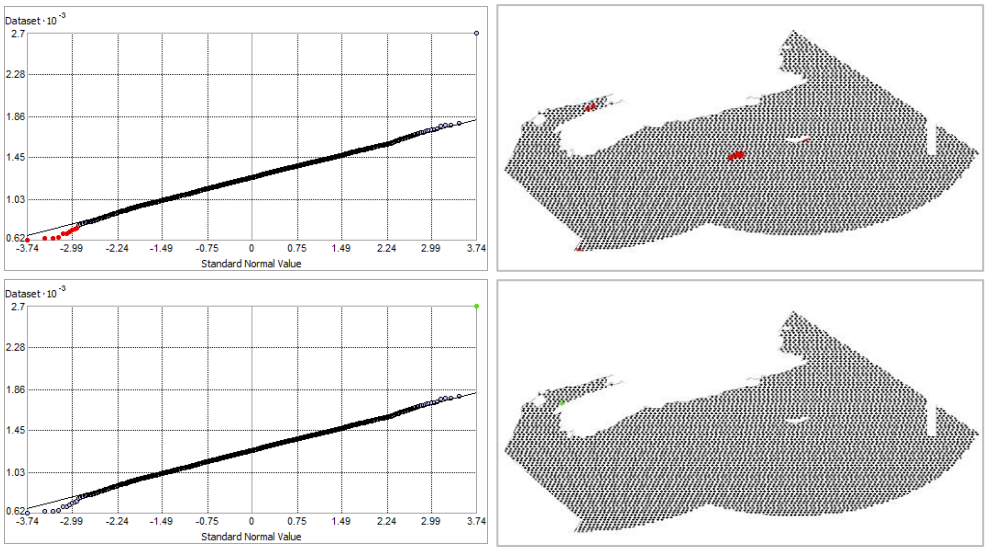

Fig. 492. Normal Q-Q plot for data values of Annual Primary Production Range (mg C m^{-2} day^{-1}). Points falling under (upper panel) and over (bottom panel) the reference line are mapped.

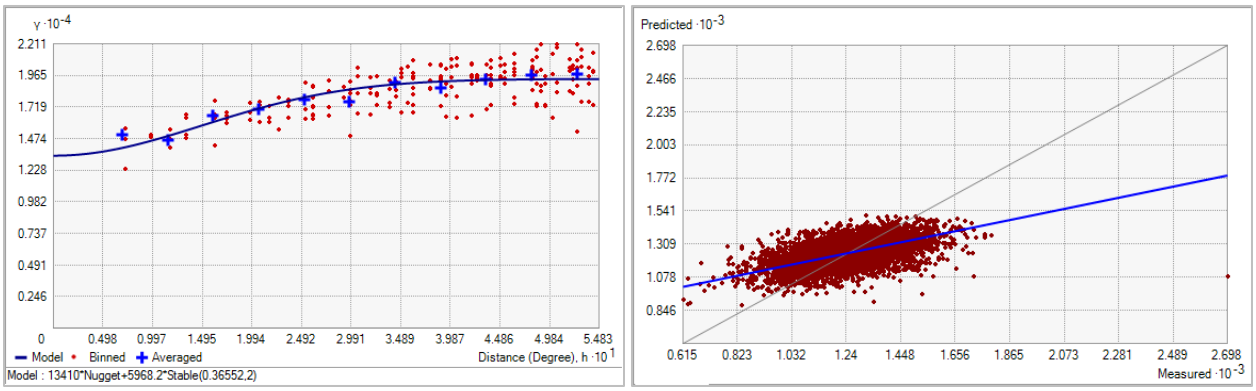

Fig. 493. Left panel: Semivariogram of Annual Primary Production Range (mg C m^{-2} day^{-1}). Binned values are shown as red dots; average points are shown as blue crosses; the model fit to the averaged values is shown as a blue line. Lag size: 0.046 degrees; number of lags: 12; Parameter: 2; Range: 0.366 degrees; Partial Sill: 5968.154. Right panel: Scatterplot of predicted values versus observed values for the variable Annual Primary Production Range (mg C m^{-2} day^{-1}).

Table 198. Results of cross-validation of the kriged model for Annual Primary Production Range (mg C m^{-2} day^{-1}).

Prediction error	**Value**
Number of Observations	5330
Overall Mean Error	0.179
Root Mean Square Prediction Error	128.527
Standardized Mean	1.287×10^{-3}
Standardized Root Mean Square Prediction Error	1.024
Average Standard Error	125.205

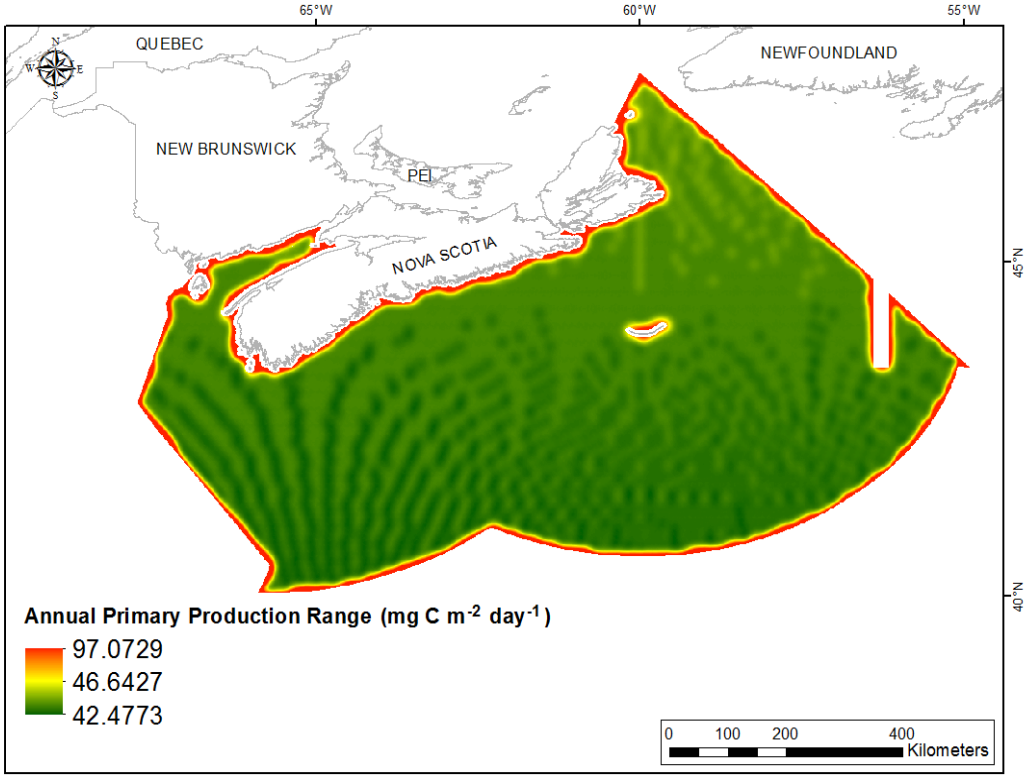

Fig. 494. Prediction standard error surface of Annual Primary Production Range (mg C m^{-2} day^{-1}).

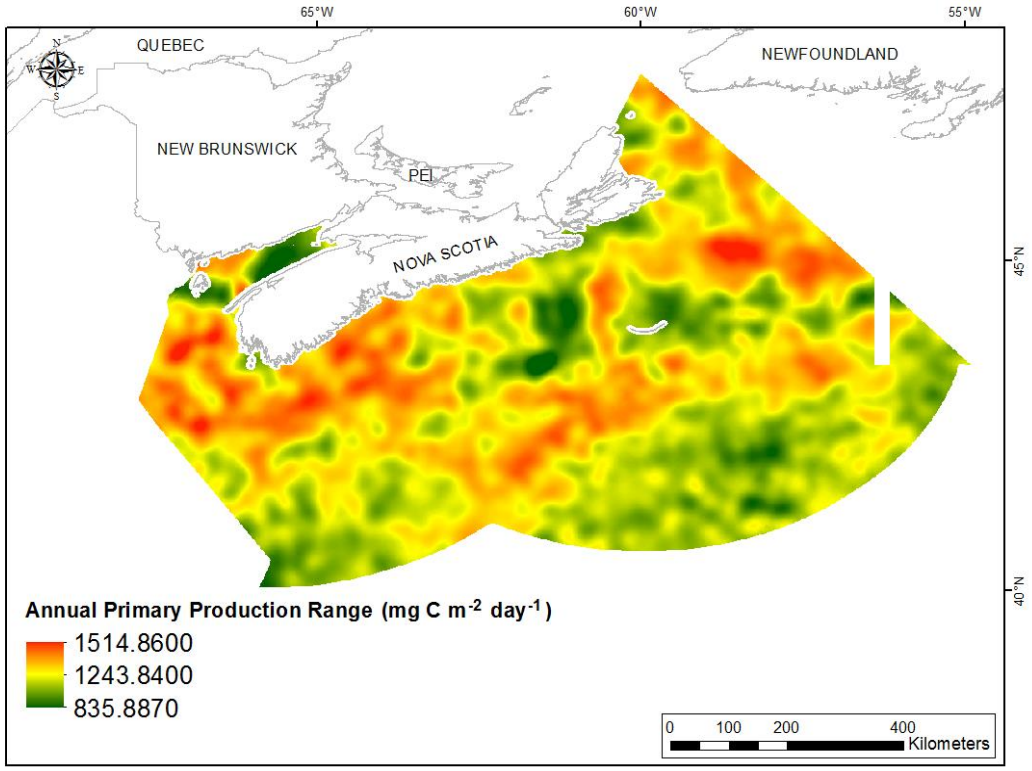

Fig. 495. Interpolated prediction surface of Annual Primary Production Range (mg C m^{-2} day^{-1}).

Annual Primary Production Average Minimum

This variable displayed a leptokurtic distribution with outlying data in the upper range (Table 199, Fig. 496). The data were higher than predicted by a normal distribution at both tails, however, the mid-region was well-predicted (Fig. 497). The areas of over-prediction showed little spatial pattern over the study extent (Fig. 497).

The semivariogram showed moderate autocorrelation present in the data (Fig. 498). The model showed a poor fit between measured and predicted values (Fig. 498), with over-prediction of small values and under-prediction of large values. Nonetheless, good performance of the model was indicated by the cross-validation results (Table 200). The error map showed high error along the edges of the study extent (Fig. 499). The kriged surface is presented in Fig. 500.

Table 199. Distributional properties of Annual Primary Production Average Minimum (mg C m^{-2} day^{-1}).

Property	Value
Number of Observations	5330
Minimum	168.570
Maximum	804.370
Mean	324.180
Median	3324.180
Standard Deviation	56.056
Skewness	0.458
Kurtosis	4.360

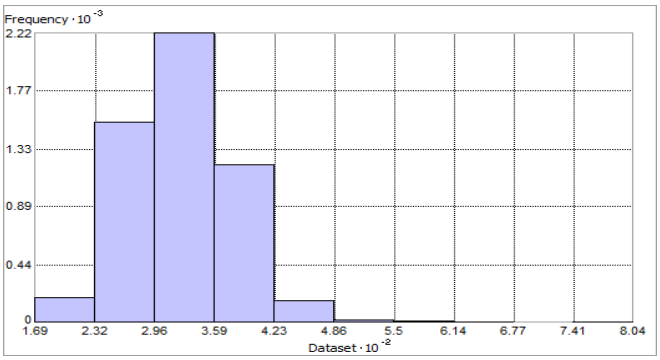

Fig. 496. Distribution of Annual Primary Production Average Minimum (mg C m^{-2} day^{-1}). Histogram was illustrated using 10 bins. X axis is shown at 10^{-2}; Y axis is shown at 10^{-3}.

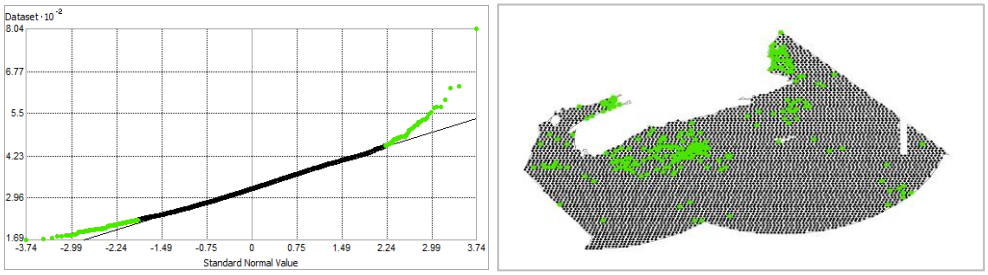

Fig. 497. Normal Q-Q plot for data values of Annual Primary Production Average Minimum (mg C m^{-2} day^{-1}). Points falling over the reference line are mapped. No points fall under the reference line.

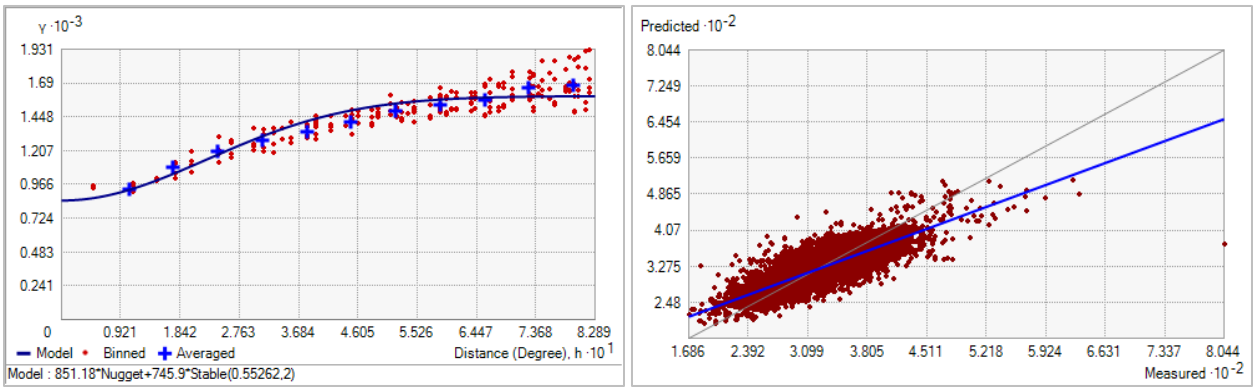

Fig. 498. Semivariogram of Annual Primary Production Average Minimum (mg C m^{-2} day^{-1}). Binned values are shown as red dots; average points are shown as blue crosses; the model fit to the averaged values is shown as a blue line. Lag size: 0.069 degrees; number of lags: 12; Parameter: 2; Range: 0.553 degrees; Partial Sill: 745.901. Right panel: Scatterplot of predicted values versus observed values for the model of Annual Primary Production Average Minimum (mg C m^{-2} day^{-1}).

Table 200. Results of cross-validation of the kriged model for Annual Primary Production Average Minimum (mg C m^{-2} day^{-1}).

Prediction error	**Value**
Number of Observations	5330
Overall Mean Error	-0.081
Root Mean Square Prediction Error	32.097
Standardized Mean	-1.863×10^{-3}
Standardized Root Mean Square Prediction Error	1.030
Average Standard Error	31.061

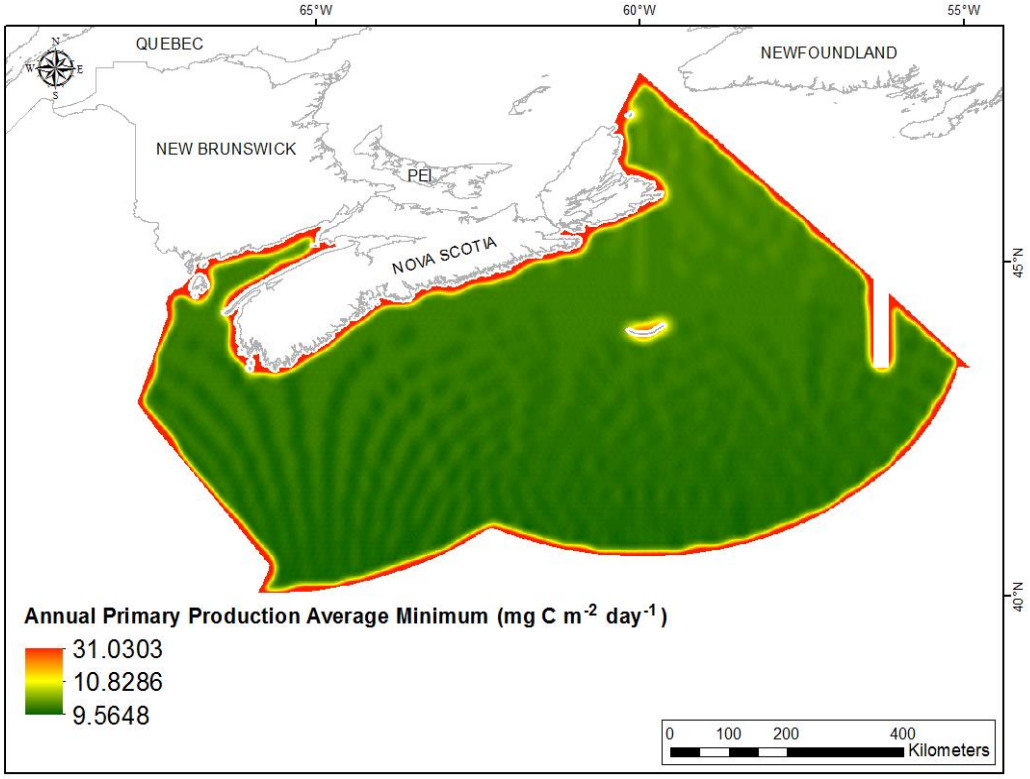

Fig. 499. Prediction standard error surface of Annual Primary Production Average Minimum (mg C m^{-2} day^{-1}).

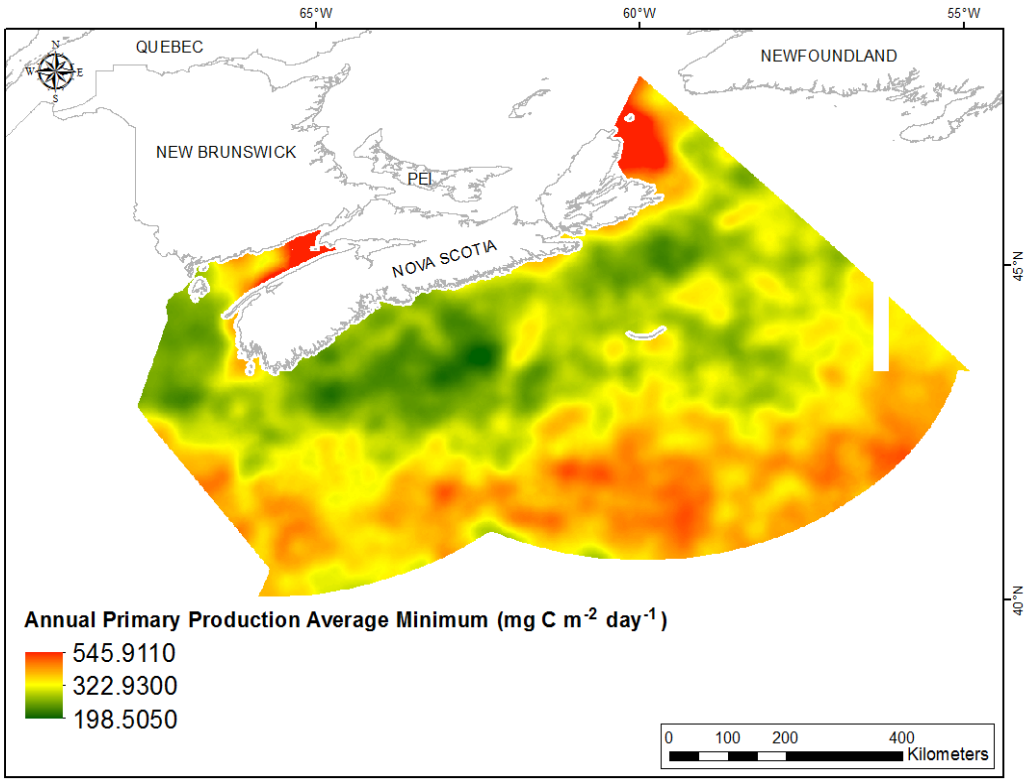

Fig. 500. Interpolated prediction surface of Annual Primary Production Average Minimum (mg C m^{-2} day^{-1}).

Annual Primary Production Average Maximum

This variable displayed a near-normal distribution with slight negative skew and leptokurtosis prior to interpolation (Table 201, Fig. 501). The data were lower than predicted by a normal distribution at both tails, however the mid-region was well-predicted (Fig. 502). The areas of under-prediction showed no spatial pattern over the study extent (Fig. 502).

The semivariogram showed moderate autocorrelation present in the data (Fig. 503). The model showed a poor fit between measured and predicted values (Fig. 503), with over-prediction of small values and under-prediction of large values. Nonetheless, good performance of the model was indicated by the cross-validation results (Table 202). The error map showed high error along the edges of the study extent (Fig. 504). The kriged surface is presented in Fig. 505.

Table 201. Distributional properties of Annual Primary Production Average Maximum (mg C m^{-2} day^{-1}).

Property	Value
Number of Observations	5330
Minimum	598.620
Maximum	1570.800
Mean	1199.300
Median	1199.800
Standard Deviation	109.960
Skewness	-0.152
Kurtosis	3.362

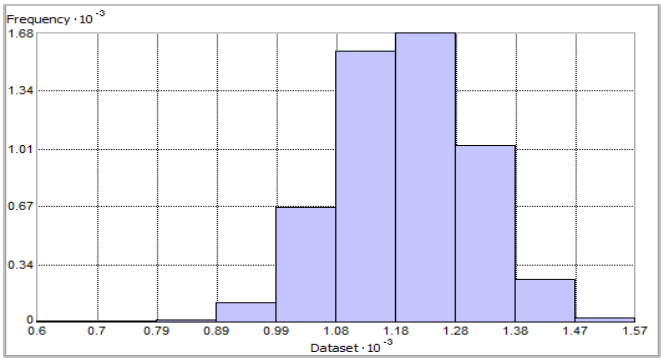

Fig. 501. Distribution of Annual Primary Production Average Maximum (mg C m^{-2} day^{-1}). Histogram was illustrated using 10 bins. X and Y axes are shown at 10^{-3}.

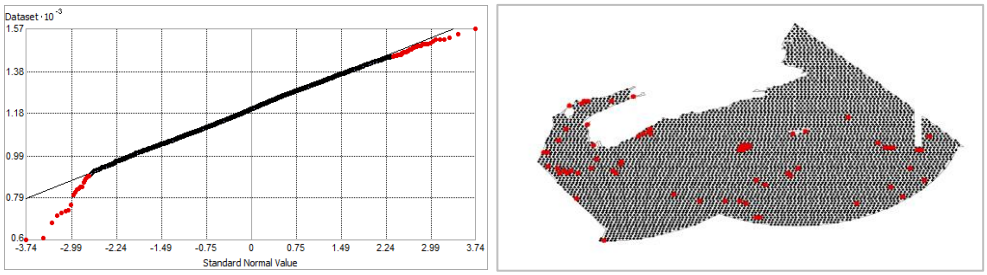

Fig. 502. Normal Q-Q plot for data values of Annual Primary Production Average Maximum (mg C m^{-2} day^{-1}). Points falling under the reference line are mapped. No points fall over the reference line.

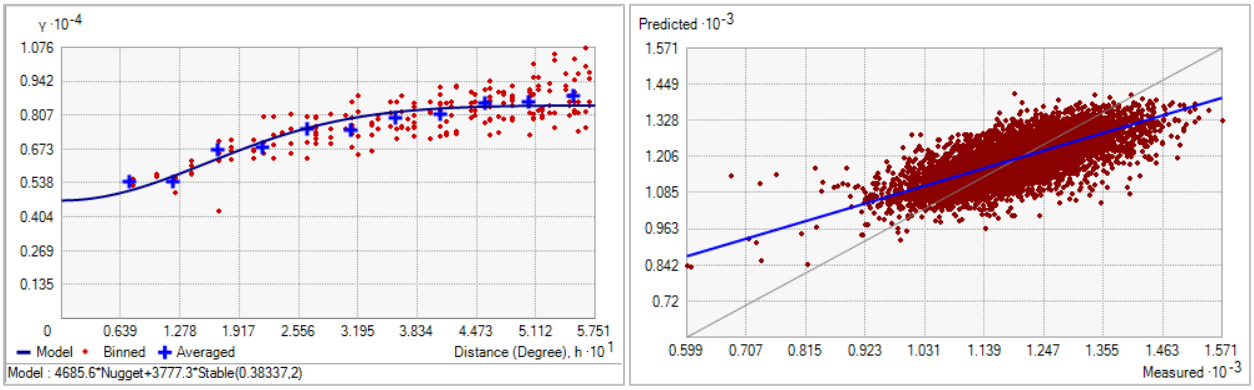

Fig. 503. Semivariogram of Annual Primary Production Average Maximum (mg C m^{-2} day^{-1}). Binned values are shown as red dots; average points are shown as blue crosses; the model fit to the averaged values is shown as a blue line. Lag size: 0.048 degrees; number of lags: 12; Parameter: 2; Range: 0.383 degrees; Partial Sill: 3777.334. Right panel: Scatterplot of predicted values versus observed values for the model of Annual Primary Production Average Maximum (mg C m^{-2} day^{-1}).

Table 202. Results of cross-validation of the kriged model for Annual Primary Production Average Maximum (mg C m^{-2} day^{-1}).

Prediction error	**Value**
Number of Observations	5330
Overall Mean Error	0.057
Root Mean Square Prediction Error	76.820
Standardized Mean	4.581×10^{-4}
Standardized Root Mean Square Prediction Error	1.018
Average Standard Error	75.348

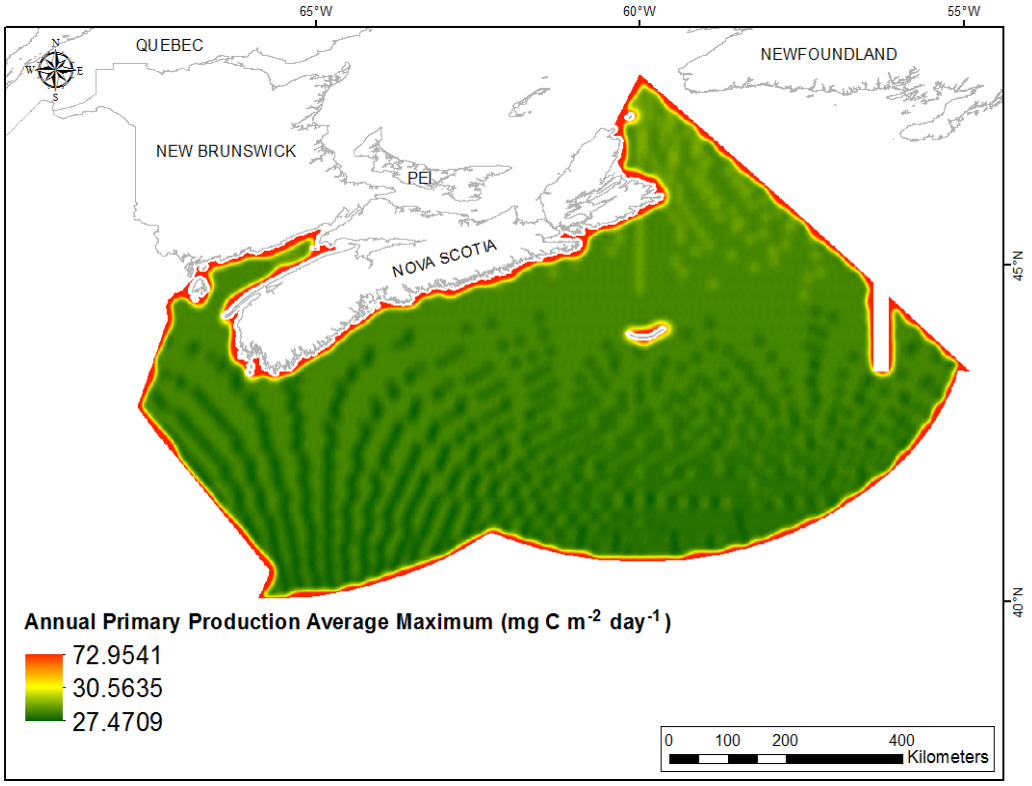

Fig. 504. Prediction standard error surface of Annual Primary Production Average Maximum (mg C m^{-2} day^{-1}).

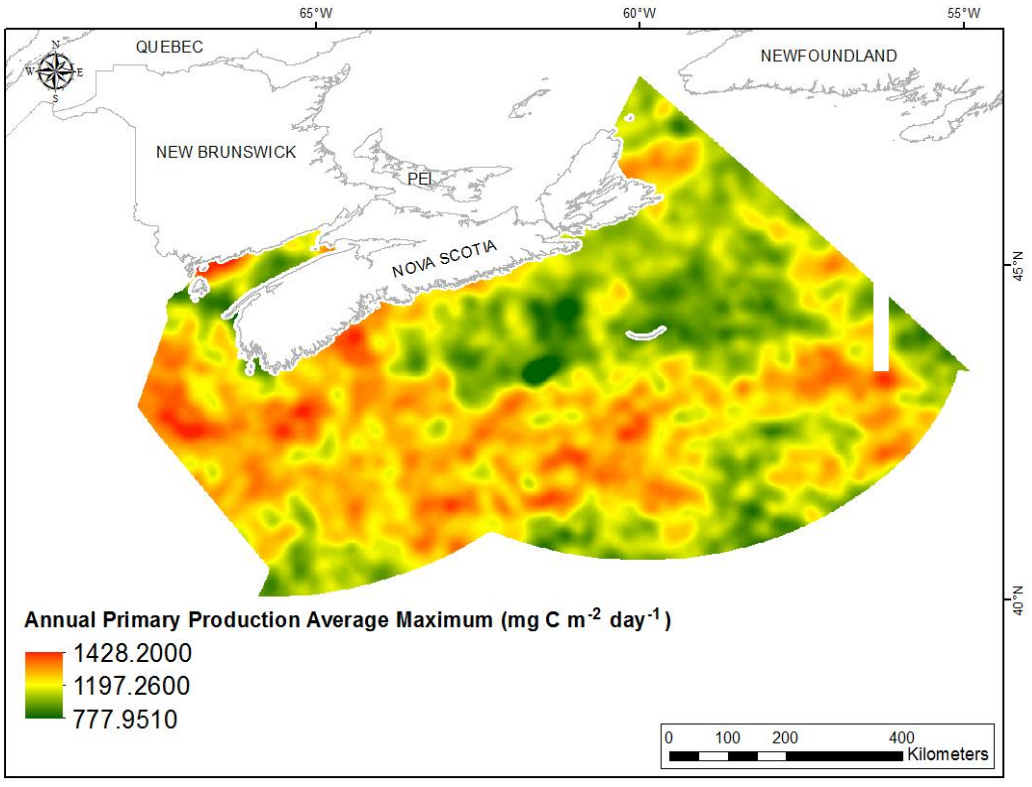

Fig. 505. Interpolated prediction surface of Annual Primary Production Average Maximum (mg C m^{-2} day^{-1}).

Annual Primary Production Average Range

This variable displayed a near-normal distribution with slight negative skew prior to interpolation (Table 203, Fig. 506). The data were lower than predicted by a normal distribution at both tails, however the mid-values were well predicted (Fig. 507). The areas of under-prediction showed no spatial pattern over the study extent (Fig. 507).

The semivariogram showed moderate autocorrelation present in the data (Fig. 508). The model showed a poor fit between measured and predicted values (Fig. 508), with over-prediction of small values and under-prediction of large values. Nonetheless, good performance of the model was indicated by the cross-validation results (Table 204). The error map showed high error along the edges of the study extent (Fig. 509). The kriged surface is presented in Fig. 510.

Table 203. Distributional properties of Annual Primary Production Average Range (mg C m^{-2} day^{-1}).

Property	Value
Number of Observations	5330
Minimum	242.500
Maximum	1237.400
Mean	875.160
Median	873.38
Standard Deviation	120.11
Skewness	-0.062
Kurtosis	3.191

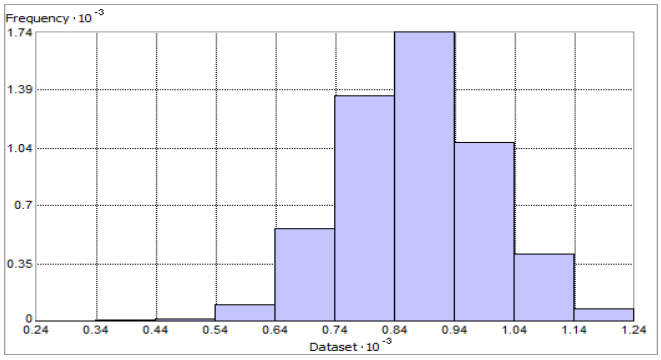

Fig. 506. Distribution of Annual Primary Production Average Range (mg C m^{-2} day^{-1}). Histogram was illustrated using 10 bins. X and Y axes are shown at 10^{-3}.

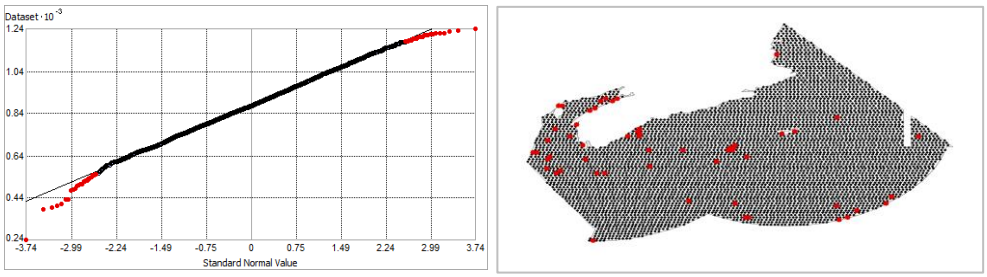

Fig. 507. Normal Q-Q plot for data values of Annual Primary Production Average Range (mg C m^{-2} day^{-1}). Points falling under the reference line are mapped. No points fall over the reference line.

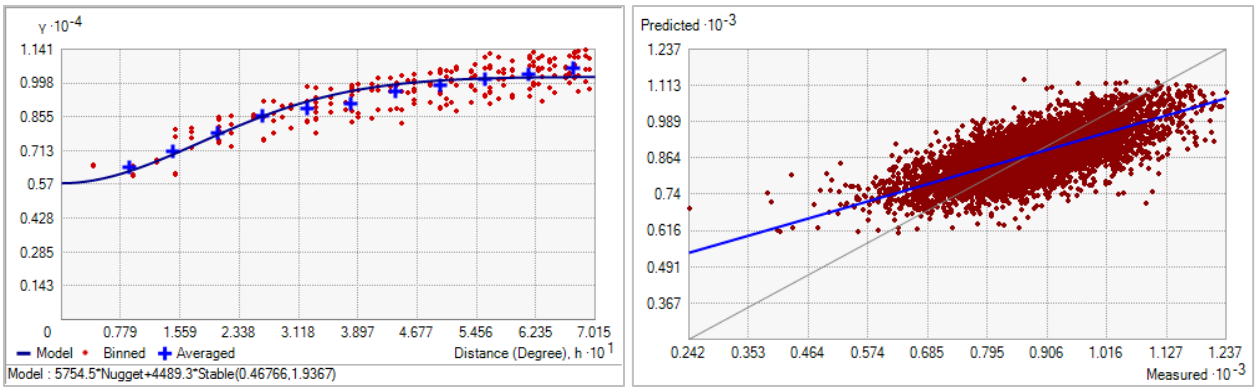

Fig. 508. Semivariogram of Annual Primary Production Average Range (mg C m^{-2} day^{-1}). Binned values are shown as red dots; average points are shown as blue crosses; the model fit to the averaged values is shown as a blue line. Lag size: 0.058 degrees; number of lags: 12; Parameter: 1.937 Range: 0.468 degrees; Partial Sill: 4489.26. Right panel: Scatterplot of predicted values versus observed values for the model of Annual Primary Production Average Range (mg C m^{-2} day^{-1}).

Table 204. Results of cross-validation of the kriged model for Annual Primary Production Average Range (mg C m^{-2} day^{-1}).

Prediction error	**Value**
Number of Observations	5330
Overall Mean Error	0.161
Root Mean Square Prediction Error	83.366
Standardized Mean	1.433×10^{-3}
Standardized Root Mean Square Prediction Error	1.014
Average Standard Error	82.097

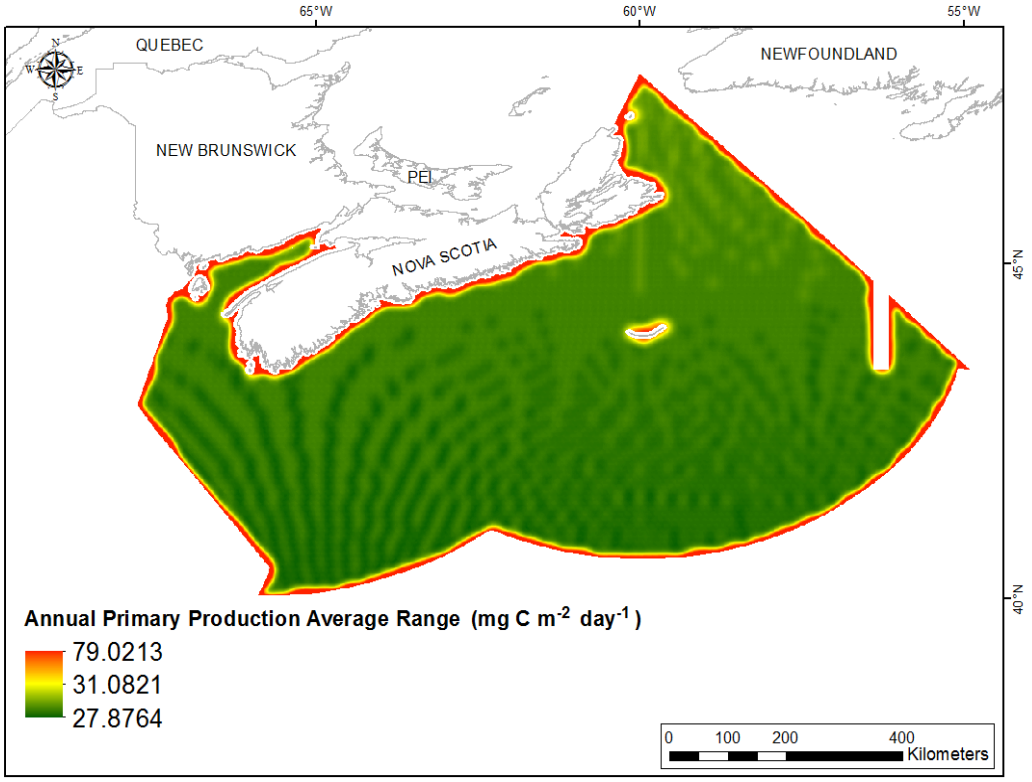

Fig. 509. Prediction standard error surface of Annual Primary Production Average Range (mg C m^{-2} day^{-1}).

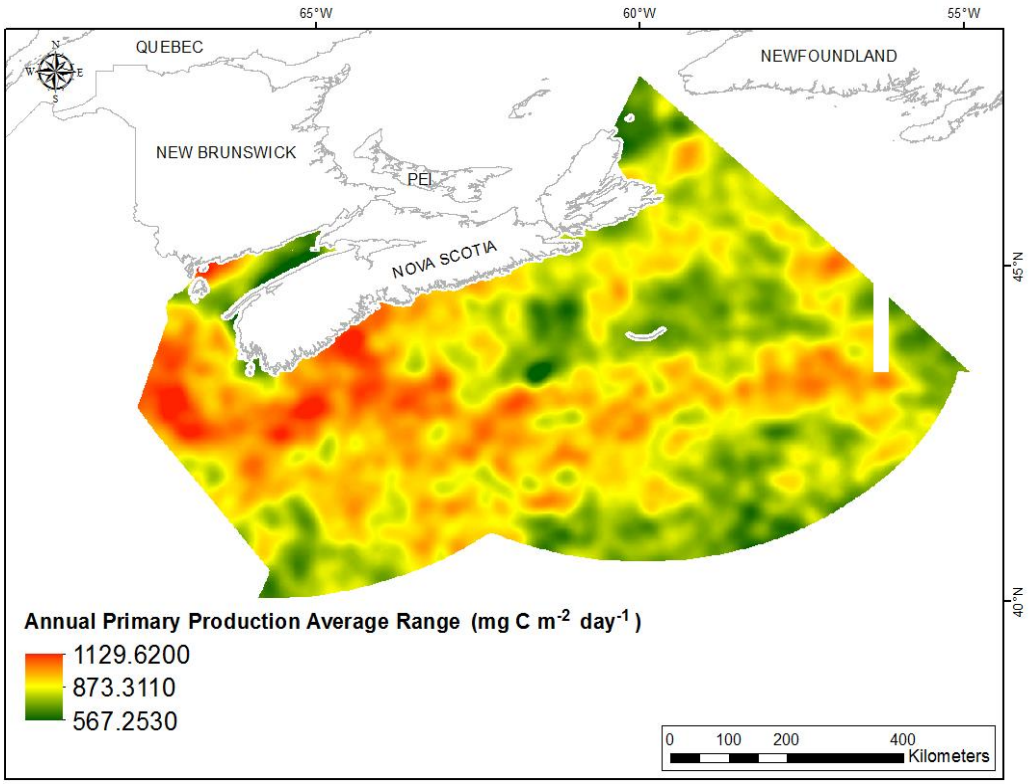

Fig. 510. Interpolated prediction surface of Annual Primary Production Average Range (mg C m^{-2} day^{-1}).

Dissolved Oxygen

Dissolved oxygen affects the distribution of marine animals, and is produced in the marine environment. The ratio of dissolved oxygen to carbon is used to estimate net primary production during a bloom period (Queste et al., 2015). Generally, as water stratification develops in the spring, nitrate, phosphate, and silicate nutrients are consumed and drawn down to deeper water by phytoplankton and remain low throughout the rest of the year, while dissolved oxygen decreases (Manasrah et al., 2006).

Dissolved Oxygen

This variable displayed a bimodal distribution prior to interpolation (Table 205, Fig. 511). The data were higher than predicted by a normal distribution at the lowest and upper mid-range values, and lower than the reference line at mid-values (Fig. 512). The areas of under- and over-prediction showed no spatial pattern over the study extent (Fig. 512).

The semivariogram showed weak autocorrelation present in the data (Fig. 513). The model showed poor fit between measured and predicted values (Fig. 513), with over-prediction of low values and under-prediction of high values. Poor model performance was also indicated by the cross-validation statistics (Table 206). The error map showed a highly discontinuous and patchy pattern over the study extent with low error at the location of data observations (Fig. 514). The kriged surface, which is also patchy and discontinuous, is presented in Fig. 515.

Table 205. Distributional properties of Dissolved Oxygen (ml l^{-1}).

Property	Value
Number of Observations	1867
Minimum	2.963
Maximum	9.564
Mean	5.560
Median	5.266
Standard Deviation	1.201
Skewness	0.389
Kurtosis	2.396

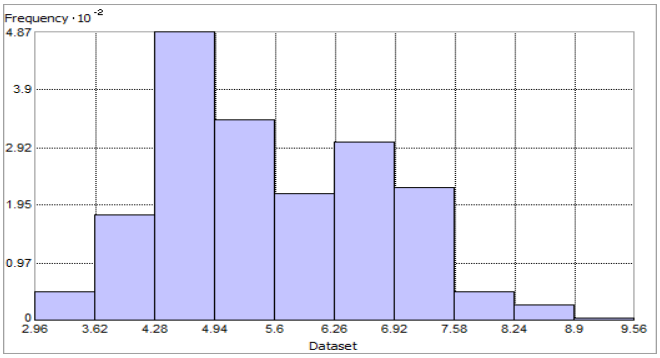

Fig. 511. Distribution of Dissolved Oxygen (ml l^{-1}). Histogram was illustrated using 10 bins. Y axis is shown at 10^{-2}.

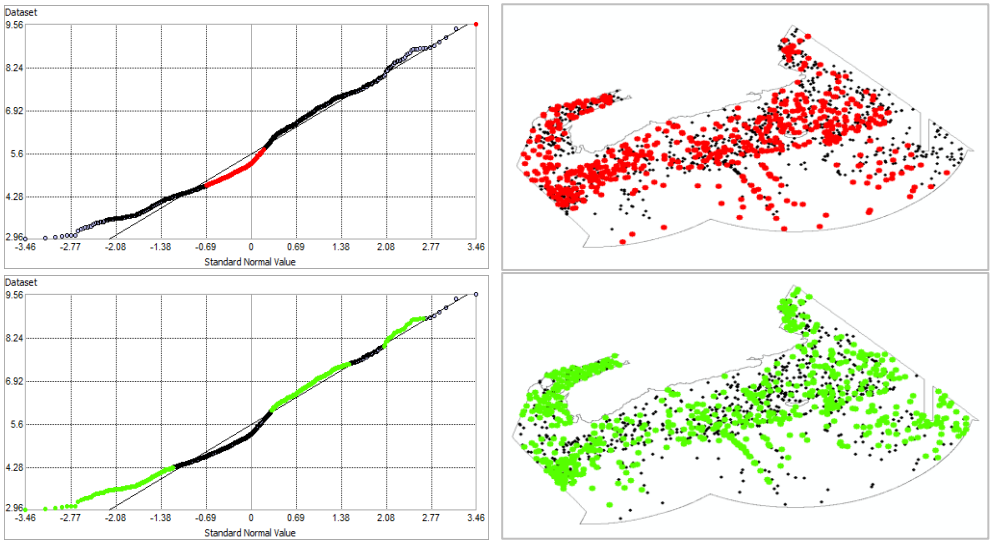

Fig. 512. Normal Q-Q plot for data values of Dissolved Oxygen (ml l^{-1}). Points falling under (upper panel) and over (bottom panel) the reference line are mapped.

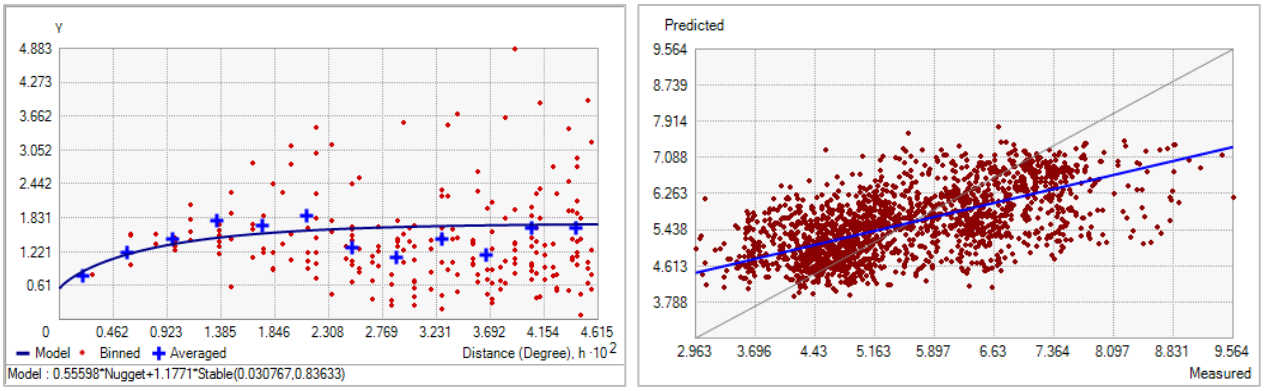

Fig. 513. Left panel: Semivariogram of Dissolved Oxygen (ml l^{-1}). Binned values are shown as red dots; average points are shown as blue crosses; the model fit to the averaged values is shown as a blue line. Lag size: 0.004 degrees; number of lags: 12; Parameter: 0.836; Range: 0.031 degrees; Partial Sill: 1.177. Right panel: Scatterplot of predicted values versus observed values for the variable Dissolved Oxygen (ml l^{-1}).

Table 206. Results of cross-validation of the kriged model for Dissolved Oxygen (ml l^{-1}).

Prediction error	**Value**
Number of Observations	1867
Overall Mean Error	0.021
Root Mean Square Prediction Error	0.970
Standardized Mean	0.008
Standardized Root Mean Square Prediction Error	0.753
Average Standard Error	1.326

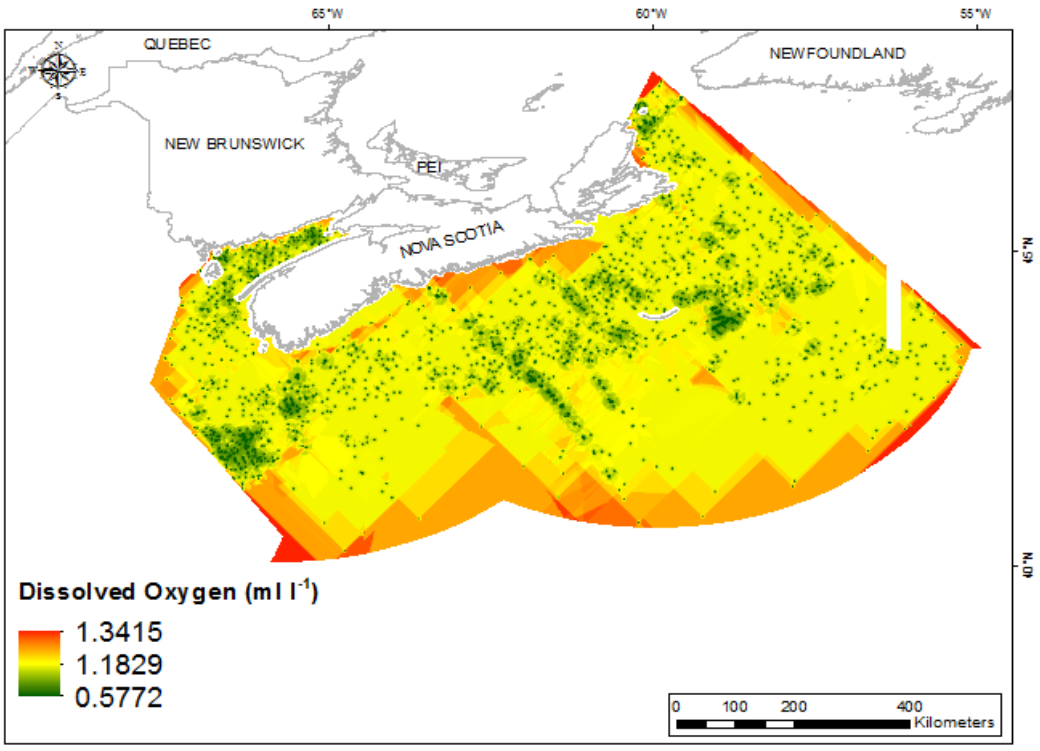

Fig. 514. Prediction standard error surface of Dissolved Oxygen (ml l^{-1}).

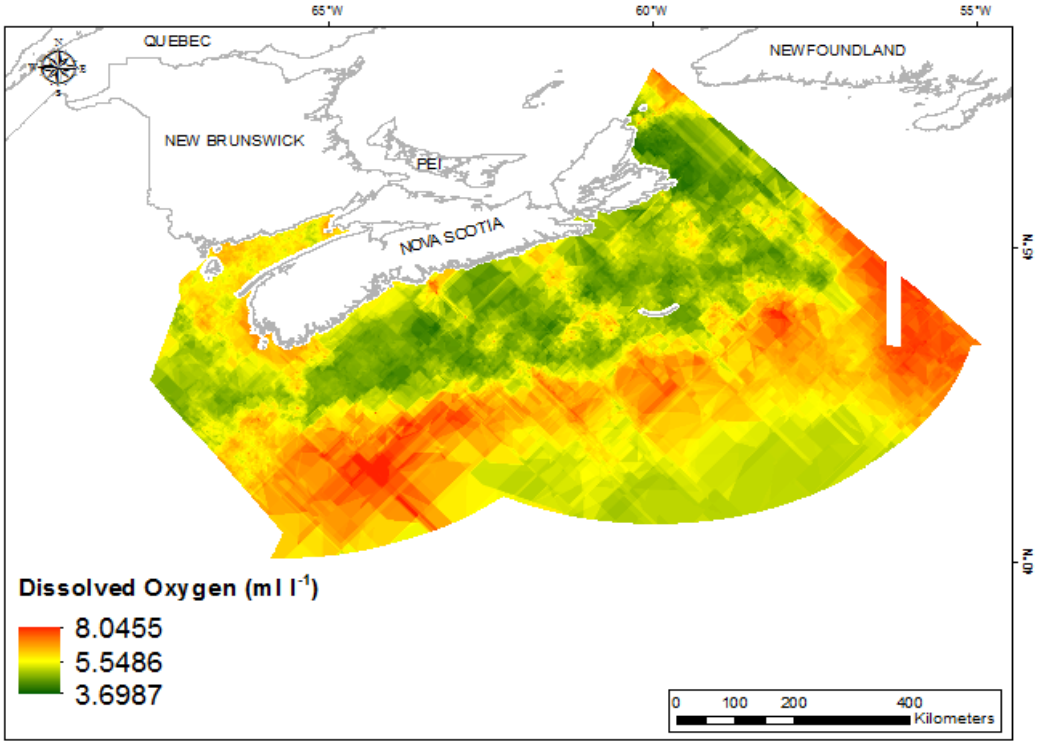

Fig. 515. Interpolated prediction surface of Dissolved Oxygen (ml l^{-1}).

ACKNOWLEDGMENTS

Funding for this technical report was received from a Strategic Program for Ecosystem-Based Research and Advice (SPERA) project to E. Kenchington. We thank C. Fuentes-Yaco and G. White (DFO-MAR) for providing the chlorophyll *a* and primary production data, respectively. We thank J. Murillo and A. Serdynska (DFO) for their review of this document.

REFERENCES

Beazley, L., Kenchington, E., Murillo, F.J., Lirette, C., Guijarro, J., McMillan, A., and Knudby, A. 2016a. Species Distribution Modelling of Corals and Sponges in the Maritimes Region for Use in the Identification of Significant Benthic Areas. Can. Tech. Rep. Fish. Aquat. Sci. 3172: vi + 189p.

Beazley, L., Lirette, C., Sabaniel, J., Wang, Z., Knudby, A., and Kenchington, E. 2016b. Characteristics of Environmental Data Layers for Use in Species Distribution Modelling in the Gulf of St. Lawrence. Can. Tech. Rep. Fish. Aquat. Sci. 3154: viii + 357p.

Beazley, L., Kenchington, E., and Lirette, C. 2017. Species Distribution Modelling and Kernel Density Analysis of Benthic Ecologically and Biologically Significant Areas (EBSAs) and Other Benthic Fauna in the Maritimes Region. Can. Tech. Rep. Fish. Aquat. Sci. 3204: vi + 159p.

Beazley, L.I., Kenchington, E.L., Murillo, F.J., and Sacau, M. 2013. Deep-sea sponge grounds enhance diversity and abundance of epibenthic megafauna in the Northwest Atlantic. ICES J. Mar. Sci. 70: 1471–1490.

Bender, M., Grande, K., and Johnson, K. 1987. A comparison of four methods for determining planktonic community production. Limnol. Oceanogr. 32: 1085-1098.

Boyer, T.P., Antonov, J.I., Baranova, O.K., and 12 others. 2013, World Ocean Database 2013. Sydney Levitus, Ed.; Alexey Mishonov, Technical Ed.; NOAA Atlas NESDIS 72, 209 pp.

Carney, R.S. 2005. Zonation of deep-sea biota on continental margins. Oceanogr. Mar. Biol. Annu. Rev. 43: 211–279.

Carstensen, J., Conley, D.J., Lophaven, S., Danielsson, A., Rahm, L., and Toompuu, A. 2002. Statistical Analysis and Modelling of Phytoplankton Dynamics: Exploitation of Data in the Nordic and Baltic Monitoring Programs, Nordic Council of Ministers.

Cheng, R.T., Ling, C-H, and Gartner, J.W. 1999. Estimates of bottom roughness length and bottom shear stress in South San Francisco Bay, California. J. Geophys. Res. 104: 7715-7728.

de Boyer Montégut, C., Madec, G., Fischer, A.S., Lazar, A., and Iudicone, D. 2004. Mixed layer depth over the global ocean: An examination of profile data and a profile-based climatology. J Geophys Res 109, C12003, doi:10.1029/2004JC002378.

DeCarlo, L.T. On the meaning and use of kurtosis. Psychol. Methods, 2(3): 292-307.

Deutsch, C.V. 1996. Correcting for negative weights in ordinary kriging. Comput. Geosci. 22: 765-773.

Drinkwater, K.F., Petrie, B., and Smith, P.C. 2003. Climate variability on the Scotian Shelf during the 1990s. ICES Mar. Sci. Symp. 219: 40-49.

Feldman, G.C., and McClain, C.R. 2012. Ocean Color Web, SeaWiFS Reprocessing 2010.0, NASA Goddard Space Flight Centre. Eds. Kuring, N. and Bailey, S.W. June, 2012. http://oceancolor.gsfc.nasa.gov/

Goovaerts, P. 1997. Geostatistics for Natural Resources Evaluation. Oxford University Press. 483 pp.

Goovaerts, P. 2000. Geostatistical approaches for incorporating elevation into the spatial interpolation of rainfall. J. Hydrol. 228: 113–129.

Guijarro, J., Beazley, L., Lirette, C., Wang, Z., and Kenchington, E. 2016. Characteristics of Environmental Data Layers for Use in Species Distribution Modelling in the Newfoundland and Labrador Region. Can. Tech. Rep. Fish. Aquat. Sci. 3187: viii + 325p.

Harrison, W.G., Martin, J.L. and Maass, H. 2007. Phytoplankton Early Warning Approaches for Finfish Aquaculture in Southwestern New Brunswick: Utility of Satellite-based Remote-sensing of Ocean Colour. Can. Tech. Rep. Fish. Aquat. Sci. 2706: iii + 27 p.

Hebert, D., Pettipas, R., Brickman, D., and Dever M. 2013. Meteorological, Sea Ice and Physical Oceanographic Conditions on the Scotian Shelf and in the Gulf of Maine during 2012. DFO Can. Sci. Advis. Sec. Res. Doc. 2013/058. v + 46 p.

Johnston, K., Ver Hoef, J.M., Krivoruchko, K., and Lucas, N. 2001. Using ArcGIS Geostatistical Analyst. ArcGIS User manual, ESRI. California, Redlands. 1-300 pp.

Knudby, A., Kenchington, E., and Murillo, F.J. 2013. Modeling the distribution of *Geodia* sponges and sponge grounds in the northwest Atlantic Ocean. PLoS ONE 8(12): e82306. doi:10.1371/journal.pone.0082306.

Kravchenko, A., and Bullock, D.G. 1999. A comparative study of interpolation methods for mapping soil properties. Agron. J. 91: 393–400.

Krivoruchko, K. 2011. Spatial Statistical Data Analysis for GIS Users. ESRI Press, Redlands, CA. 928 pp.

Levin, L.A., Etter, R. J., Rex, M.A., Gooday, A.J., Smith, C. R., Pineda, J., Stuart, C. T., et al. 2001. Environmental influences on regional deep-sea species diversity. Annu. Rev. Ecol. Syst., 32: 51–93.

Li, J. and Heap, A.D. 2008. A Review of Spatial Interpolation Methods for Environmental Scientists. Geoscience Australia, Record 2008/23, 137 pp.

Lutz, M.J., Caldeira, K., Dunbar, R.B., and Behrenfeld, M.J. 2007. Seasonal rhythms of net primary production and particulate organic carbon flux to depth describe the efficiency of biological pump in the global ocean. J Geophys Res-Oceans 112: C10011.

Ly, S., Charles, C., and Degré, A. 2011. Geostatistical interpolation of daily rainfall at catchment scale: the use of several variogram models in the Ourthe and Ambleve catchments, Belgium. Hydrol. Earth Syst. Sci. 15: 2259-2274.

MacDonald, I. R., Bluhm, B. A., Iken, K., Gavaev, S., and Strong, S. 2010. Benthic macrofauna and megafauna assemblages in the Arctic Deep-Sea Canada Basin. Deep Sea Res. II 57: 136–152.

Manasrah, R., Raheed, M., and Badran, M.I. 2006. Relationships between water temperature, nutrients and dissolved oxygen in the northern Gulf of Aqaba, Red Sea. Oceanologia 48: 237-253.

Mercier, A., Hamel, J-F. 2011. Contrasting reproductive strategies in three deep- sea octocorals from eastern Canada: *Primnoa resedaeformis*, *Keratoisis ornata*, and *Anthomastus grandiflorus*. Coral Reefs 30: 337–350.

Moses, W.J., Gitelson, A.A., and Povazhnyy, A. 2009. Estimation of chlorophyll-*a* concentration in case II waters using MODIS and MERIS data- successes and challenges. Environ. Res. Lett., 4, doi:10.1088/1748-9326/4/4/045005, 8 pp.

Papiol, V., Cartes, J. E., Fanelli, E., and Maynou, F. 2012. Influence of environmental variables on the spatio-temporal dynamics of the bentho-pelagic assemblages in the middle slope of the Balearic Basin (NW Mediterranean). Deep Sea Res. I, 61: 84–99.

Platt, T., Sathyendranath, S., Forget, M-H., White III, G.N., Caverhill, C., Bouman, H., Devred, E., and Son, S. 2008. Operational estimation of primary production at large geographical scales. Remote Sens. Environ., 112: 3437-3448.

Polovina, J.J., Mitchum, G.T., and Evans, G.T. 1995. Decadal and basin-scale variation in mixed layer depth and the impact on biological production in the Central and North Pacific, 1960-88. Deep-Sea Res. 42: 1701-1716.

Queste, B.Y., Heywood, K.J., Smith Jr., W.O., Kaufman, D.E., Jickells, T.D., and Dinniman, M.S. 2015. Dissolved oxygen dynamics during a phytoplankton bloom in the Ross Sea polynya. Antarct. Sci. 27(4): 362-372.

Robinson, T.P., and Metternicht, G. 2006. Testing the performance of spatial techniques for mapping soil properties. Comput. Electron. Agric. 50: 97-108.

Soltwedel, T., Jaeckisch, N., Ritter, N., Hasemann, C., Bergmann, M., and Klages, M. 2009. Bathymetric patterns of megafaunal assemblages from the arctic deep-sea observatory HAUSGARTEN. Deep Sea Res. I 56: 1856–1872.

Spetland, F., Rapp, H.T., Hoffmann, F., and Tendal, O.S. 2007. Sexual reproduction of *Geodia barretti* Bowerbank 1858 (Porifera, Astrophorida) in two Scandinavian fjords. In: Custódio, M.R., Lôbo-Hajdu, G., Hajdu, E., and Muricy, G (eds). Porifera Research: Biodiversity, Innovation and Sustainability. Rio de Janeiro, Brazil: Museu. Nacional: 613-620.

Sun, Z., Hamel,J.-F., Edinger, E., Mercier, A. 2010a. Reproductive biology of the deep-sea octocoral *Drifa glomerata* in the Northwest Atlantic. Mar. Biol. 157: 863–873.

Sun, Z., Hamel, J.-F., Mercier, A. 2010b. Planulation periodicity, settlement preferences and growth of two deep-sea octocorals from the Northwest Atlantic. Mar. Ecol. Prog. Ser. 410: 71–87.

Sun, Z., Hamel, J.-F., Mercier, A. 2011. Planulation, larval biology, and early growth of the deep-sea soft corals *Gersemia fruticosa* and *Duva florida* (Octocorallia: Alcyonacea). Invert. Biol. 130: 91–99.

Sutherland, B.R., Barrett K.J. and Gingras, M.K. 2014. Clay settling in fresh and salt water. Environ. Fluid Mech. 15: 147-160.

Vance, R.R. 1973. On reproductive strategies in marine benthic invertebrates. Amer. Nat. 107: 339-352.

Yamamoto, J.K. 2007. On unbiased backtransform of lognormal kriging estimates. Comput. Geosci. 11: 219-234.

APPENDIX I - Summary of Variables with Negative Values in the Interpolated Prediction Surface Resulting from Ordinary Kriging

Appendix 1 shows a map of each of the seven variables with negative values resulting in the prediction surfaces after spatial interpolation using ordinary kriging. The location of the negative values is highlighted in blue. The data distribution prior to modeling and the numbers of cells with negative values for each variable is presented in Table A1. Negative values associated with temperature and salinity were found along the continental slope.

Table A1. Summary of environmental variables with negative prediction values resulting from ordinary kriging.

Variable	Negative values in input	Data distribution	Total number of cells	Cells with negative values	Range of negative values
Bottom Temperature Range	No	Right-skewed	326,283	1970	-0.78 to -2.43×10^{-6}
Bottom Temperature Average Range	No	Right-skewed, single large outlier	326,283	5470	-0.68 to -5.26×10^{-6}
Bottom Salinity Range	No	Right-skewed, single large outlier	326,283	4032	-0.18 to -2.83×10^{-6}
Bottom Salinity Average Range	No	Right-skewed, single large outlier	326,283	11390	-0.13 to -1.39×10^{-6}
Spring Chlorophyll *a* Range	No	Right-skewed	326,283	2	-0.06, -0.03
Annual Chlorophyll *a* Range	No	Right-skewed; outliers	326,283	1	-0.02

Bottom Temperature Range

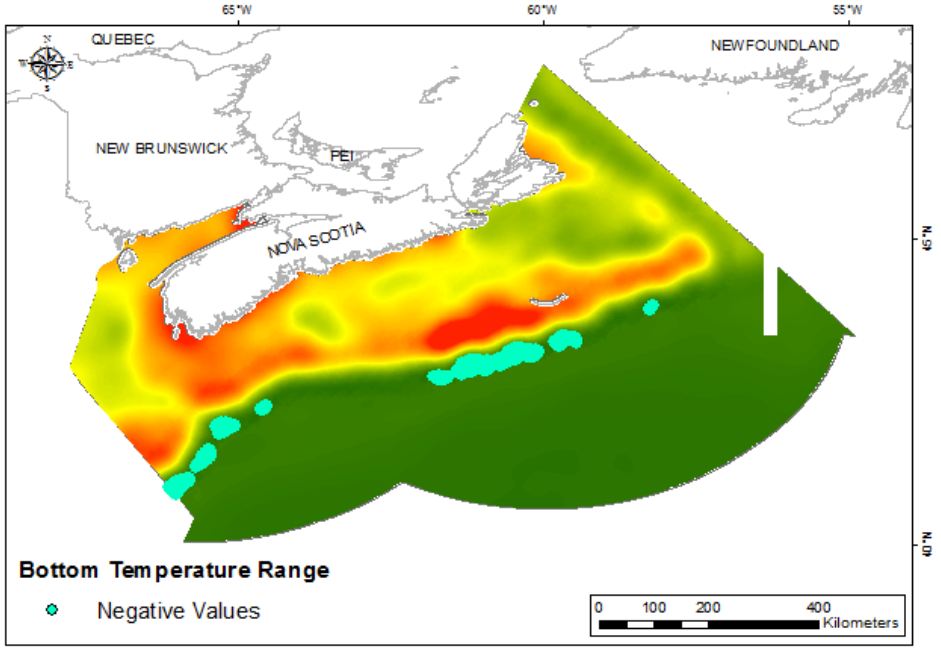

Fig. A1. Negative values generated in the interpolated prediction surface of Bottom Temperature Range.

Bottom Temperature Average Range

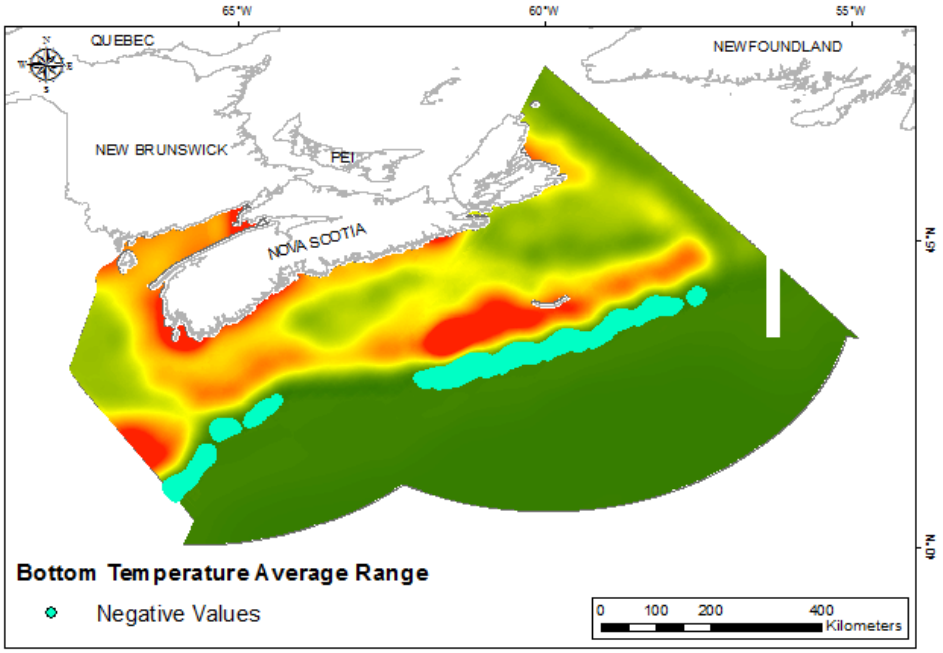

Fig. A2. Negative values generated in the interpolated prediction surface of Bottom Temperature Average Range.

Bottom Salinity Range

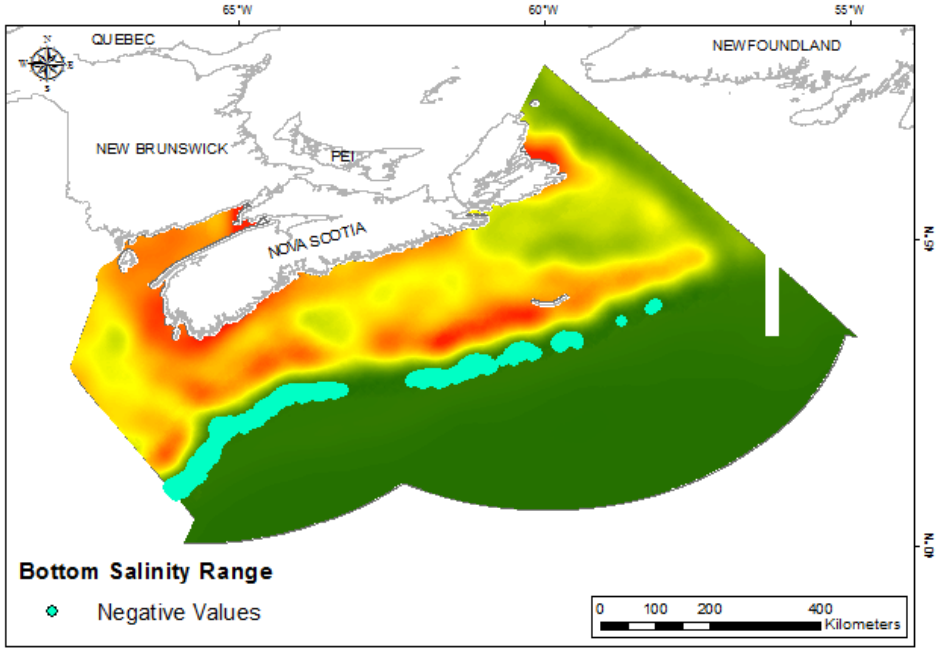

Fig. A3. Negative values generated in the interpolated prediction surface of Bottom Salinity Range.

Bottom Salinity Average Range

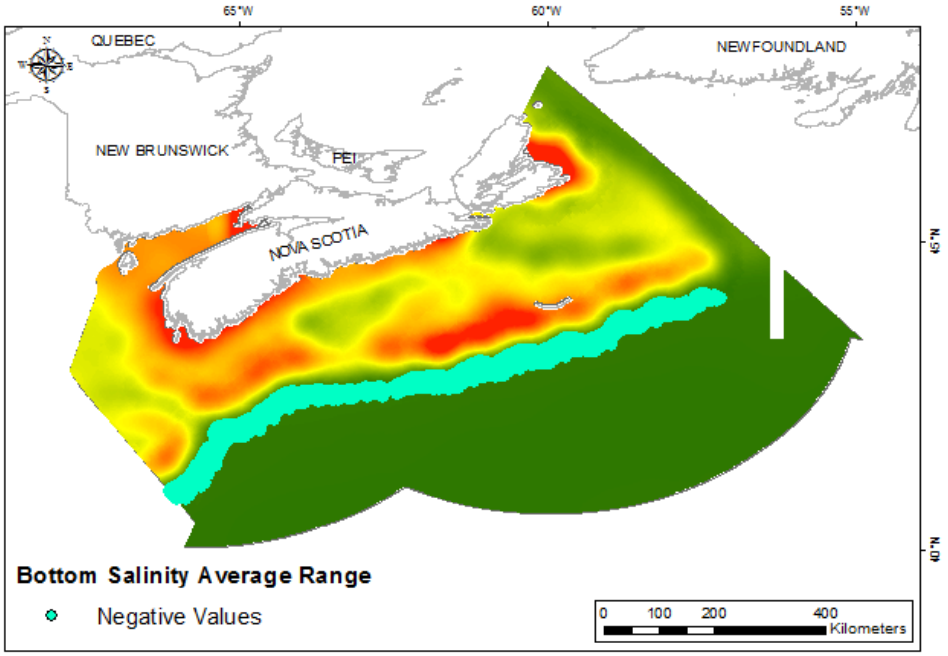

Fig. A4. Negative values generated in the interpolated prediction surface of Bottom Salinity Average Range.

Spring Chlorophyll *a* Range

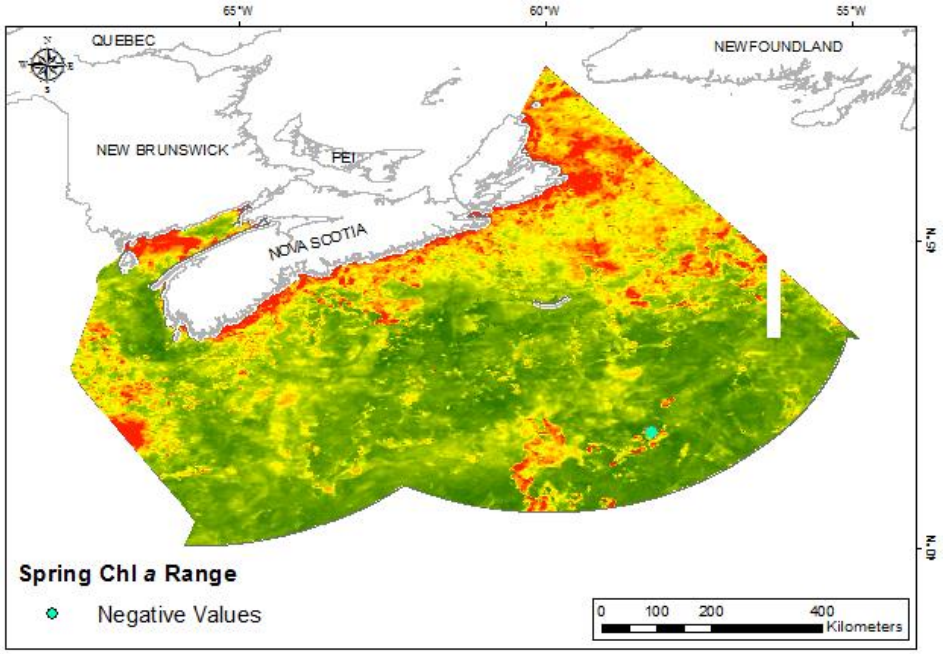

Fig. A5. Negative values generated in the interpolated prediction surface of Spring Chlorophyll *a* Range.

Annual Chlorophyll *a* Range

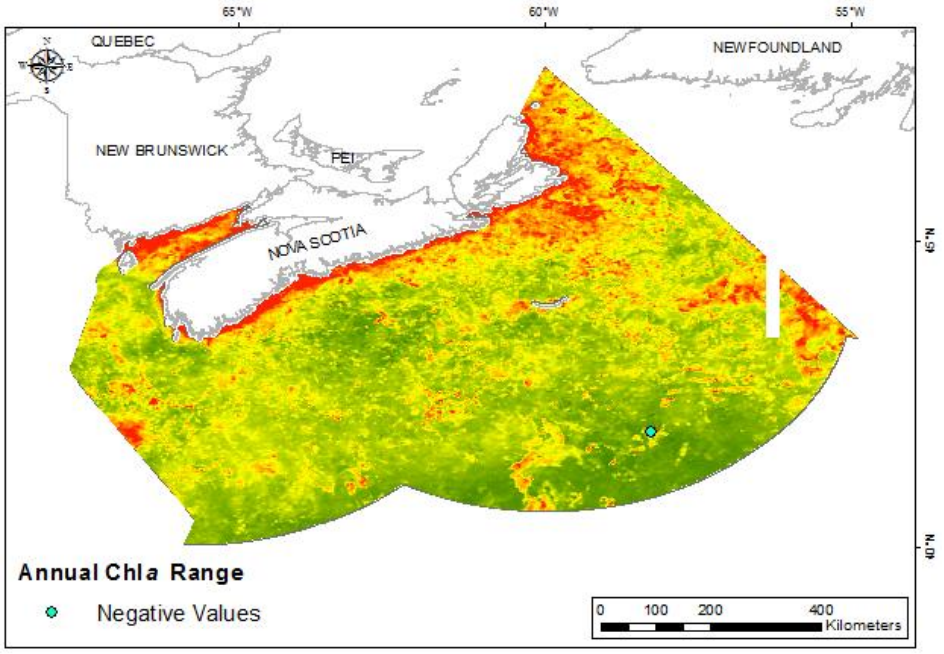

Fig. A6. Negative values generated in the interpolated prediction surface of Annual Chlorophyll *a* Range.